

Examining the TRPV3 cation channel in a culture model of human epidermis

Ciara Larkin, B.A. (Mod.)

This thesis is submitted to
Dublin City University
for the award of
PhD

School of Biotechnology,
Dublin City University,
Ireland.


This work was supervised by:

Dr. Jianghui Meng
Dr. Jiafu Wang
Dr. Dermot Walls, and
Dr. Sandra O'Neill.

August 2023

Declaration and Statement of Plagiarism

I hereby certify that this material, which I now submit for assessment on the programme of study leading to the award of Doctor of Philosophy is entirely my own work, and that I have exercised reasonable care to ensure that the work is original, and does not to the best of my knowledge breach any law of copyright, and has not been taken from the work of others save and to the extent that such work has been cited and acknowledged within the text of my work.

Signed: X 
Ciara Larkin

ID No.: 17210338

Date: 22/08/2023

Acknowledgements

This research was funded by the Science Foundation Ireland Starting Investigator Research Grant (15/SIRG/3508T). This grant was supplemented by the Orla Benson Postgraduate Research Scholarship (2019/20, DCU), which covered my work at the University of Debrecen, Hungary. Additional funding was provided by the Higher Education Authority and DCU.

I would like to acknowledge and thank my supervisor, Dr. Jianghui Meng. Thank you for the guidance and encouragement; thank you for giving me the space to explore. This project encountered more than one obstacle, but you remained calm and helped keep me focused. This work would have been impossible without you.

I would also like to extend my sincerest thanks to my co-supervisor, Dr. Jiafu Wang, and mentors: Dr. Anne Parle-McDermott, Dr. Dermot Walls, and Dr. Sandra O'Neill. Each of you provided invaluable support and advice; from the bottom of my heart, thank you.

This research would not have been possible without our incredible collaborators. Many thanks to Dr. Andrea Szegedi, Dr. Imre Lőrinc Szabó, and Dr. Zsolt Dajnoki in Debrecen, Hungary. Thanks also to Dr. Martin Steinhoff in Qatar; to Dr. Timo Buhl in Germany; and to Dr. Weiwei Chen, Dr. Song Xiao, Dr. Wenke Cheng, and Dr. Yuanyuan Fan in China.

I also wish to highlight the many DCU colleagues and friends who were always willing to share their expertise or lend a sympathetic ear. Thank you to the Meng/Wang team: Dr. ChunXu Shan, Mr. John Nealon, Dr. Kim Orange, and Dr. Minhong Tang. Thank you to my lab mates in the School of Biotechnology, the Nano Research Facility, and the National Institute for Cellular Biotechnology. Special thanks to Ms. Aoife Connolly, Dr. Antonios Dougalis, Dr. Damian O'Donohue, Dr. Orla Moriarty, Dr. Richard Lalor, Dr. Seshu Kumar Kaza, and Dr. Tom Zurawski.

This project is thanks to the phenomenal staff working behind the scenes in DCU. These incredible humans kept my research going and my sanity intact. Thank you to Ms. Josephine Ozoani, Ms. Leah Nolan, Mr. Maurice Burke, Mr. Robbie Sinnott, and Dr. Úna Prendergast from the Nano Research Facility. Thank you to Dr. Donal O'Gorman, Dr. Finbarr O'Sullivan, Ms. Mairead Callan, and Dr. Michael Henry from the National Institute for Cellular Biotechnology. Special thanks to Dr. Rosaleen Devery and Ms. Sharon Whyte. I would like to extend my deepest gratitude to Mr. Michael Burke: your unwavering support and commitment will never be forgotten.

Finally, thank you to my wonderful family and friends. To my parents, Denise and Padraic, who always believed in me; thank you. To my sister and brother, Michelle and Cathal, who picked up the slack when birthdays came around; thank you. To my friends and housemates who always knew when not to ask; thank you. Thank you to everyone who championed my successes and endured my rants – I couldn't have done it without you!

Table of Contents

Title Page.....	i
Declaration and Statement of Plagiarism	iii
Acknowledgements	v
Table of Contents	vi
List of Abbreviations.....	ix
List of Tables.....	xiii
List of Figures.....	xiv
Value of Research.....	xix
Aims and Objectives.....	xix
Publications	xx
Other Publications	xx
Abstract.....	xxi
1. Introduction.....	1
1.1. The skin.....	2
1.1.1. Structure of the skin	2
1.1.2. Immunology of the skin.....	6
1.1.3. Cutaneous neural networks	8
1.2. Skin disease and itch	10
1.2.1. Inflammatory skin disease	10
1.2.2. Chronic itch (pruritus).....	12
1.3. Acute itch pathways and their role in pruritus	16
1.3.1. Acute itch vs. pain.....	16
1.3.2. Types of acute itch	16
1.3.3. Chemical itch pathways in the periphery	20
1.3.4. Nonneuronal cells in itch transduction.....	23
1.4. TRP channels and pruritus	29
1.4.1. TRPV1 in histaminergic itch and pruritic conditions	30
1.4.2. TRPA1 in nonhistaminergic itch and pruritic conditions	31
1.4.3. Emerging TRP channels in itch research	32
1.5. The TRPV3 cation channel	33
1.5.1. TRPV3 expression and protein structure	33
1.5.2. Biophysical and molecular features of the TRPV3 channel	35
1.5.3. TRPV3 as a coordinator of epidermal patterning	39
1.5.4. TRPV3 mutations and Olmsted syndrome.....	42
1.5.5. TRPV3 as an inducer of inflammation, itch, and dermatitis.....	43
1.5.6. Targeting TRPV3.....	46

2.	Materials and Methods	49
2.1.	Materials	50
2.1.1.	Primary epidermal keratinocytes from human donors.....	50
2.1.2.	Reagents, compounds, kits, and consumables	50
2.1.3.	Primary antibodies.....	54
2.1.4.	Secondary antibodies.....	55
2.1.5.	Equipment and software	56
2.2.	Methods	57
2.2.1.	Culturing normal human epidermal keratinocytes (NHEK).....	57
2.2.2.	Lentivirus-mediated protein knockdown: reducing VAMP3 expression	59
2.2.3.	Pre-treatments, inhibitors, and stimulations	60
2.2.4.	Phospho-kinase array: comparing activation of kinase proteins	64
2.2.5.	Cytokine array: comparing mediator release.....	65
2.2.6.	Calcium imaging: monitoring calcium in live keratinocytes.....	66
2.2.7.	Classifying calcium responses using <i>k</i> -means clustering	68
2.2.8.	SDS-PAGE and western blotting: comparing protein expression.....	69
2.2.9.	Immunocytochemistry	70
2.2.10.	Data analyses	72
3.	Examining the Signalling Pathways Acting Downstream of the TRPV3 Channel... 73	73
3.1.	Overview	74
3.2.	Results	75
3.2.1.	Keratinocytes in our NHEK model express key cytoskeletal and TRPV3 proteins	75
3.2.2.	TRP channel agonists activate distinct intracellular signalling	77
3.2.3.	TRPA1 and TRPV1 agonists fail to promote consistent mediator release	89
3.2.4.	The TRPV3 agonist promotes mediator release	107
3.2.5.	TRPV3-linked mediator release is independent of JNK signalling.....	111
3.2.6.	Keratinocytes in our NHEK model express key SNARE proteins.....	114
3.2.7.	Knockdown of VAMP3 alters TRPV3-linked mediator release	118
3.3.	Discussion.....	130
3.3.1.	Summary.....	130
3.3.2.	Specificity of TRP agonists	132
3.3.3.	TRPV3-linked mediators: their role in skin health and disease.....	134
3.3.4.	Conclusion.....	136
4.	Examining the Dynamics of TRPV3-mediated Calcium Fluctuations..... 137	137
4.1.	Overview	138
4.2.	Results	139
4.2.1.	TRPA1, TRPV1, and TRPV3 agonists enhance calcium flux in subsets of cultured epidermal keratinocytes.....	139
4.2.2.	The TRPV3 agonist induces a phasic calcium response	145

4.2.3.	Pharmacological blockade of endocytosis alters the temporal features of the TRPV3 calcium response.....	152
4.2.4.	Knockdown of VAMP3 alters TRPV3-linked calcium responses; however, issues with controls negate robust conclusions.....	161
4.2.5.	TRPV3 undergoes activation-induced trafficking	167
4.3.	Discussion	171
4.3.1.	Summary	171
4.3.2.	Are TRPV1 and TRPA1 functional in human keratinocytes?	173
4.3.3.	Properties of the TRPV3 channel.....	174
4.3.4.	Clustering analyses: a method for detecting subtle changes in calcium channel activity	175
4.3.5.	Conclusion	176
5.	Assessing the Impact of BNP on TRPV3 Sensitivity, Signalling, and Trafficking	177
5.1.	Overview.....	178
5.2.	Results.....	179
5.2.1.	Keratinocytes in our NHEK model express receptors for BNP: NPRA and NPRB	179
5.2.2.	BNP sensitises TRPV3-mediated calcium fluctuations	180
5.2.3.	BNP fails to enhance TRPV3-linked mediator release	191
5.2.4.	BNP promotes TRPV3 trafficking and membrane insertion	194
5.2.5.	BNP-induced TRPV3 trafficking is mediated by GSK-3 α/β , JNK-pan, and p38 α kinase proteins	199
5.3.	Discussion	206
5.3.1.	Summary	206
5.3.2.	Inter-experimental differences in number of calcium clusters.....	208
5.3.3.	BNP: an inducer of early epidermal alterations?	211
5.3.4.	Targeting BNP	212
5.3.5.	Conclusion	212
6.	Discussion of Work in Context.....	213
6.1.	TRPV3 and the role of cation gradients in the skin	214
6.2.	TRPV3-linked itch and the microbiome	217
6.3.	TRPV3 and Piezo channels.....	222
6.4.	TRPV3 and the wider cutaneous system.....	226
6.5.	Limitations and questions for future research.....	232
6.5.1.	The impact of culture conditions and donor genetics on TRPV3-linked signalling.....	232
6.5.2.	Measuring TRPV3-linked signalling	235
6.5.3.	Assessing TRPV3-linked calcium responses	236
6.5.4.	Tracking TRPV3 activation dynamics and trafficking	238
6.6.	Statement of impact, summary, and conclusions	240
7.	Bibliography	241

List of Abbreviations

2-APB	2-Aminoethoxydiphenyl borate	CER	Ceramide
5-HT	Serotonin	CGRP	Calcitonin gene-related peptide
a.u.	Arbitrary units	CHIR.	CHIR99021
ACD	Allergic contact dermatitis	Chk2	Checkpoint kinase 2
AD	Atopic dermatitis	CHOL	Cholesterol
AITC	Allyl isothiocyanate	c-Jun	AP-1 transcription factor subunit
AL.	AL8697	CN	Cuneate nucleus
ARD	Ankyrin repeat domain	CXCL1	Chemokine (C-X-C motif) ligand 1
ATP	Adenosine triphosphate	D250	Drofenine (250 μ M)
AUC	Area under the curve	D500	Drofenine (500 μ M)
BA	Bile acids	DAPI	4',6-diamidino-2-phenylindole
BCA	Bicinchoninic acid assay	D_B	Densitometry from basal samples
BChE	Butyrylcholinesterase	Dkk-1	Dickkopf-1
BNP	B-type natriuretic peptide	DPBA	Diphenylboronic anhydride
BoNT	Botulinum neurotoxins	DPBS	Dulbecco's phosphate-buffered saline
BSG	Basigin	DRG	Dorsal root ganglion
CE	Cornified envelope	Drof.	Drofenine

D_s	Densitometry from stimulated samples	GPCR	G protein-coupled receptors
DYN	Dynorphin	GSK3	Glycogen synthase kinase-3
EC	Endothelial cells	h	hour(s)
ECM	Extracellular matrix	Hck	Hematopoietic cell kinase
ECN	External cuneate nucleus	HDP	Host defence peptides
EGF	Epidermal growth factor	HEPES	HEPES buffered saline solution
EGFR	EGF receptor	HF	Hair follicle
eNOS	Endothelial nitric oxide synthase	HRP	Horseradish peroxidase
ER	Endoplasmic reticulum	HUVEC	Human umbilical vein endothelial cells
FCER	Fc epsilon receptor	ICC	Immunocytochemistry
FCH	Fold change	IFNγ	Interferon gamma
FDF-19	Fibroblast growth factor 19	IgE	Immunoglobulin E
FFA	Free fatty acid	IgG	Immunoglobulin G
FGF	Fibroblast growth factor	IL	Interleukin
Fyn	FYN proto-oncogene	IL-1ra	Interleukin 1 receptor antagonist
FA/F0	Change in fluorescence	IMQ	Imiquimod
FA/F0_{max}	Amplitude of calcium peak	JAK	Janus kinase
GN	Gracile nucleus	JNK	Jun N-terminal kinase

JNK.	JNK-IN-8	NP	Nonpeptidergic
JNK1/2/3	c-Jun N-terminal kinase 1/2/3	NPRA/B/C	Natriuretic peptide receptor type A/B/C
kDa	kilodalton	ns	not significant
KLK	Kallikrein	NT	Nontargeted
Kv	Voltage-gated potassium channel	p38α	p38 α mitogen-activated protein kinase
LC	Langerhans cells	p53	Cellular tumour antigen p53
LEKTI	Lympho-epithelial Kazal type inhibitor	p70S6K	Ribosomal protein S6 kinase
LTMR	Low-threshold mechanoreceptor	PAI-1	Plasminogen activator inhibitor 1
MAPK	Mitogen-activated protein kinase	PDGFA	Platelet-derived growth factors
M-CSF	Macrophage colony-stimulating factor 1	PKC	Protein kinase C
MIF	Migration inhibitory factor	PLCγ1	Phospholipase C-gamma-1
min	minute(s)	PTX3	Pentraxin-related protein PTX3
MMP	Matrix metalloproteinase	Q¹ - Q³	25th percentile – 75th percentile
Mrgpr	Mas-related G protein-coupled receptors	QOL	Quality of life
MW	Molecular weight marker	ROI	Region of interest
NF	Neurofilament	S	Serine residue
NGAL	Neutrophil gelatinase-associated lipocalin	s.p.i.	seconds post initiation
NHEK	Normal human epidermal keratinocytes	SC	Stratum corneum

SEM	Standard error of the mean	TRPA1	Transient receptor potential ankyrin 1
shRNA	Short hairpin RNA	TRPC	Transient receptor potential canonical
SNAP	Soluble NSF attachment protein	TRPML	Transient receptor potential mucolipin
SNARE	Soluble N-ethylmaleimide-sensitive factor activating protein receptor	TRPV	Transient receptor potential vanilloid
SP.	SP600125	TSLP	Thymic stromal lymphopoietin
SPF	Specific pathogen free	TSLPR	Thymic stromal lymphopoietin receptor
SPRR	Small proline-rich proteins	TSP-1	Thrombospondin-1
STAT	Signal transducer and activation of transcription	V3T	VAMP3-targeted
SYK	Spleen tyrosine kinase	VAMP	Vesicle-associated membrane protein
T	Threonine residue	VDBP	Vitamin D binding protein
TBS	Tris Buffered Saline	VEGF	Vascular endothelial growth factor
TEWL	Trans-epidermal water loss	VSLD	Voltage sensing-like domain
TfR	Transferrin receptor	WB	Western blot
TGF-α	Transforming growth factor alpha	WNK1	Lysine deficient protein kinase 1
Th	T helper	WT	Wild type
Time_{max}	Latency of calcium peak	Y	Tyrosine residue
TNF	Tumour necrosis factor	Yes	Yamaguchi sarcoma virus oncogene
TPA	Total peak area		

List of Tables

Table 2.1.	Basic characteristics of each adult donor.....	50
Table 2.2.	Reagents, compounds, kits, and consumables.....	51
Table 2.3.	Primary antibodies.....	54
Table 2.4.	Secondary antibodies.....	55
Table 2.5.	Key equipment and software.....	56
Table 3.1.	Representative images of duplicate antibody spots from phospho-kinase array showing effect of TRP agonists on intracellular protein phosphorylation.....	78
Table 3.2.	Representative images of duplicate antibody spots from cytokine array showing effect of TRP agonists on mediator release.....	89
Table 3.3.	Representative images of duplicate antibody spots from cytokine array showing effect of TRPV3 agonist on mediator release.....	108
Table 3.4.	Representative images of duplicate antibody spots from cytokine array showing effect of JNK inhibitor on TRPV3 agonist-induced mediator release.....	112
Table 3.5.	Representative images of duplicate antibody spots from cytokine array showing effect of VAMP3 knockdown on TRPV3 agonist-induced mediator release.....	120
Table 4.1.	Calcium response parameters in TRP agonist-sensitive keratinocytes.....	140
Table 4.2.	Basic cellular parameters: TRP agonist-sensitive vs. TRP agonist-insensitive keratinocytes.....	143
Table 4.3.	Calcium response parameters following TRPV3 agonist stimulation: effect of endocytosis inhibitor Pitstop2 vs. control.....	157
Table 4.4.	Basic cellular parameters: TRPV3-positive vs. TRPV3-negative keratinocytes.....	168
Table 5.1.	Range of peak latency values included in each cluster.....	188
Table 5.2.	Representative images of duplicate antibody spots from cytokine array showing effect of BNP pre-treatment on TRPV3-associated mediator release.....	192
Table 5.3.	Basic cellular parameters: TRPV3-positive vs. TRPV3-negative keratinocytes.....	195
Table 5.4.	Range of peak latency values in each cluster: Section 4.2.3 vs. Section 5.2.2.....	209

List of Figures

Figure 1.1. Structure of mammalian skin.	2
Figure 1.2. Structure of mammalian epidermis.	3
Figure 1.3. Keratinocyte differentiation and stratum corneum formation.	4
Figure 1.4. Model of epidermal desquamation.	5
Figure 1.5. Immunological anatomy of the epidermis.	6
Figure 1.6. The diverse contribution of keratinocytes to immune responses in skin.	7
Figure 1.7. Sensory afferents in hairy and glabrous skin.	9
Figure 1.8. Comparison of inflammation and immune cell responses in psoriasis and atopic dermatitis.	11
Figure 1.9. Conditions and disorders associated with chronic pruritus.	12
Figure 1.10. Schematic representation of cells and mediators involved in peripheral itch.	14
Figure 1.11. BNP and itch transduction.	15
Figure 1.12. Neural pathways underpinning acute mechanical and chemical itch transduction.	17
Figure 1.13. Schematic of proposed peripheral itch circuits in mice.	20
Figure 1.14. Direct pruritogens secreted from nonneuronal cutaneous cells.	24
Figure 1.15. Mast cell-evoked itch.	25
Figure 1.16. Basophils promote allergen-induced acute itch flares in atopic patients.	26
Figure 1.17. Keratinocyte-evoked itch.	27
Figure 1.18. Phylogeny of TRP channels.	29
Figure 1.19. TRPV3 is expressed in epidermal keratinocytes.	33
Figure 1.20. Polypeptide sequence of human TRPV3.	34
Figure 1.21. Structural characterisation of human TRPV3.	35
Figure 1.22. Two physical constrictions along the ion pore of TRPV3 in a lipid bilayer.	36
Figure 1.23. Activators, inhibitors, and modulators of TRPV3.	38
Figure 1.24. TRPV3 deficient mice exhibit curly whiskers, misaligned hair follicles, and a thin stratum corneum.	40
Figure 1.25. Carvacrol induces hyperplasia in wild type but not TRPV3 knockout mice.	41
Figure 1.26. Schematic structure of TRPV3 showing location of reported mutations in people with Olmsted syndrome.	42
Figure 1.27. Knockout of TRPV3 suppresses carvacrol-induced scratching in C57BL/6J mice.	44
Figure 1.28. TRPV3 proteins are upregulated in the epidermis of atopic dermatitis lesions.	45
Figure 1.29. Several skin conditions are associated with elevated epidermal TRPV3.	45
Figure 2.1. Culturing normal human epidermal keratinocytes.	57
Figure 2.2. VAMP3 AlphaFold structure prediction.	59
Figure 2.3. Chemical information on pre-treatments, inhibitors, and stimulations.	60
Figure 2.4. Example of phospho-kinase array membrane.	64
Figure 2.5. Example of cytokine array membrane.	65

Figure 3.1. Keratinocytes in our NHEK model express key cytoskeletal and TRPV3 proteins.	76
Figure 3.2. Effect of TRP agonists on activation of Chk2.	79
Figure 3.3. Effect of TRP agonists on activation of c-Jun.	80
Figure 3.4. Effect of TRP agonists on activation of eNOS.	81
Figure 3.5. Effect of TRP agonists on activation of Fyn.	81
Figure 3.6. Effect of TRP agonists on activation of Hck.	82
Figure 3.7. Effect of TRP agonists on activation of p53.	83
Figure 3.8. Effect of TRP agonists on activation of p70S6K.	83
Figure 3.9. Effect of TRP agonists on activation of PLC γ 1.	84
Figure 3.10. Effect of TRP agonists on activation of STAT5A.	85
Figure 3.11. Effect of TRP agonists on activation of WNK1.	86
Figure 3.12. Effect of TRP agonists on activation of Yes.	86
Figure 3.13. Effect of TRP agonists on activation of p38 α	87
Figure 3.14. Effect of TRP agonists on BSG release.	91
Figure 3.15. Effect of TRP agonists on CXCL1 release.	92
Figure 3.16. Effect of TRP agonists on Dkk-1 release.	93
Figure 3.17. Effect of TRP agonists on EGF release.	93
Figure 3.18. Effect of TRP agonists on FGF-2 release.	94
Figure 3.19. Effect of TRP agonists on FGF-19 release.	95
Figure 3.20. Effect of TRP agonists on IFN γ release.	95
Figure 3.21. Effect of TRP agonists on IL-1 α release.	96
Figure 3.22. Effect of TRP agonists on IL-1ra release.	97
Figure 3.23. Effect of TRP agonists on IL-8 release.	97
Figure 3.24. Effect of TRP agonists on IL-17A release.	98
Figure 3.25. Effect of TRP agonists on KLK3 release.	99
Figure 3.26. Effect of TRP agonists on M-CSF release.	99
Figure 3.27. Effect of TRP agonists on MIF release.	100
Figure 3.28. Effect of TRP agonists on NGAL release.	101
Figure 3.29. Effect of TRP agonists on PAI-1 release.	101
Figure 3.30. Effect of TRP agonists on PDGFA release.	102
Figure 3.31. Effect of TRP agonists on PTX3 release.	103
Figure 3.32. Effect of TRP agonists on Tfr release.	104
Figure 3.33. Effect of TRP agonists on TGF- α release.	104
Figure 3.34. Effect of TRP agonists on TSP-1 release.	105
Figure 3.35. Effect of TRP agonists on VDBP release.	106
Figure 3.36. Further analyses investigating effect of the TRPV3 agonist on mediator release.	110
Figure 3.37. TRPV3 agonist-evoked mediator release is independent of JNK signalling.	113

Figure 3.38. Keratinocytes in our NHEK model express SNAP23 and syntaxin 3 SNARE proteins.....	114
Figure 3.39. Keratinocytes in our NHEK model express SNAP29 and syntaxin 16 SNARE proteins.....	115
Figure 3.40. Keratinocytes in our NHEK model express VAMP3 and syntaxin 4 SNARE proteins.....	116
Figure 3.41. Keratinocytes in our NHEK model express VAMP3 and VAMP7 SNARE proteins.....	117
Figure 3.42. VAMP3-targeted shRNA successfully reduced VAMP3 expression.	118
Figure 3.43. Effect of VAMP3 knockdown on TRPV3 agonist-evoked BSG release.	121
Figure 3.44. Effect of VAMP3 knockdown on TRPV3 agonist-evoked Dkk-1 release.....	122
Figure 3.45. Effect of VAMP3 knockdown on TRPV3 agonist-evoked EGF release.	123
Figure 3.46. Effect of VAMP3 knockdown on TRPV3 agonist-evoked IL-1 α release.....	124
Figure 3.47. Effect of VAMP3 knockdown on TRPV3 agonist-evoked IL-1ra release.....	125
Figure 3.48. Effect of VAMP3 knockdown on TRPV3 agonist-evoked MIF release.....	126
Figure 3.49. Effect of VAMP3 knockdown on TRPV3 agonist-evoked PAI-1 release.....	127
Figure 3.50. Effect of VAMP3 knockdown on TRPV3 agonist-evoked PDGFA release.....	128
Figure 3.51. Effect of VAMP3 knockdown on TRPV3 agonist-evoked TGF- α release.....	129
Figure 3.52. Schematic showing putative kinase pathways acting downstream of TRP channels in epidermal keratinocytes.	130
Figure 3.53. Schematic showing putative pathways involved in release of TRPV3- linked mediators from epidermal keratinocytes.	131
Figure 4.1. Schematic showing timing of TRPA1, TRPV1, and TRPV3 agonist stimulation and calcium recording.....	139
Figure 4.2. Single-cell traces showing effect of basal medium on cellular calcium flux.....	140
Figure 4.3. Single-cell traces showing effect of TRPA1 agonist on cellular calcium flux.	141
Figure 4.4. Single-cell traces showing effect of TRPV1 agonist on cellular calcium flux.	141
Figure 4.5. Single-cell traces, representative images, and population analysis showing effect of TRPV3 agonist on cellular calcium flux.	142
Figure 4.6. Schematic showing timing of TRPV3 agonist stimulation and calcium recording.	145
Figure 4.7. Temporal variation within the TRPV3 agonist-mediated calcium response.....	146
Figure 4.8. Population analysis showing effect drofenine on cellular calcium flux.....	147
Figure 4.9. TRPV3 response profile: Single-cell analysis showing effect of drofenine on cellular calcium peaks.....	148
Figure 4.10. Clustering analysis highlights phasic nature of the TRPV3 agonist-induced calcium response.....	149
Figure 4.11. Cluster subgroups show distinct overall and peak calcium response parameters.....	150
Figure 4.12. Schematic showing timing of Pitstop2 pre-treatment, TRPV3 agonist stimulation, and calcium recording.....	152
Figure 4.13. Raw temporal response data correlates with stage position.....	153

Figure 4.14. Endocytosis inhibitor fails to significantly affect proportion of TRPV3 agonist insensitive keratinocytes.	154
Figure 4.15. Endocytosis inhibitor fails to significantly affect the number of drofenine-induced calcium peaks per cell.	155
Figure 4.16. Endocytosis inhibitor alters the later phases of the TRPV3 agonist-induced calcium response.	156
Figure 4.17. Clustering analysis of control TRPV3-linked calcium response profile.	158
Figure 4.18. Endocytosis inhibitor alters phasic nature of the TRPV3-linked calcium response.	159
Figure 4.19. VAMP3-targeted shRNA successfully reduced VAMP3 expression.	161
Figure 4.20. Schematic showing timing of TRPV3 agonist stimulation in keratinocytes treated with control nontargeted or VAMP3-targeted lentiviral particles.	162
Figure 4.21. Knockdown of VAMP3 increases proportion of TRPV3 agonist insensitive cells.	162
Figure 4.22. Knockdown of VAMP3 altered the TRPV3 agonist-induced calcium response.	163
Figure 4.23. Comparison of TRPV3 agonist-induced calcium responses in normal and lentiviral-treated keratinocytes.	165
Figure 4.24. Surface TRPV3 proteins were detected in cultured epidermal keratinocytes.	167
Figure 4.25. TRPV3 channels undergo activation induced trafficking.	169
Figure 4.26. Graphical summary showing putative pathways underpinning the phasic TRPV3 calcium response.	172
Figure 5.1. Keratinocytes in our NHEK model express receptors for BNP: NPRA and NPRB.	179
Figure 5.2. Schematic showing timing of BNP pre-treatment, TRPV3 agonist stimulation, and calcium recording.	180
Figure 5.3. Raw fluorescence data and single-cell traces showing effect of BNP pre-treatment on TRPV3 agonist-induced calcium response.	181
Figure 5.4. BNP pre-treatment enhances average TRPV3 agonist-induced calcium response.	182
Figure 5.5. BNP pre-treatment increases AUC of TRPV3 agonist-induced calcium response.	183
Figure 5.6. BNP pre-treatment fails to increase amplitude of TRPV3-linked calcium peaks.	184
Figure 5.7. BNP pre-treatment accelerates TRPV3-linked calcium peaks.	185
Figure 5.8. BNP pre-treatment alters TRPV3-linked response profiles.	186
Figure 5.9. Optimum number of clusters (k) within each TRPV3-linked response profile.	187
Figure 5.10. Clustering of TRPV3-linked response profiles using k-means clustering.	188
Figure 5.11. BNP pre-treatment increases amplitude of rapid TRPV3-linked calcium peaks.	189
Figure 5.12. BNP pre-treatment alters phasic nature of the TRPV3-linked calcium response.	190
Figure 5.13. BNP pre-treatment fails to enhance TRPV3 agonist-induced mediator release.	193

Figure 5.14. Representative images showing surface expression of TRPV3 proteins in cultured epidermal keratinocytes.	194
Figure 5.15. Representative images showing effect of BNP on surface expression of TRPV3 proteins in cultured epidermal keratinocytes.	196
Figure 5.16. BNP promotes TRPV3 trafficking.	197
Figure 5.17. BNP alters proportion of TRPV3-positive and TRPV3-negative keratinocytes.	197
Figure 5.18. BNP promotes TRPV3 trafficking in TRPV3-positive keratinocytes.	198
Figure 5.19. Representative images showing surface expression of TRPV3 proteins in cultured epidermal keratinocytes.	199
Figure 5.20. Nonspecific fluorescence is unaffected by kinase inhibitor pre-treatment.	202
Figure 5.21. Inhibition of GSK-3 α/β and JNK1/2/3 reduces BNP-induced TRPV3 trafficking.	203
Figure 5.22. Stimulation with BNP \pm kinase inhibitors alter the proportion of TRPV3-positive and TRPV3-negative keratinocytes.	204
Figure 5.23. Inhibition of p38 α , GSK-3 α/β , and JNK1/2/3 reduces BNP-induced TRPV3 trafficking in TRPV3-positive keratinocytes.	205
Figure 5.24. Graphical summary showing putative pathways underpinning TRPV3 upregulation and sensitisation in atopic dermatitis.	207
Figure 5.25. Clustering ranges from Section 4.2.3 and Section 5.2.2 are comparable.	210
Figure 6.1. Calcium and magnesium gradients in the skin.	215
Figure 6.2. Sequence comparison of TRPV channels.	216
Figure 6.3. Antibiotics improve dermatitis indicators in ADAM17 knockout mice.	219
Figure 6.4. TRPV3 mutation promotes dermatitis and itch in DS-Nh mice housed under conventional, but not specific pathogen free, conditions.	220
Figure 6.5. PAR2, TRPA1, and TRPV1 are upregulated in porcine skin with scabies.	221
Figure 6.6. Merkel cells express TRPV3.	222
Figure 6.7. Piezo1 is expressed in human skin.	225
Figure 6.8. TRPV3, TRPV4, Piezo1, and Piezo 2 are expressed in human oesophageal tissue.	225
Figure 6.9. Mass spectrometry-based proteomic analysis of skin layers and cellular subsets.	226
Figure 6.10. Matrisome genes expressed in dermal fibroblasts.	229
Figure 6.11. The LabSkin™ 3D model of human skin.	233

Value of Research

Chronic itch is a surprisingly common issue: up to 1 in 5 people will experience it at some point in their lifetime (Weisshaar, 2016; Hay *et al.*, 2014). Current estimates from the USA indicate that each chronic itch patient costs the state almost \$300,000 over their lifetime – a societal burden of about \$88.8 billion (Whang *et al.*, 2021). Despite these shocking figures, current anti-itch drugs are largely ineffective. Our group works to develop targeted anti-itch compounds; the *in vitro* work described herein forms the basis of *in vivo* work and guides our drug development.

Aims and Objectives

The primary aim of this project is to further our understanding of the TRPV3 channel in epidermal keratinocytes of the skin.

This aim encompasses several objectives:

1. Delineate the signalling pathways acting downstream of TRPA1, TRPV1, and TRPV3 channels.
2. Outline the kinase and exocytotic pathways involved in TRPV3-evoked mediator release.
3. Examine the functional properties of the TRPV3 channel, focusing on the role of SNARE proteins and receptor cycling.
4. Assess the effect of B-type natriuretic peptide (BNP), a key itch-linked neuropeptide, on epidermal TRPV3 responses.

Together, our research group endeavours to develop targeted anti-itch therapeutics. This project represents the *in vitro* component of our work: team members and international collaborators use these data to guide *in vivo* work and drug development.

Publications

Larkin, C., Chen, W., Szabó, I. L., Shan, C., Dajnoki, Z., Szegedi, A., Buhl, T., Fan, Y., O'Neill, S., Walls, D., Cheng, W., Xiao, S., Wang, J., & Meng, J. (2021). Novel insights into the TRPV3-mediated itch in atopic dermatitis. *Journal of Allergy and Clinical Immunology*, **147**: 1110–1114.

Lu, Z., Xiao, S., Chen, W., Zhu, R., Yang, H., Steinhoff, M., Li, Y., Cheng, W., Yan, X., Li, L., Xue, S., Larkin, C., Zhang, W., Fan, Q., Wang, R., Wang, J., & Meng, J. (2022). IL-20 promotes cutaneous inflammation and peripheral itch sensation in atopic dermatitis. *FASEB Journal*, **36**: 22334.

Yang, H., Zhu, R., Zhang, W., Chen, W., Yan, X., Shan, C., Xue, S., Wang, R., Dai, X., Wang, J., Larkin, C., Wang, J., & Meng, J. (2023). Urotensin II/GPR14 Pathway Regulates Chronic Itch in Mice. *The Journal of Investigative Dermatology* (online ahead of print).

Other Publications

Dempsey, C., Rubio Araiz, A., Bryson, K. J., Finucane, O., Larkin, C., Mills, E. L., Robertson, A. A. B., Cooper, M. A., O'Neill, L. A. J., & Lynch, M. A. (2017). Inhibiting the NLRP3 inflammasome with MCC950 promotes non-phlogistic clearance of amyloid- β and cognitive function in APP/PS1 mice. *Brain, Behavior, and Immunity*, **61**: 306–316.

Examining the Transient Receptor Potential Vanilloid 3 (TRPV3) channel in a culture model of human epidermis

Ciara Larkin

Abstract

Chronic itch affects about to 1 in 5 people worldwide (Hay *et al.*, 2014; Weisshaar, 2016). Current anti-itch drugs and treatment options are highly nonspecific and largely ineffective. Thus, for most patients, chronic itch is intractable. Mounting evidence suggests that dysregulation or overactivation of transient receptor potential vanilloid 3 (TRPV3) could drive chronic itch; however, basic TRPV3 research is lacking. This project investigated how the TRPV3 channel functions in the epidermal layer of human skin and asks what role it plays in dermatitis and skin-derived itch.

Specifically, this work examines TRPV3 signalling, functional activity, sensitisation, and trafficking in normal human epidermal keratinocytes – a key culture model for human epidermis. A variety of methods including phospho-kinase arrays, cytokine arrays, live calcium imaging, and immunocytochemistry were employed. This work also utilised unsupervised clustering analyses to assess calcium imaging data. The data described herein confirm TRPV3 as a potent inducer of epidermal inflammation, with collaborators revealing a clear link between TRPV3-evoked PAI-1 release and skin-derived itch. Unsupervised clustering analyses revealed the phasic nature of TRPV3- induced calcium flux and highlighted the role of SNARE-mediated receptor cycling in normal TRPV3 activity. Lastly, this work exposed a novel neuro-epidermal link: B-type natriuretic peptide (BNP) – a key neuropeptide driving human itch – sensitised TRPV3 activity and promoted kinase-dependent TRPV3 trafficking.

This basic work demonstrated the impact of TRPV3 in human skin and, together with *in vivo* data from collaborators, identified several novel targets for anti-dermatitis and anti-itch therapeutics. Overall, we believe that interruption of the TRPV3-associated pathways outlined herein would alleviate both inflammation and itch in human patients with atopic dermatitis, psoriasis, and other pruritic dermatoses.

1. Introduction

1.1. The skin

The skin is a complex, stratified, and highly dynamic tissue (Kabashima *et al.*, 2019). The skin contains an interconnected network of cells, structural proteins, and signalling mediators. Together, the skin functions as both an inert structural barrier and an active component of the immune and nervous systems, with the dermis and epidermis representing key sites for neuro-immune communication.

1.1.1. Structure of the skin

The skin is organised into 3 distinct layers termed the hypodermis, dermis, and epidermis (**Figure 1.1.**). These layers play crucial and specific roles in cutaneous physiology and pathophysiology.

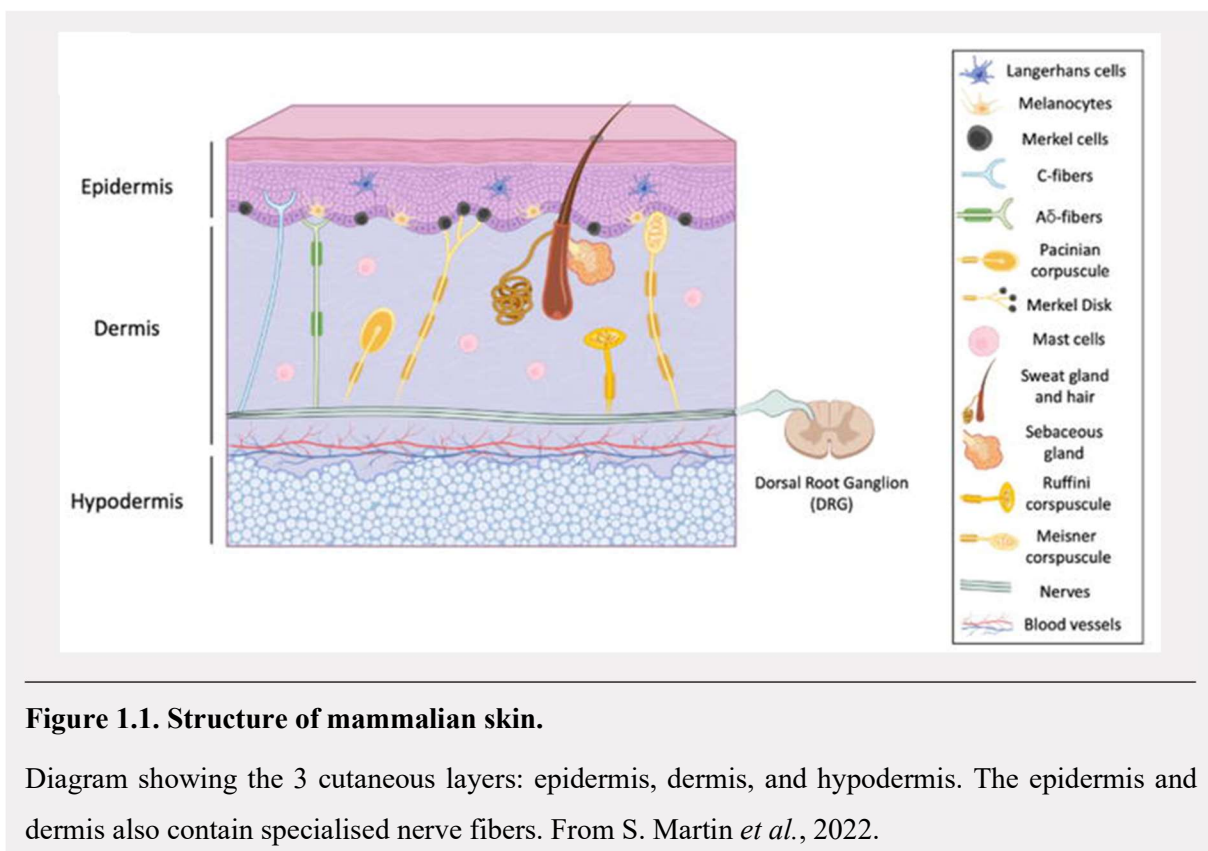


Figure 1.1. Structure of mammalian skin.

Diagram showing the 3 cutaneous layers: epidermis, dermis, and hypodermis. The epidermis and dermis also contain specialised nerve fibers. From S. Martin *et al.*, 2022.

1.1.1.1. Hypodermis

The hypodermis – the innermost layer – enables movement of the skin, protects against mechanical insults and plays an important role in homeostasis, thermoregulation and energy storage (Kabashima, 2016). The hypodermis is a subcutaneous fatty layer: this layer contains a loose lattice of fibrous bundles interspersed through adipose tissue. The hypodermis also contains a microvascular system and represents an essential source of endocrine and paracrine mediators (Mohamed-Ali *et al.*, 1998). These mediators support the upper layers of the skin and are essential for wound healing (Schmidt and Horsley, 2013).

1.1.1.2. Dermis

The dermis confers the mechanical strength and elasticity to the skin. This layer is primarily fibrous, with collagen and elastic fibers producing a mesh of connective tissue. These fibers, in combination with extracellular matrix proteins, stabilise the skin and provide a scaffold for cell migration (Nyström and Bruckner-Tuderman, 2019). The dermis is also a dynamic and immune cell-rich tissue (Kabashima *et al.*, 2019; Kabashima, 2016). Together, this cellular network coordinates homeostatic, inflammatory and repair processes in the skin.

1.1.1.3. Epidermis

The epidermis, the outermost section of the skin, acts as a physical barrier against exogenous insults and is often altered in patients with skin disease. This layer, and the keratinocytes within it, are the focus of this project.

Structurally, the epidermis exists as continuous but stratified system of keratinocytes (**Figure 1.2**). These strata – stratum basale, stratum spinosum, stratum granulosum, and stratum corneum – are produced through a process of progressive differentiation: as basal keratinocytes proliferate, cells migrate outward and undergo terminal differentiation (Watt, 1989; Eckert, 1989). This process culminates in the generation of the outer stratum corneum. The stratum corneum is a cornified layer of enucleated keratinocytes held together by tight junctions and surrounded by a dense matrix of cross-linked proteins and insoluble lipids (Matsui and Amagai, 2017). This semi-permeable barrier protects against water loss and external agents and is often impaired in clinical skin conditions.

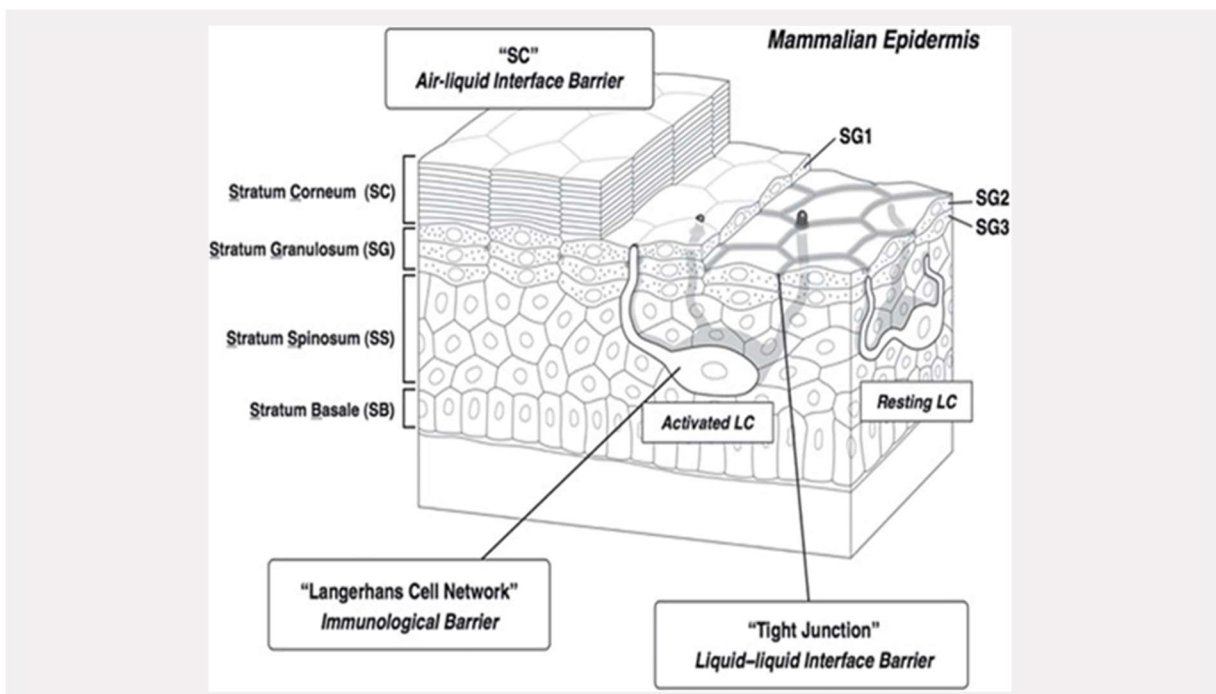


Figure 1.2. Structure of mammalian epidermis.

Diagram also highlights three barrier elements within the epidermis: the stratum corneum; tight junctions; and Langerhans cells (LC) and the cutaneous immune response. From Matsui and Amagai, 2017.

During the differentiation process, epidermal keratinocytes express a number of layer-specific proteins (**Figure 1.3**). Keratins, a family of intermediate filaments, are tightly regulated and highly correlated with epidermal layer: keratin 5 and keratin 14 are expressed in the stratum basale, while keratin 1 and keratin 10 are expressed in the stratum spinosum. Keratins assemble into heterodimers and form an intracellular cytoskeletal network. At the cell boundary, keratin filament bundles bind to desmosomes and anchor the cell-to-cell junctions. Keratinocytes of the middle stratum granulosum (SG2) also form tight junctions with adjacent keratinocytes (Hashimoto, 1971). These cell-to-cell junctions are dependent on tight junction proteins such as claudins, occludins, and junctional adhesion molecules; these proteins also show a layer-specific expression profile (Bäsler *et al.*, 2016). The SG2-tight junction layer represents additional barrier underneath the stratum corneum.

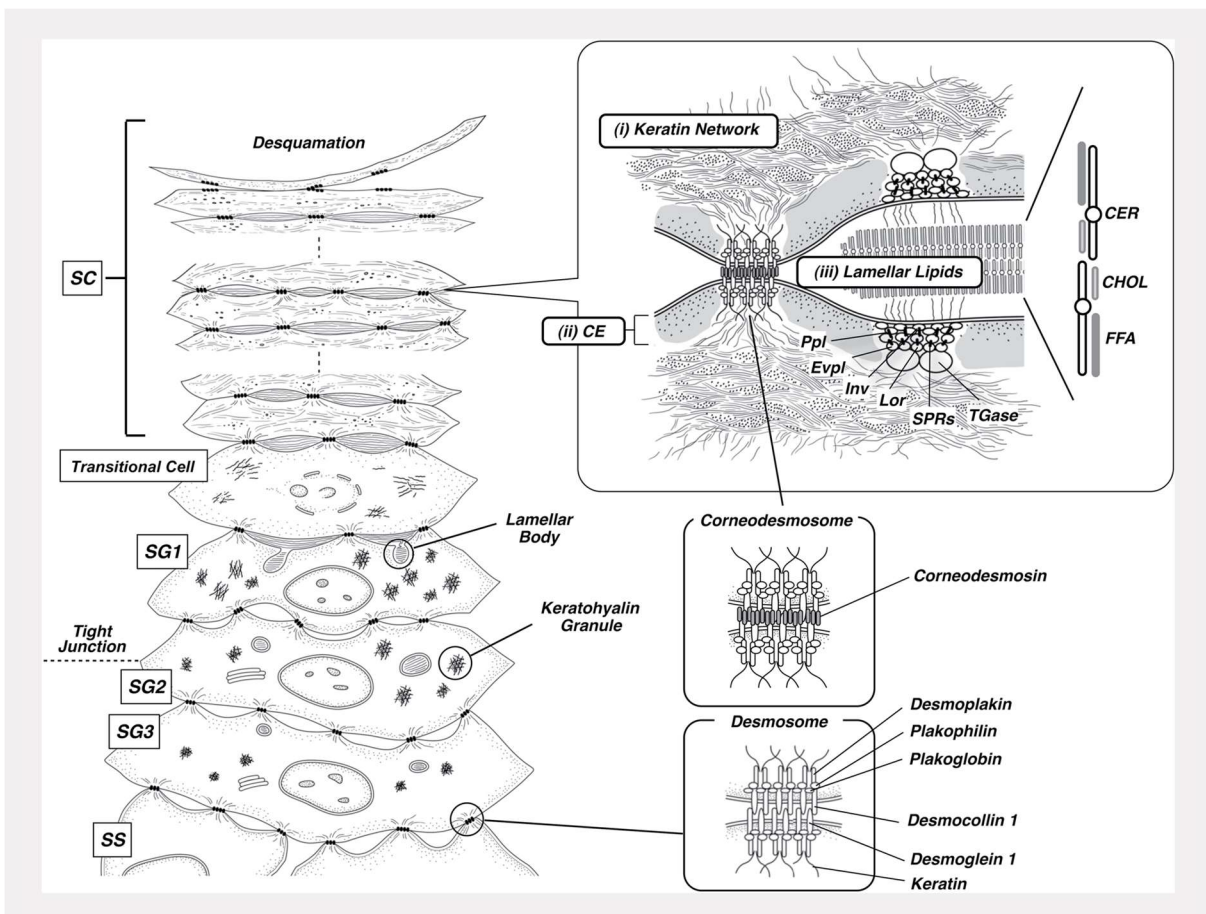


Figure 1.3. Keratinocyte differentiation and stratum corneum formation.

Abbreviations: CE, cornified envelope; CER, ceramide; CHOL, cholesterol; Evpl, envoplakin; FFA, free fatty acid; Lor, loricrin; Ppl, periplakin; SG, stratum granulosum; SPRR, small proline-rich proteins; SS, stratum spinosum; TGase, transglutaminase. From Matsui and Amagai, 2017.

Cornification – the conversion of keratinocytes from live to enucleated cells (corneocytes) – is a key step in stratum corneum formation. Keratinocytes of the stratum granulosum (and the outer layer of the stratum spinosum) produce keratohyalin granules; these cytoplasmic structures contain a mixture of keratin and keratin-binding proteins such as profilaggrin, loricrin, and trichohyalin (Freeman and Sonthalia, 2019). As keratinocytes differentiate, keratohyalin granules expand and mature; as granules mature, keratin and keratin-binding proteins aggregate and crosslink to form a homogenous keratin matrix (Freeman and Sonthalia, 2019). Following a similar pattern to keratohyalin granules, mature lamellar bodies are located in the outer layers of the stratum granulosum (SG1); these cytoplasmic structures contain a mixture of antimicrobial peptides, enzymes, and lipid precursors (ceramides, cholesterol, and free fatty acids) (Feingold, 2007; Elias and Choi, 2005). During cornification, SG1 keratinocytes lose their organelles and nuclei; secrete the contents of their lamellar bodies; and, using the transglutaminase enzyme (TGase), crosslink extracellular lipids and intracellular proteins to form the cornified envelope of the stratum corneum barrier.

In healthy skin, the outermost corneocyte layer (or stratum corneum) is shed through a protease-dependent process called desquamation (**Figure 1.4**). These corneocytes are then replaced by underlying cells, as described above. Kallikrein proteases, KLK5 and KLK7, cleave corneodesmosomes and are particularly important for desquamation (Egelrud and Lundström, 1991). KLK are secreted from lamellar bodies at the SG-SC interface; however, lamellar bodies also contain a serine proteinase inhibitor, LEKTI (lympho-epithelial Kazal type inhibitor), which tightly controls the proteolytic activity of the KLK desquamation enzymes (Deraison *et al.*, 2007). This KLK-LEKTI interaction is pH dependent and modulated by the pH gradient of the stratum corneum: as the extracellular matrix acidifies, LEKTI dissociates from KLK, and desquamation can occur. This system allows for constant renewal and repair of the exposed epidermal tissue, ensuring the integrity of the stratum corneum barrier and the underlying cutaneous tissue.

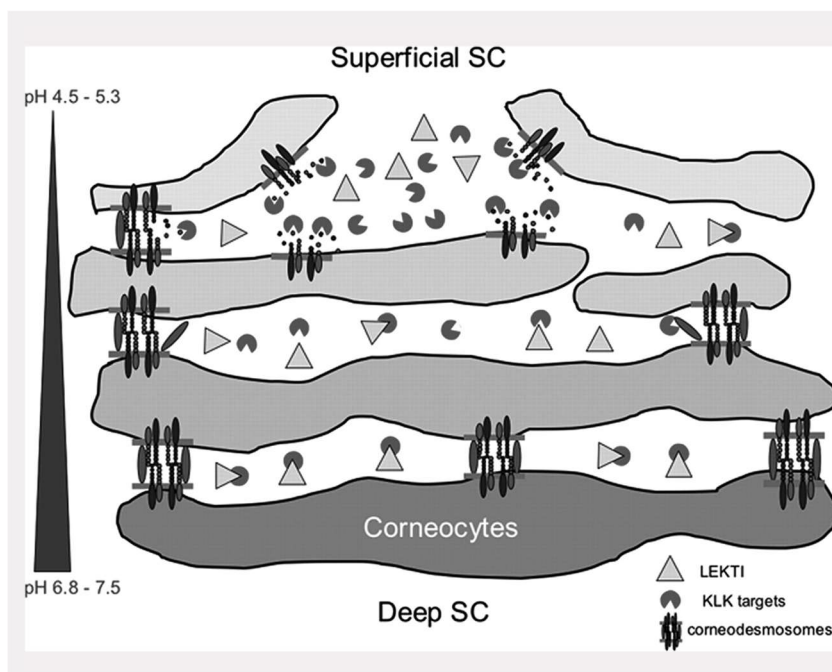


Figure 1.4. Model of epidermal desquamation.

Diagram highlights effect of pH on the KLK-LEKTI interaction. *Abbreviations:* KLK, kallikreins; LEKTI, lympho-epithelial Kazal type inhibitor; stratum corneum, SC. From Deraison *et al.*, 2007.

1.1.2. Immunology of the skin

The skin is primarily a barrier organ, protecting the body from exogenous agents, chemicals, and pathogens. The stratum corneum – the outermost layer of the epidermis – acts as an inert physical barrier. Damage to the stratum corneum activates the cutaneous immune response, with layer-specific cells facilitating both innate and adaptive immunity (**Figure 1.5**) (Kabashima *et al.*, 2019). Epidermal immune responses are largely mediated by keratinocytes, Langerhans cells (LC), and tissue resident memory T (TRM) cells. The murine epidermis also contains $\gamma\delta$ T cells. Early dermal immune responses are mediated by resident fibroblasts, dermal dendritic cells, and mast cells. The dermal vascular network allows circulating neutrophils and lymphocytes to enter the cutaneous tissue; this network also represents a key site for T cell activation. Together, these cutaneous cells coordinate the local response, eliminating exogenous insults, and restoring homeostasis. This system is essential for wound healing and is often dysregulated in skin disease.

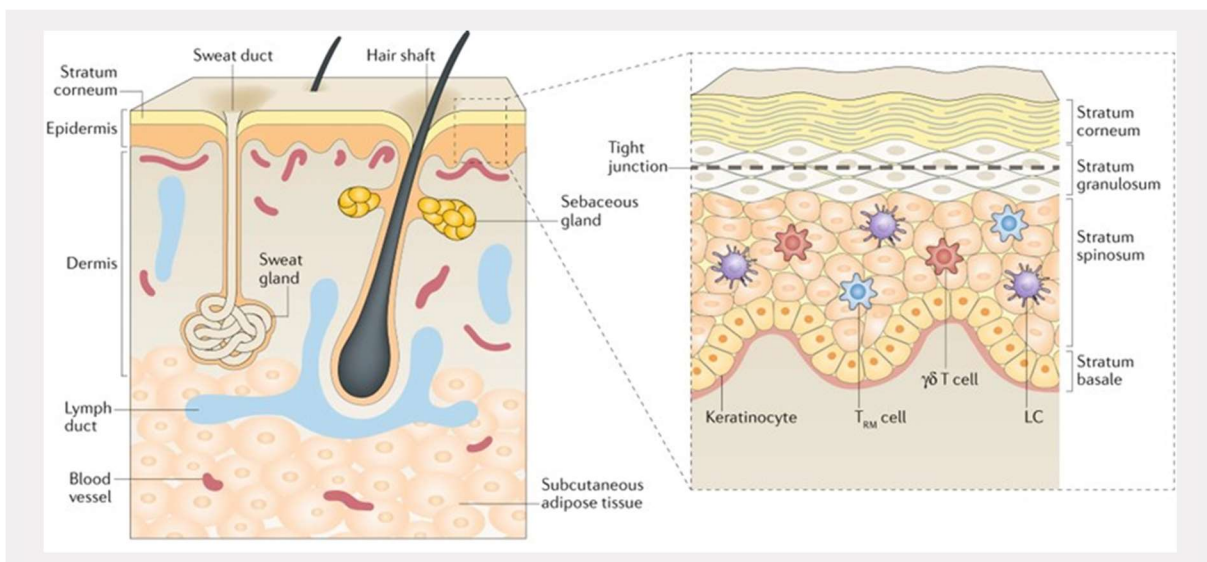


Figure 1.5. Immunological anatomy of the epidermis.

In the epidermis, tight junctions are formed underneath the stratum corneum (in the stratum granulosum). The epidermal layer contains keratinocytes, Langerhans cells (LCs), $\gamma\delta$ T cells, and resident memory T (TRM) cells). From Kabashima *et al.*, 2019.

1.1.2.1. Keratinocytes: more than just a physical barrier

This project focuses on epidermal keratinocytes. In addition to their barrier function, mounting evidence suggests that keratinocytes also play a role in epidermal immunity and clinical dermatitis.

Keratinocytes promote the cutaneous immune response and pathological inflammation (**Figure 1.6**). Keratinocytes detect exogenous pathogens and endogenous alarm signals. These cells express a broad array of pattern recognition receptors, including toll-like receptors, nucleotide-binding oligomerisation domain-like receptors, RIG-I-like receptors, and C-type lectin receptors (van den Berg *et al.*, 2014; Lebre *et al.*, 2007; Feldmeyer *et al.*, 2007; Kalali *et al.*, 2008; Jiang *et al.*, 2020; Terhorst *et al.*, 2010; Köllisch *et al.*, 2005; Baker *et al.*, 2003). Keratinocytes also interact with a

variety of immune cells, releasing and responding to a plethora of inflammatory mediators and antimicrobial peptides (Jiang *et al.*, 2020). In a similar manner, keratinocytes can also interact with peripheral neurons, driving neuronal activation and neurogenic inflammation. Keratinocytes may even process and display major histocompatibility complexes on their surface, promoting the induction of adaptive immune responses (Black *et al.*, 2007; Kennedy-Crispin *et al.*, 2012). These reports highlight the active and nuanced role of keratinocytes in the skin.

This project examines the inflammatory capacity of primary human keratinocytes, with collaborators comparing these *in vitro* results to data from clinical skin disease. Together, this work aims to delineate the role of keratinocytes in cutaneous immunity and inflammatory skin disease.

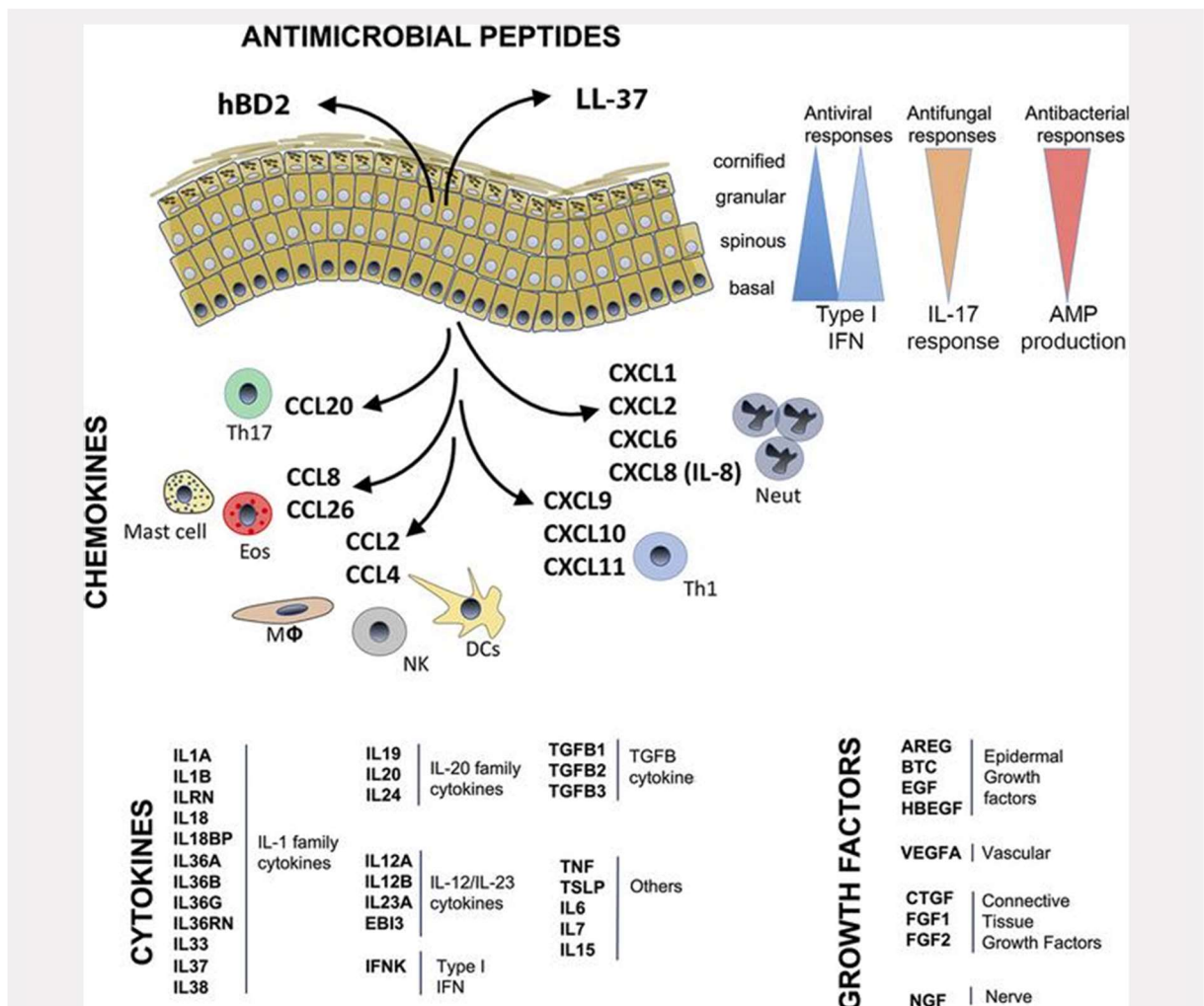


Figure 1.6. The diverse contribution of keratinocytes to immune responses in skin.

Immune responses are highly varied across the epidermal layers: antiviral responses are highest in the basal region, while antifungal and antibacterial responses are highest in the upper regions. Keratinocytes express and secrete a variety of chemokines, cytokines, and growth factors that affect nearby immune cells, cutaneous cells, and neurons. From Jiang *et al.*, 2020.

1.1.3. Cutaneous neural networks

The skin contains a complex network of autonomic and somatosensory neurons. Bidirectional communication between the nervous system and the skin forms an integral part of any cutaneous response. This neuro-cutaneous and neuro-immune link is often altered in clinical skin conditions and is a key focus for ongoing itch and dermatitis research.

1.1.3.1. Autonomic system

Cholinergic and noradrenergic autonomic fibers regulate cutaneous secretions, control vascular tone, and underpin the local physiological changes required for immune cell infiltration (Roosterman *et al.*, 2006; Glatte *et al.*, 2019). Currently, little is known regarding the role of autonomic nerves in skin disease, though this is a particularly interesting avenue for future investigations.

1.1.3.2. Somatosensory system

The cutaneous somatosensory system allows the skin to function as a type of sensory organ: peripheral sensory neurons detect and translate multimodal external stimuli into a collection of discernible properties. These primary sensory neurons extend from the skin to the spinal cord, with their cell bodies located in the dorsal root or trigeminal ganglia. Cutaneous sensory neurons are often polymodal and are classified into 3 broad categories: A β fibers, A δ fibers and C fibers. The distribution of these sensory afferents is highly dependent on the skin type: hairy *vs.* glabrous (hairless) skin (**Figure 1.7**).

A β fibers are heavily myelinated, with large diameter axons and cell bodies; these neurons transmit mechanical touch and are termed low-threshold mechanoreceptors (LTMR). Activation of LTMR is mediated by highly specialised nerve endings such as Pacinian corpuscles, Merkel disks, Ruffini corpuscles, and Meisner corpuscles. These nerve endings are located in the dermal layer, with A β fibers unable to enter the epidermis. A δ fibers are lightly myelinated, with medium diameter axons and cell bodies; these fibers lose their myelination before entering the dermal layer (Provitiera *et al.*, 2007). C fibers are unmyelinated, with small diameter axons and cell bodies. Both A δ and C fibers innervate the dermal and epidermal layers. These fibers terminate as free nerve endings, directly interacting with the surrounding keratinocytes and other cutaneous or immune cells. A subpopulation of mechano-sensitive A δ and C fibers also act as LTMR: A δ -LTMR and C-LTMR, respectively (Abraira and Ginty, 2013). Polymodal A δ and C fibers respond to multiple distinct stimuli including temperature (thermosensitive neurons); pain (nociceptors); and/or itch (pruriceptors). Adding to this complexity, mounting evidence indicates that nociceptors and pruriceptors represent distinct, but overlapping, subsets of sensory neurons (Lay and Dong, 2020; Chen and Sun, 2020; Usoskin *et al.*, 2015). Putative pruriceptors and itch-sensitive pathways represent key targets for anti-itch therapeutics and are discussed in more detail in **Section 1.3**.

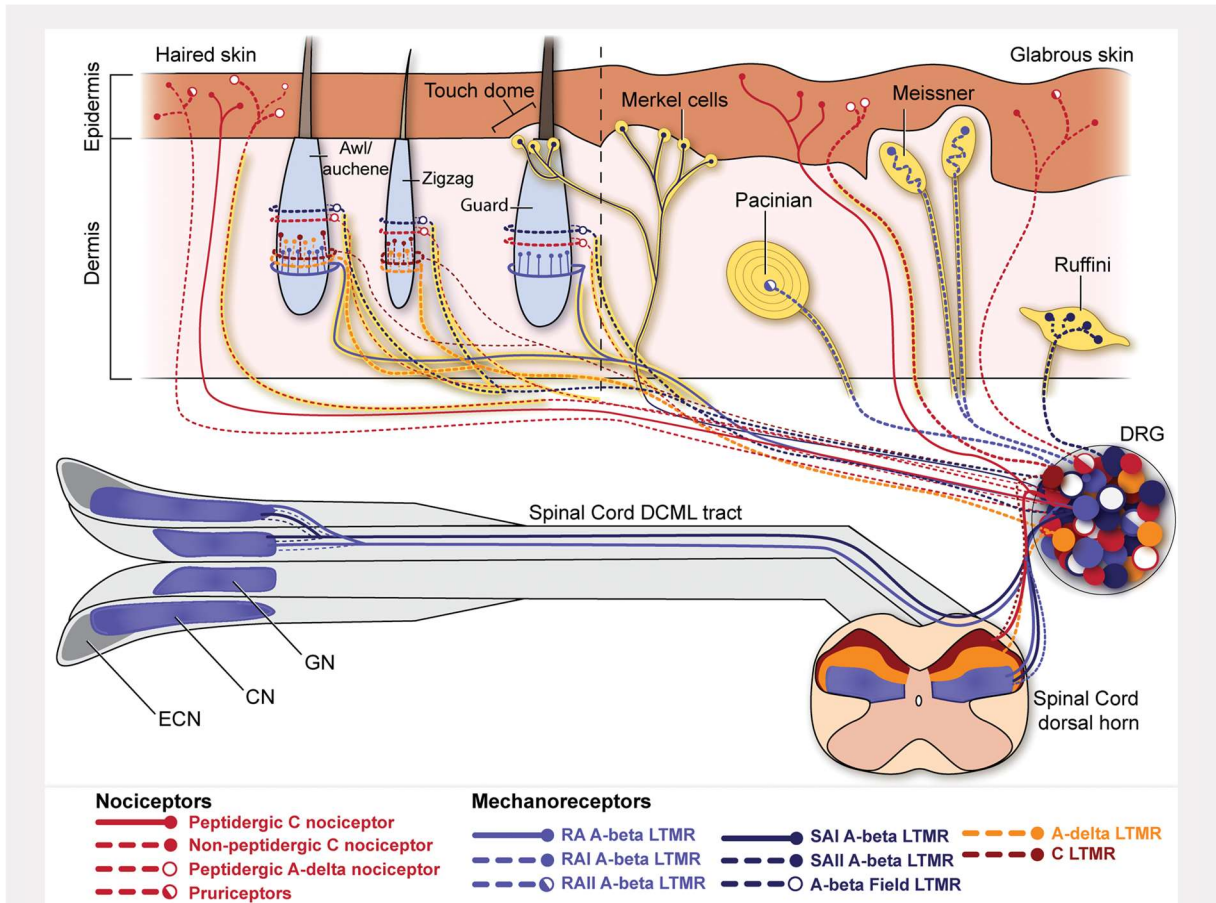


Figure 1.7. Sensory afferents in hairy and glabrous skin.

Diagram highlights the complexity of the cutaneous somatosensory system. *Abbreviations:* CN, cuneate nucleus; DRG, dorsal root ganglion; ECN, external cuneate nucleus; GN, gracile nucleus; LTMR, low-threshold mechanoreceptors. From Crawford and Caterina, 2020.

1.2. Skin disease and itch

The skin is a barrier tissue and an essential component of both the immune and nervous systems. Conditions that affect the skin have a profoundly negative impact on patients' quality of life: skin disease is the 4th leading cause of nonfatal disability worldwide (Hay *et al.*, 2014; Karimkhani *et al.*, 2017). Skin disease is also widespread, affecting nearly 1-in-3 people in the USA every day (Johnson and Roberts, 1978; Johnson, 2004). The term skin disease encompasses a plethora of disorders including abscess, acne vulgaris, alopecia areata, atopic dermatitis, cellulitis, impetigo, prurigo nodularis, psoriasis, scabies, and urticaria. Although the aetiologies of these diseases are complex, each can be categorised as either inflammatory or noninflammatory.

1.2.1. Inflammatory skin disease

Atopic dermatitis and psoriasis are examples of common inflammatory skin diseases. As with most conditions, inflammatory skin diseases are driven by both genetic and environmental factors. Though their aetiologies are distinct, many inflammatory skin diseases display similar clinical and histological features, suggesting overlap in the pathophysiological mechanisms. Current evidence suggests 3 broad and highly interlinked mechanisms underpin inflammatory skin disease: epidermal barrier alteration; abnormal immune cell infiltration; and exaggerated pro-inflammatory mediator expression (**Figure 1.8**) (Pezzolo and Naldi, 2020).

Specific subsets of T lymphocytes play particularly important roles in atopic dermatitis and psoriasis, with disease-specific inflammation resulting in clear cutaneous lesions (Guttman-Yassky and Krueger, 2017). These patients often exhibit systemic inflammation and develop non-cutaneous comorbidities such as metabolic and cardiovascular diseases (Guttman-Yassky *et al.*, 2018). Together, these features highlight the importance of balance within the cutaneous tissue: communication between cutaneous cells, immune cells and peripheral neurons must be tightly controlled.

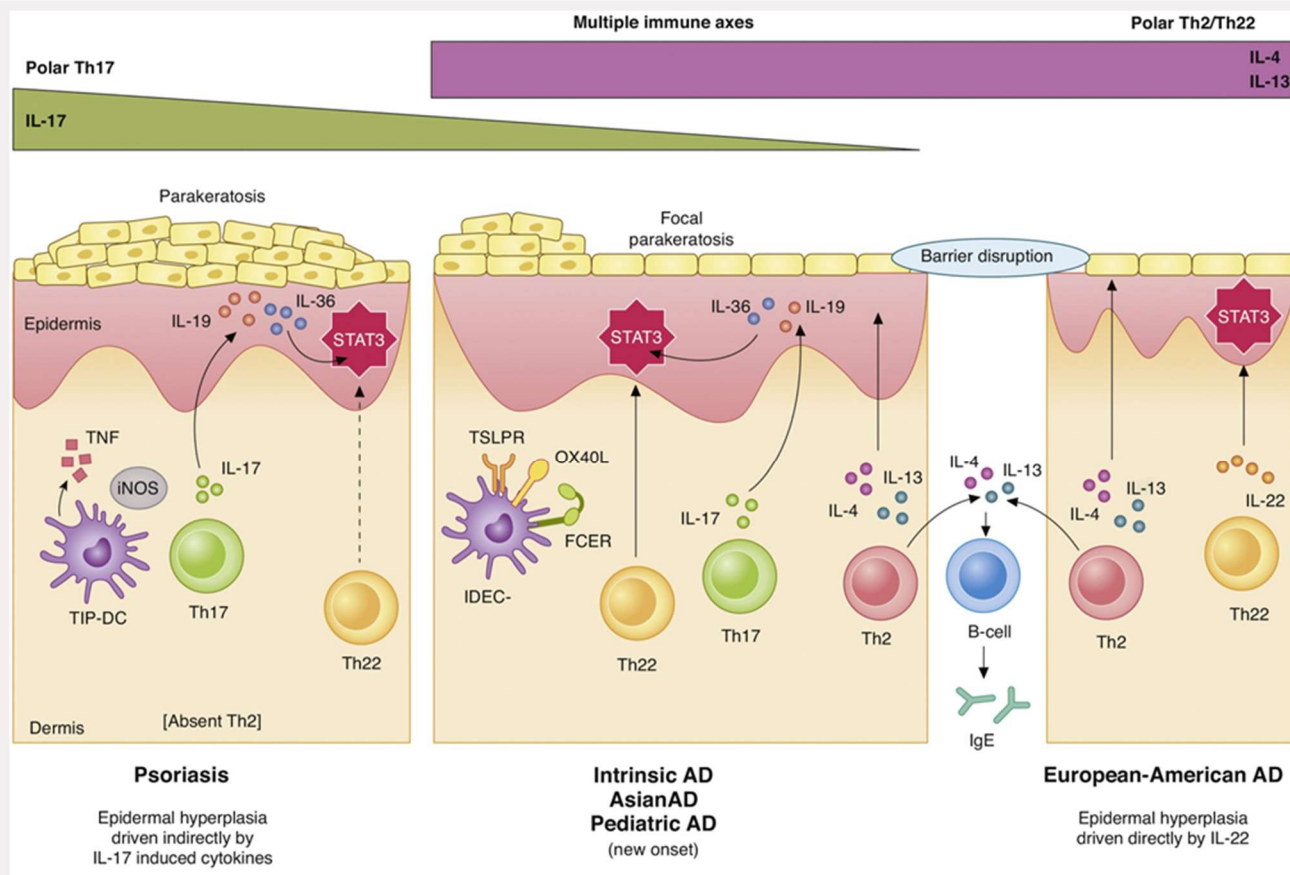


Figure 1.8. Comparison of inflammation and immune cell responses in psoriasis and atopic dermatitis.

Diagram also highlights the key differences between atopic dermatitis (AD) subtypes (Intrinsic, Asian, and Paediatric AD vs. European-American AD). *Abbreviations:* FCER, Fc epsilon receptor (also known as IgE receptor); IDEC, inflammatory dendritic epidermal cells; IgE, immunoglobulin E; IL, interleukin; iNOS, inducible nitric oxide synthase; OX40L, OX40-Ligand; STAT, signal transducer and activator of transcription; Th, T helper cell; TSLPR, thymic stromal lymphopoietin receptor. From Guttman-Yassky and Krueger, 2017.

1.2.2. Chronic itch (pruritus)

Chronic itch is broadly classified as itch lasting longer than 6 weeks. Clinically, this itch is termed pruritus. Although progress is being made, anti-itch agents are largely nonspecific and ineffective.

Pruritus is a surprisingly common phenomenon: up to 1-in-5 people will experience chronic pruritus at some point in their lifetime (Weisshaar, 2016; Hay *et al.*, 2014). This high prevalence may be explained by the broad array of conditions associated with chronic pruritus: dermatologic, systemic, neuropathic, and psychogenic (**Figure 1.9**) (Ständer and Grundmann, 2012). Pruritus is particularly common in inflammatory skin conditions. In a recent multi-centre study, chronic pruritus was reported in more than 60% of atopic dermatitis patients and almost 50% of psoriasis patients (Schut *et al.*, 2019). However, irrespective of the inducing stimuli or condition, itch is perceived to exist on the external surface and promotes scratching of this external site. In patients with chronic pruritus, this recurrent itch-scratch cycle damages the epidermal barrier, promotes cutaneous inflammation, and significantly impairs overall quality of life (Kini *et al.*, 2011; Matteredne *et al.*, 2011).

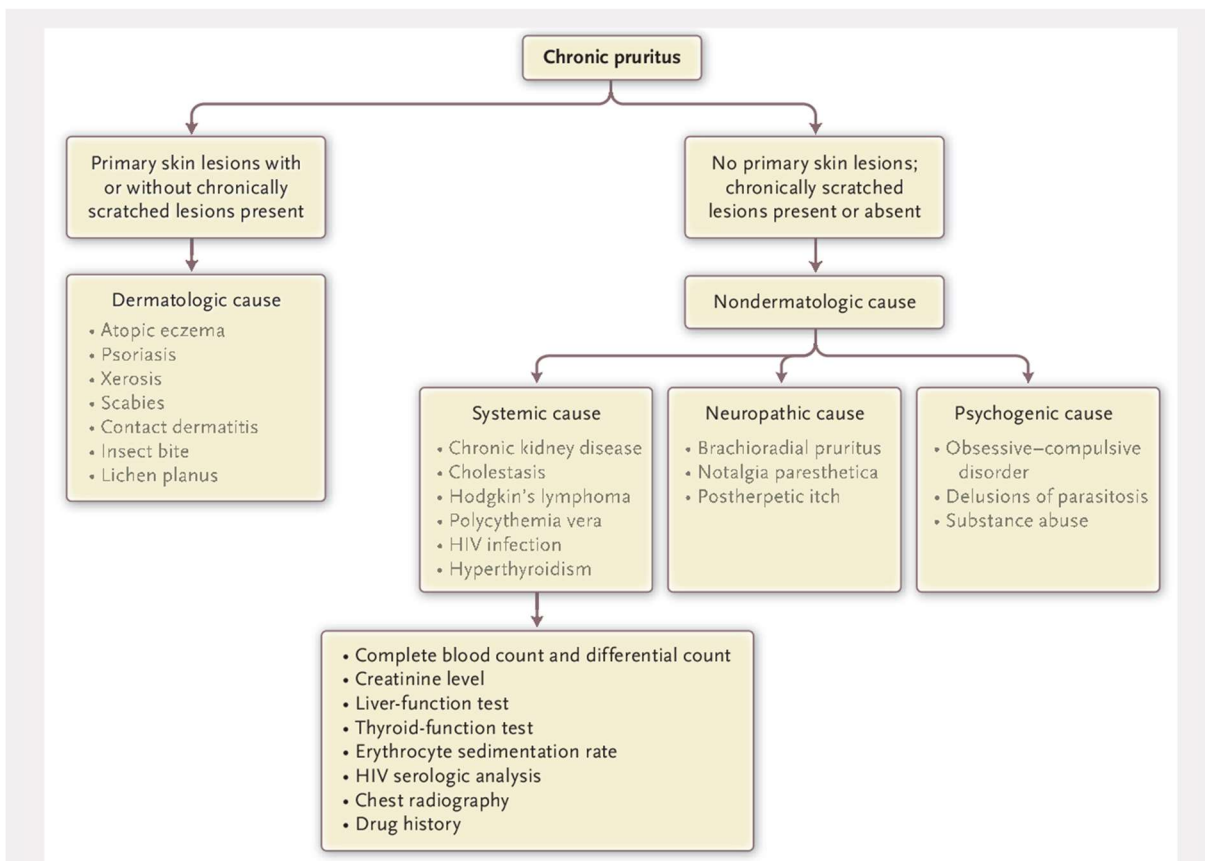


Figure 1.9. Conditions and disorders associated with chronic pruritus.

From Yosipovitch and Bernhard, 2013.

Chronic pruritus is caused by abnormal activation of normal itch pathways. This activation may be triggered by issues at any stage of itch signalling, transduction, or perception. Thus, pathological itch sensations are also classified with regard to the mechanism or site of dysfunction: pruritoceptive (skin), systemic, neuropathic, and/or psychogenic (Kahremany *et al.*, 2020). Pruritoceptive itch originates in the skin, mucosal membranes, or cornea, and represents the primary system for induction of normal acute itch responses. Briefly, pruritogens (itch-inducers) activate itch-sensitive sensory neurons in the skin; these fibers transmit the signal to the spinal cord, activating spinal circuits and ascending pathways, and culminating in the perception of itch. Overactivation of pruritoceptive itch is common in patients with inflammatory skin conditions. Systemic, neuropathic, and psychogenic itch involve dysfunctional or maladaptive activation of pruritoceptive itch pathways. Systemic itch is induced by pruritic compounds in the bloodstream (Krajnik and Zyllicz, 2001). Neuropathic itch is caused by damage to neuronal and/or glial cells resulting in neurogenic inflammation and sensitisation of itch circuitry (Misery *et al.*, 2014; Yosipovitch and Samuel, 2008). Psychogenic itch has no known origin and may be caused by psychological disturbances, psychiatric disease and/or substance abuse (Yosipovitch and Samuel, 2008). Pruritic disorders may involve more than one system of itch induction and, thus, may require several distinct therapeutic interventions.

Itch involves a complex interplay between epidermal keratinocytes, immune cells, and cutaneous sensory neurons (**Figure 1.10**) (Dong and Dong, 2018). In inflammatory skin conditions, this communication is facilitated and exacerbated by disease-specific inflammation and dysregulated peripheral signalling. Mapping of these pathways has revealed several endogenous pruritogenic factors including 5-HT, CXCL1, IL-31, IL-33, and TSLP; each of these factors provoke scratching behaviour in healthy mice (Wilson, Thé, *et al.*, 2013; Yamaguchi *et al.*, 1999; Walsh *et al.*, 2019; Cevikbas *et al.*, 2014; Liu *et al.*, 2016). Several of these factors are specifically elevated in pruritic lesions from atopic dermatitis and/or psoriasis patients (Nattkemper *et al.*, 2018). Although complex and interconnected, these dysregulated signalling pathways underpin disease progression and the recurrent itch/scratch cycle. Thus, our work attempts to identify novel disease-relevant pathways and the mechanisms driving their dysregulation.

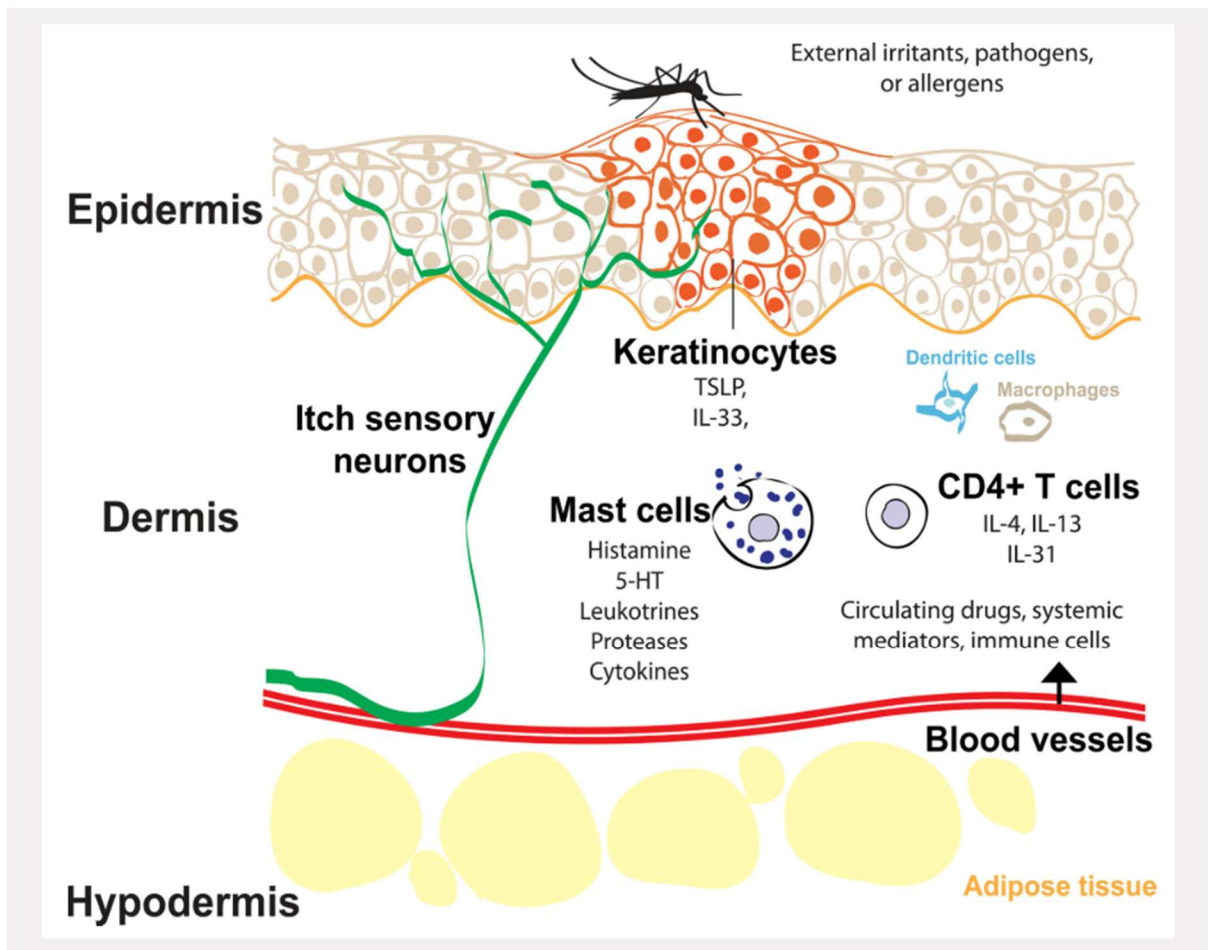


Figure 1.10. Schematic representation of cells and mediators involved in peripheral itch.

Keratinocytes, mast cells, CD4 T cells, and other cutaneous immune cells release mediators that activate peripheral itch-sensitive neurons in the skin. From Dong and Dong, 2018.

In addition to dysregulated intracellular signalling, the peripheral nervous system is also altered in samples from pruritic inflammatory skin conditions. Functional changes include sensitisation of central and peripheral itch pathways, and reduction of descending inhibition (Pogatzki-Zahn *et al.*, 2020; Dong and Dong, 2018; Nattkemper *et al.*, 2018). Under certain conditions, peripheral sensory neurons can promote neurogenic inflammation, secreting neuropeptides that act on adjacent keratinocytes, fibroblasts, and immune cells. These neuropeptides include B-type natriuretic peptide (BNP), calcitonin gene-related peptide (CGRP), and substance P (SP) (De Logu *et al.*, 2019; Roosterman *et al.*, 2006; Usoskin *et al.*, 2015; Story *et al.*, 2003; Boillat *et al.*, 2014). In pruritic inflammatory skin conditions, neuropeptides stimulate epidermal cells and exacerbate inflammation.

BNP is a key factor in both central and peripheral itch transduction (**Figure 1.11**). BNP is produced in itch-selective sensory neurons where it co-localises with TRPV1, MrgprA3, and MrgprC11 (Mishra and Hoon, 2013; Usoskin *et al.*, 2015). Following release, BNP binds to its cognate receptors: NPRA, NPRB, or NPRC. In the murine spinal cord, BNP is both necessary and sufficient for itch transduction; intrathecal BNP produces scratching behaviour via activation of NPRA⁺ neurons (Mishra and Hoon, 2013). In the skin, BNP is localised to a subset of IL-31-responsive

peptidergic neurons, while NPRA and NPRB are expressed in cells of the dermal and epidermal layers (Meng *et al.*, 2018; Usoskin *et al.*, 2015; Changlin Li *et al.*, 2018). IL-31 activates sensory neurons to release BNP – a pathway that is elevated in mouse models of peripheral itch and in pruritic skin conditions such as atopic dermatitis and psoriasis (Meng *et al.*, 2018; Ewald *et al.*, 2015; Liu *et al.*, 2016; Nattkemper *et al.*, 2018). A recent review by members of our group detailed the role of BNP in itch transduction and the possible effect of anti-BNP agents for the treatment of human itch (Meng *et al.*, 2020). The project herein builds on this theory, examining the impact of BNP on epidermal keratinocytes.

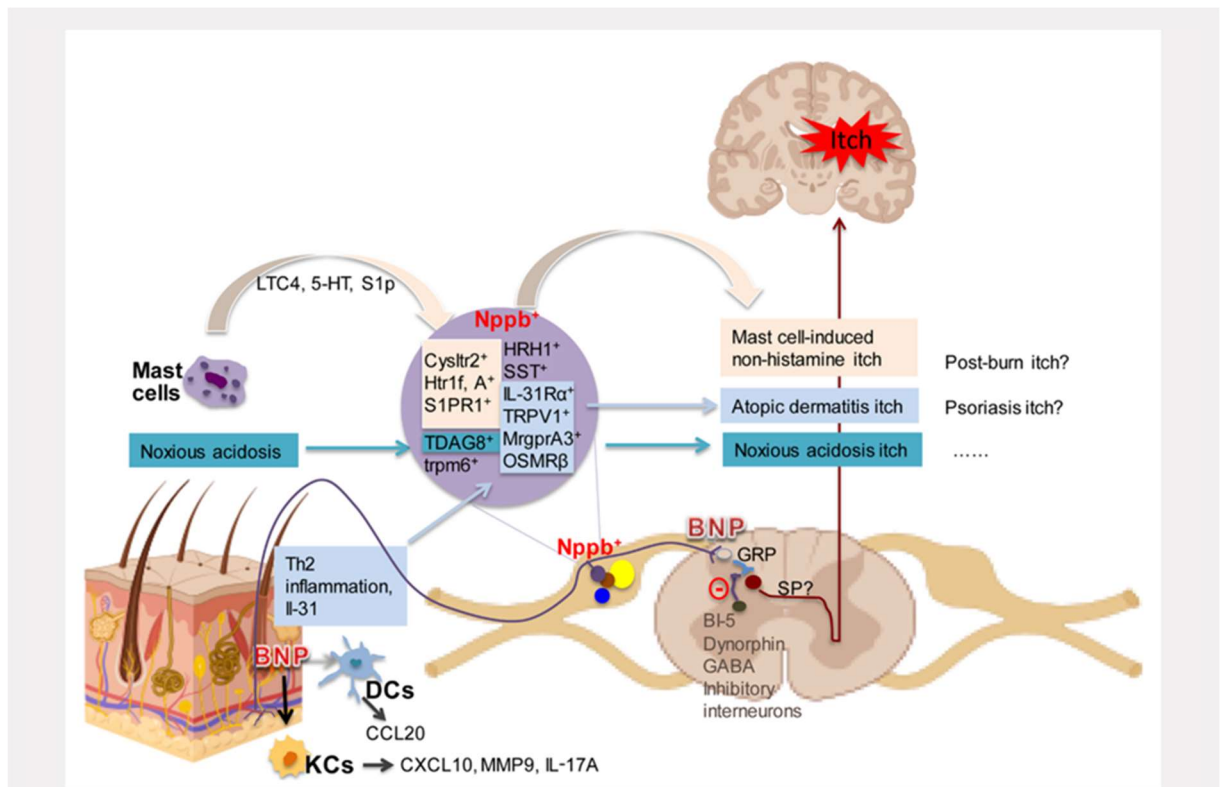


Figure 1.11. BNP and itch transduction.

Mast cell activation promotes release of leucotrine C4 (LTC4), serotonin (5-HT), and sphingosine 1-phosphate (S1P). These mast cell-derived mediators activate Nppb-positive (Nppb⁺) neurons, promoting mast cell-induced non-histamine itch. Acidic citrate (model for noxious acidosis) activate Nppb⁺ neurons, promoting noxious acidosis itch. IL-31 activates keratinocytes, promoting BNP release. Epidermal BNP activates keratinocytes and dendritic cells (DC), potentiating epidermal inflammation. These inflammatory mediators activate Nppb⁺ neurons, promoting atopic dermatitis (AD) itch. Lastly, BNP is expressed in spinal itch-sensitive neurons; in the spine, BNP activates gastrin-releasing peptide expressing neurons (GRP⁺) and facilitates central itch transduction. From Meng, Chen and Wang, 2020.

1.3. Acute itch pathways and their role in pruritus

Acute itch is a common sensation that provokes a desire to scratch (Savin, 1998). When acute, the itch-scratch response is a beneficial and protective reflex; this reflex ensures the removal of insects, irritants, and other external hazards. Scratching of the affected area stimulates a local immune reaction, priming and enhancing the protective capacity of the underlying epidermal population (Furue *et al.*, 2020). In patients with clinical pruritus, these acute responses become overactivated or dysregulated. Thus, to develop targeted anti-itch agents, researchers work to delineate the neural and intercellular pathways involved in itch transduction.

1.3.1. Acute itch vs. pain

Both itch and pain are transmitted by subsets of sensory neurons. Historically, itch was regarded as a submodality of pain, with early investigations suggesting that itch could arise from low intensity activation of nociceptors (Bishop, 1943; McMahon and Koltzenburg, 1992). Scientists have since proposed alternative theories suggesting that discrimination of itch and pain is based on specific neuronal pathways (labelled-line theory); is due to population coding (selectivity theory); and/or is reflective of the pattern of the neural activation (spatial contrast theory) (Hu *et al.*, 2021). These theories remain incomplete and disputed (Ikoma *et al.*, 2006; Ma, 2010; Braz *et al.*, 2014; Prescott *et al.*, 2014; Koch *et al.*, 2018; Chen and Sun, 2020). As mentioned previously, researchers now believe that acute itch and pain are transmitted via distinct, but overlapping, populations of sensory neurons (Chen and Sun, 2020; Lay and Dong, 2020; Usoskin *et al.*, 2015). In recent years, researchers have identified several itch-selective receptors, peptides and neuronal pathways (Chen and Sun, 2020; Lay and Dong, 2020). Thus, though our understanding is far from complete, acute itch and pain are likely transduced by distinct, but overlapping, populations of sensory neurons (Usoskin *et al.*, 2015). However, as nociceptive and pruriceptive systems share many of the same components, oversimplification and segregation of itch and pain research should be avoided.

1.3.2. Types of acute itch

Acute itch begins in the skin: certain stimuli or itch-inducers (pruritogens) activate specialised sensory neurons in the skin; these peripheral neurons enter the spinal cord, relaying the itch message to specific second-order neurons; these spinal neurons ascend via the contralateral spinothalamic tract to the thalamus. Researchers have now identified 2 discrete subtypes of acute itch sensation – mechanical itch and chemical itch – with each being coordinated by distinct mediators, receptors, and neural pathways. These pathways are discussed below and outlined in **Figure 1.12**.

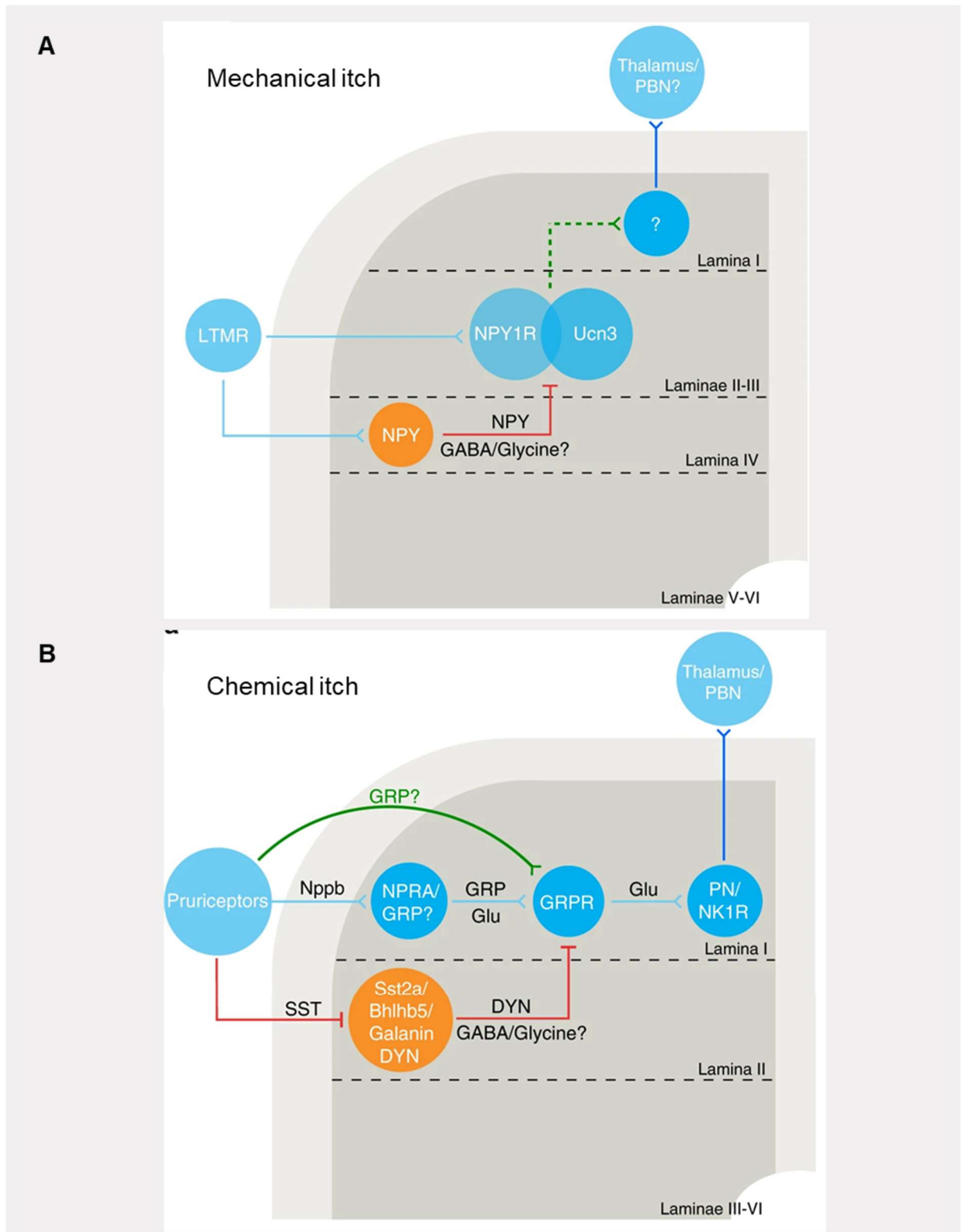


Figure 1.12. Neural pathways underpinning acute mechanical and chemical itch transduction.

A, Mechanical itch pathways. **B**, Chemical itch pathways. *Abbreviations:* DYN, dynorphin; gastrin-releasing peptide, GRP; gastrin-releasing peptide receptor, GRPR; glutamate, Glu; LTMR, low-threshold mechanoreceptors; NK1R, neurokinin 1 receptor; Nppb, natriuretic peptide B (also known as BNP); NPRA, natriuretic peptide receptor A; NPY, neuropeptide Y; PN, projection neuron; spinothalamic tract, STT; Ucn3, urocortin 3. From Chen and Sun, 2020.

1.3.2.1. Mechanical itch

Fine touch, weak electrical stimulation and other mechanical stimuli can provoke mechanical itch sensations (Ikoma *et al.*, 2005; Rothman, 1922; Shelley and Arthur, 1957; Fukuoka *et al.*, 2013; Pan *et al.*, 2019). Mechanical itch is thought to represent a type of innocuous touch initiated by cutaneous mechanotransducers and transduced by mechano-sensitive sensory neurons (Feng *et al.*, 2018; Woo *et al.*, 2014). Both gentle and noxious touch are transmitted by low-threshold mechanoreceptors (LTMRs), including myelinated A β and A δ fibers and unmyelinated C fibers (Zimmerman *et al.*, 2014). Touch-evoked itch may be mediated by a subgroup of A β -LTMRs expressing toll-like receptor 5 (TLR5). Pharmacological inhibition of these peripheral TLR5⁺ neurons reduced scratching responses associated with weak von Frey filament stimulation (Pan *et al.*, 2019). Furthermore, specific spinal interneuron populations have been linked to mechanical itch: neuropeptide Y-positive (NPY⁺) interneurons and a subset of urocortin 3-positive (Ucn3⁺) interneurons (Acton *et al.*, 2019; Bourane, Duan, *et al.*, 2015; Pan *et al.*, 2019). More recently, researchers identified the Piezo channels as key detectors and transducers of mechanical stimuli (Ernfors *et al.*, 2021; Coste *et al.*, 2010). Despite these advances, the exact neural pathways underpinning mechanical itch remain elusive.

Alterations to mechanical itch pathways, termed alloknesis and hyperknesis, are common in patients with chronic pruritus (Andersen *et al.*, 2017; Sakai and Akiyama, 2020; Andersen *et al.*, 2018). Briefly, alloknesis refers to itch induced by a non-pruritic stimulus, while hyperknesis denotes a heightened intensity of itch evoked by a normally pruritic stimulus. Mechanical alloknesis is mediated by TLR5⁺ sensory neurons, with targeted blockage reducing touch-evoked itch in histamine-treated mice and a murine model of dermatitis (Pan *et al.*, 2019). Surprisingly, blockade of Merkel cell mechanotransducers promotes sensitisation of mechanical itch pathways and may underpin aging-associated and dry skin-induced alloknesis (Feng *et al.*, 2018).

Although mechanical itch likely plays an important role in chronic pruritus, itch-associated LTMRs remain poorly defined and are largely unaffected by current anti-itch strategies.

1.3.2.2. Chemical itch

Chemical itch is induced by various endogenous mediators and exogenous agents (Kahremany *et al.*, 2020). Following binding to their cognate receptors, these pruritogens activate itch-sensitive neural pathways, often promoting opening of transient receptor potential (TRP) and other cation channels and culminating in the generation of NaV1.7-dependent action potentials (Dong and Dong, 2018; Kahremany *et al.*, 2020).

Histamine represents the archetypal pruritogen: chemical itch is often defined as either histamine-dependent or histamine-independent (Andersen *et al.*, 2015). When activated by allergens or inflammation, mast cells rapidly release histamine (Benditt *et al.*, 1955; Tal and Liberman, 1997). Histamine stimulates and primes the local immune response, activating various innate and adaptive

immune cells (Damaj *et al.*, 2007; Ling *et al.*, 2004; László *et al.*, 2001; Jutel *et al.*, 2001). Histamine directly evokes acute itch sensations, activating peripheral C fibers via the H1R and H4R histamine receptors (Tani and Ishikawa, 1990; Schmelz *et al.*, 1997; Rossbach *et al.*, 2011). However, chronic itch is largely refractory to antihistamine treatment and is broadly histamine-independent (Ikoma *et al.*, 2006).

To date, several non-histaminergic pruritogens been identified. These include endogenous and exogenous compounds: serotonin (5-HT); cathepsin S, mucunain and other proteases; leukotriene C₄, sphingosine 1-phosphate and other bioactive lipid mediators; and various inflammatory compounds (interleukin-4 [IL-4], IL-13, IL-31, IL-33, and thymic stromal lymphopoietin [TSLP]) (Voisin *et al.*, 2021; Hill *et al.*, 2018; Morita *et al.*, 2015; Kim *et al.*, 2012; Reddy *et al.*, 2008; Ui *et al.*, 2006; Campion *et al.*, 2019; Cevikbas *et al.*, 2014; Wilson, Thé, *et al.*, 2013; Liu *et al.*, 2016). These pruritogens, and their associated signalling pathways, are often dysregulated in pruritic skin.

In both healthy and diseased skin, pruritogens activate itch-sensitive sensory neurons. Some bind directly to neuronal receptors, while others act indirectly: binding to receptors on cutaneous cell and evoking secretion of direct pruritogens and/or inflammatory factors. These direct and indirect pathways are discussed in detail below.

1.3.3. Chemical itch pathways in the periphery

A number of recent breakthroughs have transformed our understanding of pruritoceptive itch processing (Chiu *et al.*, 2014; Usoskin *et al.*, 2015; Goswami *et al.*, 2014; Reynders and Moqrish, 2015; Thakur *et al.*, 2014). These advances were enabled by the development of next generation RNA sequencing (RNAseq): expression-based classification of murine neurons led to the discovery of functional subpopulations within the sensory network. Mounting evidence now indicates that, in mice, chemical pruritoceptive itch is transduced by a specific populations of small diameter sensory neurons. These neurons express key itch-linked receptors and neuropeptides (**Figure 1.13**).

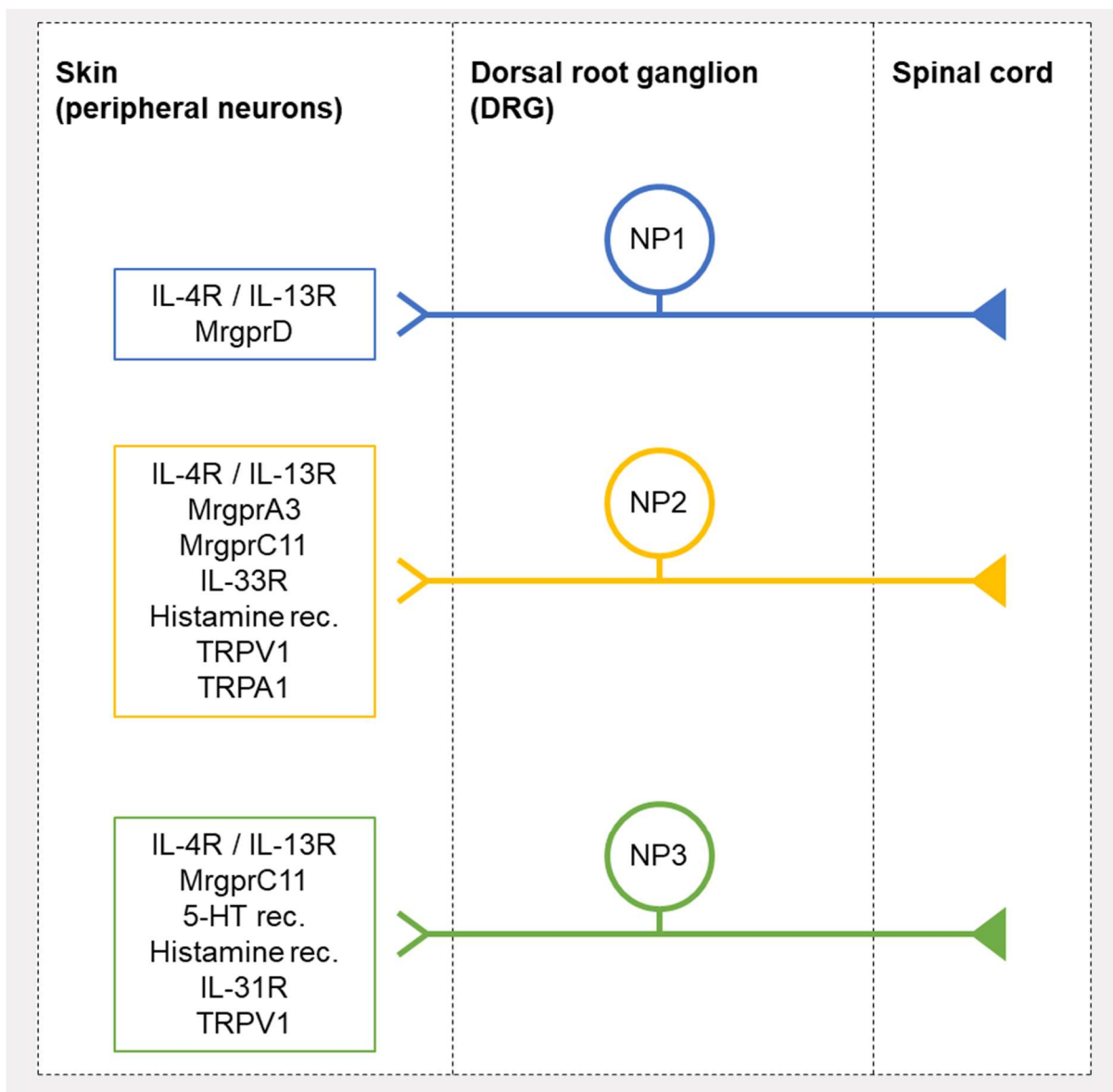


Figure 1.13. Schematic of proposed peripheral itch circuits in mice.

Abbreviations: IL, interleukin; Mrgpr, Mas-related G protein-coupled receptors; NP, nonpeptidergic; TRPA1, transient receptor potential ankyrin 1; TRPV1, transient receptor potential vanilloid 1. Taken and modified without permission from Dong and Dong, 2018.

1.3.3.1. Nonpeptidergic (NP) neurons

One pivotal study categorised itch-sensitive neurons into 3 overlapping groups; these neurons are NP nociceptors: NP1, NP2, and NP3 (Usoskin *et al.*, 2015). All 3 NP groups express IL-4 and IL-13 receptors, supporting the assertion that inflammatory factors exacerbate itch signalling (Usoskin *et al.*, 2015; Oetjen *et al.*, 2017; Chiu *et al.*, 2014). Each of the NP groups express distinct itch-linked receptors, indicating a high level of functional specificity within the murine pruriceptor population. NP3 neurons express receptors for proteases, 5-HT, leukotrienes, IL-31, and endothelin-1 (ET-1); thus, NP3 neurons are thought to mediate inflammatory itch (Usoskin *et al.*, 2015; Kardon *et al.*, 2014). Both NP2 and NP3 neurons express varying but notable levels of histamine and IL-33 receptors (Usoskin *et al.*, 2015). NP3 neurons express BNP, a key itch-linked neuropeptide and driver of dysregulated epidermal signalling (Mishra and Hoon, 2013; Usoskin *et al.*, 2015; Meng *et al.*, 2018; Meng *et al.*, 2020). Thus, NP3 neurons facilitate inflammatory itch transduction and potentiate AD-associated neurogenic inflammation.

1.3.3.2. Mas-related G protein-coupled receptors

Researchers identified certain mas-related G protein-coupled receptors (Mrgpr) as key itch-linked receptors and markers of murine itch-sensitive peripheral neurons (Dong *et al.*, 2001; Zylka *et al.*, 2003; Liu *et al.*, 2009). The Mrgpr family consists of more than 50 distinct G protein-coupled receptors (GPCRs): MrgprA1-A22, MrgprB1-B13, MrgprC1-C14, and MrgprD-G. Expression of MrgprA3, MrgprC11, and MrgprD is restricted to small diameter sensory neurons – putative itch-sensitive neurons (Dong *et al.*, 2001; Zylka *et al.*, 2003). MrgprA3 is expressed in the NP2 subgroup; these MrgprA3⁺ neurons exclusively innervate the epidermal layer (Usoskin *et al.*, 2015; Dong *et al.*, 2001; Liu *et al.*, 2009; Zylka *et al.*, 2003; Liu *et al.*, 2008; Han *et al.*, 2013; Sharif *et al.*, 2020). Injection of chloroquine, an antimalarial drug and MrgprA3 agonist, directly activates itch-sensitive neurons and promotes scratching bouts in mice (Ru *et al.*, 2017; Liu *et al.*, 2009; Akiyama *et al.*, 2012). MrgprC11 is expressed in both NP2 and NP3 (Usoskin *et al.*, 2015; Zylka *et al.*, 2003; Liu *et al.*, 2009). MrgprC11 agonists, including endogenous BAM8-22 and exogenous tick peptides, act directly on MrgprC11⁺ neurons and induce significant acute scratching behaviour (Qin Liu *et al.*, 2011; Xueke Li *et al.*, 2021; Liu *et al.*, 2009). The MrgprC11 receptor is now thought to be involved in both acute and chronic itch, with recent findings suggesting that MrgprC11⁺ fibers are particularly important for itch in glabrous skin (Steele *et al.*, 2021; Qin Liu *et al.*, 2011). Lastly, MrgprD is expressed in murine NP1 neurons (Usoskin *et al.*, 2015). Intracutaneous injection of β -alanine, a specific agonist for MrgprD, evokes scratching behaviour in mice and induces itch sensations in humans (Wooten *et al.*, 2014; Rau *et al.*, 2009; Shinohara *et al.*, 2004; Liu *et al.*, 2012).

1.3.3.3. Human Mrgpr-like proteins: MRGPRX

In humans, our understanding of neural pruritoceptive pathways is incomplete. The human MRGPR family consists of 4 Mrgpr-like proteins (MRGPRX1-4), with MRGPRX1 showing high sequence and functional homology with mouse MrgprA and MrgprC proteins (Lembo *et al.*, 2002). Expression of this MRGPRX1 protein is restricted to small diameter C fibers where it underpins both chloroquine and BAM8-22-evoked itch in humans (Sikand *et al.*, 2011; Lembo *et al.*, 2002; Liu *et al.*, 2009; Xueke Li *et al.*, 2021; Sanjel *et al.*, 2019). Thus, the murine labelled-line theory may also be applicable to human systems; however, further research is required.

1.3.3.4. Transient receptor potential channels

Transient receptor potential (TRP) channels function as membrane-associated cation pores. TRPV1 and TRPA1 channels are expressed on subsets of peripheral sensory neurons. In mice, approximately 12% of sensory neurons are TRPV1-positive (TRPV1⁺); although just 30% of TRPV1⁺ neurons express TRPA1, almost 97% of TRPA1⁺ cells are also TRPV1⁺ (Story *et al.*, 2003; Jordt *et al.*, 2004; Kobayashi *et al.*, 2005). Of the NP neurons, TRPV1 is detected in NP2 and NP3 but TRPA1 is restricted to NP2 (Usoskin *et al.*, 2015).

TRPV1⁺ neurons are polymodal, with a subset being itch-sensitive: selective ablation of TRPV1⁺ neurons impairs thermal sensitivity, pain, and itch-like behaviour (Woodbury *et al.*, 2004; Mishra and Hoon, 2010; Mishra *et al.*, 2011; Imamachi *et al.*, 2009; Solinski, Kriegbaum, *et al.*, 2019; Cavanaugh *et al.*, 2009). The TRPV1⁺/TRPA1⁺ NP3 neurons express BNP, CGRP SP (De Logu *et al.*, 2019; Roosterman *et al.*, 2006; Usoskin *et al.*, 2015; Story *et al.*, 2003; Boillat *et al.*, 2014). In these neurons, direct activation of the TRPV1 channel promotes neuropeptide release (Boillat *et al.*, 2014) highlighting the role of TRPV1 and TRPV1⁺/TRPA1⁺ neurons in neuro-epidermal communication and itch. Thus, TRPV1 and TRPA1 channels represent important markers for both nociceptors and putative pruriceptors.

1.3.4. Nonneuronal cells in itch transduction

Sensory neurons are essential for the transmission of itch signals; however, nonneuronal cutaneous cells are required for induction of indirect itch pathways. This neuro-immune and neuro-epidermal communication underpins both normal pruritoceptive itch transduction and pathological pruritus (Wang and Kim, 2020). Certain stimuli activate nonneuronal cells in the skin; these cells then secrete direct pruritogens and/or inflammatory mediators leading to the activation of adjacent itch-sensitive sensory neurons (**Figure 1.14**). When activated, mast cells, basophils, and keratinocytes release high levels of endogenous pruritogens – many of which are now implicated in pruritic inflammatory skin conditions. Thus, modulation of these complex and disease-specific pathways represents a key aim of ongoing research.

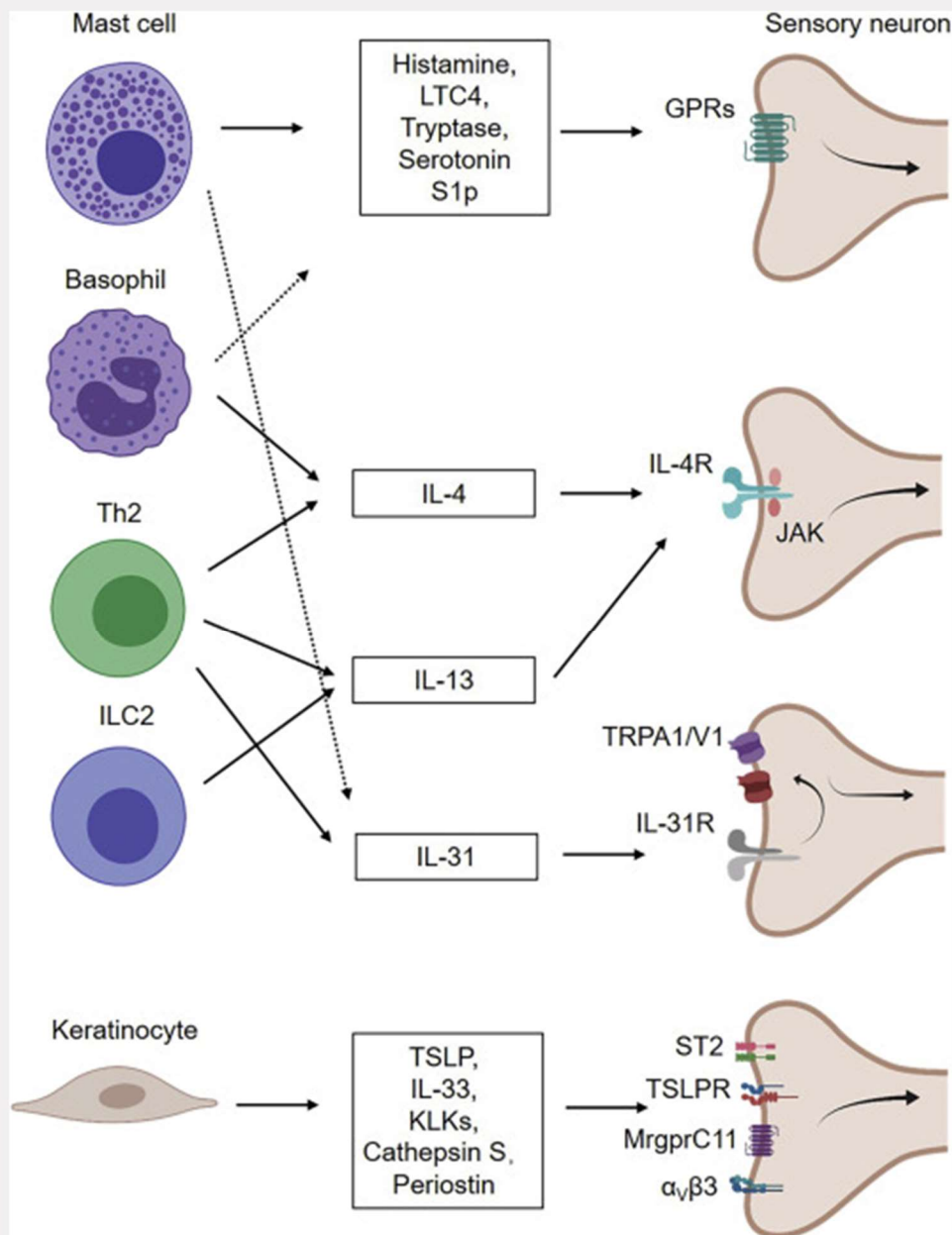


Figure 1.14. Direct pruritogens secreted from nonneuronal cutaneous cells.

Diagram highlights the role of mast cells, basophils, T helper cell (Th), group 2 innate lymphoid cells (ILC2) and keratinocytes in pruritogenic itch. *Abbreviations:* $\alpha_v\beta_3$, alpha v beta 3 (integrin); GPRs, G-protein-coupled receptors; IL, interleukin; ILC2, group 2 innate lymphoid cells; JAK, Janus kinase; KLK, kallikrein; LTC4, Leukotriene C4; MrgprC11, Mas-related G protein-coupled receptor C11; ST2, suppression of tumorigenicity 2 (IL-33R); S1P, sphingosine-1-phosphate; TSLP, thymic stromal lymphopoietin. From Wang and Kim, 2020.

1.3.4.1. Mast cells

To date, much of our understanding of indirect itch induction or endogenous pruritogen release has centred on mast cells and their role in histamine-dependent itch. Basic secretagogues activate mast cells, binding to murine Mrgprb2 or human MRGPRX2 to induce degranulation (**Figure 1.15**) (Ferry *et al.*, 2002; McNeil *et al.*, 2015; Wang *et al.*, 2020). Immunoglobulin E antibodies also induce degranulation. Mast cell granules contain a plethora of inflammatory factors and direct pruritogens: histamine, 5-HT, prostaglandins, leukotrienes, proteases, and various cytokines (Metcalf *et al.*, 1997; Lagunoff *et al.*, 1983; Wang *et al.*, 2020). In addition to these atopy-related mediators, MRGPRX2 is upregulated in pruritic atopic dermatitis and psoriasis skin (Nattkemper *et al.*, 2018). Thus, mast cells mediate indirect itch pathways, facilitating both acute and atopic itch.

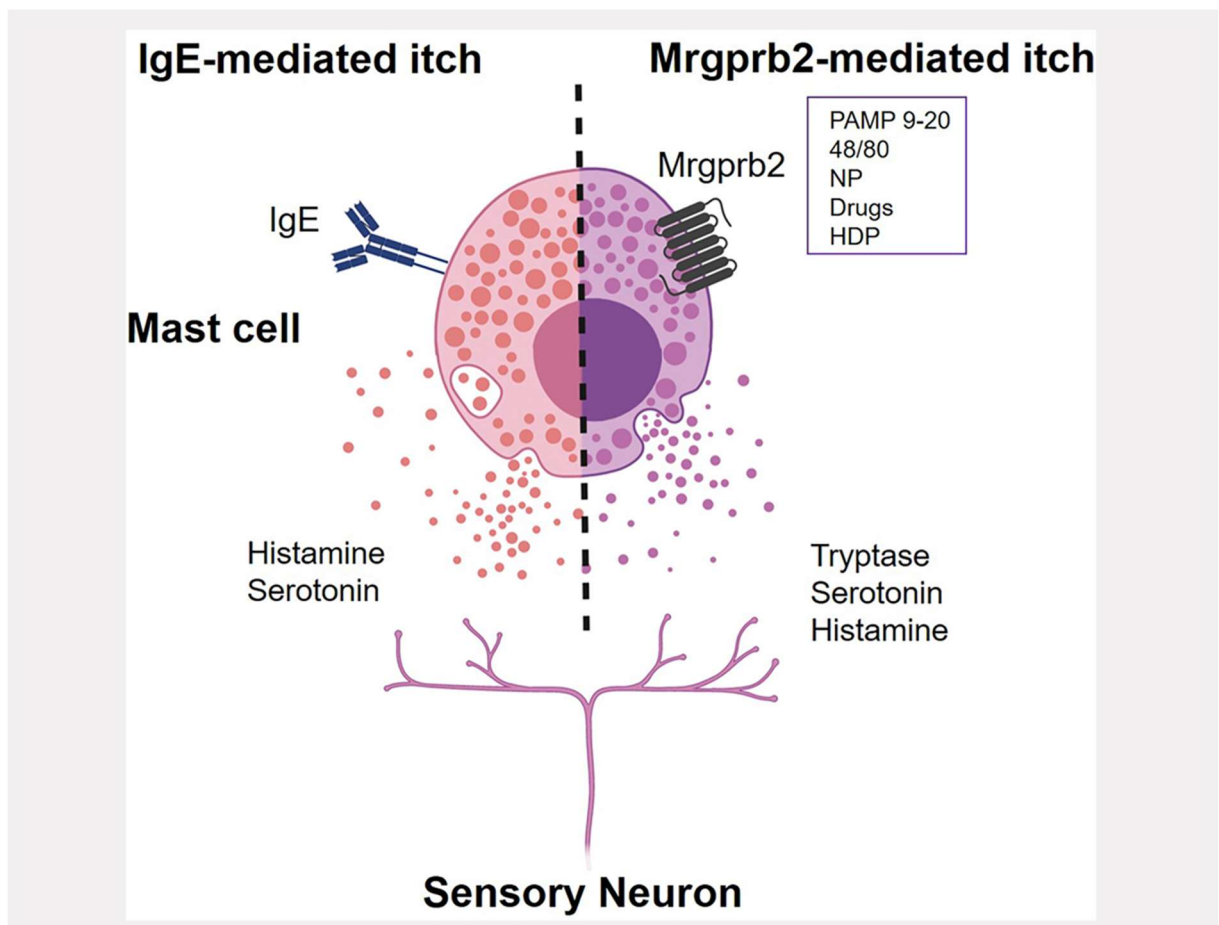


Figure 1.15. Mast cell-evoked itch.

Diagram illustrates IgE- and Mrgprb2-evoked degranulation and itch. *Abbreviations:* HDPs, host defence peptides; IgE, immunoglobulin E; Mrgpr/MRGPR, Mas-related G protein-coupled receptor; NPs, neuropeptides; PAMP 9-20, pro-adrenomedullin peptide 9–20. From Wang, Yang and Kim, 2020.

1.3.4.2. Basophils

Basophils evoke indirect itch in a similar manner to mast cells: IgE activates basophils to induce degranulation. Basophil granules contain histamine, IL-31, TSLP, proteases, prostaglandins, and other direct activators of itch-sensitive neurons (Hashimoto *et al.*, 2019). Basophil populations are elevated and highly active in atopic dermatitis lesions and chronic itch conditions (Mashiko *et al.*, 2017; Kim *et al.*, 2014; Hashimoto *et al.*, 2019). In atopic patients, basophil-derived leukotriene C4 promotes acute allergen-induced itch flares (**Figure 1.16**) (Fang Wang *et al.*, 2021). Thus, basophils are key drivers of indirect pruritogenic itch.

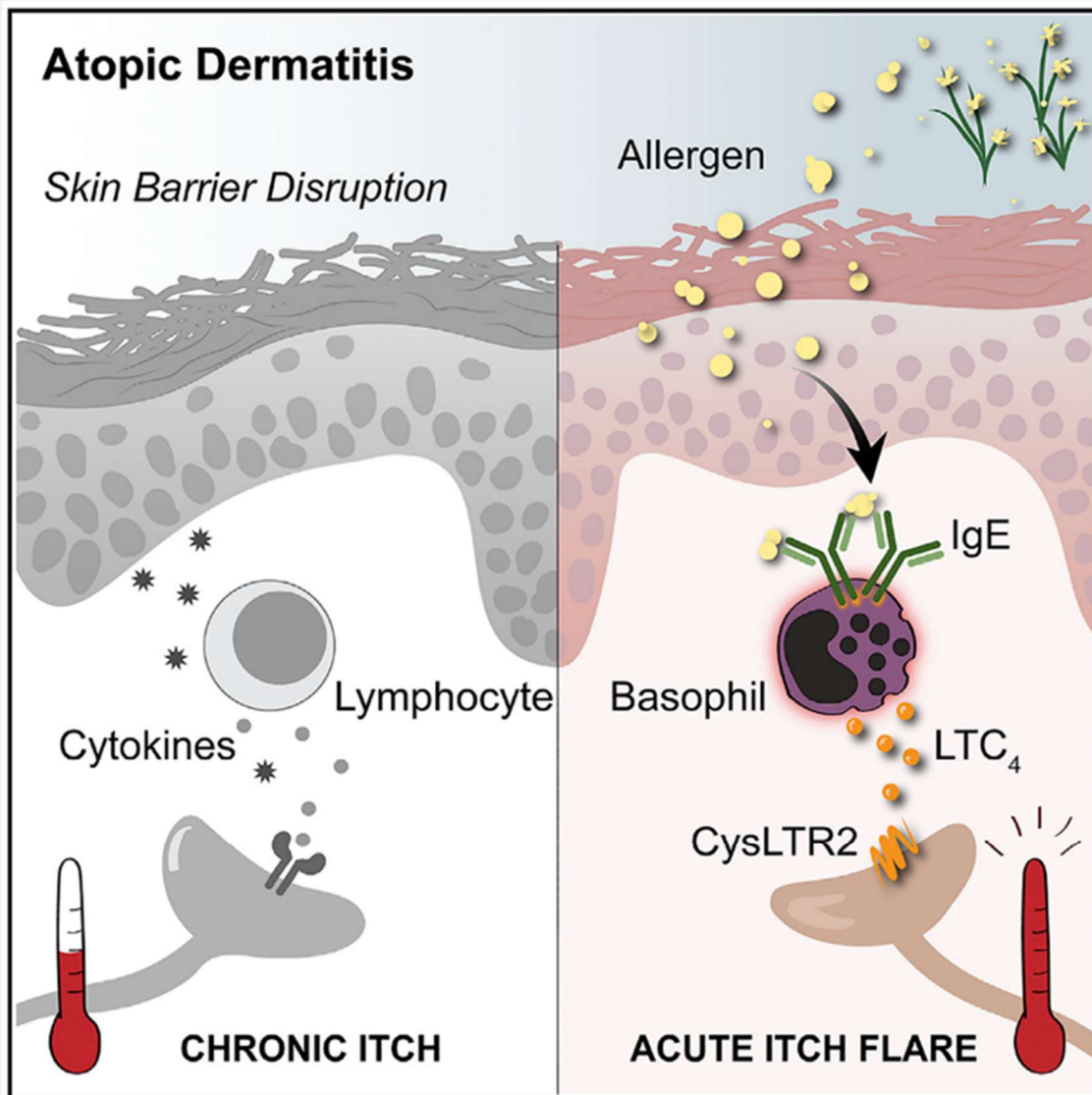


Figure 1.16. Basophils promote allergen-induced acute itch flares in atopic patients.

Chronic itch in atopic patients is characterised by barrier disruption and lymphocyte-derived signalling. Acute itch flares in atopic patients are driven by external allergens and basophil cell-derived signalling. Allergens stimulate IgE-dependent degranulation of basophils; released leukotriene C4 (LC₄) activates adjacent CysLTR2-positive sensory neurons inducing acute itch transduction. From Wang *et al.*, 2021.

1.3.4.3. Keratinocytes

As mentioned previously, keratinocytes represent an active component of the cutaneous immune response. Following epidermal damage, keratinocytes secrete a wide variety of inflammatory mediators, growth factors and antimicrobial peptides (**Figure 1.17**). In addition to promoting and potentiating cutaneous inflammation, several of these keratinocyte-derived mediators function as direct pruritogens: TSLP, IL-33, cathepsin S, and various kallikreins (Wilson, Thé, *et al.*, 2013; Liu *et al.*, 2016; Reddy *et al.*, 2010; Hagermark, 1974; Guo *et al.*, 2020).

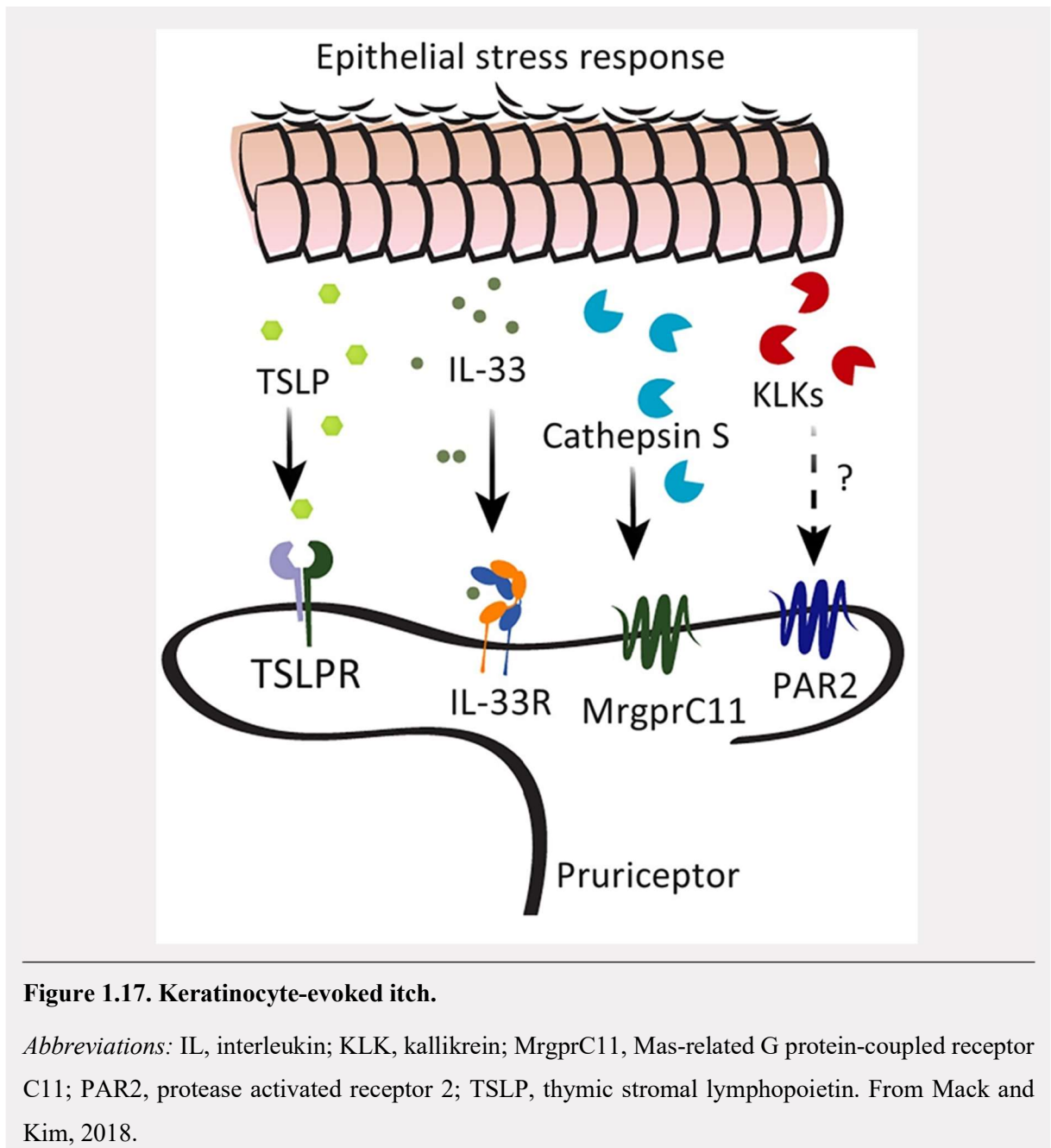


Figure 1.17. Keratinocyte-evoked itch.

Abbreviations: IL, interleukin; KLK, kallikrein; MrgprC11, Mas-related G protein-coupled receptor C11; PAR2, protease activated receptor 2; TSLP, thymic stromal lymphopoietin. From Mack and Kim, 2018.

TSLP activates dendritic cells, promotes Th2 differentiation, and stimulates Th2-type inflammatory responses (Soumelis *et al.*, 2002; Watanabe *et al.*, 2004; Wallmeyer *et al.*, 2017). Binding to the neuronal TSLP receptor (TSLPR), TSLP activates sensory neurons and evokes striking scratching behaviours in mice (Wilson, Thé, *et al.*, 2013). Specific overexpression of TSLP in epidermal keratinocytes promotes significant spontaneous scratching and AD-like dermatitis in mice (Li *et al.*, 2005). Consistent with this finding, TSLP is highly overexpressed in keratinocytes from atopic dermatitis patients and likely is involved in atopic itch (Soumelis *et al.*, 2002).

IL-33 also promotes Th2-type inflammation, induces mast cell degranulation, and stimulates neurons to produce itch (Liu *et al.*, 2016; Komai-Koma *et al.*, 2012; Kondo *et al.*, 2008; Moro *et al.*, 2010). IL-33 is also increased in lesional atopic dermatitis and, when over expressed in the skin, can promote AD-like alterations and spontaneous scratching in mice (Savinko *et al.*, 2012; Imai *et al.*, 2013; Nakamura *et al.*, 2019).

Cathepsin S, an endogenous cysteine protease, promotes rapid itch sensation in humans (Reddy *et al.*, 2010). Overexpression of cathepsin S upregulates protease activated receptor (PAR) 2 expression on dendritic cells, enhances cutaneous Th2-type inflammatory mediators, and promotes itchy mast cell-associated dermatitis in mice (Kim *et al.*, 2012). Cathepsin S activates several itch-associated receptors, namely PAR2, PAR4, and MrgprC11; thus, the exact pathway for cathepsin S-evoked itch remains unclear (Reddy *et al.*, 2010; Reddy *et al.*, 2015; Chung *et al.*, 2019).

Kallikreins (KLK) – a group of serine protease involved in desquamation – have been linked to keratinocyte-driven itch (Nauroy and Nyström, 2020). Several KLKs are upregulated in pruritic lesional atopic dermatitis and AD-like murine models, with KLK7 proving particularly important (Komatsu *et al.*, 2007; Morizane *et al.*, 2012; Nattkemper *et al.*, 2018). Th2-type cytokines promote KLK7 expression and drive KLK7-mediated barrier dysfunction (Morizane *et al.*, 2012). Though KLK7 is unable to directly promote itch sensations, KLK7 knockdown attenuates scratching behaviour in a murine model of atopic dermatitis (Guo *et al.*, 2020), suggesting that KLK7 may facilitate itch transduction through cleavage and processing of cutaneous pruritogens.

Though these reports suggest a clear role for epidermal keratinocytes in pruritus, the development of specific keratinocyte-targeting compounds remains slow. This project aims to further our understanding of keratinocyte signalling and identify novel neuro-epidermal pathways.

1.4. TRP channels and pruritus

The TRP channel superfamily is highly conserved: some members have been identified in insects, helminths, and even protozoa (Wolstenholme *et al.*, 2011; Tsagareli and Nozadze, 2020). In humans, the TRP family contains 28 members split into 6 subgroups on the basis of sequence homology: TRPV (vanilloid), TRPC (canonical), TRPM (melastatin), TRPA (ankyrin), TRPP (polycystin), and TRPML (mucolipin) (**Figure 1.18**) (Tsagareli and Nozadze, 2020; Montell *et al.*, 2002). Although all TRP channels act as functional membrane-associated cation pores, each displays a distinct expression pattern, ion selectivity, and activation mechanism (Montell *et al.*, 2002).

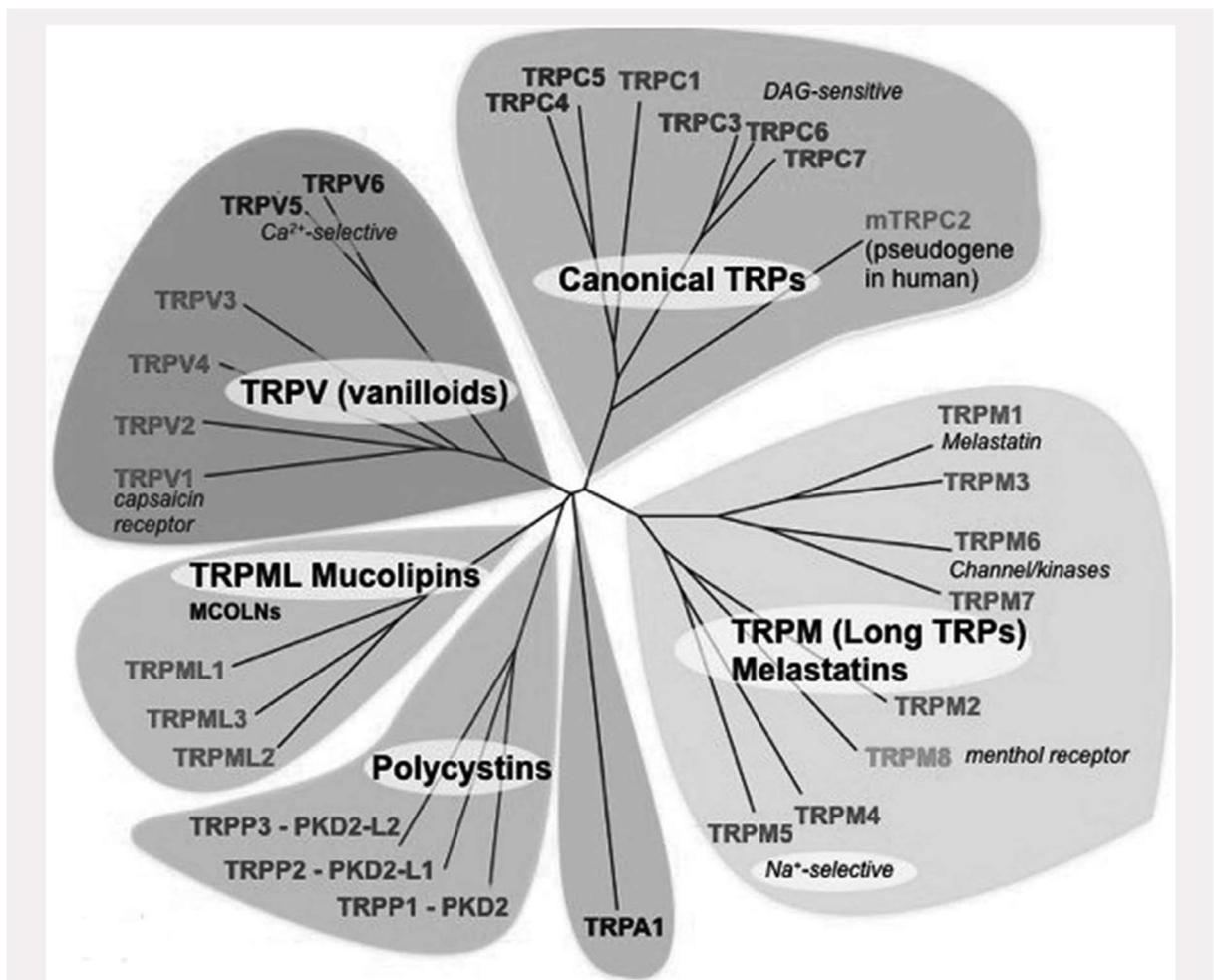


Figure 1.18. Phylogeny of TRP channels.

From Tsagareli and Nozadze, 2020.

Previous sections described TRPV1 and TRPA1 as markers of neural itch pathways. Here, we discuss the function of these TRP channels and their role in pruritus. We also outline emerging TRP channels in itch research.

1.4.1. TRPV1 in histaminergic itch and pruritic conditions

TRPV1 channels are activated by capsaicin, pH or protons, and noxious heat (>43°C) (Caterina *et al.*, 1997; Caterina *et al.*, 2000). Here, capsaicin is used as the experimental TRPV1 agonist.

In sensory neurons, TRPV1 channels function as cellular sensors, integrating cellular signals and promoting action potential generation. TRPV1 is functionally coupled to both H1R and H4R histamine receptors (Shim *et al.*, 2007; Jian *et al.*, 2016; Imamachi *et al.*, 2009). Knockout of TRPV1 channels and ablation of TRPV1⁺ neurons attenuate histamine-evoked scratching in mice. This itch-like behaviour is dependent on phospholipase A₂, phospholipase β₃, lipoxygenase signalling (Shim *et al.*, 2007; Imamachi *et al.*, 2009). H4R-mediated itch is also dependent on phospholipase C (Jian *et al.*, 2016). In addition to histamine, TRPV1 channels have been linked to bradykinin, nerve growth factor (NGF), 5-HT, and prostaglandins (Sugiura *et al.*, 2004; Chuang *et al.*, 2001; Moriyama *et al.*, 2005).

Several cutaneous cells express TRPV1 proteins: mast cells, sebocytes and keratinocytes (Bíró *et al.*, 1998; Bodó *et al.*, 2005; Southall *et al.*, 2003; Inoue *et al.*, 2002; Denda *et al.*, 2001; Bodó *et al.*, 2004; Ständer *et al.*, 2004). In keratinocytes, TRPV1 agonists modulate differentiation, proliferation and apoptosis, and mediator release; capsaicin stimulated HaCaTs release prostaglandin E₂ and IL-8 (Bodó *et al.*, 2005; Southall *et al.*, 2003). However, the effects of nonneuronal TRPV1 remain poorly characterised.

The TRPV1 channel has also been linked to several dermatological disorders. Cutaneous TRPV1 transcripts are increased in erythematotelangiectatic and phymatous rosacea, but not in papulopustular rosacea (Sulk *et al.*, 2012). Patients with prurigo nodularis, an intensely pruritic dermatological disease, also show elevated numbers TRPV1⁺ keratinocytes (Ständer *et al.*, 2004). Moreover, TRPV1 expression is elevated in both pruritic atopic dermatitis and pruritic psoriasis, with skin staining revealing notable increases when compared with nonpruritic/nonlesional disease-matched samples (Nattkemper *et al.*, 2018).

To date, targeting of TRPV1 has been shown to alleviate itch in both murine AD-like disease and human atopic dermatitis patients. Thus, dysregulation of TRPV1 expression and activity may be involved in the development of pruritic skin conditions.

1.4.2. TRPA1 in nonhistaminergic itch and pruritic conditions

TRPA1 channels are activated by allyl isothiocyanate (AITC), cinnamaldehyde, hydrogen peroxide, and other noxious electrophilic chemicals and endogenous reactive oxygen (Jordt *et al.*, 2004; Sawada *et al.*, 2008; Alpizar *et al.*, 2013). Here, AITC is used as the experimental TRPA1 agonist.

In sensory neurons, TRPA1 channels function in a similar manner to TRPV1, responding to cellular signals and promoting action potential generation. Mounting evidence suggests that TRPA1 may integrate and transmit nonhistaminergic itch-inducing signals. Neuronal TRPA1 channel is functionally coupled to TSLPR and MrgprC11, facilitating TSLP- and BAM8-22-induced itch, respectively (Wilson, Thé, *et al.*, 2013; Wilson *et al.*, 2011). TRPA1 may mediate chloroquine and 5-HT-evoked itch, though reports are conflicting at present (Wilson *et al.*, 2011; Ru *et al.*, 2017; Morita *et al.*, 2015; Akiyama *et al.*, 2016). In addition to dermatologic itch, TRPA1 also plays an important role in cholestatic itch. Bile acids (BA) promote itch-like behaviour in mice and underpin the intractable pruritus associated with clinical cholestasis; BA-induced itch is mediated by activation of the BA receptor, TGR5, with TRPA1 facilitating neuronal activation and itch transduction (Lieu *et al.*, 2014).

Several cutaneous cells express TRPA1: melanocytes, fibroblasts and keratinocytes; albeit at very low levels (Atoyan *et al.*, 2009; Bellono *et al.*, 2013). A recent study indicated that nonneuronal TRPA1 may be affected by inflammation, with tumour necrosis factor (TNF) significantly increasing TRPA1 expression and activity in a keratinocyte cell-line (HaCaTs) (Luostarinen *et al.*, 2021). In keratinocytes, TRPA1 agonists enhance expression of pro-inflammatory cytokines (Atoyan *et al.*, 2009). Similar to TRPV1, the effects of nonneuronal TRPA1 remain poorly characterised.

Pruritus is largely mediated by histamine-independent mechanisms; the TRPA1 channel has been linked to pruritic inflammatory skin conditions such as AD, allergic contact dermatitis, dry skin-associated itch, and inflammatory itch models (Liu *et al.*, 2013; Kang *et al.*, 2017; Oh *et al.*, 2013; Cevikbas *et al.*, 2014; Wilson, Nelson, *et al.*, 2013). TRPA1 is specifically upregulated in pruritic AD, but not pruritic psoriasis (Nattkemper *et al.*, 2018). Genetic and pharmacological blockade of TRPA1 exacerbates imiquimod-induced alterations in mice (Kemény *et al.*, 2018), suggesting that TRPA1 may be protective in psoriasis. However, as much of our understanding is based on broad TRPA1 antagonists or TRPA1^{-/-} mice, the cells responsible for these effects remain elusive. Thus, cell-specific TRPA1 knockdowns may reveal important insights into these disease-specific TRPA1 pathways.

1.4.3. Emerging TRP channels in itch research

Several members of the TRP family have been associated with acute itch transmission and chronic pruritus (Moore *et al.*, 2018; Dong and Dong, 2018; Feng *et al.*, 2017; Luo *et al.*, 2015; Kittaka and Tominaga, 2017; Caterina and Pang, 2016; Sun and Dong, 2016; Foster *et al.*, 2017; Xie and Hu, 2018). In addition to TRPV1 and TRPA1, several other TRP channels have now been linked to both the physiology and pathophysiology of the skin (Caterina and Pang, 2016). These include TRPC4, TRPV4 and TRPV3 (Xie and Hu, 2018). Briefly, TRPC4 channels are involved in pruritic reactions induced by selective serotonin reuptake inhibitor treatment (Lee *et al.*, 2018; Warnock and Morris, 2002). TRPV4 has been linked to a variety of pruritogens and may play a role in both allergic and non-allergic chronic itch (Luo *et al.*, 2018; Chen *et al.*, 2016; Akiyama *et al.*, 2016; Kim *et al.*, 2016). TRPV3 plays a crucial role in skin physiology and pathophysiology, with current evidence suggesting a link between TRPV3 and pruritic dermatitis. This project aims to further investigate TRPV3-associated processes and their role in human skin conditions.

TRPV1 and TRPA1 remain the most extensively studied of the itch-associated TRP channels. However, several other channels have now been linked to both the physiology and pathophysiology of the skin (Caterina and Pang, 2016). These include TRPC4, TRPV4, and TRPV3 (Xie and Hu, 2018). Briefly, TRPC4 channels are involved in pruritic reactions induced by selective serotonin reuptake inhibitor treatment (Lee *et al.*, 2018; Warnock and Morris, 2002). TRPV4 has been linked to a variety of pruritogens and may play a role in both allergic and non-allergic chronic itch (Luo *et al.*, 2018; Chen *et al.*, 2016; Akiyama *et al.*, 2016; Kim *et al.*, 2016). TRPV3 plays a crucial role in skin physiology and pathophysiology, with current evidence suggesting a link between TRPV3 and pruritic skin conditions.

1.5. The TRPV3 cation channel

This project aims to further investigate TRPV3 and its role in human skin conditions.

1.5.1. TRPV3 expression and protein structure

TRPV3 expression is largely restricted to the skin, with the Genotype-Tissue Expression (GTEx) project describing the skin as the primary location of TRPV3 transcripts in humans (Xu *et al.*, 2006; Peier *et al.*, 2002; Moqrich *et al.*, 2005; Lonsdale *et al.*, 2013). TRPV3 is abundantly expressed in epidermal keratinocytes (**Figure 1.19**), with strong staining localised to the basal keratinocyte layer (Peier *et al.*, 2002; Facer *et al.*, 2007; Asakawa *et al.*, 2006). TRPV3 is also expressed in hair follicle and mucosal epithelial cells (Xu *et al.*, 2006; Aijima *et al.*, 2015; Peier *et al.*, 2002; Xu *et al.*, 2002; Borb r  *et al.*, 2011).

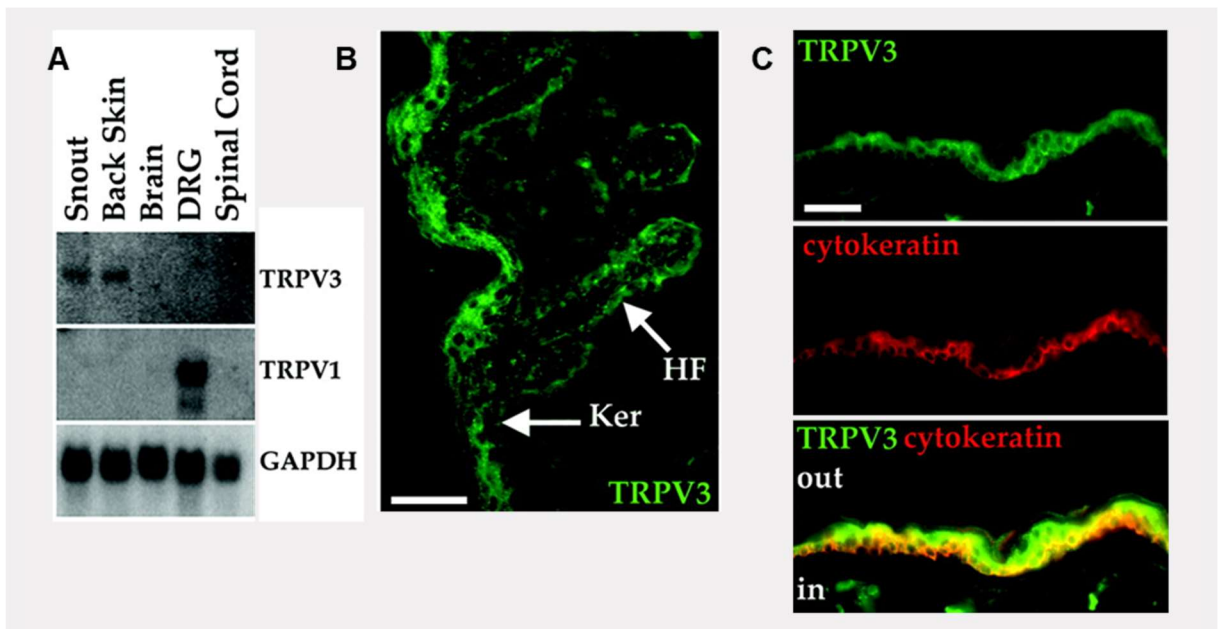


Figure 1.19. TRPV3 is expressed in epidermal keratinocytes.

A, Northern blot analysis of adult rat tissues showing TRPV3, TRPV1 and glyceraldehyde phosphate dehydrogenase (GAPDH) transcript expression. **B**, Immunostaining showing TRPV3 in the keratinocytes (Ker) and hair follicle (HF) of newborn mice. **C**, Immunostaining showing TRPV3 and basal pan-cytokeratin in epidermal layer of adult rat skin. Scale bars =50 μ m. From Peier *et al.*, 2002.

Reports of neuronal TRPV3 remain controversial. TRPV3 transcripts have been detected in spinal cord, DRG and brain tissue from human and non-human primates (Xu *et al.*, 2002; Smith *et al.*, 2002; Peier *et al.*, 2002) but are minimal in rodent neuronal samples (Peier *et al.*, 2002; Moqrich *et al.*, 2005; Smith *et al.*, 2002). Surprisingly, hippocampal slices from TRPV3 knockout mice show impaired induction of synaptic plasticity, suggesting a role for TRPV3 in the neuronal circuits of the hippocampus (Brown *et al.*, 2013). Whether these extra-epidermal TRPV3 channels will impede the utility of TRPV3-targeting agents remains unclear.

In humans, the TRPV3 sequence is mapped to chromosome 17p13, with the complete open reading frame measuring 2,370 base pairs and coding for a protein of 790 amino acids (**Figure 1.20**) (Smith *et al.*, 2002; Xu *et al.*, 2002). This TRPV3 protein contains 6 putative transmembrane regions (S1 - S6), with the S1 - S4 helices representing a voltage sensor-like domain and S5- S6 lining the cation pore. These S1- S6 regions are flanked by a TRP helix at the C-terminus and ankyrin repeat domain (ARD) at the N-terminus (Zubcevic *et al.*, 2018; Singh *et al.*, 2018). The TRP helix is a short but highly conserved sequence, which acts as an intracellular sensor for phosphatidylinositol 4,5-bisphosphate (PIP₂) and represents an important site for PIP₂-mediated modulation of TRPV3 activity (Doerner *et al.*, 2011). Similar to other TRPV proteins, the TRPV3-ARD contains 6 ankyrin repeats and acts to facilitate protein-protein interactions. This region controls the assembly of TRPV3 subunits, trafficking of functional TRPV3 channels, and induction of downstream TRPV3 signalling. Both the TRP domain and ARD represent characteristic features of the TRPV family, underpinning the regulation, gating, and trafficking of these channels. However, research into the specific residues required for both normal and pathological TRPV3 functioning is ongoing.

```

M K A H P K E M V P L M G K R V A A P S G N P A V L P E K R 30
P A E I T P T K K S A H F F L E I E G F E P N P T V A K T S 60
P P V F S K P M D S N I R Q C I S G N C D D M D S P Q S P Q 90
D D V T E T P S N P N S P S A Q L A K E E Q R R K K G R L K 120
K R I F A A V S E G C V E E L V E L L V E L Q E L C R R R H 150
D E D V P D F L M H K L T A S D T G K T C L M K A L L N I N 180
P N T K E I V R I L L A F A E E N D I L G R F I N A E Y T E 210
E A Y E G Q T A L N I A I E R R O G D I A A L L I A A G A D 240
V N A H A K G A F F N P K Y Q H E G F Y F G E T P L A L A A 270
C T N Q P E I V Q L L M E H E Q T D I T S R D S R G N N I L 300
H A L V T V A E D F K T Q N D F V K R M Y D M I L L R S G N 330
W E L E T T R N N D G L T P L Q L A A K M G K A E I L K Y I 360
L S R E I K E K R L R S L S R K F T D W A Y G P V S S S L Y 390
D L T N V D T T T D N S V L E I T V Y N T N I D N R H E M L 420
T L E P L H T L L H M K W K K F A K H M F F L S F C F Y F F 450
Y N I T L T L V S Y Y R P R E E E A I P H P L A L T H K M G 480
W L Q L L G R M F V L I W A M C I S V K E G I A I F L L R P 510
S D L Q S I L S D A W F H F V F F I Q A V L V I L S V F L Y 540
L F A Y K E Y L A C L V L A M A L G W A N M L Y Y T R G F Q 570
S M G M Y S V M I Q K V I L H D V L K F L F V Y I V F L L G 600
F G V A L A S L I E K C P K D N K D C S S Y G S F S D A V L 630
E L F K L T I G L G D L N I Q Q N S K Y P I L F L F L L I T 660
Y V I L T F V L L L N M L I A L M G E T V E N V S K E S E R 690
I W R L Q R A R T I L E F E K M L P E W L R S R F R M G E L 720
C K V A E D D F R L C L R I N E V K W T E W K T H V S F L N 750
E D P G P V R R T D F N K I Q D S S R N N S K T T L N A F E 780
E V E E F P E T S V * 790

```

Figure 1.20. Polypeptide sequence of human TRPV3.

Amino acid residues number shown in margin (1 – 790). Solid lines indicate predicted transmembrane regions (S1 – S6). Dashed lines indicate predicted ankyrin repeat domain (ARD). Consensus sites for protein kinase A (filled diamonds) and protein kinase C (filled circles) are also shown. From Smith *et al.*, 2002.

1.5.2. Biophysical and molecular features of the TRPV3 channel

TRPV3 proteins assemble to form a symmetric homotetrameric complex (**Figure 1.21**) (Zubcevic *et al.*, 2018). TRPV3 may also complex with TRPV1, though the functional relevance of these heterotetramers remains unknown (Smith *et al.*, 2002; Cheng *et al.*, 2007; Cheng *et al.*, 2012; Hellwig *et al.*, 2005). Following assembly and insertion, the TRPV3 complex functions as a nonselective, plasma membrane-spanning cation channel (Zubcevic *et al.*, 2018; Peier *et al.*, 2002; Xu *et al.*, 2002). Human TRPV3 channels contain 2 clear constriction sites, with G638 residues forming the outer ion selectivity filter (4.5 Å) and I674 side chains creating a hydrophobic intracellular gate (5.3 Å) (**Figure 1.22**) (Deng *et al.*, 2020). Channel opening is dependent on subtle but global structural rearrangements, ultimately resulting in separation of the pore-lining S6 helices, lipid rearrangement and cation influx (Deng *et al.*, 2020). While TRPV3 is cation nonselective, this channel is highly permeable to calcium (Ca^{2+}) ions ($\text{Ca}^{2+} > \text{Na}^+ \approx \text{K}^+ \approx \text{Cs}^+$) (Xu *et al.*, 2002) and facilitates global calcium fluctuations.

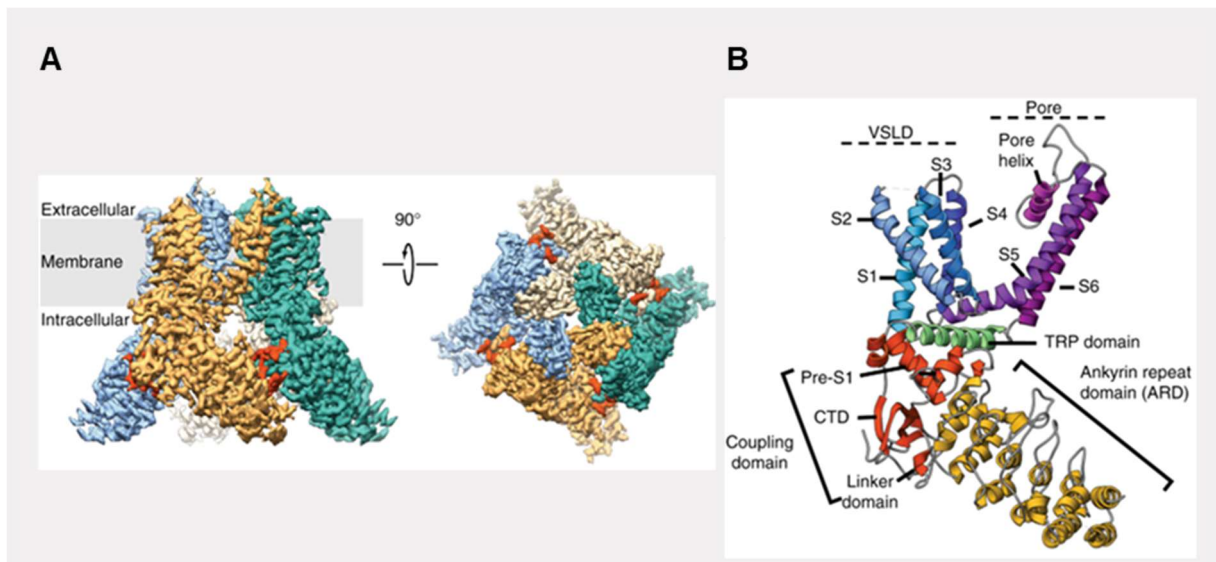


Figure 1.21. Structural characterisation of human TRPV3.

A, 3D cryo-EM reconstruction of apo human TRPV3 tetramer, coloured by protomer. The C-terminal domain is shown in red. **B**, Overview of structural elements within single TRPV3 protomer: Ankyrin repeat domain (ARD) is shown in yellow; Coupling domain, consisting of linker domain, pre-S1 and the C-terminal domain, is shown in red; Voltage sensing-like domain (VSLD), consisting of helices S1–S4, is shown in blue, the pore domain, consisting of helices S5–S6 and the pore helix, is coloured in purple; the TRP domain is shown in green. From Zubcevic *et al.*, 2018.

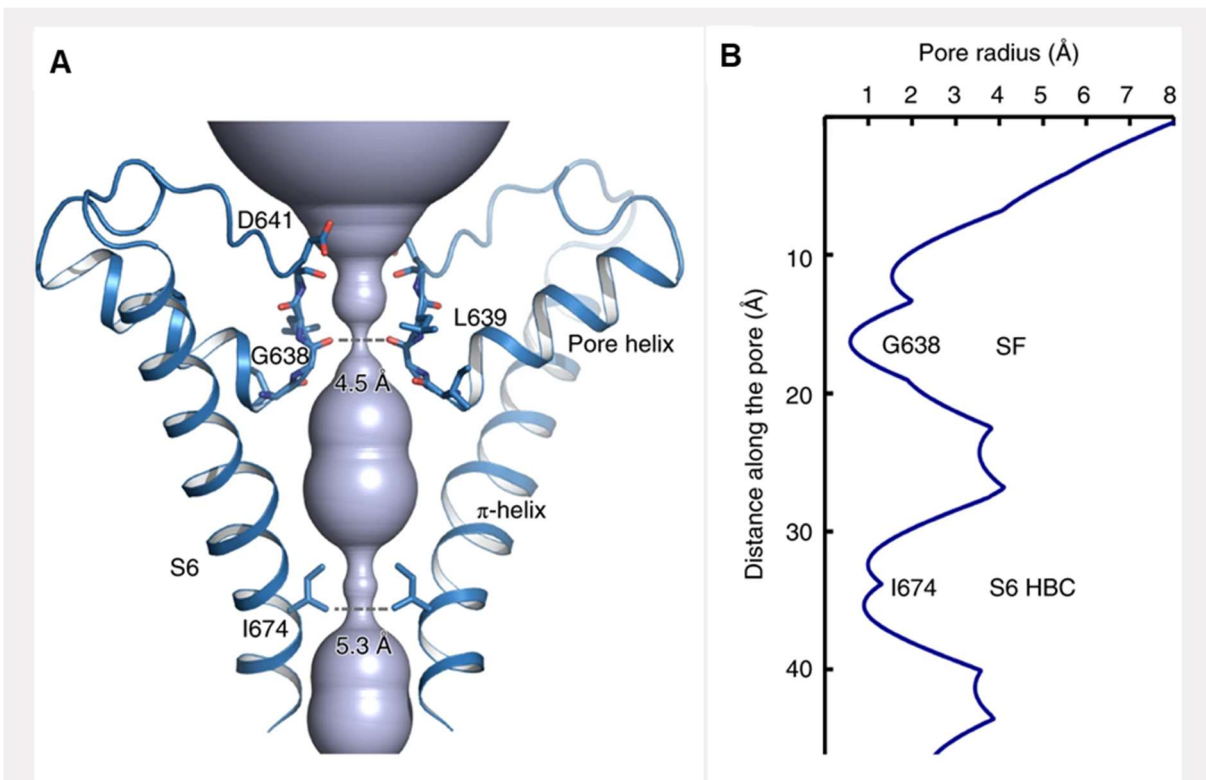


Figure 1.22. Two physical constrictions along the ion pore of TRPV3 in a lipid bilayer.

A, Ion-conduction pore of TRPV3 in a lipid bilayer, shown as a light blue surface calculated with the program HOLE. The front and back subunits are removed for clarity. Two narrow constrictions at the selectivity filter and the intracellular S6 bundle-crossing regions are illustrated. **B**, Dimensions of the ion-conduction pore. From Deng *et al.*, 2020.

Like many other TRPs, TRPV3 channels are thermosensitive. With a temperature threshold of between 33°C and 42°C, TRPV3 opens in response to innocuous physiologically-relevant temperatures (Peier *et al.*, 2002; Xu *et al.*, 2002; Smith *et al.*, 2002). Mutagenesis screening identified the pore-spanning S6 region as the key site mediating thermal activation of TRPV3 (Grandl *et al.*, 2008). Findings from co-culture systems suggest that keratinocyte-expressed TRPV3 channels may facilitate thermo-transduction: keratinocytes detect warm temperatures via TRPV3 and coordinate thermosensation through release of ATP and subsequent activation of adjacent sensory neurons (Mandadi *et al.*, 2009). However, though early reports from TRPV3 knockout mice supported a role for TRPV3 in thermo-transduction (Moqrich *et al.*, 2005), a later group failed to replicate these *in vivo* findings (Huang *et al.*, 2011).

In a similar manner to TRPV1 and TRPA1, TRPV3 channels function as signal integrators. Consistent with this theory, several agonists and intracellular signalling pathways potentiate TRPV3 activity (**Figure 1.23**). TRPV3 currents are sensitised by protein kinase C (PKC) and activation of G_{q/11}-coupled receptors, with phospholipase C (PLC) facilitating the GPCR-induced potentiation (Cheng *et al.*, 2010; Xu *et al.*, 2006; Hu *et al.*, 2006). PLC-mediated sensitisation is dependent on hydrolysis of phosphatidylinositol (4,5) biphosphate (PI(4,5)P₂), indicating that resting levels of plasma membrane PIP₂ function to negatively regulate TRPV3 activity (Doerner *et al.*, 2011). TRPV3 activity is also potentiated by unsaturated fatty acids such as arachidonic acid, an important component in cutaneous inflammatory pathways (Hu *et al.*, 2006). Reports suggest that TRPV3 channels show enhanced activity upon repeated stimulation (Chung *et al.*, 2004; Chung *et al.*, 2005). This unusual feature remains poorly understood, though it may be mediated by binding of calmodulin to the N-terminal and pore regions of the TRPV3 channel (Xiao, Tang, *et al.*, 2008; Phelps *et al.*, 2010). In addition to these signalling pathways, TRPV3 has also been linked with histamine (H1R), bradykinin (B2R), muscarinic (HM1) and PAR2 receptors (Xu *et al.*, 2006; Park *et al.*, 2017; Zhao *et al.*, 2020). Thus, though the exact *in vivo* activation and sensitisation mechanisms remain unclear, TRPV3 represents a potent polymodal thermosensitive sensor.

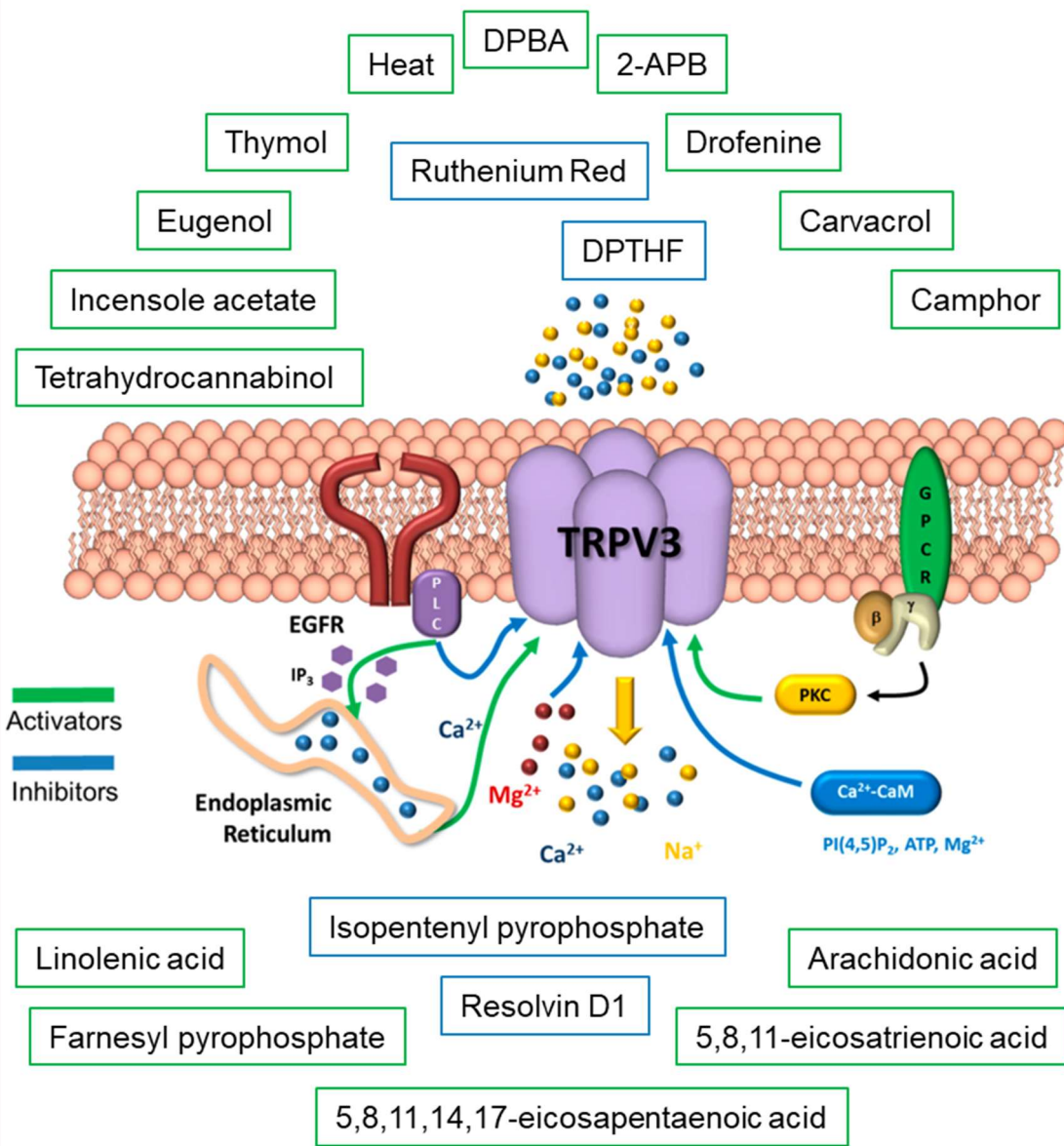


Figure 1.23. Activators, inhibitors, and modulators of TRPV3.

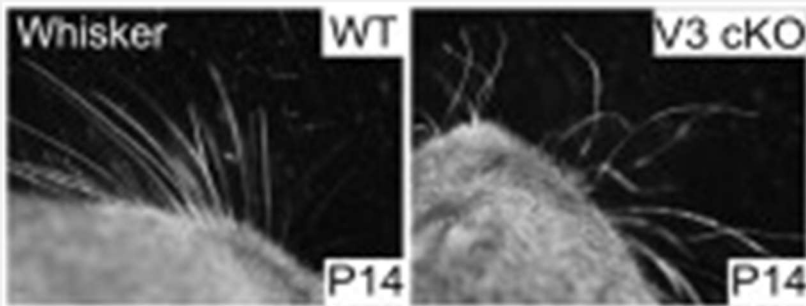
Abbreviations: 2-APB, 2-Aminoethoxydiphenyl borate; DPBA, diphenylboronic anhydride; EGF receptor (EGFR), extracellular growth factor receptor; GPCR, G-protein coupled receptor; PKC, protein kinase C; and PLC, phospholipase C. Figure modified from Broad *et al.*, 2016.

1.5.3. TRPV3 as a coordinator of epidermal patterning

As described previously, generation of the stratified epidermal barrier is dependent on proliferation and differentiation of keratinocytes. These essential processes are primarily mediated by the epidermal growth factor (EGF) pathway, with the skin displaying extraordinary sensitivity to under- and/or overactivation of this system. Briefly, release of transforming growth factor alpha (TGF α) leads to activation of the EGF receptor (EGFR) and induction of the tightly controlled system of keratinocyte proliferation and differentiation. TGF α and EGFR loss-of-function murine models highlight the importance of this pathway in epidermal morphogenesis, hair patterning and wound healing (Threadgill *et al.*, 1995; Sibilian and Wagner, 1995; Murillas *et al.*, 1995; Mann *et al.*, 1993; Luetkeke *et al.*, 1993; Luetkeke *et al.*, 1994).

Surprisingly, TRPV3 knockout mice resemble TGF α and EGFR mutants (**Figure 1.24**) (Schneider *et al.*, 2008), suggesting that TRPV3 may be linked to the TGF α /EGFR pathway. Though the overall architecture of the skin is unaffected, TRPV3 knockout (TRPV3^{-/-}) mice exhibit clear abnormalities in keratinocyte differentiation, epidermal barrier, and hair morphology and follicle patterning (Cheng *et al.*, 2010). TRPV3^{-/-} mice are characterised by a thin SC, a wavy coat, and curly whiskers (Cheng *et al.*, 2010; Moqrich *et al.*, 2005). Keratinocyte-specific deletion of TRPV3 is sufficient for induction of this phenotype (Cheng *et al.*, 2010). TRPV3-deficient mutants also display reduced expression of TGF α mRNA and impaired EGFR phosphorylation (Cheng *et al.*, 2010).

A



B

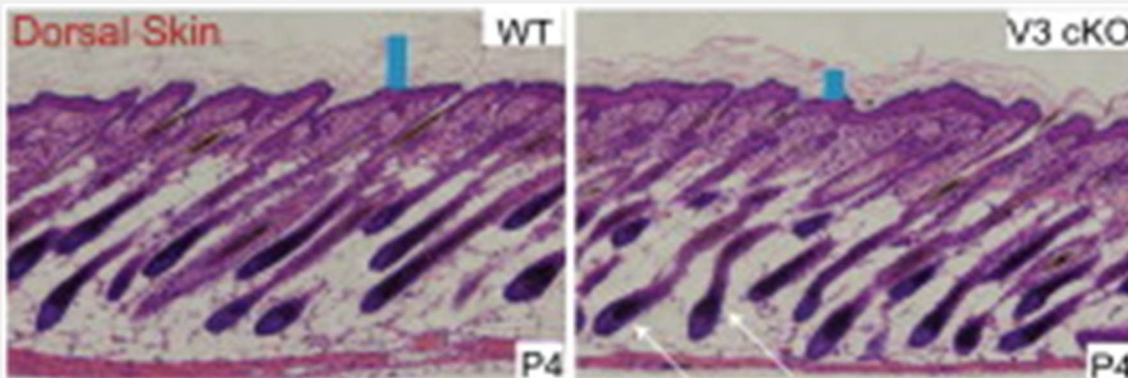


Figure 1.24. TRPV3 deficient mice exhibit curly whiskers, misaligned hair follicles, and a thin stratum corneum.

A, Whiskers of wildtype (WT) and TRPV3 knockout mice (V3 cKO; fl/fl: K14 Cre). Whiskers of wildtype (WT) mice were straight, while whiskers of TRPV3 knockout mice (V3 cKO) were curly and hooked. **B**, H&E staining of dorsal skin reveals abnormalities in V3 cKO mice: thin stratum corneum layer (blue rectangle) and misaligned hair follicles. From Cheng *et al.*, 2010.

The TRPV3 channel may directly interact with EGFR and drive epidermal hyperplasia. TGF- α enhances TRPV3 channel activity and promotes phosphorylation of a TRPV3 tyrosine residue (Cheng *et al.*, 2010). TRPV3 activation stimulates ADAM17-dependent cleavage and release of TGF α , activating EGFR and enhancing keratinocyte proliferation, differentiation and apoptosis (Cheng *et al.*, 2010; Yujing Wang *et al.*, 2021; Aijima *et al.*, 2015; Szöllösi *et al.*, 2018). Similarly, application of carvacrol, a TRPV3 agonist, promotes epidermal thickening in mice (**Figure 1.25**) (Yujing Wang *et al.*, 2021; Yan *et al.*, 2019). These reports suggest that TRPV3 plays a direct role in TGF- α /EGFR signalling and epidermal hyperplasia.

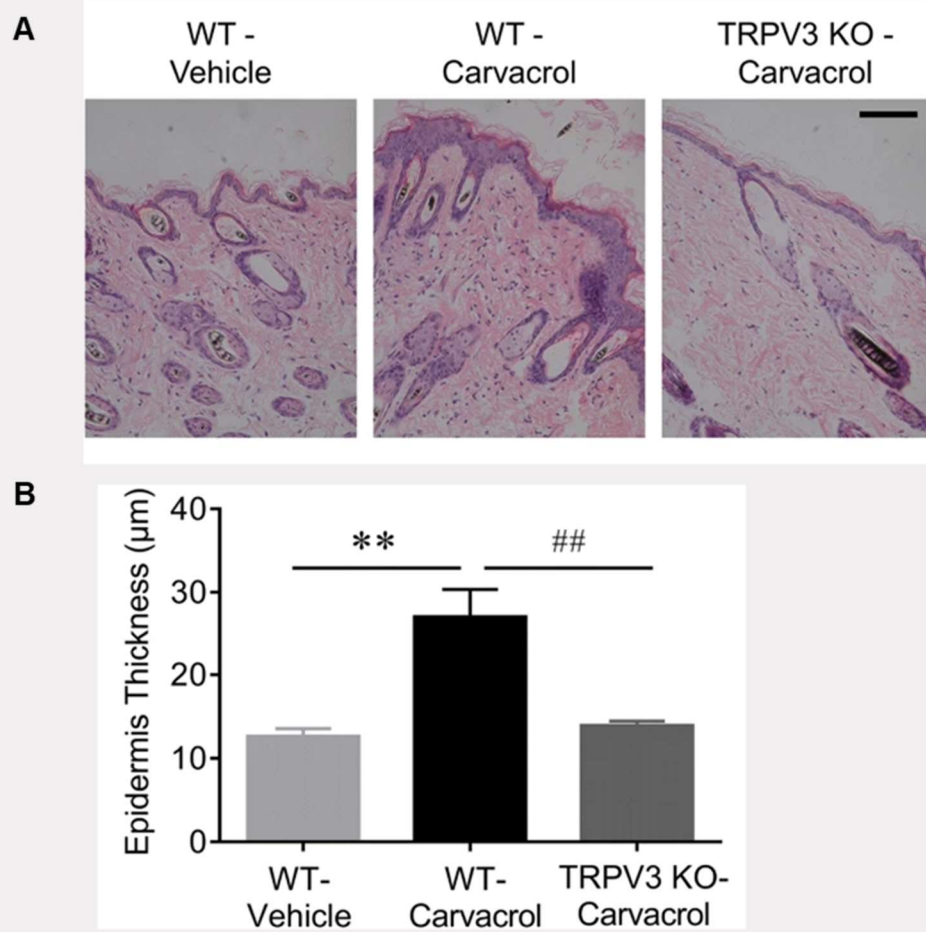


Figure 1.25. Carvacrol induces hyperplasia in wild type but not TRPV3 knockout mice.

Wild type (WT) and TRPV3 knockout (KO) mice were treated with vehicle or 1% carvacrol. Images show H&E staining (A); and quantification of epidermis thickness (B). Scale =100 μm. **, ## $P < 0.01$, N =5. From Wang *et al.*, 2020.

1.5.4. TRPV3 mutations and Olmsted syndrome

Olmsted syndrome, a rare and debilitating genodermatosis, is primarily caused by point mutations in the TRPV3 channel (Cambiaghi *et al.*, 1995; Larregue *et al.*, 2000; Rivers *et al.*, 1985; Lin *et al.*, 2012). Patients present with thick skin on the palms of hands and/or soles of feet, and dry pruritic lesions around the eyes, mouth, nose, ears, genitals or naval (Olmsted, 1927; Duchatelet and Hovnanian, 2015; Tao *et al.*, 2008; Mevorah *et al.*, 2005). Although the severity of the syndrome varies, pain and itch are common (Nofal *et al.*, 2010; Tao *et al.*, 2008; Mevorah *et al.*, 2005; Duchatelet and Hovnanian, 2015).

Patients with Olmsted syndrome display point mutations at several distinct regions within the *TRPV3* gene (Figure 1.26) (Eytan *et al.*, 2014; Lai-Cheong *et al.*, 2012; Danso-Abeam *et al.*, 2013; Sabine Duchatelet *et al.*, 2014; S. Duchatelet *et al.*, 2014; He *et al.*, 2015; Kariminejad *et al.*, 2014). Similar *TRPV3* mutations have also been identified in rodents, with affected mice and rats displaying significant dermatitis and itch-like behaviours (Asakawa *et al.*, 2006; Imura *et al.*, 2009; Yamamoto-Kasai *et al.*, 2013). Findings from heterologous expression systems suggest that these point mutations increase the likelihood of channel opening, promoting cell death, and interrupting the normal physiological functions of TRPV3 (Lin *et al.*, 2012; Xiao, Tian, *et al.*, 2008). Thus, overactivation or sensitisation of TRPV3 dysregulates epidermal signalling and promotes pruritus. Though research is ongoing, the TRPV3/TGF α /EGFR pathway represents an important target for hyperplastic skin conditions such as Olmsted syndrome, atopic dermatitis, and psoriasis.

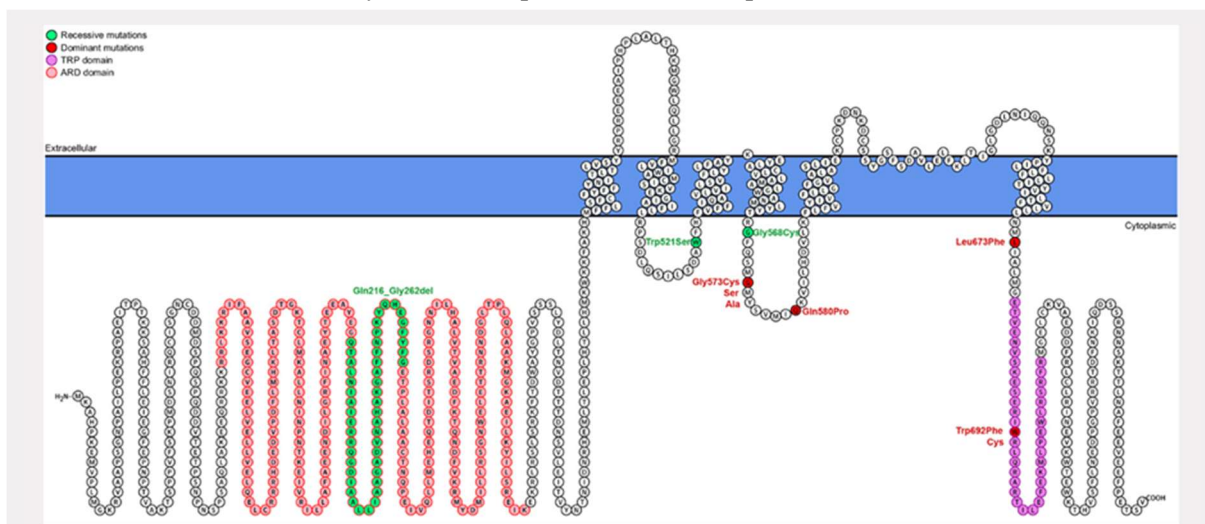


Figure 1.26. Schematic structure of TRPV3 showing location of reported mutations in people with Olmsted syndrome.

All Olmsted syndrome-linked TRPV3 mutations effect the cytoplasmic region. Green represents recessive mutations. Red represents dominant mutations. Pink indicates the transient receptor potential (TRP) domain, while light red indicates the ankyrin repeat domain (ARD). From Wang *et al.*, 2020.

1.5.5. TRPV3 as an inducer of inflammation, itch, and dermatitis

Keratinocytes coordinate cutaneous inflammation, itch, and skin disease. However, our understanding of the role of TRPV3 in these pathological processes remains incomplete.

TRPV3 activation enhances keratinocyte-derived inflammation, promoting secretion of IL-1 α , IL-6, IL-8, and TNF α (Szöllösi *et al.*, 2018; Xu *et al.*, 2006). TRPV3 activation may also promotes secretion of prostaglandin E2 (PGE2), adenosine triphosphate (ATP), nitric oxide (NO), nerve growth factor, and TSLP, each representing potent inducers of itch, pain or dermatitis (Seo *et al.*, 2020; Yamamoto-Kasai *et al.*, 2013; Cals-Grierson and Ormerod, 2004; Miyamoto *et al.*, 2011; Zhao *et al.*, 2020; Mandadi *et al.*, 2009; Huang *et al.*, 2008). In both humans and mice, genetic TRPV3 overactivation elevates epidermal inflammation and inflammatory cell infiltration (Yoshioka *et al.*, 2009; Danso-Abeam *et al.*, 2013). These rodents exhibit high serological levels of AD-linked inflammatory factors such as IgE, IL-1 α , IL-13, IL-17, CCL11, CCL17, and MCP-1 (Yoshioka *et al.*, 2009; Imura *et al.*, 2009). Blockade of TRPV3 reduces cutaneous inflammation in experimental AD-like models, including 2,4-Dinitrofluorobenzene (DNFB)-treated and calcipotriol (MC903)-treated mice (Zhao *et al.*, 2020; Seo *et al.*, 2020; Qu *et al.*, 2019). These data highlight the inflammatory capacity of the TRPV3 channel in epidermal keratinocytes.

As discussed previously, indirect pruritoceptive itch is dependent on cutaneous cells including keratinocytes. These cells secrete inflammatory factors and direct pruritogens to activate adjacent itch-sensitive neurons. Reports now suggest that keratinocyte-expressed TRPV3 may a role in this indirect pathway. Intradermal injection of a TRPV3 agonist promotes acute TRPV3-dependent scratching behaviour in mice (**Figure 1.27**) (Cui *et al.*, 2018; Zhang *et al.*, 2019; Seo *et al.*, 2020). This itch-like response is characterised by 2 distinct phases, an initial phase (0 - 20min post-injection) and a sustained phase (20 - 60min post-injection) (Cui *et al.*, 2018). TRPV3 has also been linked to PAR2-mediated itch (Zhao *et al.*, 2020; Park *et al.*, 2017), suggesting that TRPV3 may coordinate inflammatory itch induction. Inhibition of NO, a TRPV3-linked pruritogen, reduces scratching in a variety of acute and prolonged murine itch models (Ostadhadi *et al.*, 2016; Andoh and Kuraishi, 2003; Foroutan *et al.*, 2015; Ostadhadi *et al.*, 2015; Haddadi *et al.*, 2017). TRPV3 expression is specifically upregulated in pruritic burns, relative to nonpruritic burn tissue (Park *et al.*, 2017; Yang *et al.*, 2015). Together, these reports suggest that keratinocyte TRPV3 may be involved in indirect itch induction in the skin.

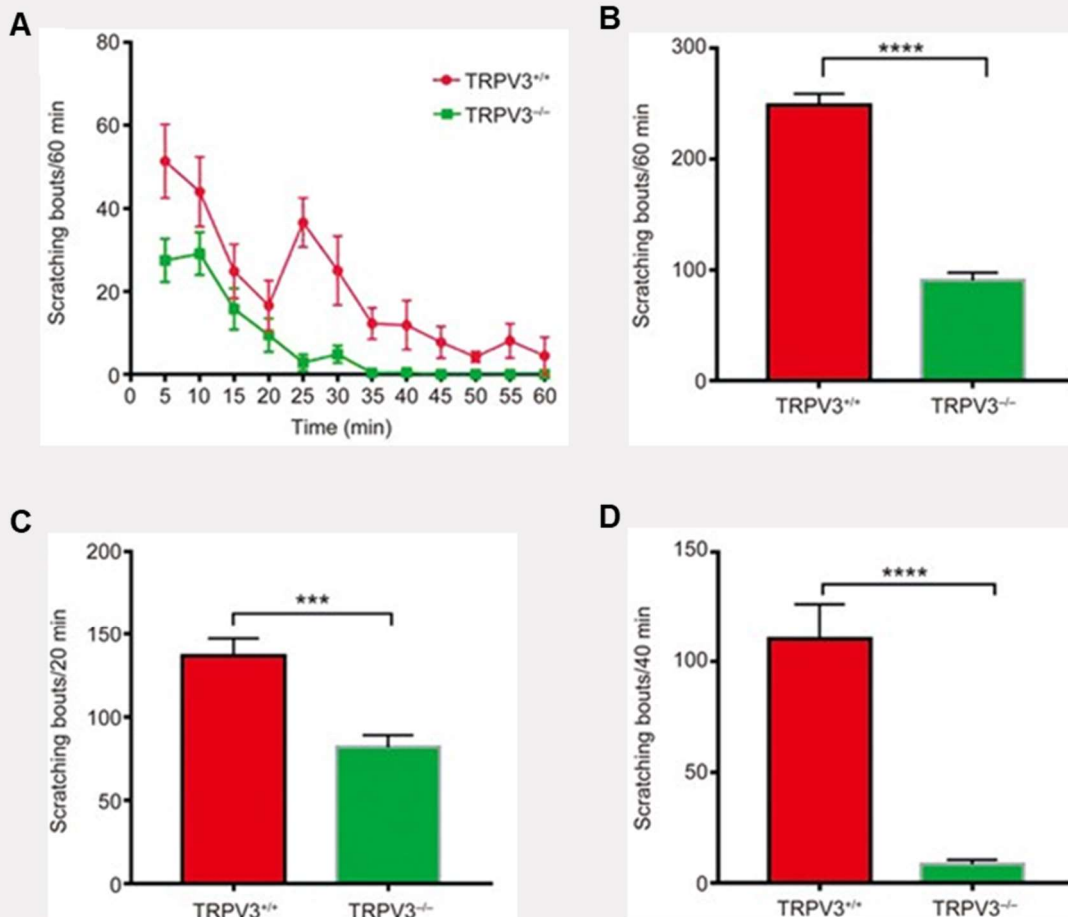


Figure 1.27. Knockout of TRPV3 suppresses carvacrol-induced scratching in C57BL/6J mice.

A, Time course of scratching bouts. **B – D**, Quantification of scratching bouts: overall- 60 minutes (**B**); first 20 minutes (**C**); last 40 minutes (**D**). *** $P \leq 0.001$, **** $P \leq 0.0001$, Student's t-test, TRPV3 knockout (TRPV3^{-/-}) compared with wild type (TRPV3^{+/+}). From Cui *et al.*, 2018.

Mounting evidence now suggests that TRPV3 is involved in pruritic inflammatory skin conditions. TRPV3 transcription and expression is increased in AD, psoriasis, acute contact dermatitis, rosacea and several animal models of dermatitis (**Figure 1.28** and **Figure 1.29**) (Seo *et al.*, 2020; Zhao *et al.*, 2020; Nattkemper *et al.*, 2018; Qu *et al.*, 2019; Sulk *et al.*, 2012; Larkin *et al.*, 2021). TRPV3 activity is sensitised in keratinocytes isolated from atopic dermatitis patients (Seo *et al.*, 2020). Experimental TRPV3 activation promotes epidermal hyperplasia and induces AD-like lesions in mice (Qu *et al.*, 2019; Yujing Wang *et al.*, 2021). Genetic and pharmacological TRPV3 blockade alleviates inflammation and histological alterations in a murine dermatitis model (MC903) (Zhao *et al.*, 2020). Together, these findings support the notion that TRPV3 is involved in human dermatitis and suggest that modulation of TRPV3 activity may represent an effective strategy for the treatment of pruritic skin conditions.

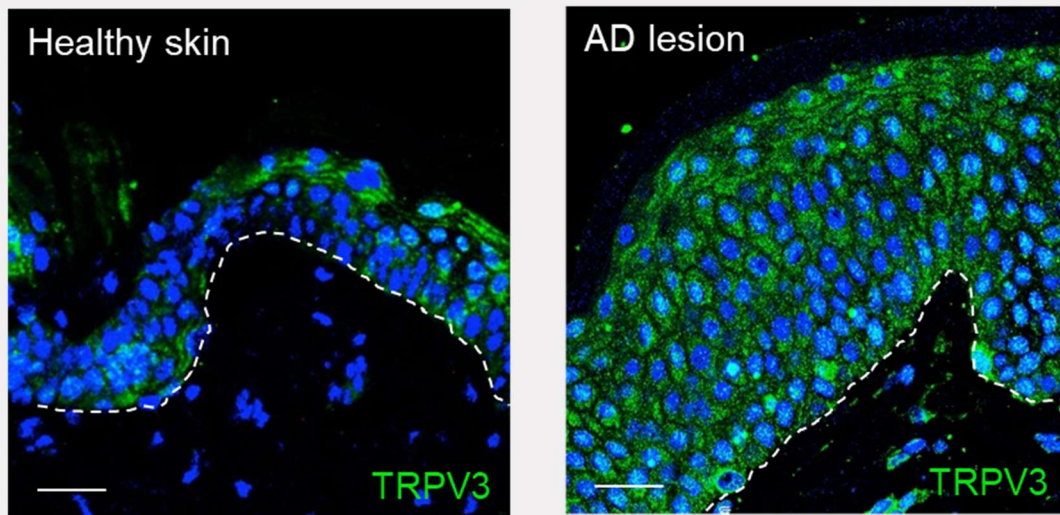


Figure 1.28. TRPV3 proteins are upregulated in the epidermis of atopic dermatitis lesions.

Representative immunostaining of TRPV3 (green) in healthy skin and atopic dermatitis (AD) lesions from human donors. Dotted line indicates the dermal-epidermal junction. Scale =20 μ m. Images included in Larkin *et al.*, 2021.

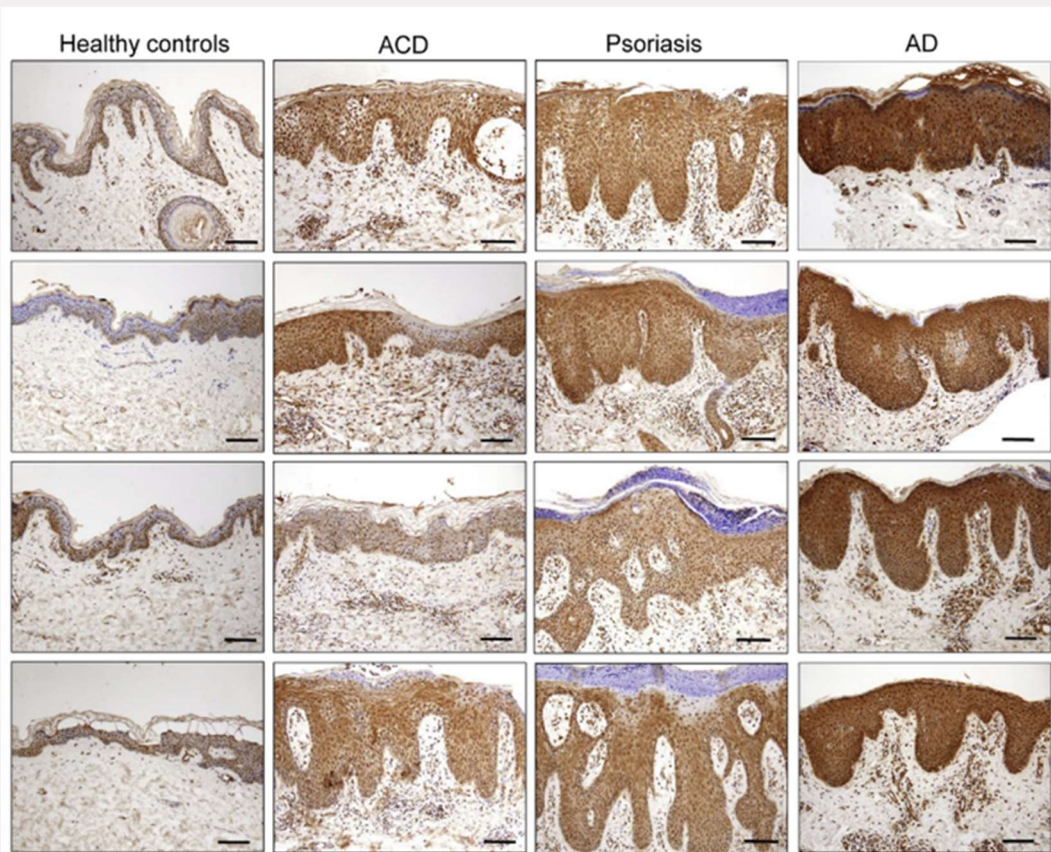


Figure 1.29. Several skin conditions are associated with elevated epidermal TRPV3.

Representative immunostaining of TRPV3 (brown) in samples from healthy controls, allergic contact dermatitis (ACD), psoriasis, and atopic dermatitis (AD). Each image represents a different human donor. Scale =100 μ m. From Seo *et al.*, 2020.

1.5.6. Targeting TRPV3

1.5.6.1. TRPV3 agonists

Several TRPV3 agonists and modulators have been described; however, many show high levels of promiscuity and low levels of potency.

Although neither act specifically on the TRPV3 channel, 2-aminoethyl diphenylborinate (2-APB) and carvacrol are commonly used as experimental TRPV3 agonists. 2-APB also acts on a multitude of other receptors and channels including several members of the TRP family; inositol 1,4,5-trisphosphate receptors (IP3R); and certain gap junction channels (Bai *et al.*, 2006; Maruyama *et al.*, 1997; Hu *et al.*, 2004; Chung *et al.*, 2004). Carvacrol, camphor, thymol, eugenol, and other skin-sensitising organic monoterpenes also activate TRPV3 (Xu *et al.*, 2006; Vogt-Eisele *et al.*, 2007; Moqrich *et al.*, 2005). Again, many of these organic compounds are highly promiscuous and do not represent specific TRPV3 agonists. Unfortunately, much of our knowledge of *in vitro* TRPV3 signalling is based on 2-APB and/or carvacrol stimulations.

Drofenine, 2-APB analogue, was discovered during a screen of the Microsource Spectrum Collection (Deering-Rice *et al.*, 2014). Drofenine shows comparable potency to 2-APB and carvacrol, but higher TRPV3 selectivity: drofenine exhibits minimal activity at TRPV1 and TRPA1; thus, drofenine was chosen as the TRPV3 agonist for the studies described herein. Drofenine is also reported to inhibit the Kv2.1 voltage-gated potassium channel, the enzyme butyrylcholinesterase (BChE) and the muscarinic M1 receptor (Xu *et al.*, 2020; Kunysz *et al.*, 1988; Bodur *et al.*, 2001).

1.5.6.2. TRPV3 antagonists

Although some TRPV3 antagonists have been discovered, specific inhibitors are lacking. Thus, researchers often use the nonselective TRP channel blocker, ruthenium red, to block TRPV3 activity.

Forsythoside B is a plant derived compound that is commonly used in traditional Chinese medicine. In TRPV3-expressing HEK293, Forsythoside B reduces TRPV3 activity – even minimising the deleterious effect of the OS-associated mutation (Zhang *et al.*, 2019). Carvacrol promotes hair loss in mouse skin, a common process in Olmsted syndrome and lesional skin; Forsythoside B alleviates this effect, minimising cell death within the outer root sheath (Yan *et al.*, 2019). Forsythoside B also reduces scratching behaviour in murine itch models: TRPV3-induced; histamine-induced; and dry skin-induced (Zhang *et al.*, 2019). Recent data suggests that Forsythoside B may be anti-pruritic in humans, with topical application reducing carvacrol-evoked itch sensations (Jin Cheol Kim *et al.*, 2021). Verbascoside, a structurally similar compound, also inhibits TRPV3 activity (Sun *et al.*, 2020). This compound reduces TRPV3-evoked scratching and has proven effective in experimental atopic dermatitis models and atopic dermatitis in dogs (Biasibetti *et al.*, 2018; Yongxi Li *et al.*, 2018; Sun *et al.*, 2020).

Osthole – another plant derived compound commonly used in traditional Chinese medicine – binds directly to TRPV3 to block agonist-induced channel opening and calcium influx (Neuberger *et al.*, 2021; Sun *et al.*, 2018). In mice, Osthole reduces scratching in models of TRPV3-induced itch; dry skin-induced itch; and irritant-induced itch (Qu *et al.*, 2019; Sun *et al.*, 2018).

Dyclonine, a clinical anaesthetic, alleviates inflammatory itch in mucous membranes and the skin (Morginson *et al.*, 1956). Dyclonine modulates activity TRPV3, suppressing activation of normal and OS-mutant channels (Liu *et al.*, 2021). This group also found that Dyclonine alleviates carvacrol-induced acute scratching behaviour in mice.

Despite the clear link between TRPV3 and itch conditions, clinical and preclinical data are lacking. Small molecule selective TRPV3 inhibitors have been developed and tested by Hydra Bioscience, Glenmark Pharmaceuticals and AbbVie, however, they have yet to be assessed in the context of itch (Broad *et al.*, 2016).

1.5.6.3. Therapeutic development

New anti-itch therapies attempt to target specific inflammatory pathways and neural circuits (Fowler and Yosipovitch, 2020); thus, these compounds must be tailored to the pruritic condition and underlying signalling. TRPV3 is overexpressed and overactivated in pruritic inflammatory skin conditions (Larkin *et al.*, 2021; Seo *et al.*, 2020). However, specific TRPV3-targeting agents are lacking.

Anti-inflammatory compounds are currently being trialled for the treatment of pruritic inflammatory skin conditions such as atopic dermatitis and psoriasis. Drugs targeting IL-4 (Dupilumab), IL-13 (Lebrikizumab), and IL-31 (Nemolizumab) are being developed for the treatment of atopic itch (Loh *et al.*, 2020; Ruzicka *et al.*, 2017; Han *et al.*, 2017; Yosipovitch *et al.*, 2019). Drugs targeting IL-17A (Secukinumab) are being developed for psoriatic-itch (Langley *et al.*, 2014; Théréné *et al.*, 2018).

Other anti-itch agents target intracellular signalling pathways. The Janus kinase (JAK)/signal transducer and activation of transcription (STAT) pathway coordinates the release of various cytokines and growth factors. A topical JAK inhibitor, Tofacitinib, alleviates itch in both atopic dermatitis and psoriasis patients (Théréné *et al.*, 2018; Mamolo *et al.*, 2013; Bissonnette *et al.*, 2016; Ständer *et al.*, 2018; Feldman *et al.*, 2016). Another kinase inhibitor, Cerdulatinib, targets both JAK and spleen tyrosine kinase (SYK) to reduce inflammation in patients with mild-to-moderate atopic dermatitis (Piscitelli *et al.*, 2021).

Another particularly interesting group of emerging anti-itch agents are the botulinum neurotoxins (BoNT). Briefly, BoNT cleave specific cellular SNARE proteins, blocking vesicle fusion and thus reducing cytokine release and modulating receptor upregulation (Pirazzini *et al.*, 2017). To date, BoNT have been used for a variety of clinical and aesthetic purposes, including both pain and itch, with BoNT proving to be broadly antipruritic (Gazerani, 2018). However, usage and development of

BoNT-based therapeutics requires a thorough understanding of the specific SNARE proteins and their role in diseased patients and healthy controls. BoNT block membrane insertion of TRPV1 and TRPA1 in cultured sensory neurons (Meng *et al.*, 2016). VAMP3, a SNARE protein, has proven to be particularly important for keratinocyte-derived inflammation, suggesting that VAMP3-targeting BoNT may alleviate dermatitis (Meng *et al.*, 2019).

This project aims to identify the inflammatory mediators, kinase pathways and SNARE proteins acting downstream of TRPV3. We believe that these insights will aid the development of TRPV3-targeting agents and advance the treatment of pruritic inflammatory skin conditions.

2. Materials and Methods

2.1. Materials

2.1.1. Primary epidermal keratinocytes from human donors

Cryopreserved normal human epidermal keratinocytes from a single adult donor (NHEK-Ad) were purchased from Lonza (Switzerland). The experiments described herein used a number of different donor batches. The basic characteristics of each adult donor are detailed in **Table 2.1**.

Table 2.1. Basic characteristics of each adult donor.

Batch Number	Material Number	Age (years)	Sex (M/F)	Race (B/C/H)	Experimental Notes
18TL180364	00192627	33	F	H	
18TL053546	00192627	75	F	C	Issues with PAI-1 release
18TL099145	00192627	38	F	B	
0000549412	00192627	32	F	H	
18TL073811	00192627	55	F	B	
0000530069	00192627	20	M	C	Issues with PAI-1 release
0000249305	00192627	32	F	B/C	

Note: All batches were purchased from Lonza. *Abbreviations:* B, Black; C, Caucasian; F, female; H, Hispanic; M, male; PAI-1, Plasminogen activator inhibitor-1.

2.1.2. Reagents, compounds, kits, and consumables

General materials were purchased from: Acros Organics (Belgium); Axon Medchem BV (Netherlands); Calbiochem (via Merck Millipore, Ireland); Fisher BioReagents (via Thermo Fisher Scientific, Ireland); ibidi (Germany); Invitrogen (via Bio-Sciences, Ireland); Li-Cor (Germany); Lonza (Switzerland); Merck Millipore (Ireland); R&D Systems (via Bio-Techne, Ireland); Sigma-Aldrich (Ireland); Thermo Fisher Scientific (Ireland); and Tocris Bioscience (via Bio-Techne, Ireland). Catalogue numbers of each item are listed in **Table 2.2**.

Table 2.2. Reagents, compounds, kits, and consumables.

Name	Category	Supplier	Catalogue Number
μ-Dish 35 mm	Cell Culture Reagent or Consumable	ibidi	81156
μ-Slide 8 well ibiTreat	Cell Culture Reagent or Consumable	ibidi	80826
4x Protein Sample Loading Buffer	General Reagent or Chemical	Li-Cor	928-40004
AL8697 (AL.)	Pharmacological Agonist or Inhibitor	R&D Systems	4753
Allyl Isothiocyanate (AITC)	Pharmacological Agonist or Inhibitor	Sigma-Aldrich	377430
BCA assay	Kit	Merck Millipore	71285-3
Bolt 4 - 12%, Bis-Tris Gels	SDS-PAGE and Western Blotting	Invitrogen	NM04125BOX
Bovine Serum Albumin (BSA)	General Reagent or Chemical	Sigma-Aldrich	A7030
Brain Natriuretic Peptide (BNP) (1-32) (human)	Pharmacological Agonist or Inhibitor	Tocris	3522
Calcitonin Gene Related Peptide (CGRP) (human)	Pharmacological Agonist or Inhibitor	Sigma-Aldrich	C0167
Capsaicin	Pharmacological Agonist or Inhibitor	Sigma-Aldrich	M2028
Chameleon Duo Pre-stained Protein Ladder	SDS-PAGE and Western Blotting	Li-Cor	928-60001
CHIR99021 (CHIR.)	Pharmacological Agonist or Inhibitor	Sigma-Aldrich	SML1046
Cytiva Amersham ECL Prime Western Blotting Detection Reagent	General Reagent or Chemical	Thermo Fisher Scientific	45-002-401
Dimethyl sulfoxide (DMSO)	General Reagent or Chemical	Sigma-Aldrich	D2650
Drofenine hydrochloride	Pharmacological Agonist or Inhibitor	Sigma-Aldrich	D7402
Dulbecco's Phosphate Buffered Saline (DPBS)	General Reagent or Chemical	Sigma-Aldrich	D8537
Duolink In Situ Mounting Medium with DAPI	Immunocytochemistry	Sigma-Aldrich	DUO82040
Fluo-4 AM	General Reagent or Chemical	Invitrogen	F14201
Formaldehyde solution (37 wt. % in H ₂ O)	General Reagent or Chemical	Sigma-Aldrich	F1635
Glycine	General Reagent or Chemical	Fisher BioReagents	BP381-1
<i>Continued overleaf</i>			

Table 2.2 continued. Reagents, compounds, kits, and consumables.

Name	Category	Supplier	Catalogue Number
Immobilon-FL transfer membrane 0.45 µm	SDS-PAGE and Western Blotting	Merck Millipore	IPFL00010
Intercept® Blocking Buffer	General Reagent or Chemical	Li-Cor	927-60001
JNK-IN-8 (JNK.)	Pharmacological Agonist or Inhibitor	Axon Medchem BV	2361
KBM-Gold Keratinocyte Basal Medium	Cell Culture Reagent or Consumable	Lonza	00192151
KGM-Gold Keratinocyte SingleQuots Kit	Cell Culture Reagent or Consumable	Lonza	00192152
Lentiviral Transduction Particles: non-targeted (NT)	Cell Culture Reagent or Consumable	Sigma-Aldrich	SHC016
Lentiviral Transduction Particles: VAMP3-targeted (V3T)	Cell Culture Reagent or Consumable	Sigma-Aldrich	TRCN000330914 (sequence: GCAGCCAAGTTG AAGAGGAAA)
Lysis Buffer 6	General Reagent or Chemical	R&D Systems	895561
Methanol	General Reagent or Chemical	Acros Organics	444310050
Pitstop2	Pharmacological Agonist or Inhibitor	Sigma-Aldrich	SML1169
ProLong Diamond Antifade Mountant	Immunocytochemistry	Invitrogen	P36961
Protease Inhibitor Cocktail Set II	General Reagent or Chemical	Calbiochem	539134
Proteome Profiler Human Phospho-Kinase Array Kit	Kit	R&D Systems	ARY003B
Proteome Profiler Human XL Cytokine Array Kit	Kit	R&D Systems	ARY022B
Puromycin	General Reagent or Chemical	Sigma-Aldrich	P8833
ReagentPack Subculture Reagents	Cell Culture Reagent or Consumable	Lonza	CC-5034
Revert 700 Total Protein Stain and Wash Kit	SDS-PAGE and Western Blotting	Li-Cor	926-11015
Sodium Chloride	General Reagent or Chemical	Acros Organics	42290010
SP600125 (SP.)	Pharmacological Agonist or Inhibitor	Sigma-Aldrich	S5567
			<i>Continued overleaf</i>

Table 2.2 continued. Reagents, compounds, kits, and consumables.

Name	Category	Supplier	Catalogue Number
Substance P	Pharmacological Agonist or Inhibitor	Sigma-Aldrich	S6883
Tris	General Reagent or Chemical	Fisher BioReagents	BP152
Sodium Chloride	General Reagent or Chemical	Acros Organics	42290010
SP600125 (SP.)	Pharmacological Agonist or Inhibitor	Sigma-Aldrich	S5567
Substance P	Pharmacological Agonist or Inhibitor	Sigma-Aldrich	S6883
Tris	General Reagent or Chemical	Fisher BioReagents	BP152
Triton X-100	General Reagent or Chemical	Sigma-Aldrich	T8787
Tween 20	General Reagent or Chemical	Sigma-Aldrich	P1379
β -mercaptoethanol	General Reagent or Chemical	Sigma-Aldrich	M3148

2.1.3. Primary antibodies

Primary antibodies were purchased from: Abcam (U.K.); Alomone Labs (Israel); BioLegend (U.K.); Novus Biologicals (via Bio-Techne, Ireland); and Synaptic Systems (Germany). Details of each antibody are listed in **Table 2.3**.

Table 2.3. Primary antibodies.

Target Protein	Host/Isotype	Supplier	Catalogue Number	Dilution
Cytokeratin 14	Mouse	Abcam	ab7800	1:1000 (ICC)
NPRA	Rabbit	Abcam	ab14356	1:250 (ICC)
NPRB	Mouse	Abcam	ab55724	1:25 (ICC)
SNAP23	Mouse	Novus Biologicals	H00008773-M01	1:500 (ICC)
SNAP29	Mouse	Novus Biologicals	H00009342-M01	1:50 (ICC); 1:250 (WB)
Syntaxin 3	Rabbit	Synaptic Systems	110 032	1:250 (ICC)
Syntaxin 4	Mouse	Novus Biologicals	H00006810-M04	1:50 (ICC)
Syntaxin 16	Rabbit	Synaptic Systems	110 162	1:250 (ICC); 1:1000 (WB)
TRPV3	Mouse	Abcam	ab85022	1:1000 (ICC)
TRPV3 (extracellular)	Rabbit	Alomone Labs	ACC 033	1:100 (modified ICC)
VAMP1/2/3	Rabbit	Synaptic Systems	104 102	1:500 (ICC); 1:1000 (WB)
VAMP7	Mouse	Synaptic Systems	232 011	1:25 (ICC)
Vimentin (594-conjugated)	Mouse	BioLegend	677804	1:200 (ICC)

Abbreviations: ICC, immunocytochemistry; NPRA, natriuretic peptide receptor type A; NPRB, natriuretic peptide receptor type B; SNAP, soluble NSF attachment protein; TRPV3, transient receptor potential vanilloid 3; VAMP, vesicle-associated membrane protein; WB, western blot.

2.1.4. Secondary antibodies

Secondary antibodies were purchased from: Abcam (U.K.); Invitrogen (via Bio-Sciences, Ireland); Jackson ImmunoResearch (U.K.); and Li-Cor (Germany). Details of each antibody are listed in **Table 2.4**.

Table 2.4. Secondary antibodies.

Species Reactivity	Host / Isotype	Clonality	Conjugate	Supplier	Catalogue Number
Mouse	Goat / IgG (H + L)	Monoclonal	Alexa Fluor 488	Abcam	ab150113
Mouse	Goat / IgG (H + L)	Polyclonal	Alexa Fluor 594	Invitrogen	A-11005
Mouse	Goat / IgG (H + L)	Polyclonal	IRDye 690RD	Li-Cor	926-68070
Rabbit	Donkey / IgG (H + L)	Polyclonal	HRP	Jackson ImmunoResearch	711-035-152
Rabbit	Goat / IgG (H + L)	Polyclonal	Alexa Fluor 555	Abcam	ab150078
Rabbit	Goat / IgG (H + L)	Polyclonal	Alexa Fluor 488	Invitrogen	A-11008
Rabbit	Goat / IgG (H + L)	Polyclonal	IRDye 800CW	Li-Cor	926-32211

Abbreviations: H, heavy; HRP, horseradish peroxidase; IgG, immunoglobulin G; L, light.

2.1.5. Equipment and software

Key equipment and software are listed in **Table 2.5**.

Table 2.5. Key equipment and software.

Name	Company	Function
G:BOX Chemi XT4 System	Syngene, Cambridge, UK	Western Blot and Membrane Imaging (chemiluminescent)
ImageJ (plus FIJI)	National Institutes of Health, Bethesda, MD, USA	Software
LSM710 Confocal	Zeiss, Oberkochen, Germany	Confocal Microscopy
Mini Gel Tank	Invitrogen, Waltham, MA, USA	SDS-PAGE Electrophoresis
Odyssey Imaging System	Li-Cor, Lincoln, NE, USA	Western Blot Imaging (fluorescent)
Prism 6	GraphPad, La Jolla, CA, USA	Software
RStudio 2019	RStudio, Boston, MA, USA	Software
TCS SP8 Confocal	Leica, Wetzlar, Germany	Confocal Microscopy
TE22 Mighty Small Transfer Tank	Hofer, Holliston, MA, USA	Western Blot Transfer
Zen 2012 (black edition)	Zeiss, Oberkochen, Germany	Software

2.2. Methods

2.2.1. Culturing normal human epidermal keratinocytes (NHEK)

Cryopreserved normal human epidermal keratinocytes (NHEK) were purchased from Lonza (Switzerland) (see Section 2.1.1). Upon arrival, keratinocytes were placed in liquid nitrogen storage for future use.

Passage zero cells were seeded as per manufacturer's instructions. Briefly, the cryovial was thawed in a 37°C water bath; in a sterile field, cells were gently resuspended and added to a T-75 culture flask containing pre-equilibrated growth medium (37°C, 5% CO₂, 30 minutes [min]). Growth medium consisted of KBM-Gold Keratinocyte Basal Medium supplemented with KGM-Gold Keratinocyte SingleQuots. Seeded keratinocytes were incubated and grown to a confluency of 70% (37°C, 5% CO₂, 2 – 3 days) (Figure 2.1). If a confluency of >80% was reached, keratinocytes were appropriately discarded. This monolayer culture system was used as a model of human epidermis.

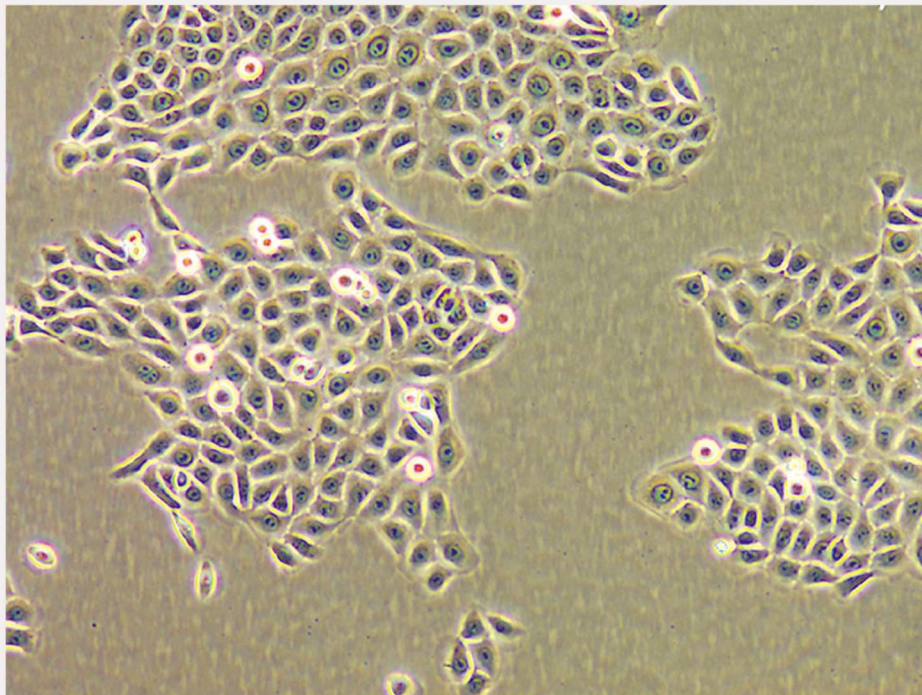


Figure 2.1. Culturing normal human epidermal keratinocytes.

Image shows cultured normal human epidermal keratinocytes (NHEK) from a single adult donor. Image from Lonza website (product code: 00192627).

Keratinocytes were subcultured as per manufacturer's instructions using the recommended subculture reagents: ReagentPack Subculture Reagents. Briefly, at about 70% confluency, growth medium was removed and trypsin/EDTA was added to the cells (room temperature). The flask was incubated, warming the trypsin solution (37°C, 5% CO₂, 2 min). Keratinocytes were then examined under the microscope, rapping the flask at intervals of 30 seconds until about 90% of cells were round in shape and/or floating. The trypsin solution was neutralised with trypsin neutralising solution; cell solution was transferred to a sterile microcentrifuge tube. The flask was rinsed with HEPES buffered saline solution (HEPES-BSS); this rinse was added to the cell solution. Harvested cells were centrifuged and pelleted (220 x g, 5 min). Pellets were resuspended in growth medium and added to pre-prepared culture flasks for further culturing or dishes and chambers for experiments.

For experiments, keratinocytes were seeded at 1×10^4 cells/cm² in experiment-specific cell culture dishes or chambers. Seeded keratinocytes were cultured in growth medium, incubated, and grown to a confluency of <70% (37°C, 5% CO₂, 1 – 3 days). Growth medium was removed at least 24 hours prior to stimulation and replaced with basal medium: growth medium minus hydrocortisone. All experiments were carried out using keratinocytes \leq passage 4.

2.2.2. Lentivirus-mediated protein knockdown: reducing VAMP3 expression

Lentiviral particles were used to interrupt expression of the Vesicle-associated membrane protein 3 (VAMP3) SNARE protein in cultured keratinocytes (NHEK) (**Figure 2.2**). This infection and selection work was primarily managed by Dr. Meng, as described previously (Meng *et al.*, 2019).

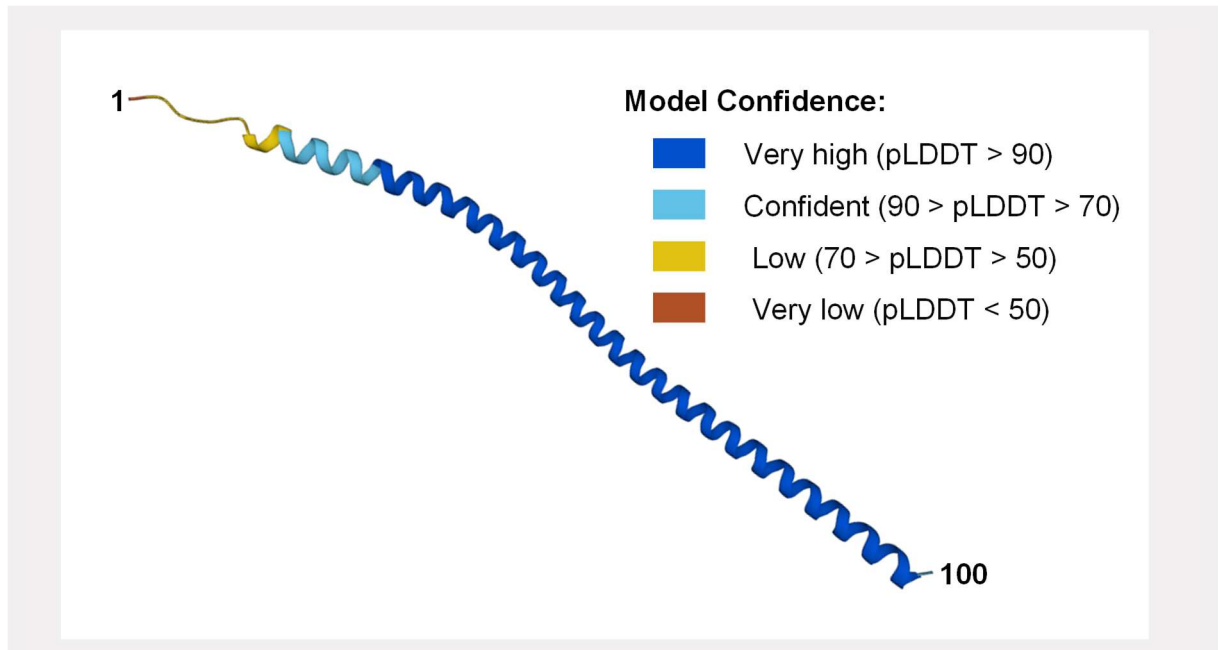


Figure 2.2. VAMP3 AlphaFold structure prediction.

Image depicts the predicted 3D structure of the VAMP3 protein (amino acid residues 1 and 100 are shown). The AlphaFold model produces a per-residue confidence score (pLDDT) of between 0 and 100, with values above 90 denoting very high confidence. From the AlphaFold protein structure database (Varadi *et al.*, 2022; Jumper *et al.*, 2021).

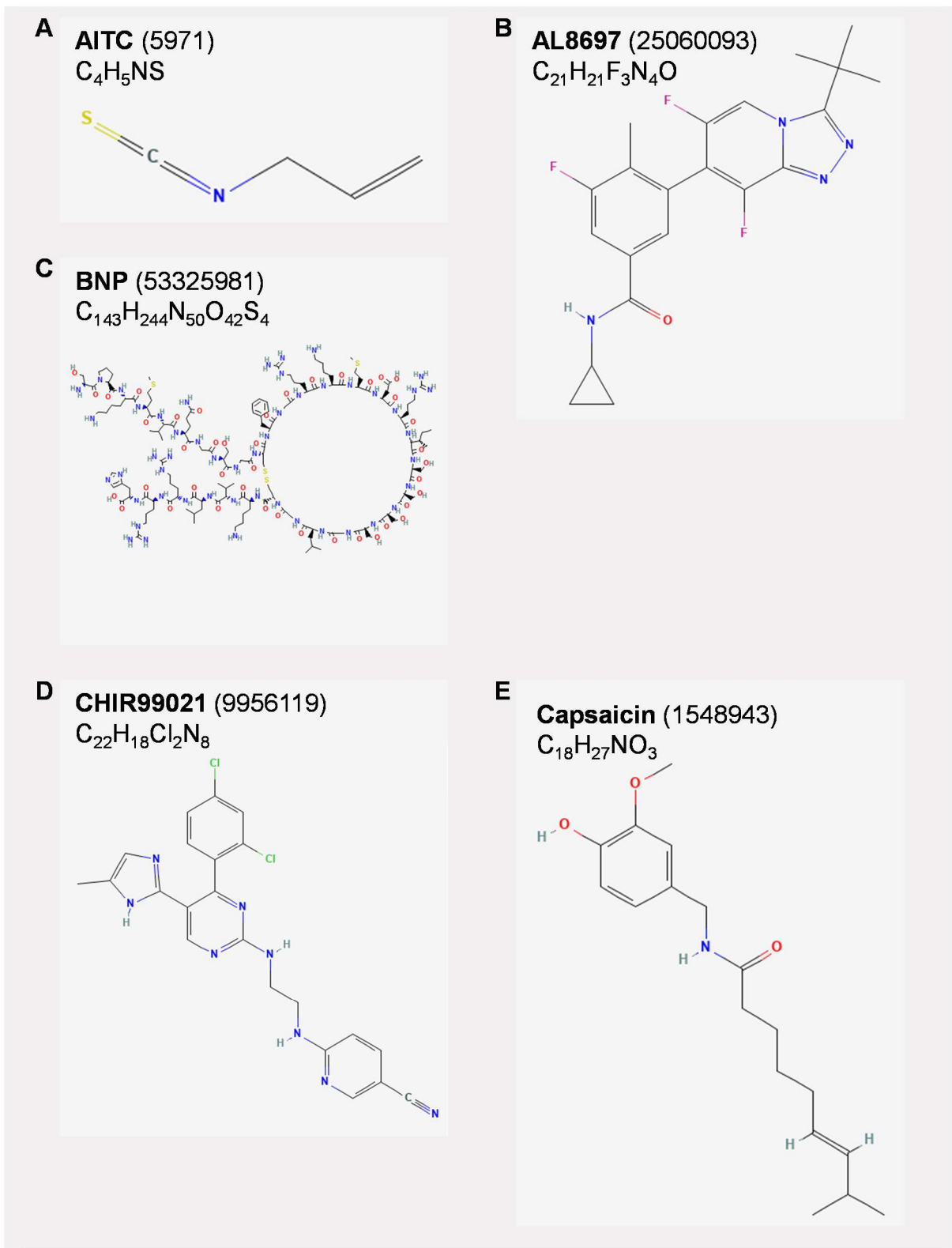
Seeded keratinocytes were cultured in growth medium (37°C, 5% CO₂, 2 days). Keratinocytes were treated with medium containing either nontargeted (NT) control PLK0.1-puro lentiviral particles or short-hairpin RNA lentiviral particles that specifically target VAMP3 (V3T) (400 transducing units/well). Treated keratinocytes were incubated for 48 hours (h) (replicate 1) or 72 h (replicate 2). Infected cells were selected by addition of puromycin (1 µg/ml, 72 h). NT and V3T keratinocytes were used in TRPV3 stimulation and cytokine release assays (see **Section 2.2.3.4** and **Section 2.2.5**), and live calcium imaging experiments (see **Section 2.2.6**). VAMP3 expression was examined in NT and V3T keratinocytes by SDS-PAGE and western blotting (see **Section 2.2.8**).

Targeted gene/protein ID and validated sequence for shRNA lentiviral transduction particles is as follows: NM_004781, V3:

CCGGGCAGCCAAGTTGAAGAGGAAACTCGAGTTTCTCTTCAACTTGGCTGCTTTTTG

2.2.3. Pre-treatments, inhibitors, and stimulations

This section details the relevant pre-treatments, inhibitors, and stimulations. Molecular formulas and 2D chemical structures are shown in **Figure 2.3**. All treatments were carried out in a sterile field and diluted in basal medium: growth medium minus hydrocortisone. Incubation times are specific to the treatment (37°C, 5% CO₂).



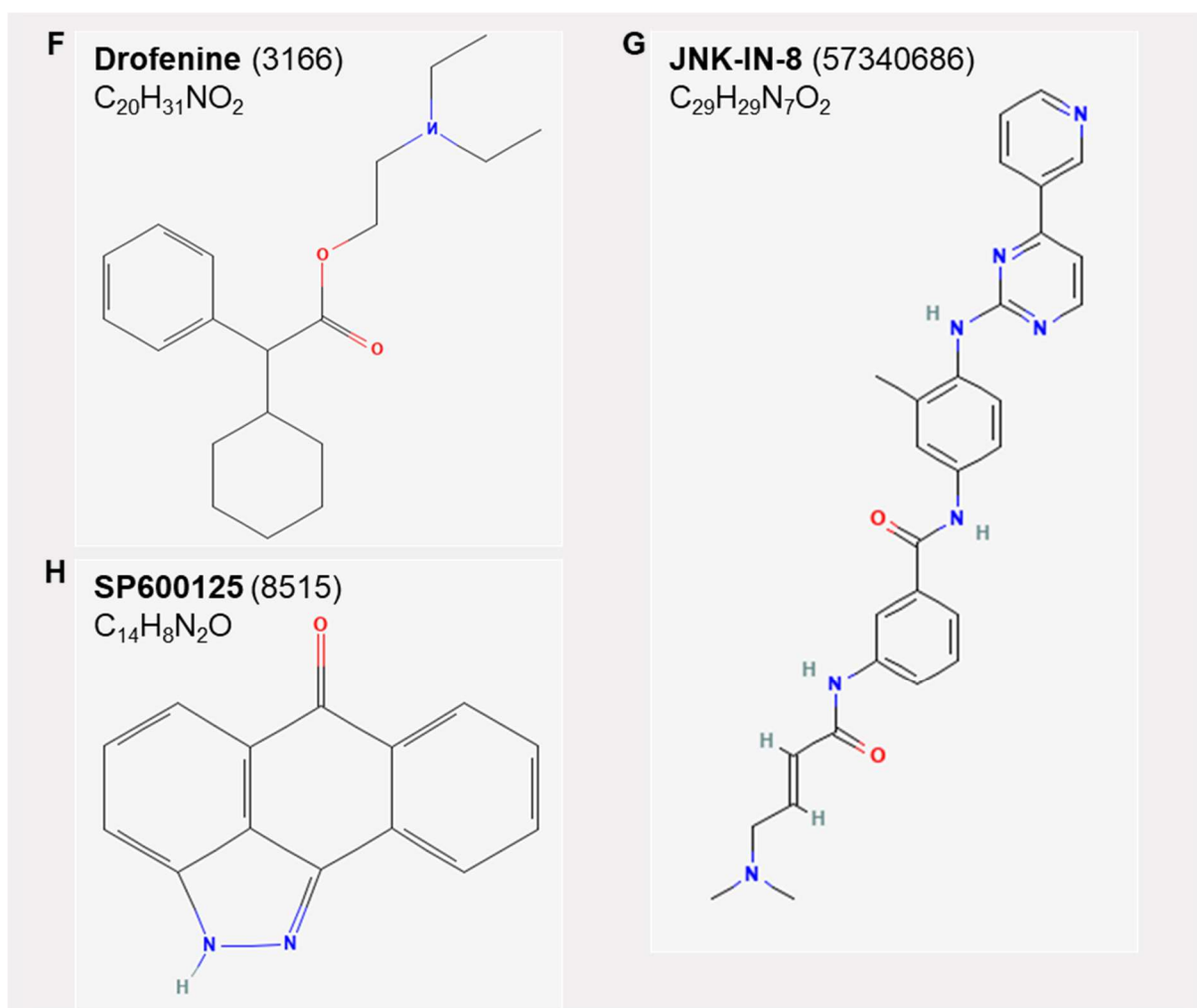


Figure 2.3. Chemical information on pre-treatments, inhibitors, and stimulations.

Images show the molecular formulas and 2D chemical structures of each named compound. Figures in brackets indicate the PubChem compound identification number. Produced using information and figures from PubChem Compounds: National Center for Biotechnology Information (2022).

2.2.3.1. Pre-treating with B-type natriuretic peptide (BNP)

To examine the effect of BNP on TRPV3-evoked mediator release, keratinocytes were pre-treated with basal medium \pm BNP (1 μ M, 4 h) (control *vs.* BNP). Pre-treated keratinocytes were stimulated with basal medium \pm drofenine (TRPV3 agonist; 500 μ M) \pm BNP (1 μ M) (1 h). Cell culture supernatants were removed and pooled; released mediators were measured using cytokine array (see **Section 2.2.5**).

To examine the effect of BNP on TRPV3-linked calcium responses, keratinocytes cultured in μ -Slide 8 well imaging chambers were pre-treated with basal medium \pm BNP (1 μ M, 4 h): control *vs.* BNP. TRPV3 agonist-induced fluctuations were then monitored using live calcium imaging and analysed (see **Section 2.2.6**).

To examine the effect of BNP on TRPV3 trafficking, keratinocytes cultured in μ -Slide 8 well imaging chambers were stimulated with basal medium + BNP (1 μ M) for 0 h, 3 h or 24 h. Surface TRPV3 channels were then detected using a modified immunocytochemistry method (see **Section 2.2.9.2**).

2.2.3.2. Pre-treating with kinase inhibitors

To examine the effect of JNK inhibition on TRPV3-evoked mediator release, keratinocytes were pre-treated with basal medium \pm JNK-IN-8 (1 μ M, 1 h). Pre-treated keratinocytes were stimulated with basal medium \pm drofenine (TRPV3 agonist; 500 μ M) \pm JNK-IN-8 (1 μ M) (1 h). Cell culture supernatants were removed and pooled; released mediators were measured using cytokine array (see **Section 2.2.5**).

To examine the effect of kinase inhibition on BNP-induced TRPV3 trafficking, keratinocytes were pre-treated with basal medium \pm kinase inhibitor (all 1 μ M, 1 h):

- p38 α inhibitor: AL8697 (Al.)
- GSK3 inhibitor: CHIR99021 (CHIR.)
- JNK-pan inhibitor: JNK-IN-8 (JNK.), or
- c-Jun inhibitor: SP600125 (SP.).

Keratinocytes pre-treated with kinase inhibitors were stimulated with basal medium \pm BNP (1 μ M) \pm kinase inhibitor (3 h). Surface TRPV3 channels were then detected using a modified immunocytochemistry method (see **Section 2.2.9.2**).

2.2.3.3. Pre-treating with endocytosis inhibitor

To examine the effect of endocytosis inhibition on TRPV3-linked calcium responses, keratinocytes cultured in μ -Dish 35 mm imaging chamber were pre-treated with basal medium \pm Pitstop2 (25 μ M, 30 min): control *vs.* Pitstop2. TRPV3-linked fluctuations were then monitored using live calcium imaging and analysed (see **Section 2.2.6**). For information on time data equalisation: see **Section 2.2.6.1**.

2.2.3.4. Stimulating TRP channels

To examine the effect of TRP agonists on intracellular signalling, keratinocytes were treated with basal medium \pm TRP agonists: AITC (TRPA1 agonist, 100 μ M); capsaicin (TRPV1 agonist, 1 μ M); or drofenine (TRPV3 agonist, 500 μ M) (15 min). Keratinocytes were scraped, lysate was pooled, and protein phosphorylation was measured using the phospho-kinase array (see **Section 2.2.4**).

To examine the effect of TRP agonists on intercellular signalling, keratinocytes were treated with basal medium \pm TRP agonists: AITC (TRPA1 agonist, 100 μ M); capsaicin (TRPV1 agonist, 1 μ M); or drofenine (TRPV3 agonist, 500 μ M) (1 h). In some experiments, keratinocytes also received a pre-treatment or inhibitor (BNP or JNK-IN-8; detailed above). In other experiments, keratinocytes were cultured with control nontargeted (NT) or VAMP3-targeted (V3T) lentiviral particles to produce NT and V3T cultures (detailed above). Following TRP agonist stimulation, cell culture supernatants were removed and pooled; released mediators were measured using cytokine array (see **Section 2.2.5**).

2.2.4. Phospho-kinase array: comparing activation of kinase proteins

The Proteome Profiler Human Phospho-Kinase Array Kit was used to compare kinase protein activation. This kit uses “sandwich” immunoassay technology to simultaneously detect phosphorylation of 43 protein residues (protein [residue]): AKT1/2/3 [S473]; AKT 1/2/3 [T308]; AMPK α 1 [T183]; AMPK α 2 [T172]; β -Catenin [-]; Chk-2 [T68]; CREB [S133]; c-Jun [S63]; EGFR [Y1086]; eNOS [S1177]; ERK1/2 [T202/Y204, T185/Y187]; FAK [Y397]; Fgr [Y412]; Fyn [Y420]; GSK3 $\alpha\beta$ [S21/S9]; Hck [Y411]; HSP27 [S78/S82]; HSP60 [-]; JNK 1/2/3 [T183/Y185, T221/Y223]; Lck [Y394]; Lyn [Y397]; MSK1/2 [S376/S360]; PDGF R β [Y751]; PLC- γ 1 [Y783]; PRAS40 [T246]; PYK2 [Y402]; p27 [T198]; p38 α [T180/Y182]; p53 [S15]; p53 [S392]; p53 [S46]; p70S6K [T389]; p70S6K [T421/S424]; RSK1/2/3 [S380/S386/S377]; Src [Y419]; STAT2 [Y689]; STAT3 [S727]; STAT3 [Y705]; STAT5A [Y694]; STAT5A/B [Y694/Y699]; STAT5B [Y699]; STAT6 [Y641]; TOR [S2448]; WNK1 [T60]; Yes [Y426].

Following TRP agonist treatments, keratinocytes were scraped, lysate was pooled, and protein phosphorylation was measured as per the manufacturer’s instructions. Lysate was added to specialised nitrocellulose membranes. These membranes are dotted with highly specific capture antibodies which bind to the phosphorylated proteins within the samples. Membranes were then probed with biotinylated detection antibody and relative phosphorylation was visualised using chemiluminescent detection reagents and the G:BOX imaging system (**Figure 2.4**). The densitometry of each positive signal was measured using ImageJ software. Each phospho-residue is represented by a pair of duplicated spots; average signal for each phospho-residue was calculated. Data were expressed as the fold change (FCH) of phosphorylation relative to unstimulated basal controls. FCH is given as $(D_S - D_B) / D_B$, where D_B represents densitometry values from basal samples and D_S represents densitometry values from stimulated samples. Presented data indicate all proteins which show significant (or close to significant) increases in relative phosphorylation following stimulation vs. basal levels. Several proteins were unaffected by stimulation; p38 α [Y180/Y182] was included as an example of one such protein.

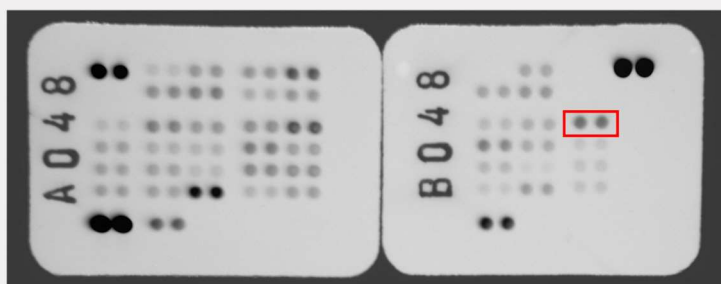


Figure 2.4. Example of phospho-kinase array membrane.

Image shows one set of membranes from the phospho-kinase array kit following chemiluminescent detection. Each named kinase is represented by 2 adjacent spots (red box highlights one duplicate). Duplicate spots are quantified using densitometry; these values are then averaged: this average is the value used for each replicate (i.e. D_S or D_B in the equation above).

2.2.5. Cytokine array: comparing mediator release

The Proteome Profiler Human XL Cytokine Array Kit was used to compare mediator release. This kit uses “sandwich” immunoassay technology to simultaneously detect 105 different mediators: Adiponectin; Apolipoprotein A-I; Angiogenin; Angiopoietin-1; Angiopoietin-2; BAFF; BDNF; BSG; Complement Component C5/C5a; CD14; CD30; CD40 ligand; Chitinase 3-like 1; Complement Factor D; C-Reactive Protein; Cripto-1; CXCL1; Cystatin C; Dkk-1; DPPIV; EGF; ENA-78; Endoglin; Fas Ligand; FGF-2; FGF-7; FGF-19; Flt-3 Ligand; G-CSF; GDF-15; GM-CSF; Growth Hormone; HGF; ICAM-1; IFN γ ; IGFBP-2; IGFBP-3; IL-1 α ; IL-1 β ; IL-1ra; IL-2; IL-3; IL-4; IL-5; IL-6; IL-8; IL-10; IL-11; IL-12 p70; IL-13; IL-15; IL-16; IL-17A; IL-18Bpa; IL-19; IL-22; IL-23; IL-24; IL-27; IL-31; IL-32; IL-33; IL-34; IP-10; I-TAC; KLK3; Leptin; LIF; MCP-1; MCP-3; M-CSF; MIF; MIG; MIP-1 α /MIP-1 β ; MIP-3 α ; MIP-3 β ; MMP-9; Myeloperoxidase; NGAL; Osteopontin; PAI-1; PDGFA; PDGF-AB/BB; PTX3; PF4; RAGE; RANTES; RBP-4; Relaxin-2; Resistin; SDF-1 α ; SHBG; ST2; TARC; TFF3; Tfr; TGF- α ; TSP-1; TNF- α ; uPAR; VEGF; VDBP; CD31; TIM-3; VCAM-1.

Following pre-treatments and treatments, cell culture supernatants were removed and pooled; released mediators were measured as per the manufacturer’s instructions. Supernatants were added to specialised nitrocellulose membranes. These membranes are dotted with highly specific capture antibodies which bind to the mediators within the samples. Membranes were then probed with biotinylated detection antibody and relative release was visualised using chemiluminescent detection reagents and the G:BOX imaging system (**Figure 2.5**). The densitometry of each positive signal was measured using ImageJ software. Each phospho-residue is represented by a pair of duplicated spots; average signal for each phospho-residue was calculated. Data were expressed as the fold change (FCH) of phosphorylation relative to unstimulated basal controls. FCH is given as $(D_S - D_B) / D_B$, where D_B and D_S represent densitometry values from basal and stimulated samples, respectively. Presented data indicate all proteins which were consistently detected. To specifically examine the impact of pre-treatments on TRPV3-evoked release, data were also expressed as a percentage of normal drofenine-induced release (i.e. allowing the control TRPV3 group to equal 100%, matched).

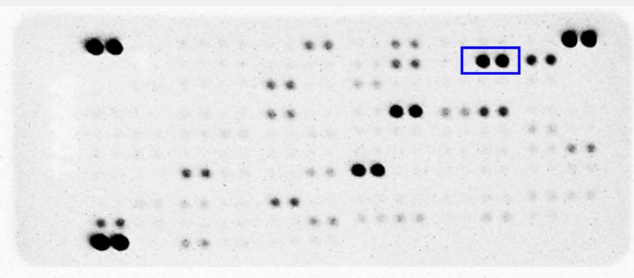


Figure 2.5. Example of cytokine array membrane.

Image shows one set of membranes from the cytokine array kit following chemiluminescent detection. Each named cytokine is represented by 2 adjacent spots (blue box highlights one duplicate). Duplicate spots are quantified using densitometry; these values are then averaged: this average is the value used for each replicate (i.e. D_S or D_B in the equation above).

2.2.6. Calcium imaging: monitoring calcium in live keratinocytes

Live calcium imaging was used to monitor the effect of TRP stimulation on intracellular calcium levels. Here, keratinocytes were cultured in either μ -Slide 8 well or μ -Dish 35 mm imaging chambers. In some experiments, keratinocytes were pre-treated with BNP or endocytosis inhibitor (Pitstop2) (detailed above). Keratinocytes were treated with calcium dye and incubated (37°C, 5% CO₂, 30 min). Visualisation of this dye (Fluo-4 AM) is dependent on removal the acetoxymethyl (AM) ester which only occurs when inside the cell. When bound to calcium, the fluorescence intensity of Fluo-4 increases by more than 100-fold. Thus, enhanced fluorescent signal indicates elevated cytosolic calcium.

Following incubation, the calcium dye solution was removed, keratinocytes were washed, and fresh basal medium (\pm pre-treatment/inhibitor solution) was added. Loaded keratinocytes were equilibrated to room temperature prior to imaging (more than 10 min). Loaded keratinocytes were excited and fluorescence was recorded using a Leica TCS SP8 or Zeiss LSM710 confocal microscope, with images acquired at 5 or 10 s intervals. After a baseline recording (\geq 100 s), TRP agonists were added and fluorescence was recorded. Agonists were diluted in basal medium: AITC (TRPA1, 50 μ M); capsaicin (TRPV1, 1 μ M); drofenine (TRPV3, 250 or 500 μ M) (all room temperature).

Raw image data were examined using Zen 2012 (black edition) or ImageJ software. Manual region of interest (ROI) selection was used to outline each cell. The software then quantified the fluorescence within each ROI at each time point. These fluorescence data were then imported to Excel for management and manipulation. For each ROI, fluorescence data were normalised to $F\Delta/F_0$, where $F\Delta$ denotes the change in fluorescence and F_0 the baseline fluorescence. The activation threshold was set at 30% ($F\Delta/F_0 \geq 0.3$), a figure which is commonly used in the literature. $F\Delta/F_0$ values were graphed relative to time; these time course graphs show either single-cell calcium traces or average $F\Delta/F_0$ in a population of cells.

Calcium response parameters were measured: mean fluorescence change ($F\Delta/F_0$); area under the curve (AUC, arbitrary units [a.u.]); total peak area (TPA, a.u.); peak amplitude ($F\Delta/F_0$); peak latency (s). Comparison of overall calcium responses focused on AUC values. Comparison of peak calcium responses focused on the amplitude and latency of the peaks. Response profiles were generated for TRPV3 experiments: peak latency vs. peak amplitude. These plots were examined for clusters using *k*-means clustering (see **Section 2.2.7**).

ImageJ software also allowed for measurement of cellular parameters such as area, perimeter, and various shape descriptors (circularity and roundness). The definitions and formulas below are taken from the ImageJ user guide:

Circularity $4\pi \times \frac{[Area]}{[Perimeter]^2}$, with a value of 1.0 indicating a perfect circle.

Values closer to 0.0 indicate an increasingly elongated shape.

Roundness $4 \times \frac{[Area]}{\pi \times [Major\ axis]^2}$; also known as the inverse of aspect ratio.

2.2.6.1. Equalising time data from endocytosis inhibition experiment

The endocytosis inhibition experiment showed notable variation. We noticed striking differences in the time data when compared with previous work. To investigate whether these differences were indicative of inhibitor-induced effects or experimental noise, correlation analyses were carried out (Pearson r correlation).

ROI fluorescence data was examined and converted to $F\Delta/F0$ over time (as above). The initiation point in each stimulation was identified. Initiation point refers to the time (in seconds) between addition of stimulation and the earliest incidence of cellular activation ($F\Delta/F0 \geq 0.3$). Correlation analyses were carried out, comparing initiation point data to pre-treatment (control vs. Pitstop2) and to the stage position on the x-axis (μm). Initiation time only correlated with the stage position: the variation was indicative of noise. Thus, time values were equalised across stimulations. The initiation point of each stimulation was defined as time zero. Time data were then converted to seconds pre/post- initiation point (s.p.i.) and analysed as normal.

2.2.7. Classifying calcium responses using *k*-means clustering

An unsupervised machine-learning algorithm – *k*-means clustering – was used to assess TRPV3 response profiles to determine whether functional subgroups existed within the TRPV3-positive population. A similar framework was used to compare compounds targeting GPCRs (Gupta *et al.*, 2017).

Response profiles were imported to RStudio: each cell was represented by its peak latency (Time_{\max}) and peak amplitude ($F\Delta/F0_{\max}$). Data were filtered to include only responsive cells ($F\Delta/F0 \geq 0.3$). Responsive datasets were then examined for subgroups using *k*-means clustering (RStudio).

In early analyses, the optimum number of clusters (*k*) was determined using both direct (silhouette and elbow) and statistical testing methods (gap statistic). The gap statistic testing method (Tibshirani *et al.*, 2001) was deemed sufficient and was the sole method used in later analyses. This testing method compares the total within-cluster variation for different values of *k* with their predicted values under null reference distribution of the data. The estimate of the optimal clusters is defined as the *k* value at which the gap statistic is maximised, indicating that the clustering structure is distinct from the random uniform distribution of points. The gap statistic plot shows the gap statistic associated with each value of *k* (\pm SEM) and the optimal *k* is marked with a vertical dashed blue line.

Responsive datasets were partitioned using the *k*-means algorithm (RStudio) to produce a given number of clusters (*k*). This approach groups similar data points together, minimising the within group variation. When examining the impact of the endocytosis inhibitor (Pitstop2), experimental groups were partitioned using the cluster limits from control data. When examining the impact of BNP pre-treatment, groups were partitioned independently. Partitioned data were compared using nonparametric statistics and contingency analyses.

2.2.8. SDS-PAGE and western blotting: comparing protein expression

SDS-PAGE and western blotting were used to examine protein expression in keratinocyte lysate. Keratinocytes were lysed in ice-cold lysis buffer (Lysis Buffer 6) plus protease inhibitors (1% [v/v]). Lysate was clarified by centrifugation (14,000 x g, 4°C, 10 min). Protein concentration was quantified (bicinchoninic acid assay [BCA] assay). Samples were equalised and diluted in loading buffer (4x Protein Loading Buffer) plus β -mercaptoethanol (5% [v/v]). Samples were denatured (95°C, 5 min) and allowed to cool to room temperature.

Denatured protein samples were loaded into precast polyacrylamide gels (Bolt 4 - 12%, Bis-Tris). Gels were run at 120 volts (room temperature, 90 min) in MOPS/SDS running buffer: 50 mM MOPS, 50 mM Tris, 3.5 mM SDS, 1 mM EDTA. Separated proteins were transferred by wet transfer (28 mA, 4°C, 4 h) in Towbin buffer: 25 mM Tris, 192 mM glycine, pH 8.3, plus 20% methanol [v/v]. Membranes were rinsed with Tris Buffered Saline (TBS): 50 mM Tris, 150 mM Sodium Chloride, pH 7.5. Membranes were blocked with Intercept Blocking Buffer or Marvel solution: 5% Marvel [w/v] in TBS. Blocked membranes were then probed with primary antibody diluted in blocking buffer (4°C, 16 h). Unbound primary antibody was removed by washing with TBS plus Tween 20 (TBS-T; 0.1% Tween 20 [v/v] in TBS). Primary antibodies were detected with either HRP-conjugated or IRDye (800CW / 680RD) secondary antibodies diluted in TBS-T (room temperature, 1 h). Unbound secondary antibody was removed by washing with TBS-T. Residual Tween 20 was removed by washing with TBS. HRP-conjugates were imaged with chemiluminescent detection reagents and the G:BOX imaging system. IRDye antibodies were visualised on an Odyssey 9120 imaging system.

2.2.9. Immunocytochemistry

2.2.9.1. Detecting total protein expression

Standard immunocytochemistry was used to visualise protein expression. Here, keratinocytes were cultured in μ -Slide 8 well imaging chambers. Medium was removed by washing with Dulbecco's Phosphate Buffered Saline (DPBS). Cells were fixed using 3.7% formaldehyde solution: 10% formaldehyde (37% in H₂O) [v/v] in DPBS (15 min, room temperature). Fixation solution was removed by washing (DPBS). Cells were permeabilised using Triton X solution: 0.1% Triton X [v/v] in DPBS (room temperature, 9 min). Permeabilisation solution was removed by washing (DPBS). Samples were incubated with blocking solution: 1% bovine serum albumin (BSA) [w/v]; 0.1% Tween 20 [v/v]; 22.52 mg/ml glycine [w/v]; in DPBS. Samples were probed with primary antibody diluted in blocking solution (4°C, 16 h). Unbound primary antibody was removed by washing (DPBS). Primary antibodies were detected with suitable fluorescent secondary antibodies diluted in DPBS (room temperature, 1 h). Unbound secondary antibody was removed by washing (DPBS; followed by d.H₂O). Samples were mounted and dried before imaging. All images were acquired using a Leica TCS SP8 confocal microscope.

2.2.9.2. Detecting surface TRPV3 protein expression

A modified immunocytochemistry protocol was used to visualise surface TRPV3 expression. Here, keratinocytes were cultured in μ -Slide 8 well imaging chambers. Following pre-treatments and/or stimulations (described above), live keratinocytes were probed with a TRPV3-ecto antibody. This highly specific antibody binds the extracellular region of the TRPV3 channel. TRPV3-ecto was added to the basal medium \pm stimulation at a concentration of 85 μ g/ml. Keratinocytes were incubated (5% CO₂, 37°C, 15 min). Unbound TRPV3-ecto was removed by washing with basal medium. Fluorescent secondary antibody solution was then added: Alexa Fluor 555, anti-rabbit at 10 μ g/ml in basal medium (5% CO₂, 37°C, 1 h). Unbound secondary antibody and medium was removed by washing with DPBS. Samples were fixed using 3.7% formaldehyde solution (room temperature, 4 min). Fixation solution was removed by washing (DPBS; followed by d.H₂O). Samples were mounted and dried before imaging. All images were acquired using a Leica TCS SP8 Confocal Laser Scanning Microscope. All images were acquired using a Leica TCS SP8 confocal microscope.

2.2.9.2.1. Quantification and comparison

Prior to measurement and analysis of surface TRPV3 proteins, images were coded to minimise subjective bias. Coded images were examined using ImageJ software. Image analyses were carried out using ImageJ software. Manual ROI selection was used to outline each cell. Fluorescent signal per ROI was quantified using the “Find Maxima” tool (prominence > 60.00, strict, exclude edge maxima). Cellular characteristics were also noted for each ROI: area, perimeter, circularity, and roundness. Once fluorescence was quantified, blinding was removed.

To minimise the impact of cell size on fluorescent signal count, maxima data were equalised to the number of intracellular particles per 1500 μm^2 . This measure was used to indicate TRPV3 expression and nonspecific fluorescence. These experiments also compared the percentage of TRPV3-positive (TRPV3⁺) keratinocytes within each group, where TRPV3⁺ cells express ≥ 5 intracellular particles per 1500 μm^2 .

2.2.10. Data analyses

Prior to analyses, all data were examined for normality (Shapiro-Wilk normality test). Broadly, these data did not follow the normal distribution. Thus, nonparametric statistical analyses were employed. Nonparametric numerical data are described as median and range (25th percentile [Q¹] – 75th percentile [Q³]), unless otherwise stated. Nonparametric data were analysed using Wilcoxon signed rank test, Mann-Whitney U-test or Kruskal-Wallis test (plus Dunn with Bonferroni adjustment). Categorical data were analysed using Fisher's exact or Chi-squared tests. For all analyses, 0.5 was chosen as the significance threshold: ns $P > .05$; * $P \leq .05$; ** $P \leq .01$; *** $P \leq .001$. Statistical analyses were performed with Prism software and RStudio.

3. Examining the Signalling Pathways Acting Downstream of the TRPV3 Channel

3.1. Overview

TRP channels are expressed in a variety of cell types, including both neuronal and nonneuronal cells. To date, itch research has focused on the role of TRPA1 and TRPV1 channels in sensory neurons. Although accepted as key transducers of histamine-dependent and histamine-independent itch, the effect of TRPV1 and TRPA1 channels in nonneuronal skin cells remained elusive. TRPV3 is primarily expressed in the basal keratinocytes of the epidermal layer (Peier *et al.*, 2002; Lonsdale *et al.*, 2013). In healthy skin, TRPV3 modulates keratinocyte proliferation, barrier formation and healing, and hair morphogenesis (Cheng *et al.*, 2010). Recently, findings from our group showed that TRPV3 is highly and specifically upregulated in lesional regions of human atopic dermatitis, human psoriasis and a murine model of dermatitis (Larkin *et al.*, 2021). Herein, we examine the signalling pathways associated with TRPA1, TRPV1, and TRPV3 channels in human epidermal keratinocytes. Specifically, this work aims to delineate the intracellular kinases and intercellular mediators associated with these epidermal channels, with a particular focus on TRPV3-associated signalling.

Cultured normal human epidermal keratinocytes (NHEK) represent a common model for various dermatological studies, including wound healing, skin modelling, and oncology. These primary keratinocytes are known to express native and functional TRPV3 channels (Szöllösi *et al.*, 2018) and represent a useful culture model for investigating TRP signalling *in vitro*. These experiments utilised several methods including fluorescent immunocytochemistry, cytokine array, phospho-kinase array, pharmacological inhibition, and shRNA-mediated knockdown.

This chapter outlines TRP-associated intracellular and intercellular signalling in epidermal keratinocytes. The studies described herein identified novel TRP-associated kinase pathways, SNARE proteins, and signalling mediators. These *in vitro* findings formed the basis of further work carried out by our collaborators, culminating in the identification a novel itch-inducer. Together, these data underline the role of TRPV3 signalling in wound healing and dermatitis-linked signalling.

3.2. Results

3.2.1. Keratinocytes in our NHEK model express key cytoskeletal and TRPV3 proteins

This project aims to further our understanding of the TRPV3 channel in the human epidermis. To do this, normal human epidermal keratinocytes (NHEK) donated by healthy adults were grown in culture; this keratinocyte monolayer represents a commonly utilised model of the epidermis. Prior to signalling analyses, fluorescent immunocytochemistry was used to confirm the expression of cytoskeletal proteins (vimentin and cytokeratin 14) and TRPV3.

Keratinocytes (NHEK) were labelled with antibodies targeting vimentin and cytokeratin 14, and/or TRPV3 (see **Table 2.3** for details). Vimentin staining revealed a cytosolic and filamentous signal, both of which are characteristic features of the vimentin protein (**Figure 3.1A**). Cytokeratin 14 staining revealed a cytosolic, mesh-like pattern (**Figure 3.1B**). TRPV3 staining displayed a widespread nuclear or perinuclear expression pattern (**Figure 3.1C, upper panel**). Importantly, some keratinocytes also showed clear cytosolic or membrane-like TRPV3 expression, suggesting that these cells may be responsive to TRPV3 agonists. Comparable fluorescence was not detected in the negative control staining (**Figure 3.1C, lower panel**), indicating that the visible signal represents TRPV3 and cytokeratin 14 proteins.

These findings suggest that our NHEK culture model expresses the TRPV3 protein. These data are supported by the literature and unpublished qPCR data from our lab. This NHEK culture model is used throughout this project.

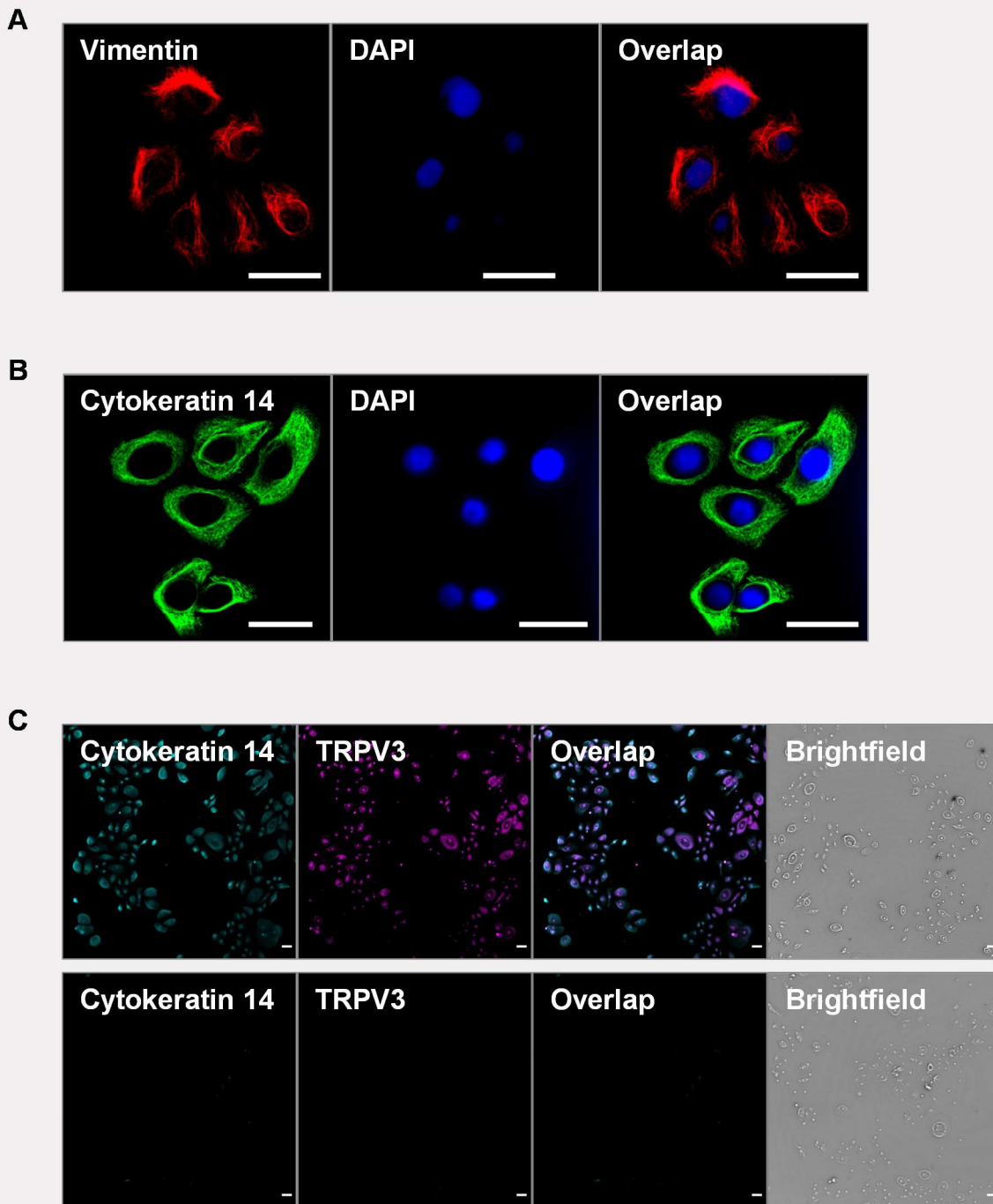


Figure 3.1. Keratinocytes in our NHEK model express key cytoskeletal and TRPV3 proteins.

A – B, Immunostaining of keratinocytes (NHEK) indicating expression of named proteins: vimentin and DAPI (**A**); cytokeratin 14 and DAPI (**B**). Original magnification 63x. **C**, Immunostaining of keratinocytes indicating expression of cytokeratin 14 and TRPV3 (*upper panel*) vs. negative control (*lower panel*). Original magnification 20x. All scale bars =50 μ m.

3.2.2. TRP channel agonists activate distinct intracellular signalling

To date, much of transient receptor potential (TRP) research has centred on neuronal TRPA1 and TRPV1 channels. This project examines TRPA1, TRPV1, and TRPV3 in normal human epidermal keratinocytes (NHEK), a common culture model of the epidermis. This section focuses on the kinase proteins acting downstream of these TRP channels. Kinase proteins coordinate intracellular signalling and promote specific biological effects. Kinase proteins also represent important targets for modulation of inflammation: several Janus kinase (JAK) inhibitors are currently under development and in clinical trials for the treatment of skin disease (Sideris *et al.*, 2020; Cohen, 2002). Thus, downstream kinase pathways could represent effective targets for TRP-associated inflammation and skin disease.

Kinase proteins are activated by phosphorylation at specific residues. This feature allows us to assess kinase activation. Here, NHEK were stimulated with basal medium \pm TRP agonists: AITC (TRPA1, 100 μ M); capsaicin (TRPV1, 1 μ M); or drofenine (TRPV3, 500 μ M) [15 min, 37°C]. Following stimulation, cells were lysed and samples clarified. Levels of intracellular kinase phosphorylation were compared using the phospho-kinase array. This array simultaneously detects residue-specific phosphorylation of 39 human proteins (43 residues): AKT1/2/3; AMPK α 1; AMPK α 2; β -Catenin; Chk2; CREB; c-Jun; EGFR; eNOS; ERK1/2; FAK; Fgr; Fyn; GSK-3 α β ; Hck; HSP27; HSP60; JNK1/2/3; Lck; Lyn; MSK1/2; PDGF R β ; PLC γ 1 PRAS40; PYK2; p38 α ; p53; p70S6K; RSK1/2/3; Src; STAT2; STAT3; STAT5A; STAT5B; STAT5A/B; STAT6; TOR; WNK1; and Yes. Briefly, when phosphorylated (at a specific residue), the named protein binds to capture antibodies located at duplicate spots on a nitrocellulose membrane. Chemiluminescent development reveals the relative levels of each phosphorylated protein. Here, 11 kinase proteins displayed varied levels of phosphorylation following experimental stimulation: Chk2, c-Jun, eNOS, Fyn, Hck, p53, p70S6K, PLC γ 1, STAT5A, WNK1, and Yes (**Table 3.1**). Several kinase proteins were detected but unaffected by TRP agonist stimulation: p38 α is included as an example of one such protein.

Table 3.1. Representative images of duplicate antibody spots from phospho-kinase array showing effect of TRP agonists on intracellular protein phosphorylation.

Protein	Residue	Basal	TRPA1	TRPV1	TRPV3
Chk2	[T68]				
c-Jun	[S63]				
eNOS	[S1177]				
Fyn	[Y420]				
Hck	[Y411]				
p53	[S15]				
p70S6K	[T389]				
PLCγ1	[Y783]				
STAT5A	[Y694]				
WNK1	[T60]				
Yes	[Y426]				
p38α	[Y180/2]				

Note: Table includes images of duplicate spots; antibodies at each spot bind to the phosphorylated version of the named kinase protein. p38α is included as an example of a kinase protein that is unaffected by TRP agonist stimulation. *Abbreviations:* Chk2, checkpoint kinase 2; c-Jun, activator protein 1 transcription factor subunit; eNOS, endothelial nitric oxide synthase; Fyn, Fyn proto-oncogene; Hck, hematopoietic cell kinase; p38α, mitogen-activated protein kinase 14; p53, cellular tumour antigen p53; p70S6K, ribosomal protein S6 kinase; PLCγ1, phospholipase C-gamma-1; S, serine; STAT5A, signal transducer and activator of transcription 5A; T, threonine; TRPA1, transient receptor potential ankyrin 1; TRPV1, transient receptor potential vanilloid 1; TRPV3, transient receptor potential vanilloid 3; WNK1, lysine deficient protein kinase 1; Y, tyrosine; and Yes, Yamaguchi sarcoma virus oncogene.

Duplicate antibody spots were then measured using densitometry. Average pixel density of each duplicate pair represents one experimental replicate. Average pixel density data were expressed as fold change (FCH) relative to basal medium-treated samples ($n = 3$). FCH data were presented as median FCH and interquartile range ($Q^1 - Q^3$) and were analysed using the nonparametric Kruskal-Wallis test plus Dunn's multiple comparison post-test (all *vs.* basal). The graphs below reveal the relative change in phosphorylation of each named protein, highlighting the link between TRP stimulation and kinase activation.

Check point kinase 2 (Chk2) is a multifunctional enzyme which initiates cell cycle arrest and apoptosis following DNA damage. Phosphorylation of Chk2 at threonine 68 [T68] was detected but, although approaching significance, was not significantly affected by TRP agonist stimulation: $H(2) = 6.787$, $P = .0568$ (**Figure 3.2**). Median Chk2 phosphorylation was increased in TRPV1 samples; however, this trend did not reach significance (FCH = 0.613 *vs.* 0; $P = .050$). Though increased phosphorylation was detected in one TRPV3 replicate, levels were statistically unchanged in TRPA1 and TRPV3 groups ($P = .1205$ and $P = .2618$, respectively). Thus, Chk2 may act downstream of the TRPV1 receptor in human epidermal keratinocytes.

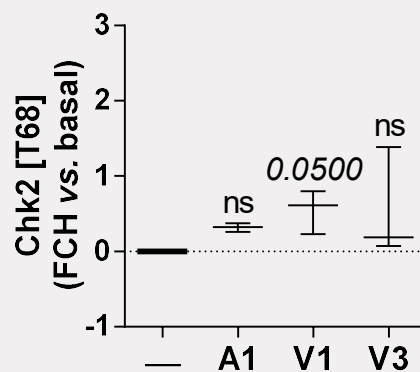


Figure 3.2. Effect of TRP agonists on activation of Chk2.

Graph compares phosphorylation of check point kinase 2 (Chk2) at threonine 68 [T68] in keratinocytes (NHEK) following application of basal medium \pm TRP agonists [15 min]: AITC (TRPA1 agonist [A1], 100 μ M); capsaicin (TRPV1 agonist [V1], 1 μ M); drofenine (TRPV3 agonist [V3], 500 μ M). Data expressed as fold change (FCH) over basal level (represented by — and dotted line). Plots indicate median of 3 independent experiments, with bars outlining min and max values. P -values calculated using Kruskal-Wallis test: ns $P > .05$.

Activator protein 1 transcription factor subunit (c-Jun) functions downstream of Jun N-terminal kinase (JNK), acting as a transcription factor and positive regulator of cellular proliferation (Johnson and Nakamura, 2007). Phosphorylation of c-Jun at serine 63 [S63] was detected and was significantly affected by TRP agonist stimulation: $H(2) = 7.931$, $P = .0198$ (**Figure 3.3**). c-Jun phosphorylation was significantly increased in TRPV3 samples, with median levels reaching more than 200% above baseline (FCH = 2.60 *vs.* 0; $P = .0187$). Though increased phosphorylation was detected in 2 TRPA1

replicates, levels were statistically unchanged in TRPA1 and TRPV1 groups ($P = .1579$ and $P = .4149$, respectively). Thus, c-Jun acts downstream of the TRPV3 receptor in human epidermal keratinocytes.

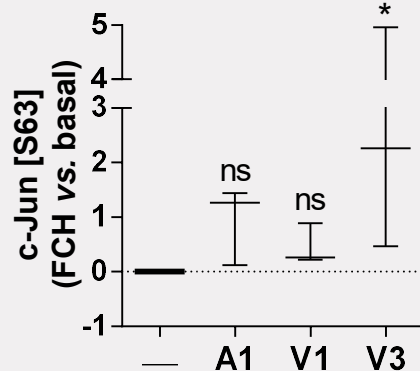


Figure 3.3. Effect of TRP agonists on activation of c-Jun.

Graph compares phosphorylation of activator protein 1 transcription factor subunit (c-Jun) at serine 63 [S63] in keratinocytes (NHEK) following application of basal medium \pm TRP agonists [15 min]: AITC (TRPA1 agonist [A1], 100 μ M); capsaicin (TRPV1 agonist [V1], 1 μ M); drofenine (TRPV3 agonist [V3], 500 μ M). Data expressed as fold change (FCH) over basal level (represented by — and dotted line). Plots indicate median of 3 independent experiments, with bars outlining min and max values. P -values calculated using Kruskal-Wallis test: ns $P > .05$; * $P \leq .05$.

Endothelial nitric oxide synthase (eNOS) is a key inducer of NO production in the skin and driver of NO-mediated wound healing. Phosphorylation of eNOS at serine 1177 [S1177] was detected and was significantly affected by TRP agonist stimulation: $H(2) = 6.995$, $P = .0469$ (**Figure 3.4**). Each of the groups show elevated levels of eNOS phosphorylation: median FCH values reached 1.052 (TRPA1); 0.6495 (TRPV1); and 1.013 (TRPV3). This trend reached significance in the TRPA1 group ($P = .0365$); phosphorylation was statistically unchanged in TRPV1 and TRPV3 groups ($P = .2618$ and $P = .1579$, respectively). Thus, eNOS acts downstream of the TRPA1 receptor in human epidermal keratinocytes.

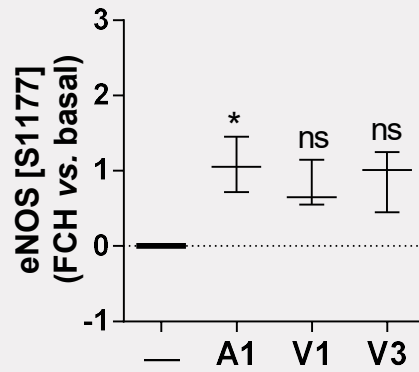


Figure 3.4. Effect of TRP agonists on activation of eNOS.

Graph compares phosphorylation of endothelial nitric oxide synthase (eNOS) at serine 1177 (S1177) in keratinocytes (NHEK) following application of basal medium \pm TRP agonists [15 min]: AITC (TRPA1 agonist [A1], 100 μ M); capsaicin (TRPV1 agonist [V1], 1 μ M); drofenine (TRPV3 agonist [V3], 500 μ M). Data expressed as fold change (FCH) over basal level (represented by — and dotted line). Plots indicate median of 3 independent experiments, with bars outlining min and max values. P-values calculated using Kruskal-Wallis test: ns $P > .05$; * $P \leq .05$.

Fyn proto-oncogene (Fyn), a member of the Src family, represents a key regulator of keratinocyte growth and differentiation. Phosphorylation of Fyn at tyrosine 420 [Y420] was detected and was significantly affected by TRP agonist stimulation: $H(2) = 8.191$, $P = .0159$ (**Figure 3.5**). Fyn phosphorylation was significantly increased in TRPV3 samples (FCH = 0.4993 vs. 0; $P = .0187$). Though increased phosphorylation was detected in one TRPV1 replicate, levels were statistically unchanged in TRPA1 and TRPV1 groups ($P = .5138$ and $P = .1205$, respectively). Thus, Fyn acts downstream of the TRPV3 receptor in human epidermal keratinocytes.

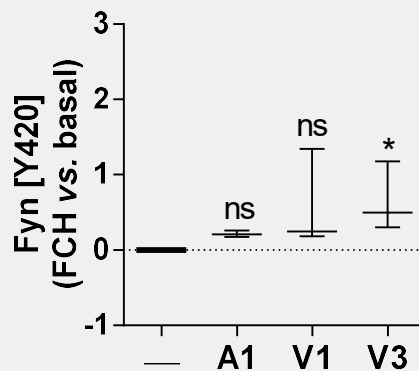


Figure 3.5. Effect of TRP agonists on activation of Fyn.

Graph compares phosphorylation of Fyn proto-oncogene (Fyn) at tyrosine 420 [Y420] in keratinocytes (NHEK) following application of basal medium \pm TRP agonists [15 min]: AITC (TRPA1 agonist [A1], 100 μ M); capsaicin (TRPV1 agonist [V1], 1 μ M); drofenine (TRPV3 agonist [V3], 500 μ M). Data expressed as fold change (FCH) over basal level (represented by — and dotted

line). Plots indicate median of 3 independent experiments, with bars outlining min and max values. *P*-values calculated using Kruskal-Wallis test: ns $P > .05$; * $P \leq .05$.

Hematopoietic cell kinase (Hck), also a member of the Src family, is associated with a cellular proliferation and survival, chemokine signalling, and immune cell activation. Phosphorylation of Hck at tyrosine 411 [Y411] was detected and was significantly affected by TRP agonist stimulation: $H(2) = 8.243$, $P = .0144$ (**Figure 3.6**). Hck phosphorylation was significantly increased in TRPV3 samples, with median levels reaching more than 150% above baseline (FCH = 1.541 vs. 0; $P = .0131$). Though increased phosphorylation was detected in one TRPV1 replicate, levels were statistically unchanged in TRPA1 and TRPV1 groups ($P = .3314$ and $P = .2618$, respectively). Thus, Hck acts downstream of the TRPV3 receptor in human epidermal keratinocytes.

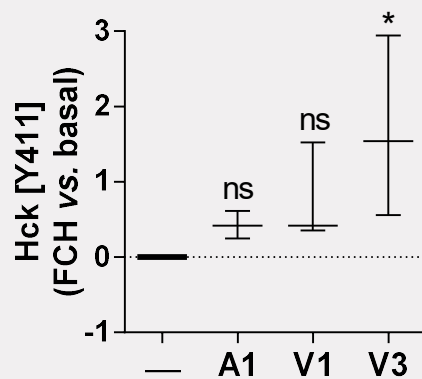


Figure 3.6. Effect of TRP agonists on activation of Hck.

Graph compares phosphorylation of hematopoietic cell kinase (Hck) at tyrosine 411 [Y411] in keratinocytes (NHEK) following application of basal medium \pm TRP agonists [15 min]: AITC (TRPA1 agonist [A1], 100 μ M); capsaicin (TRPV1 agonist [V1], 1 μ M); drofenine (TRPV3 agonist [V3], 500 μ M). Data expressed as fold change (FCH) over basal level (represented by — and dotted line). Plots indicate median of 3 independent experiments, with bars outlining min and max values. *P*-values calculated using Kruskal-Wallis test: ns $P > .05$; * $P \leq .05$.

Cellular tumour antigen p53 (p53) is a pleiotropic transcription factor which interacts with tumour suppressor genes and modulates cell cycle arrest. Phosphorylation of p53 at serine 15 [S15] was detected and was significantly affected by TRP agonist stimulation: $H(2) = 7.931$, $P = .0198$ (**Figure 3.7**). p53 phosphorylation was significantly increased in TRPA1 samples, with median levels measuring more than 100% above baseline (FCH = 1.048 vs. 0; $P = .0187$). Though increased phosphorylation was detected in one TRPV3 replicate, levels were statistically unchanged in TRPV1 and TRPV3 groups ($P = .4149$ and $P = .1579$, respectively). Thus, p53 acts downstream of the TRPA1 receptor in human epidermal keratinocytes.

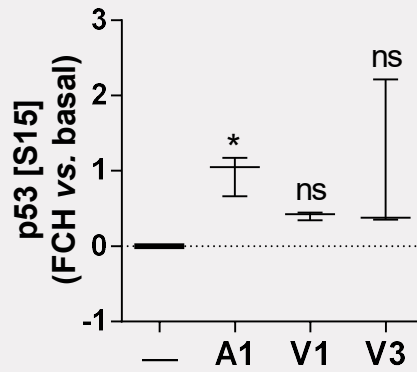


Figure 3.7. Effect of TRP agonists on activation of p53.

Graph compares phosphorylation of cellular tumour antigen p53 (p53) at serine 15 [S15] in keratinocytes (NHEK) following application of basal medium \pm TRP agonists [15 min]: AITC (TRPA1 agonist [A1], 100 μ M); capsaicin (TRPV1 agonist [V1], 1 μ M); drofenine (TRPV3 agonist [V3], 500 μ M). Data expressed as fold change (FCH) over basal level (represented by — and dotted line). Plots indicate median of 3 independent experiments, with bars outlining min and max values. *P*-values calculated using Kruskal-Wallis test: ns $P > .05$; * $P \leq .05$.

Ribosomal protein S6 kinase (p70S6K) is a mitogen-activated serine/threonine protein kinase, driving cell growth and stimulating G1 cell cycle progression. Phosphorylation of p70S6K at threonine 389 [T389] was detected and was significantly affected by TRP agonist stimulation: $H(2) = 7.775$, $P = .0223$ (Figure 3.8). p70S6K phosphorylation was significantly increased in TRPA1 samples, with median levels measuring more almost 150% above baseline (FCH = 1.461 vs. 0; $P = .0187$). Though increased phosphorylation was detected in one TRPV3 replicate, levels were statistically unchanged in TRPV1 and TRPV3 groups ($P = .3314$ and $P = .2044$, respectively). Thus, p70S6K acts downstream of the TRPA1 receptor in human epidermal keratinocytes.

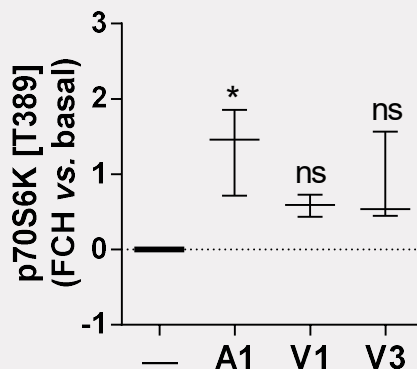


Figure 3.8. Effect of TRP agonists on activation of p70S6K.

Graph compares phosphorylation of ribosomal protein S6 kinase (p70S6K) at threonine 389 [T389] in keratinocytes (NHEK) following application of basal medium \pm TRP agonists [15 min]: AITC (TRPA1 agonist [A1], 100 μ M); capsaicin (TRPV1 agonist [V1], 1 μ M); drofenine (TRPV3 agonist

[V3], 500 μ M). Data expressed as fold change (FCH) over basal level (represented by — and dotted line). Plots indicate median of 3 independent experiments, with bars outlining min and max values. *P*-values calculated using Kruskal-Wallis test: ns *P* > .05; * *P* \leq .05.

Phospholipase C-gamma-1 (PLC γ 1) functions downstream of epidermal growth factors, promoting keratinocyte migration and wound healing (Kim *et al.*, 2019). Phosphorylation of PLC γ 1 at tyrosine 783 [Y783] was detected but, although approaching significance, was not significantly affected by TRP agonist stimulation: $H(2) = 6.527$, $P = .0707$ (**Figure 3.9**). Each of the groups show elevated levels of PLC γ 1 phosphorylation: median FCH values reached 0.9415 (TRPA1); 0.7462 (TRPV1); and 0.6692 (TRPV3). Though phosphorylation was statistically unchanged in TRPA1 and TRPV3 groups ($P = .1205$ and $P = .2044$, respectively), this trend was approaching significance in the TRPV1 group ($P = .0678$). Thus, PLC γ 1 may act downstream of the TRPV1 receptor in human epidermal keratinocytes.

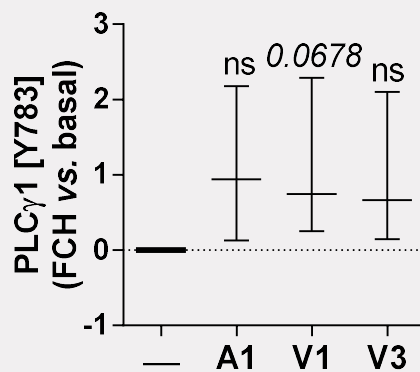


Figure 3.9. Effect of TRP agonists on activation of PLC γ 1.

Graph compares phosphorylation of phospholipase C-gamma-1 (PLC γ 1) at tyrosine 783 [Y783] in keratinocytes (NHEK) following application of basal medium \pm TRP agonists [15 min]: AITC (TRPA1 agonist [A1], 100 μ M); capsaicin (TRPV1 agonist [V1], 1 μ M); drofenine (TRPV3 agonist [V3], 500 μ M). Data expressed as fold change (FCH) over basal level (represented by — and dotted line). Plots indicate median of 3 independent experiments, with bars outlining min and max values. *P*-values calculated using Kruskal-Wallis test: ns *P* > .05.

Signal transducer and activator of transcription 5A (STAT5A) is a member of the JAK/STAT (Janus kinase/signal transducers and activators of transcription) pathway and a key coordinator of inflammatory signalling. Phosphorylation of STAT5A at tyrosine 694 [Y694] was detected but, although approaching significance, was not significantly affected by TRP agonist stimulation: $H(2) = 6.787$, $P = .0515$ (**Figure 3.10**). Median STAT5A phosphorylation was increased in TRPV3 samples; however, this trend did not reach significance (FCH = 0.5078 vs. 0; $P = .050$). Phosphorylation was statistically unchanged in TRPA1 and TRPV1 groups ($P > .9999$ for both, respectively). Thus, STAT5A may act downstream of the TRPV3 receptor in human epidermal keratinocytes.

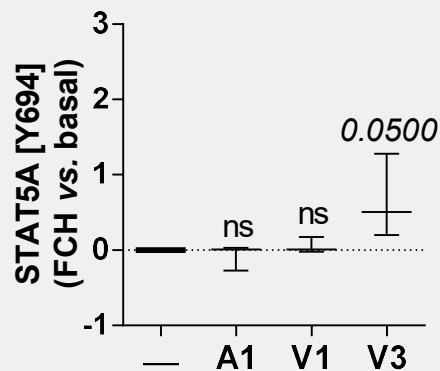


Figure 3.10. Effect of TRP agonists on activation of STAT5A.

Graph compares phosphorylation of signal transducer and activator of transcription 5A (STAT5A) at tyrosine 694 [Y694] in keratinocytes (NHEK) following application of basal medium \pm TRP agonists [15 min]: AITC (TRPA1 agonist [A1], 100 μ M); capsaicin (TRPV1 agonist [V1], 1 μ M); drofenine (TRPV3 agonist [V3], 500 μ M). Data expressed as fold change (FCH) over basal level (represented by — and dotted line). Plots indicate median of 3 independent experiments, with bars outlining min and max values. P -values calculated using Kruskal-Wallis test: ns $P > .05$.

Lysine deficient protein kinase 1 (WNK1) is a pleiotropic serine/threonine kinase which regulates cross-membrane ion transport. Phosphorylation of WNK1 at threonine 60 [T60] was detected but, although approaching significance, was not significantly affected by TRP agonist stimulation: $H(2) = 6.527$, $P = .0673$ (**Figure 3.11**). WNK1 phosphorylation was significantly increased in TRPA1 samples, with median levels reaching more than 100% above baseline (FCH = 1.192 vs. 0; $P = .0365$). Though increased phosphorylation was detected in one TRPV3 replicate, levels were statistically unchanged in TRPV1 and TRPV3 groups ($P = .5138$ and $P > .9999$, respectively). Thus, WNK1 acts downstream of the TRPA1 receptor in human epidermal keratinocytes.

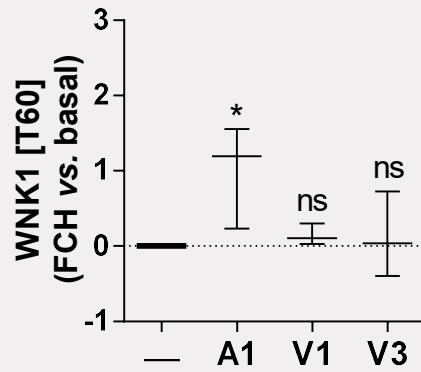


Figure 3.11. Effect of TRP agonists on activation of WNK1.

Graph compares phosphorylation of lysine deficient protein kinase 1 (WNK1) at threonine 60 [T60] in keratinocytes (NHEK) following application of basal medium \pm TRP agonists [15 min]: AITC (TRPA1 agonist [A1], 100 μ M); capsaicin (TRPV1 agonist [V1], 1 μ M); drofenine (TRPV3 agonist [V3], 500 μ M). Data expressed as fold change (FCH) over basal level (represented by — and dotted line). Plots indicate median of 3 independent experiments, with bars outlining min and max values. *P*-values calculated using Kruskal-Wallis test: ns $P > .05$; * $P \leq .05$.

Yamaguchi sarcoma virus oncogene (Yes), a member of the Src family, has recently been implicated in IL-17A signalling in epidermal keratinocytes (Tohyama *et al.*, 2021). Phosphorylation of Yes at tyrosine 426 [Y426] was detected but, although approaching significance, was not significantly affected by TRP agonist stimulation: $H(2) = 6.683$, $P = .0642$ (**Figure 3.12**). Median Yes phosphorylation was increased in TRPV1 samples; however, this trend did not reach significance (FCH = 0.287 vs. 0; $P = .0500$). Though increased phosphorylation was detected in one TRPV3 replicate, levels were statistically unchanged in TRPA1 and TRPV3 groups ($P = .1579$ and $P = .2044$, respectively). Thus, Yes may act downstream of the TRPV1 receptor in human epidermal keratinocytes.

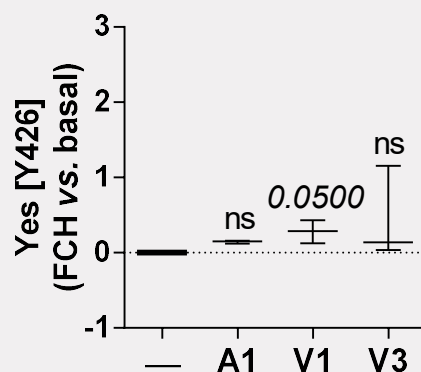


Figure 3.12. Effect of TRP agonists on activation of Yes.

Graph compares phosphorylation of Yamaguchi sarcoma virus oncogene (Yes) at tyrosine 426 [Y426] in keratinocytes (NHEK) following application of basal medium \pm TRP agonists [15 min]: AITC (TRPA1 agonist [A1], 100 μ M); capsaicin (TRPV1 agonist [V1], 1 μ M); drofenine (TRPV3 agonist [V3], 500 μ M). Data expressed as fold change (FCH) over basal level (represented by — and dotted line). Plots indicate median of 3 independent experiments, with bars outlining min and max values. *P*-values calculated using Kruskal-Wallis test: ns $P > .05$.

Mitogen-activated protein kinase 14 (p38 α), a member of the p38 mitogen-activated protein kinase (MAPK) family, facilitates UVB-induced chemokine release from primary murine keratinocytes (Kim *et al.*, 2008). Phosphorylation of p38 α at threonine 180 or tyrosine 182 was detected but was not significantly affected by TRP agonist stimulation: $H(2) = 0.058$, $P = .9922$ (**Figure 3.13**). Median p38 α phosphorylation was unaffected by TRP agonist application (FCH = 0 for all; $P > .9999$). These data underline the specificity of this assay and strengthen the positive results.

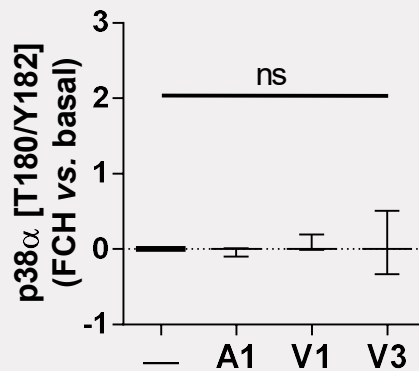


Figure 3.13. Effect of TRP agonists on activation of p38 α .

Graph compares phosphorylation of mitogen-activated protein kinase 14 (p38 α) at tyrosine 180 or tyrosine 182 [T180/Y182] in keratinocytes (NHEK) following application of basal medium \pm TRP agonists [15 min]: AITC (TRPA1 agonist [A1], 100 μ M); capsaicin (TRPV1 agonist [V1], 1 μ M); drofenine (TRPV3 agonist [V3], 500 μ M). Data expressed as fold change (FCH) over basal level (represented by — and dotted line). Plots indicate median of 3 independent experiments, with bars outlining min and max values. *P*-values calculated using Kruskal-Wallis test: ns $P > .05$.

Where noted above, variation was largely grouped into specific replicates: for TRPA1, outliers were in replicate 3; for TRPV1, outliers were in replicate 1; and for TRPV3, outliers were in replicate 2. Phosphorylation and dephosphorylation is a rapid process; this pattern suggests that some of the variation may be caused by differences in stimulation time.

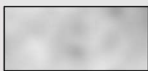
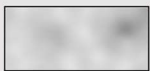


































In summary, agonists targeting TRPA1, TRPV1, and TRPV3 channels induce measurable changes in intracellular signalling. This finding indicates that these TRP channels are functional in our NHEK culture model. Stimulation of TRPA1 increased phosphorylation of p53, p70S6K, eNOS, and WNK1, with all reaching significance. Stimulation of TRPV1 increased phosphorylation of Yes, Chk2, and PLC γ 1, though none reached significance. Stimulation of TRPV3 increased phosphorylation of c-Jun, STAT5A, Fyn, and Hck, though STAT5A failed to reach significance. Together, these results highlight the distinct signalling pathways acting downstream of TRPA1, TRPV1, and TRPV3 channels in a culture model of human epidermis.

3.2.3. TRPA1 and TRPV1 agonists fail to promote consistent mediator release

Neuronal TRPA1 and TRPV1 have been extensively studied: current evidence implicates these channels in the transduction of histamine-independent and -dependent itch, respectively. While both channels have been detected in the skin, their role in epidermal inflammation remains poorly understood. These experiments aim to address this knowledge gap, comparing the effect of TRPA1, TRPV1, and TRPV3 agonists on mediator release from normal human epidermal keratinocytes (NHEK), a common culture model of the epidermis.



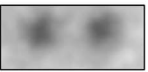
















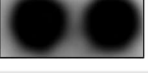















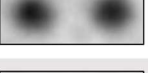
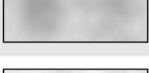
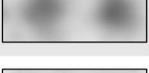
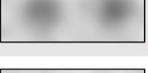
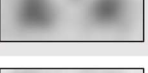








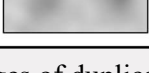

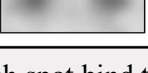
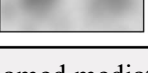
NHEK were stimulated with basal medium \pm TRP agonists: AITC (TRPA1, 100 μ M); capsaicin (TRPV1, 1 μ M); or drofenine (TRPV3, 500 μ M) [1 h, 37°C]. Following stimulation, cell supernatant was collected and pooled. Mediator release was compared using the cytokine array. Briefly, when present in the supernatant sample, the named protein binds to capture antibodies located at duplicate spots on a nitrocellulose membrane. Chemiluminescent development reveals the relative levels of each released protein. Here, a number of proteins were consistently detected: BSG, CXCL1, Dkk-1, EGF, FGF-2, FGF-19, IFN γ , IL-1 α , IL-1ra, IL-8, IL-17A, KLK3, M-CSF, MIF, NGAL, PAI-1, PDGFA, PTX3, Tfr, TGF- α , TSP-1, and VDBP (Table 3.2).

Table 3.2. Representative images of duplicate antibody spots from cytokine array showing effect of TRP agonists on mediator release.

Mediator	Basal	TRPA1	TRPV1	TRPV3
BSG				
CXCL1				
Dkk-1				
EGF				
FGF-2				
FGF-19				
IFN γ				
IL-1 α				
IL-1ra				

Continued overleaf

Table 3.2 continued. Representative images of duplicate antibody spots from cytokine array showing effect of TRP agonists on mediator release.

Mediator	Basal	TRPA1	TRPV1	TRPV3
IL-8				
IL-17A				
KLK3				
M-CSF				
MIF				
NGAL				
PAI-1				
PDGFA				
PTX3				
TfR				
TGF- α				
TSP-1				
VDBP				

Note: Table includes images of duplicate spots; antibodies at each spot bind to the named mediator. *Abbreviations:* BSG, basigin; CXCL1, chemokine C-X-C motif ligand 1; Dkk-1, dickkopf-1; EGF, epidermal growth factor; FGF-2, fibroblast growth factor 2; FGF-19, fibroblast growth factor 19; IFN γ , interferon gamma; IL-1 α , interleukin-1 alpha; IL-1ra, interleukin 1 receptor antagonist; IL-8, interleukin-8; IL-17A, interleukin-17A; KLK3, kallikrein-3; M-CSF, macrophage colony-stimulating factor 1; MIF, macrophage migration inhibitory factor; NGAL, neutrophil gelatinase-associated lipocalin; PAI-1, plasminogen activator inhibitor 1; PDGFA, platelet derived growth factor subunit A; PTX3, pentraxin-related protein PTX3; TfR, transferrin receptor protein 1; TGF- α , transforming growth factor alpha; TRPA1, transient receptor potential ankyrin 1; TRPV1, transient receptor potential vanilloid 1; TRPV3, transient receptor potential vanilloid 3; TSP-1, thrombospondin-1; and VDBP, vitamin D binding protein.

Duplicate antibody spots were then measured using densitometry. Average pixel density of each duplicate pair represents one experimental replicate. Average pixel density data were expressed as fold change (FCH) relative to basal medium-treated samples (n=4). FCH data were presented as median FCH and interquartile range ($Q^1 - Q^3$) and were analysed using the nonparametric Kruskal-Wallis test plus Dunn's multiple comparison post-test (all vs. basal). The graphs below reveal the relative change of each named protein, highlighting the link between TRP stimulation and mediator release.

Basigin (BSG) is also known as extracellular matrix metalloproteinase inducer (EMMPRIN) or CD147. In the skin, BSG is involved in wound healing and tissue remodelling, enhancing fibroblast production of matrix metalloproteinases (Guo *et al.*, 1997). Here, BSG was detected in cellular supernatant; relative levels were significantly affected by agonist stimulation: $H(3) = 8.597$, $P = .0184$ (**Figure 3.14**). TRPA1 and TRPV1 agonists failed to increase median BSG levels. These data were statistically comparable to baseline ($P > .9999$ for both). The TRPV3 agonist increased median BSG levels by more than 400% above baseline. This increase was approaching significance (FCH = 4.470; $P = .0501$). Thus, activation of the TRPV3 channel may promote BSG release from human epidermal keratinocytes.

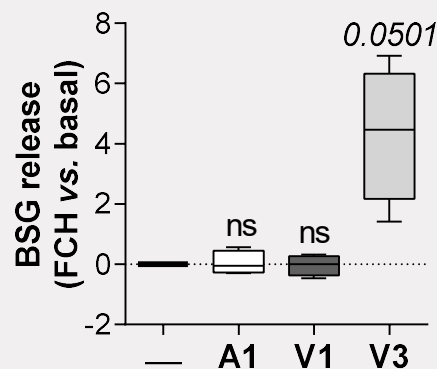


Figure 3.14. Effect of TRP agonists on BSG release.

Graph compares release of basigin (BSG) from keratinocytes (NHEK) following application of basal medium \pm TRP agonists [1 h]: AITC (TRPA1 agonist [A1], 100 μ M); capsaicin (TRPV1 agonist [V1], 1 μ M); drofenine (TRPV3 agonist [V3], 500 μ M). Data expressed as fold change (FCH) over basal level (represented by — and dotted line). Boxplots indicate median ($Q^1 - Q^3$) of 4 independent experiments, with bars outlining min and max values. P -values calculated using Kruskal-Wallis test: ns $P > .05$.

Chemokine C-X-C motif ligand 1 (CXCL1) promotes chemotaxis of neutrophils and facilitates UVB-induced inflammatory responses (Kunisada *et al.*, 2017). Here, CXCL1 was detected in cellular supernatant; however, relative levels were statistically unchanged by agonist stimulation: $H(3) = 1.909$, $P = .6275$ (**Figure 3.15**). The post-hoc comparison failed to detect significant differences between agonist groups and baseline levels ($P > .9999$ [TRPA1]; $P = .5247$ [TRPV1]; $P > .9999$ [TRPV3]). Although TRPA1 and TRPV1 agonists affected CXCL1 secretion – with later replicates showing increases of around 600% (FCH = 5.970 and 7.675, respectively) – this effect was highly varied. As TRP agonists fail to evoke consistent CXCL1 release, further experiments are required to investigate the potential link between TRPA1, TRPV1, or TRPV3 activation and CXCL1 release from human epidermal keratinocytes.

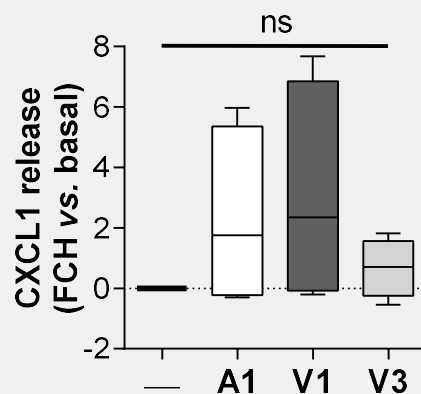


Figure 3.15. Effect of TRP agonists on CXCL1 release.

Graph compares release of chemokine C-X-C motif ligand 1 (CXCL1) from keratinocytes (NHEK) following application of basal medium \pm TRP agonists [1 h]: AITC (TRPA1 agonist [A1], 100 μ M); capsaicin (TRPV1 agonist [V1], 1 μ M); drofenine (TRPV3 agonist [V3], 500 μ M). Data expressed as fold change (FCH) over basal level (represented by — and dotted line). Boxplots indicate median ($Q^1 - Q^3$) of 4 independent experiments, with bars outlining min and max values. P -values calculated using Kruskal-Wallis test: ns $P > .05$.

Dickkopf-1 (Dkk-1) inhibits the Wnt/ β -catenin pathway, regulating skin pigmentation, epidermal thickness, and the hair cycle (Kwack *et al.*, 2012; Yamaguchi *et al.*, 2008). Here, Dkk-1 was detected in cellular supernatant; relative levels were significantly affected by agonist stimulation: $H(3) = 10.50$, $P = .0028$ (**Figure 3.16**). TRPA1 and TRPV1 agonists failed to increase median Dkk-1 levels. These data were statistically comparable to baseline ($P = .4039$ and $P = .6105$, respectively). The TRPV3 agonist significantly increased median Dkk-1 levels, with relative values peaking at almost 1500% above baseline (FCH = 14.836; $P = .0039$). Thus, activation of the TRPV3 channel promotes Dkk-1 release from human epidermal keratinocytes.

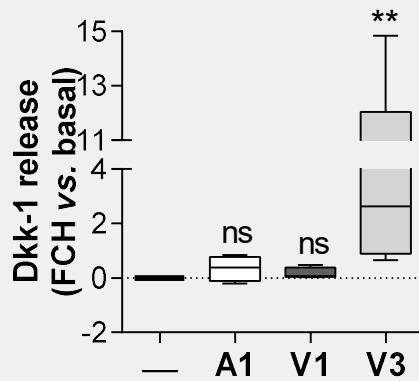


Figure 3.16. Effect of TRP agonists on Dkk-1 release.

Graph compares release of dickkopf-1 (Dkk-1) from keratinocytes (NHEK) following application of basal medium \pm TRP agonists [1 h]: AITC (TRPA1 agonist [A1], 100 μ M); capsaicin (TRPV1 agonist [V1], 1 μ M); drofenine (TRPV3 agonist [V3], 500 μ M). Data expressed as fold change (FCH) over basal level (represented by — and dotted line). Boxplots indicate median (Q¹ – Q³) of 4 independent experiments, with bars outlining min and max values. *P*-values calculated using Kruskal-Wallis test: ns *P* > .05; ** *P* \leq .01.

Epidermal growth factor (EGF) promotes migration and proliferation of cutaneous cells – key steps in wound healing (Wells, 1999). Here, EGF was detected in cellular supernatant; relative levels were significantly affected by agonist stimulation: $H(3) = 18.477$, $P = .0210$ (**Figure 3.17**). Although increased release was noted in one TRPA1 replicate, TRPA1 and TRPV1 agonists failed to consistently increase median EGF levels. These data were statistically comparable to baseline ($P = .1046$ and $P = .2491$, respectively). The TRPV3 agonist significantly increased median EGF secretion ($P = .0159$). Thus, activation of the TRPV3 channel promotes EGF release from human epidermal keratinocytes.

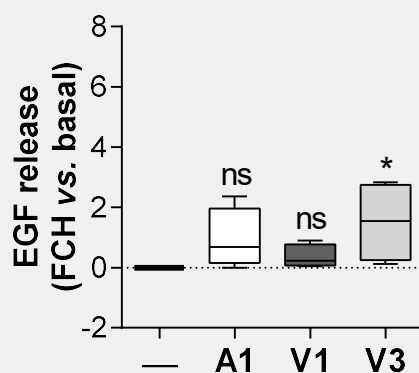


Figure 3.17. Effect of TRP agonists on EGF release.

Graph compares release of extracellular growth factor (EGF) from keratinocytes (NHEK) following application of basal medium \pm TRP agonists [1 h]: AITC (TRPA1 agonist [A1], 100 μ M); capsaicin (TRPV1 agonist [V1], 1 μ M); drofenine (TRPV3 agonist [V3], 500 μ M). Data expressed as fold

change (FCH) over basal level (represented by — and dotted line). Boxplots indicate median ($Q^1 - Q^3$) of 4 independent experiments, with bars outlining min and max values. P -values calculated using Kruskal-Wallis test: ns $P > .05$; * $P \leq .05$.

Fibroblast growth factor 2 (FGF-2) is a potent angiogenic and mitogenic factor involved in a wide variety of biological processes including wound healing (Koike *et al.*, 2020). Here, FGF-2 was detected in cellular supernatant; however, relative levels were statistically unchanged by agonist stimulation: $H(3) = 2.575$, $P = .4933$ (**Figure 3.18**). The post-hoc comparison failed to detect significant differences between agonist groups and baseline levels ($P > .9999$ [TRPA1]; $P > .9999$ [TRPV1]; $P = .4657$ [TRPV3]). Thus, TRPA1, TRPV1, and TRPV3 agonists fail to evoke FGF-2 release from human epidermal keratinocytes.

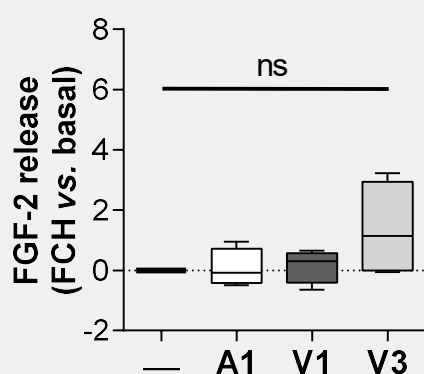


Figure 3.18. Effect of TRP agonists on FGF-2 release.

Graph compares release of fibroblast growth factor 2 (FGF-2) from keratinocytes (NHEK) following application of basal medium \pm TRP agonists [1 h]: AITC (TRPA1 agonist [A1], 100 μ M); capsaicin (TRPV1 agonist [V1], 1 μ M); drofenine (TRPV3 agonist [V3], 500 μ M). Data expressed as fold change (FCH) over basal level (represented by — and dotted line). Boxplots indicate median ($Q^1 - Q^3$) of 4 independent experiments, with bars outlining min and max values. P -values calculated using Kruskal-Wallis test: ns $P > .05$.

Fibroblast growth factor 19 (FGF-19) is involved in a variety of physiological and pathological processes. In the skin, FGF-19 binds to its cognate receptor (FGFR4) to promote Wnt/ β -catenin signalling and drive keratinocyte proliferation (Yu *et al.*, 2019). Here, FGF-19 was detected in cellular supernatant; relative levels were significantly affected by agonist stimulation: $H(3) = 8.037$, $P = .0289$ (**Figure 3.19**). TRPA1 and TRPV1 agonists failed to increase median FGF-19 levels. These data were statistically comparable to baseline ($P = .5345$ and $P = .1845$, respectively). The TRPV3 agonist evoked a small but significant increase in FGF-19 secretion, with median levels reaching about 70% above baseline (FCH = 0.699; $P = .0170$). Thus, activation of the TRPV3 channel may promote FGF-19 release from human epidermal keratinocytes.

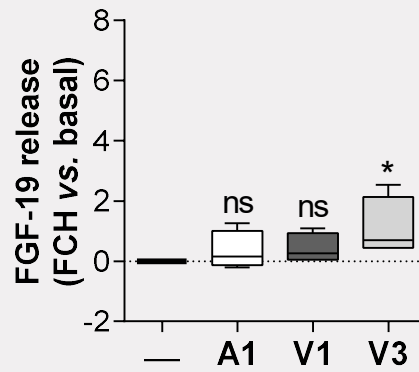


Figure 3.19. Effect of TRP agonists on FGF-19 release.

Graph compares release of fibroblast growth factor 19 (FGF-19) from keratinocytes (NHEK) following application of basal medium \pm TRP agonists [1 h]: AITC (TRPA1 agonist [A1], 100 μ M); capsaicin (TRPV1 agonist [V1], 1 μ M); drofenine (TRPV3 agonist [V3], 500 μ M). Data expressed as fold change (FCH) over basal level (represented by — and dotted line). Boxplots indicate median ($Q^1 - Q^3$) of 4 independent experiments, with bars outlining min and max values. P -values calculated using Kruskal-Wallis test: ns $P > .05$; * $P \leq .05$.

Interferon gamma ($IFN\gamma$), or type II interferon, is primarily produced by natural killer and T cells; this Th1 cytokine coordinates both innate and adaptive immune responses (Schoenborn and Wilson, 2007). Here, FGF-2 was detected in cellular supernatant; however, relative levels were statistically unchanged by agonist stimulation: $H(3) = 2.843$, $P = .4445$ (**Figure 3.20**). The post-hoc comparison failed to detect significant differences between agonist groups and baseline levels ($P = .2995$ [TRPA1]; $P > .9999$ [TRPV1]; $P = .7855$ [TRPV3]). Thus, TRPA1, TRPV1, and TRPV3 agonists fail to evoke $IFN\gamma$ release from human epidermal keratinocytes.

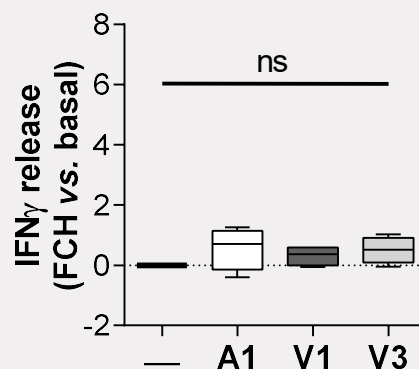


Figure 3.20. Effect of TRP agonists on $IFN\gamma$ release.

Graph compares release of interferon gamma ($IFN\gamma$) from keratinocytes (NHEK) following application of basal medium \pm TRP agonists [1 h]: AITC (TRPA1 agonist [A1], 100 μ M); capsaicin (TRPV1 agonist [V1], 1 μ M); drofenine (TRPV3 agonist [V3], 500 μ M). Data expressed as fold change (FCH) over basal level (represented by — and dotted line). Boxplots indicate median ($Q^1 -$

Q³) of 4 independent experiments, with bars outlining min and max values. *P*-values calculated using Kruskal-Wallis test: ns *P* > .05.

Interleukin-1 alpha (IL-1 α) acts as an “alarmin”, a key initiator of early inflammation following infection, cell stress, or tissue damage (Di Paolo and Shayakhmetov, 2016; Garlanda *et al.*, 2013). Here, IL-1 α was detected in cellular supernatant; however, although approaching significance, relative levels were statistically unchanged by agonist stimulation: $H(3) = 6.457$, $P = .0801$ (**Figure 3.21**). TRPA1 and TRPV1 agonists failed to increase median IL-1 α levels. These data were statistically comparable to baseline levels ($P > .9999$ for both). The TRPV3 agonist evoked a significant but varied increase in IL-1 α secretion, with the median change values ranging from 50% to 730% above baseline (FCH = 0.497 and 7.282) ($P = .0499$). Thus, activation of the TRPV3 channel promotes IL-1 α release from human epidermal keratinocytes.

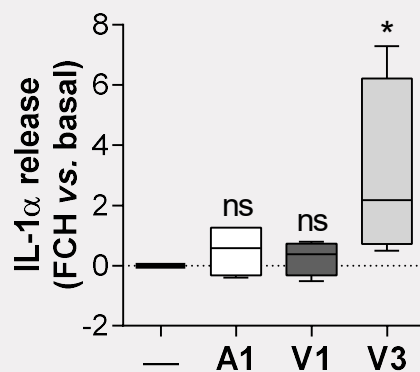


Figure 3.21. Effect of TRP agonists on IL-1 α release.

Graph compares release of interleukin-1 alpha (IL-1 α) from keratinocytes (NHEK) following application of basal medium \pm TRP agonists [1 h]: AITC (TRPA1 agonist [A1], 100 μ M); capsaicin (TRPV1 agonist [V1], 1 μ M); drofenine (TRPV3 agonist [V3], 500 μ M). Data expressed as fold change (FCH) over basal level (represented by — and dotted line). Boxplots indicate median (Q¹ – Q³) of 4 independent experiments, with bars outlining min and max values. *P*-values calculated using Kruskal-Wallis test: ns *P* > .05; * *P* \leq .05.

Interleukin 1 receptor antagonist (IL-1ra) binds to the IL-1 receptor (IL-1R1), blocking the action of both IL-1 α and IL-1 β (Garlanda *et al.*, 2013). Here, IL-1ra was detected in cellular supernatant; however, relative levels were statistically unchanged by agonist stimulation: $H(3) = 5.821$, $P = .1141$ (**Figure 3.22**). TRPA1 and TRPV1 agonists failed to increase median IL-1ra levels. These data were statistically comparable to baseline ($P = .8849$ and $P = .5345$, respectively). The TRPV3 agonist promoted a slight increase in IL-1ra secretion; this difference was approaching significance ($P = .0501$). Thus, activation of the TRPV3 channel may promote IL-1ra release from human epidermal keratinocytes.

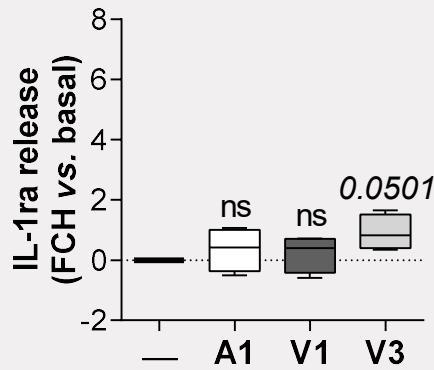


Figure 3.22. Effect of TRP agonists on IL-1ra release.

Graph compares release of interleukin 1 receptor antagonist (IL-1ra) from keratinocytes (NHEK) following application of basal medium \pm TRP agonists [1 h]: AITC (TRPA1 agonist [A1], 100 μ M); capsaicin (TRPV1 agonist [V1], 1 μ M); drofenine (TRPV3 agonist [V3], 500 μ M). Data expressed as fold change (FCH) over basal level (represented by — and dotted line). Boxplots indicate median ($Q^1 - Q^3$) of 4 independent experiments, with bars outlining min and max values. P -values calculated using Kruskal-Wallis test: ns $P > .05$.

Interleukin-8 (IL-8), also known as CXCL8, promotes neutrophil activation and chemotaxis (Bernhard *et al.*, 2021). Here, IL-8 was detected in cellular supernatant; however, relative levels were statistically unchanged by agonist stimulation: $H(3) = 1.097$, $P = .8039$ (**Figure 3.23**). The post-hoc comparison failed to detect significant differences between agonist groups and baseline levels ($P > .9999$ for all). Thus, TRPA1, TRPV1, and TRPV3 agonists fail to evoke IL-8 release from human epidermal keratinocytes.

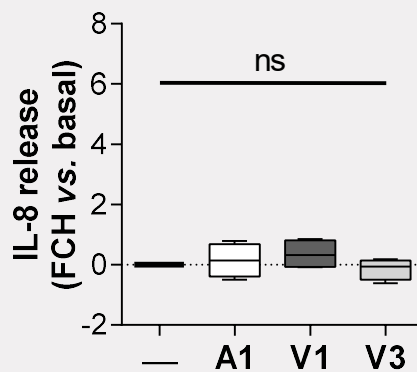


Figure 3.23. Effect of TRP agonists on IL-8 release.

Graph compares release of interleukin-8 (IL-8) from keratinocytes (NHEK) following application of basal medium \pm TRP agonists [1 h]: AITC (TRPA1 agonist [A1], 100 μ M); capsaicin (TRPV1 agonist [V1], 1 μ M); drofenine (TRPV3 agonist [V3], 500 μ M). Data expressed as fold change (FCH) over basal level (represented by — and dotted line). Boxplots indicate median ($Q^1 - Q^3$) of 4

independent experiments, with bars outlining min and max values. *P*-values calculated using Kruskal-Wallis test: ns $P > .05$.

Interleukin-17A (IL-17A) is primarily produced by innate lymphoid and Th17 cells, a specific subset of CD4⁺ T helper cells (Liu *et al.*, 2020). IL-17A activates cutaneous cells such as keratinocytes, neutrophils, and fibroblasts, and is associated with psoriasis, hidradenitis suppurativa, and other inflammatory skin diseases. Here, IL-17A was detected in cellular supernatant; however, relative levels were statistically unchanged by agonist stimulation: $H(3) = 4.590$, $P = .2087$ (**Figure 3.24**). FCH data suggests that TRP agonists may alter IL-17A release; however, raw array images highlight the low level of IL-17A present in each sample (**Table 3.2**). The post-hoc comparison failed to detect significant differences between the agonist groups and baseline levels ($P = .6105$ [TRPA1]; $P = .4657$ [TRPV1]; $P = .1087$ [TRPV3]). Thus, TRPA1, TRPV1, and TRPV3 agonists fail to evoke IL-17A release from human epidermal keratinocytes.

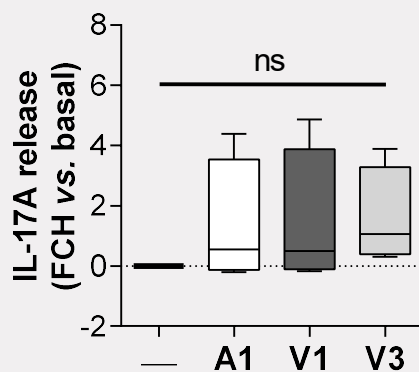


Figure 3.24. Effect of TRP agonists on IL-17A release.

Graph compares release of interleukin-17A (IL-17A) from keratinocytes (NHEK) following application of basal medium \pm TRP agonists [1 h]: AITC (TRPA1 agonist [A1], 100 μ M); capsaicin (TRPV1 agonist [V1], 1 μ M); drofenine (TRPV3 agonist [V3], 500 μ M). Data expressed as fold change (FCH) over basal level (represented by — and dotted line). Boxplots indicate median ($Q^1 - Q^3$) of 4 independent experiments, with bars outlining min and max values. *P*-values calculated using Kruskal-Wallis test: ns $P > .05$.

Kallikrein-3 (KLK3) is a serine protease which is primarily expressed in seminal plasma (Shaw and Diamandis, 2007). Here, KLK3 was detected in cellular supernatant; however, relative levels were statistically unchanged by agonist stimulation: $H(3) = 1.545$, $P = .7060$ (**Figure 3.25**). The post-hoc comparison failed to detect significant differences between agonist groups and baseline levels ($P = .7855$ [TRPA1]; $P > .9999$ [TRPV1]; $P > .9999$ [TRPV3]). Thus, TRPA1, TRPV1, and TRPV3 agonists fail to evoke KLK3 release from human epidermal keratinocytes.

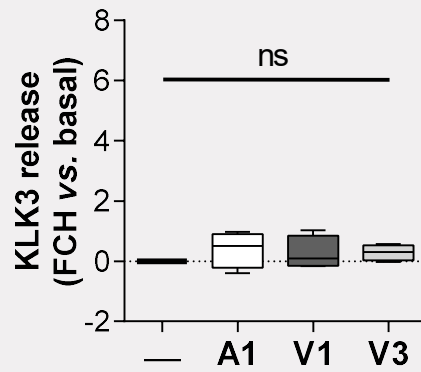


Figure 3.25. Effect of TRP agonists on KLK3 release.

Graph compares release of kallikrein-3 (KLK3) from keratinocytes (NHEK) following application of basal medium \pm TRP agonists [1 h]: AITC (TRPA1 agonist [A1], 100 μ M); capsaicin (TRPV1 agonist [V1], 1 μ M); drofenine (TRPV3 agonist [V3], 500 μ M). Data expressed as fold change (FCH) over basal level (represented by — and dotted line). Boxplots indicate median ($Q^1 - Q^3$) of 4 independent experiments, with bars outlining min and max values. P -values calculated using Kruskal-Wallis test: ns $P > .05$.

Macrophage colony-stimulating factor (M-CSF), also known as colony-stimulating factor-1 (CSF-1), functions as a hematopoietic growth factor (Stanley *et al.*, 1997). Here, M-CSF was detected in cellular supernatant; however, relative levels were statistically unchanged by agonist stimulation: $H(3) = 4.052$, $P = .2685$ (**Figure 3.26**). The post-hoc comparison failed to detect significant differences between agonist groups and baseline levels ($P = .1845$ [TRPA1]; $P = .4657$ [TRPV1]; $P = .4039$ [TRPV3]). Thus, TRPA1, TRPV1, and TRPV3 agonists fail to evoke M-CSF release from human epidermal keratinocytes.

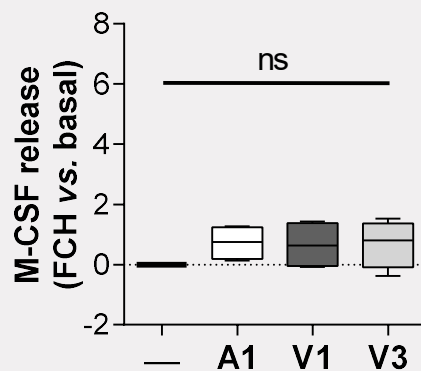


Figure 3.26. Effect of TRP agonists on M-CSF release.

Graph compares release of macrophage colony-stimulating factor (M-CSF) from keratinocytes (NHEK) following application of basal medium \pm TRP agonists [1 h]: AITC (TRPA1 agonist [A1], 100 μ M); capsaicin (TRPV1 agonist [V1], 1 μ M); drofenine (TRPV3 agonist [V3], 500 μ M). Data expressed as fold change (FCH) over basal level (represented by — and dotted line). Boxplots

indicate median ($Q^1 - Q^3$) of 4 independent experiments, with bars outlining min and max values. P -values calculated using Kruskal-Wallis test: ns $P > .05$.

Macrophage migration inhibitory factor (MIF) is a highly pleiotropic mediator that primarily evokes innate immune responses and inflammation (Calandra and Roger, 2003). Here, MIF was detected in cellular supernatant; however, relative levels were statistically unchanged by agonist stimulation: $H(3) = 5.642$, $P = .1257$ (**Figure 3.27**). TRPA1 and TRPV1 agonists failed to increase median MIF levels. These data were statistically comparable to baseline ($P > .9999$ for both). The TRPV3 agonist altered MIF secretion, however, this change was highly varied. FCH values ranged from 16% to 444% above baseline (FCH = 0.160 and 4.439). This trend was approaching significance ($P = .0746$). Thus, activation of the TRPV3 channel may promote MIF release from human epidermal keratinocytes.

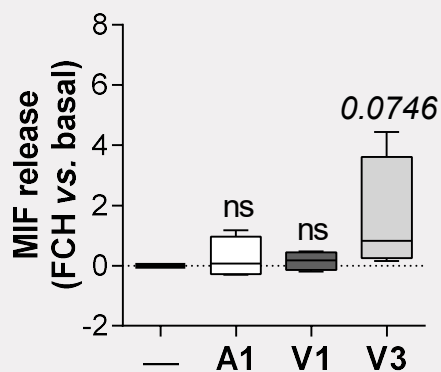


Figure 3.27. Effect of TRP agonists on MIF release.

Graph compares release of macrophage migration inhibitory factor (MIF) from keratinocytes (NHEK) following application of basal medium \pm TRP agonists [1 h]: AITC (TRPA1 agonist [A1], 100 μ M); capsaicin (TRPV1 agonist [V1], 1 μ M); drofenine (TRPV3 agonist [V3], 500 μ M). Data expressed as fold change (FCH) over basal level (represented by — and dotted line). Boxplots indicate median ($Q^1 - Q^3$) of 4 independent experiments, with bars outlining min and max values. P -values calculated using Kruskal-Wallis test: ns $P > .05$.

Neutrophil gelatinase-associated lipocalin (NGAL) is potent bacteriostatic agent, which is released from neutrophil granules at the site of infection or inflammation (Goetz *et al.*, 2002). Here, NGAL was detected in cellular supernatant; however, relative levels were statistically unchanged by agonist stimulation: $H(3) = 1.545$, $P = .7060$ (**Figure 3.28**). The post-hoc comparison failed to detect significant differences between agonist groups and baseline levels ($P = .7855$ [TRPA1]; $P > .9999$ [TRPV1]; $P > .9999$ [TRPV3]). Thus, TRPA1, TRPV1, and TRPV3 agonists fail to evoke NGAL release from human epidermal keratinocytes.

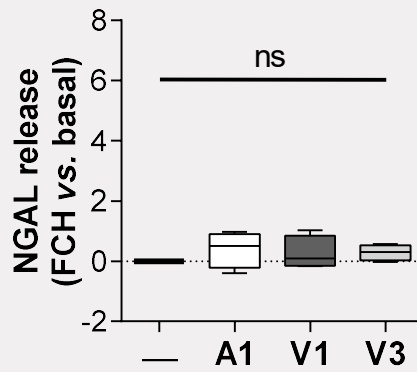


Figure 3.28. Effect of TRP agonists on NGAL release.

Graph compares release of neutrophil gelatinase-associated lipocalin (NGAL) from keratinocytes (NHEK) following application of basal medium \pm TRP agonists [1 h]: AITC (TRPA1 agonist [A1], 100 μ M); capsaicin (TRPV1 agonist [V1], 1 μ M); drofenine (TRPV3 agonist [V3], 500 μ M). Data expressed as fold change (FCH) over basal level (represented by — and dotted line). Boxplots indicate median ($Q^1 - Q^3$) of 4 independent experiments, with bars outlining min and max values. P -values calculated using Kruskal-Wallis test: ns $P > .05$.

Plasminogen activator inhibitor 1 (PAI-1), also known as serine protease inhibitor E1 (Serpin E1), regulates fibrinolysis – a key step in wound healing – through inhibition of tissue-type plasminogen activator (t-PA) and urokinase-type plasminogen activator (u-PA) (Lijnen, 2005). Here, PAI-1 was detected in cellular supernatant; however, although approaching significance, relative levels were statistically unchanged by agonist stimulation: $H(3) = 6.336$, $P = .0861$ (**Figure 3.29**). Relative PAI-1 levels showed high levels of variation, with later TRPA1 and TRPV3 replicates showing increases of more than 200% (FCH = 2.290 and 2.790, respectively). Although the post-hoc comparison failed to detect significant differences between agonist groups and baseline levels, FCH data from the TRPV3 group were approaching significance ($P = .0613$). Thus, the TRPV3 agonist may promote PAI-1 release from human epidermal keratinocytes.

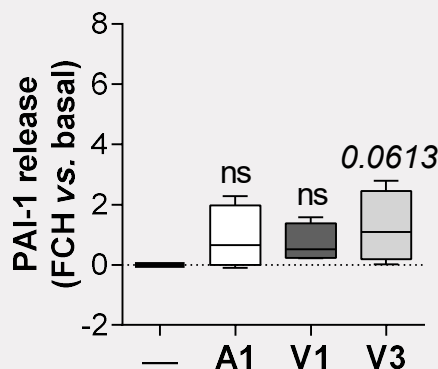


Figure 3.29. Effect of TRP agonists on PAI-1 release.

Graph compares release of plasminogen activator inhibitor 1 (PAI-1) from keratinocytes (NHEK) following application of basal medium \pm TRP agonists [1 h]: AITC (TRPA1 agonist [A1], 100 μ M); capsaicin (TRPV1 agonist [V1], 1 μ M); drofenine (TRPV3 agonist [V3], 500 μ M). Data expressed as fold change (FCH) over basal level (represented by — and dotted line). Boxplots indicate median ($Q^1 - Q^3$) of 4 independent experiments, with bars outlining min and max values. P -values calculated using Kruskal-Wallis test: ns $P > .05$.

Platelet derived growth factor subunit A (PDGFA) activates cutaneous mesenchymal cells and facilitates tissue repair (Heldin and Westermark, 1999). Here, PDGFA was detected in cellular supernatant; however, although approaching significance, relative levels were statistically unchanged by agonist stimulation: $H(3) = 7.142$, $P = .0531$ (**Figure 3.30**). TRPA1 and TRPV1 agonists failed to consistently increase median PDGFA levels. These data were statistically comparable to baseline ($P = .2995$ and $P = .2561$, respectively). The TRPV3 agonist evoked a small but significant increase in PDGFA secretion, with median levels reaching about 160% above baseline (FCH = 1.684; $P = .0266$). Thus, the TRPV3 agonist may promote PDGFA release from human epidermal keratinocytes.

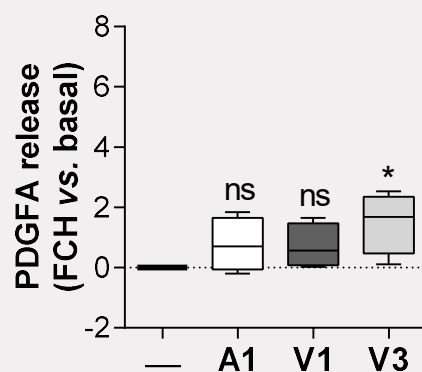


Figure 3.30. Effect of TRP agonists on PDGFA release.

Graph compares release of platelet derived growth factor subunit A (PDGFA) from keratinocytes (NHEK) following application of basal medium \pm TRP agonists [1 h]: AITC (TRPA1 agonist [A1], 100 μ M); capsaicin (TRPV1 agonist [V1], 1 μ M); drofenine (TRPV3 agonist [V3], 500 μ M). Data expressed as fold change (FCH) over basal level (represented by — and dotted line). Boxplots indicate median ($Q^1 - Q^3$) of 4 independent experiments, with bars outlining min and max values. P -values calculated using Kruskal-Wallis test: ns $P > .05$; * $P \leq .05$.

Pentraxin-related protein PTX3 (PTX3) is an innate immune protein and activator of the classical complement pathway (Garlanda *et al.*, 2018). Here, PTX3 was detected in cellular supernatant; however, relative levels were statistically unchanged by agonist stimulation: $H(3) = 6.179$, $P = .0943$ (**Figure 3.31**). Although the post-hoc comparison failed to detect significant differences between agonist groups and baseline levels, FCH data from the TRPV3 group were approaching significance ($P = .0746$). Thus, the TRPV3 agonist may promote PTX3 release from human epidermal keratinocytes.

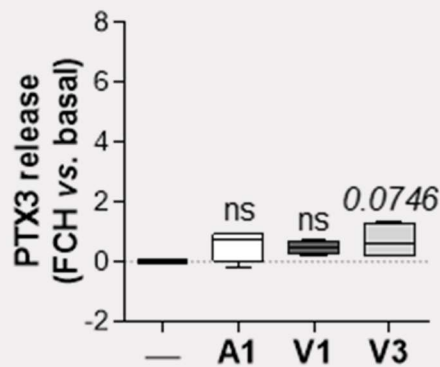


Figure 3.31. Effect of TRP agonists on PTX3 release.

Graph compares release of pentraxin-related protein PTX3 (PTX3) from keratinocytes (NHEK) following application of basal medium \pm TRP agonists [1 h]: AITC (TRPA1 agonist [A1], 100 μ M); capsaicin (TRPV1 agonist [V1], 1 μ M); drofenine (TRPV3 agonist [V3], 500 μ M). Data expressed as fold change (FCH) over basal level (represented by — and dotted line). Boxplots indicate median ($Q^1 - Q^3$) of 4 independent experiments, with bars outlining min and max values. P -values calculated using Kruskal-Wallis test: ns $P > .05$.

Transferrin receptor protein 1 (TfR) facilitates cellular iron uptake, binding to transferrin and stimulating receptor-mediated endocytosis of the transferrin-iron complex (Mayle *et al.*, 2012). Here, TfR was detected in cellular supernatant; however, although approaching significance, relative levels were statistically unchanged by agonist stimulation: $H(3) = 6.784$, $P = .0658$ (**Figure 3.32**). TRPA1 and TRPV1 agonists failed to increase median TfR levels. These data were statistically comparable to baseline ($P = .3487$ and $P = .1554$, respectively). The TRPV3 agonist evoked a small but significant increase in TfR secretion, with median levels reaching more than 90% above baseline (FCH = 0.914; $P = .0408$). Thus, the TRPV3 agonist may promote TfR release from human epidermal keratinocytes.

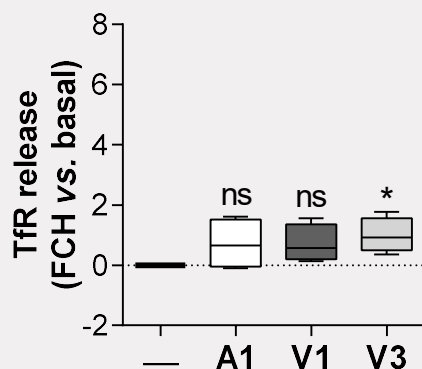


Figure 3.32. Effect of TRP agonists on Tfr release.

Graph compares release of transferrin receptor protein 1 (Tfr) from keratinocytes (NHEK) following application of basal medium \pm TRP agonists [1 h]: AITC (TRPA1 agonist [A1], 100 μ M); capsaicin (TRPV1 agonist [V1], 1 μ M); drofenine (TRPV3 agonist [V3], 500 μ M). Data expressed as fold change (FCH) over basal level (represented by — and dotted line). Boxplots indicate median ($Q^1 - Q^3$) of 4 independent experiments, with bars outlining min and max values. P -values calculated using Kruskal-Wallis test: ns $P > .05$.

Transforming growth factor alpha (TGF- α) is a key inducer of EGF signalling and epithelial development (Wee and Wang, 2017). Here, TGF- α was detected in cellular supernatant; relative levels were significantly affected by agonist stimulation: $H(3) = 9.112$, $P = .0112$ (**Figure 3.33**). TRPA1 and TRPV1 agonists failed to increase median TGF- α levels. These data were statistically comparable to baseline ($P = .8849$ and $P > .9999$, respectively). The TRPV3 agonist significantly increased median TGF- α levels ($P = .0106$). Thus, activation of the TRPV3 channel promotes TGF- α release from human epidermal keratinocytes.

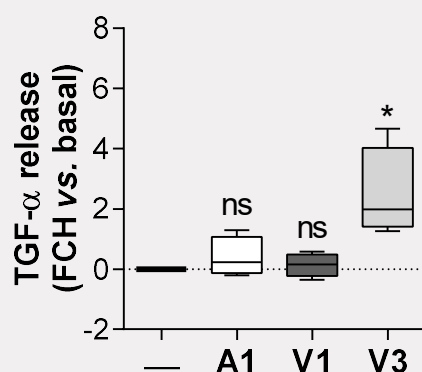


Figure 3.33. Effect of TRP agonists on TGF- α release.

Graph compares release of transforming growth factor alpha (TGF- α) from keratinocytes (NHEK) following application of basal medium \pm TRP agonists [1 h]: AITC (TRPA1 agonist [A1], 100 μ M); capsaicin (TRPV1 agonist [V1], 1 μ M); drofenine (TRPV3 agonist [V3], 500 μ M). Data expressed as fold change (FCH) over basal level (represented by — and dotted line). Boxplots indicate median

($Q^1 - Q^3$) of 4 independent experiments, with bars outlining min and max values. P -values calculated using Kruskal-Wallis test: ns $P > .05$; * $P \leq .05$.

Thrombospondin-1 (TSP-1) is an extracellular matrix factor involved in tissue remodelling (Murphy-Ullrich, 2019). Here, TSP-1 was detected in cellular supernatant; however, relative levels were statistically unchanged by agonist stimulation: $H(3) = 5.664$, $P = .1244$ (**Figure 3.34**). The post-hoc comparison failed to detect significant differences between agonist groups and baseline levels ($P = .6105$ [TRPA1]; $P = .1087$ [TRPV1]; $P > .9999$ [TRPV3]). Thus, TRPA1, TRPV1, and TRPV3 agonists fail to evoke TSP-1 release from human epidermal keratinocytes.

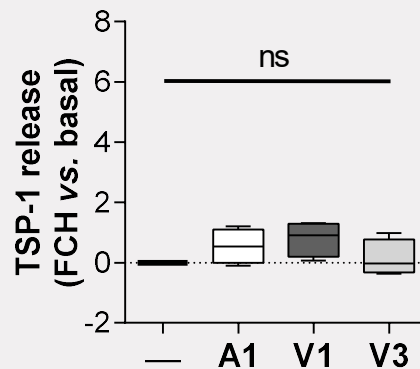


Figure 3.34. Effect of TRP agonists on TSP-1 release.

Graph compares release of thrombospondin-1 (TSP-1) from keratinocytes (NHEK) following application of basal medium \pm TRP agonists [1 h]: AITC (TRPA1 agonist [A1], 100 μ M); capsaicin (TRPV1 agonist [V1], 1 μ M); drofenine (TRPV3 agonist [V3], 500 μ M). Data expressed as fold change (FCH) over basal level (represented by — and dotted line). Boxplots indicate median ($Q^1 - Q^3$) of 4 independent experiments, with bars outlining min and max values. P -values calculated using Kruskal-Wallis test: ns $P > .05$.

Vitamin D binding protein (VDBP) acts as the primary carrier of Vitamin D and its metabolites, transporting them from the skin to the liver and kidneys and modulating their delivery to target tissues (Pop *et al.*, 2022). Here, VDBP was detected in cellular supernatant; however, relative levels were statistically unchanged by agonist stimulation: $H(3) = 2.306$, $P = .5447$ (**Figure 3.35**). Post-hoc comparison failed to detect significant differences between agonist groups and baseline levels ($P = .5345$ [TRPA1]; $P = .6105$ [TRPV1]; $P = .9924$ [TRPV3]). Thus, TRPA1, TRPV1, and TRPV3 agonists fail to evoke consistent VDBP release from human epidermal keratinocytes.

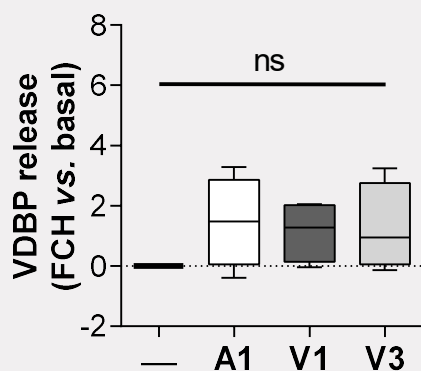


Figure 3.35. Effect of TRP agonists on VDBP release.

Graph compares release of vitamin D binding protein (VDBP) from keratinocytes (NHEK) following application of basal medium \pm TRP agonists [1 h]: AITC (TRPA1 agonist [A1], 100 μ M); capsaicin (TRPV1 agonist [V1], 1 μ M); drofenine (TRPV3 agonist [V3], 500 μ M). Data expressed as fold change (FCH) over basal level (represented by — and dotted line). Boxplots indicate median ($Q^1 - Q^3$) of 4 independent experiments, with bars outlining min and max values. *P*-values calculated using Kruskal-Wallis test: ns $P > .05$.













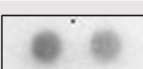




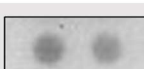




Together, these data suggest that TRPV1 and TRPA1 agonists are unable to induce consistent mediator release from cultured epidermal keratinocytes. Conversely, the TRPV3 agonist evoked significant release of Dkk-1, EGF, FGF-19, IL-1 α , PDGFA, TfR, and TGF- α . These TRPV3-linked mediators coordinate cellular proliferation, migration, and differentiation to modulate cutaneous tissue repair. Here, we noted a high level of inter-replicate variability, reducing the statistical power of our analyses. Other mediators (BSG, IL-1ra, MIF, PAI-1, and PTX3) showed a trend towards a statistical increase following TRPV3 agonist application. These factors coordinate innate immune responses, modulate IL-1 inflammation, and facilitate wound healing. Future replicates are required to establish whether TRPV3 activation could promote the secretion of these epidermal mediators.

3.2.4. The TRPV3 agonist promotes mediator release

TRPV3 expression is upregulated in skin from patients with atopic dermatitis and psoriasis – 2 key inflammatory skin conditions (Seo *et al.*, 2020; Larkin *et al.*, 2021). Though work is ongoing, our understanding of the link between TRPV3 activation and inflammation remains incomplete. In the previous section, our data suggested that the TRPV3 channel may act as a coordinator of epidermal signalling and tissue repair; however, high levels of inter-replicate variation reduced the statistical power of this work. Thus, this section employs further replication to establish whether TRPV3 activation can promote the secretion of key mediators from normal human epidermal keratinocytes (NHEK), a culture model of human epidermis.

NHEK were stimulated with basal medium \pm TRPV3 agonist (drofenine, 500 μ M) [1 h, 37°C]. Following stimulation, cell supernatant was collected and pooled. Mediator release was compared using the cytokine array. Briefly, when present in the supernatant sample, the named protein binds to capture antibodies located at duplicate spots on a nitrocellulose membrane. Chemiluminescent development reveals the relative levels of each released protein. Here, a number of proteins were consistently detected: Basigin (BSG), dickkopf-1 (Dkk-1), epidermal growth factor (EGF), interleukin-1 alpha (IL-1 α), interleukin 1 receptor antagonist (IL-1ra), macrophage migration inhibitory factor (MIF), neutrophil gelatinase-associated lipocalin (NGAL), plasminogen activator inhibitor 1 (PAI-1), platelet derived growth factor subunit A (PDGFA), transforming growth factor alpha (TGF- α), and thrombospondin-1 (TSP-1) (**Table 3.3**).

Table 3.3. Representative images of duplicate antibody spots from cytokine array showing effect of TRPV3 agonist on mediator release.

Mediator	Basal	TRPV3
BSG		
Dkk-1		
EGF		
IL-1 α		
IL-1ra		
MIF		
NGAL		
PAI-1		
PDGFA		
TGF- α		
TSP-1		

Note: Table includes images of duplicate spots; antibodies at each spot bind to a named mediator. Average densitometry of these duplicates equals one experimental replicate. *Abbreviations:* BSG, basigin; Dkk-1, dickkopf-1; EGF, epidermal growth factor; IL-1 α , interleukin-1 alpha; IL-1ra, interleukin 1 receptor antagonist; MIF, macrophage migration inhibitory factor; NGAL, neutrophil gelatinase-associated lipocalin; PAI-1, plasminogen activator inhibitor 1; PDGFA, platelet derived growth factor subunit A; TGF- α , transforming growth factor alpha; TRPV3, transient receptor potential vanilloid 3; and TSP-1, thrombospondin-1.

Duplicate antibody spots were then measured using densitometry. Average pixel density of each duplicate pair represents one experimental replicate. Average pixel density data were expressed as fold change (FCH) relative to basal medium-treated samples (n=12). Prior to statistical analyses, the distribution of TRPV3 (FCH) data were examined using the Shapiro-Wilk normality test. Several sets failed the normality test indicating that they departed significantly from the Gaussian distribution: BSG ($P = .0024$); Dkk-1 ($P = .0003$); EGF ($P = .0027$); IL-1 α ($P = .0306$); IL-1ra ($P = .0002$); MIF ($P = .0020$); and PDGFA ($P = .0120$). Other sets passed the normality test: NGAL ($P = .2363$); PAI-1 ($P = .8641$); TGF- α ($P = .1284$); and TSP-1 ($P = .4917$). To account for this deviation from the Gaussian distribution, FCH data were presented as median FCH and interquartile range ($Q^1 - Q^3$) and were analysed using the nonparametric Kruskal-Wallis test plus Dunn's multiple comparison post-test (Basal vs. TRPV3).

The graph below reveals the relative change of each named protein, highlighting the link between TRPV3 stimulation and mediator release (**Figure 3.36**). This comparison revealed several important changes. Release of BSG, a protein involved in tissue remodelling, was significantly increased in the TRPV3 group ($P = .0005$). Release of Dkk-1, a negative regulator of Wnt signalling, was significantly increased in the TRPV3 group ($P = .0010$). Release of EGF, a potent growth factor, was significantly increased in the TRPV3 group ($P = .0005$). Release of IL-1 α , a key initiator of early inflammation, was significantly increased in the TRPV3 group ($P = .0005$). Release of IL-1ra, a competitive inhibitor of IL-1 signalling, was significantly increased in the TRPV3 group ($P = .0010$). Release of MIF, a highly pleiotropic mediator, was significantly increased in the TRPV3 group ($P = .0024$). Release of NGAL, a bacteriostatic agent, was statistically unchanged in the TRPV3 group ($P = .0923$). Release of PAI-1, a modulator of wound healing, was significantly increased in the TRPV3 group ($P = .0068$). Release of PDGFA, a mitogenic factor, was significantly increased in the TRPV3 group ($P = .0369$). Release of TGF- α , a key inducer of EGF signalling and epithelial development, was significantly increased in the TRPV3 ($P = .0005$). Release of TSP-1, an extracellular matrix factor, was statistically unchanged in the TRPV3 group ($P = .7910$). Together, the TRPV3 agonist evoked significant release of 9 mediators from epidermal keratinocytes: BSG, Dkk-1, EGF, IL-1 α , IL-1ra, MIF, PAI-1, PDGFA, and TGF- α . These data confirm that TRPV3 is expressed and functional in the NHEK model, with agonist-mediated activation driving notable mediator release. Together with findings from the previous section, these data suggest that the TRPV3 channel functions as a coordinator of epidermal signalling and tissue repair.

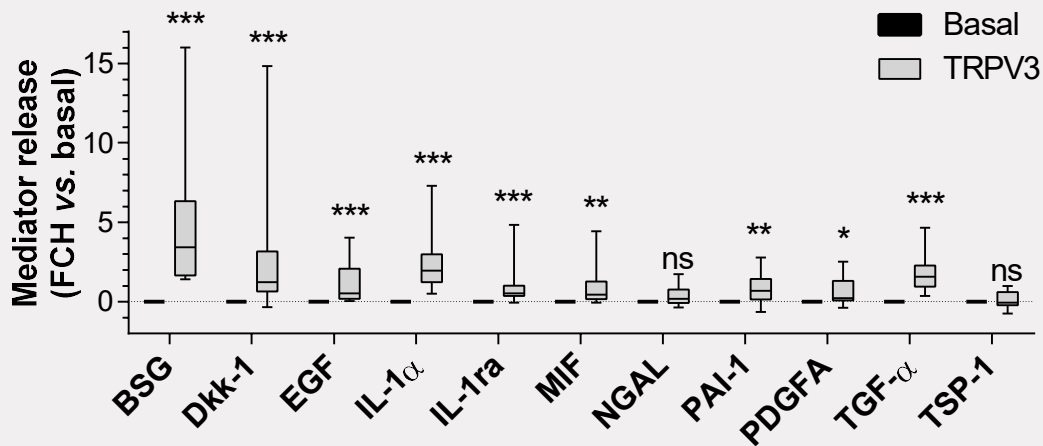


Figure 3.36. Further analyses investigating effect of the TRPV3 agonist on mediator release.

Graph shows relative release of named mediators from keratinocytes (NHEK). Keratinocytes were stimulated with basal medium \pm drofenine (TRPV3 agonist, 500 μ M): Basal vs. TRPV3. Data expressed relative to basal levels (represented by — and dotted line). Plots indicate median of 12 independent experiments, with bars outlining min and max values. *P*-values calculated using one-sample Wilcoxon signed rank test; ns *P* > .05.


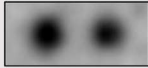
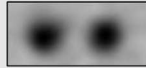






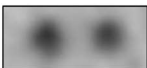

















TRPV3-linked mediators have been associated with inflammatory skin conditions. Briefly, BSG, Dkk-1 and TGF- α are increased in psoriatic skin; dysregulated IL-1 α drives hidradenitis suppurativa; and PAI-1 promotes acute and atopic itch (Peng *et al.*, 2017; Okubo *et al.*, 2022; Seifert *et al.*, 2015; Tzanetakou *et al.*, 2016; Kanni *et al.*, 2018; Larkin *et al.*, 2021). Together, these findings reveal the nuanced role of TRPV3 in the skin and highlight the potential impact of dysregulated epidermal TRPV3 signalling in human skin conditions.

3.2.5. TRPV3-linked mediator release is independent of JNK signalling

Kinase proteins coordinate downstream signalling, promote specific biological effects, and represent important targets for drug development. Mediator release experiments suggested that TRPV3 may play a role in epidermal signaling in normal and diseased skin. Phospho-kinase experiments revealed a link between TRPV3 agonist application and phosphorylation of c-Jun at the serine 63 (S63) residue. This residue is phosphorylated by the Jun N-terminal kinase (JNK) proteins (Dunn *et al.*, 2002). Here, we use a pan-JNK inhibitor to investigate whether the JNK/c-Jun signalling axis regulates TRPV3-linked mediator release from normal human epidermal keratinocytes (NHEK), a common culture model of human epidermis.

NHEK were pre-treated with basal medium \pm JNK-IN-8 (JNK inhibitor; 1 μ M) [1 h, 37°C]. Following inhibitor pre-treatment, cells were stimulated with drofenine (TRPV3 agonist; 500 μ M) \pm JNK-IN-8 (1 μ M) [1 h, 37°C]. Following stimulation, cell supernatant was collected and pooled. Mediator release was compared using the cytokine array. Briefly, when present in the supernatant sample, the named protein binds to capture antibodies located at duplicate spots on a nitrocellulose membrane. Chemiluminescent development reveals the relative levels of each released protein. Here, a number of proteins were consistently detected: Basigin (BSG), dickkopf-1 (Dkk-1), epidermal growth factor (EGF), interleukin-1 alpha (IL-1 α), interleukin 1 receptor antagonist (IL-1ra), macrophage migration inhibitory factor (MIF), plasminogen activator inhibitor 1 (PAI-1), platelet derived growth factor subunit A (PDGFA), and transforming growth factor alpha (TGF- α) (**Table 3.4**).

Table 3.4. Representative images of duplicate antibody spots from cytokine array showing effect of JNK inhibitor on TRPV3 agonist-induced mediator release.

Mediator	Basal [Control]	TRPV3 [Control]	TRPV3 [JNK-IN-8]
BSG			
Dkk-1			
EGF			
IL-1 α			
IL-1ra			
MIF			
PAI-1			
PDGFA			
TGF- α			

Note: JNK-IN-8 inhibits the JNK kinase protein. Table includes images of duplicate spots; antibodies at each spot bind to a named mediator. Average densitometry of these duplicates equals one experimental replicate. *Abbreviations:* BSG, basigin; Dkk-1, dickkopf-1; EGF, epidermal growth factor; IL-1 α , interleukin-1 alpha; IL-1ra, interleukin 1 receptor antagonist; MIF, macrophage migration inhibitory factor; PAI-1, plasminogen activator inhibitor 1; PDGFA, platelet derived growth factor subunit A; TGF- α , transforming growth factor alpha; and TRPV3, transient receptor potential vanilloid 3.

Duplicate antibody spots were then measured using densitometry. Average pixel density of each duplicate pair represents one experimental replicate. Average pixel density data were expressed as fold change (FCH) relative to basal medium-treated samples (n = 3). To examine the impact of JNK inhibition on drofenine-induced mediator release, FCH data were expressed as a percentage of normal TRPV3 agonist-induced release (i.e. allowing the control TRPV3 group to equal 100%, matched). Data were presented as median and interquartile range ($Q^1 - Q^3$) and were analysed using the nonparametric Wilcoxon signed rank test (vs. 100%: TRPV3 [Control]).

The JNK inhibitor, JNK-IN-8, was unable to significantly reduce TRPV3-associated mediator release in human epidermal keratinocytes (**Figure 3.37**). Median evoked BSG levels were 5% higher in TRPV3 [JNK-IN-8] (105.1%; $P=1.000$). Median evoked Dkk-1 levels were 7% higher in TRPV3 [JNK-IN-8] (107.2%; $P=1.000$). Median evoked EGF levels were 6% higher in TRPV3 [JNK-IN-8] (106.4%; $P=1.000$). Median evoked IL-1 α levels were 3% higher in TRPV3 [JNK-IN-8] (102.8%; $P=1.000$). Median evoked IL-1ra levels were 7% higher in TRPV3 [JNK-IN-8] (106.6%; $P=1.000$). Median evoked MIF levels were unchanged in TRPV3 [JNK-IN-8] (99.8%; $P=1.000$). Median evoked PAI-1 levels were 3% higher in TRPV3 [JNK-IN-8] (103.3%; $P=.7500$). Median evoked PDGFA levels were 6% higher in TRPV3 [JNK-IN-8] (106.4%; $P=.7500$). Median evoked TGF- α levels were 6% higher in TRPV3 [JNK-IN-8] (106.0%; $P=.5000$). Overall, TRPV3-linked secretion was statistically comparable in control and JNK-IN-8 pre-treated keratinocytes.

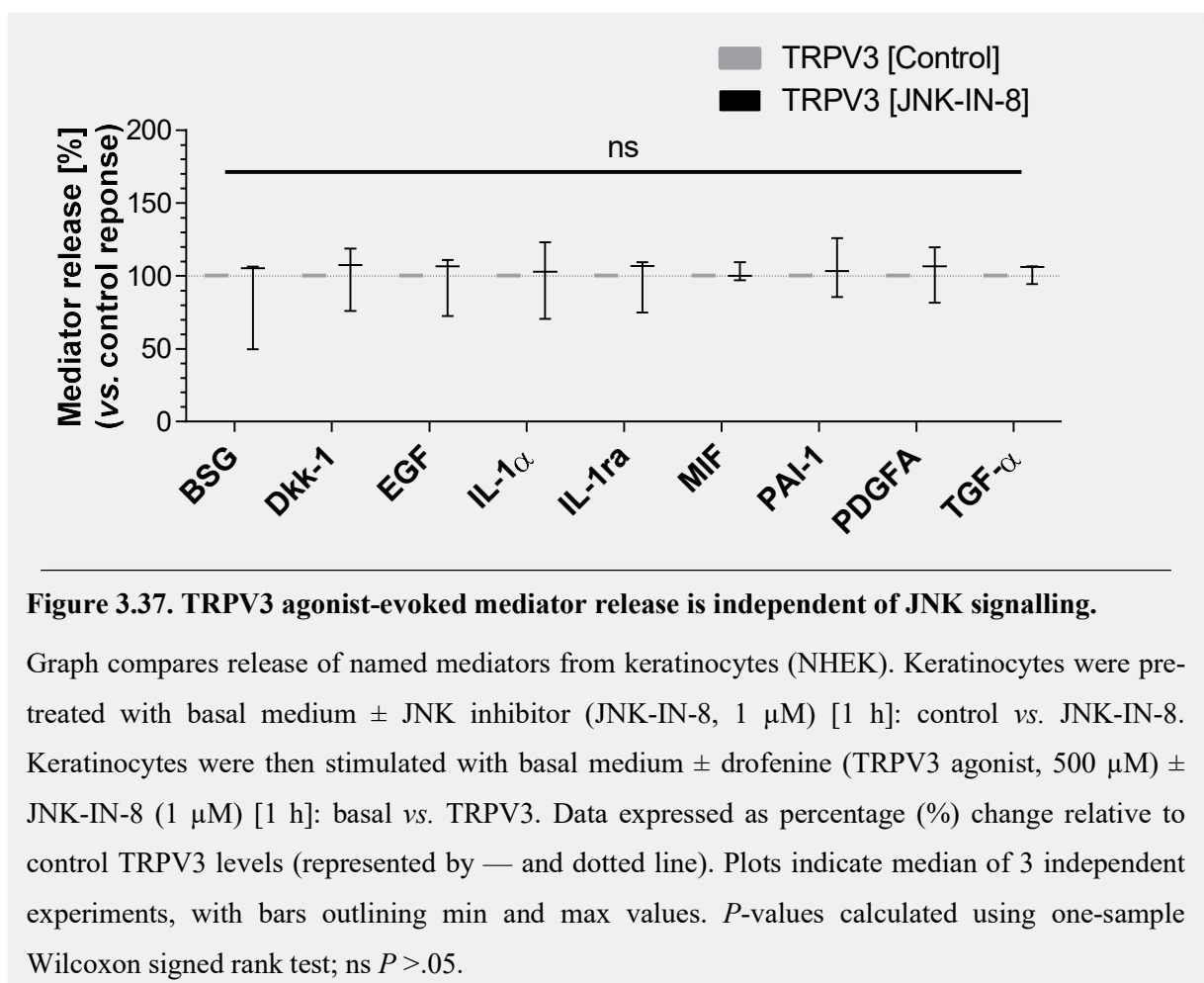


Figure 3.37. TRPV3 agonist-evoked mediator release is independent of JNK signalling.

Graph compares release of named mediators from keratinocytes (NHEK). Keratinocytes were pre-treated with basal medium \pm JNK inhibitor (JNK-IN-8, 1 μ M) [1 h]: control vs. JNK-IN-8. Keratinocytes were then stimulated with basal medium \pm drofenine (TRPV3 agonist, 500 μ M) \pm JNK-IN-8 (1 μ M) [1 h]: basal vs. TRPV3. Data expressed as percentage (%) change relative to control TRPV3 levels (represented by — and dotted line). Plots indicate median of 3 independent experiments, with bars outlining min and max values. P -values calculated using one-sample Wilcoxon signed rank test; ns $P > .05$.

Together, these data indicate that TRPV3-associated mediator release is independent of JNK signalling in the NHEK model of human epidermis. Other kinase proteins are also capable of phosphorylating c-Jun. These include RhoA/ROCK, CDK5, and VRK1. Thus, c-Jun may drive TRPV3-linked mediator release via a JNK-independent pathway.

3.2.6. Keratinocytes in our NHEK model express key SNARE proteins

Soluble N-ethylmaleimide-sensitive fusion protein attachment protein receptors, or SNAREs, facilitate membrane fusion. This process underpins both the controlled release of certain mediators and the trafficking of membrane-bound receptors. Briefly, SNARE-dependent fusion involves a high-affinity interaction between vesicle-SNAREs (v-SNAREs) and plasma membrane target SNAREs (t-SNAREs). The SNARE complex draws vesicle and plasma membranes together, facilitating membrane fusion. Thus, when identified, SNARE proteins represent important and highly specific targets for the modulation of inflammation and/or functional receptor upregulation.

Fluorescent immunocytochemistry was used to examine the expression of key SNARE proteins in cultured normal human epidermal keratinocytes (NHEK). NHEK were labelled with antibodies targeting SNAP23, SNAP29, syntaxin 3, syntaxin 4, syntaxin 16, VAMP3, and/or VAMP7 (see **Table 2.3** for details). Samples were then imaged using confocal microscopy.

SNAP23 and syntaxin 3 signals were detected in all stained keratinocytes (**Figure 3.38, upper panel**). Overlap images suggest that SNAP23 and syntaxin 3 are associated with distinct cellular regions: while both were detected in the perinuclear and nuclear regions, SNAP23 was also localised to the plasma membrane. These signals were not detected in negative control samples (**Figure 3.38, lower panel**).

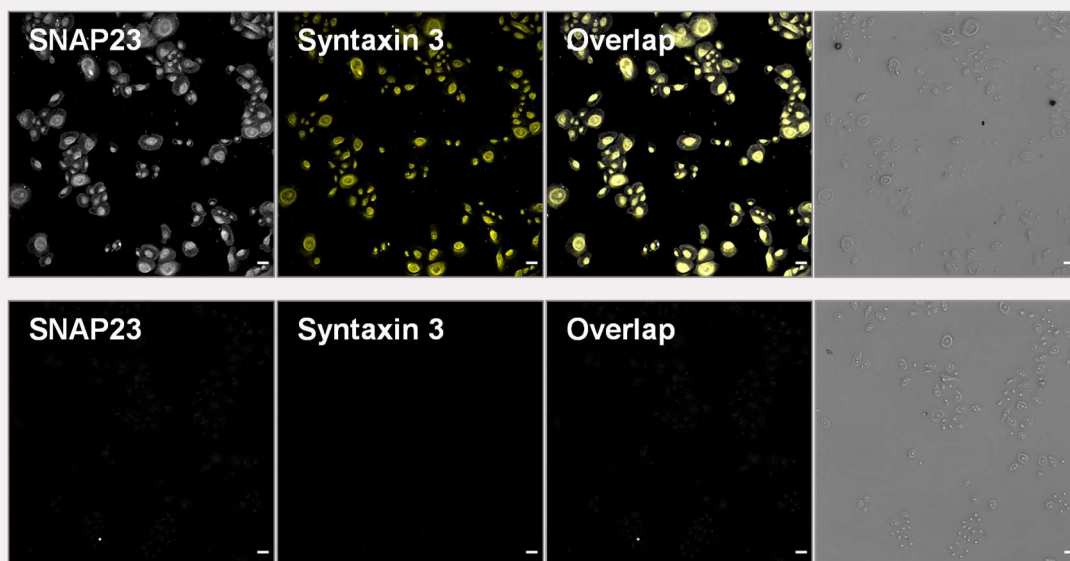


Figure 3.38. Keratinocytes in our NHEK model express SNAP23 and syntaxin 3 SNARE proteins.

Immunostaining of keratinocytes (NHEK) indicating expression of named proteins: SNAP23 and syntaxin 3 (*upper panel*) vs. negative control (*lower panel*). Original magnification 20x. Scale bars =50 μm .

Both SNAP29 and syntaxin 16 signals were detected in all stained keratinocytes, however, levels of SNAP29 expression were highly varied (**Figure 3.39**, *upper panel*). Although both are localised to the perinuclear and nuclear regions, syntaxin 16 is also detected in the cytoplasmic area. These signals were not detected in negative control samples (**Figure 3.39**, *lower panel*).

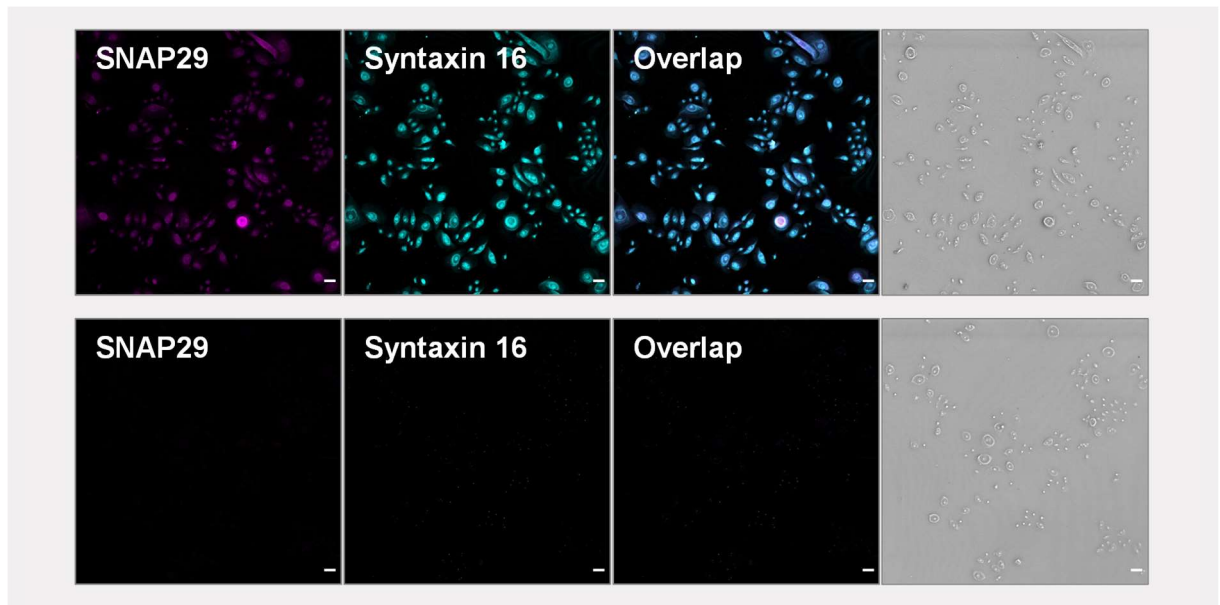


Figure 3.39. Keratinocytes in our NHEK model express SNAP29 and syntaxin 16 SNARE proteins.

Immunostaining of keratinocytes (NHEK) indicating expression of SNAP29 and syntaxin 16 (*upper panel*) vs. negative control (*lower panel*). Original magnification 20x. Scale bars =50 μ m.

VAMP3 and syntaxin 4 signals were detected in all stained keratinocytes (**Figure 3.40**, *upper panel*). Syntaxin 4 was primarily localised to the cytoplasmic area. In contrast, the cellular location of VAMP3 was varied, with larger cells showing higher levels of cytoplasmic expression. These signals were not detected in negative control samples (**Figure 3.40**, *lower panel*).

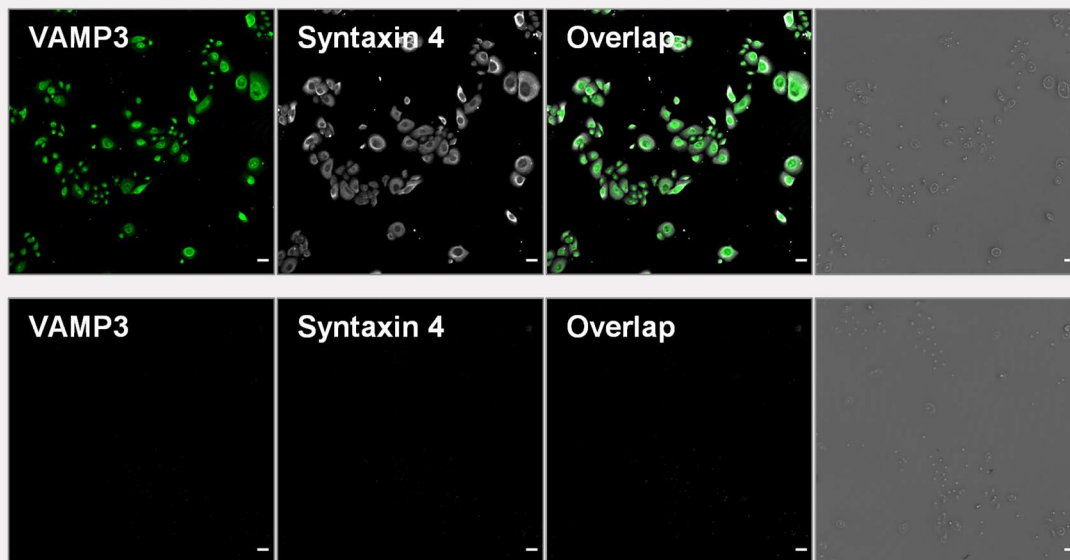
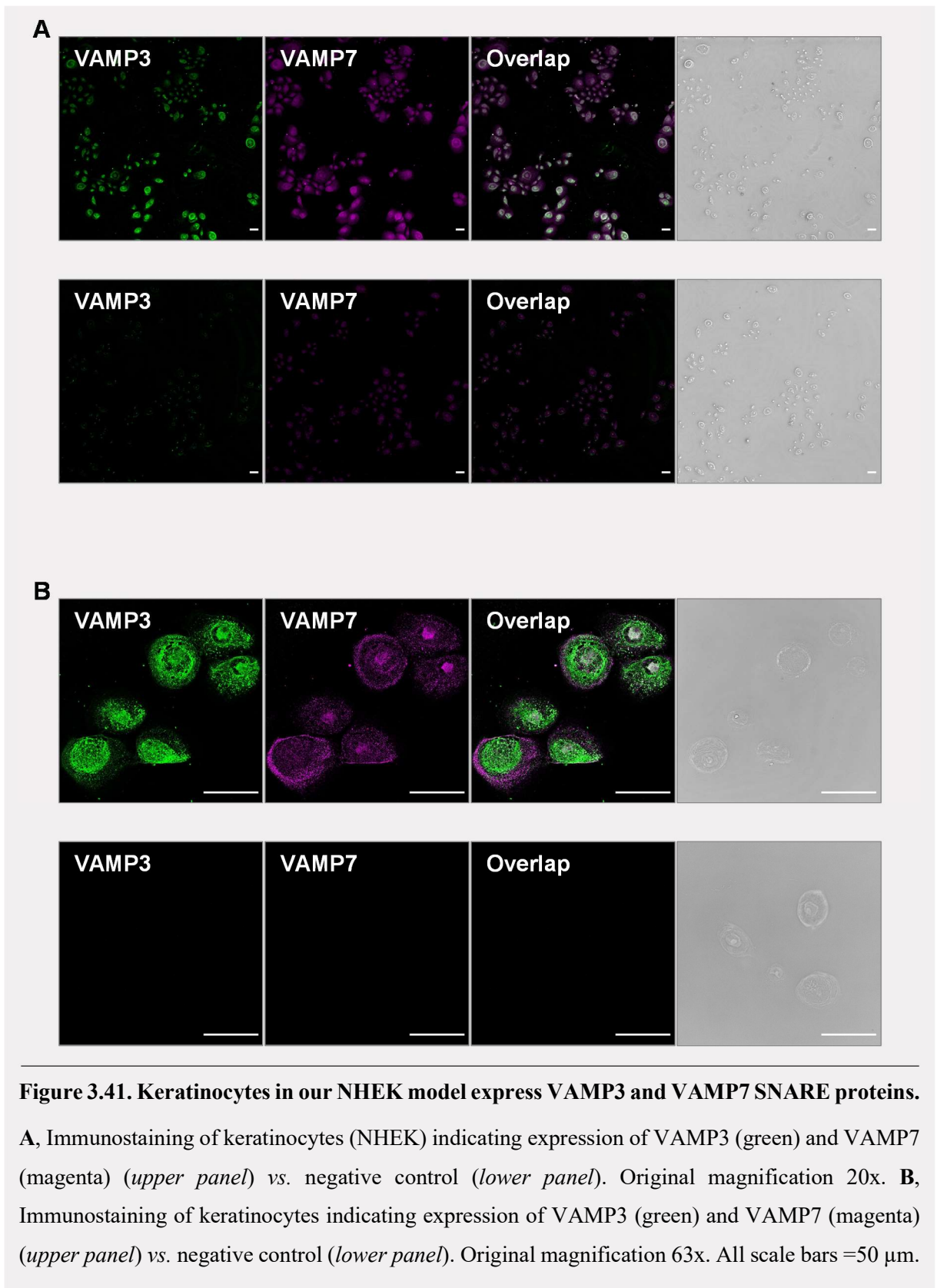


Figure 3.40. Keratinocytes in our NHEK model express VAMP3 and syntaxin 4 SNARE proteins.

Immunostaining of keratinocytes (NHEK) indicating expression of VAMP3 and syntaxin 4 (*upper panel*) vs. negative control (*lower panel*). Original magnification 20x. Scale bars =50 μm .

VAMP7 signals were detected in all stained keratinocytes (**Figure 3.41A, upper panel**). VAMP7 was localised to the cytoplasmic and perinuclear areas. VAMP3 was detected in perinuclear and nuclear regions, though larger cells showed higher levels of cytoplasmic expression. These signals were not detected in negative control samples (**Figure 3.41A, lower panel**). To further examine VAMP3 and VAMP7 staining, samples were also examined at a higher magnification. These images confirmed VAMP3 and VAMP7 expression in keratinocytes and revealed distinct differences in protein expression (**Figure 3.41B, upper panel**). While both VAMP3 and VAMP7 displayed punctate staining in the cytoplasmic and perinuclear regions, some cells also showed high levels of VAMP7 at the cell surface. Moreover, closer examination of the overlap image indicates that VAMP3 and VAMP7 may label distinct and non-overlapping populations of exocytotic vesicles. Importantly, these signals were not detected in negative control samples (**Figure 3.41B, lower panel**). Together, these images confirm that keratinocytes in our NHEK model express crucial SNARE proteins.



3.2.7. Knockdown of VAMP3 alters TRPV3-linked mediator release

Soluble N-ethylmaleimide-sensitive fusion protein attachment protein receptors, or SNAREs, facilitate intracellular vesicle fusion and mediate the controlled release of a variety of cytokines, chemokines, and other signalling mediators. Briefly, SNARE-dependent fusion involves a high-affinity interaction between vesicle-SNAREs (v-SNAREs) and plasma membrane target SNAREs (t-SNAREs); the SNARE complex draws vesicle and plasma membranes together, facilitating membrane fusion. Recent publications have highlighted the importance of the VAMP3 v-SNARE in epidermal inflammation (Meng *et al.*, 2019). Here, we examined whether TRPV3-linked mediator release was facilitated by VAMP3-dependent exocytosis in normal human epidermal keratinocytes (NHEK). Using short-hairpin RNA (shRNA), we assessed impact of VAMP3 knockdown on TRPV3 agonist-induced mediator release.

NHEK were treated with control nontargeted (NT) or VAMP3-targeted (V3T) shRNA particles. After puromycin-mediated selection, shRNA-expressing keratinocytes were termed NT and V3T. Successful VAMP3 knockdown was confirmed by western blotting (**Figure 3.42A**): in V3T cells, VAMP3 expression was reduced by about 97% relative to NT basal levels (**Figure 3.42B**).

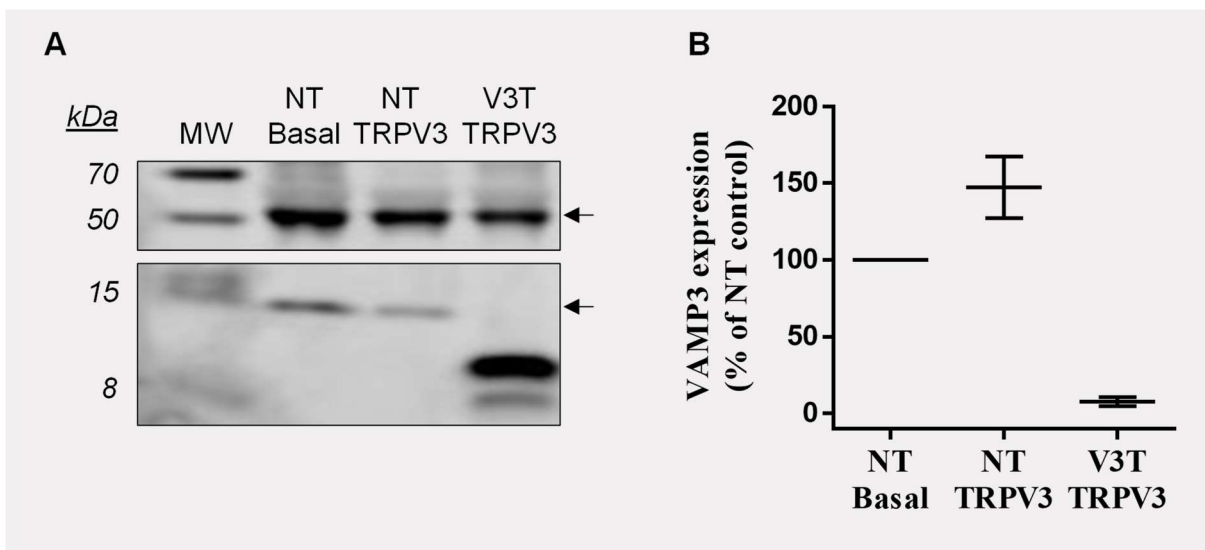


Figure 3.42. VAMP3-targeted shRNA successfully reduced VAMP3 expression.

Keratinocytes (NHEK) were treated with nontargeted (NT) and VAMP3-targeted (V3T) lentiviral particles. NT and V3T cultures were stimulated with basal medium \pm TRPV3 agonist: basal vs. TRPV3. **A**, Western blot analysis of VAMP3 expression in NT and V3T lysate. Upper arrow represents SNAP29 (internal control). **B**, Comparison of VAMP3 expression as a percentage of NT basal level. Plots indicate median ($Q^1 - Q^3$) of 2 independent knockdown events, with bars outlining min and max values.

NT and V3T NHEK cultures were stimulated with basal medium \pm TRPV3 agonist (drofenine, 500 μ M) [1 h, 37°C]: NT cultures received basal medium \pm drofenine (500 μ M), while V3T cultures received basal medium + drofenine (500 μ M). Following stimulation, cell supernatant was collected and pooled. Mediator release was compared using the cytokine array. Briefly, when present in the supernatant sample, the named protein binds to capture antibodies located at duplicate spots on a nitrocellulose membrane. Chemiluminescent development reveals the relative levels of each released protein. Here, a number of mediators were consistently detected: Basigin (BSG), dickkopf-1 (Dkk-1), epidermal growth factor (EGF), interleukin-1 alpha (IL-1 α), interleukin 1 receptor antagonist (IL-1ra), macrophage migration inhibitory factor (MIF), plasminogen activator inhibitor 1 (PAI-1), platelet derived growth factor subunit A (PDGFA), and transforming growth factor alpha (TGF- α) (**Table 3.5**).

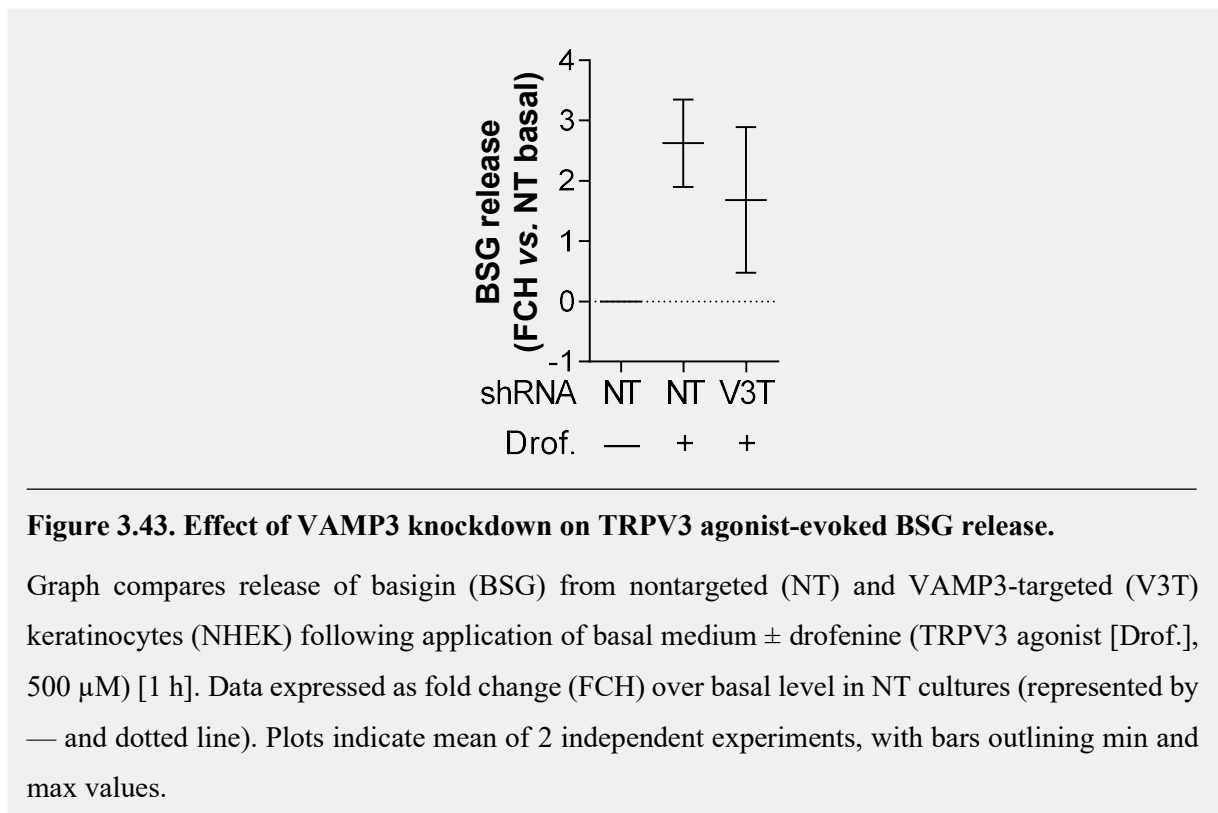
Table 3.5. Representative images of duplicate antibody spots from cytokine array showing effect of VAMP3 knockdown on TRPV3 agonist-induced mediator release.

Mediator	NT Basal	NT TRPV3	V3T TRPV3
BSG			
Dkk-1			
EGF			
IL-1 α			
IL-1ra			
MIF			
PAI-1			
PDGFA			
TGF- α			

Note: Keratinocytes were treated with nontargeted (NT) and VAMP3-targeted (V3T) lentiviral particles. NT and V3T cultures were stimulated with basal medium \pm TRPV3 agonist: basal vs. TRPV3. Table includes images of duplicate spots; antibodies at each spot bind to a named mediator. Average densitometry of these duplicates equals one experimental replicate. *Abbreviations:* BSG, basigin; Dkk-1, dickkopf-1; EGF, epidermal growth factor; IL-1 α , interleukin-1 alpha; IL-1ra, interleukin 1 receptor antagonist; MIF, macrophage migration inhibitory factor; PAI-1, plasminogen activator inhibitor 1; PDGFA, platelet derived growth factor subunit A; TGF- α , transforming growth factor alpha; and TRPV3, transient receptor potential vanilloid 3.

Duplicate antibody spots were then measured using densitometry. Average pixel density of each duplicate pair represents one experimental replicate. Average pixel density data were expressed as fold change (FCH) relative to NT basal medium-treated samples (n=2). FCH data were presented as median FCH (\pm min/max values). This data require further replication before statistical analyses can be undertaken; these experiments are included as an indication of future works. The graphs below reveal the relative change of each named protein, highlighting the role of VAMP3-dependent exocytosis in TRPV3-linked mediator release.

Basigin (BSG) is involved in wound healing and cutaneous remodelling (Guo *et al.*, 1997). BSG secretion was detected in cellular supernatant from NT and V3T keratinocytes (**Figure 3.43**). In NT cultures, TRPV3 stimulation enhanced BSG secretion relative to NT baseline levels (FCH =2.623 vs. 0). In V3T cultures, TRPV3 stimulation also enhanced BSG secretion relative to NT basal (FCH =1.682). This BSG release was notably lower than that from stimulated NT cultures. Specifically, VAMP3 knockdown reduced drofenine-evoked BSG release by about 35%. Thus, TRPV3-linked BSG secretion may be facilitated by VAMP3-dependent exocytosis in human epidermal keratinocytes.



Dickkopf-1 (Dkk-1) regulates skin pigmentation, epidermal thickness, and the hair cycle (Kwack *et al.*, 2012; Yamaguchi *et al.*, 2008). Dkk-1 secretion was detected in cellular supernatant from NT and V3T keratinocytes (**Figure 3.44**). In NT cultures, TRPV3 stimulation enhanced Dkk-1 secretion relative to NT baseline levels (FCH =1.023 vs. 0). In V3T cultures, TRPV3 stimulation failed to enhance Dkk-1 secretion relative to NT basal (FCH=0.137). This Dkk-1 release was notably lower than that from stimulated NT cultures. Specifically, VAMP3 knockdown reduced drofenine-evoked Dkk-1 release by about 87%. Thus, TRPV3-linked Dkk-1 secretion may be facilitated by VAMP3-dependent exocytosis in human epidermal keratinocytes.

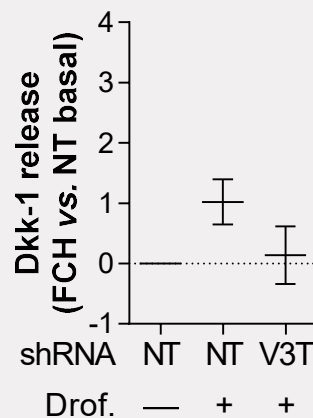


Figure 3.44. Effect of VAMP3 knockdown on TRPV3 agonist-evoked Dkk-1 release.

Graph compares release of dickkopf-1 (Dkk-1) from nontargeted (NT) and VAMP3-targeted (V3T) keratinocytes (NHEK) following application of basal medium ± drofenine (TRPV3 agonist [Drof.], 500 μM) [1 h]. Data expressed as fold change (FCH) over basal level in NT cultures (represented by — and dotted line). Plots indicate mean of 2 independent experiments, with bars outlining min and max values.

Epidermal growth factor (EGF) plays a key role in wound healing (Wells, 1999). EGF secretion was detected in cellular supernatant from NT and V3T keratinocytes (**Figure 3.45**). In NT cultures, TRPV3 stimulation enhanced EGF secretion relative to NT baseline levels, though this increase was minimal (FCH =0.400 vs. 0). In V3T cultures, TRPV3 stimulation failed to enhance EGF secretion relative to NT basal (FCH =0.124). This EGF release was notably lower than that from stimulated NT cultures. Thus, TRPV3-linked EGF secretion may be facilitated by VAMP3-dependent exocytosis in human epidermal keratinocytes.

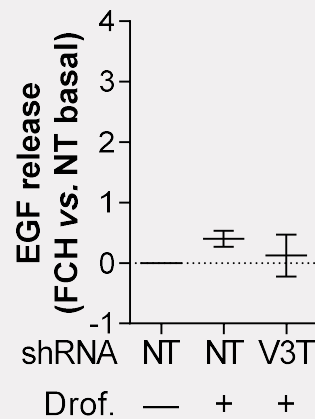


Figure 3.45. Effect of VAMP3 knockdown on TRPV3 agonist-evoked EGF release.

Graph compares release of extracellular growth factor (EGF) from nontargeted (NT) and VAMP3-targeted (V3T) keratinocytes (NHEK) following application of basal medium \pm drofenine (TRPV3 agonist [Drof.], 500 μ M) [1 h]. Data expressed as fold change (FCH) over basal level in NT cultures (represented by — and dotted line). Plots indicate mean of 2 independent experiments, with bars outlining min and max values.

Interleukin-1 alpha (IL-1 α) initiates early inflammation following infection, cell stress, or tissue damage (Di Paolo and Shayakhmetov, 2016; Garlanda *et al.*, 2013). IL-1 α secretion was detected in cellular supernatant from NT and V3T keratinocytes (**Figure 3.46**). In NT cultures, TRPV3 stimulation enhanced IL-1 α secretion relative to NT baseline levels (FCH =2.083 vs. 0). In V3T cultures, TRPV3 stimulation also enhanced IL-1 α secretion relative to NT basal (FCH =0.692). This IL-1 α release was notably lower than that from stimulated NT cultures. Specifically, VAMP3 knockdown reduced drofenine-evoked BSG release by more than 65%. Thus, TRPV3-linked IL-1 α secretion may be facilitated by VAMP3-dependent exocytosis in human epidermal keratinocytes.

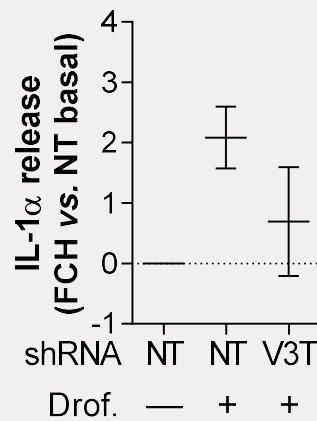


Figure 3.46. Effect of VAMP3 knockdown on TRPV3 agonist-evoked IL-1 α release.

Graph compares release of interleukin-1 alpha (IL-1 α) from nontargeted (NT) and VAMP3-targeted (V3T) keratinocytes (NHEK) following application of basal medium \pm drofenine (TRPV3 agonist [Drof.], 500 μ M) [1 h]. Data expressed as fold change (FCH) over basal level in NT cultures (represented by — and dotted line). Plots indicate mean of 2 independent experiments, with bars outlining min and max values.

Interleukin 1 receptor antagonist (IL-1ra) inhibits the IL-1 receptor (IL-1R1), blocking the action of both IL-1 α and IL-1 β (Garlanda *et al.*, 2013). IL-1ra secretion was detected in cellular supernatant from NT and V3T keratinocytes (**Figure 3.47**). In NT cultures, TRPV3 stimulation enhanced IL-1ra secretion relative to basal, though this increase was minimal (FCH =0.474 vs. 0). In V3T cultures, TRPV3 stimulation also enhanced IL-1ra secretion relative to NT basal (FCH =0.991). This IL-1ra release was actually higher than that from stimulated NT cultures. Whether this V3T-associated change was caused by an increase in basal or evoked IL-1ra release is unclear. However, TRPV3-linked IL-1ra secretion is likely independent of VAMP3-mediated exocytosis in human epidermal keratinocytes.

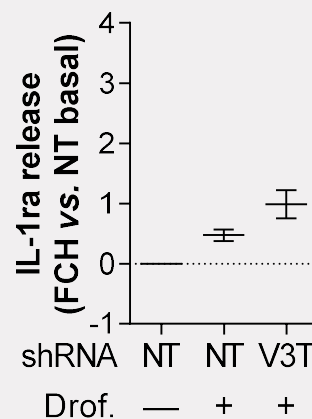


Figure 3.47. Effect of VAMP3 knockdown on TRPV3 agonist-evoked IL-1ra release.

Graph compares release of interleukin 1 receptor antagonist (IL-1ra) from nontargeted (NT) and VAMP3-targeted (V3T) keratinocytes (NHEK) following application of basal medium \pm drofenine (TRPV3 agonist [Drof.], 500 μ M) [1 h]. Data expressed as fold change (FCH) over basal level in NT cultures (represented by — and dotted line). Plots indicate mean of 2 independent experiments, with bars outlining min and max values.

Macrophage migration inhibitory factor (MIF) is a highly pleiotropic mediator that primarily evokes innate immune responses and inflammation (Calandra and Roger, 2003). MIF secretion was detected in cellular supernatant from NT and V3T keratinocytes (**Figure 3.48**). In both NT and V3T cultures, TRPV3 stimulation failed to enhance MIF secretion relative to basal (FCH =0.198 and 0.105, respectively). These MIF data are inconsistent with previous findings from NHEK. Thus, shRNA treatment may underpin these discrepancies. Further studies should be carried out using a different method. However, at present, it is unclear whether TRPV3-linked MIF secretion is dependent on VAMP3- mediated exocytosis in human epidermal keratinocytes.

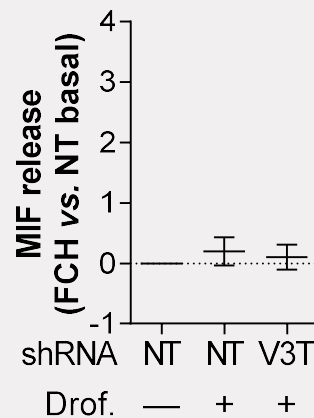


Figure 3.48. Effect of VAMP3 knockdown on TRPV3 agonist-evoked MIF release.

Graph compares release of macrophage migration inhibitory factor (MIF) from nontargeted (NT) and VAMP3-targeted (V3T) keratinocytes (NHEK) following application of basal medium ± drofenine (TRPV3 agonist [Drof.], 500 μ M) [1 h]. Data expressed as fold change (FCH) over basal level in NT cultures (represented by — and dotted line). Plots indicate mean of 2 independent experiments, with bars outlining min and max values.

Plasminogen activator inhibitor 1 (PAI-1) is a regulator of fibrinolysis (Lijnen, 2005). PAI-1 secretion was detected in cellular supernatant from NT and V3T keratinocytes (**Figure 3.49**). In NT cultures, TRPV3 stimulation enhanced PAI-1 secretion relative to basal (FCH =0.841 vs. 0). In V3T cultures, TRPV3 stimulation failed to enhance PAI-1 secretion relative to NT basal (FCH =-0.306). This PAI-1 release was notably lower than that from stimulated NT cultures. Specifically, VAMP3 knockdown reduced drofenine-evoked PAI-1 release by almost 140%. This striking decrease brought PAI-1 levels below baseline values, suggesting that VAMP3 knockdown may also reduce homeostatic PAI-1 release. Thus, both TRPV3-linked and normal homeostatic PAI-1 secretion may be facilitated by VAMP3-dependent exocytosis in human epidermal keratinocytes.

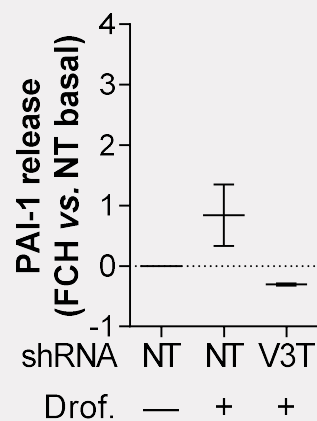


Figure 3.49. Effect of VAMP3 knockdown on TRPV3 agonist-evoked PAI-1 release.

Graph compares release of plasminogen activator inhibitor 1 (PAI-1) from nontargeted (NT) and VAMP3-targeted (V3T) keratinocytes (NHEK) following application of basal medium ± drofenine (TRPV3 agonist [Drof.], 500 μM) [1 h]. Data expressed as fold change (FCH) over basal level in NT cultures (represented by — and dotted line). Plots indicate mean of 2 independent experiments, with bars outlining min and max values.

Platelet derived growth factor subunit A (PDGFA) activates cutaneous mesenchymal cells and facilitates tissue repair (Heldin and Westermark, 1999). PDGFA secretion was detected in cellular supernatant from NT and V3T keratinocytes (**Figure 3.50**). In both NT and V3T cultures, TRPV3 stimulation failed to enhance PDGFA secretion relative to basal (FCH =0.124 and -0.073, respectively). These PDGFA data are inconsistent with previous findings from NHEK. Thus, shRNA treatment may underpin these discrepancies. Further studies should be carried out using a different method. However, at present, it is unclear whether TRPV3-linked PDGFA secretion is dependent on VAMP3- mediated exocytosis in human epidermal keratinocytes.

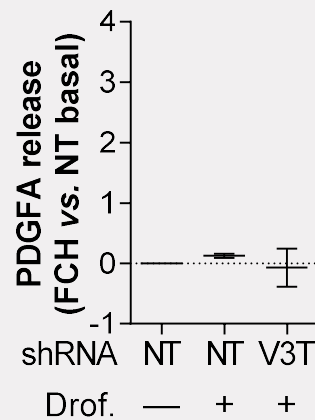


Figure 3.50. Effect of VAMP3 knockdown on TRPV3 agonist-evoked PDGFA release.

Graph compares release of platelet derived growth factor subunit A (PDGFA) from nontargeted (NT) and VAMP3-targeted (V3T) keratinocytes (NHEK) following application of basal medium \pm drofenine (TRPV3 agonist [Drof.], 500 μ M) [1 h]. Data expressed as fold change (FCH) over basal level in NT cultures (represented by — and dotted line). Plots indicate mean of 2 independent experiments, with bars outlining min and max values.

Transforming growth factor alpha (TGF- α) is a key inducer of EGF signalling and epithelial development (Wee and Wang, 2017). TGF- α secretion was detected in cellular supernatant from NT and V3T keratinocytes (**Figure 3.51**). In NT cultures, TRPV3 stimulation enhanced TGF- α secretion relative to basal (FCH =0.948 vs. 0). In V3T cultures, TRPV3 stimulation also enhanced median TGF- α secretion relative to NT basal (FCH=0.722). This TGF- α release was comparable to that from stimulated NT cultures. Thus, TRPV3-linked TGF- α secretion is likely independent of VAMP3-mediated exocytosis in human epidermal keratinocytes.

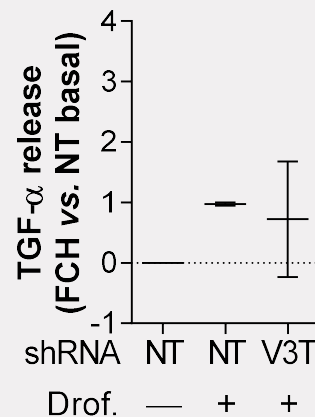


Figure 3.51. Effect of VAMP3 knockdown on TRPV3 agonist-evoked TGF- α release.

Graph compares release of transforming growth factor alpha (TGF- α) from nontargeted (NT) and VAMP3-targeted (V3T) keratinocytes (NHEK) following application of basal medium \pm drofenine (TRPV3 agonist [Drof.], 500 μ M) [1 h]. Data expressed as fold change (FCH) over basal level in NT cultures (represented by — and dotted line). Plots indicate mean of 2 independent experiments, with bars outlining min and max values.

These data suggest that, in a culture model of human epidermis, activation of TRPV3 promotes VAMP3-mediated exocytosis of BSG, Dkk-1, EGF, IL-1 α , and PAI-1. VAMP3 was not required for induced IL-1 α release, suggesting that this anti-inflammatory compound would be unaffected by VAMP3-targeting agents. Many of these TRPV3-linked mediators have been associated with inflammatory skin conditions: BSG, Dkk-1, and TGF- α are increased in psoriatic skin; dysregulated IL-1 α drives hidradenitis suppurativa; and PAI-1 promotes acute itch and atopic dermatitis (Peng *et al.*, 2017; Okubo *et al.*, 2022; Seifert *et al.*, 2015; Tzanetakou *et al.*, 2016; Kanni *et al.*, 2018; Larkin *et al.*, 2021). Thus, VAMP3-targeting agents could interrupt TRPV3-linked signalling in these inflammatory skin conditions. Although this study requires further replication, we hypothesize that targeting of VAMP3 could reduce TRPV3-associated signalling and inflammation in the skin.

3.3. Discussion

3.3.1. Summary

Herein, we provide evidence for TRPA1, TRPV1, and TRPV3 activity in a culture model of human epidermis. Phospho-kinase analyses revealed the intracellular pathways acting downstream of TRPA1, TRPV1, and TRPV3 channels (**Figure 3.52**). Application of the TRPA1 agonist (AITC) enhanced phosphorylation of p53 ($P = .0187$), p70S6K ($P = .0187$), eNOS ($P = .0365$), and WNK1 ($P = .0365$). Application of the TRPV1 agonist (capsaicin) enhanced phosphorylation of Yes ($P = .0500$), Chk2 ($P = .0500$), and PLC γ 1 ($P = .0678$) – though no changes reached significance. Application of the TRPV3 agonist (drofenine) enhanced phosphorylation of c-Jun ($P = .0187$), STAT5A ($P = .0500$), Fyn ($P = .0187$), and Hck ($P = .0131$). Together, these data indicate that TRPA1, TRPV1, and TRPV3 channels are expressed and functional in the NHEK model of human epidermis.

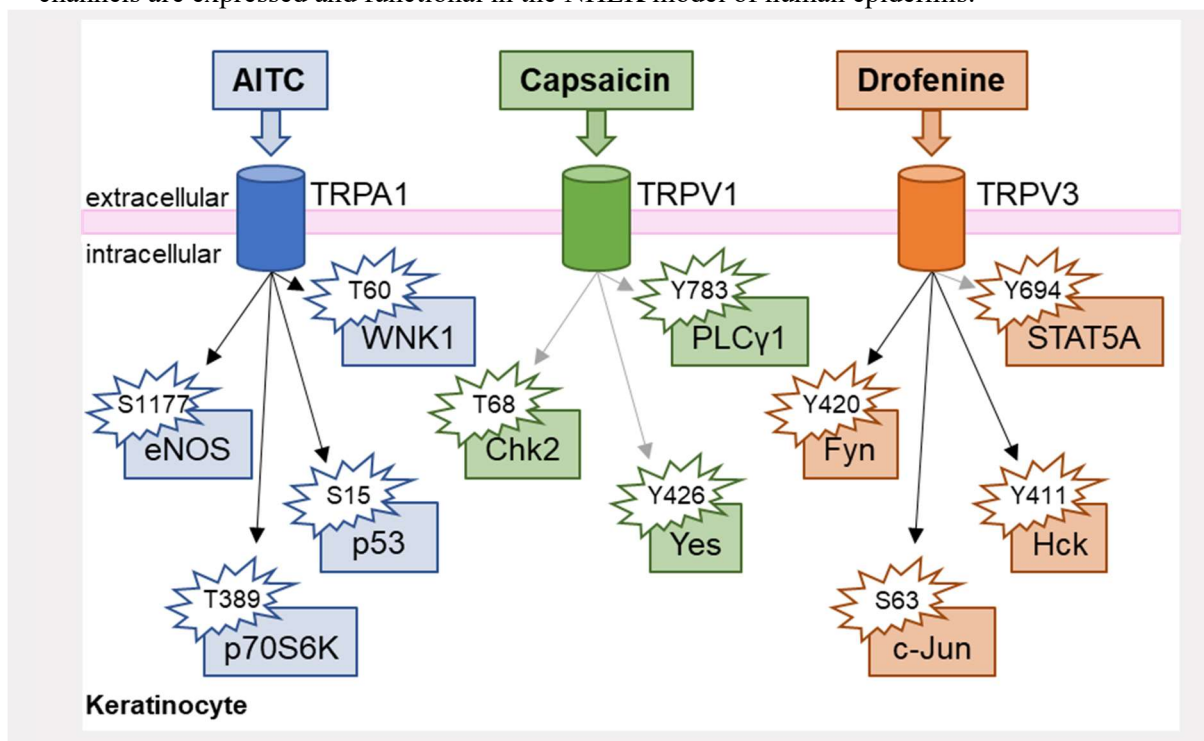


Figure 3.52. Schematic showing putative kinase pathways acting downstream of TRP channels in epidermal keratinocytes.

Diagram highlights the intracellular proteins that show increased phosphorylation in keratinocytes (NHEK) following TRP agonist application. Black arrows indicate that statistical significance was reached. Phosphorylated residues of each protein are also shown. *Abbreviations:* Chk2, checkpoint kinase 2; c-Jun, activator protein 1 transcription factor subunit; eNOS, endothelial nitric oxide synthase; Fyn, Fyn proto-oncogene; Hck, hematopoietic cell kinase; p53, cellular tumour antigen p53; p70S6K, ribosomal protein S6 kinase; PLC γ 1, phospholipase C-gamma-1; S, serine; STAT5A, signal transducer and activator of transcription 5A; T, threonine; TRPA1, transient receptor potential ankyrin 1; TRPV1/TRPV3, transient receptor potential vanilloid 1/3; WNK1, lysine deficient protein kinase 1; Y, tyrosine; and Yes, Yamaguchi sarcoma virus oncogene.

Following agonist-mediated TRPV3 activation, human epidermal keratinocytes released potent signalling mediators: BSG, Dkk-1, IL-1 α , PAI-1 and TGF- α (**Figure 3.53**). TRPV1 and TRPA1 agonists failed to induce significant mediator release. Although TRPV3 activation enhanced c-Jun phosphorylation, TRPV3-linked release was independent of JNK/c-Jun signalling. Knockdown of VAMP3 reduced BSG, Dkk-1, IL-1 α , and PAI-1 release. Although these knockdown experiments require further replication, our data suggest that VAMP3-dependent exocytosis may contribute to evoked secretion of these TRPV3-linked mediators. Work by our collaborators found that PAI-1 is increased in lesional atopic dermatitis and drives scratching behaviour in a murine model of acute and prolonged itch (Larkin *et al.*, 2021). Together, these studies solidified cultured NHEK as an appropriate and robust model for investigation of the TRPV3 channel. TRPV3 activation alters cutaneous inflammation, enhances pruritic signalling, and dysregulates normal repair processes. Thus, we propose that overactivation of the epidermal TRPV3 channel may drive pruritic and inflammatory skin conditions. This work identified novel epidermal signalling pathways, revealing several targets for the treatment of TRPV3-associated inflammation and disease.

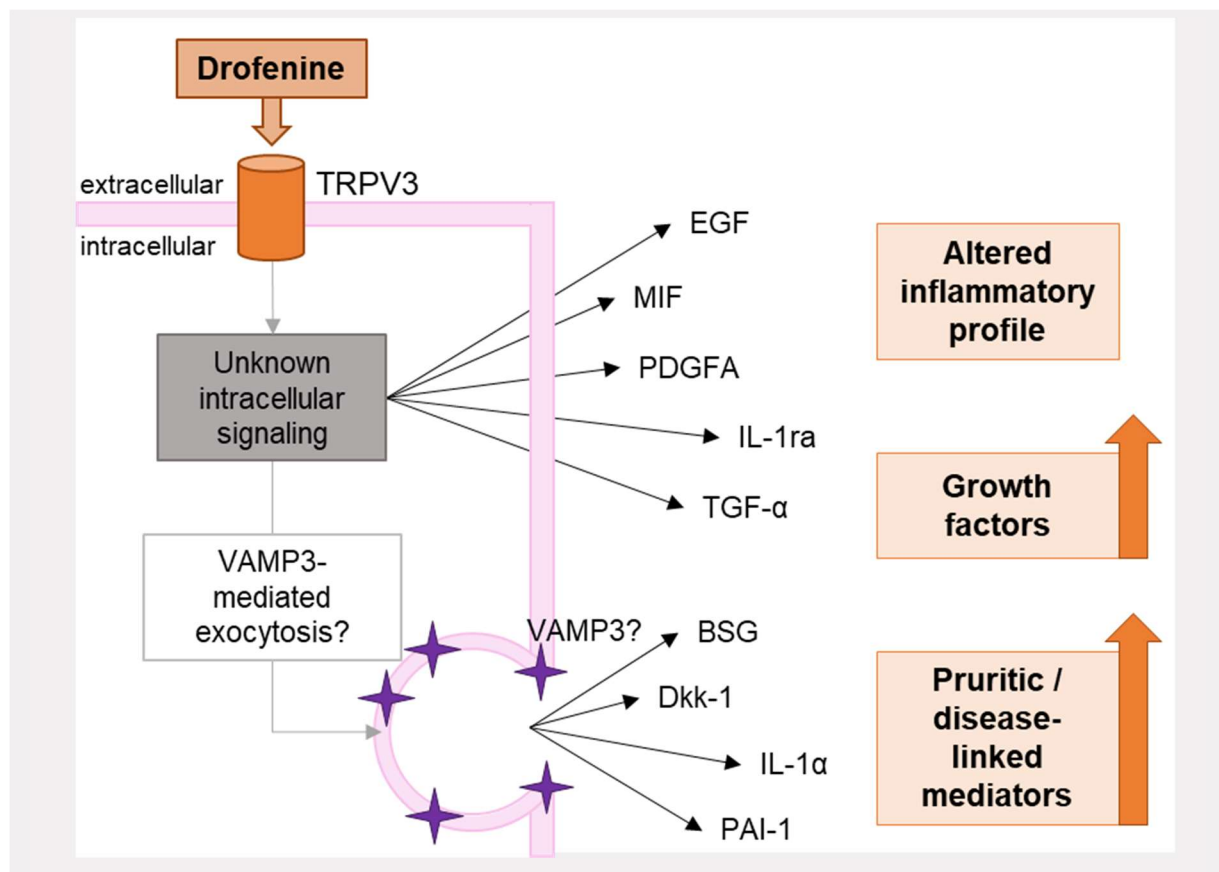


Figure 3.53. Schematic showing putative pathways involved in release of TRPV3-linked mediators from epidermal keratinocytes.

Diagram highlights the intercellular signalling pathways acting downstream of the TRPV3 channel in the NHEK model of human epidermis. *Abbreviations:* BSG, basigin; Dkk-1, dickkopf-1; EGF, epidermal growth factor; IL-1 α , interleukin-1 alpha; IL-1ra, interleukin 1 receptor antagonist; MIF, macrophage migration inhibitory factor; PAI-1, plasminogen activator inhibitor 1; PDGFA, platelet derived growth factor subunit A; TGF- α , transforming growth factor alpha.

3.3.2. Specificity of TRP agonists

Robust signalling analyses require potent and specific agonists, antagonists, and modulators. This process is complicated by the polymodal nature of TRP channels. To date, several TRP agonists have been developed, though the specificity of these agents varies. Here, we used AITC to activate TRPA1; capsaicin to activate TRPV1; and drofenine to activate TRPV3.

AITC is a component of mustard oil and a potent TRPA1 agonist (Jordt *et al.*, 2004; Capasso *et al.*, 2012). AITC binds to the intracellular region of the TRPA1 channel, covalently modifying cysteine residues and promoting pore opening (Hinman *et al.*, 2006; Macpherson *et al.*, 2007). Reports have described some TRPA1-independent effects. AITC enhances MAPK signalling in fibroblast cells and modulates contractions in isolated mouse colon (Capasso *et al.*, 2012; Yap *et al.*, 2021). At higher concentrations, AITC can sensitise and even activate TRPV1 channels (Ohta *et al.*, 2007; Everaerts *et al.*, 2011; Alpizar *et al.*, 2014). However, at the concentrations used herein, AITC is unable to activate TRPV1-expressing neurons from *Trpa1* knockout mice (Everaerts *et al.*, 2011). Thus, we conclude that our AITC results likely represent TRPA1-linked signaling in human epidermal keratinocytes.

Capsaicin is a small lipophilic compound found in chili peppers and a key agonist of the TRPV1 channel (Hayes *et al.*, 2000). Following binding, capsaicin lowers the temperature threshold of TRPV1 allowing channel opening at room temperature (Jordt *et al.*, 2000). A number of TRPV1-independent effects have been reported, with data suggesting that capsaicin could inhibit neuronal voltage-gated potassium (Kv) channels and reduce VEGF-mediated angiogenesis in endothelial cells (Min *et al.*, 2004; Braga Ferreira *et al.*, 2020; Yang *et al.*, 2014). However, TRPV1 remains the primary target of capsaicin. Thus, we conclude that our capsaicin results likely represent TRPV1-linked signaling in human epidermal keratinocytes.

Drofenine is a specific, albeit underutilised, TRPV3 agonist (Deering-Rice *et al.*, 2014). To date, TRPV3 research has depended on nonselective agents such as camphor, carvacrol, eugenol, and 2-APB (Hu *et al.*, 2004; Moqrich *et al.*, 2005; Vogt-Eisele *et al.*, 2007; Xu *et al.*, 2006). Recently, researchers used drofenine to investigate the role of TRPV3 in liver cirrhosis and pollutant-induced respiratory disorders (Nguyen *et al.*, 2020; Yan *et al.*, 2021). However, off-target effects must be noted. Drofenine inhibits butyrylcholinesterase in the blood; modulates M1 and M2 muscarinic receptors in smooth muscle; and reduces the transcription of Kv channels and the amplitude Kv2.1 currents in DRG neurons (Xu *et al.*, 2020; Bodur *et al.*, 2001; Kunysz *et al.*, 1988). Here, we found that drofenine activated TRPV3-expressing keratinocytes, enhancing the secretion of PAI-1 and other mediators. Work by our collaborators confirmed that this PAI-1 release was dependent on TRPV3 expression in NHEK (Larkin *et al.*, 2021). Thus, we conclude that our drofenine results likely represent TRPV3-linked signaling in human epidermal keratinocytes.

These assays outlined the effect of TRPA1, TRPV1, and TRPV3 agonists on cellular signalling, providing evidence for these channels in human epidermal keratinocytes. However, further investigations would be strengthened by concurrent pharmacological inhibition or channel knockdown.

3.3.3. TRPV3-linked mediators: their role in skin health and disease

Here, we identified 9 mediators acting downstream of the TRPV3 channel in human keratinocytes. These proteins are involved in a wide variety of processes such as skin repair, inflammation, and skin disease.

In healthy skin, TRPV3 interacts with the EGF/EGFR/TGF- α pathway to coordinate epidermal growth, patterning, and repair. This function was echoed in our release assays: TRPV3 activation enhanced EGF and TGF- α release. Published reports described comparable levels of TGF- α following application of a TRPV3 agonist cocktail (2-APB plus carvacrol) (Cheng *et al.*, 2010). TRPV3 has also been linked to in skin patterning *in vivo*. TRPV3 knockout mice are characterised by a thin SC, wavy coat and whiskers, and impaired EGFR/TGF- α signalling (Cheng *et al.*, 2010; Moqrich *et al.*, 2005). Together, these reports validate our *in vitro* findings and highlight the role of TRPV3-linked signalling in healthy skin.

TRPV3 may modulate the inflammatory environment within the epidermis. Here, TRPV3 activation promoted the release of IL-1 α – a potent stimulator of CD4 T cell responses (Ben-Sasson *et al.*, 2009). IL-1 α has previously been linked to TRPV3: eugenol-mediated TRPV3 activation enhanced IL-1 α secretion in a mouse keratinocyte cell-line; while carvacrol increased IL-1 α , IL-8, and TNF α transcripts in NHEK (Szöllösi *et al.*, 2018; Xu *et al.*, 2006). Carvacrol also elevated the release of TSLP, NGF, and PGE2 in NHEK (Seo *et al.*, 2020). In addition to these inflammatory and pruritogenic compounds, we found the TRPV3 activation could induce anti-inflammatory signalling pathways such as IL-1ra. This finding indicates that TRPV3 is more than a “pro-inflammatory” channel and suggests that TRPV3 may regulate the inflammatory environment in healthy skin. Together, these reports act to strengthen the validity of our signalling analyses and further confirm drofenine as a potent agonist of the TRPV3 channel.

Recent reports, including work from our laboratory, have described a link between TRPV3 expression and dermatitis (Larkin *et al.*, 2021; Vasas *et al.*, 2022). Dysregulated TRPV3 signalling may also play a role in skin conditions. BSG is increased in psoriatic skin lesions where it drives differentiation of a subtype of T helper cell (Th17) – a key step in disease development (Okubo *et al.*, 2022; Peng *et al.*, 2017). Reports suggest that a polymorphism in *BSG* could even affect psoriasis susceptibility (Wu *et al.*, 2011). Dkk-1 regulates skin pigmentation and epidermal thickness, promoting the development of palmoplantar-like skin in *ex vivo* experiments (Yamaguchi *et al.*, 2008; Yamaguchi *et al.*, 2009). Dkk-1 is highly upregulated in patients with plaque psoriasis, though this increase is restricted to nonlesional skin and peripheral blood mononuclear cells (Seifert *et al.*, 2015). Overexpression of IL-1 α initiates spontaneous inflammatory epidermal lesions in transgenic mice (Groves *et al.*, 1995). Dysregulated IL-1 α signalling also underpins the pathogenesis of hidradenitis suppurativa, a neutrophilic autoinflammatory skin condition: IL-1 α -targeting drugs and antibodies have proved clinically efficacious for patients with hidradenitis suppurativa (Tzanetakou *et al.*, 2016; Kanni *et al.*, 2018). PAI-1 is a potent itch-inducer in murine models of acute and

prolonged itch (Larkin *et al.*, 2021). Experiments carried out by Dr. Meng showed PAI-1 to be highly and specifically increased in lesional atopic dermatitis, with no significant change found in nonlesional atopic dermatitis or psoriatic skin (Larkin *et al.*, 2021). Dr. Meng found that TGF- α is highly and specifically upregulated in lesional psoriasis, with levels unchanged in nonlesional psoriasis or in atopic dermatitis skin (Larkin *et al.*, 2021). These clinical and translational findings highlight the true impact of dysregulated TRPV3 signalling in the human epidermis.

Together, these results highlight the nuanced role of TRPV3 in the skin. TRPV3 represents an important target for both anti-itch and anti-dermatitis agents. However, researchers must ensure that these drugs modulate TRPV3 overactivation, while leaving normal functioning intact. Later chapters will examine the pathways involved in TRPV3 trafficking and sensitisation. We believe that these data could facilitate the development of modulatory compounds and targeted therapeutics.

3.3.4. Conclusion

This chapter outlined the signalling pathways acting downstream of TRPA1, TRPV1, and TRPV3 receptors in the NHEK culture model of human epidermis.

These data failed to provide consistent and clear evidence of functional TRPA1 and TRPV1 channels in the NHEK culture model. Although TRPA1 and TRPV1 agonists promoted detectable kinase activation, these agonists failed to evoke significant mediator release. It is possible that TRPA1 and TRPV1 are expressed in a small subpopulation of keratinocytes; however, this theory remains unexplored.

Conversely, our data clearly highlighted the impact of TRPV3 on the epidermal environment. The TRPV3 agonist promoted significant kinase activation and mediator release. These results showed high levels of inter-replicate variability. Thus, TRPV3 expression and activity may be related to donor genetics or epigenetic modifications. This *in vitro* work formed the basis of further work carried out by our collaborators, culminating in the identification a novel itch-inducer and solidifying TRPV3 as a key coordinator of dermatitis-linked signalling.

4. Examining the Dynamics of TRPV3-mediated Calcium Fluctuations

4.1. Overview

TRPA1, TRPV1, and TRPV3 channels function as calcium-permeable cation channels. When associated with the plasma membrane, these channels facilitate cation influx and downstream signalling. Results outlined in Chapter 3 suggest that TRPA1 and TRPV1 channels may induce intracellular signalling in subsets of epidermal keratinocytes. However, whether these channels evoke calcium fluctuations remained unknown. Conversely, activation of TRPV3 promotes rapid calcium influx in a variety of expression systems, cell-lines, and primary cells (Peier *et al.*, 2002; Deering-Rice *et al.*, 2014; Smith *et al.*, 2002; Xu *et al.*, 2002; Szöllösi *et al.*, 2018). Reports suggest that the TRPV3 channel exhibits unusual properties such as sensitisation upon repeated activation (Chung *et al.*, 2004; Xiao, Tang, *et al.*, 2008; Chung *et al.*, 2005). However, the dynamics of the TRPV3 calcium response remain poorly defined. This chapter aims to confirm the functional expression of TRPA1, TRPV1, and TRPV3 in cultured normal human epidermal keratinocytes (NHEK). This work then focuses on TRPV3, examining the population dynamics of the calcium response and the mechanisms underpinning these phasic fluctuations.

Confocal imaging, in conjunction with fluorescent calcium dyes, allows researchers to monitor the activity of calcium channels in real-time. The variation within these data can reveal key features of the functional response. Commonly used methods and analyses often mask this variation and may conceal important elements of the response. Gupta and team sought instead to utilise normal variation, using unsupervised machine-learning algorithms to characterise and compare response profiles (Gupta *et al.*, 2017). Herein, a similar framework was used to assess calcium fluctuations. This method allowed us to quantify the effect of inhibitors and genetic knockdown on TRPV3 activity.

These experiments identified functional subgroups within the keratinocyte population and highlighted the importance receptor cycling in normal TRPV3-linked calcium responses.

4.2. Results

4.2.1. TRPA1, TRPV1, and TRPV3 agonists enhance calcium flux in subsets of cultured epidermal keratinocytes

TRPA1, TRPV1, and TRPV3 agonists may promote intracellular signalling in epidermal keratinocytes. Here, we examine whether agonist-mediated activation of these TRP channels evokes measurable changes in intracellular calcium.

Normal human epidermal keratinocytes (NHEK) were loaded with a cell-permeant fluorescent calcium indicator (Fluo-4 AM) and recorded using confocal microscopy. Following a baseline recording [100 seconds (s)], keratinocytes were stimulated with medium \pm TRP agonists: AITC (TRPA1 agonist, 50 μ M); capsaicin (TRPV1 agonist, 1 μ M); or drofenine (TRPV3 agonist, 500 μ M) (**Figure 4.1**). Calcium levels were monitored for 400 s. All stimulations were associated with some level of calcium response; however, these fluctuations were highly varied (**Table 4.1**).

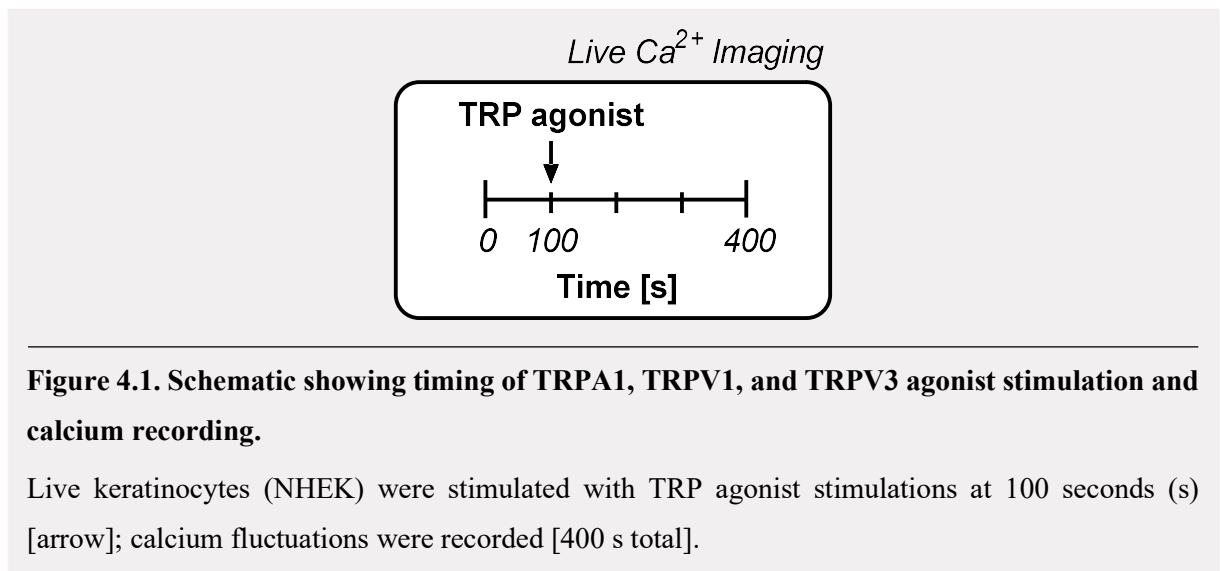
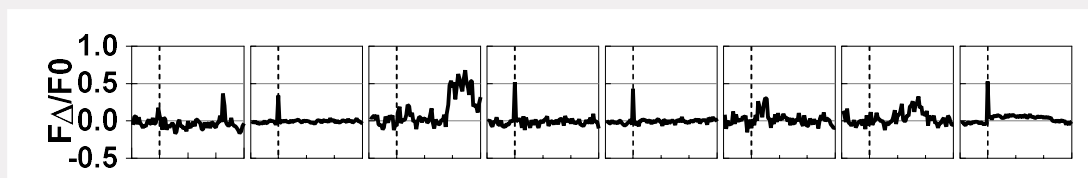


Table 4.1. Calcium response parameters in TRP agonist-sensitive keratinocytes.

Parameter	Nonspecific	TRPA1	TRPV1	TRPV3
Mean fl. change (FΔ/F0)	0.02 (0.00 – 0.65)	0.09 (0.06 – 0.13)	0.02 (0.00 – 0.07)	1.18 (0.93 – 1.48)
Peak amplitude (FΔ/F0)	0.40 (0.33 – 0.53)	0.37 (0.34 – 0.45)	0.37 (0.33 – 0.44)	4.77 (3.92 – 5.59)
Peak latency (s)	155 (0 – 225)	263 (191 – 290)	180 (110 – 250)	50 (40 – 65)
AUC (a.u.)	21.4 (13.9 – 35.9)	41.6 (30.8 – 54.5)	29.3 (10.9 – 39.7)	473.4 (375.2 – 592.0)
TPA (a.u.)	8.0 (1.9 – 20.1)	35.1 (12.5 – 49.5)	8.7 (2.1 – 25.1)	470.0 (371.4 – 588.8)

Note: Data expressed as median (Q¹ – Q³). Abbreviations: AITC, allyl isothiocyanate; a.u., arbitrary unit; μm, micrometre; fl, fluorescence; FΔ/F0, change in fluorescence; s, seconds; AUC, area under the curve; TPA, total peak area.

Addition of basal medium alone enhanced fluorescence in 2.03% ± 1.08 (M ± SEM) of keratinocytes (**Figure 4.2**). These fluctuations were low in amplitude (**Table 4.1**). Responsive cells were significantly smaller in size than non-responsive ($P < .01$ [perimeter] and $P < .05$ [area]) (**Table 4.2**). These data indicate that the addition of basal solution can activate a subset of keratinocytes.

**Figure 4.2. Single-cell traces showing effect of basal medium on cellular calcium flux.**

Representative traces showing change in fluorescence (FΔ/F0) over time following addition of basal medium. Dotted line indicates addition at 100 seconds.

AITC solution enhanced fluorescence in 5.43% ± 2.43 of keratinocytes (**Figure 4.3**). AITC-evoked fluctuations appeared to build with time: responsive cells were slow to peak — with some taking more than 4 minutes. Overall, these putative TRPA1-positive (TRPA1⁺) cells showed notable calcium increases as evident in area under the curve (AUC) and total peak area (TPA) values (**Table 4.1**). AITC-responsive keratinocytes were significantly smaller in size than non-responsive ($P < .001$ [perimeter] and $P < .0001$ [area]) (**Table 4.2**). These data suggest that functional TRPA1 channels are expressed in a subset of small diameter keratinocytes.

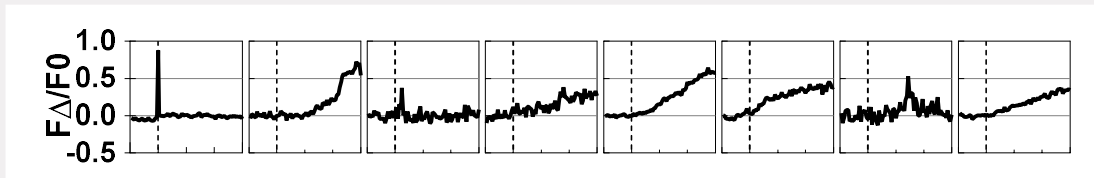


Figure 4.3. Single-cell traces showing effect of TRPA1 agonist on cellular calcium flux.

Representative traces showing change in fluorescence ($F\Delta/F0$) over time following addition of basal medium + AITC ($50\ \mu\text{M}$). Dotted line indicates addition at 100 seconds.

Capsaicin solution enhanced fluorescence in $3.22\% \pm 1.06$ of keratinocytes (**Figure 4.4**). These fluctuations were comparable to those evoked by basal medium alone: when compared with the medium-evoked responses, only max change (seconds post-stimulation) showed a significant difference ($P < .0001$) (**Table 4.1**). Comparison of cellular parameters also failed to detect significant differences between medium-responsive and capsaicin-responsive cells (**Table 4.2**). TRPA1⁺ and putative TRPV1⁺ cells were similar in size; however, TRPV1⁺ appeared more circular ($P < .0001$) and, to a lesser degree, more round ($P < .05$). Further work is required to establish whether these keratinocytes express functional TRPV1 channels.

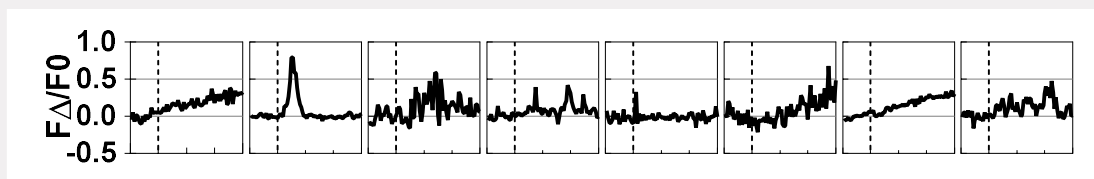


Figure 4.4. Single-cell traces showing effect of TRPV1 agonist on cellular calcium flux.

Representative traces showing change in fluorescence ($F\Delta/F0$) over time following addition of basal medium + capsaicin ($1\ \mu\text{M}$). Dotted line indicates addition at 100 seconds.

Drofenine solution enhanced fluorescence in $98.66\% \pm 0.62$ of keratinocytes (**Figure 4.5A**). These calcium responses were striking and consistent, with the average fluorescence peaking at just 70 s post-stimulation (**Figure 4.5B** and **Figure 4.5C**). Drofenine-evoked fluctuations were also high in amplitude—reaching more than 400% above baseline (**Table 4.1**). Drofenine-insensitive keratinocytes were primarily small in size ($P < .001$ [perimeter]) and circular in shape ($P < .0001$ [circularity] and $P < .0001$ [roundness]) (**Table 4.2**). Drofenine-insensitive cells were also significantly rounder than TRPA1⁺ and putative TRPV1⁺ ($P < .0001$ and $P < .05$, respectively). Thus, this small proportion of drofenine-insensitive cells may be undergoing programmed cell death.

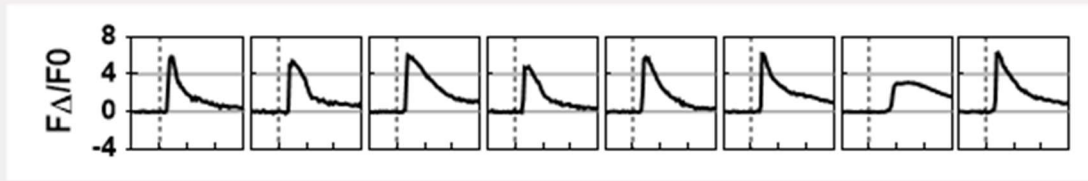
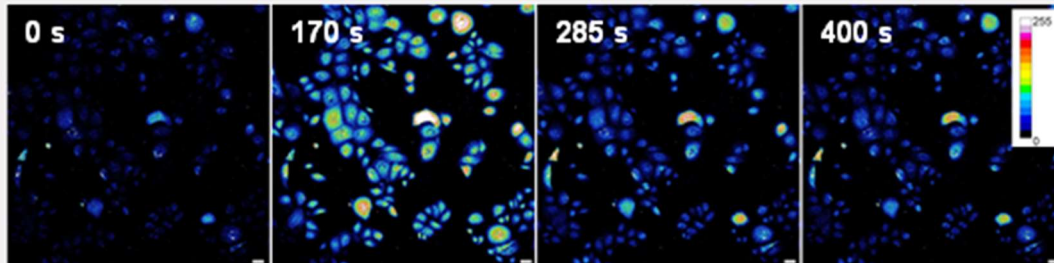
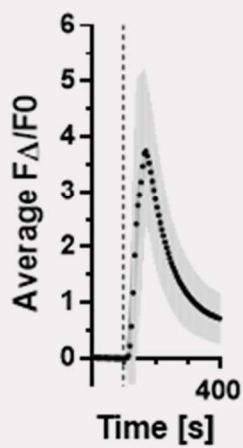
A**B****C**

Figure 4.5. Single-cell traces, representative images, and population analysis showing effect of TRPV3 agonist on cellular calcium flux.

A, Representative single-cell traces showing change in fluorescence ($F\Delta/F0$) over 400 seconds (s) following addition of basal medium + drofenine ($500\ \mu\text{M}$). Dotted line indicates addition (100 s). **B**, Representative images showing fluorescence at each named timepoint: 0 s, 170 s, 285 s, 400 s. White indicates the highest signal. Scale bars = $50\ \mu\text{m}$. **C**, Graph depicts average $F\Delta/F0$ over 400 s following addition of drofenine $500\ \mu\text{M}$. Grey region indicates SEM. Data represent 5 independent stimulations ($n=205$ keratinocytes).

Table 4.2. Basic cellular parameters: TRP agonist-sensitive vs. TRP agonist-insensitive keratinocytes.

Parameter	Nonspecific		TRPA1		TRPV1		TRPV3	
	Sensitive [1.9%]	Insensitive [98.1%]	Sensitive [4.5%]	Insensitive [95.5%]	Sensitive [3.4%]	Insensitive [96.6%]	Sensitive [98.6%]	Insensitive [1.4%]
Perimeter (μm)	79 (74 – 128)	127 (89 – 183)	107 (80 – 149)	132 (98 – 186)	79 (66 – 128)	120 (84 – 160)	141 (110 – 193)	84 (70 – 104)
Area (μm^2)	414 (309 – 860)	922 (492 – 1774)	491 (247 – 1119)	885 (524 – 1724)	428 (276 – 1105)	878 (438 – 1503)	890 (420 – 1903)	524 (357 – 767)
Circularity (a.u.)	0.81 (0.67 – 0.84)	0.74 (0.65 – 0.81)	0.69 (0.45 – 0.79)	0.71 (0.60 – 0.78)	0.80 (0.71 – 0.85)	0.78 (0.70 – 0.85)	0.70 (0.49 – 0.78)	0.91 (0.88 – 0.93)
Roundness (a.u.)	0.77 (0.58 – 0.86)	0.64 (0.54 – 0.75)	0.60 (0.29 – 0.74)	0.61 (0.50 – 0.72)	0.66 (0.59 – 0.79)	0.67 (0.56 – 0.77)	0.58 (0.32 – 0.71)	0.88 (0.83 – 0.92)

Note: Data expressed as median ($Q^1 - Q^3$). *Abbreviations:* a.u., arbitrary unit; μm , micrometre. Square brackets indicate the proportion of stimulated cells per group: agonist-sensitive vs. agonist-insensitive.

Together, these findings indicate that TRPA1, TRPV1, and TRPV3 channels are functional in cultured human keratinocytes. This work revealed novel subgroups within the keratinocyte population, with putative TRPA1⁺ and TRPV1⁺ cells representing subsets within the larger TRPV3⁺ population.

Cellular parameter data suggest that TRPA1⁺ and TRPV1⁺ cells may be small in size. Median cellular area was comparable across treatment groups: 907.3 μm^2 [media stimulated]; 877.7 μm^2 [AITC stimulated]; 863.3 μm^2 [capsaicin stimulated]; and 867.0 μm^2 [drofenine-stimulated] (data not shown). However, putative TRPA1⁺ and TRPV1⁺ cells measured just 491 μm^2 and 428 μm^2 , respectively. Conversely, putative TRPV3⁺ cells measured 890 μm^2 . Although similar in size, these TRPA1⁺ and TRPV1⁺ subpopulations are largely non-overlapping: just 0.27% of the total keratinocyte population responded to both agonists (data not shown). Thus, TRPA1 and TRPV1 may be expressed on different subsets of small epidermal keratinocytes – a potentially important finding for the development of targeted anti-TRPA1 and anti-TRPV1 therapeutics. That said, further investigations are required to establish the clinical significance of these functional subgroups in the epidermis.

TRPV3 experiments revealed a strong calcium fluctuation following drofenine application. Published reports suggest that TRPV3 channels are sensitised by intracellular calcium (Xiao, Tang, *et al.*, 2008). To investigate later phases of the TRPV3 response, further investigations of TRPV3 agonist-induced fluctuations must include a longer recording time.

4.2.2. The TRPV3 agonist induces a phasic calcium response

Drofenine evokes a rapid and high amplitude calcium response in epidermal keratinocytes. During pilot stimulations, we noted a later phase of activation that warranted further investigation. Here, we examined the complete TRPV3 response and, using unsupervised machine-learning algorithms, identified functional subgroups within the TRPV3-positive keratinocyte population.

Normal human epidermal keratinocytes (NHEK) were loaded with a cell-permeant fluorescent calcium indicator (Fluo-4 AM) and calcium dynamics were recorded using confocal imaging. Following a baseline recording [100 s], keratinocytes were stimulated with basal medium + drofenine (TRPV3 agonist, 500 μ M) (D500); calcium levels were monitored for 1000 seconds (s) (**Figure 4.6**).

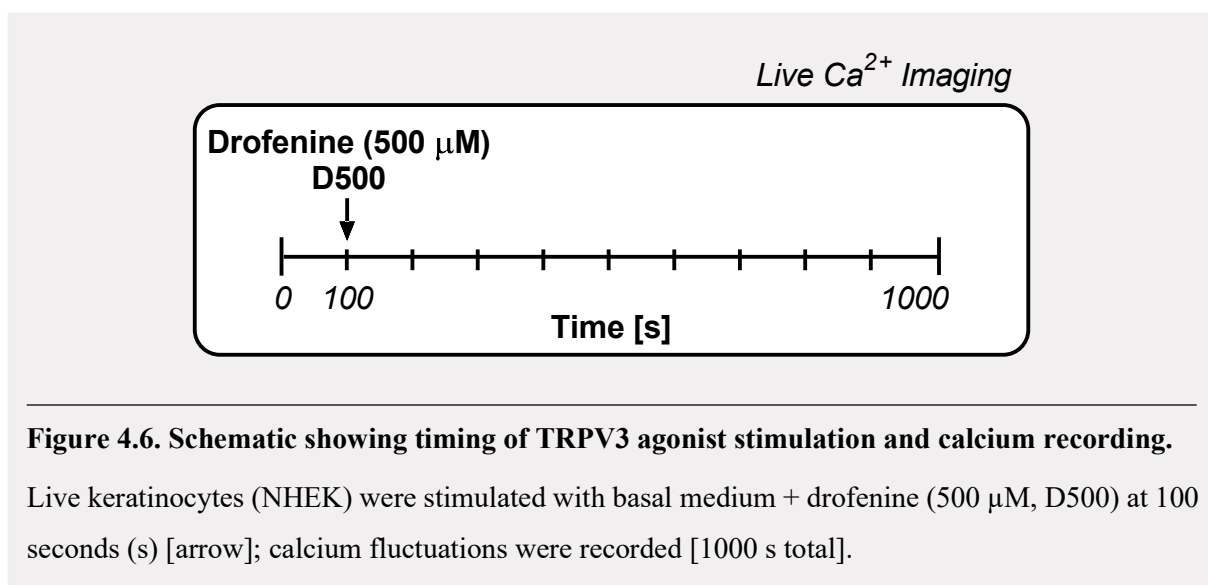


Figure 4.6. Schematic showing timing of TRPV3 agonist stimulation and calcium recording.

Live keratinocytes (NHEK) were stimulated with basal medium + drofenine (500 μ M, D500) at 100 seconds (s) [arrow]; calcium fluctuations were recorded [1000 s total].

Addition of D500 enhanced the intracellular fluorescent signal; however, single-cell traces highlight the variation within the population response (Time [s] vs. $F\Delta/F_0$; **Figure 4.7A**). Although most cells displayed the characteristic rapid peak (82.4%), images revealed a subgroup of cells showing a distinctly slow and often oscillatory response (**Figure 4.7B**).

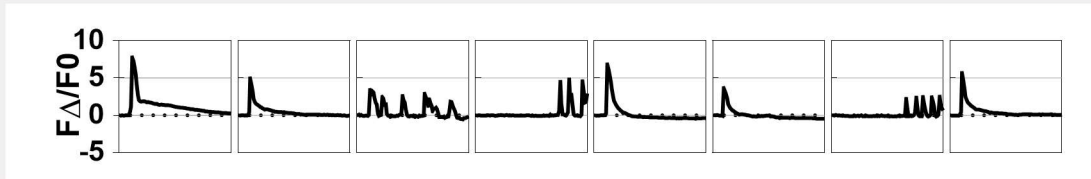
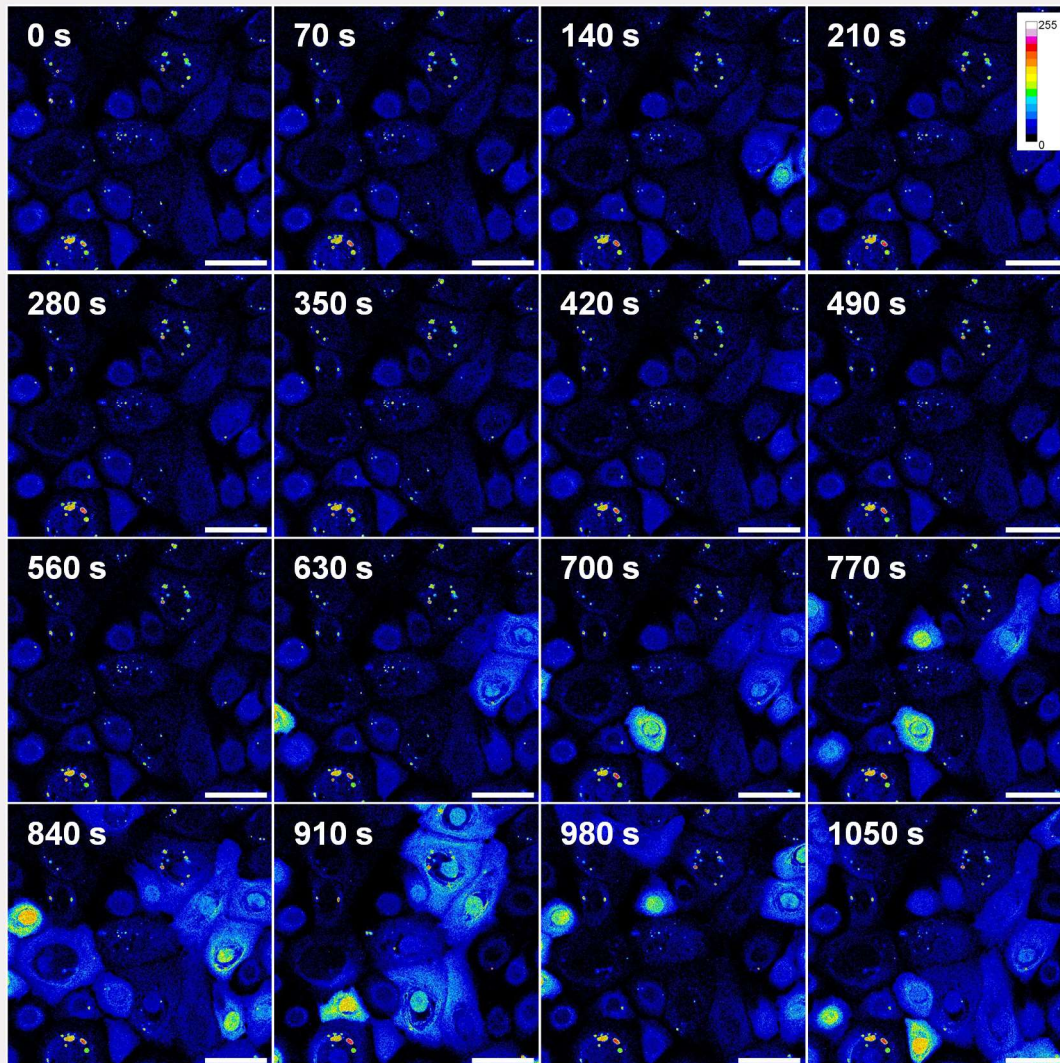
A**B**

Figure 4.7. Temporal variation within the TRPV3 agonist-mediated calcium response.

A, Representative single-cell traces showing change in fluorescence ($F\Delta/F_0$) over 1000 seconds (s) following addition of basal medium + drofenine (500 μ M). Dotted line indicates addition (100 s). **B**, Representative images fluorescence at each named timepoint: 0 s, 70 s, 140 s, 210 s, 280 s, 350 s, 420 s, 490 s, 560 s, 630 s, 700 s, 770 s, 840 s, 910 s, 980 s, 1050 s. White indicates the highest signal. Scale bars = 50 μ m.

D500-evoked calcium dynamics were first evaluated with respect to the population average; time course fluorescence data was plotted as the average change in fluorescence at each time point. Graphing of population responses highlighted the consistency of the early phase. This graph depicts the average change in intracellular fluorescence at each time point (**Figure 4.8**). Similar to previous findings, D500 elicited a rapid increase in intracellular calcium, with levels peaking just 30 s post-stimulation. This peak was high in amplitude, reaching more than 300% above baseline (mean $F\Delta/F_0 = 3.163$, SEM = .145). However, the later phases of the calcium response were absent from this average trace.

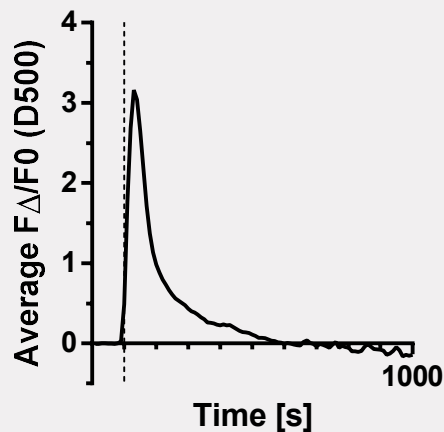


Figure 4.8. Population analysis showing effect drofenine on cellular calcium flux.

Graph depicts average change in fluorescence ($F\Delta/F_0$) over 1000 seconds (s) following addition of drofenine 500 μM (D500). Dotted line indicates addition [100 s] Data represent 5 independent stimulations (n =205 keratinocytes).

We propose that the complexity of the TRPV3 response may be better represented by single-cell focused analyses. This work focused on peak calcium changes in each D500-stimulated keratinocyte. The amplitude and latency of each peak was calculated: peak amplitude ($F\Delta/F_{0\text{max}}$) and peak latency (Time_{max}). These values were then plotted to create a D500 response profile. Each point represents a single cell (**Figure 4.9**). This plot shows the slowest responders on the right (i.e. highest peak latency values) and suggests that the D500 response may consist of distinct phases.

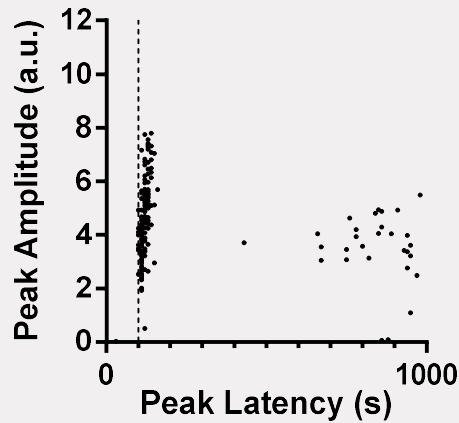


Figure 4.9. TRPV3 response profile: Single-cell analysis showing effect of drofenine on cellular calcium peaks.

Graph depicts response profile: peak latency (Time_{\max} , seconds [s]) vs. peak amplitude ($F\Delta/F0_{\max}$, arbitrary units [a.u.]) following addition of drofenine 500 μM (D500). Each dot represents a single cell. Data represent 5 independent stimulations ($n = 205$ keratinocytes).

The putative phasic activity revealed in raw recordings and single-cell plots may represent an important functional feature of the TRPV3 channel. Here, we investigated the validity of this hypothesis. Unsupervised machine-learning algorithms assessed whether the D500 response profile contained functional subgroups (i.e. clusters). D500 response profile data were imported to RStudio (**Figure 4.10A**). D500-responsive cells were identified and graphed (**Figure 4.10B**). This D500-responsive data was examined for clusters using both direct testing methods (**Figure 4.10C** [silhouette]; **Figure 4.10D** [elbow]) and statistical testing methods (**Figure 4.10E** [gap statistic]). All 3 methods determined 2 to be the optimum number of clusters (k) within the D500 response profile. These D500-responsive data, or response profile, were partitioned using k -means clustering ($k = 2$) to produce 2 distinct subgroups (**Figure 4.10F**). D500 responders were primarily assigned to cluster 1, though the proportion was varied (average = 82.4%, SEM = 17.6) (**Figure 4.10G**). The proportion of D500-insensitive cells was consistently low and was comparable to previous findings (average = 1.8%, SEM = 1.8; 1.8% vs. 1.4%). These unsupervised analyses appear to partition the D500 response profile into rapid and slow responders, supporting our hypothesis that the TRPV3 channel is associated with a phasic calcium response.

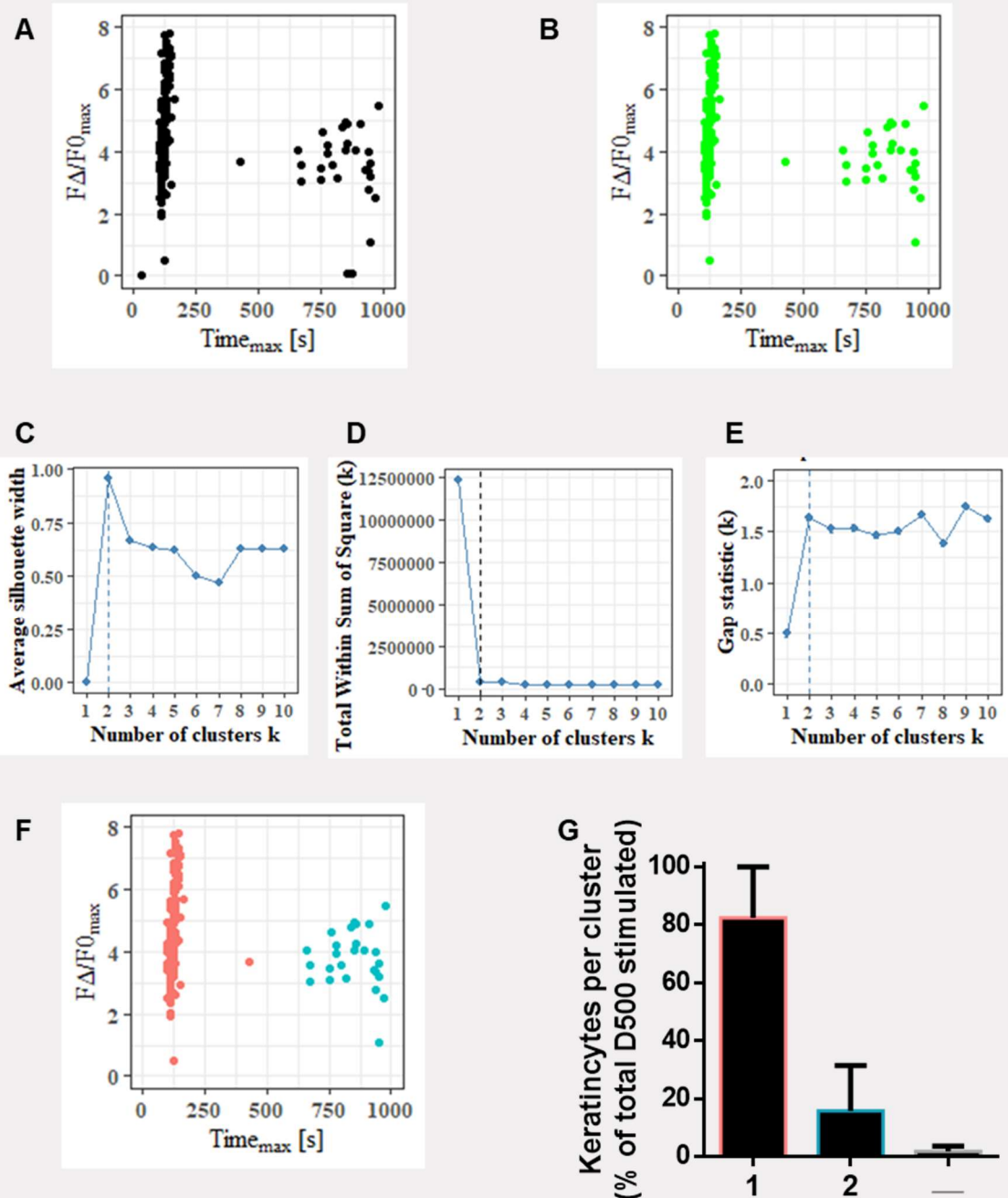


Figure 4.10. Clustering analysis highlights phasic nature of the TRPV3 agonist-induced calcium response.

A—B, TRPV3 response profile graphed in RStudio: all recorded cells (**A**) and only D500-responsive cells (**B**). Each dot represents a single cell. **C—E**, Determination of optimal number of clusters (k) using silhouette (**C**), elbow (**D**), and gap statistic (**E**) methods: optimal $k=2$ (dotted line). **F**, TRPV3 response profile showing drofenine-responsive cells coloured by cluster ($k=2$): orange [cluster 1] and blue [2]. **G**, Percentage of D500-stimulated cells assigned to each cluster, with bars indicating mean + SEM. Percentage of drofenine-insensitive cells (–) also shown. Boxplots indicate median (Q¹ – Q³), with bars outlining min and max values. Data represent 5 independent stimulations ($n=205$ keratinocytes). P -values calculated using Mann-Whitney test: ** $P \leq .01$; *** $P \leq .001$.

Visual examination of the partitioned D500 response profile suggests that the subgroups are defined by distinct peak latencies. Here, we examined whether the parameters of the calcium response were significantly different in cluster 1 and cluster 2 keratinocytes (Mann-Whitney). AUC is a measure of the overall calcium response, with values incorporating both the duration and magnitude of cellular activation. AUC values were significantly different in each cluster ($P < .0001$). The median AUC of cluster 1 was almost double that of cluster 2 (385 vs. 198 arbitrary units [a.u.]) (**Figure 4.11A**). Peak amplitude values were significantly different in each cluster ($P < .0001$). In cluster 1, calcium peaks reached about 440% above baseline; in cluster 2, peaks reached about 370% ($F\Delta/F0_{\max} = 4.41$ vs. 3.76 a.u.) (**Figure 4.11B**). As expected, peak latency values were significantly different in each cluster ($P < .0001$). Cluster 1 covered cells peaking between 100 and 430 s, while cluster 2 covered cells peaking between 660 and 980 s (**Figure 4.11C**). Thus, this unsupervised clustering segregated the D500 response profile into rapid and slow responders.

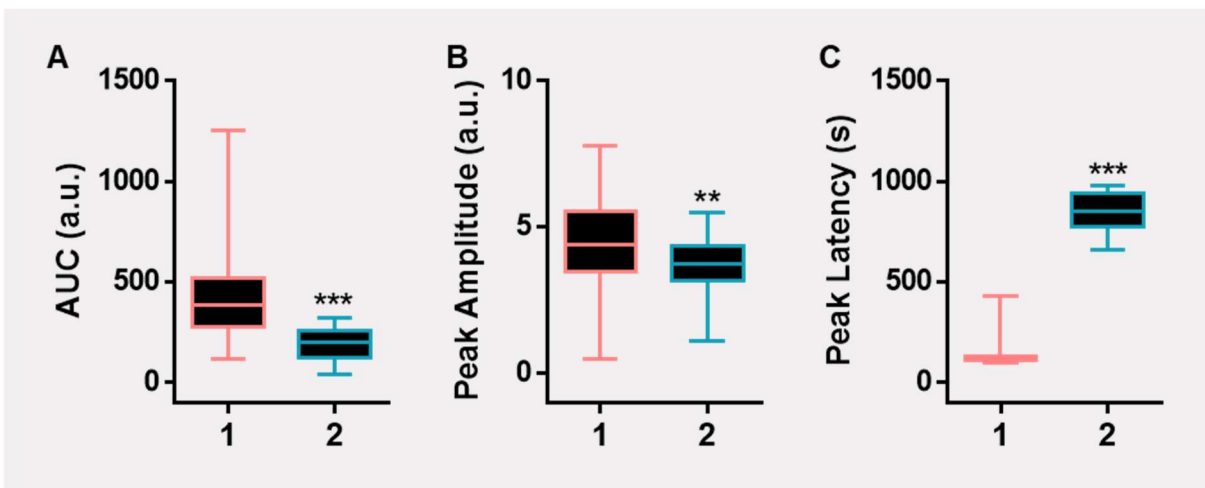


Figure 4.11. Cluster subgroups show distinct overall and peak calcium response parameters.

A–C, Comparison of clusters with respect to area under the curve (AUC, arbitrary units [a.u.]) (A); peak amplitude ($F\Delta/F0_{\max}$, a.u.) (B); and peak latency (Time_{\max} , s) (C). Boxplots indicate median ($Q^1 - Q^3$), with bars outlining min and max values. Data represent 5 independent stimulations ($n = 205$ keratinocytes). P -values calculated using Mann-Whitney test: ** $P \leq .01$; *** $P \leq .001$.

Though the biological relevance remains unclear, activation of TRPV3 elicits a phasic calcium response in cultured human epidermal keratinocytes. A similar temporal pattern has been described in *in vivo* itch studies. Intradermal injection of a TRPV3 agonist solution (carvacrol, 1%) evoked 2 phases of TRPV3-dependent scratching in mice: scratching bouts peaked between 0- and 5-minutes post-injection and again between 20- and 25-minutes post-injection (see **Figure 1.27**) (Cui *et al.*, 2018). The link between these *in vivo* findings and our *in vitro* work remains theoretical. However, it is possible that this phasic scratching behaviour is linked to the activation dynamics of the TRPV3 channel. The work outlined herein also represents a useful proof-of-principle, highlighting the value of both single-cell analyses and the clustering framework. Future experiments should record at lower magnification to include a higher number of cells per stimulation. This experimental modification should enhance the utility of the method and permit robust comparative analyses.

4.2.3. Pharmacological blockade of endocytosis alters the temporal features of the TRPV3 calcium response

Earlier findings showed that D500 evokes phasic activation in epidermal keratinocytes, with cellular calcium peaks clustering into distinct temporal subgroups: rapid vs. slow responders. A similar phasic pattern was described in a mouse model of TRPV3-evoked scratching (Cui *et al.*, 2018). We hypothesised that this itch-like behaviour may be linked to the functional dynamics of TRPV3 calcium response. However, the mechanisms driving these functional dynamics remained unknown; here, we investigated the role of endocytosis and receptor cycling. Specifically, using single-cell analyses and the clustering framework, we quantified the effect of an endocytosis inhibitor on drofenine-evoked calcium flux. This work aims to validate previous findings, assess the power of the framework for comparative analyses, and examine the mechanisms underpinning the phasic TRPV3 response.

Normal human epidermal keratinocytes (NHEK) were cultured in specialised imaging dishes (μ -Dish 35 mm). Keratinocytes were loaded with a cell-permeant fluorescent calcium indicator (Fluo-4 AM) and treated with basal medium \pm Pitstop2 (25 μ M; 30 min), an inhibitor of clatherin-dependent and -independent endocytosis. Fluorescence was monitored using confocal microscopy (1400 seconds [s] total). As suggested in the previous section, a lower magnification (10x) was used to better capture the population and increase the overall sampling rate. Following a baseline recording (100 s), all keratinocytes were stimulated with medium + drofenine (500 μ M) (D500): the only difference between the 2 D500 groups was the pre-treatment (control vs. Pitstop2) (**Figure 4.12**).

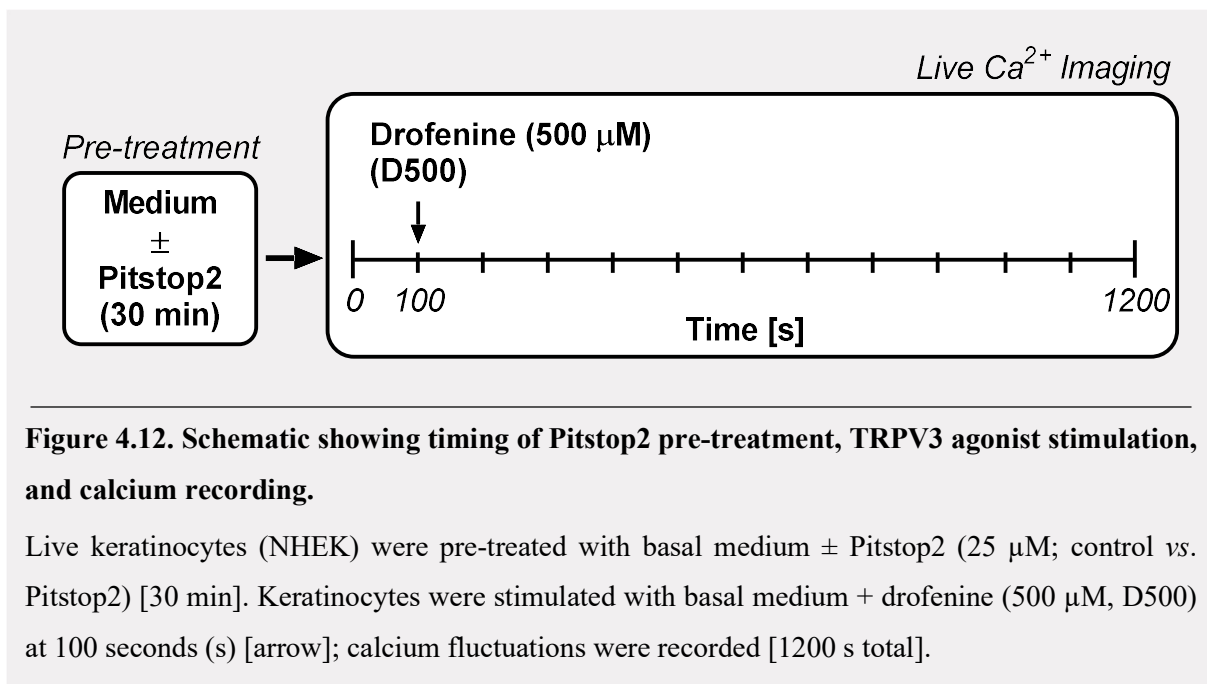


Figure 4.12. Schematic showing timing of Pitstop2 pre-treatment, TRPV3 agonist stimulation, and calcium recording.

Live keratinocytes (NHEK) were pre-treated with basal medium \pm Pitstop2 (25 μ M; control vs. Pitstop2) [30 min]. Keratinocytes were stimulated with basal medium + drofenine (500 μ M, D500) at 100 seconds (s) [arrow]; calcium fluctuations were recorded [1200 s total].

D500-evoked calcium dynamics were first evaluated with respect to the population average; time course fluorescence data was plotted as the average change in fluorescence at each time point. In both groups, addition of D500 enhanced the fluorescent signal: control (**Figure 4.13A**) and Pitstop2 (**Figure 4.13B**). Visual examination of these time course traces revealed notable variation –some stimulations took almost 4 minutes to induce any change in fluorescence. This delay or initiation latency was inconsistent with previous results, where D500 consistently elicited rapid calcium fluctuations. Initiation latency was not correlated with pre-treatment (control vs. Pitstop2; Pearson correlation, $P = .5717$) but was strongly correlated with stage position on the x-axis (Pearson correlation, $P = .0001$) (**Figure 4.13C**). We concluded that initiation latency represents experimental noise and was likely a by-product of the physical experimental setup (i.e. the comparatively larger imaging dishes). To minimise the impact of this noise, time values were equalised to seconds post initiation (s.p.i.) (see section 2.2.6.1 for further details).

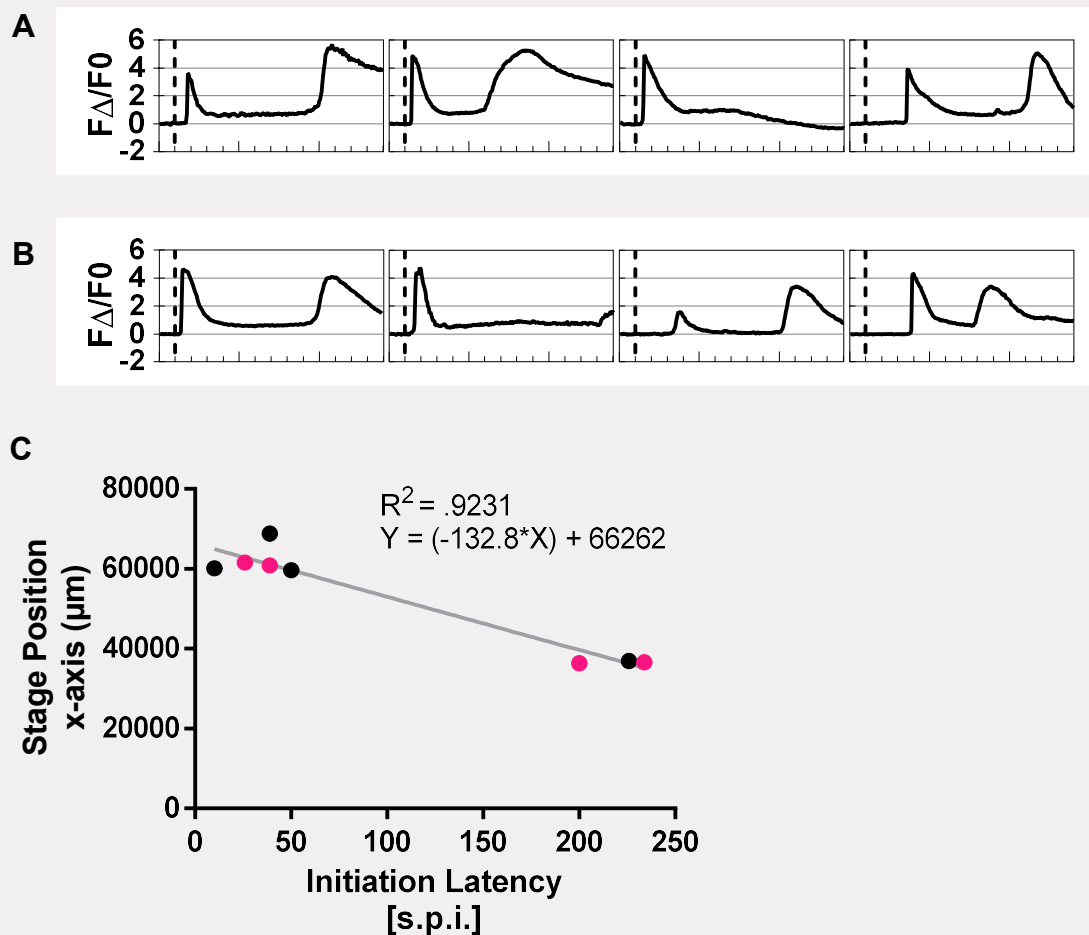


Figure 4.13. Raw temporal response data correlates with stage position.

A—B, Representative single-cell traces of 8 drofenine-responsive cells showing D500-evoked change in fluorescence (F_{Δ}/F_0) over time: control (**A**) and Pitstop2 (**B**). The x-axis of each trace represents 1400 seconds (s). **C**, Correlation of initiation latency (seconds post initiation [s.p.i.]) vs. stage position on the x-axis (μm). Stimulations are coloured by experimental group: control (black) and Pitstop2 (pink).

We first examined whether endocytosis inhibition would affect the overall proportion of D500-sensitive vs. -insensitive keratinocytes. D500-insensitive cells are defined as those which fail to reach $F \Delta / F_0 \geq 0.3$ following stimulation. Here, Pitstop2 caused a slight, but insignificant, reduction in the percentage of drofenine-insensitive cells (2.2% vs. 1.2%; Chi-squared, $P = .6212$) (**Figure 4.14**). These data suggest that overall expression of the TRPV3 channel is unchanged.

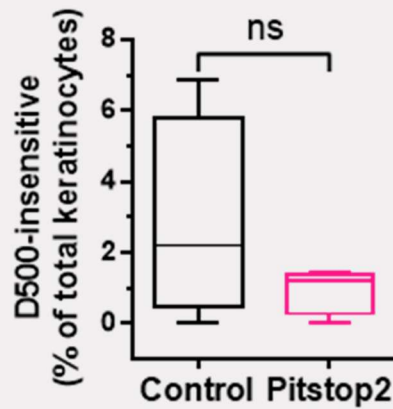


Figure 4.14. Endocytosis inhibitor fails to significantly affect proportion of TRPV3 agonist insensitive keratinocytes.

Graph depicts percentage of keratinocytes (NHEK) that failed to respond to drofenine (500 μM , D500) in control and Pitstop2 populations. Boxplots indicate median ($Q^1 - Q^3$), with bars outlining min and max values. Data represent 4 independent stimulations ($n \geq 797$ keratinocytes per group). P -values calculated using Fisher's exact test: ns $P > .05$.

We then assessed whether endocytosis inhibition would affect the number of calcium peaks in each of the D500-sensitive cells. In control samples, D500 primarily evoked a single calcium peak (64% of cells); 2 and even 3 peaks were detected in a smaller number of cells (35% and 1%, respectively) (**Figure 4.15**). Where D500 induced a single peak, calcium responses were generally rapid: these cells crossed the activation threshold (i.e. $F \Delta / F_0 \geq 0.3$) at just 20 s.p.i. (15 – 25) and peaked at 50 s.p.i. (30 – 870). In pitstop2 samples, D500 was associated with statistically comparable proportions (Chi-squared, $P = .2511$). These data suggest that kinetics of the TRPV3 channel are unchanged.

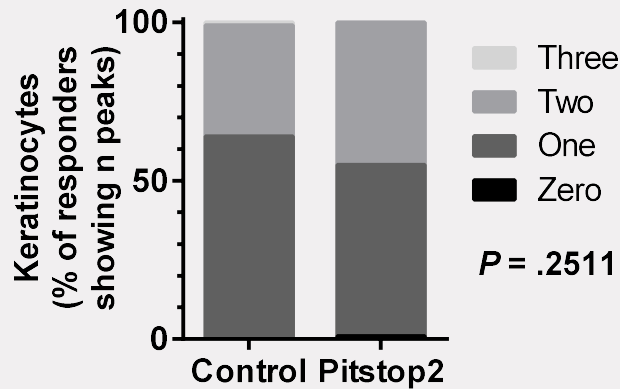


Figure 4.15. Endocytosis inhibitor fails to significantly affect the number of drofenine-induced calcium peaks per cell.

Graph depicts the proportion of drofenine-responsive keratinocytes showing zero, one, 2, or 3 calcium peaks ($P = .2511$; ns). Data represent 4 independent stimulations ($n \geq 797$ keratinocytes per group). P -values calculated using Chi-squared test.

The average $F\Delta/F0$ graph revealed a clear difference between the D500 response in control and Pitstop2 groups; this graph depicts the average change in cellular fluorescence at each time point (control [black] vs. Pitstop2 [pink]) (Figure 4.16A). Similar to previous findings, D500 evoked a rapid increase in average intracellular calcium. The amplitude of this rapid phase was unaffected by Pitstop2: in both groups, this phase peaked at more than 300% above baseline (mean $F\Delta/F0 = 3.08$ vs. 3.14; at 45 s.p.i.). Unlike previous data, the average transients shown here highlight the later phases of the calcium response; this is likely explained by the comparatively higher sampling rate. Here, Pitstop2 reduced the amplitude of the later D500-evoked peaks. At 615 s.p.i., the average amplitude in Pitstop2 samples was more than 70% lower than control levels (mean $F\Delta/F0 = 1.47$ vs. 0.42; Mann-Whitney, $P < .0001$). At 955 s.p.i., the average amplitude in Pitstop2 samples was around 40% lower than control levels (mean $F\Delta/F0 = 1.95$ vs. 1.23; Mann-Whitney, $P < .0001$). This difference is illustrated in representative images (Figure 4.16B [control] and Figure 4.16C [Pitstop2]). Pitstop2 also significantly alters the parameters of the calcium response, including area under the curve (AUC) and total peak area (TPA) (Mann-Whitney, $P < .0001$ for all measures) (Table 4.3). Together, these data suggest that inhibition of endocytosis alters the dynamics of the TRPV3 calcium response in populations of epidermal keratinocytes.

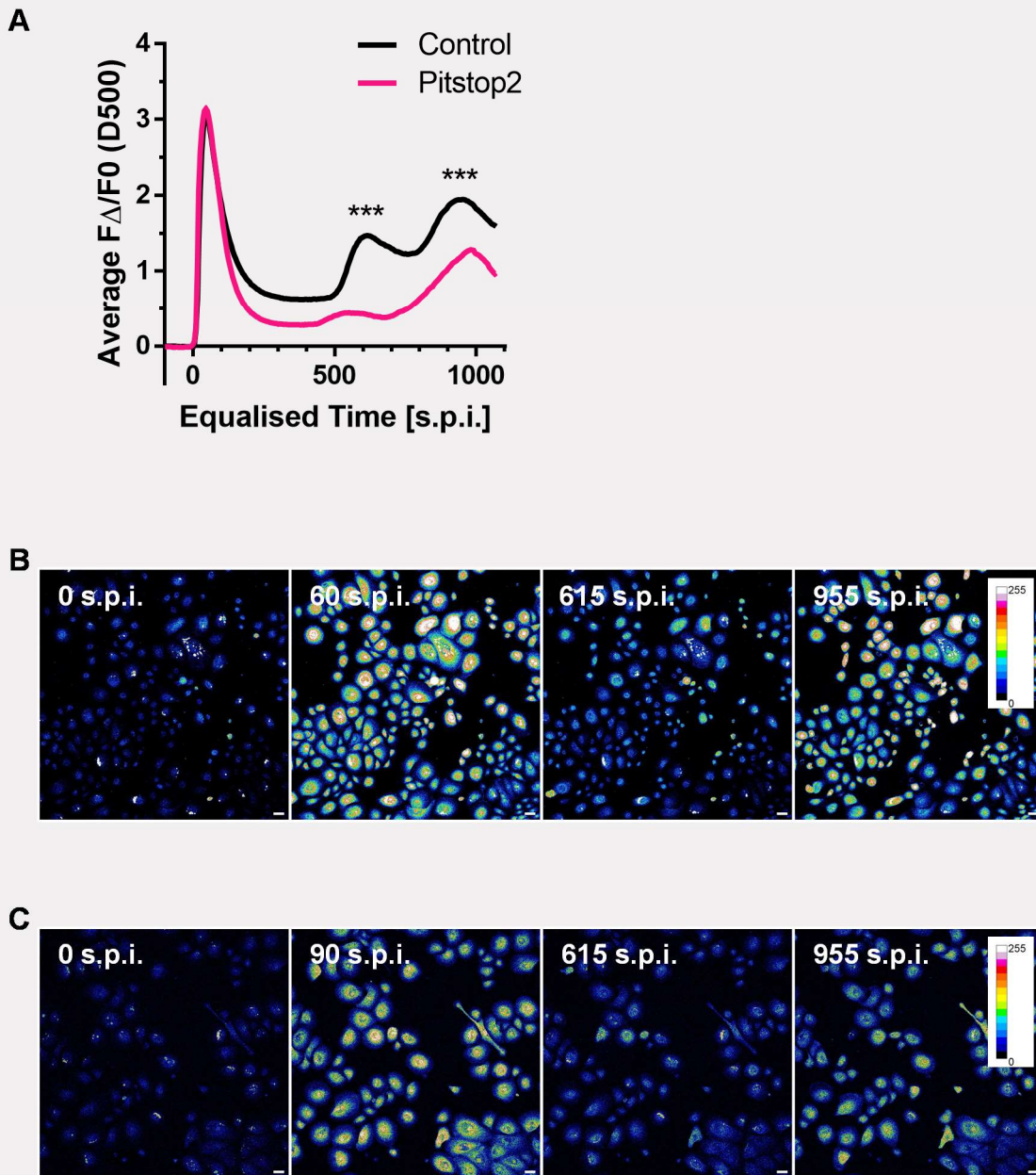


Figure 4.16. Endocytosis inhibitor alters the later phases of the TRPV3 agonist-induced calcium response.

A, Graph depicts average change in fluorescence (F_{Δ}/F_0) over time following addition of drofenine 500 μM (D500) in control (black) and Pitstop2 (pink) populations. Significance refers to the difference in F_{Δ}/F_0 values at 615 seconds post initiation (s.p.i.) and 955 s.p.i. (control vs. Pitstop2). Data represent 4 independent stimulations ($n \geq 797$ keratinocytes per group). **B—C**, Representative images showing fluorescence following drofenine (500 μM) application at each named timepoint (0, 60/90, 615, and 955 s.p.i.) in control (**B**) and Pitstop2 populations (**C**). White indicates highest signal. Scale bar = 50 μm .

Table 4.3. Calcium response parameters following TRPV3 agonist stimulation: effect of endocytosis inhibitor Pitstop2 vs. control.

Parameter	Control [797]	Pitstop2 [816]	<i>P</i>
Mean fl. change (FΔ/F0)	1.16 (0.86 – 1.50)	0.64 (0.37 – 0.96)	***
Peak amplitude (FΔ/F0)	4.25 (3.53 – 5.10)	3.97 (2.73 – 5.24)	***
Peak latency (s.p.i.)	585 (30 – 880)	45 (25 – 65)	***
AUC (a.u.)	1090 (783 – 1493)	626 (490 – 867)	***
TPA (a.u.)	1041 (707 – 1449)	488 (264 – 813)	***

Note: Data are expressed as median ($Q^1 - Q^3$). *Abbreviations:* a.u., arbitrary unit; F., fluorescence; FΔ/F0, change in fluorescence; s, seconds; AUC, area under the curve; TPA, total peak area. Square brackets indicate cells per group from 4 independent stimulations.

Single-cell focused analyses were then undertaken. This work examined the peak calcium change in each D500-stimulated keratinocyte, calculating the amplitude ($F\Delta/F0_{max}$) and latency ($Time_{max}$) of each peak. Response profiles from control populations were imported to RStudio and examined for clusters. Gap statistic testing revealed 4 to be the optimum number of clusters in this control dataset (**Figure 4.17A**). Control data were partitioned using *k*-means clustering ($k = 4$) (**Figure 4.17B**). Although clustering is unsupervised, peak latency values represent a key factor in cluster determination. Clusters in control data show distinct median latency values: 30 s.p.i. (10 – 100 [Min. – Max.], Cluster 1); 625 s.p.i. (335 – 735, Cluster 2); 865 s.p.i. (740 – 920, Cluster 3); 980 s.p.i. (925 – 1070, Cluster 4) ($P < .0001$). These data solidify previous results and reveal the high proportion of cells which show these later calcium peaks.

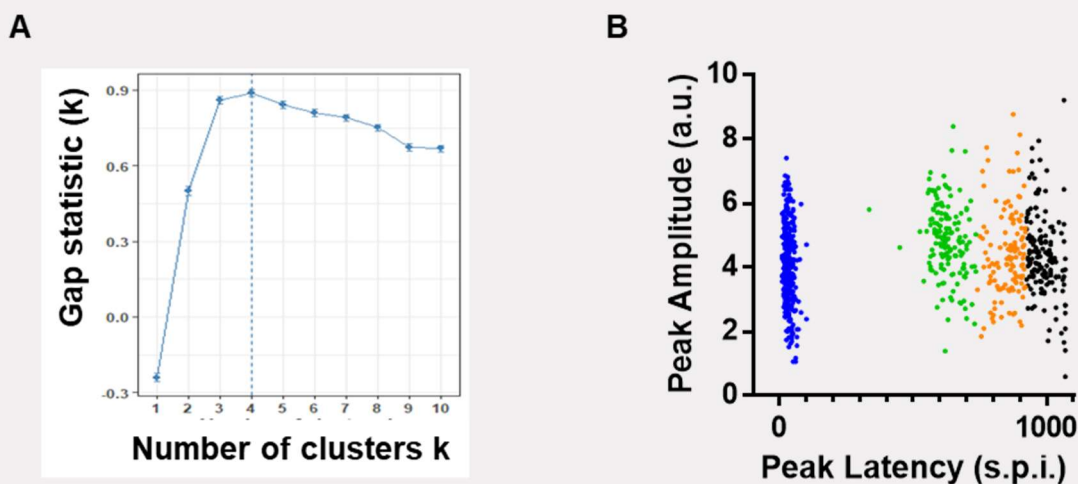
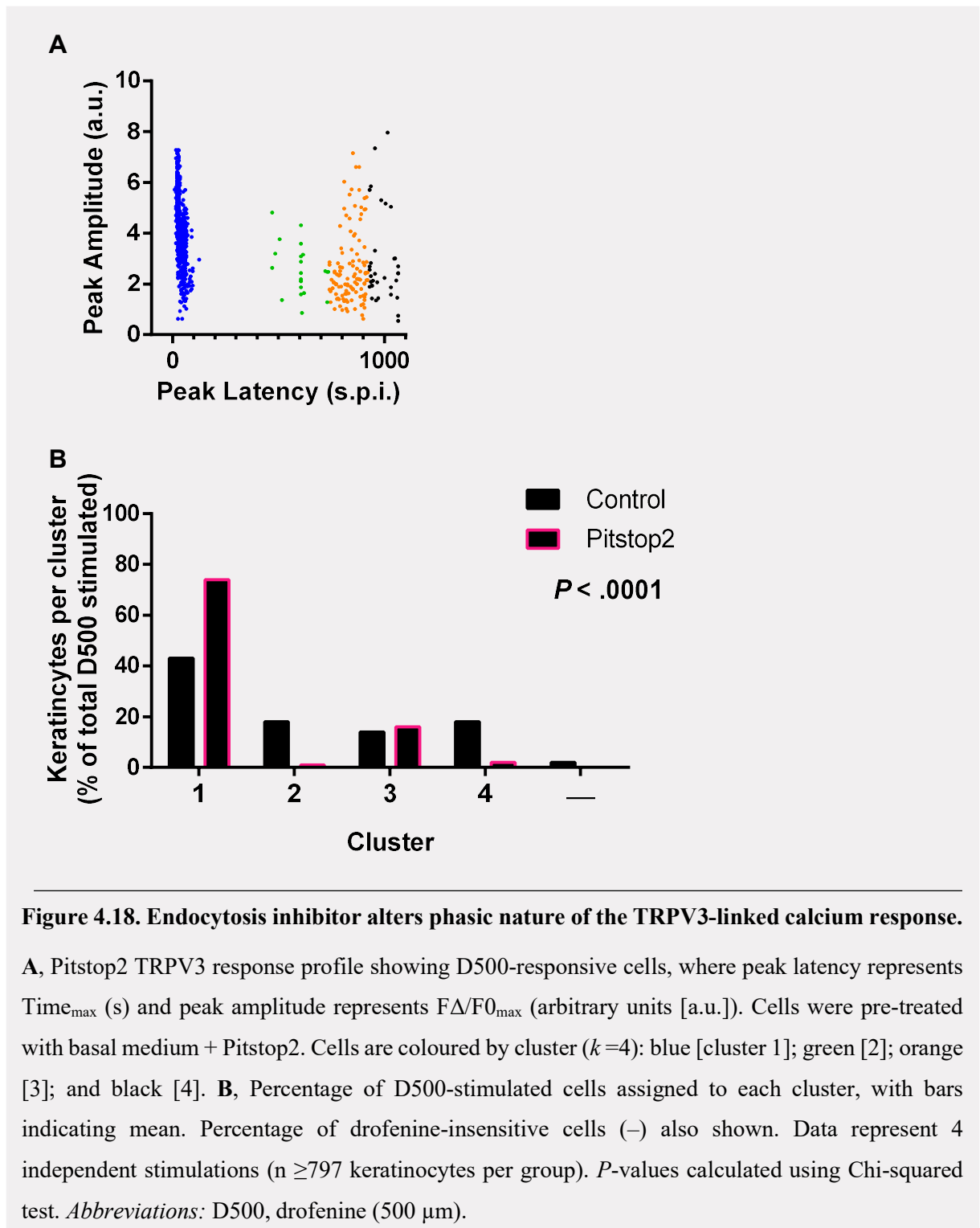


Figure 4.17. Clustering analysis of control TRPV3-linked calcium response profile.

A, Determination of optimal number of clusters (k) within the control TRPV3 response profile using gap statistic method: optimal $k = 4$ (dotted line). **B**, Control TRPV3 response profile showing D500-responsive cells, where peak latency represents Time_{\max} (s) and peak amplitude represents $F\Delta/F0_{\max}$ (arbitrary units [a.u.]). Cells were pre-treated with basal medium. Cells are coloured by cluster ($k = 4$): blue [cluster 1]; green [2]; orange [3]; and black [4]. Data represent 4 independent stimulations ($n \geq 797$). *Abbreviations*: D500, drofenine (500 μm).

Experimental data (Pitstop2) were then assigned to clusters using the limits of each control cluster. This method allows us to assess the effect of Pitstop2 on D500-evoked calcium peaks. Visual comparison of D500 response profiles revealed clear differences: control (**Figure 4.17B**) and Pitstop2 (**Figure 4.18A**). Pitstop2 was associated with a striking reduction in number of cells displaying the later calcium peaks. This effect was also illustrated in the proportion of responders assigned to each cluster (**Figure 4.18B**). Cluster 2 and 4 were almost absent in Pitstop2 samples: although control populations averaged about 18% for both clusters, Pitstop2 averaged at just 2% and 3%, respectively – a reduction of more than 80%. Cluster 3 responders were unchanged (14% vs. 16%). Quantification revealed a dramatic change in the proportion of cluster 1 responders: Pitstop2 increased the average percentage of rapid responders from around 43% to more than 70%. As discussed previously, the average percentage of drofenine-insensitive cells was low in each of the groups ($\leq 3\%$). Overall, Pitstop2 significantly altered the proportion of D500-responsive cells assigned to each cluster (Chi-squared, $P < .0001$). These data reinforce the hypothesis that inhibition of endocytosis alters the dynamics of the TRPV3 calcium response in populations of epidermal keratinocytes.



This work used calcium imaging and unsupervised clustering analyses to reveal subtle differences in the TRPV3 response. TRPV3 drives a phasic calcium response in epidermal keratinocytes; these dynamics are dependent on endocytosis. We propose that the rapid phase may be mediated by TRPV3 channels located on the plasma membrane, with cluster 1 cells likely expressing high levels of surface TRPV3. We postulate that Pitstop2 interrupts normal recycling of TRPV3, trapping the channels on the cell surface and increasing the proportion of cluster 1, rapid responders. These findings suggest that TRPV3 channels undergo high levels of receptor cycling, even under basal conditions. Pitstop2

caused a striking reduction in the later phases of the TRPV3 calcium response. These later responders were likely converted to rapid responders through inhibition of normal receptor cycling. However, this effect was specific to cluster 2 and cluster 4 cells – cluster 3 cells were unaffected – suggesting that these later phases may be mediated by distinct mechanisms. Together, these findings delineate TRPV3 response profiles in human epidermal keratinocytes, solidifying earlier results and highlighting the utility of the analysis framework. Response profiles were highly dependent on endocytosis pathways suggesting that receptor cycling underpins the temporal features of the TRPV3 channel in human epidermal keratinocytes.

4.2.4. Knockdown of VAMP3 alters TRPV3-linked calcium responses; however, issues with controls negate robust conclusions

Pharmacological activation of TRPV3 is associated with a phasic calcium response in human keratinocytes. This temporal pattern is dependent on functional endocytosis pathways, suggesting that receptor cycling underpins the phasic activity. However, the SNARE proteins involved in TRPV3 membrane insertion and trafficking remained unknown. VAMP1/2/3 is a particularly important SNARE protein in neuronal TRP trafficking and keratinocyte-derived inflammation (Meng *et al.*, 2016; Meng *et al.*, 2019). Here, we investigated the effect of VAMP3 knockdown on drofenine-evoked calcium fluctuations.

Normal human epidermal keratinocytes (NHEK) were treated with control nontargeting (NT) or VAMP3-targeting (V3T) lentiviral particles. Infected keratinocytes were selected with puromycin and VAMP3 expression was examined by western blot. VAMP3 was reduced in V3T cultures relative to NT controls (**Figure 4.19A**). Densitometry data were transformed and shown as a percentage of control VAMP3 level (**Figure 4.19B**). In V3T cultures, VAMP3 expression was reduced by almost 80% relative to NT control levels indicating that VAMP3 was successfully knocked down.

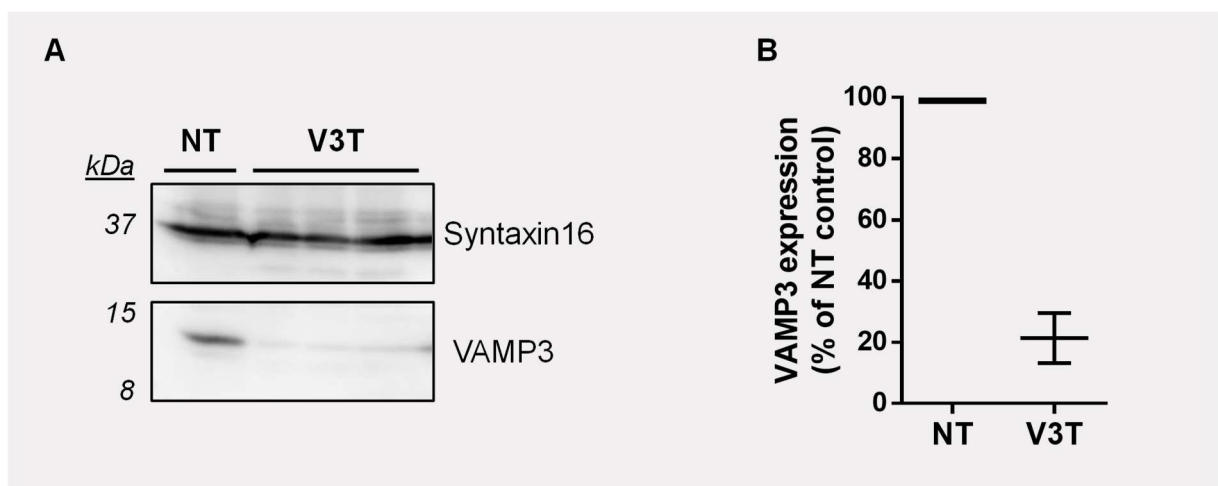


Figure 4.19. VAMP3-targeted shRNA successfully reduced VAMP3 expression.

Keratinocytes (NHEK) were treated with nontargeted (NT) and (VAMP3-targeted) V3T lentiviral particles. **A**, Western blot analysis of VAMP3 expression in NT and V3T lysate. Syntaxin16 is also shown (internal control). **B**, Comparison of VAMP3 expression as a percentage of NT level. Plots indicate median ($Q^1 - Q^3$) of 2 independent knockdown events, with bars outlining min and max values.

NT and V3T keratinocytes were loaded with a cell-permeant fluorescent calcium indicator (Fluo-4 AM) and calcium dynamics were recorded using confocal imaging. The experimental setup was identical to Section 4.2.2 (**Figure 4.20**). Following a baseline recording, keratinocytes were stimulated with a TRPV3 agonist, drofenine (500 μ M) (D500), and cellular responses were monitored for 1000 s.

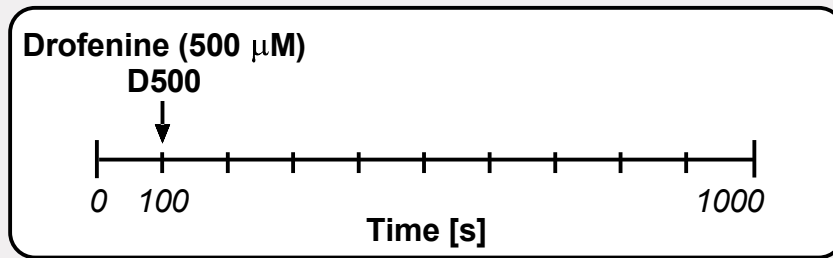


Figure 4.20. Schematic showing timing of TRPV3 agonist stimulation in keratinocytes treated with control nontargeted or VAMP3-targeted lentiviral particles.

Live nontargeted (NT) and VAMP3-targeted (V3T) keratinocytes (NHEK) were stimulated with basal medium + drofenine (500 μ M, D500) at 100 seconds (s) [arrow]; calcium fluctuations were recorded [1000 s total].

We first examined whether VAMP3 knockdown would affect the overall proportion of D500-sensitive vs. -insensitive keratinocytes. D500-insensitive cells are defined as those which fail to reach $F\Delta/F_0 \geq 0.3$ following stimulation. Addition of D500 was associated with elevated fluorescence in both NT and V3T populations. However, VAMP3 knockdown significantly altered the sensitivity of keratinocytes to D500 (Fisher's exact, $P < .0001$) (**Figure 4.21**). In NT cultures, less than 1% of cells were D500-insensitive; this figure increased to almost 20% in V3T cultures (0.76% vs. 18.49%). Thus, VAMP3 knockdown reduced the number of functional TRPV3⁺ keratinocytes. These data indicate that VAMP3 is essential for normal TRPV3 trafficking and plasma membrane insertion.

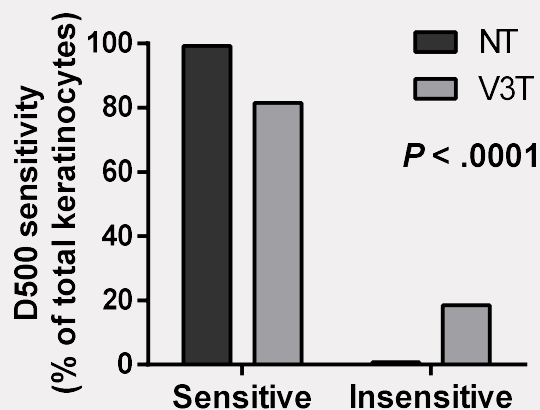


Figure 4.21. Knockdown of VAMP3 increases proportion of TRPV3 agonist insensitive cells.

Graph depicts percentage of keratinocytes (NHEK) that responded or failed to respond to drofenine (500 μ M, D500) in nontargeted (NT) and VAMP3-targeted (V3T) cultures. Plots indicate mean values. Data represent ≥ 4 independent stimulations per group (n =162 [NT] or 424 [V3T] keratinocytes; 2 independent knockdown events). P -values calculated using Fisher's exact test.

Drofenine-evoked calcium dynamics were then evaluated with respect to the population average; time course fluorescence data was plotted as the average change in fluorescence at each time point. These graphs revealed a surprising difference. The amplitude of the characteristic rapid peak was notably reduced in NT controls (black), with the average trace being almost 40% lower than that of the V3T group (grey) (**Figure 4.22A**). NT controls also displayed a striking overshoot of calcium normalisation; this feature was not evident in previous data. These strange results were echoed in the analyses of cellular activation (area under the curve [AUC]) and peak calcium responses (peak amplitude [$F\Delta/F0_{max}$] and peak latency [$Time_{max}$]). Both AUC and peak amplitude were significantly higher in V3T samples, relative to NT controls (Mann-Whitney, $P < .0001$ for both) (**Figure 4.22B** and **Figure 4.22C**), indicating that the amplitude of the calcium response was altered. Median peak latency was also higher in V3T samples, relative to NT controls (Mann-Whitney, $P = .0431$) (**Figure 4.22D**), indicating that the speed of the response was altered. These data suggested that the NT particles may have impaired the calcium response.

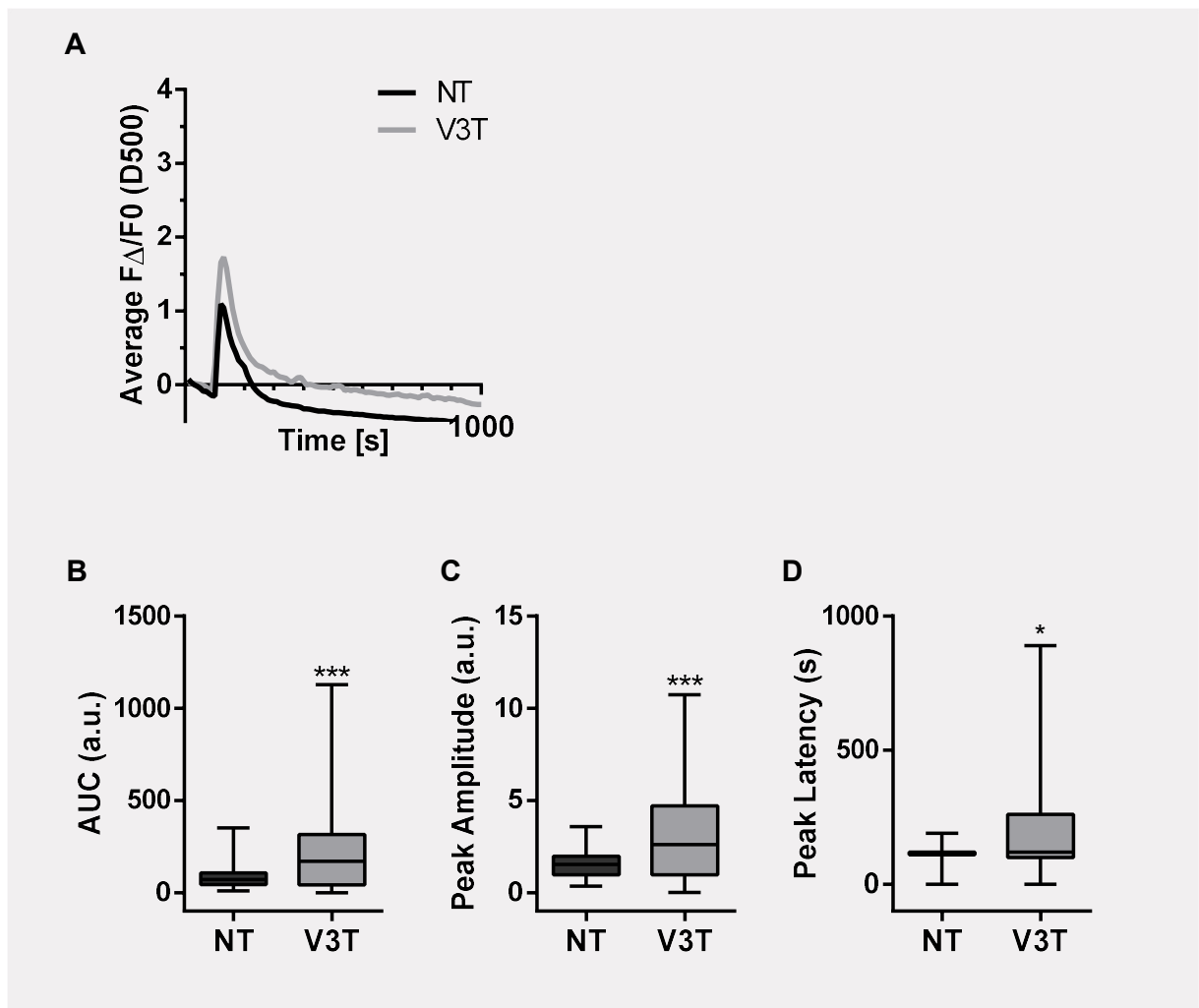


Figure 4.22. Knockdown of VAMP3 altered the TRPV3 agonist-induced calcium response.

A, Graph depicts average change in fluorescence ($F\Delta/F0$) over time following addition of drofenine 500 μ M (D500) in nontargeted (NT) controls (black) and VAMP3-targeted (V3T) (grey) populations. **B–D**, Comparison of calcium peak parameters in NT and V3T populations: area under the curve (AUC, arbitrary units [a.u.]) (**B**); peak amplitude ($F\Delta/F0_{max}$, a.u.) (**C**); and peak latency ($Time_{max}$, s) (**D**).

(D). Boxplots indicate median ($Q^1 - Q^3$), with bars outlining min and max values. Data represent ≥ 4 independent stimulations per group (n =162 [NT] or 424 [V3T] keratinocytes; 2 independent knockdown events). *P*-values calculated using Mann-Whitney test: * $P \leq .05$; *** $P \leq .001$.

This work followed the experimental setup and imaging settings described in section 4.2.2. Experiments were carried out using the same donor batch of keratinocytes. Thus, data from this previous section represents a comparable normal control response. Here, we compared NT and V3T results to these normal data. Visual comparison of the population average transients ($F\Delta/F0$) revealed clear differences: V3T samples (black) showed a striking reduction in their average transient relative to the normal control (red) (**Figure 4.23A**). Single-cell analyses of cellular activation and peak calcium responses also showed significant differences relative to normal controls. AUC, peak amplitude, and peak latency were altered in NT cells relative to normal (Kruskal-Wallis, $P < .0001$ for all measures) (**Figure 4.23B**, **Figure 4.23C**, and **Figure 4.23D**). Comparisons also suggest that VAMP3 knockdown may alter D500-evoked calcium responses: all measures were significantly different in V3T cells relative to normal controls (Kruskal-Wallis, $P < .0001$). We also compared the D500 response profile of each group: normal control (**Figure 4.23E**); NT control (**Figure 4.23F**); and V3T (**Figure 4.23G**). NT controls displayed rapid, low amplitude calcium peaks. In contrast with normal controls, calcium peaks in V3T populations were highly varied suggesting that knockdown of VAMP3 dysregulates the phasic nature of the TRPV3 response. These comparisons illustrate the shift in the NT control response, while also outlining a possible V3T-induced effect. Thus, the temporal features of TRPV3 activation are likely dependent on VAMP3 expression.

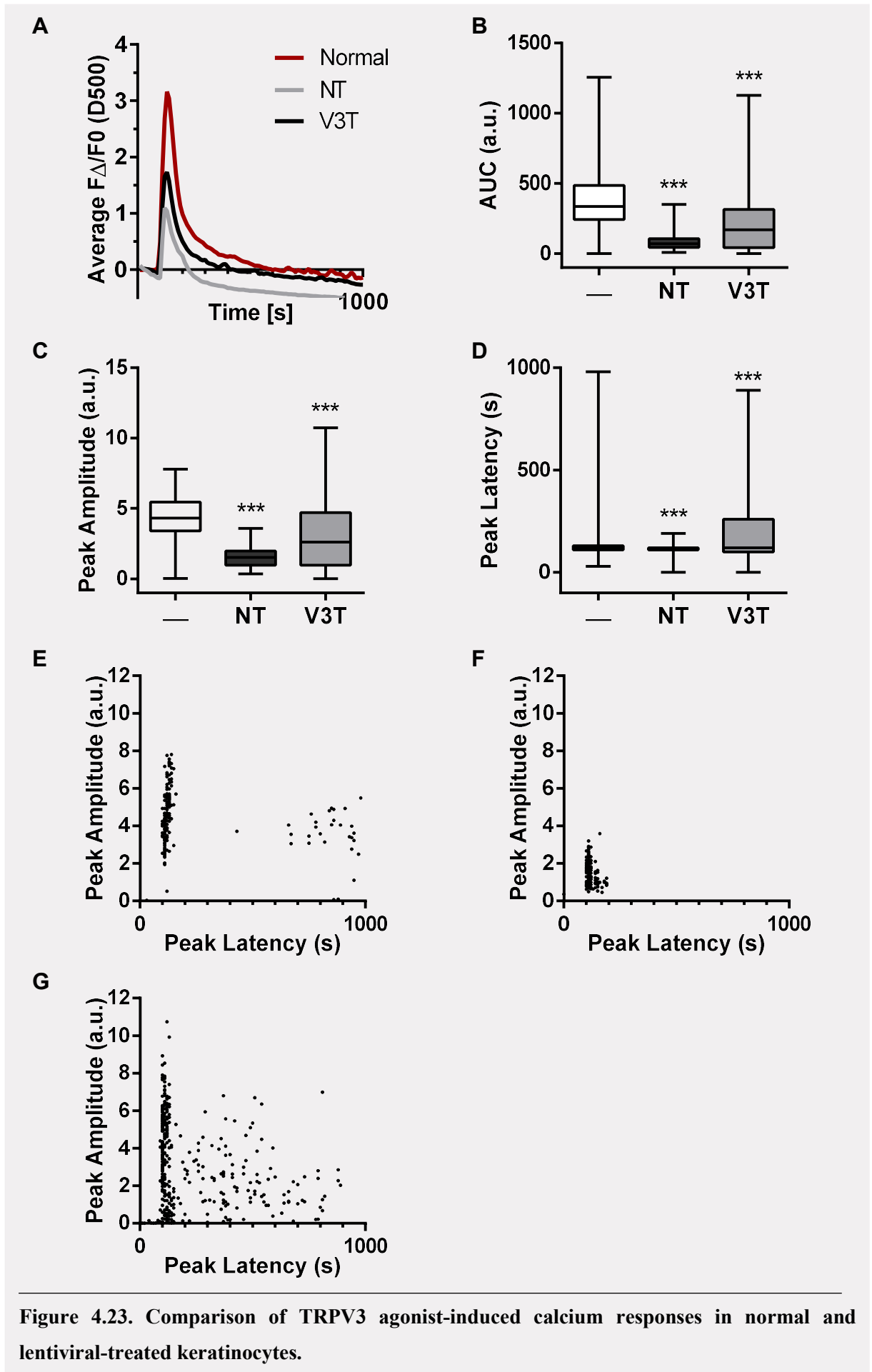


Figure 4.23. Comparison of TRPV3 agonist-induced calcium responses in normal and lentiviral-treated keratinocytes.

A, Graph depicts average change in fluorescence ($F\Delta/F0$) over time following addition of drofenine 500 μ M (D500) in normal controls (red), nontargeted (NT) controls (grey), and VAMP3-targeted (V3T) (black). **B—D**, Comparison of D500-evoked calcium response parameters in normal controls (–), NT controls, and V3T: area under the curve (AUC, arbitrary units [a.u.]) (**B**); peak amplitude ($F\Delta/F0_{\max}$, a.u.) (**C**); and peak latency (Time_{\max} , s) (**D**). **E—G**, Response profiles showing all recorded cells, where peak latency represents Time_{\max} (s) and peak amplitude represents $F\Delta/F0_{\max}$ (arbitrary units [a.u.]): normal control (**E**); NT control (**F**); and V3T (**G**) populations. Boxplots indicate median ($Q^1 - Q^3$), with bars outlining min and max values. Data represent ≥ 4 independent stimulations per group (n =162 [NT] or 424 [V3T] keratinocytes; 2 independent knockdown events). Normal control data from a previous section was used for comparison (n =205 keratinocytes). *P*-values calculated using Kruskal-Wallis test (vs. normal control [–]): *** $P \leq .001$.

Together, these findings highlight the importance of VAMP3 expression, while also illustrating the deleterious effect of NT particles on normal calcium flux. VAMP3 knockdown reduced the proportion of D500-sensitive cells and dysregulated the phasic response. We propose that basal TRPV3 trafficking, and membrane insertion is, in part, mediated by VAMP3-dependent exocytosis; however, this hypothesis requires further investigation.

4.2.5. TRPV3 undergoes activation-induced trafficking

Both *in vitro* and *in vivo*, TRPV3 activation is associated with 2 broad phases of activation, with the later phase peaking at approximately 15 minutes. This secondary activation is highly consistent and is dependent on receptor cycling. Our data indicates that this later activation is an important feature of the TRPV3 response, perhaps mediated by trafficking of latent TRPV3 channels to the plasma membrane. Here, we used a highly specific antibody targeting the extracellular region of the TRPV3 channel to examine the impact of drofenine stimulation (15 minutes [min]) on surface TRPV3 expression.

Normal human epidermal keratinocytes (NHEK) were stimulated with basal medium \pm drofenine (500 μ M; 15 min, 5% CO₂, 37°C). The ecto-TRPV3 channel antibody was added to this stimulation buffer (ACC-033; 85 μ g/ml, 15 min). Following stimulation, keratinocytes were probed with secondary antibody, fixed, and mounted. Samples were imaged using confocal microscopy, images were processed and measured using Image J software, and data were analysed using GraphPad Prism.

TRPV3 membrane expression was detected in a subpopulation of untreated control keratinocytes (**Figure 4.24**). This TRPV3 signal was not restricted to the cell surface suggesting that bound TRPV3 channels may have been internalised prior to fixation. TRPV3-positive (TRPV3⁺) cells were larger in size relative to the TRPV3-negative (TRPV3⁻) group; however, basal TRPV3 membrane expression was largely independent of cell shape (**Table 4.4**).

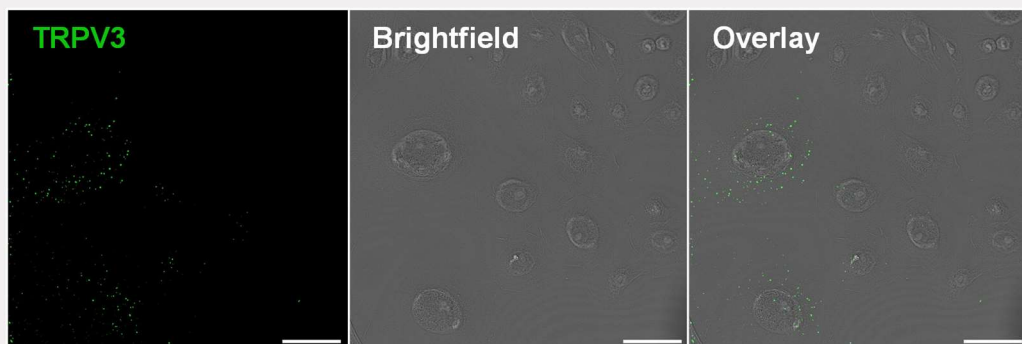


Figure 4.24. Surface TRPV3 proteins were detected in cultured epidermal keratinocytes.

Immunostaining of keratinocytes (NHEK) indicating expression of surface TRPV3 (green) and brightfield signals. Scale bars =50 μ m.

Table 4.4. Basic cellular parameters: TRPV3-positive vs. TRPV3-negative keratinocytes.

Parameter	TRPV3 ⁺ [34.3%]	TRPV3 ⁻ [65.7%]	<i>P</i>
Perimeter (μm)	207 (160 – 280)	131 (89 – 178)	***
Area (μm^2)	2600 (1542 – 5141)	1068 (491 – 1954)	***
Circularity (a.u.)	0.84 (0.78 – 0.90)	0.86 (0.77 – 0.91)	ns
Roundness (a.u.)	0.73 (0.64 – 0.82)	0.76 (0.62 – 0.85)	ns

Note: Data expressed as median ($Q^1 - Q^3$). Square brackets indicate the proportion of cells per group. *Abbreviations:* a.u., arbitrary unit; μm , micrometre; TRPV3⁺, TRPV3-positive; and TRPV3⁻, TRPV3-negative.

We then examined the effect of drofenine (500 μM) stimulation [15 min] on TRPV3 trafficking. Raw image data suggest that drofenine application may strengthen the fluorescence signal, indicating a higher level of TRPV3 membrane expression (**Figure 4.25A**). Again, this signal was not restricted to the cell surface.

Membrane TRPV3 expression is represented by the number of intracellular fluorescent particles per 1500 μm^2 . After just 15 min, drofenine significantly increased membrane TRPV3 expression (Mann-Whitney, $P < .0001$) (**Figure 4.25B**). Drofenine-stimulated cells contained about 10.52 intracellular fluorescent particles per 1500 μm^2 , while the median basal cell contained just 0.87. This increased fluorescent signal suggests that drofenine promotes TRPV3 trafficking. The notable intracellular signal suggests that activated TRPV3 may be internalised. Whether this internalisation leads to further signalling or TRPV3 degradation remains unexplored.

TRPV3⁺ cells were defined as those that express ≥ 5 intracellular fluorescent particles per 1500 μm^2 . Drofenine significantly increased the percentage of TRPV3⁺ cells (Fisher's exact, $P = .0001$) (**Figure 4.25C**). These drofenine-stimulated TRPV3⁺ cells also displayed significantly higher levels of membrane TRPV3 expression, relative to basal TRPV3⁺ cells (Mann-Whitney, $P < .0001$) (**Figure 4.25D**). These data suggest the TRPV3 agonist increases the proportion and sensitivity of TRPV3⁺ cells. Again, this suggests that TRPV3 may undergo activation-induced membrane insertion and trafficking. However, whether this functional upregulation is mediated by intracellular or intercellular signalling remains unknown.

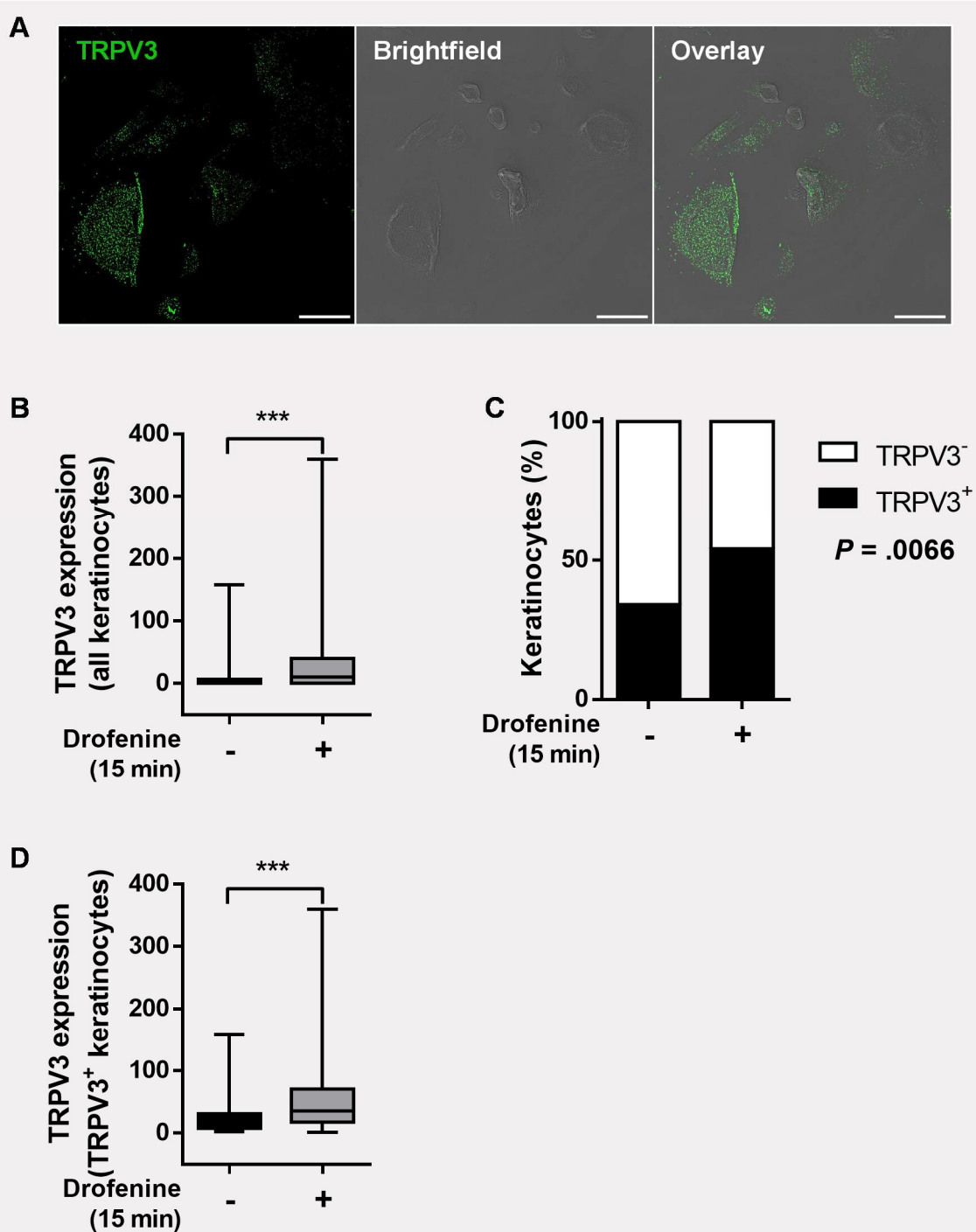


Figure 4.25. TRPV3 channels undergo activation induced trafficking.

A, Immunostaining of drofenine-treated keratinocytes (NHEK) indicating expression of surface TRPV3 (green) and brightfield signals. Scale bars =50 μm . **B—D**, Comparison of control and drofenine-treated populations: surface TRPV3 expression in all imaged cells (**B**); proportion of TRPV3⁺ cells (**C**); and surface TRPV3 expression in TRPV3⁺ cells (**D**). Boxplots indicate median ($Q^1 - Q^3$), with bars outlining min and max values. Data represent 3 independent stimulations (≥ 34 images per group, ≥ 357 keratinocytes per group). P -values calculated using Mann-Whitney (**B** and **D**) and Fisher's exact (**C**) tests: *** $P \leq .001$.

These data confirm TRPV3 membrane expression in human keratinocytes and highlight the role of trafficking in the phasic TRPV3 calcium response. As TRPV3-evoked scratching shows a similar phasic pattern (Cui *et al.*, 2018), these findings may also be important for TRPV3-linked itch.

In a previous section (**Table 4.2**), median cell area values were calculated at about 900 μm^2 . Here, median cell area values are notably higher. This discrepancy is likely explained by differences in the culture conditions. In the earlier example, keratinocytes were cultured and maintained for calcium imaging. To allow population responses, cells were grown to about 70% confluency before imaging. Here, cells were grown at a much lower density (about 40%). This is a common practice in immunocytochemistry as it gives a better view of each cell. In the skin and in culture, keratinocytes will extend their processes and attempt to connect with a nearby cell. This means that cells grown at a lower density will spread out and take up a larger area. This effect likely explains the discrepancies in cell size. Here, membrane TRPV3 expression was represented by the number of intracellular fluorescent particles per 1500 μm^2 . This minimises cell size-related variation and permits cross-experiment comparisons.

Based on the findings herein, we propose that TRPV3⁺ cells and cluster 1 responders may represent the same population within the NHEK model. About 34% of unstimulated keratinocytes were deemed TRPV3⁺; while 43% of cells showed a fast calcium peak (**Figure 4.18B**). Although there is about 9% in the difference, this could be explained by low sensitivity of the TRPV3 immunocytochemistry method.

Together, these data strengthen the hypothesis that surface TRPV3 expression underpins rapid D500-evoked fluctuations. Our data suggests that activation of TRPV3 promotes channel trafficking, increasing the proportion of TRPV3⁺ cells and enhancing TRPV3 membrane expression. Although other mechanisms may play a role, these data suggest that trafficking may be an important factor in the later stages of the TRPV3 calcium response. Thus, blocking receptor cycling could interrupt the phasic TRPV3 calcium response and the delayed component of TRPV3-associated itch.

4.3. Discussion

4.3.1. Summary

This work confirmed the functional expression of TRPA1, TRPV1, and TRPV3 in human epidermal keratinocytes. We identified functional subgroups within the keratinocyte population: TRPA1⁺ and TRPV1⁺ cells likely represent small, non-overlapping subsets within the larger TRPV3⁺ population. Pharmacological activation of TRPV3 was characterised by a biphasic or even multiphasic calcium response in populations of human epidermal keratinocytes. These temporal dynamics were dependent on receptor cycling, with drofenine promoting membrane insertion and trafficking of the TRPV3 channel (**Figure 4.26**). VAMP3 may also play a role in basal TRPV3 trafficking and membrane insertion, though results are inconclusive at present. Together, these findings solidify previous signalling results and add to our understanding of TRP activity in human epidermal keratinocytes.

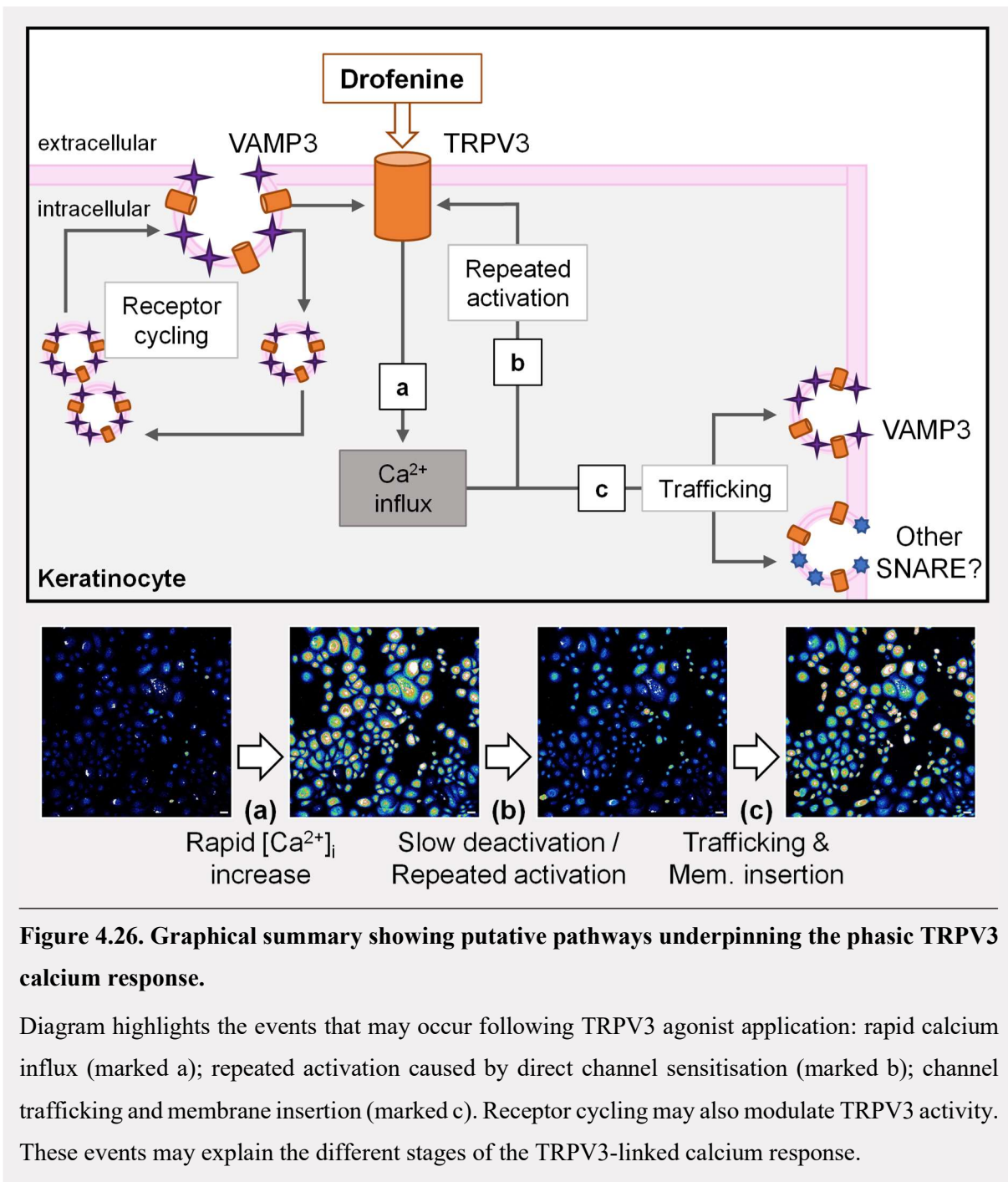


Figure 4.26. Graphical summary showing putative pathways underpinning the phasic TRPV3 calcium response.

Diagram highlights the events that may occur following TRPV3 agonist application: rapid calcium influx (marked a); repeated activation caused by direct channel sensitisation (marked b); channel trafficking and membrane insertion (marked c). Receptor cycling may also modulate TRPV3 activity. These events may explain the different stages of the TRPV3-linked calcium response.

4.3.2. Are TRPV1 and TRPA1 functional in human keratinocytes?

TRPA1 and TRPV1 are well studied in neuronal cells. However, our understanding of their function in keratinocytes is incomplete. TRPA1 and TRPV1 proteins have been detected in human keratinocytes and skin biopsies (Atoyan *et al.*, 2009; Denda *et al.*, 2001). While reports suggest that both channels are functional in epidermal keratinocytes, conclusive results are lacking. Herein, less than 4% of keratinocytes were responsive to capsaicin (1 μ M) (77 of 2047 cells). A comparable published study –using the same cell model (NHEK) and agonist concentration – claimed that approximately 12% of cells were responsive to capsaicin (83 of 690 cells) (Inoue *et al.*, 2002). Another study found that capsaicin (1 μ M) was unable to significantly increase intracellular calcium in HaCaT keratinocytes, despite the higher relative level of TRPV1 transcripts in HaCaTs vs. NHEK (Bodó *et al.*, 2005). While a separate group found that capsaicin (1 μ M) could significantly increase intracellular calcium in HaCaT keratinocytes (Southall *et al.*, 2003). These discrepancies may be linked to the relatively low expression of these channels in primary keratinocytes. These contradictory findings may also be explained by the nature of these channels: TRPV1 and TRPA1 channels function as heat-sensitive polymodal sensors, integrating a variety of environmental and inflammatory signals. Increasing ambient temperature from 22°C to 37°C enhances capsaicin-evoked calcium flux in TRPV1-expressing HEK293 cells (Sprague *et al.*, 2001). However, whether changes in ambient temperature, or a variety of other sensitising factors, could produce these contradictory results remains unclear but plausible. Together, these data suggest that TRPA1 and TRPV1 channels are functional in human epidermal keratinocytes; however, this finding requires further examination.

4.3.3. Properties of the TRPV3 channel

Drofenine evoked a phasic calcium response in primary epidermal keratinocytes. Work by our collaborators showed that this calcium flux was mediated by TRPV3: siRNA-mediated TRPV3 knockdown reduced drofenine-evoked fluctuations (Larkin *et al.*, 2021). At the cellular level, most drofenine-responsive keratinocytes displayed a single calcium peak (64% of cells), with a smaller subgroup displaying 2 distinct peaks (35%). These figures are in line with published electrophysiological analyses of the TRPV3 channel in TRPV3-overexpressing keratinocytes (Chung *et al.*, 2005). These authors described 2 phases within the cellular calcium response; the secondary phase was characterised by elevated current amplitudes and distinct kinetic features. Here, we focused on the population dynamics; our data revealed distinct temporal subgroups within the TRPV3 response, with cells showing rapid or delayed calcium peaks. These findings represent the first evidence of functional subgroups within the TRPV3-responsive keratinocyte population. This phasic pattern is echoed in a mouse model of acute TRPV3-induced scratching (Cui *et al.*, 2018) suggesting that this basic finding may have *in vivo* implications. The characteristic temporal pattern is likely mediated by a number of distinct mechanisms including: 1) repeated activation or sensitisation of surface channels; 2) trafficking and insertion of latent channels to the plasma membrane; 3) activation of channels located on intracellular calcium stores. Published reports have highlighted the sensitising effect of intracellular calcium and protons on TRPV3 activity (Haiyuan Wang *et al.*, 2021; Xiao, Tang, *et al.*, 2008; Phelps *et al.*, 2010; Chung *et al.*, 2004). Other reports suggest that repeated activation is caused by intrinsic calcium-independent gating and structural modification of the native channel (Beiying Liu *et al.*, 2011). Here, agonist-mediated activation enhanced the surface expression of the TRPV3 channel. The timing of this effect overlapped with the later phases of the calcium response suggesting that this phasic pattern is, in part, mediated by TRPV3 trafficking. Lastly, TRPV3 channels are localised to the endoplasmic reticulum (ER) in embryonic stem cells and pulmonary epithelial cells (Lo *et al.*, 2016; Nguyen *et al.*, 2020). Although data from TRPV3-expressing HEK293 cells suggests that TRPV3-mediated flux is dependent on extracellular calcium (Chung *et al.*, 2004), depletion of ER calcium reduces drofenine-evoked calcium flux in primary epithelia (Nguyen *et al.*, 2020). At present, the role of intracellular TRPV3 channels in epidermal keratinocytes remains poorly defined. Each of these mechanisms likely play a role in phasic TRPV3 activity; however, the importance of these processes in the context of TRPV3-evoked itch remains unexplored.

4.3.4. Clustering analyses: a method for detecting subtle changes in calcium channel activity

In addition to the important basic findings described above, this work validated a largely underutilised approach for examination of calcium responses in large populations of cultured cells. This method allowed for unbiased classification and comparison of calcium dynamics. A similar framework has been used to examine neuronal activation and G protein-coupled receptor signalling (Gupta *et al.*, 2017; Wei *et al.*, 2020; Mölter *et al.*, 2018). This method offers many advantages over the traditional population average approach, particularly regarding spatial and temporal resolution. Moreover, this multicell imaging provides sufficient data for both comparative population average and single-cell response analyses. The framework described herein accepts that variation is intrinsic to biological responses and works to utilise this heterogeneity— using feature extraction, semi-automated clustering, and subpopulation profiling to generate representative calcium signatures. This method can be employed for any fluorescent time course data and represents a flexible and powerful approach for interrogation of population calcium dynamics. Thus, we believe this approach to be a robust and superior alternative to the commonly utilised population average analyses, particularly when examining heterogeneous populations or responses.

TRPV3 functions as a calcium-permeable cation channel. When expressed on the plasma membrane, TRPV3 enables cation influx resulting in rapid spikes in intracellular calcium (Zubcevic *et al.*, 2018; Peier *et al.*, 2002; Xu *et al.*, 2002). Previous data showed that TRPV3 calcium responses are phasic, with a proportion of cells showing this rapid spike. Herein, we hypothesised that the rapid phase is specifically mediated by surface TRPV3 proteins: only cells showing high levels of surface TRPV3 would peak during this phase. The data outlined herein support this hypothesis. On average, 43% of control keratinocytes peaked during the cluster 1 rapid phase. These proportions are comparable to drofenine EC₅₀ data (Deering-Rice *et al.*, 2014). On average, between 34% and 41% of control keratinocytes expressed detectable levels of surface TRPV3. Similarly, BNP specifically affected the rapid phase of the TRPV3 response. BNP also enhanced acute trafficking of the TRPV3 receptor. Preliminary findings suggest that BNP does not affect the overall expression of TRPV3 (*data not included*). Together, these data demonstrate the link between rapid responders and surface TRPV3 expression.

4.3.5. Conclusion

Together, these analyses highlight the dynamics of TRPV3-associated calcium responses in human epidermal keratinocytes. These temporal features were dependent on receptor cycling and may be facilitated by VAMP3-dependent membrane insertion. Further investigations are required to investigate the importance of these findings in the context of TRPV3-evoked itch.

5. Assessing the Impact of BNP on TRPV3 Sensitivity, Signalling, and Trafficking

5.1. Overview

Overactivation and overexpression of TRPV3 has been linked to both dermatitis and itch. Olmsted syndrome, a highly pruritic genodermatosis, is caused by a mutation in the TRPV3 channel leading to TRPV3 overactivation (Lin *et al.*, 2012). Keratinocytes isolated from pruritic burns scars or atopic dermatitis lesions show elevated sensitivity to heat and chemical TRPV3 agonists (Vasas *et al.*, 2022; Seo *et al.*, 2020; Park *et al.*, 2017). Reports have suggested that PAR2 may be involved (Zhao *et al.*, 2020; Park *et al.*, 2017); however, our understanding of the underlying mechanisms remains incomplete. Previously, Dr. Meng found that IL-31 evoked BNP release from sensory neurons, while BNP elevated TRPV3 transcription in human epidermal keratinocytes (Larkin *et al.*, 2021). We hypothesize that, in inflammatory skin lesions, BNP may amplify TRPV3 activation and signalling, promoting a pruritic environment, and driving the chronic itch-scratch cycle. Thus, we examine the impact of BNP on TRPV3 sensitivity, signalling, and trafficking human epidermal keratinocytes.

This work was carried out using normal human epidermal keratinocytes (NHEK), a culture model for the human epidermis. Experiments utilised a variety of methods including cytokine array, live calcium imaging, and immunocytochemistry. First, we confirm NPRA and NPRB expression in our culture model. We then show that BNP can enhance epidermal TRPV3 activity, amplifying normal calcium responses and driving GSK3- and JNK-dependent TRPV3 trafficking human keratinocytes. At present, the exact BNP receptor facilitating these effects remains unknown. This work further delineated the link between IL-31/BNP and TRPV3, a novel itch-linked neuro-epidermal pathway.

5.2. Results

5.2.1. Keratinocytes in our NHEK model express receptors for BNP: NPRA and NPRB

Natriuretic Peptide Receptor A (NPRA) and Natriuretic Peptide Receptor B (NPRB) are expressed in the epidermis of healthy human skin (Meng *et al.*, 2018). Here, we aimed to confirm the expression of these BNP receptors in our NHEK culture model of human epidermis.

NHEK were labelled with antibodies targeting NPRA or NPRB (see **Table 2.3** for details). NPRA was primarily detected in the cytosolic region (**Figure 5.1A**; *magenta*). NPRB was localised to the outer regions of each cell – a membrane-like staining pattern (**Figure 5.1A**; *green*). NPRB signal was also consistently detected in the perinuclear region. Comparable fluorescence was not detected in the negative control staining (**Figure 5.1B**), indicating that the visible signal represents NPRA and NPRB proteins.

These data are supported by the literature and indicate that NHEK represent a useful culture model for investigating the BNP/TRPV3 pathway in the human epidermis.

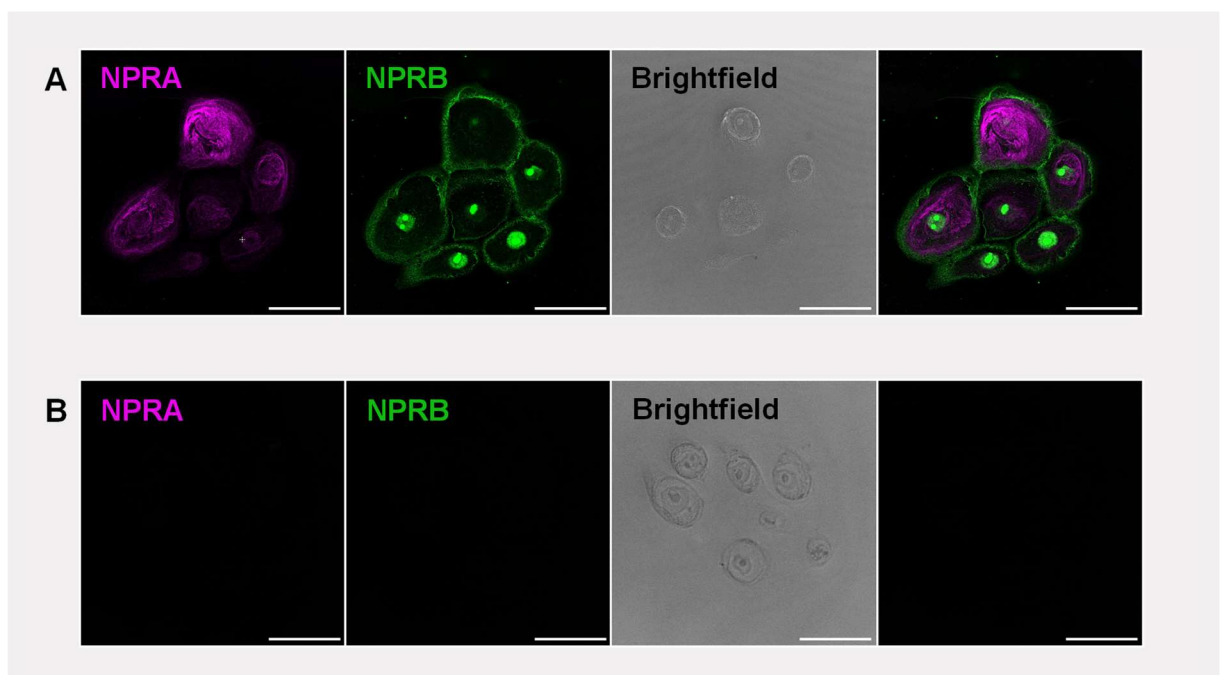


Figure 5.1. Keratinocytes in our NHEK model express receptors for BNP: NPRA and NPRB.

Keratinocytes (NHEK) were probed with solution \pm primary antibodies and imaged with confocal microscopy. **A – B**, Immunostaining showing expression of NPRA (magenta) and NPRB (green) (**A**) vs. secondary only imaging control (**B**). Original magnification 63x. Scale bars =50 μ m. *Abbreviations:* NPRA, Natriuretic Peptide Receptor A; and NPRB, Natriuretic Peptide Receptor B.

5.2.2. BNP sensitises TRPV3-mediated calcium fluctuations

Mounting evidence suggests a role for BNP in the progression and potentiation of dermatitis (Meng *et al.*, 2020). However, our understanding of the effect of BNP on keratinocytes and other cutaneous cells is incomplete. Here, we examine whether BNP pre-treatment enhances the activity of TRPV3 calcium channels in an NHEK culture model of human epidermis.

NHEK were pre-treated with basal medium \pm BNP (1 μ M; 4 h). Pre-treated keratinocytes were loaded with a cell-permeant fluorescent calcium indicator (Fluo-4 AM) and fluorescence was monitored using confocal imaging. Following a baseline recording (100 s), all keratinocytes were stimulated with TRPV3 agonist solution (basal medium + drofenine) (1000 seconds [s] total) (**Figure 5.2**). Control keratinocytes were stimulated with either drofenine 250 μ M (D250) or drofenine 500 μ M (D500); BNP pre-treated keratinocytes received just the lower concentration of drofenine (D250): the only difference between the 2 D250 groups was the pre-treatment (control vs. BNP).

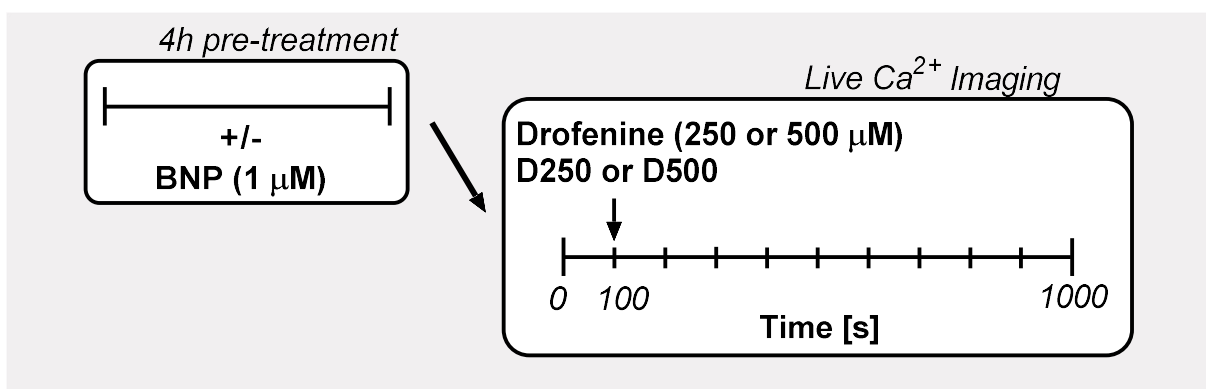


Figure 5.2. Schematic showing timing of BNP pre-treatment, TRPV3 agonist stimulation, and calcium recording.

Live keratinocytes (NHEK) were pre-treated with medium \pm BNP (1 μ M, 4h; control vs. BNP) and stimulated with TRPV3 agonist solutions; calcium fluctuations were recorded. Stimulations were added at 100 seconds (s): drofenine 250 μ M solution (D250) or drofenine 500 μ M solution (D500).

In all groups, addition of drofenine solution was associated with enhanced fluorescent signal: control D250 (**Figure 5.3A**); BNP D250 (**Figure 5.3B**); and control D500 (**Figure 5.3C**). Raw fluorescent data were normalised to change in fluorescence ($F\Delta/F_0$) over time (**Figure 5.3D**). Both images and traces confirm that drofenine solution increases intracellular calcium in keratinocytes, while also highlighting the effect of BNP and the variation within the response.

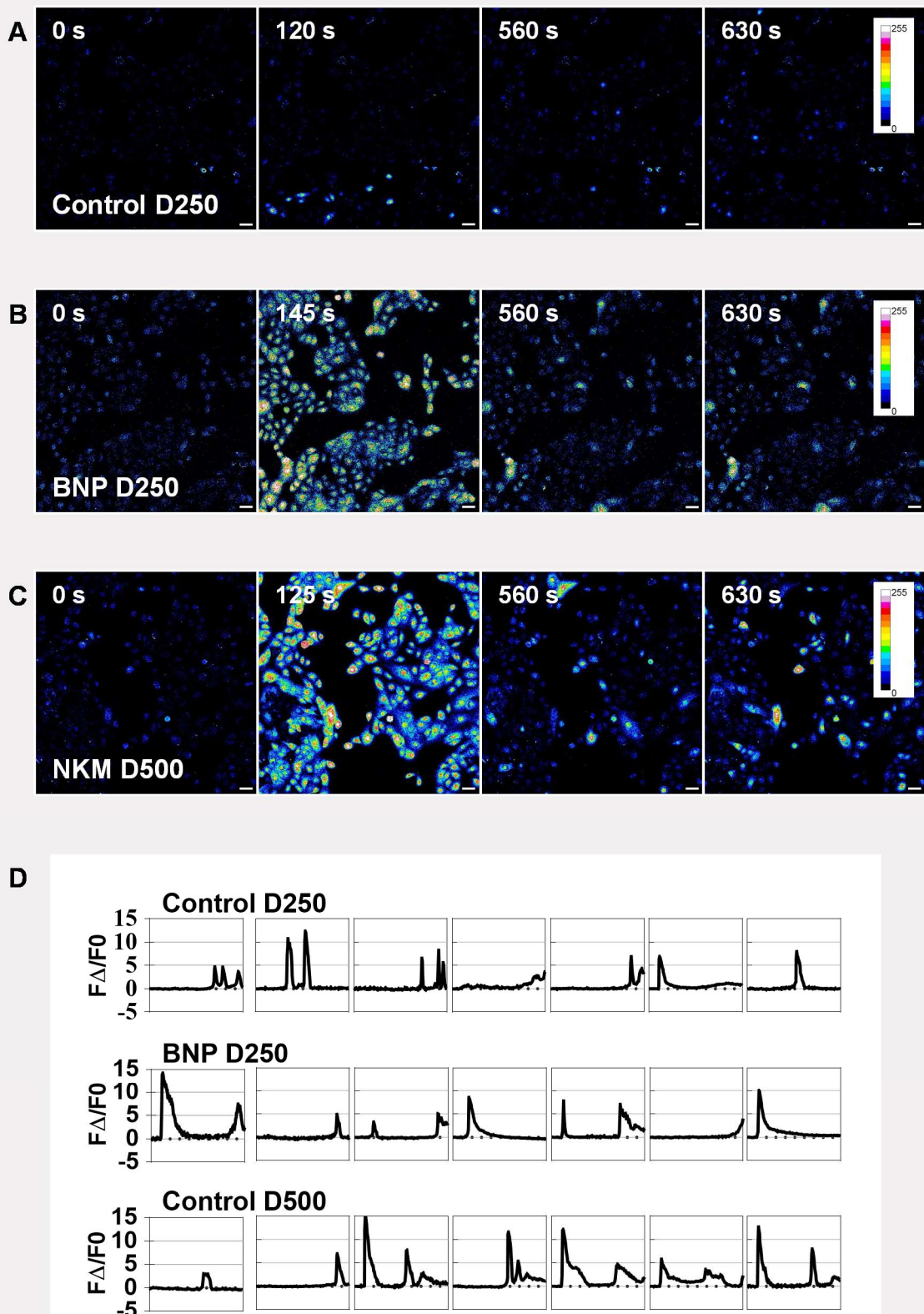


Figure 5.3. Raw fluorescence data and single-cell traces showing effect of BNP pre-treatment on TRPV3 agonist-induced calcium response.

Keratinocytes (NHEK) were pre-treated with medium \pm BNP (1 μ M, 4h; control vs. BNP) and stimulated with drofenine 250 μ M (D250) or drofenine 500 μ M (D500). A – C, Representative images showing fluorescence at each named timepoint following drofenine stimulation: control D250 (A); BNP D250 (B); control D500 (C). White indicates highest signal. Scale bars =50 μ m.

D, Representative single-cell traces from each experimental group showing change in fluorescence ($F\Delta/F_0$) over time following addition of drofenine stimulation. Each x-axis represents 1000 seconds.

Drofenine-evoked calcium dynamics were first evaluated with respect to the population average; time course fluorescence data was plotted as the average change in fluorescence at each time point. In control keratinocytes, application of D500 was associated with 2 clear peaks in the average transient (**Figure 5.4A**). The first average peak occurred at 125 seconds (s), just 25 s post-stimulation, and reached almost 400% above baseline (mean $F\Delta/F_0 = 3.797$, SEM = .192). The second peak occurred at 630 s – almost 9 minutes after D500 stimulation – and averaged at more than 200% above baseline fluorescence (mean $F\Delta/F_0 = 2.371$, SEM = .106). Application of D250, the lower concentration of drofenine, promoted a rapid peak in both control (**Figure 5.4B**) and BNP (**Figure 5.4C**) keratinocytes; however, the amplitude of this average peak showed clear differences. In control samples, the average peak reached 100% above baseline (mean $F\Delta/F_0 = 1.130$, SEM = .073). In BNP samples, the average peak reached more than 300% above baseline (mean $F\Delta/F_0 = 3.210$, SEM = .108). In both groups, D250 failed to evoke the later peak noted in the D500 stimulation (at 630 s), indicating that this later peak is specific to the higher concentration of drofenine (D500) and is not enhanced by BNP pre-treatment. These population average analyses demonstrate the concentration dependency of drofenine-evoked flux and highlight the impact of BNP on the rapid phase of TRPV3 activity in human keratinocytes.

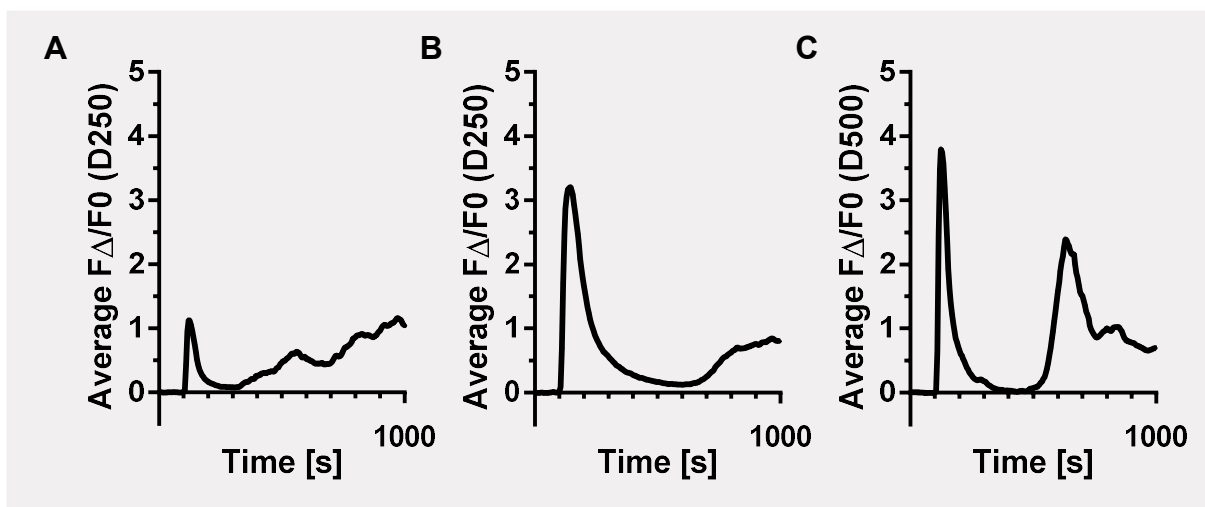
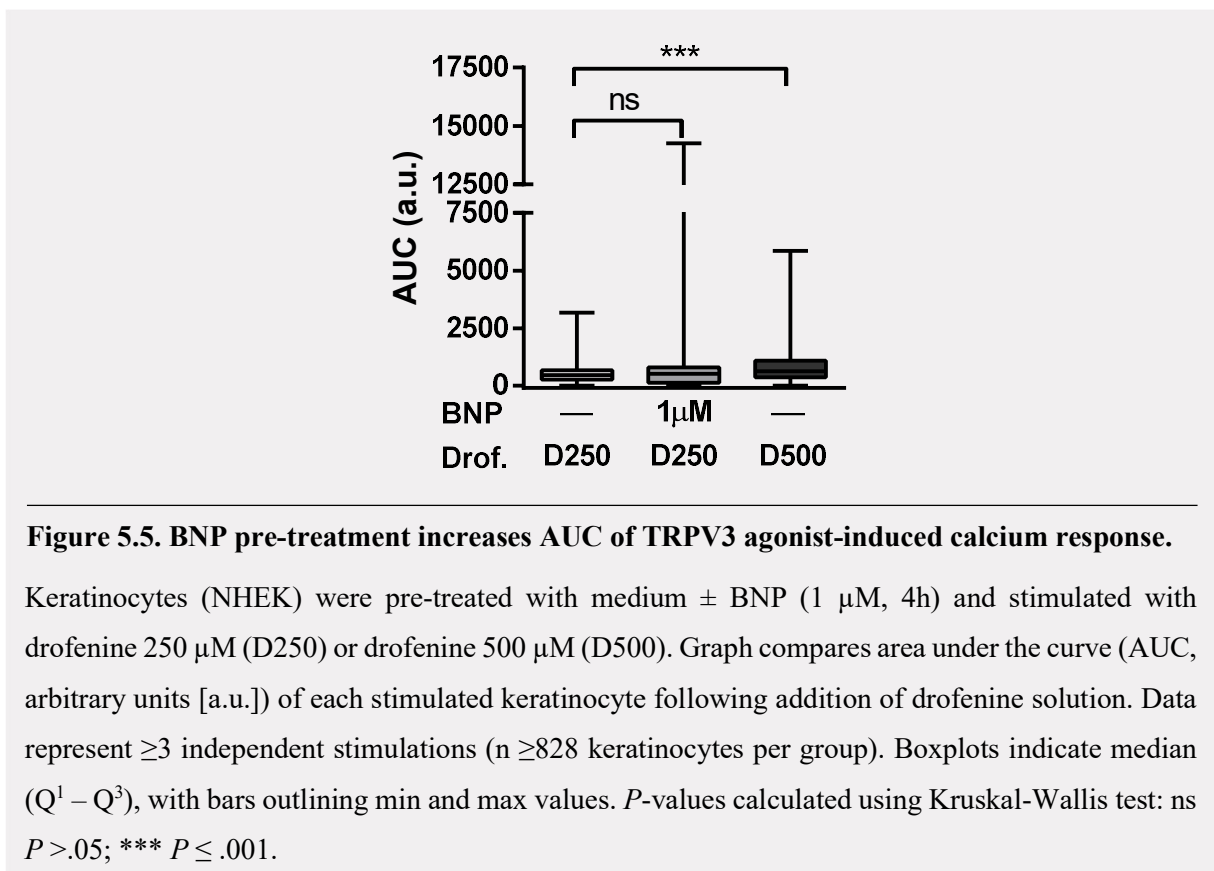


Figure 5.4. BNP pre-treatment enhances average TRPV3 agonist-induced calcium response.

Keratinocytes (NHEK) were pre-treated with medium \pm BNP (1 μ M, 4h; control vs. BNP) and stimulated with drofenine 250 μ M (D250) or drofenine 500 μ M (D500). A – C, Graphs depict average change in fluorescence ($F\Delta/F_0$) over 1000 seconds (s) following addition of drofenine stimulation: control D250 (A); BNP D250 (B); control D500 (C). Data represent ≥ 3 independent stimulations ($n \geq 828$ keratinocytes per group).

Single-cell focused analyses were then undertaken; we examined the impact of BNP on overall calcium responses and peak calcium fluctuations in each drofenine-stimulated keratinocyte.

Area under the curve (AUC) indicates the overall calcium response, with values incorporating both the duration and magnitude of cellular activation. Median AUC values from each group were significantly different (Kruskal-Wallis, $P < .0001$) (**Figure 5.5**). In control keratinocytes, levels of drofenine-evoked flux were concentration dependent. Median AUC were about 25% lower in the D250 group vs. the D500 group (466.6 vs. 621.3 arbitrary units [a.u.]). This difference was significant ($P < .0001$). Comparing the 2 D250 groups revealed the impact of BNP pre-treatment on overall drofenine-evoked flux. Here, BNP enhanced D250 AUC values relative to control D250 values (521.0 vs. 466.5 a.u.); however, this trend failed to reach significance ($P = .0898$).



Peak calcium responses are represented by peak amplitude ($F\Delta/F0_{max}$) and peak latency ($Time_{max}$). Median peak amplitude values from each group were significantly different (Kruskal-Wallis, $P < .0001$) (**Figure 5.6**). In control keratinocytes, the amplitude of drofenine-evoked calcium peaks was concentration dependent. While the control D250 group peaked at 600% above baseline (median $F\Delta/F0_{max} = 6.089$ arbitrary units [a.u.]), the D500 group reached about 800% (8.098 a.u.). This difference was significant ($P < .0001$). Comparing the 2 D250 groups revealed the impact of BNP pre-treatment on peak amplitude. Here, peak amplitude values were statistically comparable in both D250 groups ($P = .1531$) suggesting that BNP may be unable to directly sensitise the TRPV3 channel protein.

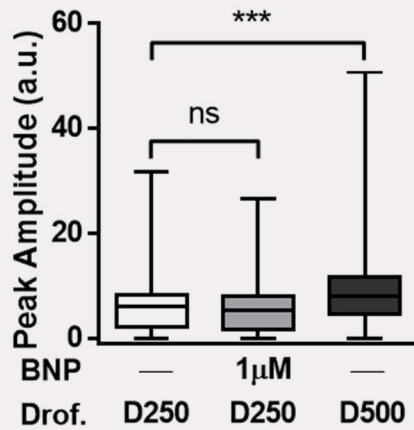


Figure 5.6. BNP pre-treatment fails to increase amplitude of TRPV3-linked calcium peaks.

Keratinocytes (NHEK) were pre-treated with medium \pm BNP (1 μ M, 4h) and stimulated with drofenine 250 μ M (D250) or drofenine 500 μ M (D500). Graph compares peak amplitude ($F\Delta/F0_{max}$, arbitrary units [a.u.]) in each stimulated keratinocyte following addition of drofenine solution. Data represent ≥ 3 independent stimulations ($n \geq 828$ keratinocytes per group). Boxplots indicate median ($Q^1 - Q^3$), with bars outlining min and max values. P -values calculated using Kruskal-Wallis test: ns $P > .05$; *** $P \leq .001$.

Peak latency ($Time_{max}$) indicates the time required for a cell to reach its maximum calcium flux. Median peak latencies values from each group were significantly different (Kruskal-Wallis test, $P < .0001$) (Figure 5.7). In control keratinocytes, the latency of drofenine-evoked calcium peaks was concentration dependent, with D500 eliciting a faster calcium response – almost 200 seconds quicker than the median D250 value (median $Time_{max} = 585$ vs. 765 seconds). This difference was significant ($P < .0001$). Comparing the 2 D250 groups revealed the impact of BNP pre-treatment on peak latency. Here, BNP accelerated the D250 response, with the BNP group reaching peak calcium just 70 seconds post-stimulation (median $Time_{max} = 170$ s). In fact, BNP group were significantly quicker than both the control D250 and D500 groups ($P < .0001$). This striking result may be explained by sensitisation or enhanced trafficking of the TRPV3 channel to the plasma membrane but requires further investigation.

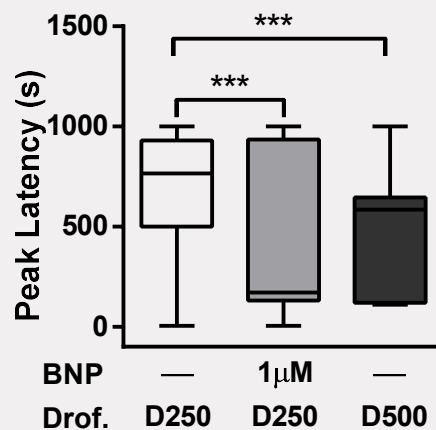


Figure 5.7. BNP pre-treatment accelerates TRPV3-linked calcium peaks.

Keratinocytes (NHEK) were pre-treated with medium \pm BNP (1 μ M, 4h) and stimulated with drofenine 250 μ M (D250) or drofenine 500 μ M (D500). Graph compares peak latency (Time_{max}, seconds [s]) in each stimulated keratinocyte following addition of drofenine solution. Data represent ≥ 3 independent stimulations ($n \geq 28$ keratinocytes per group). Boxplots indicate median (Q¹ – Q³), with bars outlining min and max values. *P*-values calculated using Kruskal-Wallis test: ns *P* > .05; *** *P* \leq .001.

Although average population traces suggested a clear link between BNP and TRPV3 activity, within group variation reduced the statistical power of traditional analyses. As discussed previously, this cell-to-cell variation may be a feature of the TRPV3 calcium response in epidermal keratinocytes: the true impact of BNP on TRPV3 activity may be better illustrated by single-cell analyses. Thus, response profiles were generated for each group (peak latency vs. peak amplitude): control D250 (**Figure 5.8A**); BNP D250 (**Figure 5.8B**); and control D500 (**Figure 5.8C**). These plots suggest functional clusters within drofenine-response, with rapid responders found on the left side of the x-axis.

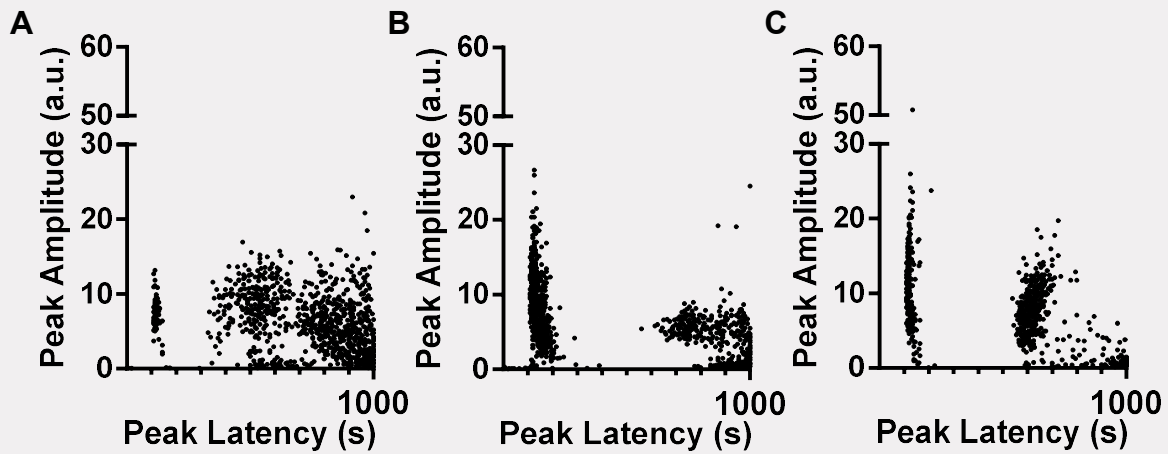


Figure 5.8. BNP pre-treatment alters TRPV3-linked response profiles.

Keratinocytes (NHEK) were pre-treated with medium \pm BNP (1 μ M, 4h) and stimulated with drofenine 250 μ M (D250) or drofenine 500 μ M (D500). A – C, Graphs depict response profiles: peak latency (Time_{max} , seconds [s]) vs. peak amplitude ($F\Delta/F0_{\text{max}}$, arbitrary units [a.u.]) following addition of drofenine stimulation: control D250 (A); BNP D250 (B); control D500 (C). Each dot represents a single cell. Data represent ≥ 3 independent stimulations ($n \geq 828$ keratinocytes per group).

Response profiles were imported to RStudio and examined for clusters, following the analysis framework developed and tested in Chapter 4. The gap statistic testing method was used to determine the optimum number of clusters (k) in each profile. In the control D250 group, the optimum k was estimated to be four (**Figure 5.9A**). In the BNP D250 group, the optimum k was estimated to be three (**Figure 5.9B**). In the control D500 group, the optimum k was estimated to be three (**Figure 5.9C**). These estimates suggest that the D250 response profile is altered following BNP pre-treatment.

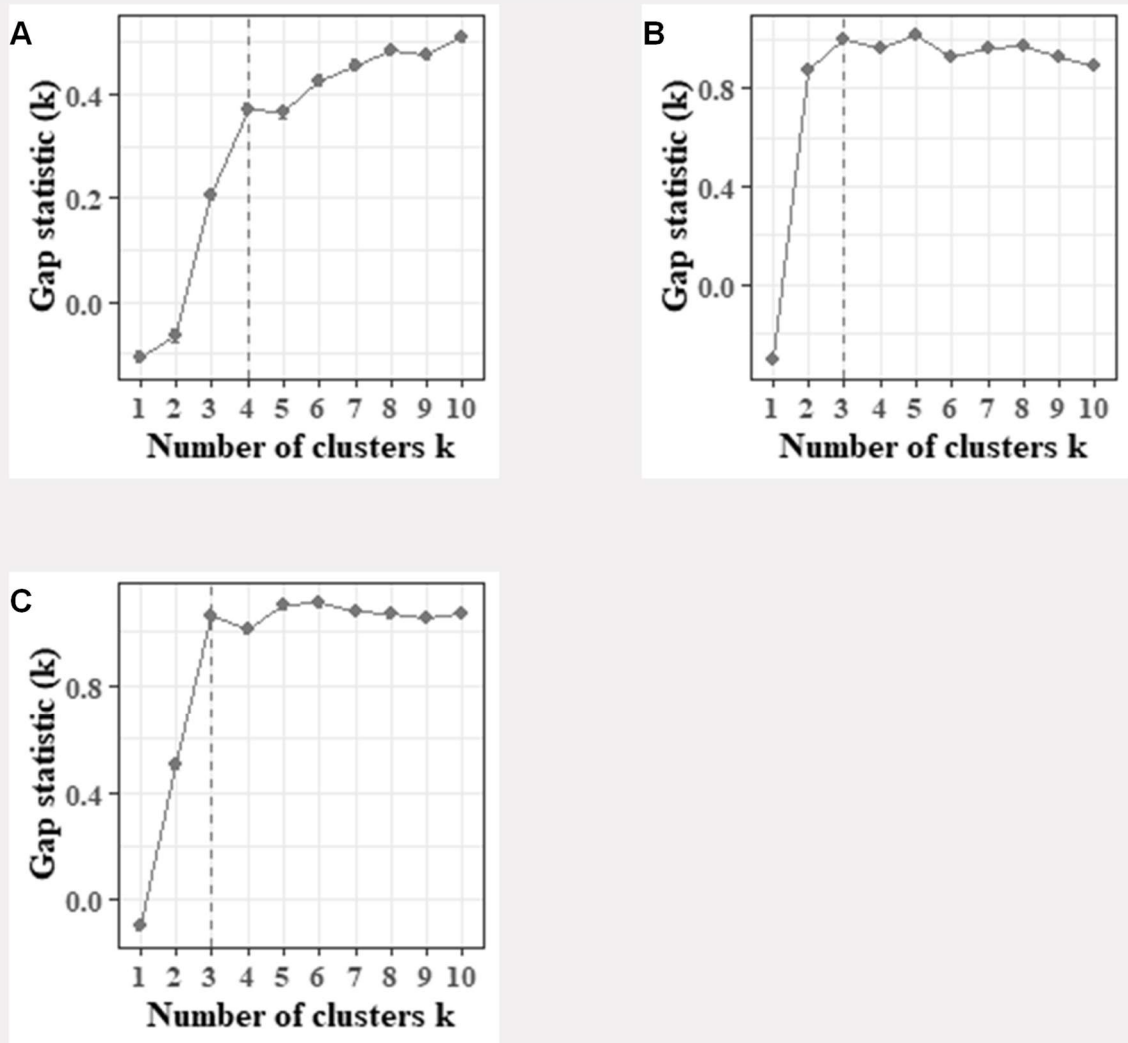


Figure 5.9. Optimum number of clusters (k) within each TRPV3-linked response profile.

Keratinocytes (NHEK) were pre-treated with medium \pm BNP (1 μ M, 4h) and stimulated with drofenine 250 μ M (D250) or drofenine 500 μ M (D500). Response profiles were examined using the Gap Statistic analysis. A – C, Graphs depict gap curve of response profile: control D250 (A); BNP D250 (B); control D500 (C). Dotted line indicates optimum k . Data represent ≥ 3 independent stimulations ($n \geq 828$ keratinocytes per group).

To allow for comparison, all 3 response profiles were partitioned using k -means clustering, where $k = 3$: control D250 (Figure 5.10A); BNP D250 (Figure 5.10B); and control D500 (Figure 5.10C). Partitioning is shown on each plot, with responders colour-coded by cluster. Although response profiles for each treatment group were clustered independently, the range of peak latency values in each cluster were comparable across treatment groups (Table 5.1). As before, this suggests that peak latency values underpin the automated partitioning of these data.

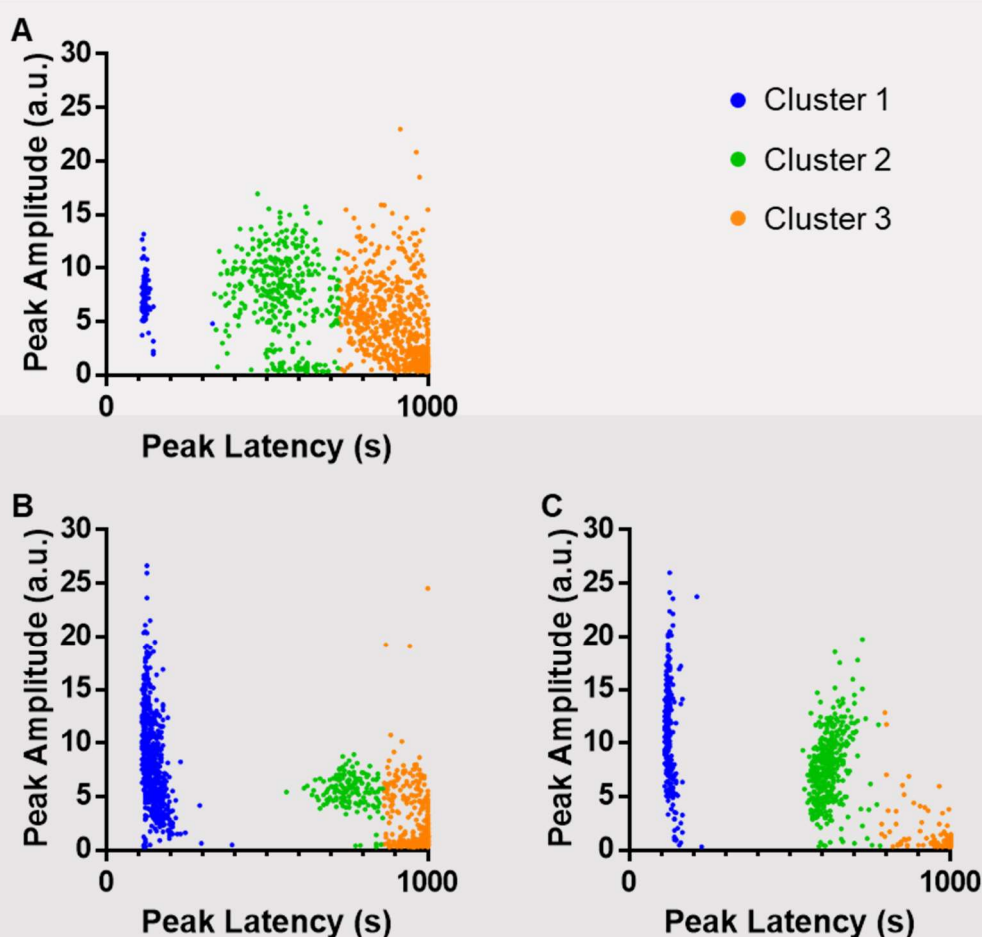


Figure 5.10. Clustering of TRPV3-linked response profiles using *k*-means clustering.

Keratinocytes (NHEK) were pre-treated with medium \pm BNP (1 μ M, 4h) and stimulated with drofenine 250 μ M (D250) or drofenine 500 μ M (D500). Response profiles were clustered using *k*-means clustering ($k=3$). **A – C**, Graphs depict response profiles: peak latency (Time_{e,max}, seconds [s]) vs. peak amplitude (F Δ /F_{0,max}, arbitrary units [a.u.]) following drofenine stimulation: control D250 (**A**); BNP D250 (**B**); control D500 (**C**). Each dot represents a single cell. Cells are coloured by cluster: blue (cluster 1); green (cluster 2); and orange (cluster 3). Data represent ≥ 3 independent stimulations ($n \geq 828$ keratinocytes per group).

Table 5.1. Range of peak latency values included in each cluster.

	Control D250	BNP D250	Control D500
Cluster 1 (seconds)	110 – 330	110 – 390	110 – 225
Cluster 2 (seconds)	335 – 720	560 – 860	540 – 780
Cluster 3 (seconds)	725 – 1000	865 – 1000	785 – 1000

Note: Data represent the min and max time values for each cluster in seconds. *Abbreviations:* D250, drofenine (250 μ M); D500, drofenine (500 μ M).

In AUC and peak amplitude analyses, BNP was unable to significantly alter the magnitude of the D250 response. We postulated that BNP may specifically impact the rapid phase. Here, cells peaking during the rapid phase (i.e. low peak latency values) were partitioned to cluster 1. Thus, we compared the peak amplitude values of cluster one cells from each of the groups (**Figure 5.11**). Again, the median values from each group were significantly different (Kruskal-Wallis test, $P < .0001$), with the amplitude of the rapid response being concentration dependent ($P < .0001$). Here, BNP significantly increased the amplitude of the D250-evoked response in cluster 1 cells ($P = .0262$) suggesting that BNP specifically enhances the rapid phase of TRPV3-mediated calcium influx.

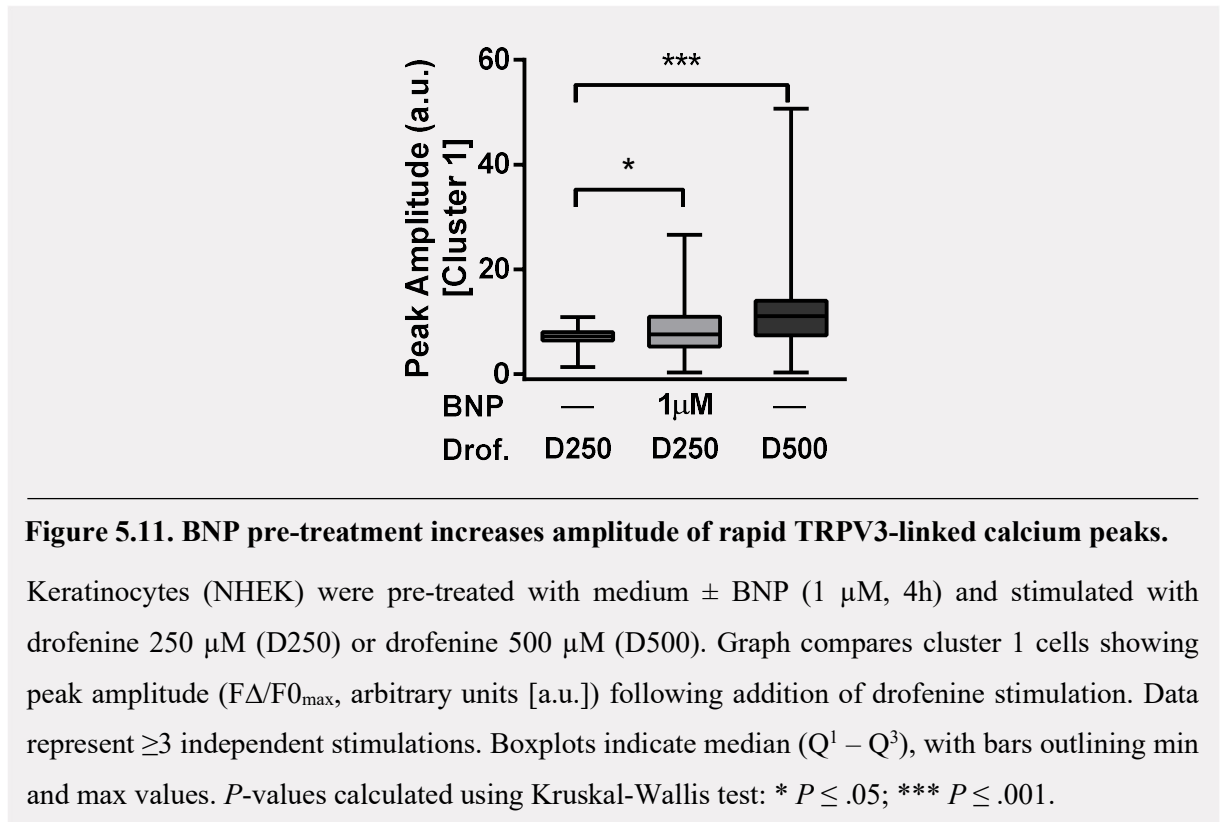


Figure 5.11. BNP pre-treatment increases amplitude of rapid TRPV3-linked calcium peaks.

Keratinocytes (NHEK) were pre-treated with medium \pm BNP (1 μ M, 4h) and stimulated with drofenine 250 μ M (D250) or drofenine 500 μ M (D500). Graph compares cluster 1 cells showing peak amplitude ($F\Delta/F0_{max}$, arbitrary units [a.u.]) following addition of drofenine stimulation. Data represent ≥ 3 independent stimulations. Boxplots indicate median ($Q^1 - Q^3$), with bars outlining min and max values. P -values calculated using Kruskal-Wallis test: * $P \leq .05$; *** $P \leq .001$.

Lastly, we graphed the proportion of responders allocated to cluster 1, 2, and 3. This analysis focuses on the impact of BNP on D250-evoked responses. The average percentage of responders allocated to each cluster was highly varied across groups (**Figure 5.12**). Examination of cluster 1 revealed a striking change: in control keratinocytes, drofenine induced rapid activation in 20% (D250) and 40% (D500) of cells; following BNP pre-treatment, D250 evoked rapid activation in 69% of cells. In control cells, clustering was associated with drofenine concentration: while D250 responders were primarily assigned to the slower cluster 3 group (56%), D500 responders were assigned to cluster 1 or cluster 2 (both 40%). In each of the groups, the average percentage of drofenine-insensitive cells was low ($\leq 4\%$). Overall, BNP significantly affected the proportion of D250-stimulated cells assigned to each cluster; Chi-square statistic: $P < .0001$. These data illustrate the clear and potent effect of BNP on the rapid phase of the TRPV3-mediated calcium responses.

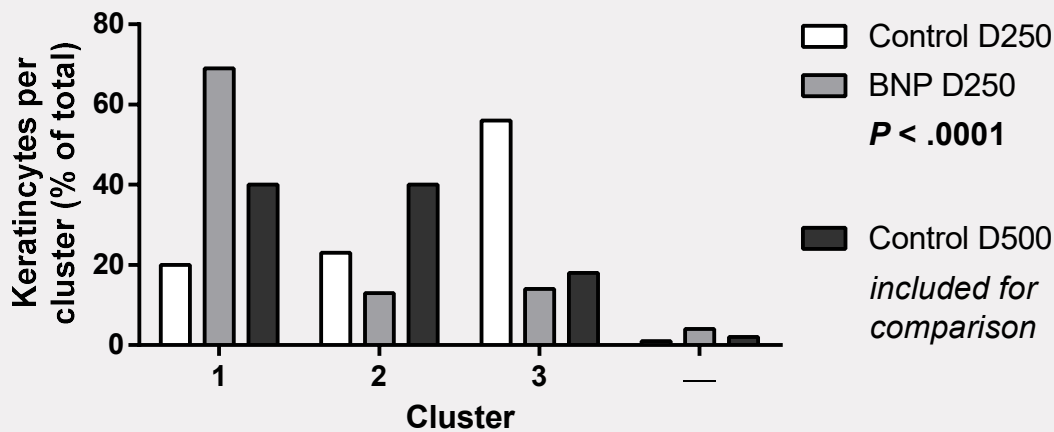


Figure 5.12. BNP pre-treatment alters phasic nature of the TRPV3-linked calcium response.

Keratinocytes (NHEK) were pre-treated with medium \pm BNP (1 μ M, 4h) and stimulated with drofenine 250 μ M (D250) or drofenine 500 μ M (D500). Response profiles were clustered using k -means clustering ($k=3$). Graph compares percentage of keratinocytes assigned to each cluster. Percentage of drofenine-insensitive (-) cells is also shown. Data represent ≥ 3 independent stimulations ($n \geq 828$ keratinocytes per treatment group). Bar graph indicates mean values. P -values calculated using Chi-squared test (control D250 vs. BNP D250): $P \leq .001$.








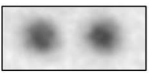




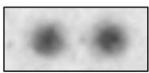

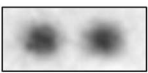





















Together, these analyses used calcium imaging to assess functional TRPV3 expression in primary human epidermal keratinocytes. Findings from control D500 stimulations were comparable to previous sections. Here, D500 evoked rapid calcium fluctuations in 40% of keratinocytes (**Figure 5.12**); previously, D500 evoked rapid calcium fluctuations in 43% of keratinocytes (**Figure 4.18B**; see cluster 1 of control group). The results outlined herein demonstrate the impact of drofenine concentration on TRPV3 activation, with the lower agonist concentration resulting in a lower and slower calcium response. This work also revealed a novel link between BNP and functional TRPV3 activity. These findings suggest that this itch-linked neuropeptide could sensitise TRPV3⁺ keratinocytes in the skin, potentially elevating inflammation and driving TRPV3-evoked itch.

5.2.3. BNP fails to enhance TRPV3-linked mediator release

TRPV3 activation drives the release of BSG, Dkk-1, EGF, IL-1 α , IL-1ra, MIF, PAI-1, PDGFA, and TGF- α from human epidermal keratinocytes. Several of the mediators are upregulated in pruritic skin conditions such as AD. We hypothesised that BNP, an itch-linked neuropeptide, would enhance TRPV3 signalling and promote the dysregulated epidermal environment common in atopic dermatitis lesions. Thus, we examined the effect of BNP pre-treatment on drofenine-induced mediator release in cultured epidermal keratinocytes.

NHEK were pre-treated with basal medium \pm BNP (1 μ M, 4 h). Following pre-treatment, cells were stimulated with basal medium \pm drofenine (TRPV3 agonist; 500 μ M) \pm BNP (1 μ M) (1 h). Supernatant was pooled and released mediators were quantified by cytokine array (**Table 5.2**). A number of mediators were consistently detected: BSG; Dkk-1; EGF; IL-1 α ; IL-1ra; MIF; PAI-1; PDGFA; TGF- α .

Table 5.2. Representative images of duplicate antibody spots from cytokine array showing effect of BNP pre-treatment on TRPV3-associated mediator release.

Mediator	Basal [Control]	TRPV3 [Control]	Basal [BNP]	TRPV3 [BNP]
BSG				
Dkk-1				
EGF				
IL-1 α				
IL-1ra				
MIF				
PAI-1				
PDGFA				
TGF- α				

Note: Table includes images of duplicate spots; antibodies at each spot bind to a named mediator. Average densitometry of these duplicates equals one experimental replicate. *Abbreviations:* BSG, basigin; BNP, B-type natriuretic peptide; Dkk-1, dickkopf-1; EGF, epidermal growth factor; IL-1 α , interleukin-1 alpha; IL-1ra, interleukin-1 receptor antagonist; MIF, macrophage migration inhibitory factor; PAI-1, plasminogen activator inhibitor-1; PDGFA, platelet derived growth factor A; TGF- α , transforming growth factor alpha; TRPV3, transient receptor potential vanilloid 3.

To examine the impact of BNP on drofenine-induced mediator release, data were expressed as a percentage of normal drofenine-induced release (i.e. allowing the control TRPV3 group to equal 100%, matched) ($n=3$). Data were presented as median and interquartile range ($Q^1 - Q^3$) and were analysed using the nonparametric Wilcoxon signed rank test (vs. 100%: TRPV3 [Control]). BNP was unable to significantly alter TRPV3-associated mediator release in human epidermal keratinocytes (**Figure 5.13**). Median evoked BSG levels were 2% higher in TRPV3 [BNP] (102.4%; $P=.750$). Median evoked Dkk-1 levels were 7% higher in TRPV3 [BNP] (107.1%; $P=1.000$). Median evoked EGF levels were 4% higher in TRPV3 [BNP] (103.8%; $P=1.000$). Median evoked IL-1 α levels were 13% higher in TRPV3 [BNP] (112.6%; $P=.500$). Median evoked IL-1ra levels were 13% lower in TRPV3 [BNP] (87.1%; $P=.250$). Median evoked MIF levels were 2% higher in TRPV3 [BNP] (101.8%; $P=.500$). Median evoked PAI-1 levels were 24% higher in TRPV3 [BNP] (124.0%; $P=.500$). Median evoked PDGFA levels were unchanged in TRPV3 [BNP] (99.8%; $P=.750$). Median evoked TGF- α levels were 2% higher in TRPV3 [BNP] (101.9%; $P=1.000$). Overall, drofenine-evoked secretion was comparable in control and BNP pre-treated keratinocytes.

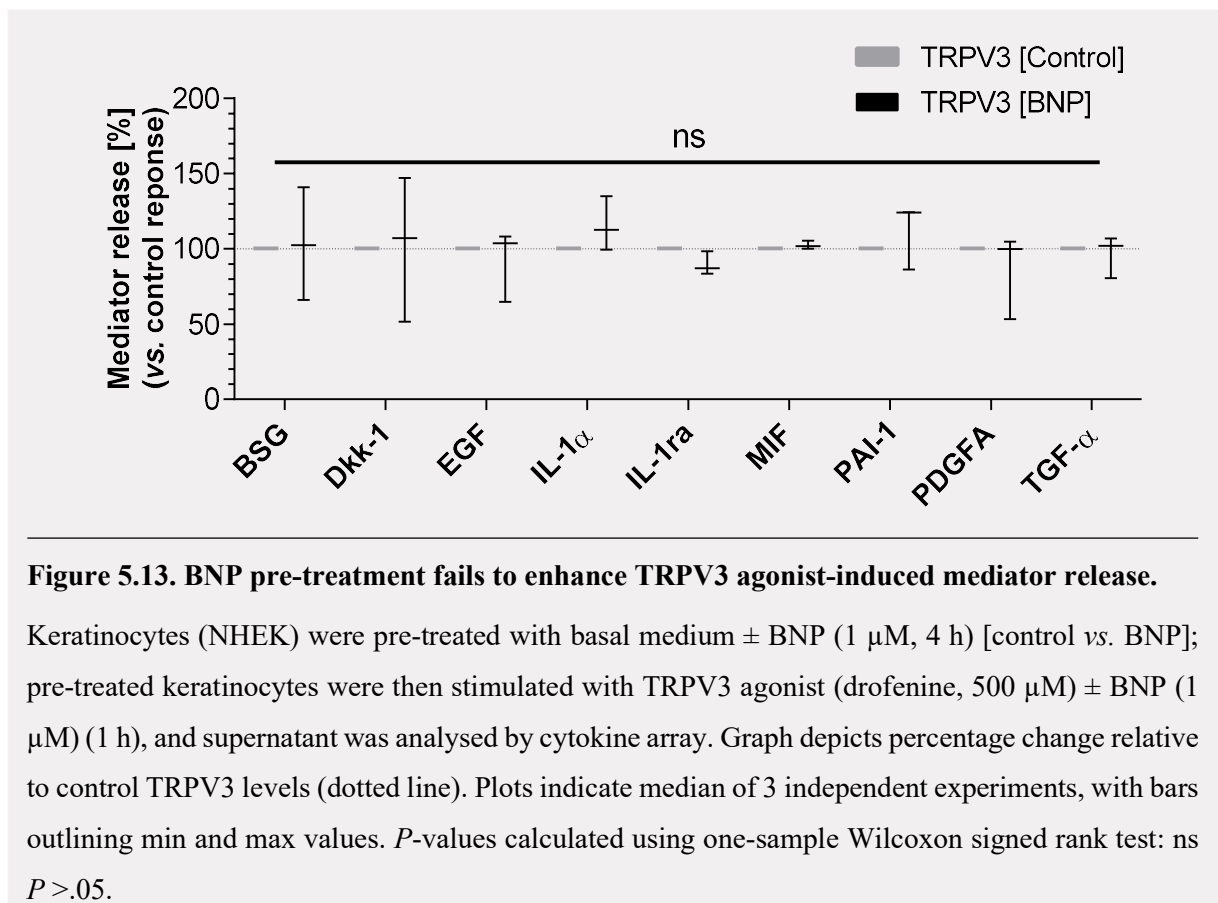


Figure 5.13. BNP pre-treatment fails to enhance TRPV3 agonist-induced mediator release.

Keratinocytes (NHEK) were pre-treated with basal medium \pm BNP (1 μ M, 4 h) [control vs. BNP]; pre-treated keratinocytes were then stimulated with TRPV3 agonist (drofenine, 500 μ M) \pm BNP (1 μ M) (1 h), and supernatant was analysed by cytokine array. Graph depicts percentage change relative to control TRPV3 levels (dotted line). Plots indicate median of 3 independent experiments, with bars outlining min and max values. P -values calculated using one-sample Wilcoxon signed rank test: ns $P > .05$.

Although BNP sensitises the TRPV3-induced calcium response, BNP fails to enhance TRPV3-associated mediator release. Whether BNP alters TSLP, or other TRPV3-linked mediators, remains unexplored. Future work should also examine the effect of co-culture and/or extended BNP incubation on TRPV3-linked mediator release.

5.2.4. BNP promotes TRPV3 trafficking and membrane insertion

Previous sections showed that BNP enhances drofenine-evoked calcium flux. This effect may be mediated by several distinct mechanisms including trafficking and membrane insertion of TRPV3 channels. Here, we assessed the impact of BNP on surface TRPV3 expression over time.

NHEK were stimulated with basal medium + BNP (1 μ M; 0, 3 and 24 hours [h]). The ecto-TRPV3 channel antibody was added to this stimulation buffer (ACC-033; 85 μ g/ml; 15 min): this highly specific antibody binds the extracellular region of the TRPV3 channel. Following stimulation, keratinocytes were probed with secondary antibody, fixed, and mounted. Samples were imaged using confocal microscopy, images were processed and measured using Image J software, and data were analysed using GraphPad Prism.

TRPV3 membrane expression was detected in a population of untreated control keratinocytes (BNP 0 h; 41% of keratinocytes) (**Figure 5.14A**). This TRPV3 signal was not restricted to the cell surface suggesting that bound TRPV3 channels may have been internalised prior to fixation. Secondary only imaging controls illustrate the specificity of this signal (**Figure 5.14B**).

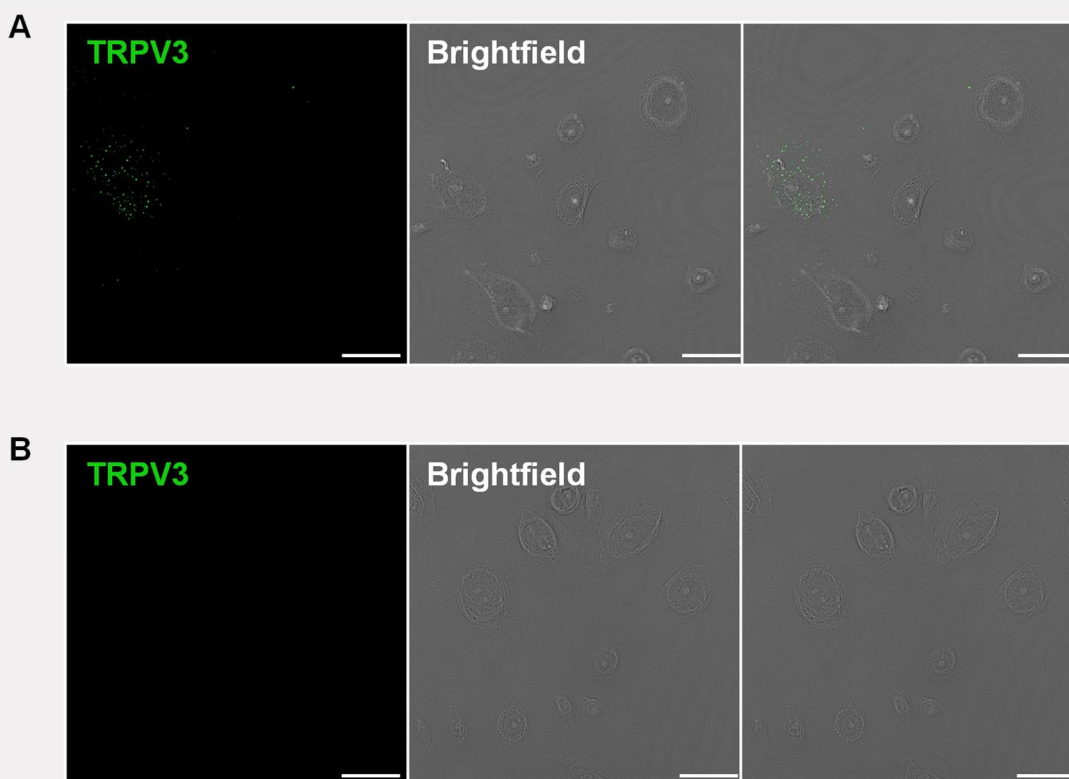


Figure 5.14. Representative images showing surface expression of TRPV3 proteins in cultured epidermal keratinocytes.

Live keratinocytes (NHEK) were probed with TRPV3-ecto antibody (85 μ g/ml, 15 min) followed by anti-rabbit (Alexa Fluor 555; 10 μ g/ml, 1 h). Keratinocytes were then fixed, mounted, and imaged using confocal microscopy. **A – B**, Representative images depict surface TRPV3 (green) and brightfield signals in basal control (BNP 0 h) (**A**) and secondary only imaging control (**B**). Scale bars =50 μ m.

TRPV3-positive (TRPV3⁺) cells were defined as those which contained ≥ 5 particles per 1500 μm^2 . Contrary to data from a previous section, TRPV3⁺ and TRPV3-negative (TRPV3⁻) keratinocytes were similar in size and shape (**Table 5.3**) suggesting that these TRPV3 expression is independent of basic cellular parameters.

Table 5.3. Basic cellular parameters: TRPV3-positive vs. TRPV3-negative keratinocytes.

Parameter	TRPV3 ⁺ [41.1%]	TRPV3 ⁻ [58.9%]	<i>P</i>
Perimeter (μm)	162 (117 – 240)	149 (114 – 224)	ns
Area (μm^2)	1701 (920 – 3604)	1351 (847 – 3102)	ns
Circularity (a.u.)	0.85 (0.80 – 0.90)	0.84 (0.76 – 0.89)	ns
Roundness (a.u.)	0.76 (0.68 – 0.84)	0.69 (0.57 – 0.82)	**

Note: Data expressed as median ($Q^1 - Q^3$). Square brackets indicate the proportion of cells per group. *Abbreviations:* a.u., arbitrary unit; μm , micrometre; TRPV3⁺, TRPV3-positive; and TRPV3⁻, TRPV3-negative.

TRPV3 membrane expression was enhanced following BNP stimulation: the visible signal was highest in the BNP 3 h samples (**Figure 5.15A**) but was also evident in BNP 24 h (**Figure 5.15B**). Although this signal was not restricted to the cell surface, these images suggest that BNP promotes TRPV3 trafficking and that this increase may wane over time.

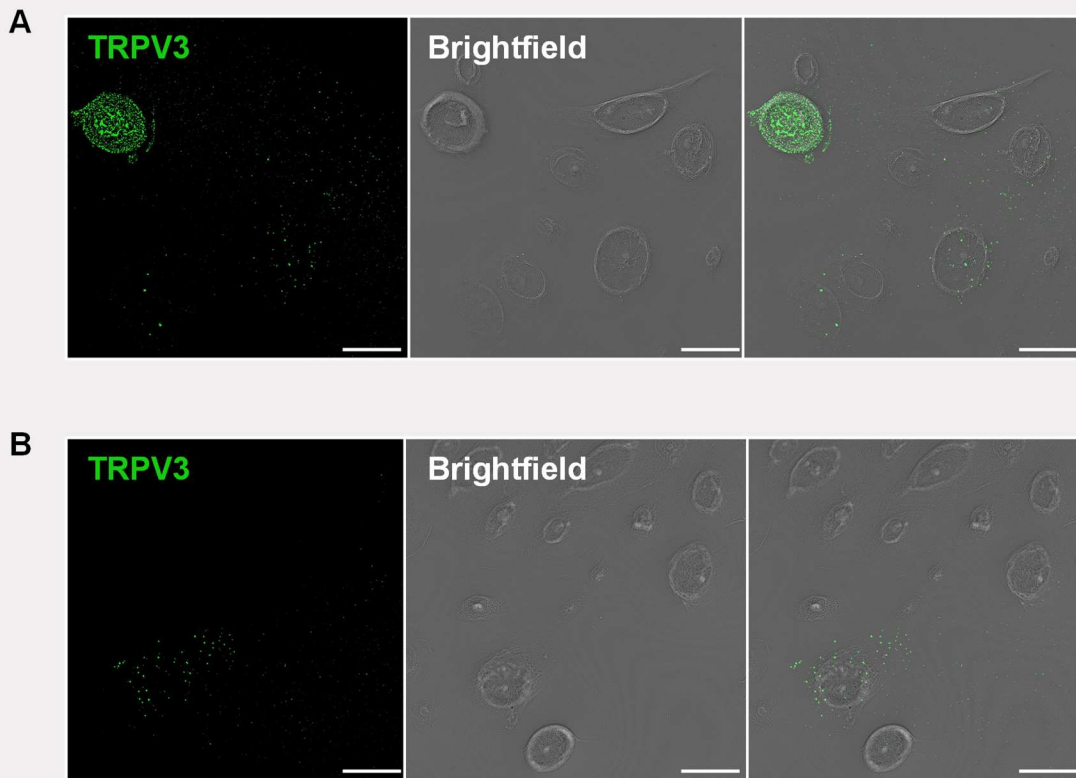


Figure 5.15. Representative images showing effect of BNP on surface expression of TRPV3 proteins in cultured epidermal keratinocytes.

Live keratinocytes (NHEK) were treated with BNP solution for 3 and 24 hours (h) and probed with basal medium \pm TRPV3-ecto antibody (85 $\mu\text{g/ml}$, 15 min) followed by anti-rabbit (Alexa Fluor 555; 10 $\mu\text{g/ml}$, 1 h). Keratinocytes were then fixed, mounted, and imaged using confocal microscopy. **A – B**, Representative images depict surface TRPV3 (green) and brightfield signals in BNP 3 h (**A**) and BNP 24 h (**B**). Scale bars =50 μm . These experiments were carried out concurrent with those depicted in **Figure 5.14**.

Quantification and comparison of fluorescence in all imaged cells emphasised this significant BNP-induced change (Kruskal-Wallis, $P < .0001$) (**Figure 5.16**). After 3 h, BNP increased the median cellular signal by more than 3-fold, relative to 0 h controls (particles per 1500 μm^2 =2.2 vs. 7.4; $P < .0001$). After 24 h, this increase was diminished, but still significant (4.61; $P = .0040$ vs. 0 h).

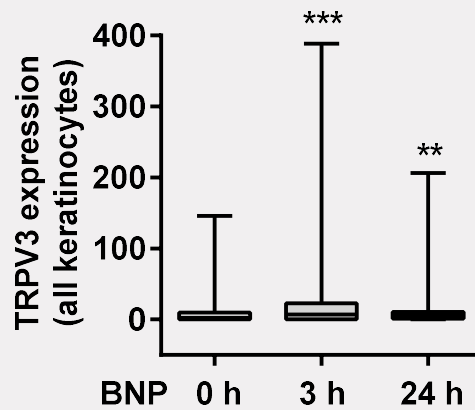


Figure 5.16. BNP promotes TRPV3 trafficking.

Graph compares TRPV3 surface expression in all imaged cells, where TRPV3 expression denotes number of intracellular fluorescent particles per $1500 \mu\text{m}^2$. Boxplots indicate median ($Q^1 - Q^3$), with bars outlining min and max values. Data represent 3 independent stimulations (≥ 30 images per group, ≥ 300 keratinocytes per group). P -values calculated using Kruskal-Wallis test: ** $P \leq .01$; *** $P \leq .001$.

BNP stimulation altered the proportion of TRPV3⁺ vs. TRPV3⁻ keratinocytes, though this trend did not reach significance (Chi-squared, $P = .0538$) (Figure 5.17). Here, the proportion of TRPV3⁺ cells went from 41% in basal samples, up to 59% after 3 h of BNP, and down to 50% after 24 h of BNP. This trend suggests that BNP can affect the trafficking of TRPV3.

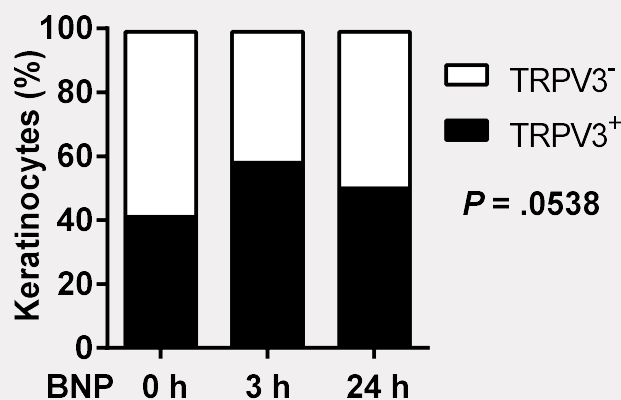


Figure 5.17. BNP alters proportion of TRPV3-positive and TRPV3-negative keratinocytes.

Graph compares percentage of cells assigned TRPV3-positive (TRPV3⁺) vs. TRPV3-negative (TRPV3⁻), where TRPV3⁺ cells express ≥ 5 intracellular fluorescent particles per $1500 \mu\text{m}^2$. Data represent 3 independent stimulations (≥ 30 images per group, ≥ 300 keratinocytes per group). P -values calculated using Chi-squared test: $P = .0538$.

BNP also affected the fluorescence in TRPV3⁺ cells (Kruskal-Wallis, $P < .0001$) (**Figure 5.18**). In these cells, BNP significantly increased the median TRPV3 signal after 3 h, relative to 0 h controls (median particles per 1500 $\mu\text{m}^2 = 12.0$ vs. 18.0; $P = .0013$). However, after 24 h, fluorescence was statistically comparable to 0 h levels (10.0; $P = .3121$ vs. 0 h). Thus, BNP promotes transient trafficking and membrane insertion of the TRPV3 channel.

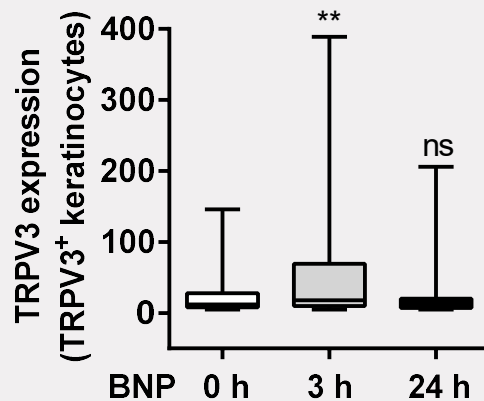


Figure 5.18. BNP promotes TRPV3 trafficking in TRPV3-positive keratinocytes.

Graph compares TRPV3 surface expression in TRPV3-positive (TRPV3⁺) cells, where TRPV3 expression denotes number of intracellular fluorescent particles per 1500 μm^2 . TRPV3⁺ cells express ≥ 5 intracellular fluorescent particles per 1500 μm^2 . Boxplots indicate median ($Q^1 - Q^3$), with bars outlining min and max values. Data represent 3 independent stimulations (≥ 30 images per group, ≥ 300 keratinocytes per group). P -values calculated using Kruskal-Wallis test: ns $P > .05$; ** $P \leq .01$.

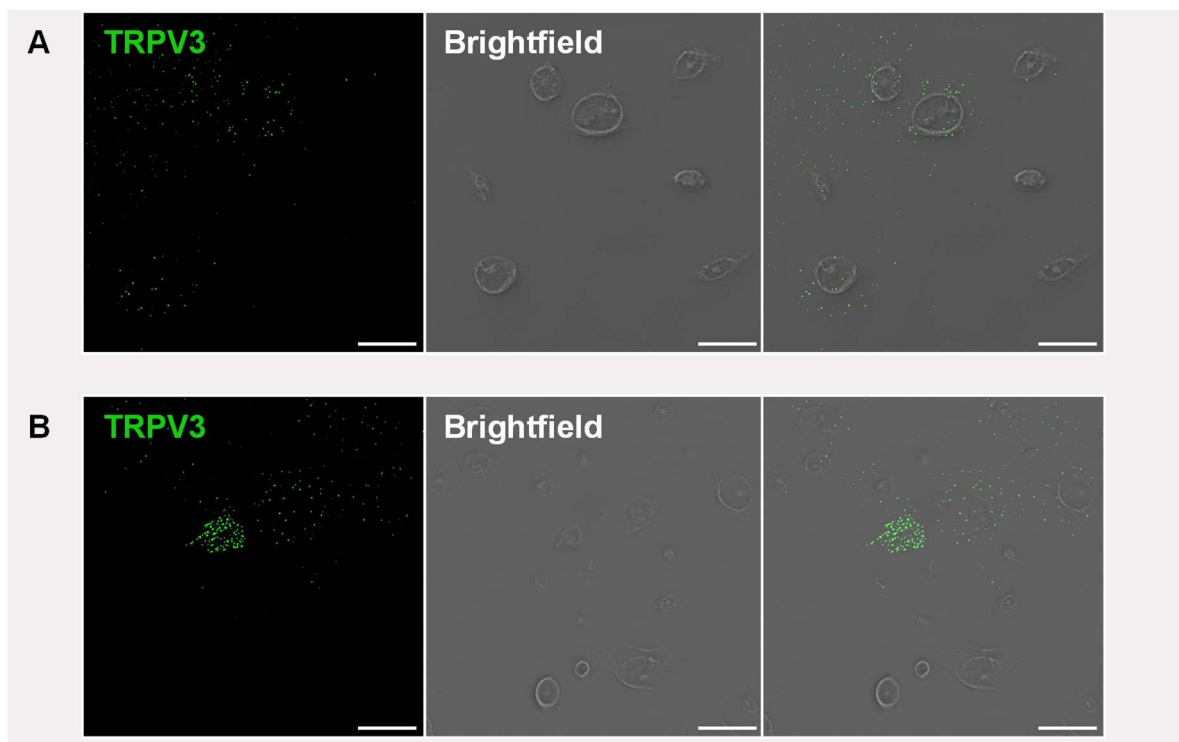
Together, these data confirm TRPV3 membrane expression in human keratinocytes. Here, approximately 41% of control keratinocytes expressed detectable levels of surface TRPV3. This value is comparable to previous staining (34%; **Figure 4.25C**) and, as discussed previously, likely represents cluster 1 rapid responders (43%; **Figure 4.18B**). BNP promoted channel trafficking after 3 h, but not after 24 h. Together with previous data, these findings suggest that this TRPV3 trafficking may underpin sensitisation of TRPV3-mediated calcium flux. Thus, the pathways underpinning this functional upregulation could represent key targets for interruption of TRPV3 overactivation in the skin.

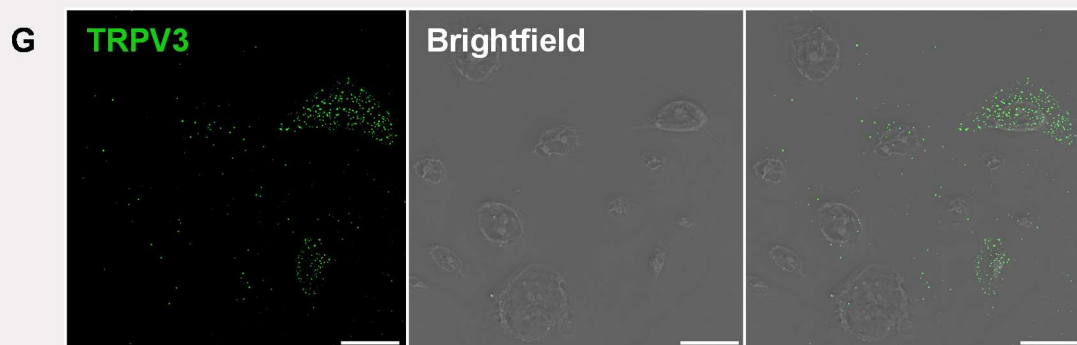
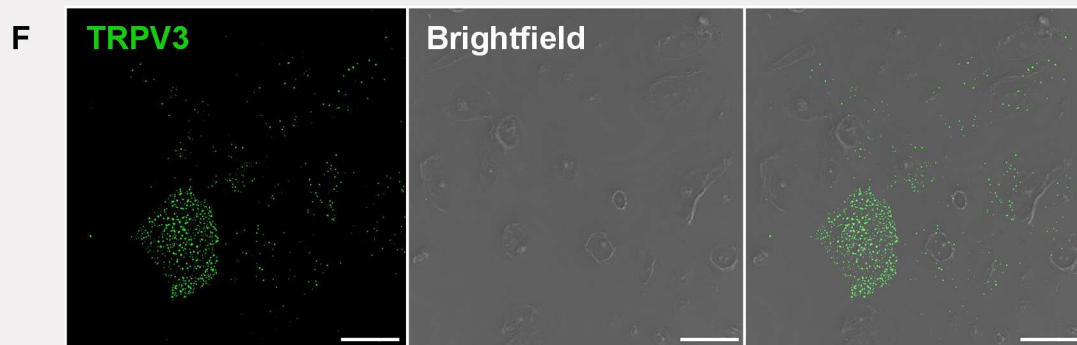
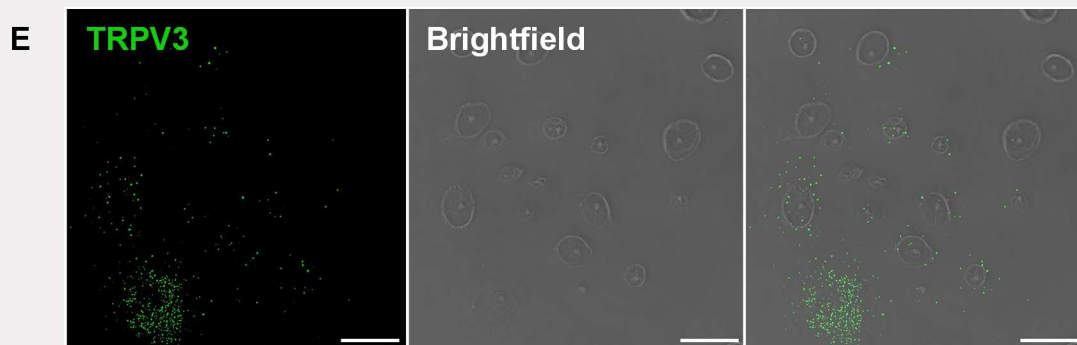
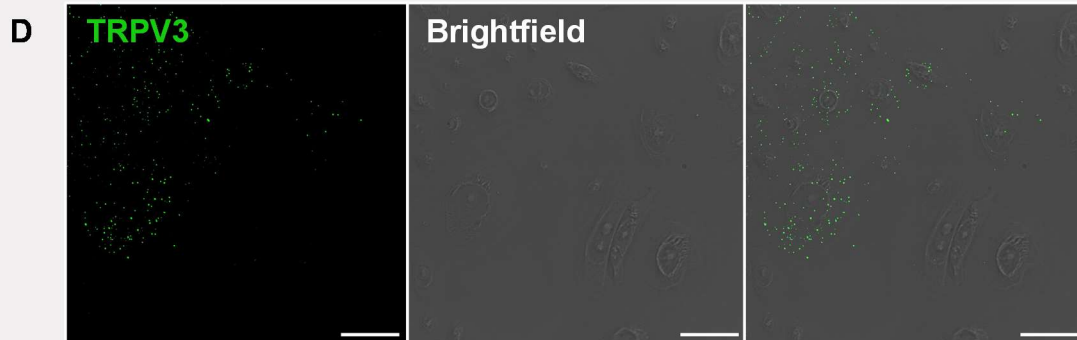
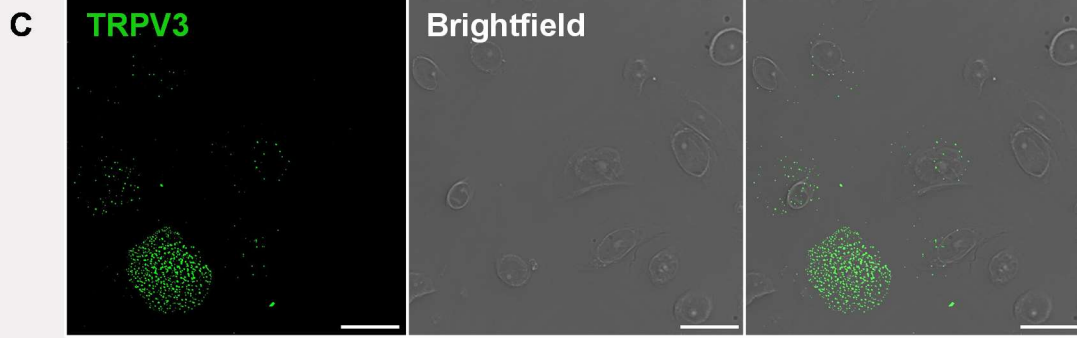
5.2.5. BNP-induced TRPV3 trafficking is mediated by GSK-3 α/β , JNK-pan, and p38 α kinase proteins

BNP stimulates TRPV3 trafficking and membrane insertion in human keratinocytes. Previous work by Dr. Meng identified kinase pathways acting downstream of BNP receptors (NPRA/B) in epidermal keratinocytes: p38 α , GSK-3 α/β , JNK-pan (Meng *et al.*, 2018). Here, we assessed the role of these kinase proteins in BNP-induced TRPV3 trafficking.

NHEK were pre-treated with basal medium \pm kinase inhibitors targeting p38 α (AL8697, AL.); GSK-3 α/β (CHIR99021, CHIR.); JNK-pan (JNK-IN-8, JNK.); or c-Jun (SP600125, SP.) (1 μ M; 1 h). Keratinocytes were then stimulated with basal medium \pm kinase inhibitors (as above) \pm BNP (1 μ M, 3 h). The ecto-TRPV3 channel antibody was added to this stimulation buffer (ACC-033; 85 μ g/ml; 15 min): this highly specific antibody binds the extracellular region of the TRPV3 channel. Following stimulation, keratinocytes were probed with secondary antibody, fixed, and mounted. Samples were imaged using confocal microscopy, images were processed and measured using Image J software, and data were analysed using GraphPad Prism. These experiments were carried out in parallel with those of **Section 5.2.4**.

TRPV3 membrane expression was detected in keratinocytes (NHEK), with groups displaying varying levels of fluorescence: basal medium alone (**Figure 5.19A**); basal medium + BNP 3 h (**Figure 5.19B**); AL. + BNP 3 h (**Figure 5.19C**); CHIR. + BNP 3 h (**Figure 5.19D**); JNK. + BNP 3 h (**Figure 5.19E**); SP. + BNP 3 h (**Figure 5.19F**); medium + BNP 24 h (**Figure 5.19G**); and secondary only imaging control (**Figure 5.19H**). The TRPV3 signal was not restricted to the cell surface suggesting that bound channels may have been internalised prior to fixation; however, secondary only imaging controls illustrate the specificity of the signal.





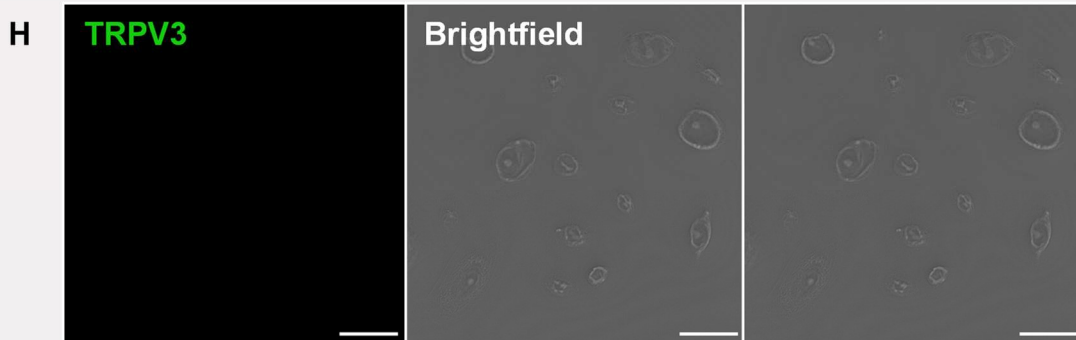


Figure 5.19. Representative images showing surface expression of TRPV3 proteins in cultured epidermal keratinocytes.

Live keratinocytes (NHEK) were pre-treated with basal medium \pm kinase inhibitors targeting p38 α (AL8697, AL.); GSK-3 α/β (CHIR99021, CHIR.); JNK1/2/3 (JNK-IN-8, JNK.); and c-Jun (SP600125, SP.). Keratinocytes were treated with basal medium \pm kinase inhibitor \pm BNP (1 μ M). Samples were then probed with basal medium \pm TRPV3-ecto antibody (85 μ g/ml, 15 min) followed by anti-rabbit (Alexa Fluor 555; 10 μ g/ml, 1 h). Probed samples were fixed, mounted, and imaged using confocal microscopy. **A – H**, Representative images showing surface TRPV3 (green) and brightfield signals: basal control (**A**); control BNP 3 h (**B**); AL. + BNP 3 h (**C**); CHIR. + BNP 3 h (**D**); JNK. + BNP 3 h (**E**); SP. + BNP 3 h (**F**); control BNP 24 h (**G**); and secondary only imaging control (**H**). Scale bars =50 μ m.

Nonspecific fluorescence was unaffected by kinase inhibitor treatment, with the median of each group measuring zero (Figure 5.20). TRPV3-positive (TRPV3⁺) cells were defined as those which contained ≥ 5 particles per 1500 μm^2 (dotted line). Here, the mean of each imaging control group was less than 5 particles per 1500 μm^2 indicating that this is a useful threshold and that kinase inhibitors do not alter nonspecific fluorescence.

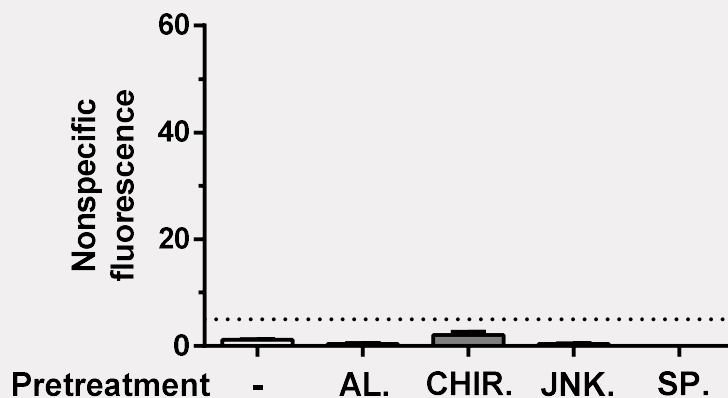


Figure 5.20. Nonspecific fluorescence is unaffected by kinase inhibitor pre-treatment.

Live keratinocytes (NHEK) were treated with basal medium \pm kinase inhibitors targeting p38 α (AL8697, AL.); GSK-3 α/β (CHIR99021, CHIR.); JNK1/2/3 (JNK-IN-8, JNK.); and c-Jun (SP600125, SP.). Samples were then probed with basal medium (15 min) followed by anti-rabbit (Alexa Fluor 555; 10 $\mu\text{g}/\text{ml}$, 1 h). Probed samples were fixed, mounted, and imaged using confocal microscopy. Graph compares fluorescence in all secondary only controls, where values denote intracellular fluorescent particles per 1500 μm^2 . Dotted line denotes 5 particles per 1500 μm^2 : the threshold for TRPV3⁺ cells. Boxplots indicate median (Q¹ - Q³), with bars outlining min and max values. Data represent 2 independent experiments.

Quantification and comparison of fluorescence in all imaged cells revealed the effect of kinase inhibitors on BNP-induced trafficking (Kruskal-Wallis, $P < .0001$) (**Figure 5.21**). As described in section 5.2.5, BNP stimulation (3 h and 24 h) significantly elevated TRPV3 surface expression relative to basal levels. Kinase inhibitor data were then compared to control BNP 3 h. GSK-3 α/β (CHIR.) and JNK-pan (JNK.) inhibitors significantly reduced BNP-induced trafficking ($P < .0001$ vs. control BNP 3 h) –in fact, these inhibitor groups were statistically comparable to basal ($P > .9999$ vs. control basal). Conversely, p38 α (AL.) and c-Jun (SP.) inhibitors were unable to modulate BNP-induced trafficking ($P = .343$ and $P > .9999$, respectively; vs. control BNP 3 h). These data suggest that GSK-3 α/β and JNK facilitate this BNP-induced TRPV3 trafficking.

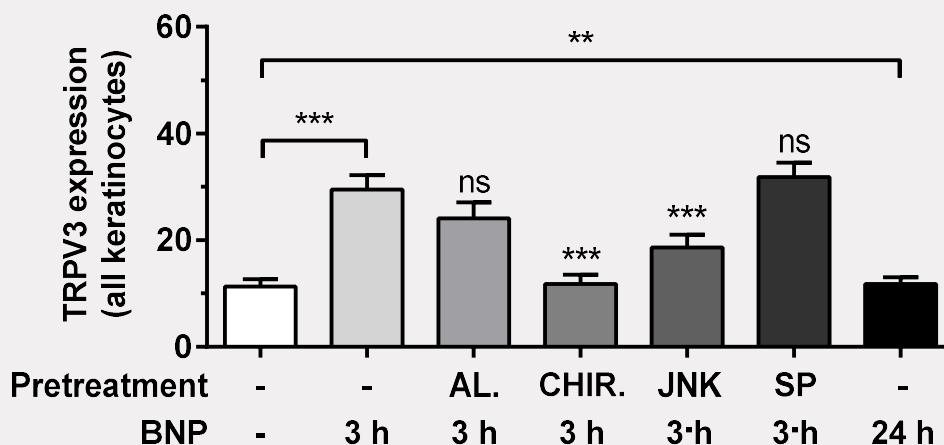


Figure 5.21. Inhibition of GSK-3 α/β and JNK1/2/3 reduces BNP-induced TRPV3 trafficking.

Live keratinocytes (NHEK) were treated with basal medium \pm kinase inhibitors targeting p38 α (AL8697, AL.); GSK-3 α/β (CHIR99021, CHIR.); JNK1/2/3 (JNK-IN-8, JNK.); and c-Jun (SP600125, SP.). Samples were then probed with basal medium (15 min) followed by anti-rabbit (Alexa Fluor 555; 10 μ g/ml, 1 h). Probed samples were fixed, mounted, and imaged using confocal microscopy. Graph compares TRPV3 surface expression in all imaged keratinocytes (NHEK), where TRPV3 expression denotes the number of intracellular fluorescent particles per 1500 μ m². Boxplots indicate median ($Q^1 - Q^3$), with bars outlining min and max values. Data represent 3 independent stimulations (≥ 30 images per group, ≥ 300 keratinocytes per group). P -values calculated using Kruskal-Wallis test (vs. control BNP 3 h, unless otherwise indicated): ns $P > .05$; ** $P \leq .01$; *** $P \leq .001$.

Kinase inhibitor treatment significantly altered the proportion of TRPV3⁺ vs. TRPV3-negative (TRPV3⁻) keratinocytes within the BNP (3 h) group (Chi-squared, $P = .0101$) (Figure 5.22). These analyses specifically compare the effect of kinase inhibition on BNP (3 h) -evoked trafficking. Statistics do not include the basal or BNP (24 h) groups. Here, the proportion of TRPV3⁺ cells went from 59% in the control BNP (3 h) group to 56% following AL. treatment; to 41% following CHIR. treatment; to 43% following JNK. treatment; and to 60% following SP. treatment. This trend again suggests that GSK-3 α/β and JNK-pan facilitate this BNP-induced TRPV3 trafficking.

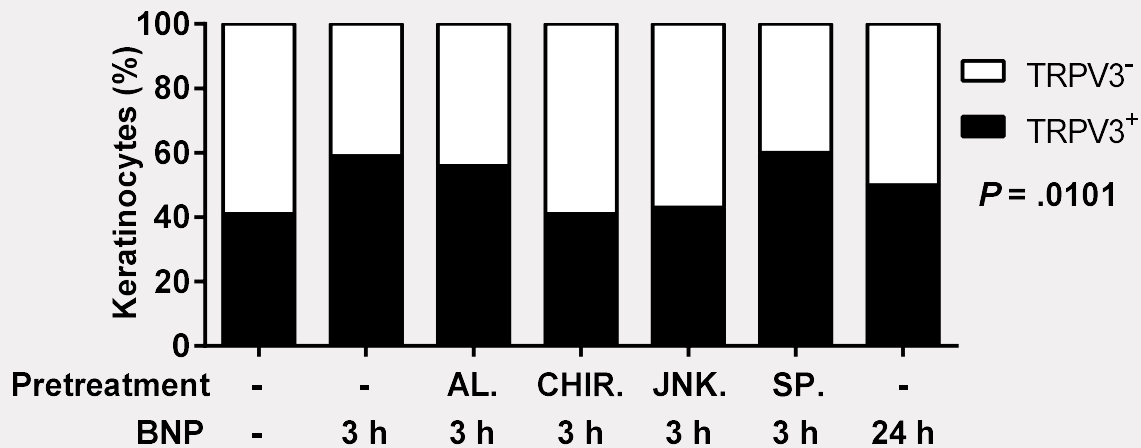


Figure 5.22. Stimulation with BNP \pm kinase inhibitors alter the proportion of TRPV3-positive and TRPV3-negative keratinocytes.

Live keratinocytes (NHEK) were treated with basal medium \pm kinase inhibitors targeting p38 α (AL8697, AL.); GSK-3 α/β (CHIR99021, CHIR.); JNK1/2/3 (JNK-IN-8, JNK.); and c-Jun (SP600125, SP.). Samples were then probed with basal medium (15 min) followed by anti-rabbit (Alexa Fluor 555; 10 $\mu\text{g}/\text{ml}$, 1 h). Probed samples were fixed, mounted, and imaged using confocal microscopy. Graph compares percentage of keratinocytes (NHEK) assigned TRPV3-positive (TRPV3⁺) vs. TRPV3-negative (TRPV3⁻), where TRPV3⁺ cells express ≥ 5 intracellular fluorescent particles per 1500 μm^2 . Data represent 3 independent stimulations (≥ 30 images per group, ≥ 300 keratinocytes per group). P -value calculated using Chi-squared test: $P = .0101$ (comparing just BNP 3 h data).

Kinase inhibitor treatment also significantly affected the fluorescence in TRPV3⁺ cells (Kruskal-Wallis, $P < .0001$) (**Figure 5.23**). Again, BNP stimulation (3 h) significantly elevated TRPV3 surface expression relative to basal levels. Kinase inhibitor data were then compared to control BNP 3 h. Here, p38 α (AL.), GSK-3 α/β (CHIR.), and JNK-pan (JNK.) inhibitors significantly reduced BNP-induced trafficking in TRPV3⁺ cells: $P = .0191$ [AL.], $P < .0001$ [CHIR.], $P = .0050$ [JNK.]; all *vs.* control BNP 3 h. Only the c-Jun (SP.) inhibitor was unable to modulate BNP-induced trafficking in TRPV3⁺ cells ($P = .1860$; *vs.* control BNP 3 h) suggesting that this TRPV3 trafficking is independent of c-Jun signalling in human keratinocytes.

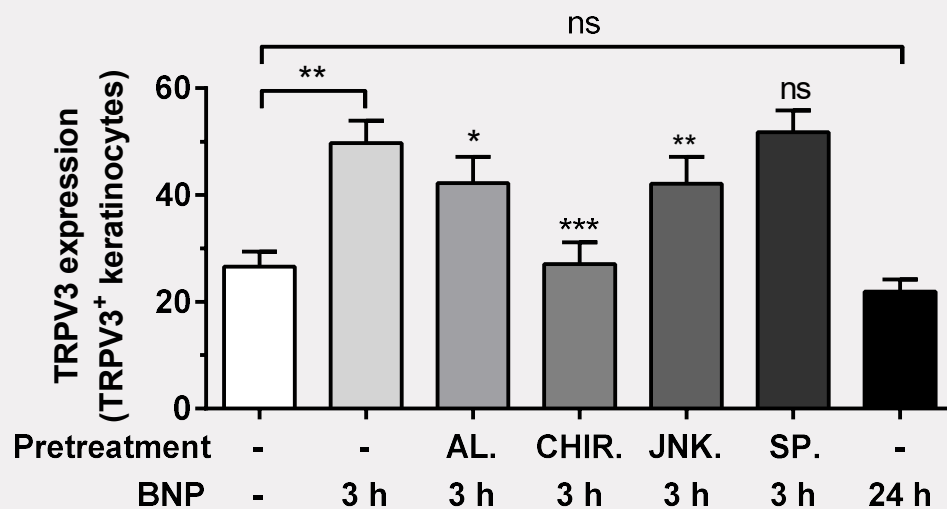


Figure 5.23. Inhibition of p38 α , GSK-3 α/β , and JNK1/2/3 reduces BNP-induced TRPV3 trafficking in TRPV3-positive keratinocytes.

Live keratinocytes (NHEK) were treated with basal medium \pm kinase inhibitors targeting p38 α (AL8697, AL.); GSK-3 α/β (CHIR99021, CHIR.); JNK1/2/3 (JNK-IN-8, JNK.); and c-Jun (SP600125, SP.). Samples were then probed with basal medium (15 min) followed by anti-rabbit (Alexa Fluor 555; 10 $\mu\text{g}/\text{ml}$, 1 h). Probed samples were fixed, mounted, and imaged using confocal microscopy. Graph compares TRPV3 surface expression in TRPV3-positive (TRPV3⁺) keratinocytes (NHEK), where TRPV3 expression denotes the number of intracellular fluorescent particles per 1500 μm^2 . TRPV3⁺ cells express ≥ 5 intracellular fluorescent particles per 1500 μm^2 . Boxplots indicate median ($Q^1 - Q^3$), with bars outlining min and max values. Data represent 3 independent stimulations (≥ 30 images per group, ≥ 300 keratinocytes per group). P -values calculated using Kruskal-Wallis test (*vs.* control BNP 3 h, unless otherwise indicated): ns $P > .05$; ** $P \leq .01$; *** $P \leq .001$.

In epidermal keratinocytes, BNP activates p38 α , GSK-3 α/β , and JNK/c-Jun signalling. The data described herein suggest that these kinase pathways then coordinate TRPV3 trafficking and membrane insertion, sensitising the TRPV3 response. Thus, targeting these kinase pathways may interrupt acute TRPV3 overexpression in atopic dermatitis and other pruritic dermatoses.

5.3. Discussion

5.3.1. Summary

The findings described herein highlight a novel neuro-epidermal pathway: BNP/TRPV3 (**Figure 5.24**). BNP sensitises TRPV3 activity, promoting rapid calcium responses. This sensitisation does not affect key TRPV3-evoked mediators. BNP promotes TRPV3 trafficking, acting via GSK-3 α/β , JNK-pan, and p38 α to elevate surface TRPV3 expression in keratinocyte populations. Together, these data outlined an AD-relevant mechanism for functional upregulation of TRPV3 channels in the skin. Thus, the pathways outlined herein represent key targets for modulation of TRPV3 activity.

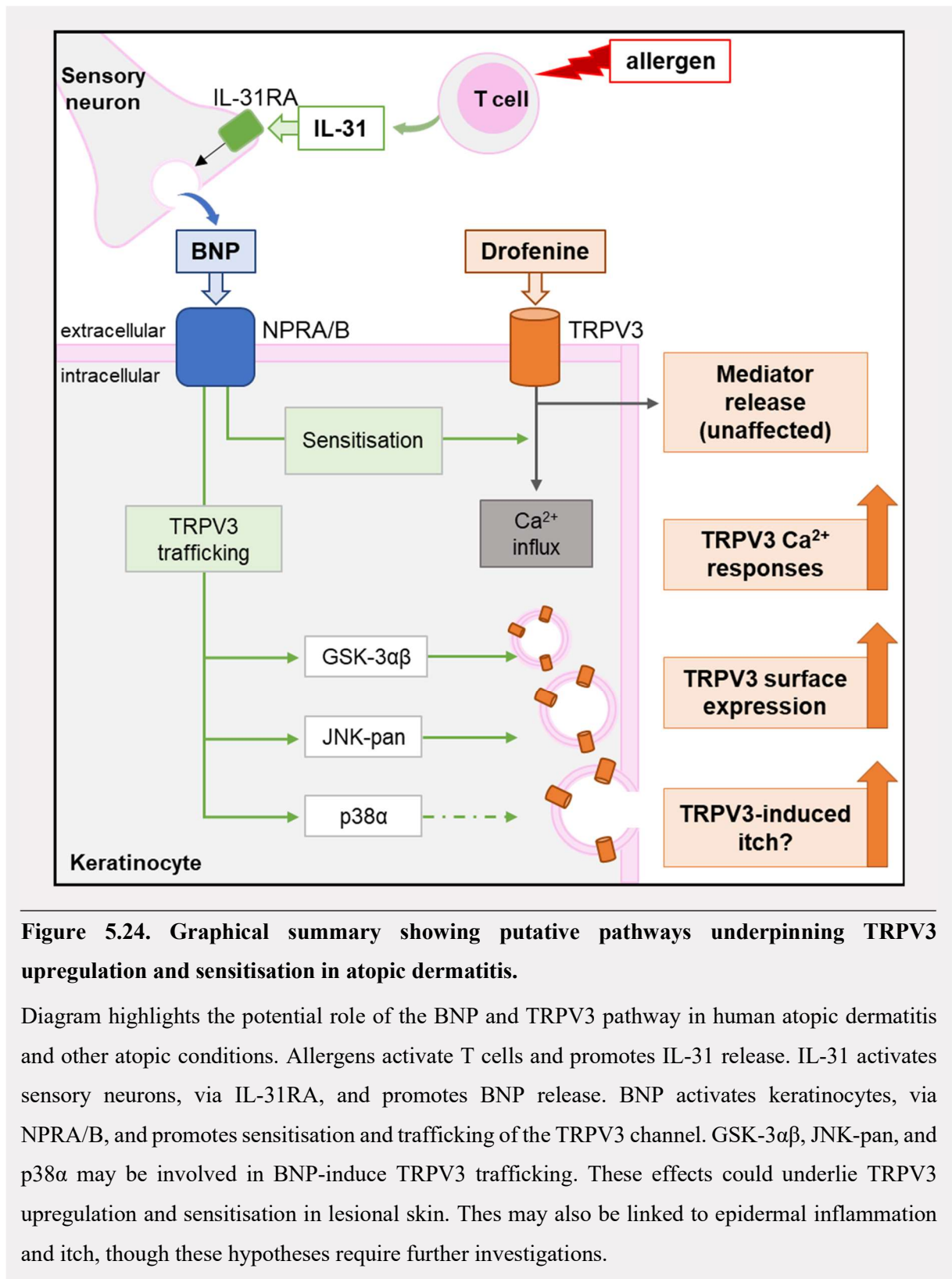


Figure 5.24. Graphical summary showing putative pathways underpinning TRPV3 upregulation and sensitisation in atopic dermatitis.

Diagram highlights the potential role of the BNP and TRPV3 pathway in human atopic dermatitis and other atopic conditions. Allergens activate T cells and promotes IL-31 release. IL-31 activates sensory neurons, via IL-31RA, and promotes BNP release. BNP activates keratinocytes, via NPRA/B, and promotes sensitisation and trafficking of the TRPV3 channel. GSK-3 $\alpha\beta$, JNK-pan, and p38 α may be involved in BNP-induce TRPV3 trafficking. These effects could underlie TRPV3 upregulation and sensitisation in lesional skin. This may also be linked to epidermal inflammation and itch, though these hypotheses require further investigations.

5.3.2. Inter-experimental differences in number of calcium clusters

This project aimed to highlight the utility of clustering analysis for integration of calcium signalling in populations of cultured cells. Our findings suggested that these clusters could represent distinct functional subpopulations within the NHEK culture model. However, this hypothesis is weakened by the differing k values across sections.

In this chapter, k -means clustering detected 3 clusters within the normal drofenine (500 μ M; D500)-evoked response profile (**Figure 5.10C**). This graph is also shown below for comparison. In this plot, peak latency was expressed in seconds, with time 0 representing the beginning of recording and time 100 marking the addition of D500. These 3 clusters covered distinct ranges of peak latency and were differentially affected by BNP pre-treatment (**Figure 5.12**) – potentially revealing an important aspect of BNP-induced TRPV3 sensitisation.

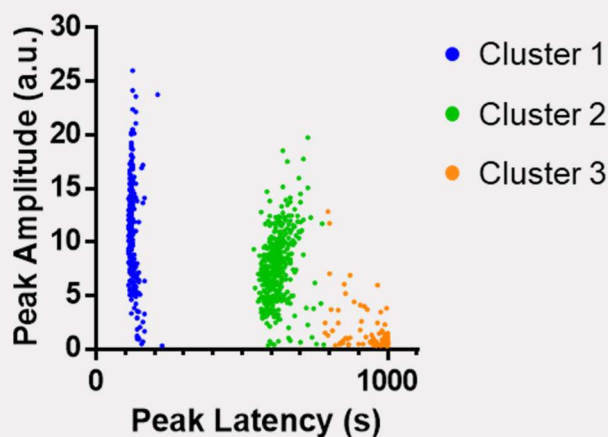


Figure 5.10C. Clustering of the D500 response profile, originally included in Section 5.2.2.

Graph depicts control D500 response profile: peak latency (Time_{max} , s) vs. peak amplitude ($F\Delta/F0_{\text{max}}$, a.u.). Each dot represents a single cell. Cells are coloured by cluster, where $k=3$. Data represent ≥ 3 independent stimulations ($n \geq 828$ keratinocytes per group, non-responders not shown). *Abbreviations:* a.u., arbitrary units; D500, drofenine (500 μ m); seconds, s.

In the previous chapter, independent k -means clustering detected 4 clusters within the normal D500 response profile (**Figure 4.17B**). Again, this graph is shown below for comparison. Peak amplitude values were lower in this experiment, compared with those of **Section 5.2.2**. This project used Fluo 4AM to measure relative calcium changes. A ratiometric calcium dye, such as fura-2, could allow for identification of inter-experimental noise and inter-experimental differences in calcium amplitude. Although notable, this difference may be explained by differences in cellular or imaging parameters.

In section 4.2.3, peak latency was expressed as seconds post initiation (s.p.i) to control for variation associated with the size of the culture dish (see **Section 2.2.6.1** for further details). In this plot, time 0 represents the initiation point: the earliest incidence of cellular activation ($F\Delta/F0 \geq 0.3$). These 4 clusters covered distinct ranges of peak latency values (**Table 5.4**). These clusters were differentially affected by Pitstop2 pre-treatment – potentially revealing an important aspect of TRPV3 trafficking.

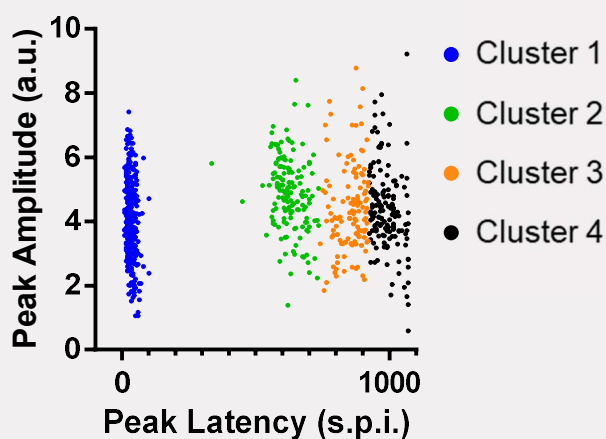


Figure 4.17B. Clustering of the D500 response profile, originally included in Section 4.2.3.

Graph depicts control D500 response profile: peak latency (Time_{\max} , s.p.i.) vs. peak amplitude ($F\Delta/F0_{\max}$, a.u.). Each dot represents a single cell. Cells are coloured by cluster, where $k=4$. Data represent 4 independent stimulations ($n \geq 797$ keratinocytes per group, non-responders not shown). *Abbreviations:* a.u., arbitrary units; D500, drofenine (500 μm); seconds post initiation, s.p.i.

Table 5.4. Range of peak latency values in each cluster: Section 4.2.3 vs. Section 5.2.2.

	Section 4.2.3	Section 5.2.2
Cluster 1 (s.p.i.)	10 – 100	10 – 120
Cluster 2 (s.p.i.)	335 – 735	440 – 675
Cluster 3 (s.p.i.)	740 – 920	680 – 895
Cluster 4 (s.p.i.)	925 – 1070	n/a

Note: Data represent the min and max s.p.i values for each cluster. *Abbreviations:* seconds post initiation, s.p.i.

To allow comparison, data from Section 5.2.2 were transformed to align with Section 4.2.3: all peak latency data were expressed as s.p.i. Following transformation, peak latency ranges were broadly comparable across sections (**Table 5.4**). Of note, the recording time for section 5.2.2 was shorter, with the cluster 4 data points absent from the dataset. This simple difference in experimental setup explains the differing k values across sections.

Graphs also highlight the clear overlap in the clustering ranges. Data from section 5.2.2 was clustered using ranges from Section 4.2.3 (**Figure 5.25A**) and Section 5.2.2 (**Figure 5.25B**). Transformed data were graphed and coloured according to cluster. Closer examination revealed that only 2% of stimulated cells were group differently when the section 4.2.3 ranges were used ($n = 14$). These comparisons suggest that the clustering analyses have detected consistent subgroups across experiments.

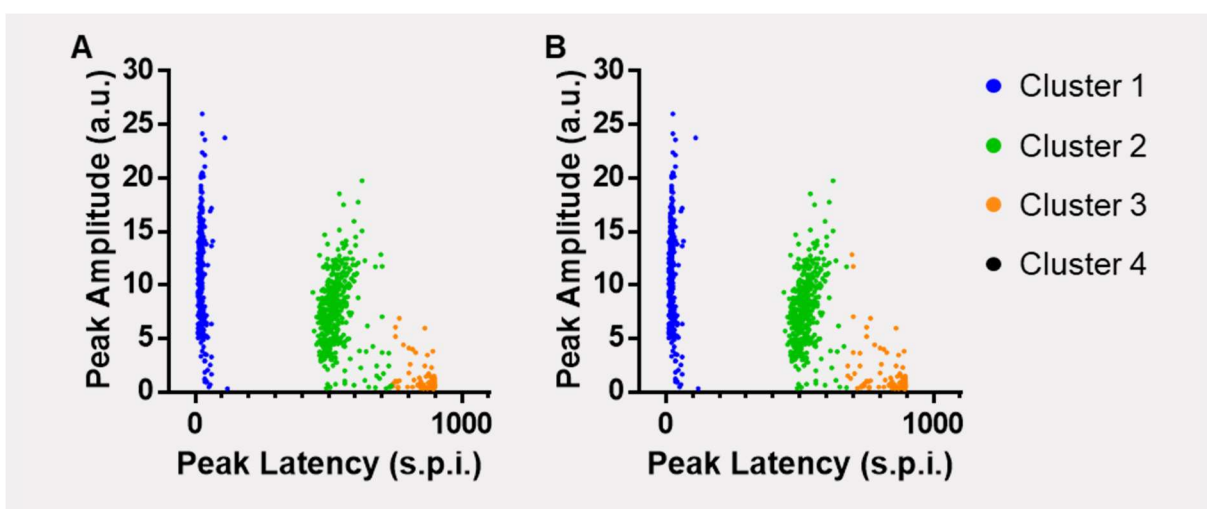


Figure 5.25. Clustering ranges from Section 4.2.3 and Section 5.2.2 are comparable.

Graphs depict the D500 response profile from section 5.2.2 following transformation: peak latency (Time_{\max} , s.p.i.) vs. peak amplitude ($F\Delta/F0_{\max}$, a.u.). Data were grouped with respect to cluster limits from section 4.2.3 (**A**) and section 5.2.2 (**B**). *Abbreviations:* a.u., arbitrary units; D500, drofenine (500 μm); seconds post initiation, s.p.i.

Future experiments should utilise a consistent experimental setup. However, our data suggests that TRPV3 calcium responses can be consistently clustered into distinct responses groups. Together, these comparisons strengthen the validity of the findings herein and aid our overall understanding of the TRPV3 calcium response.

5.3.3. BNP: an inducer of early epidermal alterations?

BNP, TRPV3, and TRPV3-linked mediators are increased in pruritic and lesional skin (Seo *et al.*, 2020; Zhao *et al.*, 2020; Nattkemper *et al.*, 2018; Qu *et al.*, 2019; Sulk *et al.*, 2012; Yang *et al.*, 2015; Park *et al.*, 2017). Thus, it was reasonable to assume that BNP would prime keratinocytes, elevating functional TRPV3 expression and TRPV3-evoked release.

Here, BNP successfully promoted TRPV3 activity and surface expression; but failed to affect mediator release. At first glance these data appear contradictory. Firstly, BNP may affect other TRPV3-linked mediators not included in these analyses: ATP, PGE2, NO, NGF or TSLP (Cals-Grierson and Ormerod, 2004; Huang *et al.*, 2008; Mandadi *et al.*, 2009; Miyamoto *et al.*, 2011; Yamamoto-Kasai *et al.*, 2013; Seo *et al.*, 2020; Zhao *et al.*, 2020). Closer inspection of calcium data suggests another possibility: BNP accelerates the calcium response without affecting the overall proportion of drofenine-sensitive keratinocytes. Thus, it is possible that BNP also accelerates mediator release without affecting the total release over one hour. This hypothesis could be easily examined using shorter incubation times; however, at present no clear conclusions can be made. BNP also induces TRPV3 trafficking at 3 h, but not at 24 h. These results are in direct contrast to findings from pruritic lesions; however, together, they demonstrate the complex interplay between cutaneous cells and sensory neurons in the skin. We propose that BNP may stimulate acute TRPV3 trafficking *in vivo*, with other lesional mediators stabilising this upregulation and potentiating mediator release. Thus, BNP, and the pathways identified herein, may drive early epidermal alterations in lesional skin and represent an important target for modulation of acute atopic dermatitis lesions, potentially interrupting the transition from acute to chronic.

5.3.4. Targeting BNP

The data outlined herein represent the first evidence of the BNP/TRPV3 neuro-epidermal link (Larkin *et al.*, 2021). BNP is released from cutaneous NP3 sensory neurons and highly elevated in pruritic lesions (Mishra and Hoon, 2013; Usoskin *et al.*, 2015; Meng *et al.*, 2018). At present, specific BNP-targeting agents are lacking. Release of BNP is dependent on VAMP1 and SNAP25 SNARE proteins (Meng *et al.*, 2018). BNP activates epidermal keratinocytes, promoting phosphorylation of GSK-3 α/β , JNK, p38 α and ERK1/2 kinases (Meng *et al.*, 2018). Herein, GSK-3 α/β , JNK, p38 α pathways coordinated functional TRPV3 upregulation. GSK-3 α/β also underpins BNP-evoked IL-17A release from keratinocytes (Meng *et al.*, 2018). In the skin BNP activates dendritic cells, promoting phosphorylation of c-Jun and release of CCL20 (Meng *et al.*, 2018). In addition to this neuro-epidermal signalling, BNP is both necessary and sufficient for central itch transduction (Mishra and Hoon, 2013). Intraperitoneal injection of JS-11, an NPRA antagonist, reduces scratching behaviour, but not inflammation, in murine models of acute and prolonged itch (Solinski, Dranchak, *et al.*, 2019). Together, these data highlight the potential impact of anti-BNP agents in the treatment of pruritic inflammatory skin conditions and reveal several novel targets for drug development.

5.3.5. Conclusion

In atopic dermatitis lesions, NP3 sensory neurons release BNP and stimulate adjacent epidermal keratinocytes. BNP alters TRPV3 responses suggesting that this pathway may promote TRPV3 overexpression and overactivation in lesional skin. Here, we identified GSK-3 α/β , JNK-pan, and p38 α kinase proteins as key coordinators of BNP-induced TRPV3 trafficking; targeting of these pathways may modulate TRPV3 responses and TRPV3-evoked itch in acute lesions. Further investigations are required to elucidate the mechanisms driving TRPV3 upregulation and sensitisation in chronic lesions.

6. Discussion of Work in Context

6.1. TRPV3 and the role of cation gradients in the skin

TRPV3 is a calcium (Ca^{2+})-permeable cation channel. Herein, calcium was used as an indicator of TRPV3 channel opening. We found that the TRPV3 agonist, drofenine, promotes rapid and widespread calcium fluctuations in an NHEK culture model of human epidermis.

TRPV3 also permits entry of sodium (Na^+), potassium (K^+), and caesium (Cs^+): $\text{Ca}^{2+} > \text{Na}^+ \approx \text{K}^+ \approx \text{Cs}^+$ (Xu *et al.*, 2002). Permeability ratios suggest that TRPV3 is moderately calcium-selective (about 12 $\text{P}_{\text{Ca}}/\text{P}_{\text{Na}}$) (Xu *et al.*, 2002). At present, reports on TRPV3-mediated magnesium currents are lacking – in fact, magnesium may represent an important negative regulator of the TRPV3 channel (Luo *et al.*, 2012). More recently, TRPV3 was shown to facilitate influx of ammonium cations – a key factors in the synthesis of filaggrin, loricrin, and involucrin (Danielyan *et al.*, 2009; Rosendahl *et al.*, 2016; Schrapers *et al.*, 2018; Liebe *et al.*, 2020, 2021). Each of these cations induce and modulate keratinocyte signalling, highlighting the potential impact of TRPV3 dysregulation on homeostasis and healing of the skin.

Reepithelialisation following cutaneous damage is dependent on a complex and tightly controlled signalling cascade, involving both calcium and magnesium cations. Both calcium and magnesium display consistent and comparable concentration gradients across the epidermal layer (**Figure 6.1**): concentration of these cations peaks in the stratum granulosum (Denda *et al.*, 2000; Haftek *et al.*, 2022). Cutaneous calcium regulates keratinocyte proliferation, differentiation, cornification, desquamation, and inflammation (Elsholz *et al.*, 2014; Bikle, 2023). Magnesium acts as a co-factor for more than 300 enzymes, regulating a plethora of processes and ion channels (Fawcett *et al.*, 1999). Certain magnesium salts promote barrier repair and reduce inflammation (Denda *et al.*, 1999; Proksch *et al.*, 2005). Calcium and magnesium also function as antimicrobial agents, reducing the viability of *s. aureus* in culture (Xie and Yang, 2016). However, although calcium concentrations are elevated in atopic dermatitis lesions (Forslind *et al.*, 1999), lesions are characterised by increased *s. aureus* (Kong *et al.*, 2012). Gradients of calcium and magnesium promote integrin-dependent migration of fibroblasts and keratinocytes – a key step in reepithelialisation (Lange *et al.*, 1995). In humans, reepithelialisation is aided by topical application of a calcium and magnesium containing Marine Mineral Complex (MXC): MXC cooled the skin and stimulated wound healing pathways in 3D-organotypic model of burn injury (Wallace *et al.*, 2020). Thus, calcium and magnesium are particularly important for epidermal function and wound healing.

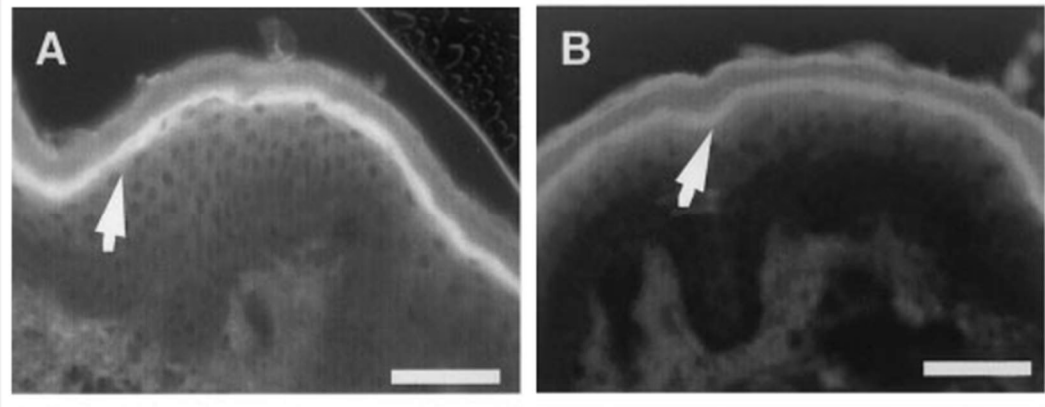


Figure 6.1. Calcium and magnesium gradients in the skin.

Calcium (*left panel*, labelled A) and magnesium (*right panel*, labelled B) are localised to the stratum granulosum in normal human skin, marked with a white arrow. Scale bars =50 μm . From Denda, Hosoi and Asida, 2000.

TRPV3 channels may facilitate calcium-dependent processes and dysfunction in the skin. TRPV3 agonists inhibit proliferation and promote apoptosis in cultured keratinocytes, with both effects being dependent on calcium influx (Borbíró *et al.*, 2011). TRPV3-mediated calcium currents promote activation of intracellular transglutaminases – key calcium-dependent enzymes involved in barrier formation and cornification (Cheng *et al.*, 2010). People with Olmsted syndrome primarily present with painful palmoplantar keratoderma: thickening of the epidermis on the palms of the hands and the soles of the feet. Several of the mutations underlying Olmsted syndrome affect the TRPV3 channel: these mutations enhance TRPV3 channel opening, elevate calcium influx, and promote apoptosis (Lin *et al.*, 2012). Keratinocytes isolated from patients with Olmsted syndrome show elevated rates of apoptosis (Lin *et al.*, 2012). TRPV3 overexpression and overactivation has also been linked to atopic dermatitis lesions (Seo *et al.*, 2020; Larkin *et al.*, 2021). In a cultured HaCaT model, application of drofenine resulted in profound and rapid cell death (data not shown), even at levels much lower than the described EC50 (Deering-Rice *et al.*, 2014). These HaCaT expressed notable levels of TRPV3 within the cellular membrane region suggesting that the drofenine-induced cell death may be mediated by TRPV3-dependent calcium-induced apoptosis (data not shown). Thus, dysregulated TRPV3 activity could alter epidermal calcium gradients and impair normal epidermal function.

Certain TRP channels are permeable to magnesium. These include TRPV1, TRPV4, TRPM6, and TRPM7 (Li *et al.*, 2007; Caterina *et al.*, 1997; Voets *et al.*, 2002). Although often termed cation nonselective, TRPV3 may be unable to conduct magnesium currents. An aspartate residue (D672) has been linked to magnesium permeability in TRPV4 channels (Nilius *et al.*, 2004; Voets *et al.*, 2002). Amino acid sequence comparison shows that this aspartate is replaced with glutamic acid (E672) in TRPV3 (**Figure 6.2**) (Nilius *et al.*, 2004). Separate reports found that intracellular and

extracellular magnesium can directly inhibit TRPV3 channel opening (Luo *et al.*, 2012). This magnesium block is, at least in part, dependent on a separate aspartate residue located in the outer pore region of the TRPV3 channel (D641) (Chung *et al.*, 2005; Luo *et al.*, 2012; Deng *et al.*, 2020). In fact, magnesium may represent a key modulator of TRPV3 activity both *in vitro* and *in vivo*. Magnesium deficiency promotes a pruritic erythematous rash and spontaneous scratching in rodents (Akamatsu *et al.*, 2006; Neckermann *et al.*, 2000). In atopic skin, topical magnesium reduces barrier damage and improves skin hydration. Thus, early hypotheses suggested that magnesium deficiency could be a driver of atopic dermatitis (Lipkin *et al.*, 1964; Maccardle *et al.*, 1941; Koppes *et al.*, 2016; Proksch *et al.*, 2005). In theory, this topical magnesium could also modulate TRPV3 activity - though this hypothesis remains unexplored. Together, these reports show that magnesium influx is independent of the TRPV3 channel; suggest that magnesium represents an important modulator of TRPV3 activity; and highlight the importance of magnesium balance in cutaneous health and disease.

TRPV1 : YNSLYSTCLEL	FKFTIGMGDL	EFTE
TRPV2 : YRGILEASLEL	FKFTIGMGEL	AFQE
TRPV3 : YGSFSDAVLEL	FKLTIGLGDL	NIQQ
TRPV4 : SETFSTFL ⁶⁷² DL	FKLTIG ⁶⁸² MGDL	EMLS
TRPV5 : YPTALFSTFEL	F-LTIIDGPA	NYSV
TRPV6 : YPMALFSTFEL	F-LTIIDGPA	NYNV

Figure 6.2. Sequence comparison of TRPV channels.

D672 is linked to magnesium permeability in TRPV4 channels. Box indicates putative selectivity filter. From Nilius *et al.*, 2004.

The results outlined herein revealed distinct phases within the drofenine-evoked calcium response. Later phases were associated with TRPV3 trafficking; while earlier phases were sensitised by BNP, an itch-linked neuropeptide. The importance of these findings in the context of epidermal calcium gradients and calcium-dependent process remains unexplored. It is possible that interruption of TRPV3 trafficking could reduce calcium-induced apoptosis – a particularly important pathway in Olmsted syndrome. It is also possible that topical BNP could promote calcium-induced reepithelization. However, it is clear that healthy skin requires a balanced and tightly regulated calcium response. Compounds that modulate TRPV3 could help to rebalance epidermal calcium gradients in atopic dermatitis, Olmsted syndrome, and other dermatoses.

6.2. TRPV3-linked itch and the microbiome

Chronic itch is a particularly common symptom in dermatology clinics (Schut *et al.*, 2019). One multi-centre study found that the incidence of chronic itch was highest in people with unclassified pruritus (78.0%, total n =39 people); prurigo and related conditions (72.2%, n =13); and atopic dermatitis (66.7%, n =96). Although lower in the ranking, this report found that almost 1-in-2 people with psoriasis reported chronic itch (49.6%, n =263). TRPV3 is upregulated and/or sensitised in a number of these pruritic conditions (Larkin *et al.*, 2021; Seo *et al.*, 2020; Qu *et al.*, 2019; Nattkemper *et al.*, 2018). Our work also showed that the TRPV3-linked mediator, PAI-1 (or Serpin E1), is increased in lesional atopic dermatitis and drives scratching behaviour in murine models of acute and prolonged itch (Larkin *et al.*, 2021). Based on these reports, it is tempting to speculate that overactivation of TRPV3 leads to immune-related itch and pruritic conditions; however, the truth is likely much more complicated.

Olmsted syndrome is caused by a TRPV3 mutation that leads to aberrant TRPV3 activity. Surprisingly, only about 1-in-5 people with Olmsted syndrome report chronic itch (Mevorah *et al.*, 2005; Tao *et al.*, 2008). These reports suggest that overactivation of TRPV3 alone is insufficient for itch induction. As discussed previously, inflammatory dermatoses are caused a complex interplay between skin cells, immune system, and peripheral neurons. These conditions are often characterised by an impaired epidermal barrier, inflammation, and refractory pruritus. Inflammatory dermatoses have also been associated with microbiome imbalance, or dysbiosis – though causal links are limited at present (Yudie Yang *et al.*, 2022). To date, cutaneous dysbiosis has been described in patients with atopic dermatitis, psoriasis, acne vulgaris, rosacea, seborrheic dermatitis, and hidradenitis suppurativa (Chopra *et al.*, 2022; Kong *et al.*, 2012; Bäsler *et al.*, 2016; Yan *et al.*, 2017; Lewis *et al.*, 2019; Fitz-Gibbon *et al.*, 2013; Marson *et al.*, 2022; Lin *et al.*, 2021). Several of these conditions have also been linked to TRPV3 overexpression or dysregulation (Toledo Mauriño *et al.*, 2020). Here, we examine the role of the microbiome in TRPV3-linked itch and skin disease.

The term “microbiome” refers to the microbes found on or in a host and the environment the inhabit and create (Berg *et al.*, 2020). In the skin, the microbiome is primarily localised to the external epidermal layers and follicular structures. This pattern is strikingly similar to that of the TRPV3 channel (Xu *et al.*, 2002). The cutaneous microbiome facilitates immunological development, immune responses, and wound healing (Liu *et al.*, 2023; Byrd *et al.*, 2018). In healthy human skin, the cutaneous microbiome contains a highly-regulated community of commensal bacteria, including: *Cutibacterium*, *Corynebacterium*, *Staphylococcus*, and *Streptococcus* species (Sinha *et al.*, 2021). This microbial diversity is related to skin location and affected by external factors, host genetics, and disease state (Perez *et al.*, 2016; Yudie Yang *et al.*, 2022).

In healthy human skin, the epidermal barrier protects against pathological microbial colonisation; however, in inflammatory lesions, this barrier is often impaired (Lee and Kim, 2022). Here, we found that the TRPV3 agonist, drofenine, enhanced cleavage and release of TGF- α . Previous reports have outlined the importance of TGF- α , and its receptor EGFR, in epidermal morphogenesis, hair patterning and wound healing (Threadgill *et al.*, 1995; Sibia and Wagner, 1995; Murillas *et al.*, 1995; Mann *et al.*, 1993; Luetkeke *et al.*, 1993; Luetkeke *et al.*, 1994). Further analyses showed that TRPV3 directly interacts with EGFR, stimulating ADAM17-dependent cleavage and release of TGF α (Cheng *et al.*, 2010; Yujing Wang *et al.*, 2021; Aijima *et al.*, 2015; Szöllösi *et al.*, 2018). This TRPV3/EGFR/ADAM17/ TGF α pathway drives epidermal barrier formation and repair. In addition to AD-like dermatitis, EGFR and ADAM17 knockout mice exhibit epidermal dysbiosis; restoration of normal bacterial diversity, using antibiotic treatment, alleviated dermatitis (**Figure 6.3**) (Kobayashi *et al.*, 2015). Similarly, EGFR inhibitors promote prolonged dysbiosis and a skin rash in healthy humans (Ashida *et al.*, 2023). Human atopic dermatitis lesions are also characterised by barrier disruption and epidermal dysbiosis, with lesions containing high levels of *Staphylococcus aureus* (*S. aureus*) (Kong *et al.*, 2012; Hammond *et al.*, 2022; Kobayashi *et al.*, 2015; Bjerre *et al.*, 2021). A recent report found that activation of TRPV3 in macrophages enhances phagocytosis and bacterial clearance (Sahu and Goswami, 2023). Although TRPV3 is overexpressed and sensitised in atopic dermatitis lesions, TGF- α levels are unchanged (Larkin *et al.*, 2021; Seo *et al.*, 2020). These data suggest that AD-linked barrier dysfunction is mediated by other factors, a topic that is well discussed in the literature (Yang *et al.*, 2020). Current data suggests that, in atopic dermatitis lesions, *S. aureus* utilises underlying barrier dysfunction; *S. aureus* also potentiates epidermal inflammation and drives further barrier dysfunction (Nakatsuji *et al.*, 2016; Hammond *et al.*, 2022). Thus, though initial barrier dysfunction is likely independent of the TRPV3/TGF- α pathway, *S. aureus*-evoked inflammation could enhance TRPV3 activity and dysregulate TRPV3-linked signalling. Herein, we found that release of TRPV3-linked mediators was unaffected by the AD-linked neuropeptide, BNP (4 h); however, longer incubation times may reveal the true impact of AD- and *S. aureus*-linked inflammation on TRPV3 signalling. Moreover, although topical TRPV3-targeting compounds may be beneficial for some conditions, whether these inhibitors would impair the epidermal barrier and facilitate dysbiosis remains unknown, but possible.

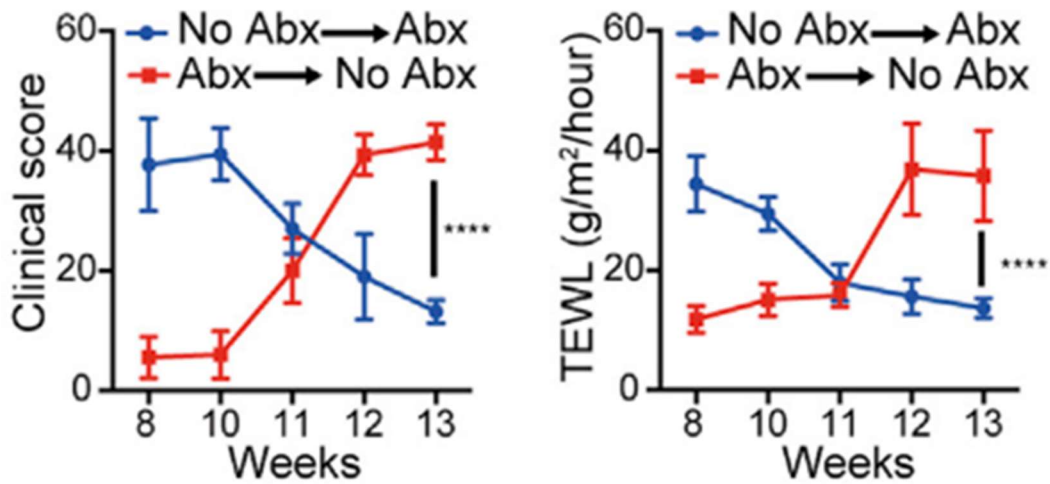
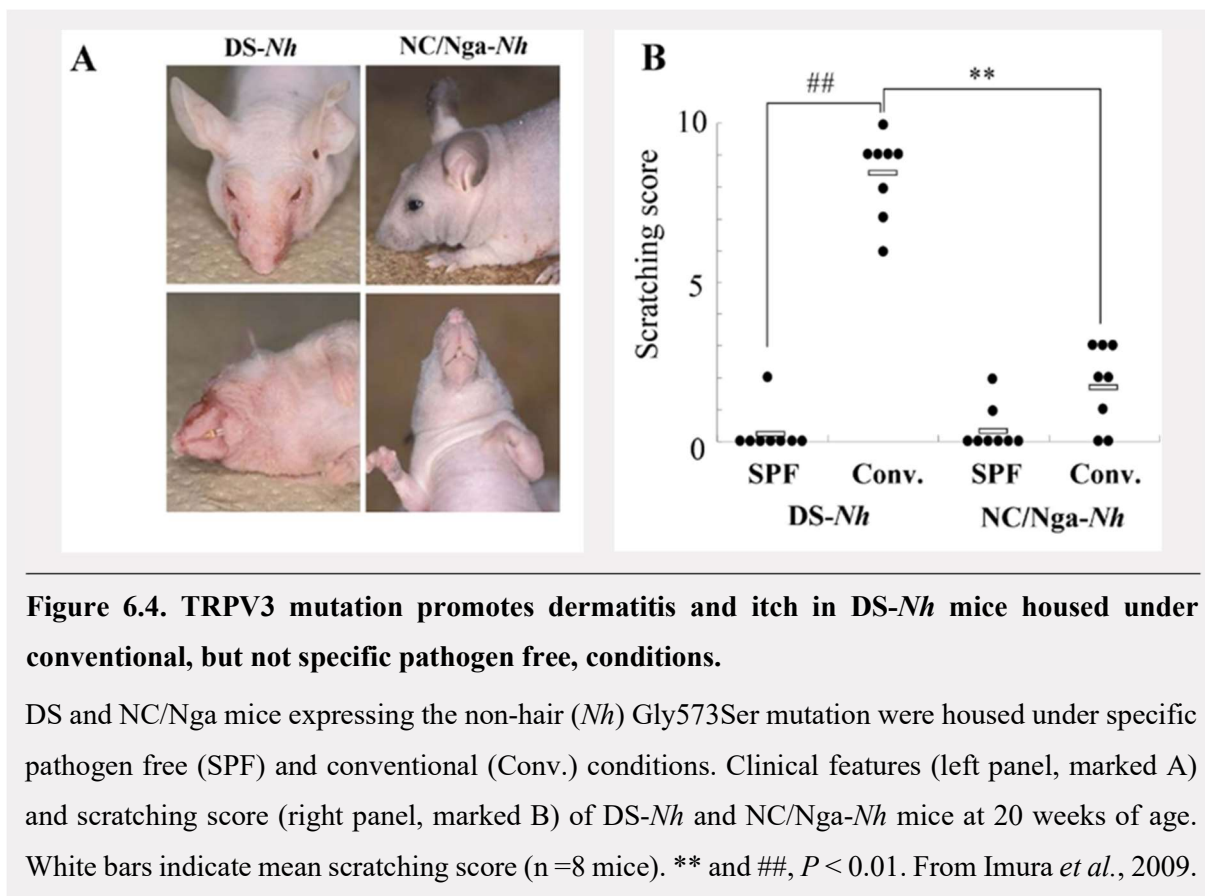


Figure 6.3. Antibiotics improve dermatitis indicators in ADAM17 knockout mice.

Graphs show effect of antibiotics (Abx) on clinical score and trans-epidermal water loss (TEWL) in Adam17 knockout mice during a crossover protocol. Data are shown as the mean \pm SD. **** $P \leq 0.0001$ determined by Student's t-test ($N = 7$). From Kobayashi *et al.*, 2015.

Overactivation of TRPV3 can provoke dermatitis and itch in murine models and humans. However, this TRPV3-linked phenotype is dependent on the external environment and cutaneous microbiome. Spontaneous TRPV3 mutants – DS-*Nh* mice and WBN/Kob-*Ht* rats – express the TRPV3Gly573Ser point mutation (Asakawa *et al.*, 2006; Imura *et al.*, 2009; Yamamoto-Kasai *et al.*, 2013). This TRPV3 Gly573Ser mutation is associated with Olmsted syndrome in humans (Lin *et al.*, 2012). When housed in conventional units, spontaneous TRPV3 mutants exhibit hairlessness, AD-like lesions, and itch-like behaviour (Asakawa *et al.*, 2006; Asakawa *et al.*, 2005; Haraguchi *et al.*, 1997; Yoshioka *et al.*, 2003; Imura *et al.*, 2009; Watanabe *et al.*, 2003). However, when housed in specific pathogen free (SPF) units, this dermatitis and itch-link behaviour is absent (**Figure 6.4**) (Imura *et al.*, 2009; Yoshioka *et al.*, 2003). Here, we found that the TRPV3 agonist, drofenine, enhanced IL-1 α release from the NHEK culture model of human epidermis. This finding was supported by the literature (Xu *et al.*, 2006). Interestingly, comparison of spontaneous TRPV3 mutants found that IL-1 α was significantly elevated in DS-Nh mice housed in conventional units, relative to those housed in SPF units (Imura *et al.*, 2009). TRPV3-linked dermatitis and itch is also dependent on the underlying genetic background. The TRPV3 Gly573Ser mutation fails to elicit dermatitis in BALB/c and NC/Nga mice irrespective of the housing condition (Imura *et al.*, 2009; Watanabe *et al.*, 2003). Moreover, the Gly573Ser mutation provokes spontaneous scratching behaviour, but not dermatitis, in C57BL/6 mice housed in conventional units (Yoshioka *et al.*, 2009). Together, these reports demonstrate the complexity of TRPV3-linked itch and dermatitis. They suggest that, in some cases, overactivation of TRPV3 may be insufficient for induction of dermatitis or itch. Thus, the TRPV3-

linked phenotype may be dependent on the cutaneous microbiome. As such, microbiome modulation may be an effective method for treatment of pruritus in Olmsted syndrome.



Cutaneous microbiota can activate itch-sensitive neurons, though the role of TRPV3 is unclear at present. Both *S. epidermidis* and *S. aureus* activate keratinocytes and promote β -defensin release (Ommori *et al.*, 2018; Ommori *et al.*, 2013; Lai *et al.*, 2010). β -defensins function as essential antimicrobial agents in the skin, but are highly upregulated in atopic dermatitis and psoriasis lesions (Tseng and Hoon, 2022). β -defensins promote mast cell degranulation, acting on Mrgpr to drive the release of IL-31 and other pruritogenic compounds (Niyonsaba *et al.*, 2010; Subramanian *et al.*, 2013; Zhang and McNeil, 2019). β -defensin 2 and 3 can also directly activate MrgprA3⁺ sensory neurons and promote scratching behaviour (Tseng and Hoon, 2022). Whether TRPV3 plays a role in these itch pathways remains unexplored. Proteases secreted by *Sarcoptes scabiei* mites, dust mites, and *S. aureus* can activate PAR2 to elicit itch sensations (Zhao *et al.*, 2020; Kato *et al.*, 2009; Chandrabalan *et al.*, 2021; H. S. Kim *et al.*, 2021). Cutaneous PAR2, TRPA1, and TRPV1 are upregulated skin from people with scabies, the pruritic condition caused by the *Sarcoptes scabiei* mite (**Figure 6.5**) (Sanders *et al.*, 2019). Activation of PAR2 in keratinocytes promotes TRPV3-dependent calcium influx and TSLP release (Zhao *et al.*, 2020; Park *et al.*, 2017). This PAR2/TRPV3/TSLP itch pathway is involved in pruritic burn scars and atopic itch (Hua Yang *et al.*, 2022; Park *et al.*, 2017). Together, these examples highlight the potential impact of TRPV3 in microbe-evoked itch.

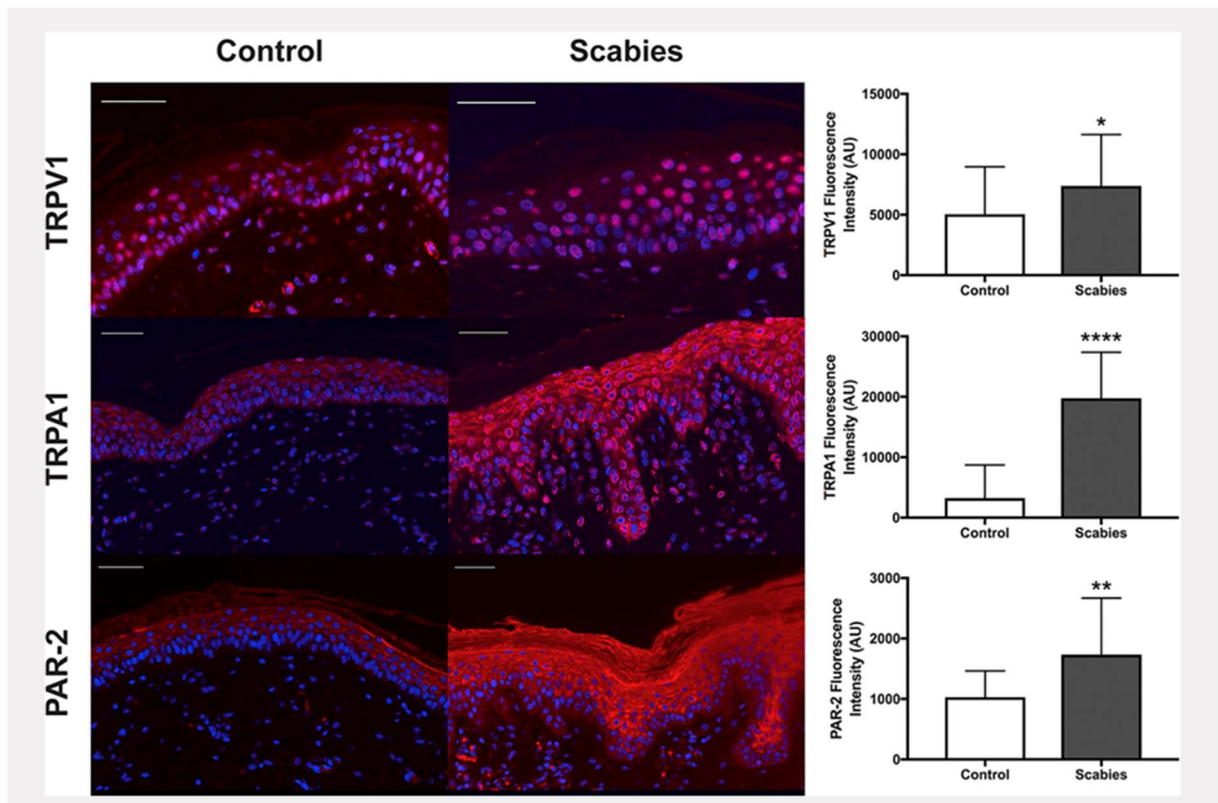


Figure 6.5. PAR2, TRPA1, and TRPV1 are upregulated in porcine skin with scabies.

Representative images and quantification of TRPV1, TRPA1, and PAR2 expression in control and scabies skin (n =3). Scale bars =50 μ m. * $P < 0.05$, ** $P < 0.01$, **** $P < 0.001$, unpaired t-test scabies versus control. AU, arbitrary unit. From Sanders *et al.*, 2019.

This project focused on TRPV3 signalling in an NHEK model of human epidermis. We hypothesised that overactivation of TRPV3 could underpin itch in pruritic skin conditions. Our group aims to identify novel itch-mediators and targets for future drug development. The reports outlined above highlight the impact of the cutaneous microbiome on TRPV3-linked itch. They suggest that the dysbiosis could underpin TRPV3 dysregulation. Thus, we propose that initial barrier dysfunction facilitates dysbiosis; dysbiosis then stimulates TRPV3, promoting further barrier disruption and driving TRPV3-dependent and -independent itch transduction.

6.3. TRPV3 and Piezo channels

In 2021, Ardem Patapoutian received a Nobel Prize for their discovery of the mechano-responsive Piezo1 and Piezo2 channels (Ernfors *et al.*, 2021; Coste *et al.*, 2010). Piezo1 and Piezo2 subunits assemble to form homotrimeric cation channels that open in response to direct mechanical pressure (Ge *et al.*, 2015; Saotome *et al.*, 2018; Wang *et al.*, 2019; Zhao *et al.*, 2018; Guo and MacKinnon, 2017; Jiang *et al.*, 2021; Feng *et al.*, 2022; Ernfors *et al.*, 2021). Piezo channels are expressed in neurons and a number of cutaneous cells, including Merkel cells, immune cells, and keratinocytes. Herein, we examine whether TRPV3 and Piezo channels could interact in the skin.

Piezo channels are expressed in mechano-sensitive LTMR, nociceptive neurons, and Merkel cells (Feng and Hu, 2019; Woo *et al.*, 2014; Maksimovic *et al.*, 2014; Ranade *et al.*, 2014; Coste *et al.*, 2010; Usoskin *et al.*, 2015). Merkel cells also express TRPV3 (**Figure 6.6**) (Bourane, Grossmann, *et al.*, 2015). Though Piezo channels are known to facilitate transduction of touch sensations and mechanical itch (Ernfors *et al.*, 2021; Coste *et al.*, 2010), the role of TRPV3 is unclear. Knockout of epidermal Piezo1 impairs behavioural responses to both light touch and noxious mechanosensation (Mikesell *et al.*, 2022). Knockout of epidermal Piezo2 impairs behavioural responses to light touch, without affecting noxious mechanosensation (Woo *et al.*, 2014). Conversely, genetic overactivation of TRPV3 (Gly573Ser mutant) impairs noxious mechanosensation, without affecting behavioural responses to light touch (Fatima *et al.*, 2022). Murine models suggest that TRPV3 and Piezo channels may also be involved in dry skin itch – a type of mechanical itch. Dry skin evoked scratching is reduced in both Piezo2 and TRPV3 knockout mice (Yamamoto-Kasai *et al.*, 2012; Feng *et al.*, 2022). Thus, epidermal TRPV3 may potentiate Piezo-mediated mechanical itch. This potentiation likely occurs via release of epidermal factors and sensitisation of Merkel cell responses, though the exact factors remain unexplored.

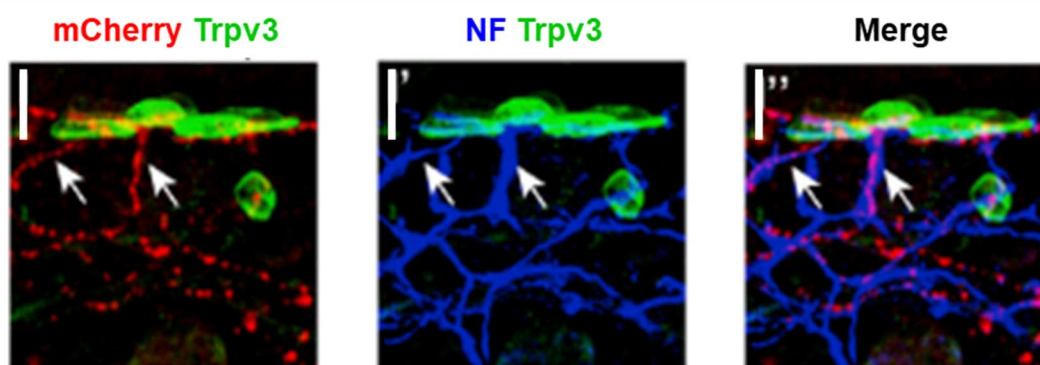


Figure 6.6. Merkel cells express TRPV3.

Hairy skin stained with mCherry (red), neurofilament (NF, blue), and Trpv3 (green). Arrows indicate double-labelled neurons. Scale bars =25 μm . From Bourane *et al.*, 2015.

Piezo1 and Piezo2 are expressed on peripheral itch-linked sensory neurons in mice and may play a role in pruriceptor-mediated itch (Hill *et al.*, 2022; Coste *et al.*, 2010; Ranade *et al.*, 2014; Usoskin *et al.*, 2015; Follansbee and Dong, 2022). In DRG samples, Piezo1 transcripts colocalise with key itch-linked receptors and neuropeptides (BNP and somatostatin) (Hill *et al.*, 2022; Liu *et al.*, 2009; Liu *et al.*, 2012). More than 80% of BNP-positive sensory neurons express Piezo1 (92% in murine DRG and 84% in human DRG) (Hill *et al.*, 2022). Piezo1 is also expressed in a subset of MrgprD-positive neurons, which underpin β -alanine-evoked itch (Hill *et al.*, 2022; Liu *et al.*, 2009; Liu *et al.*, 2012). Although at lower levels when compared with Piezo1, Piezo2 is also expressed in a subset of pruriceptive neurons. In DRG samples, about 25% of BNP-positive sensory neurons express Piezo2 (25.8% in murine DRGs and 27.1% human DRGs); while about 60% of Piezo2-positive neurons also express MrgprA3 (Hill *et al.*, 2022). These BNP findings are particularly interesting when you consider the link between BNP and TRPV3 outlined herein and in our published work (Larkin *et al.*, 2021). BNP sensitises TRPV3-positive (TRPV3⁺) keratinocytes, promoting TRPV3 transcription, sensitising TRPV3 activity, and enhancing TRPV3 trafficking (Larkin *et al.*, 2021). We also identified a novel itch circuit, with keratinocyte-derived PAI-1 activating a subset of sensory neurons and promoting scratching behaviour (Larkin *et al.*, 2021). However, whether Piezo channels are directly or indirectly involved in this BNP/TRPV3/PAI-1 pathway remains unknown.

Immune cells detect and respond to their environment, protecting the body from both exogenous and endogenous threats. This essential function is dependent on a variety of specialised receptors, including pattern recognition receptors, TRP channels, and even Piezo channels. Several immune cells express high levels of Piezo1; these include undifferentiated myeloid cells, macrophages, T cells, and microglia (Solis *et al.*, 2019; Geng *et al.*, 2021; Atcha *et al.*, 2021; Zhu *et al.*, 2023; Liu *et al.*, 2018; Syeda *et al.*, 2015). In myeloid cells, cyclical hydrostatic pressure activates Piezo1 leading to calcium influx, stabilisation of hypoxia-inducible factor 1 α , and expression of pro-inflammatory mediators (Solis *et al.*, 2019). In macrophages, Piezo1 functions downstream of TLR4, facilitating cytoskeletal remodelling and bacterial clearance (Geng *et al.*, 2021; Atcha *et al.*, 2021; Tadala *et al.*, 2022). Reports on the function of Piezo1 in T cell populations are conflicting at present, though this may be explained by differences in methodology (Du *et al.*, 2023). One group found that Piezo1 modulates regulatory T cell (T_{reg}) expansion, without effecting CD4⁺ T cell differentiation or T cell receptor signalling (Jairaman *et al.*, 2021). Another group found that Piezo1 was involved in T cell receptor signalling: Piezo1 knockdown reduced T cell priming, activation, and proliferation (Liu *et al.*, 2018). Immune-expressed Piezo1 is involved in normal inflammatory processes; similarly, dysregulated Piezo1 is associated with dysregulated inflammatory processes (Solis *et al.*, 2019). Immune cells such as macrophages and T cells also express TRPV3 (Sahu and Goswami, 2023; Majhi *et al.*, 2015; Inada *et al.*, 2006). In macrophages, TRPV3 channels are located on the lysosome and nucleolus (Sahu and Goswami, 2023). This report indicates that macrophage-expressed TRPV3 channels facilitate chemotaxis, bacterial clearance, and wound healing – though additional evidence is limited at present. Dysregulation of TRPV3 has also been linked with inflammation. Although

interesting, further work is required to establish whether TRPV3 and Piezo channels interact in immune cells.

TRPV3 and Piezo channels may interact in epidermal keratinocytes. Keratinocytes express functional Piezo1 channels, with expression peaking in the stratum granulosum and stratum spinosum (**Figure 6.7**) (Mikesell *et al.*, 2022; Coste *et al.*, 2010; Labarrade *et al.*, 2023). A small study detected TRPV3, TRPV4, Piezo1, and Piezo2 proteins in samples from murine and human larynges (**Figure 6.8**) (Foote *et al.*, 2022). Early reports have outlined a direct link between TRPV4 and Piezo1. In cultured endothelial cells (HUVECs), stimulation of Piezo1 resulted in sustained TRPV4-mediated calcium influx, with phospholipase A2 acting as the intracellular TRPV4 agonist (Swain and Liddle, 2021). A similar Piezo1/TRPV4 link was reported in osteoblastic MC3T3-E1 cells (Yoneda *et al.*, 2019). Keratinocyte-expressed Piezo1 is activated by noxious mechanical stimuli causing injury; current data suggest that this Piezo1 activation may promote reepithelialisation – a key function of epidermal TRPV3 (Gudipaty *et al.*, 2017; Eisenhoffer *et al.*, 2012; Labarrade *et al.*, 2023). Piezo1 may also play a role in the hair thinning – a common feature of androgenetic alopecia, genetic hypotrichosis, and mature skin (Xie *et al.*, 2022; Cotsarelis and Millar, 2001; Lei and Chuong, 2016; Matsumura *et al.*, 2017). A recent report suggests that hair shaft miniaturization directly activates Piezo1 leading to calcium influx, TNF- α signalling, and hair follicle stem cell apoptosis (Xie *et al.*, 2022). TRPV3 is involved in normal hair patterning and is highly expressed in follicular keratinocytes (Huang *et al.*, 2008; Peier *et al.*, 2002; Xu *et al.*, 2002; Xu *et al.*, 2006; Borb r  *et al.*, 2011; Cheng *et al.*, 2010). Pharmacological and genetic overactivation of TRPV3 is associated with hair abnormalities *in vitro*, in rodents, and in humans (Asakawa *et al.*, 2006; Xiao, Tian, *et al.*, 2008; Lin *et al.*, 2012; Yan *et al.*, 2019; Song *et al.*, 2021; Duchatelet and Hovnanian, 2015; Borb r  *et al.*, 2011). Here, we found that the TRPV3 agonist, drofenine, enhanced release Dkk-1. Dkk-1 inhibits Wnt signalling, impairs hair growth, and is upregulated in balding regions from males and females with androgenetic alopecia and alopecia areata (Bafico *et al.*, 2001; Mao *et al.*, 2001; Kwack *et al.*, 2012; Fawzi *et al.*, 2016; Mahmoud *et al.*, 2019; Jiaqi Liu *et al.*, 2022). Together, these reports suggest that TRPV3 and Piezo1 are functionally aligned in keratinocytes.

This project identified a number of TRPV3-linked mediators involved in cutaneous inflammation and inflammatory itch. Piezo channels are generally considered to be mechano-specific and involved in touch and mechanical itch transduction. However, this section highlighted a number of locations and pathways for TRPV3 and Piezo interaction. Thus, further investigations into this putative link are required and warranted. Lastly, as much of these Piezo data are derived from murine models (Follansbee and Dong, 2022), future work should examine the impact of Piezo modulation on pruritic skin conditions in humans.

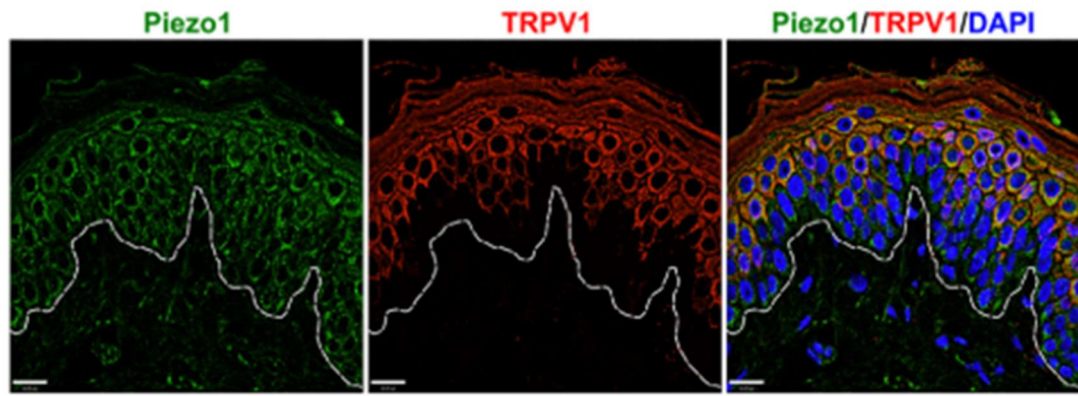


Figure 6.7. Piezo1 is expressed in human skin.

Immunostaining showing Piezo1 (green) and TRPV1 (red). Scale bars =16 μm . From Labarrade *et al.*, 2023.

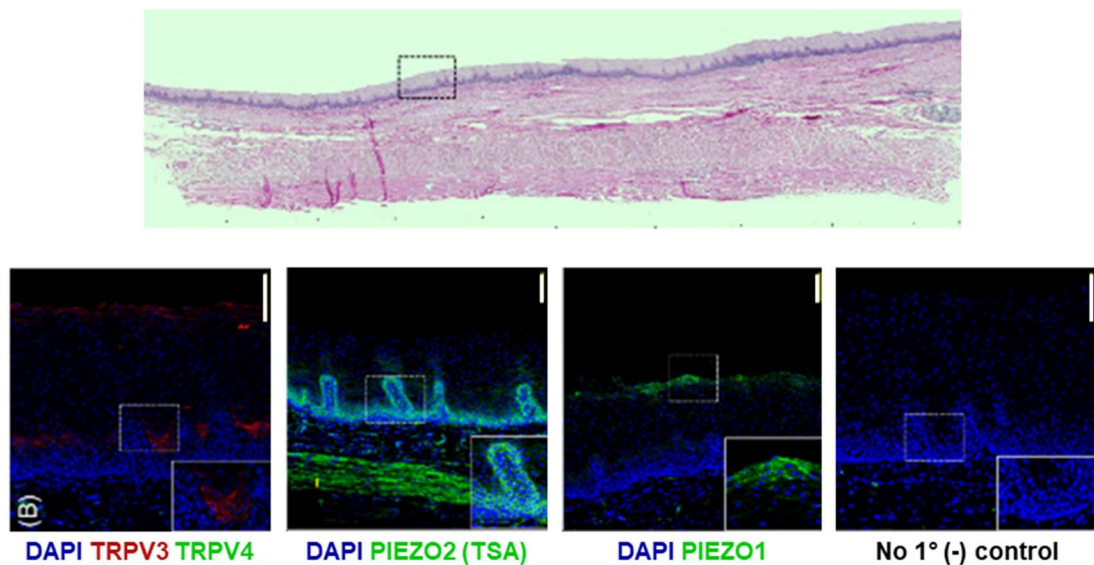


Figure 6.8. TRPV3, TRPV4, Piezo1, and Piezo 2 are expressed in human oesophageal tissue.

Low magnification H&E staining (top panel) and immunostaining showing TRPV3 (red) and TRPV4 (green), Piezo2 (green), and Piezo1 (green) (bottom pane). Images for TRPV3 and TRPV4 taken at 30x magnification; images for Piezo1 and Piezo2 taken at 20x magnification. Scale bars =100 μm . Modified for clarity from Foote *et al.*, 2022.

6.4. TRPV3 and the wider cutaneous system

This project examined the TRPV3 channel in a monolayer of normal human epidermal keratinocytes (NHEK). Functionally, this NHEK culture model likely recapitulates the inner region of the epidermis. In the skin, these keratinocytes would function as part of the wider cutaneous system, integrating stimuli from both the epidermal and dermal layers.

Recent reports have highlighted the remarkable morphological, functional, and genetic diversity of this cutaneous system. This diversity was outlined in the proteomic atlas of healthy human skin: using mass spectrometry-based proteomics, the authors identified the proteomic profiles of each cellular subset and skin layer (**Figure 6.9**) (Dyring-Andersen *et al.*, 2020). Recent technological advances have enabled researchers to examine the spatial patterns of gene expression in cells from organised tissues (Moses and Pachter, 2022). These single-cell RNA sequencing (scRNA-seq) analyses have revealed functionally distinct clusters within populations of fibroblasts (Buechler *et al.*, 2021; Korsunsky *et al.*, 2022), dermal endothelial cells (Qingyang Li *et al.*, 2021), and keratinocytes (Zou *et al.*, 2021; Cheng *et al.*, 2018). Separate analyses have described functional subgroups within peripheral sensory neurons (Chiu *et al.*, 2014; Usoskin *et al.*, 2015; Goswami *et al.*, 2014; Reynders and Moqrich, 2015; Thakur *et al.*, 2014). In this section, we outline the complexity of the cutaneous system and the impact of TRPV3-linked signalling on the function and dysfunction of the skin.

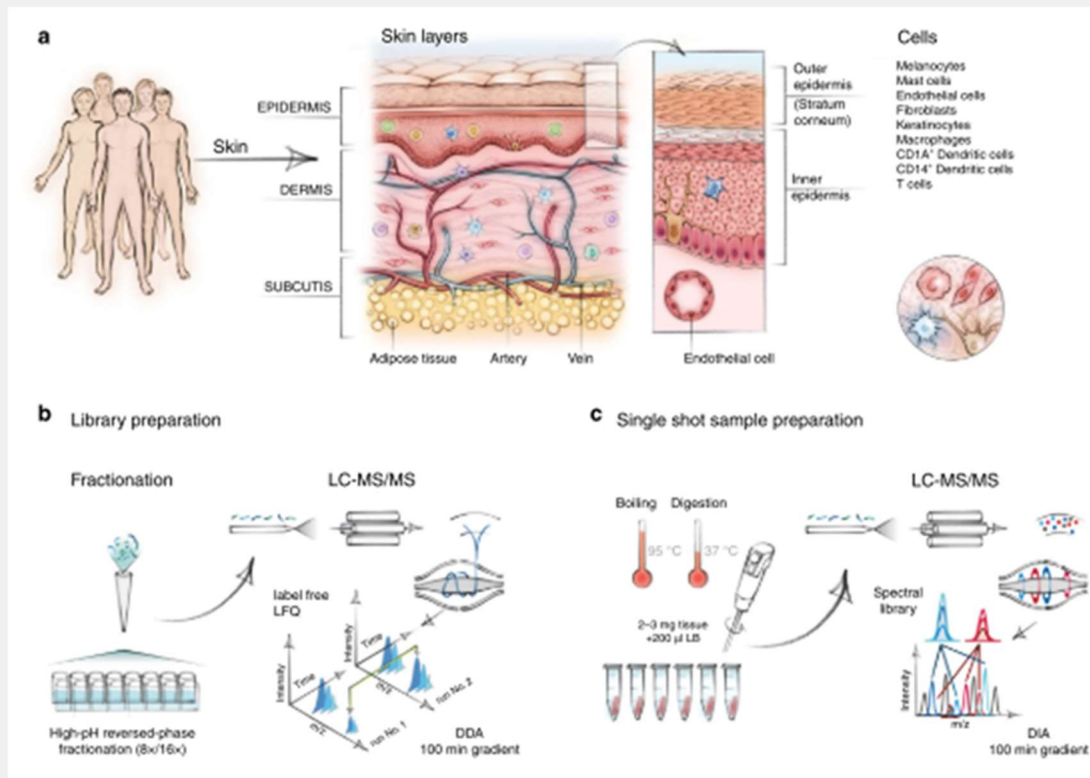


Figure 6.9. Mass spectrometry-based proteomic analysis of skin layers and cellular subsets.

Schematic shows experimental setup and workflow. From Dyring-Andersen *et al.*, 2020.

Dermal fibroblasts are broadly defined by their location within the dermis: papillary versus reticular (Korosec *et al.*, 2019). Fibroblasts are further subdivided into functional subpopulations using a variety of markers (Haydont, Neiveyans, *et al.*, 2019; Janson *et al.*, 2012; Nauroy *et al.*, 2017; Philippeos *et al.*, 2018; Solé-Boldo *et al.*, 2020; Tabib *et al.*, 2018). Even in culture, primary human fibroblasts express layer-specific markers, morphology, and functional properties (Philippeos *et al.*, 2018; Tabib *et al.*, 2018). Papillary fibroblasts are broadly characterised by Wnt signalling (Philippeos *et al.*, 2018; Rognoni *et al.*, 2016; Driskell *et al.*, 2013). Reticular fibroblasts show species-specific expression profiles: genes related to extracellular matrix (ECM) regulation were highly expressed in murine cells, while secretoglobin genes were enriched in human cells (Philippeos *et al.*, 2018). A recent report segregated human fibroblasts into 5 broad subpopulations, with each subgroup displaying a distinct gene signature: SPARC⁺COL3A1⁺ (C4 fibroblasts); FBLN1⁺ (C5 fibroblasts); PTGS2⁺ SEMA4A⁺ (C8 fibroblasts); CD34⁺ MFAP5⁺ (C9 fibroblasts); and CCL10⁺ CCL19⁺ (C11 fibroblasts) (Korsunsky *et al.*, 2022). These 5 subpopulations were consistently identified in gut, lung, salivary gland, and synovium tissue (Korsunsky *et al.*, 2022). Gene set enrichment analysis suggests that C4 fibroblasts are involved in ECM remodelling and C11 fibroblasts directly interact with immune cells and promote inflammation (Korsunsky *et al.*, 2022). C4 and C11 fibroblasts are expanded in inflamed tissues: C4 localise to perivascular regions, while C11 colocalise with T lymphocytes (Korsunsky *et al.*, 2022). C11 fibroblasts are also significantly expanded in lesional atopic dermatitis skin (Korsunsky *et al.*, 2022; He *et al.*, 2020). Following cutaneous damage, dermal fibroblasts proliferate, migrate, and differentiate to form a fibrotic scar. These processes are tightly controlled, with wound-activated fibroblasts showing distinct expression profiles at different times and at different locations within the wound site (Foster *et al.*, 2021). At the wound edge, local fibroblasts are activated and proliferate inward (Foster *et al.*, 2021). Wound-activated fibroblasts also undergo functional differentiation, with clustering revealing 4 putative subgroups linked to distinct wound healing processes: “mechano-fibrotic”, “activated-responder”, “remodelling”, and “proliferator” fibroblasts (Foster *et al.*, 2021). Together, these data highlight the genetic and functional diversity within the dermal fibroblast population.

In addition to fibroblasts, the dermal layer contains vasculature, dendritic cells (DCs), macrophages, and T cells. This cutaneous region is a key site of immune cell recruitment and interaction. Reports suggest that the dermal layer may contain immune microdomains, with infiltrating and resident immune cells localising to distinct regions (Wang *et al.*, 2014). In DCs in the superficial papillary dermis highly active and mobile (Wang *et al.*, 2014). DCs detect and present antigens; here, they may also activate and interact with basal keratinocytes in the dermal-epidermal junction. In addition to the dermal immune cells, dermal endothelial cells (EC) play an active role in cutaneous immune responses, participating in immune cell recruitment and infiltration (Zhu *et al.*, 2020; Chen *et al.*, 2021; Evans *et al.*, 2021). Using ssRNA-seq, researchers identified 5 major subtypes of EC within the human dermis (Qingyang Li *et al.*, 2021). EC subtypes displayed distinct genotypic signatures and were associated with distinct vascular regions: arteriole EC; capillary EC; post-capillary venule

EC; venule EC; and lymphatic EC (Qingyang Li *et al.*, 2021). Capillary EC are involved in immune surveillance and T cell activation, with cells expressing high levels of antigen presentation molecules (Qingyang Li *et al.*, 2021). Arteriole EC expressed angiogenesis-linked genes, while post-capillary venule EC expressed inflammation-related genes (Qingyang Li *et al.*, 2021). Together these reports underline the functional complexity of the dermal immune response.

Keratinocytes often considered a homogenous population. Similar to dermal fibroblasts, epidermal keratinocytes are broadly defined by their location within the epidermis. Basal keratinocytes, the innermost cells of the epidermis, are in fact a type of stem cell. These stem cells produce daughter keratinocytes that, through further rounds of proliferation and differentiation, underpin epidermal stratification and epidermal barrier formation (Watt, 1989; Eckert, 1989). This process creates layer-specific and differentiation-linked expression patterns (Matsui and Amagai, 2017). More recently, scRNA-seq has revealed additional functional subgroups within the keratinocyte population (Zou *et al.*, 2021). Keratinocytes clustered into 9 distinct subpopulations: proliferating undifferentiated basal cells (MC1, MC2, and MC3); quiescent undifferentiated basal cells (BC1, BC2, and BC3); differentiated spinous cells (SC1 and SC2); and terminally differentiated cells (GC) (Zou *et al.*, 2021). These findings are consistent with an earlier report (Cheng *et al.*, 2018). Staining analyses suggest that TRPV3 is localised to the stratum basale, while TRPV1 may be expressed in the upper stratum (**Figure 6.7**) (Peier *et al.*, 2002; Facer *et al.*, 2007; Asakawa *et al.*, 2006; Labarrade *et al.*, 2023). This staining pattern may explain the apparent lack of TRPV1 responses in our NHEK model. Herein, we also outlined a number of functional subgroups with respect to TRPV3-linked calcium responses in our NHEK model. Keratinocyte gene signatures are also impacted by the anatomic location of skin sampling: inflammatory genes are enriched in scalp keratinocytes, while proliferation-associated genes are enriched in foreskin keratinocytes (Cheng *et al.*, 2018). These data highlight the heterogeneity within the epidermal keratinocyte population. The experiments outlined herein failed to account for or utilise this heterogeneity.

In addition to the cellular components, the skin also contains an extracellular matrix (ECM) consisting of “core matrisome” and “matrisome-associated” components (Martin *et al.*, 1984; Naba *et al.*, 2012; Naba *et al.*, 2016). Core matrisome components support the structure of the skin and include collagens, proteoglycans, and glycoproteins (Leng *et al.*, 2020). Matrisome-associated components are signalling mediators and growth factor that are bound to core components (Leng *et al.*, 2020). The ECM mesh creates a 3-dimensional microenvironment and acts as a bioactive scaffold for cellular adhesion and migration. Similar to the cellular components, different cutaneous regions express different ECM components (Li *et al.*, 2022). In the dermis, papillary regions express higher levels of secreted factors, while reticular regions express higher levels of ECM glycoproteins (**Figure 6.10**) (Nauroy *et al.*, 2017). With regard to core matrisome components, collagen VII (COLVII) is enriched in papillary fibroblasts and elastin is enriched in reticular fibroblasts; these expression profiles reflect the distinct functions of the 2 dermal regions (Nauroy *et al.*, 2017). COLVII anchoring

fibrils are particularly important in the basement membrane – a highly specialised ECM region located between the epidermal and dermal layers (dermal-epidermal junction). Basal keratinocytes are physically anchored to the basal membrane: collagen, laminin, and integrin receptors bind the internal actin cytoskeleton to the underlying membrane (Gonzales *et al.*, 1999; Hsu *et al.*, 2014; Jones and Watt, 1993). This interaction is key to the structure and stability of the epidermis.

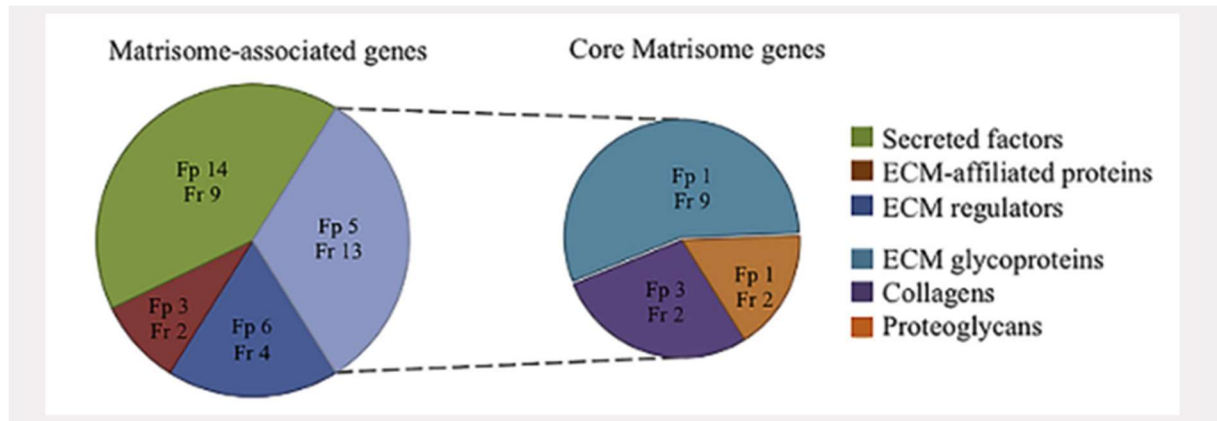


Figure 6.10. Matrisome genes expressed in dermal fibroblasts.

Pie charts highlight the proportion of Matrisome-associated and core matrisome genes expressed in papillary fibroblasts (Fp) and reticular fibroblasts (Fr). From Nauroy *et al.*, 2017.

Mature human skin displays distinct morphological and biological features, with reports suggesting these changes are caused by changes in the cutaneous ECM. Mature skin express lower levels of proteins associated with cell-matrix adhesion, response to growth factors, acute inflammatory responses, wound healing, and fungal defence; and higher levels of proteins associated with ossification, bone mineralisation, and connective tissue development (Mansheng Li *et al.*, 2021). Other reports found that mature skin showed elevated transcription of pro-inflammatory and apoptotic factors (Zou *et al.*, 2021; Haydont, Bernard, *et al.*, 2019). Relative levels of core matrisome components also changed with age (Mansheng Li *et al.*, 2021). In addition to normal skin patterning, the ECM is essential for wound healing. Skin keloids – fibroproliferative scar tissue – are caused by an imbalance in ECM deposition and degradation following tissue damage (Zhang *et al.*, 2021; Andrews *et al.*, 2016). Keloids are associated with disordered inflammation, protease activity, and ECM remodelling – leading to impaired wound healing (Zhang *et al.*, 2021). Angiogenic and inflammatory factors were significantly upregulated in keloid tissue (Zhang *et al.*, 2021). Protease-related ECM regulators, such as the Serpin (or PAI) superfamily, were dysregulated in keloid tissue: SERPINH1, SERPINA6, SERPINF1, SERPINF2, SERPINA3, SERPINB9, SERPINA4, SERPINB5, SERPINC1, and SERPINA1 were upregulated; while SERPINB7, SERPIND1, SERPINB12, SERPINB8, SERPINB6, SERPING1, SERPINA5, and SERPINB1 were downregulated (Zhang *et al.*, 2021). These data highlight the importance of the SERPIN superfamily on skin healing. Herein, we linked TRPV3 activation to SERPINE1 (or PAI-1) release from keratinocytes; future work should investigate the effect of TRPV3 activation on other members of the SERPIN superfamily.

Herein, we examined TRPV3 signalling, activity and trafficking in a monolayer NHEK model of human epidermis. This culture model allowed for investigation of cellular signalling, calcium fluctuations, and channel trafficking. We found that the TRPV3 agonist, drofenine, promoted release of BSG, Dkk-1, EGF, IL-1 α , IL-1ra, MIF, PAI-1, PDGFA, and TGF- α from cultured NHEK. However, this model fails to account for the complexity of the cutaneous system.

Each of these TRPV3-linked mediators can affect a number of cutaneous cells. Following cleavage and release, BSG stimulates fibroblasts to release MMPs, promoting a key pathway in cutaneous remodelling, cancer, and psoriasis (Taylor *et al.*, 2002; Sameshima *et al.*, 2000; Lim *et al.*, 1998; Guo *et al.*, 1997; Guindolet and Gabison, 2020; Peng *et al.*, 2017; Cui *et al.*, 2021). Though the exact receptor underpinning this BSG/MMP response remains unclear, released BSG promotes MMP-dependent cleavage of membrane-bound BSG (Tang *et al.*, 2004; Egawa *et al.*, 2006). Dkk-1 is highly upregulated in androgenetic alopecia and alopecia areata, with Dkk-1 acting directly on follicular keratinocytes to promote apoptosis and induce hair follicle regression (Fawzi *et al.*, 2016; Mahmoud *et al.*, 2019; Qingmei Liu *et al.*, 2022; Kwack *et al.*, 2012). Dkk-1 interrupts Wnt/ β -catenin signalling, directly binding and promoting internalisation of the low-density lipoprotein receptor-related proteins 5 and 6 (LRP5 and LRP6) (Bao *et al.*, 2012). In the skin, LRP5 and LRP6 transcripts have been detected in endothelial cells, sweat glands, certain fibroblasts, smooth muscle cells, and adipocytes (Uhlén *et al.*, 2015), suggesting that the cutaneous effects of Dkk-1 may be more complex than currently understood. EGF and TGF- α bind and activate EGFR, promoting epidermal growth and repair. TGF α and EGFR loss-of-function murine models highlight the importance of this pathway in epidermal morphogenesis, hair patterning and wound healing (Threadgill *et al.*, 1995; Sibilina and Wagner, 1995; Murillas *et al.*, 1995; Mann *et al.*, 1993; Luetkeke *et al.*, 1993; Luetkeke *et al.*, 1994). In the skin, EGFR is primarily localised to the epidermal keratinocytes – though expression levels vary across donors (Uhlén *et al.*, 2015). IL-1 α binds to IL1R1, while IL-1ra inhibits IL1R1 (Mosley *et al.*, 1987). IL1R1 transcripts have been detected in Langerhans cells, endothelial cells, macrophages, and fibroblasts (Karlsson *et al.*, 2021). Dysregulation of IL-1 has been linked to hidradenitis suppurativa and other autoimmune conditions (Kanni *et al.*, 2018; Lu *et al.*, 2013; Migliorini *et al.*, 2020). MIF binds to CXCR2 or CXCR4 promote recruitment and activation of monocytes, T cells, and eosinophils (Bernhagen *et al.*, 2007; Vieira-de-Abreu *et al.*, 2011). MIF has been linked to vitiligo, psoriasis, atopic dermatitis, and alopecia areata (Chen *et al.*, 2023; Bezdek *et al.*, 2018; Shimizu *et al.*, 2001; Yasuda *et al.*, 2014; Eldsouky *et al.*, 2020); however, the role of keratinocyte-expressed TRPV3 in disease-linked MIF signalling remains unknown. PAI-1 inhibits urokinase and tissue plasminogen activators (uPA and tPA), modulating ECM degradation (Ghosh and Vaughan, 2012). PAI-1 also binds to low-density lipoprotein receptor-related protein 1 (LRP1) and regulates fibroblast migration via activation of the β -catenin pathway (Kozlova *et al.*, 2015). PAI-1 also binds to peripheral sensory neurons to promote itch transduction (Larkin *et al.*, 2021). Together, these data outline the potential impact of TRPV3 function and dysfunction in the skin.

Further work should examine the impact of TRPV3 in 3D organotypic models and explants of human skin.

This section briefly describes the complexity of the cutaneous system. This work is ongoing and constantly evolving, with a recent paper outlining gene expression and cellular interactions in psoriasis (Ma *et al.*, 2023). As we look to create novel TRPV3 modulators and other topical inhibitors, we must consider the broader impact of TRPV3 pathways in the skin. TRPV3 promotes epidermal patterning and wound healing. TRPV3-linked mediators facilitate cutaneous homeostasis and immune responses. Future therapeutics should aim to rebalance, rather than inhibit, cutaneous TRPV3 signalling.

6.5. Limitations and questions for future research

This section outlines the main limitations and questions for future research, focusing on the cell culture model and experimental methods.

6.5.1. The impact of culture conditions and donor genetics on TRPV3-linked signalling

This project assessed TRPV3-linked signalling in a culture model of human epidermis: cultured normal human epidermal keratinocytes (NHEK). Like other *in vitro* systems, the NHEK model has several drawbacks and benefits.

As discussed above, epidermal keratinocytes form an integral component of the cutaneous system, interacting with dermal fibroblasts, immune cells, and peripheral neurons. Here, NHEK are grown in a single layer, at $\leq 70\%$ confluency. This monolayer likely recapitulates the inner region of the epidermis. These culture conditions are useful for signalling and staining experiments. The normal process of terminal differentiation means that, as cultures reach confluency, NHEK form a near-inert barrier-like layer. Although essential for skin patterning, this differentiation would impair functional TRPV3 analyses. Moreover, keratinocyte differentiation affects protein expression and cellular function. Our monolayer system likely included keratinocytes at a variety of differentiation stages. Here, consistent culture conditions and timing were used. However, keratinocyte differentiation may have increased the variation *in vitro* findings. In the skin, keratinocytes express a number of layer-specific markers: keratin 5 and keratin 14 are expressed in the stratum basale, while keratin 1 and keratin 10 are expressed in the stratum spinosum. These markers would have greatly improved our TRPV3 trafficking experiments. Despite this potential differentiation-linked variation, several of the *in vitro* findings detailed herein were later validated in murine models and human skin (Larkin *et al.*, 2021). However, additional experiments should consider keratinocyte differentiation and intercellular communication.

Although still an accepted method for early *in vitro* analyses, recent reports suggest that stiff culture conditions, such as those conferred by conventional tissue culture plastics, may impact cell responses. Stiff substrates activate PIEZO1 and promote an inflammatory phenotype in bone marrow-derived macrophages; effects were correlated with the degree of stiffness, with the 280 kPa substrate significantly increasing PIEZO1-mediated calcium events (Atcha *et al.*, 2021). The stiffness of standard tissue culture plastic ranges from 0.2 to 5.0 GPa – that is 200000 to 5000000 kPa (Guimarães *et al.*, 2020). To mitigate this issue, several cell culture substrates have been developed. These include Matrigel substrate, synthetic polyethylene glycol-based substrates, and alginate-based substrates. Although useful, these substrates fail to replicate the complex environment of the basement membrane and epidermis and may introduce additional substrate-linked variation (Bahr *et al.*, 2022; Sakai and Kawakami, 2007; Hughes *et al.*, 2010). Other groups have utilised

LabSkin™, a 3D-organotypic *in vitro* model of human skin. This model contains differentiated dermal and epidermal cells, which form a biologically active and histologically comparable skin sample (**Figure 6.11**) (Wallace *et al.*, 2020). However, this 3D model lacks vasculature, resident and infiltrating immune cells, and other important cutaneous cells. Nonetheless, future experiments should examine the TRPV3 channel in an *ex vivo* or 3D organotypic model on the epidermal layer.

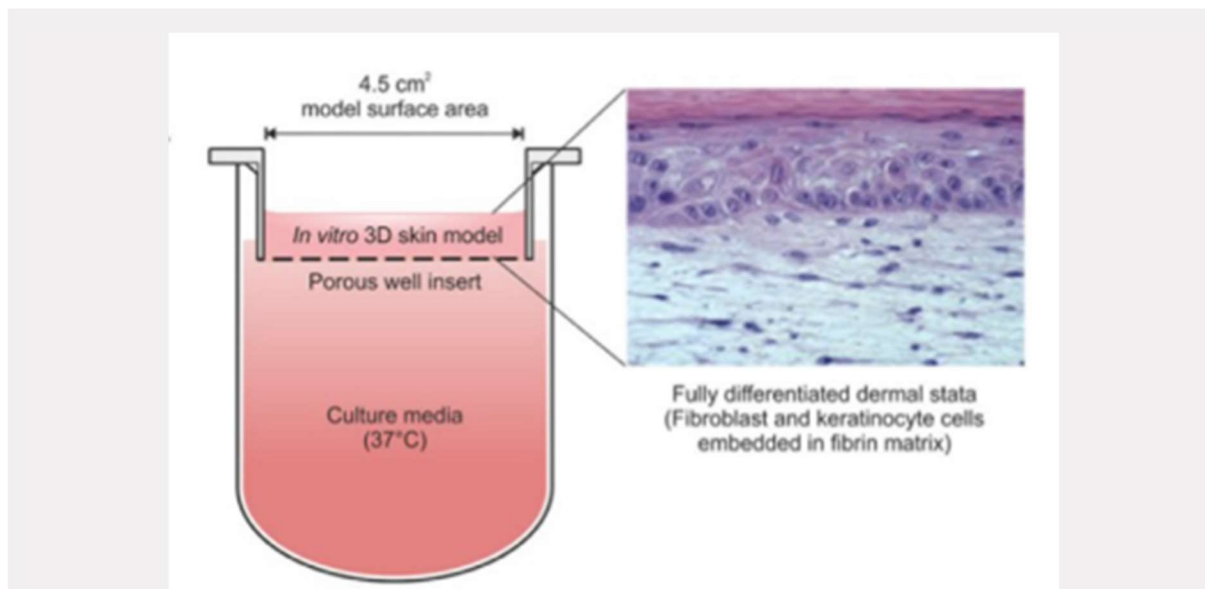


Figure 6.11. The LabSkin™ 3D model of human skin.

Schematic illustrating the LabSkin™ culture system and H&E staining of model showing clearly delineated fibroblast and keratinocyte regions. From Wallace *et al.*, 2020.

In general, controlled cultures allow for controlled experiments. This is a key tenet of *in vitro* analyses and a presumed benefit of the NHEK culture model. However, we noted a striking level of inter-experimental variation. This variation was highlighted in our signalling analyses and appears to be associated with the human donor (see **Table 2.1**). During this project we found that 2 donor batches were unable to release measurable levels of PAI-1 following drofenine application. This finding was contrary to earlier analyses. This discrepancy was first thought to be due to issues with the assay kit or experimental setup. After ruling this out, we examined the donor characteristics. Aging is linked with immunosenescence (Wang *et al.*, 2022). However, the 1st donor was 75 years old, while the 2nd was just 20-year-old. This suggests that the PAI-1 discrepancy was not related to donor age. Biological sex and sex hormones are linked with inflammatory capacity (Lau *et al.*, 2018). However, the 1st donor was female, and the 2nd was male. This suggests that the PAI-1 discrepancy was not related to donor sex. Lastly, racial and ethnic background is thought to impact systemic inflammation – though this effect may be due to social and psychological factors (Schmeer and Tarrence, 2018). Here, we noted an interesting difference: PAI-1 release was detected in NHEK donated by Hispanic, Black, and Mixed-race (Black/Caucasian) individuals; while PAI-1 release was impaired in NHEK donated by Caucasian individuals. These observations suggest that TRPV3-

evoked PAI-1 release may be related to the racial background of the donor. This putative association has been described in a number of published reports (Iso *et al.*, 1993; Festa *et al.*, 2003; Matthews *et al.*, 2005; Lutsey *et al.*, 2006). Thus, although primary human cells improve translational power, donor genetics and epigenetic variation can reduce the statistical power of *in vitro* analyses. Here, this variation was overcome by further replication.

One way to control for donor genetics is to use an immortalised cell-line. Human immortalised nontumorigenic keratinocytes (HaCaT) are an example of a widely used cell-line and culture model of human keratinocytes. This model is thought to represent a homogenous monolayer model; this means that it presents the same culture issues as NHEK but potentially without the inter-donor variation. To date, several groups have used HaCaT to examine TRPV3 *in vitro* (Deering-Rice *et al.*, 2014; Qi *et al.*, 2022; Yujing Wang *et al.*, 2021; Li *et al.*, 2016). One group found that a TRPV3 agonist promoted proliferation and TGF α release from HaCaT (Yujing Wang *et al.*, 2021). Another found that a TRPV3 antagonist reduced agonist-induced cell death agonist (Qi *et al.*, 2022). Original reports indicated that the EC₅₀ for drofenine in HaCaT was 605 μ M, though the LC₅₀ was 230 μ M following a 24 h stimulation (Deering-Rice *et al.*, 2014). During this project, HaCaT cultures were stimulated with varying concentrations of drofenine (data not shown). Surprisingly, drofenine induced rapid and profound cell death, with cells showing spindle morphology after just minutes of stimulation at levels far below LC₅₀. These observations suggest that our HaCaT could express high levels of membrane TRPV3. This theory was supported by preliminary TRPV3 staining. Thus, these examples highlight the variation within the HaCaT model and suggest that this cell-line may be inappropriate for TRPV3 assessments.

Overall, these issues increased the variation and reduced the translational power of our findings. However, work by our research group and collaborators strengthened the validity of these *in vitro* analyses (Larkin *et al.*, 2021). This thesis outlined novel TRPV3-linked signalling in monolayer cultures of primary human keratinocytes. Collaborators then investigated certain TRPV3-linked mediators in clinical dermatitis and murine models. Together, this work identified novel TRPV3-linked pathways and highlighted their role in cutaneous inflammation and pruritic skin disease. Further analyses should examine the role of other TRPV3-linked mediators in clinical dermatitis and murine models.

6.5.2. Measuring TRPV3-linked signalling

Here, we used commercially available kits to assess mediator release and kinase activation. Here, we would like to note a number of limitations and caveats associated with these arrays.

Cytokine arrays revealed that drofenine enhances release of certain mediators from cultured NHEK. A number of these mediators are upregulated in human and murine dermatitis. These reports often indicate a higher level of mediator expression - not a higher level of mediator release. For classic release mediators, like cytokines, expression and release are essentially equivalent. However, this is not the case for mediators that function as both membrane-bound and released mediators. BSG is one such mediator. BSG proteins are elevated in psoriatic lesions (Peng *et al.*, 2017) – however, the proportion of membrane-bound and released BSG remains unexplored. Here, we found that drofenine promoted cleavage and release of BSG from cultured NHEK. It is unclear whether TRPV3 upregulates the BSG protein. Current reports suggest that released BSG stimulates fibroblasts to promote MMP secretion; however, this effect may be mediated by membrane-bound BSG (Taylor *et al.*, 2002; Sameshima *et al.*, 2000; Lim *et al.*, 1998; Guo *et al.*, 1997; Guindolet and Gabison, 2020). Thus, the actual effect of enhanced BSG cleavage and release is unknown. Moreover, these kits do not account for variations in potency and local conditions. Low levels of certain mediators may result in profound effects, with impacts dependent on the sensitivity of adjacent cells. These examples highlight some of the limitations associated with these mediator release assays.

Phospho-kinase arrays revealed that drofenine enhances phosphorylation of certain intracellular kinase proteins in cultured NHEK. This array is based on the understanding that phosphorylation of these kinase proteins indicates activation. After activation, kinases proteins often undergo rapid dephosphorylation. As this can lead to sub-baseline levels of protein phosphorylation, significantly reduced protein phosphorylation could also indicate activation of the kinase pathway. This was not incorporated into the analyses herein. Thus, the power of this phospho-kinase array is limited by the transient nature of kinase activation. Future work should look to examine intracellular TRP signalling using phosphoproteomics or other spectrometry-based and high-throughput methods (Savage and Zhang, 2020; Alganem *et al.*, 2022; Zhu *et al.*, 2022; Franciosa *et al.*, 2023). These experiments could reveal important targets for TRPV3-targeting agents. The increased sensitivity of these assays may also clarify the presence or absence of functional TRPA1 and TRPV1 channels in cultured NHEK.

In addition to these methodological issues. Further studies should work to establish the SNARE proteins underlying TRPV3-linked mediator release. These data would allow for the development of targeted BoNT-based therapeutics, which could alleviate TRPV3-linked inflammation and functional upregulation in human patients.

6.5.3. Assessing TRPV3-linked calcium responses

TRPV3 is a calcium-permeable and temperature-sensitive cation channel (Peier *et al.*, 2002; Smith *et al.*, 2002; Xu *et al.*, 2002). Here, we used a cell-permeant fluorescent dye to monitor relative changes in intracellular calcium – an indicator of TRP channel activation. Fluorescent microscopy was used to record real-time calcium fluctuations in a live NHEK culture model. This method is commonly used in basic research.

TRPV3 channels facilitate influx of a variety of cations, including sodium, potassium, caesium, and ammonium cations (Xu *et al.*, 2002; Liebe *et al.*, 2021). Additional cation dyes or indicators could reveal additional features of the TRPV3 response. That said, permeability ratios suggest that TRPV3 is primarily a calcium channel. TRPV3 channels are also responsive to warm temperatures (between 33°C and 42°C) (Peier *et al.*, 2002; Xu *et al.*, 2002; Smith *et al.*, 2002). This sensitivity was noted during the calcium imaging experiments. Moreover, changes in the external environment increased cellular sensitivity and cell death. These effects may be mediated by a multitude of temperature-sensitive channels. Irrespective of the channel, these external factors likely increased the variation within our TRPV3 calcium experiments. Due to the nature of the TRPV3 channel, these issues are difficult to avoid. To minimise the impact, we allowed cells and stimulations to equilibrate to room temperature before imaging. However, it is also possible that this equilibration and prolonged imaging time could also impact cell responses.

Here, drofenine was primarily used at 500 µM concentrations. This concentration was based on data from the early drofenine analyses (Deering-Rice *et al.*, 2014). However, our live imaging experiments showed that this concentration of drofenine was capable of inducing calcium fluctuations in nearly 100% of cultured NHEK. As described previously, these fluctuations were robust and sometimes oscillating. These later responses may be explained, in part, by continued or repeated agonist-induced activation of the TRPV3 channel. Previous reports showed that TRPV3-mediated calcium flux was potentiated by repeated activation (Chung *et al.*, 2004; Chung *et al.*, 2005). This unusual feature remains poorly understood, though it may be mediated by binding of calmodulin to the N-terminal and pore regions of the TRPV3 channel (Xiao, Tang, *et al.*, 2008; Phelps *et al.*, 2010). Herein, we failed to examine the impact of repeated TRPV3 stimulation. However, we postulate that repeated stimulation would have produced similar findings to the previous reports.

Recordings of TRPV3-linked calcium fluctuations revealed a number of novel, and currently unexplained, features. Our data outlined the phasic patterns of activation, which may be linked to receptor trafficking and upregulation. In addition, recordings appeared to show fluorescent tubule-like and vesicles-shaped structures. These intercellular structures extended into the extracellular space following drofenine application. Keratinocytes produce synaptic-like protrusions to communicate with sensory neurons (Talagas *et al.*, 2020). However, the importance of these structures in TRPV3-mediated keratinocyte activation remains unknown. Observations suggested

that calcium fluctuations may spread across the cell NHEK monolayer. During a number of recordings, calcium signal appeared to originate in one cell and flow into adjacent cells. This observation may be explained by varying levels of TRPV3 expression and sensitivity. It may also represent an important feature of the TRPV3 calcium response in keratinocytes. Theoretically, this calcium flow could occur via pannexins (PANX1, PANX2, and PANX3): paracrine ion channels that are expressed in the skin (Sanchez-Pupo *et al.*, 2022; Penuela *et al.*, 2007; O'Donnell *et al.*, 2023). In addition to facilitating paracrine calcium flow, PANX3 has been linked to skin barrier function and inflammation (O'Donnell *et al.*, 2023). Thus, it is possible that recorded calcium fluctuations are mediated by rapid TRPV3-mediated calcium influx followed by pannexin-mediated calcium flow. This putative pannexin pathway may represent one or more of the later response clusters. Knockdown of PANX3 could interrupt drofenine-evoked calcium flow and dysregulate normal TRPV3-mediated wound healing and epidermal patterning. Although interesting, this theory remains unexplored.

As is the case with all projects, our methods developed and improved with every new experiment. Unfortunately, this progression resulted in different experiments having different experimental setups and leading to different data. In early studies, imaging was looking to confirm or deny the existence of functional TRPV3 channels in a live NHEK culture model. This work suggested that there may be differences in how quickly cells respond to drofenine. To examine this hypothesis, we extended the recording time and eventually used a lower magnification lens. These changes – and other experimental issues – reduced the strength of our inter-experimental comparisons. This was discussed in detail in Chapter 5 (**Section 5.3.2**). However, these experimental changes were important and revealed key insights into the population dynamics of the TRPV3 channel in keratinocytes.

6.5.4. Tracking TRPV3 activation dynamics and trafficking

This project identified several interesting features of the TRPV3-linked calcium response in NHEK. Calcium imaging revealed a phasic activation pattern. Immunocytochemistry suggested that these later phases were linked to TRPV3 channel trafficking. Moreover, calcium imaging indicated that BNP enhances TRPV3 activity. Immunocytochemistry suggested that this effect was linked to enhanced trafficking of the TRPV3 channel to the surface membrane. We identified GSK-3 $\alpha\beta$, JNK-pan, and p38 α as key drivers of this BNP-induced TRPV3 trafficking. Calcium imaging is discussed in detail in a previous section (**Section 6.5.3**). Here, we examine the issues and limitations of our surface TRPV3 imaging.

Surface TRPV3 was detected with the TRPV3-ecto antibody (Alomone Labs, ACC 033). This antibody binds to the extracellular portion of the TRPV3 channel. Using a modified immunocytochemistry approach (see **Section 2.2.9.2** for method), we attempted to detect surface TRPV3 and quantify TRPV3 trafficking. However, these images revealed notable levels of intracellular signal. During protocol optimisation, staining was tested under various environmental conditions. Although colder temperatures are known to minimise receptor internalisation, these conditions resulted in distinct morphological changes.

It is possible that this intracellular TRPV3 signal reveals important features of normal trafficking and recycling. Immunocytochemistry images suggest that, under normal conditions, TRPV3 undergoes consistent internalisation. Whether this internalisation leads to inactivation followed by degradation or recycling remains unknown. The Pitstop2 experiments highlighted the impact of endocytosis on TRPV3 activity. After just 30 min, the endocytosis inhibitor (Pitstop2) altered the temporal dynamics of the TRPV3 calcium response. Pitstop2 increased the proportion of cluster 1 responders, while decreasing the proportion of cluster 2 and cluster 4 responders (**Figure 4.18B**). We hypothesise that, under normal conditions, the TRPV3 channels would have cycled from the surface membrane to intracellular regions. Our optimised immunocytochemistry method requires about 90 minutes, from primary antibody application to cellular fixation and mounting. Thus, it is conceivable that TRPV3 channels would cycle from surface to intracellular regions, resulting in the aforementioned sub-membrane signal. In experiments where the TRPV3 signal was increased, intracellular fluorescence may represent TRPV3 proteins which have cycled from the membrane region. Thus, these findings may indicate important features of TRPV3 trafficking in a monolayer of primary human keratinocytes. Additional methods could reveal additional insights into TRPV3 trafficking. GFP-tagged TRPV3 could allow for more precise analysis of TRPV3 trafficking. However, tagging of channel proteins could impact normal cycling and function (Meyer *et al.*, 2007). Flow cytometry could improve the sensitivity and specificity of our surface TRPV3 analyses. Proximal ligation assays could also be used to identify membrane- or vesicle-associated TRPV3. This method could reveal the subcellular location of internalised TRPV3, potentially indicating whether these channels could promote further signalling or degradation. We propose that inhibitors of GSK-3 $\alpha\beta$, JNK-pan,

or p38 α may interrupt BNP-induced TRPV3 trafficking. As BNP and TRPV3 are upregulated in murine models and human dermatitis, this pathway may be clinically relevant for anti-dermatitis and anti-itch agents. This hypothesis should be examined using the aforementioned *in vitro* methods and BNP-linked murine models of dermatitis.

These calcium imaging and immunocytochemistry experiments highlighted a novel link between BNP and TRPV3 activity and trafficking. In addition, Dr. Meng showed that BNP enhances TRPV3 transcription in cultured keratinocytes (Larkin *et al.*, 2021). During this project, additional experiments attempted to assess the effect of BNP on total TRPV3 expression. These experiments appeared to suggest that neuropeptide stimulation was unable to affect TRPV3 translation. However, issues with sample preparation and antibody specificity impaired our analyses. Early western blot experiments suggested that TRPV3 was directly associated with cytoskeletal and other large proteins, with bands presenting at much high molecular weights than predicted. Indeed, preliminary blots showed that drofenine stimulation altered cytokeratin 14 detection. Other groups have shown that TRPV3 directly interacts with EGFR and other TRP proteins (Cheng *et al.*, 2010; Cheng *et al.*, 2007). These interactions are important for TRPV3 function; however, they may impact quantification of TRPV3 proteins. Further analyses should investigate the effect of BNP on total TRPV3 protein, using either improved western blot or immunocytochemistry.

Together, these experiments linked the temporal nature of TRPV3 calcium fluctuations with TRPV3 trafficking. These temporal features align with the biphasic time course of TRPV3-evoked itch (Cui *et al.*, 2018). Moreover, our data suggest that BNP enhances TRPV3 activity and trafficking – potentially highlighting a pathway for functional TRPV3 upregulation in atopic dermatitis skin. These pathways will form the basis for future anti-itch therapeutics and may help alleviate pruritus in a multitude of TRPV3-linked skin diseases.

6.6. Statement of impact, summary, and conclusions

Chronic itch is a surprisingly common issue: up to 1-in-5 people will experience it at some point in their lifetime (Weisshaar, 2016; Hay *et al.*, 2014). Our research group endeavours to develop targeted anti-itch therapeutics. This project represents the *in vitro* component of our work: team members and international collaborators use these data to guide *in vivo* work and drug development. This project represents a key step in this process, highlighting the role of TRPV3 in healthy and diseased human skin. Thus, this project will facilitate the development of novel anti-itch therapeutics for the treatment of pruritic inflammatory skin conditions.

This project identified inflammatory mediators, kinase pathways and SNARE proteins acting downstream of TRPV3 in an NHEK model of human epidermis. TRPA1, TRPV1, and TRPV3 channels activate distinct intracellular kinase proteins. Activation of TRPV3 enhances intercellular signalling, promoting both VAMP3-dependent and -independent mediator secretion. TRPV3 channels display a phasic activation profile facilitated, in part, by normal receptor cycling pathways. BNP sensitises TRPV3 responses, acting via GSK3 α/β , JNK-pan, and p38 α to drive functional TRPV3 upregulation. These *in vitro* findings outlined herein were supported by murine models and clinical samples (Larkin *et al.*, 2021). Thus, TRPV3, and the pathways outlined herein, represent key targets for future anti-itch agents. We believe that these insights will aid the development of TRPV3-targeting agents and advance the treatment of pruritic inflammatory skin conditions.

7. Bibliography

- Abraira, V.E., Ginty, D.D. (2013). The sensory neurons of touch. *Neuron*, **79**: 618–639.
- Acton, D., Ren, X., Di Costanzo, S., Dalet, A., Bourane, S., Bertocchi, I., Eva, C., Goulding, M. (2019). Spinal Neuropeptide Y1 Receptor-Expressing Neurons Form an Essential Excitatory Pathway for Mechanical Itch. *Cell Reports*, **28**: 625–639.
- Aijima, R., Wang, B., Takao, T., Mihara, H., Kashio, M., Ohsaki, Y., Zhang, J.Q., Mizuno, A., Suzuki, M., Yamashita, Y., Masuko, S., Goto, M., Tominaga, M., Kido, M.A. (2015). The thermosensitive TRPV3 channel contributes to rapid wound healing in oral epithelia. *FASEB Journal*, **29**: 182–192.
- Akamatsu, H., Makiura, M., Yamamoto, N., Yagami, A., Shimizu, Y., Matsunaga, K. (2006). The effect of fexofenadine on pruritus in a mouse model (HR-ADf) of atopic dermatitis. *Journal of International Medical Research*, **34**: 495–504.
- Akiyama, T., Ivanov, M., Nagamine, M., Davoodi, A., Carstens, M.I., Ikoma, A., Cevikbas, F., Kempkes, C., Buddenkotte, J., Steinhoff, M., Carstens, E. (2016). Involvement of TRPV4 in serotonin-evoked scratching. *Journal of Investigative Dermatology*, **136**: 154–160.
- Akiyama, T., Tominaga, M., Davoodi, A., Nagamine, M., Blansit, K., Horwitz, A., Carstens, M.I., Carstens, E. (2012). Cross-sensitization of histamine-independent itch in mouse primary sensory neurons. *Neuroscience*, **226**: 305–312.
- Alganem, K., Hamoud, A.R., Creedon, J.F., Henkel, N.D., Imami, A.S., Joyce, A.W., Ryan V, W.G., Rethman, J.B., Shukla, R., O'Donovan, S.M., Meller, J., McCullumsmith, R. (2022). The active kinome: The modern view of how active protein kinase networks fit in biological research. *Current Opinion in Pharmacology*, **62**: 117–129.
- Alpizar, Y.A., Boonen, B., Gees, M., Sanchez, A., Nilius, B., Voets, T., Talavera, K. (2014). Allyl isothiocyanate sensitizes TRPV1 to heat stimulation. *Pflugers Archiv European Journal of Physiology*, **466**: 507–515.
- Alpizar, Y.A., Gees, M., Sanchez, A., Apetrei, A., Voets, T., Nilius, B., Talavera, K. (2013). Bimodal effects of cinnamaldehyde and camphor on mouse TRPA1. *Pflugers Archiv European Journal of Physiology*, **465**: 853–864.
- Andersen, H.H., Akiyama, T., Nattkemper, L.A., Van Laarhoven, A., Elberling, J., Yosipovitch, G., Arendt-Nielsen, L. (2018). Alloeknesis and hyperknesis - Mechanisms, assessment methodology, and clinical implications of itch sensitization. *Pain*, **159**: 1185–1197.
- Andersen, H.H., Elberling, J., Arendt-Nielsen, L. (2015). Human surrogate models of histaminergic and non-histaminergic itch. *Acta Dermato-Venereologica*, **95**: 771–779.
- Andersen, H.H., Elberling, J., Sølvsten, H., Yosipovitch, G., Arendt-Nielsen, L. (2017). Nonhistaminergic and mechanical itch sensitization in atopic dermatitis. *Pain*, **158**: 1780–1791.
- Andoh, T., Kuraishi, Y. (2003). Nitric oxide enhances substance P-induced itch-associated responses in mice. *British Journal of Pharmacology*, **138**: 202–208.
- Andrews, J.P., Marttala, J., Macarak, E., Rosenbloom, J., Uitto, J. (2016). Keloids: The paradigm of skin fibrosis - Pathomechanisms and treatment. *Matrix Biology*, **51**: 37–46.
- Asakawa, M., Yoshioka, T., Hikita, I., Matsutani, T., Hirasawa, T., Arimura, A., Sakata, T., Horikawa, T. (2005). WBN/Kob-Ht rats spontaneously develop dermatitis under conventional conditions: Another possible model for atopic dermatitis. *Experimental Animals*, **54**: 461–465.
- Asakawa, M., Yoshioka, T., Matsutani, T., Hikita, I., Suzuki, M., Oshima, I., Tsukahara, K., Arimura, A., Horikawa, T., Hirasawa, T., Sakata, T. (2006). Association of a mutation in TRPV3 with defective hair growth in rodents. *Journal of Investigative Dermatology*, **126**: 2664–2672.
- Ashida, A., Tomida, S., Iwabuchi, T., Sato, Y., Kiniwa, Y., Okuyama, R. (2023). Persistent alteration of the skin microbiome in patients with skin rash after receiving EGFR inhibitor treatment. *Experimental Dermatology*, **32**: 671–677.

- Atcha, H., Jairaman, A., Holt, J.R., Meli, V.S., Nagalla, R.R., Veerasubramanian, P.K., Brumm, K.T., Lim, H.E., Othy, S., Cahalan, M.D., Pathak, M.M., Liu, W.F. (2021). Mechanically activated ion channel Piezo1 modulates macrophage polarization and stiffness sensing. *Nature Communications*, **12**: 1–14.
- Atoyan, R., Shander, D., Botchkareva, N. V. (2009). Non-neuronal expression of transient receptor potential type A1 (TRPA1) in human skin. *Journal of Investigative Dermatology*, **129**: 2312–2315.
- Bafico, A., Liu, G., Yaniv, A., Gazit, A., Aaronson, S.A. (2001). Novel mechanism of Wnt signalling inhibition mediated by Dickkopf-1 interaction with LRP6/Arrow. *Nature Cell Biology*, **3**: 683–686.
- Bahr, J.C., Li, X.Y., Feinberg, T.Y., Jiang, L., Weiss, S.J. (2022). Divergent regulation of basement membrane trafficking by human macrophages and cancer cells. *Nature Communications*, **13**: 1–20.
- Bai, D., Del Corso, C., Srinivas, M., Spray, D.C. (2006). Block of specific gap junction channel subtypes by 2-aminoethoxydiphenyl borate (2-APB). *Journal of Pharmacology and Experimental Therapeutics*, **319**: 1452–1458.
- Baker, B.S., Ovigne, J.M., Powles, A. V., Corcoran, S., Fry, L. (2003). Normal keratinocytes express Toll-like receptors (TLRs) 1, 2 and 5: Modulation of TLR expression in chronic plaque psoriasis. *British Journal of Dermatology*, **148**: 670–679.
- Bao, J., Zheng, J.J., Wu, D. (2012). The structural basis of DKK-mediated inhibition of Wnt/LRP signaling. *Science Signaling*, **5**: 22.
- Bäsler, K., Bergmann, S., Heisig, M., Naegel, A., Zorn-Kruppa, M., Brandner, J.M. (2016). The role of tight junctions in skin barrier function and dermal absorption. *Journal of Controlled Release*, **242**: 105–118.
- Bellono, N.W., Kamme, L.G., Zimmerman, A.L., Oancea, E. (2013). UV light phototransduction activates transient receptor potential A1 ion channels in human melanocytes. *Proceedings of the National Academy of Sciences of the United States of America*, **110**: 2383–2388.
- Ben-Sasson, S.Z., Hu-Li, J., Quiel, J., Cauchetaux, S., Ratner, M., Shapira, I., Dinarello, C.A., Paul, W.E. (2009). IL-1 acts directly on CD4 T cells to enhance their antigen-driven expansion and differentiation. *Proceedings of the National Academy of Sciences of the United States of America*, **106**: 7119–7124.
- Benditt, E.P., Bader, S., Lam, K.B. (1955). Studies of the mechanism of acute vascular reactions to injury. I. The relationship of mast cells and histamine to the production of edema by ovomucoid in rats. *A.M.A. Archives of Pathology*, **60**: 104–115.
- Berg, G., Rybakova, D., Fischer, D., Cernava, T., Vergès, M.C.C., Charles, T., Chen, X., Cocolin, L., Eversole, K., Corral, G.H., Kazou, M., Kinkel, L., Lange, L., Lima, N., Loy, A., Macklin, J.A., Maguin, E., Mauchline, T., McClure, R., Mitter, B., Ryan, M., Sarand, I., Smidt, H., Schelkle, B., Roume, H., Kiran, G.S., Selvin, J., Souza, R.S.C. de, Van Overbeek, L., Singh, B.K., Wagner, M., Walsh, A., Sessitsch, A., Schloter, M. (2020). Microbiome definition re-visited: old concepts and new challenges. *Microbiome*, **8**: 1–22.
- van den Berg, L.M., Zijlstra-Willems, E.M., Richters, C.D., Ulrich, M.M.W., Geijtenbeek, T.B.H. (2014). Dectin-1 activation induces proliferation and migration of human keratinocytes enhancing wound re-epithelialization. *Cellular Immunology*, **289**: 49–54.
- Bernhagen, J., Krohn, R., Lue, H., Gregory, J.L., Zernecke, A., Koenen, R.R., Dewor, M., Georgiev, I., Schober, A., Leng, L., Kooistra, T., Fingerle-Rowson, G., Ghezzi, P., Kleemann, R., McColl, S.R., Bucala, R., Hickey, M.J., Weber, C. (2007). MIF is a noncognate ligand of CXC chemokine receptors in inflammatory and atherogenic cell recruitment. *Nature Medicine*, **13**: 587–596.
- Bernhard, S., Hug, S., Stratmann, A.E.P., Erber, M., Vidoni, L., Knapp, C.L., Thomaß, B.D., Fauler, M., Nilsson, B., Nilsson Ekdahl, K., Föhr, K., Braun, C.K., Wohlgemuth, L., Huber-Lang, M., Messerer, D.A.C. (2021). Interleukin 8 elicits rapid physiological changes in neutrophils that are altered by inflammatory conditions. *Journal of Innate Immunity*, **13**: 225–241.

- Bezdek, S., Leng, L., Busch, H., Mousavi, S., Rades, D., Dahlke, M., Zillikens, D., Bucala, R., Sadik, C.D. (2018). Macrophage migration inhibitory factor (MIF) drives murine psoriasiform dermatitis. *Frontiers in Immunology*, **9**: 2262.
- Biasibetti, E., Bruni, N., Bigliati, M., Capucchio, M.T. (2018). Lactoferricin/verbascoside topical emulsion: a possible alternative treatment for atopic dermatitis in dogs. *Natural Product Research*, **32**: 2107–2110.
- Bikle, D.D. (2023). Role of vitamin D and calcium signaling in epidermal wound healing. *Journal of Endocrinological Investigation*, **46**: 205–212.
- Bíró, T., Maurer, M., Modarres, S., Lewin, N.E., Brodie, C., Ács, G., Ács, P., Paus, R., Blumberg, P.M. (1998). Characterization of functional vanilloid receptors expressed by mast cells. *Blood*, **91**: 1332–1340.
- Bishop, G.H. (1943). Responses To Electrical Stimulation of Single Sensory Units of Skin. *Journal of Neurophysiology*, **6**: 361–382.
- Bissonnette, R., Papp, K.A., Poulin, Y., Gooderham, M., Raman, M., Mallbris, L., Wang, C., Purohit, V., Mamolo, C., Papacharalambous, J., Ports, W.C. (2016). Topical tofacitinib for atopic dermatitis: a phase IIa randomized trial. *British Journal of Dermatology*, **175**: 902–911.
- Bjerre, R.D., Holm, J.B., Palleja, A., Sølberg, J., Skov, L., Johansen, J.D. (2021). Skin dysbiosis in the microbiome in atopic dermatitis is site-specific and involves bacteria, fungus and virus. *BMC Microbiology*, **21**: 256.
- Black, A.P.B., Ardern-Jones, M.R., Kasprovicz, V., Bowness, P., Jones, L., Bailey, A.S., Ogg, G.S. (2007). Human keratinocyte induction of rapid effector function in antigen-specific memory CD4⁺ and CD8⁺ T cells. *European Journal of Immunology*, **37**: 1485–1493.
- Bodó, E., Bíró, T., Telek, A., Czifra, G., Griger, Z., Tóth, B.I., Mescalchin, A., Ito, T., Bettermann, A., Kovács, L., Paus, R. (2005). A hot new twist to hair biology: Involvement of vanilloid receptor-1 (VR1/TRPV1) signaling in human hair growth control. *American Journal of Pathology*, **166**: 985–998.
- Bodó, E., Kovács, I., Telek, A., Varga, A., Paus, R., Kovács, L., Bíró, T. (2004). Vanilloid receptor-1 (VR1) is widely expressed on various epithelial and mesenchymal cell types of human skin [4]. *Journal of Investigative Dermatology*, **123**: 410–413.
- Bodur, E., Çokuğraş, A.N., Tezcan, E.F. (2001). Inhibition effects of benactyzine and drofenine on human serum butyrylcholinesterase. *Archives of Biochemistry and Biophysics*, **386**: 25–29.
- Boillat, A., Alijevic, O., Kellenberger, S. (2014). Calcium entry via TRPV1 but not ASICs induces neuropeptide release from sensory neurons. *Molecular and Cellular Neuroscience*, **61**: 13–22.
- Borbíró, I., Lisztes, E., Tóth, B.I., Czifra, G., Oláh, A., Szöllsi, A.G., Szentandrassy, N., Nánási, P.P., Péter, Z., Paus, R., Kovács, L., Bíró, T. (2011). Activation of transient receptor potential vanilloid-3 inhibits human hair growth. *Journal of Investigative Dermatology*, **131**: 1605–1614.
- Bourane, S., Duan, B., Koch, S.C., Dalet, A., Britz, O., Garcia-Campmany, L., Kim, E., Cheng, L., Ghosh, A., Ma, Q., Goulding, M. (2015). Gate control of mechanical itch by a subpopulation of spinal cord interneurons. *Science*, **350**: 550–554.
- Bourane, S., Grossmann, K.S., Britz, O., Dalet, A., Del Barrio, M.G., Stam, F.J., Garcia-Campmany, L., Koch, S., Goulding, M. (2015). Identification of a spinal circuit for light touch and fine motor control. *Cell*, **160**: 503–515.
- Braga Ferreira, L.G., Faria, J.V., dos Santos, J.P.S., Faria, R.X. (2020). Capsaicin: TRPV1-independent mechanisms and novel therapeutic possibilities. *European Journal of Pharmacology*, **887**: 173356.
- Braz, J., Solorzano, C., Wang, X., Basbaum, A.I. (2014). Transmitting Pain and Itch Messages: A Contemporary View of the Spinal Cord Circuits that Generate Gate Control. *Neuron*, **82**: 522–536.

- Broad, L.M., Mogg, A.J., Eberle, E., Tolley, M., Li, D.L., Knopp, K.L. (2016). TRPV3 in drug development. *Pharmaceuticals*, **9**: 55.
- Brown, T.E., Chirila, A.M., Schrank, B.R., Kauer, J.A. (2013). Loss of Interneuron LTD and Attenuated Pyramidal cell LTP in Trpv1 and Trpv3 KO mice. *Hippocampus*, **23**: 662–671.
- Buechler, M.B., Pradhan, R.N., Krishnamurty, A.T., Cox, C., Calviello, A.K., Wang, A.W., Yang, Y.A., Tam, L., Caothien, R., Roose-Girma, M., Modrusan, Z., Arron, J.R., Bourgon, R., Müller, S., Turley, S.J. (2021). Cross-tissue organization of the fibroblast lineage. *Nature*, **593**: 575–579.
- Byrd, A.L., Belkaid, Y., Segre, J.A. (2018). The human skin microbiome. *Nature Reviews Microbiology*, **16**: 143–155.
- Calandra, T., Roger, T. (2003). Macrophage migration inhibitory factor: A regulator of innate immunity. *Nature Reviews Immunology*, **3**: 791–800.
- Cals-Grierson, M.M., Ormerod, A.D. (2004). Nitric oxide function in the skin. *Nitric Oxide - Biology and Chemistry*, **10**: 179–193.
- Cambiaghi, S., Tadini, G., Barbareschi, M., Caputo, R. (1995). Olmsted Syndrome in Twins. *Archives of Dermatology*, **131**: 738–739.
- Campion, M., Smith, L., Gatault, S., Métails, C., Buddenkotte, J., Steinhoff, M. (2019). Interleukin-4 and interleukin-13 evoke scratching behaviour in mice. *Experimental Dermatology*, **28**: 1501–1504.
- Capasso, R., Aviello, G., Romano, B., Borrelli, F., De Petrocellis, L., Di Marzo, V., Izzo, A.A. (2012). Modulation of mouse gastrointestinal motility by allyl isothiocyanate, a constituent of cruciferous vegetables (Brassicaceae): Evidence for TRPA1-independent effects. *British Journal of Pharmacology*, **165**: 1966–1977.
- Caterina, M.J., Leffler, A., Malmberg, A.B., Martin, W.J., Trafton, J., Petersen-Zeitz, K.R., Koltzenburg, M., Basbaum, A.I., Julius, D. (2000). Impaired nociception and pain sensation in mice lacking the capsaicin receptor. *Science*, **288**: 306–313.
- Caterina, M.J., Pang, Z. (2016). TRP channels in skin biology and pathophysiology. *Pharmaceuticals*, **9**: 77.
- Caterina, M.J., Schumacher, M.A., Tominaga, M., Rosen, T.A., Levine, J.D., Julius, D. (1997). The capsaicin receptor: A heat-activated ion channel in the pain pathway. *Nature*, **389**: 816–824.
- Cavanaugh, D.J., Lee, H., Lo, L., Shields, S.D., Zylka, M.J., Basbaum, A.I., Anderson, D.J. (2009). Distinct subsets of unmyelinated primary sensory fibers mediate behavioral responses to noxious thermal and mechanical stimuli. *Proceedings of the National Academy of Sciences of the United States of America*, **106**: 9075–9080.
- Cevikbas, F., Wang, X., Akiyama, T., Kempkes, C., Savinko, T., Antal, A., Kukova, G., Buhl, T., Ikoma, A., Buddenkotte, J., Soumelis, V., Feld, M., Alenius, H., Dillon, S.R., Carstens, E., Homey, B., Basbaum, A., Steinhoff, M. (2014). A sensory neuron-expressed IL-31 receptor mediates T helper cell-dependent itch: Involvement of TRPV1 and TRPA1. *Journal of Allergy and Clinical Immunology*, **133**: 448–460.
- Chandraban, A., Thibeault, P.E., Deinhardt-Emmer, S., Nordengrün, M., Iqbal, J., Mrochen, D.M., Mittmann, L.A., Chamling, B., Reichel, C.A., Ramachandran, R., Bröker, B.M., Darisipudi, V.S.N.M. (2021). S. aureus-serine protease-like protein B (SplB) activates PAR2 and induces endothelial barrier dysfunction. *bioRxiv*.
- Chen, J., Guo, W., Du, P., Cui, T., Yang, Y., Wang, Y., Kang, P., Zhang, Z., Wang, Q., Ye, Z., Liu, L., Jian, Z., Gao, T., Bian, H., Li, S., Li, C. (2023). MIF inhibition alleviates vitiligo progression by suppressing CD8+ T cell activation and proliferation. *Journal of Pathology*, **260**: 84–96.
- Chen, J., Zhu, Z., Li, Q., Lin, Y., Dang, E., Meng, H., Sha, N., Bai, H., Wang, G., An, S., Shao, S. (2021). Neutrophils Enhance Cutaneous Vascular Dilation and Permeability to Aggravate Psoriasis

- by Releasing Matrix Metalloproteinase 9. *Journal of Investigative Dermatology*, **141**: 787–799.
- Chen, X.J., Sun, Y.G. (2020). Central circuit mechanisms of itch. *Nature Communications*, **11**: 1–10.
- Chen, Y., Fang, Q., Wang, Z., Zhang, J.Y., MacLeod, A.S., Hall, R.P., Liedtke, W.B. (2016). Transient receptor potential vanilloid 4 ion channel functions as a pruriceptor in epidermal keratinocytes to evoke histaminergic itch. *Journal of Biological Chemistry*, **291**: 10252–10262.
- Cheng, J.B., Sedgewick, A.J., Finnegan, A.I., Harirchian, P., Lee, J., Kwon, S., Fassett, M.S., Golovato, J., Gray, M., Ghadially, R., Liao, W., Perez White, B.E., Mauro, T.M., Mully, T., Kim, E.A., Sbitany, H., Neuhaus, I.M., Grekin, R.C., Yu, S.S., Gray, J.W., Purdom, E., Paus, R., Vaske, C.J., Benz, S.C., Song, J.S., Cho, R.J. (2018). Transcriptional Programming of Normal and Inflamed Human Epidermis at Single-Cell Resolution. *Cell Reports*, **25**: 871–883.
- Cheng, W., Yang, F., Liu, S., Colton, C.K., Wang, C., Cui, Y., Cao, X., Zhu, M.X., Sun, C., Wang, K.W., Zheng, J. (2012). Heteromeric heat-sensitive transient receptor potential channels exhibit distinct temperature and chemical response. *Journal of Biological Chemistry*, **287**: 7279–7288.
- Cheng, W., Yang, F., Takanishi, C.L., Zheng, J. (2007). Thermosensitive TRPV channel subunits coassemble into heteromeric channels with intermediate conductance and gating properties. *Journal of General Physiology*, **129**: 191–207.
- Cheng, X., Jin, J., Hu, L., Shen, D., Dong, X. ping, Samie, M.A., Knoff, J., Eisinger, B., Liu, M.L., Huang, S.M., Caterina, M.J., Dempsey, P., Michael, L.E., Dlugosz, A.A., Andrews, N.C., Clapham, D.E., Xu, H. (2010). TRP channel regulates EGFR signaling in hair morphogenesis and skin barrier formation. *Cell*, **141**: 331–343.
- Chiu, I.M., Barrett, L.B., Williams, E.K., Strochlic, D.E., Lee, S., Weyer, A.D., Lou, S., Bryman, G.S., Roberson, D.P., Ghasemlou, N., Piccoli, C., Ahat, E., Wang, V., Cobos, E.J., Stucky, C.L., Ma, Q., Liberles, S.D., Woolf, C.J. (2014). Transcriptional profiling at whole population and single cell levels reveals somatosensory neuron molecular diversity. *eLife*, **3**.
- Chopra, D., Arens, R.A., Amornpaibroj, W., Lowes, M.A., Tomic-Canic, M., Strbo, N., Lev-Tov, H., Pastar, I. (2022). Innate immunity and microbial dysbiosis in hidradenitis suppurativa – vicious cycle of chronic inflammation. *Frontiers in Immunology*, **13**: 1–14.
- Chuang, H.H., Prescott, E.D., Kong, H., Shields, S., Jordt, S.E., Basbaum, A.I., Chao, M. V., Julius, D. (2001). Bradykinin and nerve growth factor release the capsaicin receptor from PtdIns(4,5)P₂-mediated inhibition. *Nature*, **411**: 957–962.
- Chung, K., Pitcher, T., Grant, A.D., Hewitt, E., Lindstrom, E., Malcangio, M. (2019). Cathepsin S acts via protease-activated receptor 2 to activate sensory neurons and induce itch-like behaviour. *Neurobiology of Pain*, **6**: 100032.
- Chung, M.K., Güler, A.D., Caterina, M.J. (2005). Biphasic currents evoked by chemical or thermal activation of the heat-gated ion channel, TRPV3. *Journal of Biological Chemistry*, **280**: 15928–15941.
- Chung, M.K., Lee, H., Mizuno, A., Suzuki, M., Caterina, M.J. (2004). 2-Aminoethoxydiphenyl borate activates and sensitizes the heat-gated ion channel TRPV3. *Journal of Neuroscience*, **24**: 5177–5182.
- Cohen, P. (2002). Protein kinases - The major drug targets of the twenty-first century? *Nature Reviews Drug Discovery*, **1**: 309–315.
- Coste, B., Mathur, J., Schmidt, M., Earley, T.J., Ranade, S., Petrus, M.J., Dubin, A.E., Patapoutian, A. (2010). Piezo1 and Piezo2 are essential components of distinct mechanically activated cation channels. *Science*, **330**: 55–60.
- Cotsarelis, G., Millar, S.E. (2001). Towards a molecular understanding of hair loss and its treatment. *Trends in Molecular Medicine*, **7**: 293–301.

- Crawford, L.T.K., Caterina, M.J. (2020). Functional Anatomy of the Sensory Nervous System: Updates From the Neuroscience Bench. *Toxicologic Pathology*, **48**: 174–189.
- Cui, H.Y., Wang, S.J., Song, F., Cheng, X., Nan, G., Zhao, Y., Qian, M.R., Chen, X., Li, J.Y., Liu, F.L., Zhu, Y.M., Tian, R.F., Wang, B., Wu, B., Zhang, Y., Sun, X.X., Guo, T., Yang, X.M., Zhang, H., Li, L., Xu, J., Bian, H.J., Jiang, J.L., Chen, Z.N. (2021). CD147 receptor is essential for TFF3-mediated signaling regulating colorectal cancer progression. *Signal Transduction and Targeted Therapy*, **6**: 1–15.
- Cui, T.T., Wang, G.X., Wei, N.N., Wang, K.W. (2018). A pivotal role for the activation of TRPV3 channel in itch sensations induced by the natural skin sensitizer carvacrol. *Acta Pharmacologica Sinica*, **39**: 331–335.
- Damaj, B.B., Becerra, C.B., Esber, H.J., Wen, Y., Maghazachi, A.A. (2007). Functional Expression of H4 Histamine Receptor in Human Natural Killer Cells, Monocytes, and Dendritic Cells. *The Journal of Immunology*, **179**: 7907–7915.
- Danso-Abeam, D., Zhang, J., Dooley, J., Staats, K.A., Van Eyck, L., Van Brussel, T., Zaman, S., Hauben, E., Van De Velde, M., Morren, M.A., Renard, M., Van Geet, C., Schaballie, H., Lambrechts, D., Tao, J., Franckaert, D., Humblet-Baron, S., Meyts, I., Liston, A. (2013). Olmsted syndrome: Exploration of the immunological phenotype. *Orphanet Journal of Rare Diseases*, **8**: 1–8.
- Deering-Rice, C.E., Mitchell, V.K., Romero, E.G., Abdel Aziz, M.H., Ryskamp, D.A., Križaj, D., Venkat, R.G., Reilly, C.A. (2014). Drofenine: a 2-APB analog with improved selectivity for human TRPV3. *Pharmacology Research and Perspectives*, **2**: 62.
- Denda, M., Fuziwara, S., Inoue, K., Denda, S., Akamatsu, H., Tomitaka, A., Matsunaga, K. (2001). Immunoreactivity of VR1 on epidermal keratinocyte of human skin. *Biochemical and Biophysical Research Communications*, **285**: 1250–1252.
- Denda, M., Hosoi, J., Asida, Y. (2000). Visual imaging of ion distribution in human epidermis. *Biochemical and Biophysical Research Communications*, **272**: 134–137.
- Denda, M., Katagiri, C., Hirao, T., Maruyama, N., Takahashi, M. (1999). Some magnesium salts and a mixture of magnesium and calcium salts accelerate skin barrier recovery. *Archives of Dermatological Research*, **291**: 560–563.
- Deng, Z., MaksaeV, G., Rau, M., Xie, Z., Hu, H., Fitzpatrick, J.A.J., Yuan, P. (2020). Gating of human TRPV3 in a lipid bilayer. *Nature Structural and Molecular Biology*, **27**: 635–644.
- Deraison, C., Bonnart, C., Lopez, F., Besson, C., Robinson, R., Jayakumar, A., Wagberg, F., Brattsand, M., Hachem, J.P., Leonardsson, G., Hovnanian, A. (2007). LEKTI fragments specifically inhibit KLK5, KLK7, and KLK14 and control desquamation through a pH-dependent interaction. *Molecular Biology of the Cell*, **18**: 3607–3619.
- Doerner, J.F., Hatt, H., Ramsey, I.S. (2011). Voltage- and temperature-dependent activation of TRPV3 channels is potentiated by receptor-mediated PI(4,5)P₂ hydrolysis. *Journal of General Physiology*, **137**: 271–288.
- Dong, X., Han, S. kyoun, Zylka, M.J., Simon, M.I., Anderson, D.J. (2001). A diverse family of GPCRs expressed in specific subsets of nociceptive sensory neurons. *Cell*, **106**: 619–632.
- Dong, Xintong, Dong, Xinzhong. (2018). Peripheral and Central Mechanisms of Itch. *Neuron*, **98**: 482–494.
- Driskell, R.R., Lichtenberger, B.M., Hoste, E., Kretzschmar, K., Simons, B.D., Charalambous, M., Ferron, S.R., Herault, Y., Pavlovic, G., Ferguson-Smith, A.C., Watt, F.M. (2013). Distinct fibroblast lineages determine dermal architecture in skin development and repair. *Nature*, **504**: 277–281.
- Du, H., Bartleson, J.M., Butenko, S., Alonso, V., Liu, W.F., Winer, D.A., Butte, M.J. (2023). Tuning immunity through tissue mechanotransduction. *Nature Reviews Immunology*, **23**: 174–188.
- Duchatelet, S., Guibbal, L., De Veer, S., Fraitag, S., Nitschké, P., Zarhrate, M., Bodemer, C.,

- Hovnanian, A. (2014). Olmsted syndrome with erythromelalgia caused by recessive transient receptor potential vanilloid 3 mutations. *British Journal of Dermatology*, **171**: 675–678.
- Duchatelet, S., Hovnanian, A. (2015). Olmsted syndrome: Clinical, molecular and therapeutic aspects. *Orphanet Journal of Rare Diseases*, **10**: 3.
- Duchatelet, Sabine, Pruvost, S., De Veer, S., Fraitag, S., Nitschké, P., Bole-Feysot, C., Bodemer, C., Hovnanian, A. (2014). A new TRPV3 missense mutation in a patient with Olmsted syndrome and erythromelalgia. *JAMA Dermatology*, **150**: 303–306.
- Dunn, C., Wiltshire, C., MacLaren, A., Gillespie, D.A.F. (2002). Molecular mechanism and biological functions of c-Jun N-terminal kinase signalling via the c-Jun transcription factor. *Cellular Signalling*, **14**: 585–593.
- Dyring-Andersen, B., Løvendorf, M.B., Coscia, F., Santos, A., Møller, L.B.P., Colaço, A.R., Niu, L., Bzorek, M., Doll, S., Andersen, J.L., Clark, R.A., Skov, L., Teunissen, M.B.M., Mann, M. (2020). Spatially and cell-type resolved quantitative proteomic atlas of healthy human skin. *Nature Communications*, **11**: 1–14.
- Eckert, R.L. (1989). Structure, function, and differentiation of the keratinocyte. *Physiological Reviews*, **69**: 1316–1346.
- Egawa, N., Koshikawa, N., Tomari, T., Nabeshima, K., Isobe, T., Seiki, M. (2006). Membrane type 1 matrix metalloproteinase (MT1-MMP/MMP-14) cleaves and releases a 22-kDa extracellular matrix metalloproteinase inducer (EMMPRIN) fragment from tumor cells. *Journal of Biological Chemistry*, **281**: 37576–37585.
- Egelrud, T., Lundström, A. (1991). A chymotrypsin-like proteinase that may be involved in desquamation in plantar stratum corneum. *Archives of Dermatological Research*, **283**: 108–112.
- Eisenhoffer, G.T., Loftus, P.D., Yoshigi, M., Otsuna, H., Chien, C. Bin, Morcos, P.A., Rosenblatt, J. (2012). Crowding induces live cell extrusion to maintain homeostatic cell numbers in epithelia. *Nature*, **484**: 546–549.
- Eldesouky, F., Ibrahim, A.-S.M., Sharaf, S.M. (2020). Macrophage Migration Inhibitory Factor in Alopecia Areata and Vitiligo: A Case-Controlled Serological Study. *The Journal of clinical and aesthetic dermatology*, **13**: 24–27.
- Elias, P.M., Choi, E.H. (2005). Interactions among stratum corneum defensive functions. *Experimental Dermatology*, **14**: 719–726.
- Elsholz, F., Harteneck, C., Muller, W., Friedland, K. (2014). Calcium - A central regulator of keratinocyte differentiation in health and disease. *European Journal of Dermatology*, **24**: 650–661.
- Ernfors, P., Manira, A. El, Svenningsson, P. (2021). Discoveries of receptors for temperature and touch. *The Noble Assembly at Karolinska Institutet*, 2–5.
- Evans, C.E., Cober, N.D., Dai, Z., Stewart, D.J., Zhao, Y.Y. (2021). Endothelial cells in the pathogenesis of pulmonary arterial hypertension. *European Respiratory Journal*, **58**: 2003957.
- Everaerts, W., Gees, M., Alpizar, Y.A., Farre, R., Leten, C., Apetrei, A., Dewachter, I., Van Leuven, F., Vennekens, R., De Ridder, D., Nilius, B., Voets, T., Talavera, K. (2011). The capsaicin receptor TRPV1 is a crucial mediator of the noxious effects of mustard oil. *Current Biology*, **21**: 316–321.
- Ewald, D.A., Malajian, D., Krueger, J.G., Workman, C.T., Wang, T., Tian, S., Litman, T., Guttman-Yassky, E., Suárez-Fariñas, M. (2015). Meta-analysis derived atopic dermatitis (MADAD) transcriptome defines a robust AD signature highlighting the involvement of atherosclerosis and lipid metabolism pathways. *BMC Medical Genomics*, **8**: 1–15.
- Eytan, O., Fuchs-Telem, D., Mevorach, B., Indelman, M., Bergman, R., Sarig, O., Goldberg, I., Adir, N., Sprecher, E. (2014). Olmsted syndrome caused by a homozygous recessive mutation in TRPV3. *Journal of Investigative Dermatology*, **134**: 1752–1754.

- Facer, P., Casula, M.A., Smith, G.D., Benham, C.D., Chessell, I.P., Bountra, C., Sinisi, M., Birch, R., Anand, P. (2007). Differential expression of the capsaicin receptor TRPV1 and related novel receptors TRPV3, TRPV4 and TRPM8 in normal human tissues and changes in traumatic and diabetic neuropathy. *BMC Neurology*, **7**: 11.
- Fatima, M., Slade, H., Horwitz, L., Shi, A., Liu, J., McKinstry, D., Villani, T., Xu, H., Duan, B. (2022). Abnormal Somatosensory Behaviors Associated With a Gain-of-Function Mutation in TRPV3 Channels. *Frontiers in Molecular Neuroscience*, **14**: 340.
- Fawcett, W.J., Haxby, E.J., Male, D.A. (1999). Magnesium: physiology and pharmacology. *British Journal of Anaesthesia*, **83**: 302–322.
- Fawzi, M.M.T., Mahmoud, S.B., Shaker, O.G., Saleh, M.A. (2016). Assessment of tissue levels of dickkopf-1 in androgenetic alopecia and alopecia areata. *Journal of Cosmetic Dermatology*, **1**: 10–15.
- Feingold, K.R. (2007). The role of epidermal lipids in cutaneous permeability barrier homeostasis. *Journal of Lipid Research*, **48**: 2531–2546.
- Feldman, S.R., Thaçi, D., Gooderham, M., Augustin, M., de la Cruz, C., Mallbris, L., Buonanno, M., Tatulych, S., Kaur, M., Lan, S., Valdez, H., Mamolo, C. (2016). Tofacitinib improves pruritus and health-related quality of life up to 52 weeks: Results from 2 randomized phase III trials in patients with moderate to severe plaque psoriasis. *Journal of the American Academy of Dermatology*, **75**: 1162–1170.
- Feldmeyer, L., Keller, M., Niklaus, G., Hohl, D., Werner, S., Beer, H.D. (2007). The Inflammasome Mediates UVB-Induced Activation and Secretion of Interleukin-1 β by Keratinocytes. *Current Biology*, **17**: 1140–1145.
- Feng, J., Hu, H. (2019). A novel player in the field: Merkel disc in touch, itch and pain. *Experimental Dermatology*, **28**: 1412–1415.
- Feng, J., Luo, J., Yang, P., Du, J., Kim, B.S., Hu, H. (2018). Piezo2 channel–Merkel cell signaling modulates the conversion of touch to itch. *Science*, **360**: 530–533.
- Feng, J., Yang, P., Mack, M.R., Dryn, D., Luo, J., Gong, X., Liu, S., Oetjen, L.K., Zholos, A. V., Mei, Z., Yin, S., Kim, B.S., Hu, H. (2017). Sensory TRP channels contribute differentially to skin inflammation and persistent itch. *Nature Communications*, **8**: 1–12.
- Feng, J., Zhao, Y., Xie, Z., Zang, K., Sviben, S., Hu, X., Fitzpatrick, J.A.J., Wen, L., Liu, Y., Wang, T., Lawson, K., Liu, Q., Yan, Y., Dong, X., Han, L., Wu, G.F., Kim, B.S., Hu, H. (2022). Miswiring of Merkel cell and pruriceptive C fiber drives the itch-scratch cycle. *Science Translational Medicine*, **14**: 1–20.
- Ferry, X., Brehin, S., Kamel, R., Landry, Y. (2002). G protein-dependent activation of mast cell by peptides and basic secretagogues. *Peptides*, **23**: 1507–1515.
- Festa, A., D’Agostino, R., Rich, S.S., Jenny, N.S., Tracy, R.P., Haffner, S.M. (2003). Promoter (4G/5G) plasminogen activator inhibitor-1 genotype and plasminogen activator inhibitor-1 levels in blacks, hispanics, and non-hispanic whites: The Insulin Resistance Atherosclerosis Study. *Circulation*, **107**: 2422–2427.
- Fitz-Gibbon, S., Tomida, S., Chiu, B.H., Nguyen, L., Du, C., Liu, M., Elashoff, D., Erfe, M.C., Loncaric, A., Kim, J., Modlin, R.L., Miller, J.F., Sodergren, E., Craft, N., Weinstock, G.M., Li, H. (2013). Propionibacterium acnes strain populations in the human skin microbiome associated with acne. *Journal of Investigative Dermatology*, **133**: 2152–2160.
- Follansbee, T., Dong, X. (2022). Touch-evoked itch pinned on Piezo1 ion-channel protein. *Nature*, **607**: 36–37.
- Foote, A.G., Tibbetts, J., Bartley, S.M., Thibeault, S.L. (2022). Localization of TRPV3/4 and PIEZO1/2 sensory receptors in murine and human larynges. *Laryngoscope Investigative Otolaryngology*, **7**: 1963–1972.

- Foroutan, A., Haddadi, N.S., Ostadhadi, S., Sistany, N., Dehpour, A.R. (2015). Chloroquine-induced scratching is mediated by NO/cGMP pathway in mice. *Pharmacology Biochemistry and Behavior*, **134**: 79–84.
- Forslind, B., Werner-Linde, Y., Lindberg, M., Pallon, J. (1999). Elemental analysis mirrors epidermal differentiation. *Acta Dermato-Venereologica*, **79**: 12–17.
- Foster, D.S., Januszyk, M., Yost, K.E., Chinta, M.S., Gulati, G.S., Nguyen, A.T., Burcham, A.R., Salhotra, A., Ransom, R.C., Henn, D., Chen, K., Mascharak, S., Tolentino, K., Titan, A.L., Jones, R.E., da Silva, O., Leavitt, W.T., Marshall, C.D., des Jardins-Park, H.E., Hu, M.S., Wan, D.C., Wernig, G., Wagh, D., Coller, J., Norton, J.A., Gurtner, G.C., Newman, A.M., Chang, H.Y., Longaker, M.T. (2021). Integrated spatial multiomics reveals fibroblast fate during tissue repair. *Proceedings of the National Academy of Sciences of the United States of America*, **118**: 2110025118.
- Foster, S.L., Seehus, C.R., Woolf, C.J., Talbot, S. (2017). Sense and immunity: Context-dependent neuro-immune interplay. *Frontiers in Immunology*, **8**: 1463.
- Fowler, E., Yosipovitch, G. (2020). A new generation of treatments for itch. *Acta Dermato-Venereologica*, **100**: 37–45.
- Franciosa, G., Locard-Paulet, M., Jensen, L.J., Olsen, J. V. (2023). Recent advances in kinase signaling network profiling by mass spectrometry. *Current Opinion in Chemical Biology*, **73**: 102260.
- Freeman, S.C., Sonthalia, S. (2019). *Histology, Keratohyalin Granules*. StatPearls Publishing.
- Fukuoka, M., Miyachi, Y., Ikoma, A. (2013). Mechanically evoked itch in humans. *Pain*, **154**: 897–904.
- Furue, K., Ulzii, D., Tanaka, Y., Ito, T., Tsuji, G., Kido-Nakahara, M., Nakahara, T., Furue, M. (2020). Pathogenic implication of epidermal scratch injury in psoriasis and atopic dermatitis. *Journal of Dermatology*, **47**: 979–988.
- Garlanda, C., Bottazzi, B., Magrini, E., Inforzato, A., Mantovani, A. (2018). PTX3, a humoral pattern recognition molecule, in innate immunity, tissue repair, and cancer. *Physiological Reviews*, **98**: 623–639.
- Garlanda, C., Dinarello, C.A., Mantovani, A. (2013). The Interleukin-1 Family: Back to the Future. *Immunity*, **39**: 1003–1018.
- Gazerani, P. (2018). Antipruritic effects of botulinum neurotoxins. *Toxins*, **10**: 143.
- Ge, J., Li, W., Zhao, Q., Li, N., Chen, M., Zhi, P., Li, R., Gao, N., Xiao, B., Yang, M. (2015). Architecture of the mammalian mechanosensitive Piezo1 channel. *Nature*, **527**: 64–69.
- Geng, J., Shi, Y., Zhang, J., Yang, B., Wang, P., Yuan, W., Zhao, H., Li, J., Qin, F., Hong, L., Xie, C., Deng, X., Sun, Y., Wu, C., Chen, L., Zhou, D. (2021). TLR4 signalling via Piezo1 engages and enhances the macrophage mediated host response during bacterial infection. *Nature Communications*, **12**: 1–14.
- Ghosh, A.K., Vaughan, D.E. (2012). PAI-1 in tissue fibrosis. *Journal of Cellular Physiology*, **227**: 493–507.
- Glatte, P., Buchmann, S.J., Hijazi, M.M., Illigens, B.M.W., Siepmann, T. (2019). Architecture of the Cutaneous Autonomic Nervous System. *Frontiers in Neurology*, **10**: 970.
- Goetz, D.H., Holmes, M.A., Borregaard, N., Bluhm, M.E., Raymond, K.N., Strong, R.K. (2002). The neutrophil lipocalin NGAL is a bacteriostatic agent that interferes with siderophore-mediated iron acquisition. *Molecular Cell*, **10**: 1033–1043.
- Gonzales, M., Haan, K., Baker, S.E., Fitchmun, M., Todorov, I., Weitzman, S., Jones, J.C.R. (1999). A cell signal pathway involving laminin-5, $\alpha 3\beta 1$ integrin, and mitogen- activated protein kinase can regulate epithelial cell proliferation. *Molecular Biology of the Cell*, **10**: 259–270.

- Goswami, S.C., Mishra, S.K., Maric, D., Kaszas, K., Gonnella, G.L., Clokie, S.J., Kominsky, H.D., Gross, J.R., Keller, J.M., Mannes, A.J., Hoon, M.A., Iadarola, M.J. (2014). Molecular signatures of mouse TRPV1-lineage neurons revealed by RNA-seq transcriptome analysis. *Journal of Pain*, **15**: 1338–1359.
- Grandl, J., Hu, H., Bandell, M., Bursulaya, B., Schmidt, M., Petrus, M., Patapoutian, A. (2008). Pore region of TRPV3 ion channel is specifically required for heat activation. *Nature Neuroscience*, **11**: 1007–1013.
- Groves, R.W., Mizutani, H., Kieffer, J.D., Kupper, T.S. (1995). Inflammatory skin disease in transgenic mice that express high levels of interleukin 1 α in basal epidermis. *Proceedings of the National Academy of Sciences of the United States of America*, **92**: 11874–11878.
- Gudipaty, S.A., Lindblom, J., Loftus, P.D., Redd, M.J., Edes, K., Davey, C.F., Krishnegowda, V., Rosenblatt, J. (2017). Mechanical stretch triggers rapid epithelial cell division through Piezo1. *Nature*, **543**: 118–121.
- Guimarães, C.F., Gasperini, L., Marques, A.P., Reis, R.L. (2020). The stiffness of living tissues and its implications for tissue engineering. *Nature Reviews Materials*, **5**: 351–370.
- Guindolet, D., Gabison, E.E. (2020). Role of CD147 (EMMPRIN/Basigin) in Tissue Remodeling. *Anatomical Record*, **303**: 1584–1589.
- Guo, C.J., Mack, M.R., Oetjen, L.K., Trier, A.M., Council, M.L., Pavel, A.B., Guttman-Yassky, E., Kim, B.S., Liu, Q. (2020). Kallikrein 7 Promotes Atopic Dermatitis-Associated Itch Independently of Skin Inflammation. *Journal of Investigative Dermatology*, **140**: 1244–1252.
- Guo, H., Zucker, S., Gordon, M.K., Toole, B.P., Biswas, C. (1997). Stimulation of matrix metalloproteinase production by recombinant extracellular matrix metalloproteinase inducer from transfected Chinese hamster ovary cells. *Journal of Biological Chemistry*, **272**: 24–27.
- Guo, Y.R., MacKinnon, R. (2017). Structure-based membrane dome mechanism for piezo mechanosensitivity. *eLife*, **6**.
- Gupta, R.K., Swain, S., Kankanamge, D., Priyanka, P.D., Singh, R., Mitra, K., Karunarathne, A., Giri, L. (2017). Comparison of Calcium Dynamics and Specific Features for G Protein–Coupled Receptor–Targeting Drugs Using Live Cell Imaging and Automated Analysis. *SLAS Discovery*, **22**: 848–858.
- Guttman-Yassky, E., Krueger, J.G. (2017). Atopic dermatitis and psoriasis: two different immune diseases or one spectrum? *Current Opinion in Immunology*, **48**: 68–73.
- Guttman-Yassky, E., Krueger, J.G., Lebwohl, M.G. (2018). Systemic immune mechanisms in atopic dermatitis and psoriasis with implications for treatment. *Experimental Dermatology*, **27**: 409–417.
- Haddadi, N.S., Foroutan, A., Ostadhadi, S., Azimi, E., Rahimi, N., Nateghpour, M., Lerner, E.A., Dehpour, A.R. (2017). Peripheral NMDA receptor/NO system blockage inhibits itch responses induced by chloroquine in mice. *Acta Dermato-Venereologica*, **97**: 571–577.
- Haftak, M., Abdayem, R., Guyonnet-Debersac, P. (2022). Skin Minerals: Key Roles of Inorganic Elements in Skin Physiological Functions. *International Journal of Molecular Sciences*, **23**: 6267.
- Hagermark, O. (1974). Studies on experimental itch induced by kallikrein and bradykinin. *Acta Dermato-Venereologica*, **54**: 397–400.
- Hammond, M., Gamal, A., Mukherjee, P.K., Damiani, G., McCormick, T.S., Ghannoum, M.A., Nedorost, S. (2022). Cutaneous dysbiosis may amplify barrier dysfunction in patients with atopic dermatitis. *Frontiers in Microbiology*, **13**: 4358.
- Han, L., Ma, C., Liu, Q., Weng, H.J., Cui, Y., Tang, Z., Kim, Y., Nie, H., Qu, L., Patel, K.N., Li, Z., McNeil, B., He, S., Guan, Y., Xiao, B., Lamotte, R.H., Dong, X. (2013). A subpopulation of nociceptors specifically linked to itch. *Nature Neuroscience*, **16**: 174–182.

Han, Y., Chen, Y., Liu, X., Zhang, J., Su, H., Wen, H., Li, W., Yao, X. (2017). Efficacy and safety of dupilumab for the treatment of adult atopic dermatitis: A meta-analysis of randomized clinical trials. *Journal of Allergy and Clinical Immunology*, **140**: 888–891.

Haraguchi, M., Hino, M., Tanaka, H., Maru, M. (1997). Naturally occurring dermatitis associated with *Staphylococcus aureus* in DS-Nh mice. *Experimental animals / Japanese Association for Laboratory Animal Science*, **46**: 225–229.

Hashimoto, K. (1971). Intercellular spaces of the human epidermis as demonstrated with lanthanum. *The Journal of investigative dermatology*, **57**: 17–31.

Hashimoto, T., Rosen, J.D., Sanders, K.M., Yosipovitch, G. (2019). Possible roles of basophils in chronic itch. *Experimental Dermatology*, **28**: 1373–1379.

Hay, R.J., Johns, N.E., Williams, H.C., Bolliger, I.W., Dellavalle, R.P., Margolis, D.J., Marks, R., Naldi, L., Weinstock, M.A., Wulf, S.K., Michaud, C., J.I. Murray, C., Naghavi, M. (2014). The global burden of skin disease in 2010: An analysis of the prevalence and impact of skin conditions. *Journal of Investigative Dermatology*, **134**: 1527–1534.

Haydont, V., Bernard, B.A., Fortunel, N.O. (2019). Age-related evolutions of the dermis: Clinical signs, fibroblast and extracellular matrix dynamics. *Mechanisms of Ageing and Development*, **177**: 150–156.

Haydont, V., Neiveyans, V., Fortunel, N.O., Asselineau, D. (2019). Transcriptome profiling of human papillary and reticular fibroblasts from adult interfollicular dermis pinpoints the ‘tissue skeleton’ gene network as a component of skin chrono-ageing. *Mechanisms of Ageing and Development*, **179**: 60–77.

Hayes, P., Meadows, H.J., Gunthorpe, M.J., Harries, M.H., Duckworth, D.M., Cairns, W., Harrison, D.C., Clarke, C.E., Ellington, K., Prinjha, R.K., Barton, A.J.L., Medhurst, A.D., Smith, G.D., Topp, S., Murdock, P., Sanger, G.J., Terrett, J., Jenkins, O., Benham, C.D., Randall, A.D., Gloger, I.S., Davis, J.B. (2000). Cloning and functional expression of a human orthologue of rat vanilloid receptor-1. *Pain*, **88**: 205–215.

He, H., Suryawanshi, H., Morozov, P., Gay-Mimbrera, J., Del Duca, E., Kim, H.J., Kameyama, N., Estrada, Y., Der, E., Krueger, J.G., Ruano, J., Tuschl, T., Guttman-Yassky, E. (2020). Single-cell transcriptome analysis of human skin identifies novel fibroblast subpopulation and enrichment of immune subsets in atopic dermatitis. *Journal of Allergy and Clinical Immunology*, **145**: 1615–1628.

He, Y., Zeng, K., Zhang, X., Chen, Q., Wu, J., Li, H., Zhou, Y., Glusman, G., Roach, J., Etheridge, A., Qing, S., Tian, Q., Lee, I., Tian, X., Wang, X., Wu, Z., Hood, L., Ding, Y., Wang, K. (2015). A gain-of-function mutation in TRPV3 causes focal palmoplantar keratoderma in a chinese family. *Journal of Investigative Dermatology*, **135**: 907–909.

Heldin, C.H., Westermark, B. (1999). Mechanism of action and in vivo role of platelet-derived growth factor. *Physiological Reviews*, **79**: 1283–1316.

Hellwig, N., Albrecht, N., Harteneck, C., Schultz, G., Schaefer, M. (2005). Homo- and heteromeric assembly of TRPV channel subunits. *Journal of Cell Science*, **118**: 917–928.

Hill, R.Z., Loud, M.C., Dubin, A.E., Peet, B., Patapoutian, A. (2022). PIEZO1 transduces mechanical itch in mice. *Nature*, **607**: 104–110.

Hill, R.Z., Morita, T., Brem, R.B., Bautista, D.M. (2018). S1PR3 mediates itch and pain via distinct TRP channel-dependent pathways. *Journal of Neuroscience*, **38**: 7833–7843.

Hinman, A., Chuang, H.H., Bautista, D.M., Julius, D. (2006). TRP channel activation by reversible covalent modification. *Proceedings of the National Academy of Sciences of the United States of America*, **103**: 19564–19568.

Hsu, Y.C., Li, L., Fuchs, E. (2014). Emerging interactions between skin stem cells and their niches. *Nature Medicine*, **20**: 847–856.

- Hu, H.Z., Gu, Q., Wang, C., Colton, C.K., Tang, J., Kinoshita-Kawada, M., Lee, L.Y., Wood, J.D., Zhu, M.X. (2004). 2-Aminoethoxydiphenyl borate is a common activator of TRPV1, TRPV2, and TRPV3. *Journal of Biological Chemistry*, **279**: 35741–35748.
- Hu, H.Z., Xiao, R., Wang, C., Gao, N., Colton, C.K., Wood, J.D., Zhu, M.X. (2006). Potentiation of TRPV3 channel function by unsaturated fatty acids. *Journal of Cellular Physiology*, **208**: 201–212.
- Hu, Y., Shan, W.Q., Wu, B., Liu, T. (2021). New Insight into the Origins of Itch and Pain: How are Itch and Pain Signals Coded and Discriminated by Primary Sensory Neurons? *Neuroscience Bulletin*, **37**: 575–578.
- Huang, S.M., Lee, H., Chung, M.K., Park, U., Yin, Y.Y., Bradshaw, H.B., Coulombe, P.A., Walker, J.M., Caterina, M.J. (2008). Overexpressed transient receptor potential vanilloid 3 ion channels in skin keratinocytes modulate pain sensitivity via prostaglandin E₂. *Journal of Neuroscience*, **28**: 13727–13737.
- Huang, S.M., Li, X., Yu, Y.Y., Wang, J., Caterina, M.J. (2011). TRPV3 and TRPV4 ion channels are not major contributors to mouse heat sensation. *Molecular Pain*, **7**: 37.
- Hughes, C.S., Postovit, L.M., Lajoie, G.A. (2010). Matrigel: a complex protein mixture required for optimal growth of cell culture. *Proteomics*, **10**: 1886–1890.
- Ikoma, A., Handwerker, H., Miyachi, Y., Schmelz, M. (2005). Electrically evoked itch in humans. *Pain*, **113**: 148–154.
- Ikoma, A., Steinhoff, M., Ständer, S., Yosipovitch, G., Schmelz, M. (2006). The neurobiology of itch. *Nature Reviews Neuroscience*, **7**: 535–547.
- Imai, Y., Yasuda, K., Sakaguchi, Y., Haneda, T., Mizutani, H., Yoshimoto, T., Nakanishi, K., Yamanishi, K. (2013). Skin-specific expression of IL-33 activates group 2 innate lymphoid cells and elicits atopic dermatitis-like inflammation in mice. *Proceedings of the National Academy of Sciences of the United States of America*, **110**: 13921–13926.
- Imamachi, N., Goon, H.P., Lee, H., Anderson, D.J., Simon, M.I., Basbaum, A.I., Han, S.K. (2009). TRPV1-expressing primary afferents generate behavioral responses to pruritogens via multiple mechanisms. *Proceedings of the National Academy of Sciences of the United States of America*, **106**: 11330–11335.
- Imura, K., Yoshioka, T., Hirasawa, T., Sakata, T. (2009). Role of TRPV3 in immune response to development of dermatitis. *Journal of Inflammation*, **6**: 1–10.
- Inada, H., Iida, T., Tominaga, M. (2006). Different expression patterns of TRP genes in murine B and T lymphocytes. *Biochemical and Biophysical Research Communications*, **350**: 762–767.
- Inoue, Kaori, Koizumi, S., Fuziwara, S., Denda, S., Inoue, Kazuhide, Denda, M. (2002). Functional vanilloid receptors in cultured normal human epidermal keratinocytes. *Biochemical and Biophysical Research Communications*, **291**: 124–129.
- Iso, H., Folsom, A.R., Koike, K.A., Sato, S., Wu, K.K., Shimamoto, T., Iida, M., Komachi, Y. (1993). Antigens of tissue plasminogen activator and plasminogen activator inhibitor 1: Correlates in nonsmoking Japanese and Caucasian men and women. *Thrombosis and Haemostasis*, **70**: 475–480.
- Jairaman, A., Othy, S., Dynes, J.L., Yeromin, A. V., Zavala, A., Greenberg, M.L., Nourse, J.L., Holt, J.R., Cahalan, S.M., Marangoni, F., Parker, I., Pathak, M.M., Cahalan, M.D. (2021). Piezo1 channels restrain regulatory T cells but are dispensable for effector CD4⁺ T cell responses. *Science Advances*, **7**: 5859.
- Janson, D.G., Saintigny, G., Van Adrichem, A., Mahé, C., El Ghalbzouri, A. (2012). Different gene expression patterns in human papillary and reticular fibroblasts. *Journal of Investigative Dermatology*, **132**: 2565–2572.
- Jian, T., Yang, N., Yang, Y., Zhu, C., Yuan, X., Yu, G., Wang, C., Wang, Z., Shi, H., Tang, M., He, Q., Lan, L., Wu, G., Tang, Z. (2016). TRPV1 and PLC Participate in Histamine H₄ Receptor-Induced

Itch. *Neural Plasticity*, **2016**: 1682972.

Jiang, Y., Tsoi, L.C., Billi, A.C., Ward, N.L., Harms, P.W., Zeng, C., Maverakis, E., Michelle Kahlenberg, J., Gudjonsson, J.E. (2020). Cytokinocytes: The diverse contribution of keratinocytes to immune responses in skin. *JCI Insight*, **5**: 142067.

Jiang, Y., Yang, X., Jiang, J., Xiao, B. (2021). Structural Designs and Mechanogating Mechanisms of the Mechanosensitive Piezo Channels. *Trends in Biochemical Sciences*, **46**: 472–488.

Johnson, G.L., Nakamura, K. (2007). The c-jun kinase/stress-activated pathway: Regulation, function and role in human disease. *Biochimica et Biophysica Acta - Molecular Cell Research*, **1773**: 1341–1348.

Johnson, M.L.T. (2004). Defining the burden of skin disease in the United States - A historical perspective. *Journal of Investigative Dermatology Symposium Proceedings*, **9**: 108–110.

Johnson, M.L.T., Roberts, J. (1978). *Skin Conditions and Related Need for Medical Care among Person 1-74 Years*. Hyatsville (MD), U.S. DHEW, Public Health Service, National Center for Health Statistics Vital and Health Statistics.

Jones, P.H., Watt, F.M. (1993). Separation of human epidermal stem cells from transit amplifying cells on the basis of differences in integrin function and expression. *Cell*, **73**: 713–724.

Jordt, S.E., Bautista, D.M., Chuang, H.H., McKemy, D.D., Zygmunt, P.M., Högestätt, E.D., Meng, I.D., Julius, D. (2004). Mustard oils and cannabinoids excite sensory nerve fibres through the TRP channel ANKTM1. *Nature*, **427**: 260–265.

Jordt, S.E., Tominaga, M., Julius, D. (2000). Acid potentiation of the capsaicin receptor determined by a key extracellular site. *Proceedings of the National Academy of Sciences of the United States of America*, **97**: 8134–8139.

Jumper, J., Evans, R., Pritzel, A., Green, T., Figurnov, M., Ronneberger, O., Tunyasuvunakool, K., Bates, R., Židek, A., Potapenko, A., Bridgland, A., Meyer, C., Kohl, S.A.A., Ballard, A.J., Cowie, A., Romera-Paredes, B., Nikolov, S., Jain, R., Adler, J., Back, T., Petersen, S., Reiman, D., Clancy, E., Zielinski, M., Steinegger, M., Pacholska, M., Berghammer, T., Bodenstein, S., Silver, D., Vinyals, O., Senior, A.W., Kavukcuoglu, K., Kohli, P., Hassabis, D. (2021). Highly accurate protein structure prediction with AlphaFold. *Nature*, **596**: 583–589.

Jutel, M., Watanabe, T., Klunker, S., Akdis, M., Thomet, O.A.R., Malolepszy, J., Zak-Nejmark, T., Koga, R., Kobayashi, T., Blaser, K., Akdis, C.A. (2001). Histamine regulates T-cell and antibody responses by differential expression of H1 and H2 receptors. *Nature*, **413**: 420–425.

Kabashima, K. (2016). Overview: Immunology of the Skin. *Immunology of the Skin: Basic and Clinical Sciences in Skin Immune Responses*. Springer Japan, pp. 1–11.

Kabashima, K., Honda, T., Ginhoux, F., Egawa, G. (2019). The immunological anatomy of the skin. *Nature Reviews Immunology*, **19**: 19–30.

Kahremany, S., Hofmann, L., Gruzman, A., Cohen, G. (2020). Advances in understanding the initial steps of pruritoceptive itch: How the itch hits the switch. *International Journal of Molecular Sciences*, **21**: 1–45.

Kalali, B.N., Köllisch, G., Mages, J., Müller, T., Bauer, S., Wagner, H., Ring, J., Lang, R., Mempel, M., Ollert, M. (2008). Double-Stranded RNA Induces an Antiviral Defense Status in Epidermal Keratinocytes through TLR3-, PKR-, and MDA5/RIG-I-Mediated Differential Signaling. *The Journal of Immunology*, **181**: 2694–2704.

Kang, J., Ding, Y., Li, B., Liu, H., Yang, X., Chen, M. (2017). TRPA1 mediated aggravation of allergic contact dermatitis induced by DINP and regulated by NF- κ B activation. *Scientific Reports*, **7**: 1–9.

Kanni, T., Argyropoulou, M., Spyridopoulos, T., Pistiki, A., Stecher, M., Dinarello, C.A., Simard, J., Giamarellos-Bourboulis, E.J. (2018). MABp1 Targeting IL-1 α for Moderate to Severe

- Hidradenitis Suppurativa Not Eligible for Adalimumab: A Randomized Study. *Journal of Investigative Dermatology*, **138**: 795–801.
- Kardon, A.P., Polgár, E., Hachisuka, J., Snyder, L.M., Cameron, D., Savage, S., Cai, X., Karnup, S., Fan, C.R., Hemenway, G.M., Bernard, C.S., Schwartz, E.S., Nagase, H., Schwarzer, C., Watanabe, M., Furuta, T., Kaneko, T., Koerber, H.R., Todd, A.J., Ross, S.E. (2014). Dynorphin Acts as a Neuromodulator to Inhibit Itch in the Dorsal Horn of the Spinal Cord. *Neuron*, **82**: 573–586.
- Kariminejad, A., Barzegar, M., Abdollahimajd, F., Pramanik, R., McGrath, J.A. (2014). Olmsted syndrome in an Iranian boy with a new de novo mutation in TRPV3. *Clinical and Experimental Dermatology*, **39**: 492–495.
- Karimkhani, C., Dellavalle, R.P., Coffeng, L.E., Flohr, C., Hay, R.J., Langan, S.M., Nsoesie, E.O., Ferrari, A.J., Erskine, H.E., Silverberg, J.I., Vos, T., Naghavi, M. (2017). Global skin disease morbidity and mortality an update from the global burden of disease study 2013. *JAMA Dermatology*, **153**: 406–412.
- Karlsson, M., Zhang, C., Méar, L., Zhong, W., Digre, A., Katona, B., Sjöstedt, E., Butler, L., Odeberg, J., Dusart, P., Edfors, F., Oksvold, P., von Feilitzen, K., Zwahlen, M., Arif, M., Altay, O., Li, X., Ozcan, M., Mardonoglu, A., Fagerberg, L., Mulder, J., Luo, Y., Ponten, F., Uhlén, M., Lindskog, C. (2021). A single-cell type transcriptomics map of human tissues. *Science Advances*, **7**: 2169.
- Kato, T., Takai, T., Fujimura, T., Matsuoka, H., Ogawa, T., Murayama, K., Ishii, A., Ikeda, S., Okumura, K., Ogawa, H. (2009). Mite serine protease activates protease-activated receptor-2 and induces cytokine release in human keratinocytes. *Allergy: European Journal of Allergy and Clinical Immunology*, **64**: 1366–1374.
- Kemény, Á., Kodji, X., Horváth, S., Komlódi, R., Szóke, É., Sándor, Z., Perkecz, A., Gyömörei, C., Sétáló, G., Kelemen, B., Bíró, T., Tóth, B.I., Brain, S.D., Pintér, E., Gyulai, R. (2018). TRPA1 Acts in a Protective Manner in Imiquimod-Induced Psoriasiform Dermatitis in Mice. *Journal of Investigative Dermatology*, **138**: 1774–1784.
- Kennedy-Crispin, M., Billick, E., Mitsui, H., Gulati, N., Fujita, H., Gilleaudeau, P., Sullivan-Whalen, M., Johnson-Huang, L.M., Suárez-Fariñas, M., Krueger, J.G. (2012). Human keratinocytes' response to injury upregulates CCL20 and other genes linking innate and adaptive immunity. *Journal of Investigative Dermatology*, **132**: 105–113.
- Kim, B.S., Wang, K., Siracusa, M.C., Saenz, S.A., Brestoff, J.R., Monticelli, L.A., Noti, M., Tait Wojno, E.D., Fung, T.C., Kubo, M., Artis, D. (2014). Basophils Promote Innate Lymphoid Cell Responses in Inflamed Skin. *The Journal of Immunology*, **193**: 3717–3725.
- Kim, C., Sano, Y., Todorova, K., Carlson, B.A., Arpa, L., Celada, A., Lawrence, T., Otsu, K., Brissette, J.L., Arthur, J.S.C., Park, J.M. (2008). The kinase p38 α serves cell type-specific inflammatory functions in skin injury and coordinates pro- and anti-inflammatory gene expression. *Nature Immunology*, **9**: 1019–1027.
- Kim, C.S., Yang, X., Jacobsen, S., Masters, K.S., Kreeger, P.K. (2019). Leader cell PLC γ 1 activation during keratinocyte collective migration is induced by EGFR localization and clustering. *Bioengineering & Translational Medicine*, **4**: 10138.
- Kim, H. S., Hashimoto, T., Fischer, K., Bernigaud, C., Chosidow, O., Yosipovitch, G. (2021). Scabies itch: an update on neuroimmune interactions and novel targets. *Journal of the European Academy of Dermatology and Venereology*, **35**: 1765–1776.
- Kim, Jin Cheol, Kim, H.B., Shim, W.S., Kwak, I.S., Chung, B.Y., Kang, S.Y., Park, C.W., Kim, H.O. (2021). Activation of transient receptor potential vanilloid-3 channels in keratinocytes induces pruritus in humans. *Acta Dermato-Venereologica*, **101**: 517.
- Kim, N., Bae, K.B., Kim, M.O., Yu, D.H., Kim, H.J., Yuh, H.S., Ji, Y.R., Park, Si Jun, Kim, S., Son, K.H., Park, Sang Joon, Yoon, D., Lee, D.S., Lee, S., Lee, H.S., Kim, T.Y.K., Ryoo, Z.Y. (2012). Overexpression of cathepsin S induces chronic atopic dermatitis in mice. *Journal of Investigative*

Dermatology, **132**: 1169–1176.

Kim, S., Barry, D.M., Liu, X.Y., Yin, S., Munanairi, A., Meng, Q.T., Cheng, W., Mo, P., Wan, L., Liu, S. Bin, Ratnayake, K., Zhao, Z.Q., Gautam, N., Zheng, J., Karunaratne, W.K.A., Chen, Z.F. (2016). Facilitation of TRPV4 by TRPV1 is required for itch transmission in some sensory neuron populations. *Science Signaling*, **9**: 71.

Kini, S.P., DeLong, L.K., Veledar, E., McKenzie-Brown, A.M., Schaufele, M., Chen, S.C. (2011). The impact of pruritus on quality of life: The skin equivalent of pain. *Archives of Dermatology*, **147**: 1153–1156.

Kittaka, H., Tominaga, M. (2017). The molecular and cellular mechanisms of itch and the involvement of TRP channels in the peripheral sensory nervous system and skin. *Allergology International*, **66**: 22–30.

Kobayashi, K., Fukuoka, T., Obata, K., Yamanaka, H., Dai, Y., Tokunaga, A., Noguchi, K. (2005). Distinct expression of TRPM8, TRPA1, and TRPV1 mRNAs in rat primary afferent neurons with A δ /C-fibers and colocalization with Trk receptors. *Journal of Comparative Neurology*, **493**: 596–606.

Kobayashi, T., Glatz, M., Horiuchi, K., Kawasaki, H., Akiyama, H., Kaplan, D.H., Kong, H.H., Amagai, M., Nagao, K. (2015). Dysbiosis and *Staphylococcus aureus* Colonization Drives Inflammation in Atopic Dermatitis. *Immunity*, **42**: 756–766.

Koch, S.C., Acton, D., Goulding, M. (2018). Spinal Circuits for Touch, Pain, and Itch. *Annual Review of Physiology*, **80**: 189–217.

Koike, Y., Yozaki, M., Utani, A., Murota, H. (2020). Fibroblast growth factor 2 accelerates the epithelial–mesenchymal transition in keratinocytes during wound healing process. *Scientific Reports*, **10**: 1–13.

Köllisch, G., Kalali, B.N., Voelcker, V., Wallich, R., Behrendt, H., Ring, J., Bauer, S., Jakob, T., Mempel, M., Ollert, M. (2005). Various members of the Toll-like receptor family contribute to the innate immune response of human epidermal keratinocytes. *Immunology*, **114**: 531–541.

Komai-Koma, M., Brombacher, F., Pushparaj, P.N., Arendse, B., McSharry, C., Alexander, J., Chaudhuri, R., Thomson, N.C., McKenzie, A.N.J., McInnes, I., Liew, F.Y., Xu, D. (2012). Interleukin-33 amplifies IgE synthesis and triggers mast cell degranulation via interleukin-4 in naïve mice. *Allergy: European Journal of Allergy and Clinical Immunology*, **67**: 1118–1126.

Komatsu, N., Saijoh, K., Kuk, C., Liu, A.C., Khan, S., Shirasaki, F., Takehara, K., Diamandis, E.P. (2007). Human tissue kallikrein expression in the stratum corneum and serum of atopic dermatitis patients. *Experimental Dermatology*, **16**: 513–519.

Kondo, Y., Yoshimoto, T., Yasuda, K., Futatsugi-yumikura, S., Morimoto, M., Hayashi, N., Hoshino, T., Fujimoto, J., Nakanishi, K. (2008). Administration of IL-33 induces airway hyperresponsiveness and goblet cell hyperplasia in the lungs in the absence of adaptive immune system. *International Immunology*, **20**: 791–800.

Kong, H.H., Oh, J., Deming, C., Conlan, S., Grice, E.A., Beatson, M.A., Nomicos, E., Polley, E.C., Komarow, H.D., Mullikin, J., Thomas, J., Blakesley, R., Young, A., Chu, G., Ramsahoye, C., Lovett, S., Han, J., Legaspi, R., Sison, C., Montemayor, C., Gregory, M., Hargrove, A., Johnson, T., Riebow, N., Schmidt, B., Novotny, B., Gupta, J., Benjamin, B., Brooks, S., Coleman, H., Ho, S.L., Schandler, K., Stantripop, M., Maduro, Q., Bouffard, G., Dekhtyar, M., Guan, X., Masiello, C., Maskeri, B., McDowell, J., Park, M., Vemulapalli, M., Murray, P.R., Turner, M.L., Segre, J.A. (2012). Temporal shifts in the skin microbiome associated with disease flares and treatment in children with atopic dermatitis. *Genome Research*, **22**: 850–859.

Koppes, S.A., Charles, F., Lammers, L.A., Frings-Dresen, M., Kezic, S., Rustemeyer, T. (2016). Efficacy of a cream containing ceramides and magnesium in the treatment of mild to moderate atopic dermatitis: A randomized, double-blind, emollient- and hydrocortisone-controlled trial. *Acta Dermato-Venereologica*, **96**: 948–953.

- Korosec, A., Frech, S., Gesslbauer, B., Vierhapper, M., Radtke, C., Petzelbauer, P., Lichtenberger, B.M. (2019). Lineage Identity and Location within the Dermis Determine the Function of Papillary and Reticular Fibroblasts in Human Skin. *Journal of Investigative Dermatology*, **139**: 342–351.
- Korsunsky, I., Wei, K., Pohin, M., Kim, E.Y., Barone, F., Major, T., Taylor, E., Ravindran, R., Kemble, S., Watts, G.F.M., Jonsson, A.H., Jeong, Y., Athar, H., Windell, D., Kang, J.B., Friedrich, M., Turner, J., Nayar, S., Fisher, B.A., Raza, K., Marshall, J.L., Croft, A.P., Tamura, T., Sholl, L.M., Vivero, M., Rosas, I.O., Bowman, S.J., Coles, M., Frei, A.P., Lassen, K., Filer, A., Powrie, F., Buckley, C.D., Brenner, M.B., Raychaudhuri, S. (2022). Cross-tissue, single-cell stromal atlas identifies shared pathological fibroblast phenotypes in four chronic inflammatory diseases. *Med*, **3**: 481–518.
- Kozlova, N., Jensen, J.K., Chi, T.F., Samoylenko, A., Kietzmann, T. (2015). PAI-1 modulates cell migration in a LRP1-dependent manner via β -catenin and ERK1/2. *Thrombosis and Haemostasis*, **113**: 988–998.
- Krajnik, M., Zylicz, Z. (2001). Understanding pruritus in systemic disease. *Journal of Pain and Symptom Management*, **21**: 151–168.
- Kunisada, M., Hosaka, C., Takemori, C., Nakano, E., Nishigori, C. (2017). CXCL1 Inhibition Regulates UVB-Induced Skin Inflammation and Tumorigenesis in Xpa-Deficient Mice. *Journal of Investigative Dermatology*, **137**: 1975–1983.
- Kunysz, E.L., Michel, A.D., Whiting, R.L. (1988). Functional and direct binding studies using subtype selective muscarinic receptor antagonists. *British Journal of Pharmacology*, **93**: 491–500.
- Kwack, M.H., Kim, M.K., Kim, J.C., Sung, Y.K. (2012). Dickkopf 1 promotes regression of hair follicles. *Journal of Investigative Dermatology*, **132**: 1554–1560.
- Labarrade, F., Perrin, A., Ferreira, Y., Botto, J.M., Imbert, I. (2023). Modulation of Piezo1 influences human skin architecture and oxytocin expression. *International Journal of Cosmetic Science*, Online ahead of print.
- Lagunoff, D., Martin, T.W., Read, G. (1983). Agents that release histamine from mast cells. *Annual Review of Pharmacology and Toxicology*, **23**: 331–351.
- Lai-Cheong, J.E., Sethuraman, G., Ramam, M., Stone, K., Simpson, M.A., McGrath, J.A. (2012). Recurrent heterozygous missense mutation, p.Gly573Ser, in the TRPV3 gene in an Indian boy with sporadic Olmsted syndrome. *British Journal of Dermatology*, **167**: 440–442.
- Lai, Y., Cogen, A.L., Radek, K.A., Park, H.J., MacLeod, D.T., Leichtle, A., Ryan, A.F., Di Nardo, A., Gallo, R.L. (2010). Activation of TLR2 by a small molecule produced by staphylococcus epidermidis increases antimicrobial defense against bacterial skin infections. *Journal of Investigative Dermatology*, **130**: 2211–2221.
- Lange, T.S., Kirchberg, K., Bielinsky, A.K., Leuker, A., Bank, I., Ruzicka, T., Scharffetter-Kochanek, K. (1995). Divalent cations (Mg²⁺, Ca²⁺) differentially influence the β 1 integrin-mediated migration of human fibroblasts and keratinocytes to different extracellular matrix proteins. *Experimental Dermatology*, **4**: 130–137.
- Langley, R.G., Elewski, B.E., Lebwohl, M., Reich, K., Griffiths, C.E.M., Papp, K., Puig, L., Nakagawa, H., Spelman, L., Sigurgeirsson, B., Rivas, E., Tsai, T.-F., Wasel, N., Tying, S., Salko, T., Hampele, I., Notter, M., Karpov, A., Helou, S., Papavassilis, C. (2014). Secukinumab in Plaque Psoriasis — Results of Two Phase 3 Trials. *New England Journal of Medicine*, **371**: 326–338.
- Larkin, C., Chen, W., Szabó, I.L., Shan, C., Dajnoki, Z., Szegedi, A., Buhl, T., Fan, Y., O’Neill, S., Walls, D., Cheng, W., Xiao, S., Wang, J., Meng, J. (2021). Novel insights into the TRPV3-mediated itch in atopic dermatitis. *Journal of Allergy and Clinical Immunology*, **147**: 1110–1114.
- Larregue, M., Callot, V., Kaniakakis, J., Suau, A.M., Foret, M. (2000). Olmsted syndrome: Report of two new cases and literature review. *Journal of Dermatology*, **27**: 557–568.
- László, V., Rothe, G., Hegyesi, H., Szeberényi, J.B., Orsoó, E., Schmitz, G., Falus, A. (2001).

Increased histidine decarboxylase expression during in vitro monocyte maturation; a possible role of endogenously synthesised histamine in monocyte/macrophage differentiation. *Inflammation Research*, **50**: 428–434.

Lau, A., West, L., Tullius, S.G. (2018). The Impact of Sex on Alloimmunity. *Trends in Immunology*, **39**: 407–418.

Lay, M., Dong, X. (2020). Neural Mechanisms of Itch. *Annual Review of Neuroscience*, **43**: 187–205.

Lebre, M.C., Van Der Aar, A.M.G., Van Baarsen, L., Van Capel, T.M.M., Schuitemaker, J.H.N., Kapsenberg, M.L., De Jong, E.C. (2007). Human keratinocytes express functional toll-like receptor 3, 4, 5, and 9. *Journal of Investigative Dermatology*, **127**: 331–341.

Lee, H.J., Kim, M. (2022). Skin Barrier Function and the Microbiome. *International Journal of Molecular Sciences*, **23**: 13071.

Lee, S.H., Cho, P.S., Tonello, R., Lee, H.K., Jang, J.H., Park, G.Y., Hwang, S.W., Park, C.K., Jung, S.J., Berta, T. (2018). Peripheral serotonin receptor 2B and transient receptor potential channel 4 mediate pruritus to serotonergic antidepressants in mice. *Journal of Allergy and Clinical Immunology*, **142**: 1349–1352.

Lei, M., Chuong, C.M. (2016). Stem cells: Aging, alopecia, and stem cells. *Science*, **351**: 559–560.

Lembo, P.M.C., Grazzini, E., Groblewski, T., O'donnell, D., Roy, M.O., Zhang, J., Hoffert, C., Cao, J., Schmidt, R., Pelletier, M., Labarre, M., Gosselin, M., Fortin, Y., Banville, D., Shen, S.H., Ström, P., Payza, K., Dray, A., Walker, P., Ahmad, S. (2002). Proenkephalin A gene products activate a new family of sensory neuron-specific GPCRs. *Nature Neuroscience*, **5**: 201–209.

Leng, L., Ma, J., Sun, X., Guo, B., Li, F., Zhang, W., Chang, M., Diao, J., Wang, Yi, Wang, W., Wang, S., Zhu, Y., He, F., Reid, L.M., Wang, Yunfang. (2020). Comprehensive proteomic atlas of skin biomatrix scaffolds reveals a supportive microenvironment for epidermal development. *Journal of Tissue Engineering*, **11**: 2041731420972310.

Lewis, D.J., Chan, W.H., Hinojosa, T., Hsu, S., Feldman, S.R. (2019). Mechanisms of microbial pathogenesis and the role of the skin microbiome in psoriasis: A review. *Clinics in Dermatology*, **37**: 160–166.

Li, C., Ma, W., Yin, S., Liang, X., Shu, X., Pei, D., Egan, T.M., Huang, J., Pan, A., Li, Z. (2016). Sorting Nexin 11 Regulates Lysosomal Degradation of Plasma Membrane TRPV3. *Traffic*, **17**: 500–514.

Li, Changlin, Wang, S., Chen, Y., Zhang, X. (2018). Somatosensory Neuron Typing with High-Coverage Single-Cell RNA Sequencing and Functional Analysis. *Neuroscience Bulletin*, **34**: 200–207.

Li, J., Ma, J., Zhang, Q., Gong, H., Gao, D., Wang, Y., Li, B., Li, X., Zheng, H., Wu, Z., Zhu, Y., Leng, L. (2022). Spatially resolved proteomic map shows that extracellular matrix regulates epidermal growth. *Nature Communications*, **13**: 1–16.

Li, M., Du, J., Jiang, J., Ratzan, W., Su, L.T., Runnels, L.W., Yue, L. (2007). Molecular determinants of Mg²⁺ and Ca²⁺ permeability and pH sensitivity in TRPM6 and TRPM7. *Journal of Biological Chemistry*, **282**: 25817–25830.

Li, Mansheng, Li, X., Liu, B., Lv, L., Wang, W., Gao, D., Zhang, Q., Jiang, J., Chai, M., Yun, Z., Tan, Y., Gong, F., Wu, Z., Zhu, Y., Ma, J., Leng, L. (2021). Time-Resolved Extracellular Matrix Atlas of the Developing Human Skin Dermis. *Frontiers in Cell and Developmental Biology*, **9**: 3400.

Li, M., Messaddeq, N., Teletin, M., Pasquali, J.L., Metzger, D., Chambon, P. (2005). Retinoid X receptor ablation in adult mouse keratinocytes generates an atopic dermatitis triggered by thymic stromal lymphopoietin. *Proceedings of the National Academy of Sciences of the United States of America*, **102**: 14795–14800.

- Li, Qingyang, Zhu, Z., Wang, L., Lin, Y., Fang, H., Lei, J., Cao, T., Wang, G., Dang, E. (2021). Single-cell transcriptome profiling reveals vascular endothelial cell heterogeneity in human skin. *Theranostics*, **11**: 6461–6476.
- Li, Xueke, Yang, H., Han, Y., Yin, S., Shen, B., Wu, Y., Li, W., Cao, Z. (2021). Tick peptides evoke itch by activating MrgprC11/MRGPRX1 to sensitize TRPV1 in pruriceptors. *Journal of Allergy and Clinical Immunology*, **147**: 2236–2248.
- Li, Yongxi, Yu, H., Jin, Y., Li, M., Qu, C. (2018). Verbascoside Alleviates Atopic Dermatitis-Like Symptoms in Mice via Its Potent Anti-Inflammatory Effect. *International Archives of Allergy and Immunology*, **175**: 220–230.
- Liebe, H., Liebe, F., Sponder, G., Hedtrich, S., Stumpff, F. (2021). Beyond Ca²⁺ signalling: the role of TRPV3 in the transport of NH₄⁺. *Pflugers Archiv European Journal of Physiology*, **473**: 1859–1884.
- Lieu, T., Jayaweera, G., Zhao, P., Poole, D.P., Jensen, D., Grace, M., McIntyre, P., Bron, R., Wilson, Y.M., Krappitz, M., Haerteis, S., Korbmacher, C., Steinhoff, M.S., Nassini, R., Materazzi, S., Geppetti, P., Corvera, C.U., Bunnett, N.W. (2014). The bile acid receptor TGR5 activates the trpa1 channel to induce itch in mice. *Gastroenterology*, **147**: 1417–1428.
- Lijnen, H.R. (2005). Pleiotropic functions of plasminogen activator inhibitor-1. *Journal of Thrombosis and Haemostasis*, **3**: 35–45.
- Lim, M., Martinez, T., Jablons, D., Cameron, R., Guo, H., Toole, B., Li, J.D., Basbaum, C. (1998). Tumor-derived EMMPRIN (extracellular matrix metalloproteinase inducer) stimulates collagenase transcription through MAPK p38. *FEBS Letters*, **441**: 88–92.
- Lin, Q., Panchamukhi, A., Li, P., Shan, W., Zhou, H., Hou, L., Chen, W. (2021). Malassezia and Staphylococcus dominate scalp microbiome for seborrheic dermatitis. *Bioprocess and Biosystems Engineering*, **44**: 965–975.
- Lin, Z., Chen, Q., Lee, M., Cao, X., Zhang, J., Ma, D., Chen, L., Hu, X., Wang, H., Wang, X., Zhang, P., Liu, X., Guan, L., Tang, Y., Yang, H., Tu, P., Bu, D., Zhu, X., Wang, K., Li, R., Yang, Y. (2012). Exome sequencing reveals mutations in TRPV3 as a cause of Olmsted syndrome. *American Journal of Human Genetics*, **90**: 558–564.
- Ling, P., Ngo, K., Nguyen, S., Thurmond, R.L., Edwards, J.P., Karlsson, L., Fung-Leung, W.P. (2004). Histamine H4 receptor mediates eosinophil chemotaxis with cell shape change and adhesion molecule upregulation. *British Journal of Pharmacology*, **142**: 161–171.
- Lipkin, G., March, C., Gowdey, J. (1964). Magnesium in Epidermis, Dermis, and Whole Skin of Normal and Atopic Subjects. *The Journal of investigative dermatology*, **42**: 293–304.
- Liu, B., Escalera, J., Balakrishna, S., Fan, L., Caceres, A.I., Robinson, E., Sui, A., McKay, M.C., McAlexander, M.A., Herrick, C.A., Jordt, S.E. (2013). TRPA1 controls inflammation and pruritogen responses in allergic contact dermatitis. *FASEB Journal*, **27**: 3549–3563.
- Liu, B., Tai, Y., Achanta, S., Kaelberer, M.M., Caceres, A.I., Shao, X., Fang, J., Jordt, S.E. (2016). IL-33/ST2 signaling excites sensory neurons and mediates itch response in a mouse model of Poison ivy contact allergy. *Proceedings of the National Academy of Sciences of the United States of America*, **113**: 7572–7579.
- Liu, Beiying, Yao, J., Zhu, M.X., Qin, F. (2011). Hysteresis of gating underlines sensitization of TRPV3 channels. *Journal of General Physiology*, **138**: 509–520.
- Liu, C.S.C., Raychaudhuri, D., Paul, B., Chakrabarty, Y., Ghosh, A.R., Rahaman, O., Talukdar, A., Ganguly, D. (2018). Cutting Edge: Piezo1 Mechanosensors Optimize Human T Cell Activation. *The Journal of Immunology*, **200**: 1255–1260.
- Liu, Jiaqi, Xiao, Q., Xiao, J., Niu, C., Li, Y., Zhang, X., Zhou, Z., Shu, G., Yin, G. (2022). Wnt/ β -catenin signalling: function, biological mechanisms, and therapeutic opportunities. *Signal Transduction and Targeted Therapy*, **7**: 1–23.

- Liu, Q., Ranallo, R., Rios, C., Grice, E.A., Moon, K., Gallo, R.L. (2023). Crosstalk between skin microbiota and immune system in health and disease. *Nature Immunology*, **24**: 895–898.
- Liu, Q., Sikand, P., Ma, C., Tang, Z., Han, L., Li, Z., Sun, S., LaMotte, R.H., Dong, X. (2012). Mechanisms of itch evoked by β -alanine. *Journal of Neuroscience*, **32**: 14532–14537.
- Liu, Qingmei, Tang, Y., Huang, Y., Wang, Ji'an, Yang, K., Zhang, Yuting, Pu, W., Liu, J., Shi, X., Ma, Y., Ni, C., Zhang, Yue, Zhu, Y., Li, H., Wang, Jiucun, Lin, J., Wu, W. (2022). Insights into male androgenetic alopecia using comparative transcriptome profiling: hypoxia-inducible factor-1 and Wnt/ β -catenin signalling pathways*. *British Journal of Dermatology*, **187**: 936–947.
- Liu, Q., Tang, Z., Surdenikova, L., Kim, S., Patel, K.N., Kim, A., Ru, F., Guan, Y., Weng, H.J., Geng, Y., Undem, B.J., Kollarik, M., Chen, Z.F., Anderson, D.J., Dong, X. (2009). Sensory Neuron-Specific GPCR Mrgprs Are Itch Receptors Mediating Chloroquine-Induced Pruritus. *Cell*, **139**: 1353–1365.
- Liu, Q., Wang, J., Wei, X., Hu, J., Ping, C., Gao, Y., Xie, C., Wang, P., Cao, P., Cao, Z., Yu, Y., Li, D., Yao, J. (2021). Therapeutic inhibition of keratinocyte trpv3 sensory channel by local anesthetic dyclonine. *eLife*, **10**.
- Liu, Qin, Weng, H.J., Patel, K.N., Tang, Z., Bai, H., Steinhoff, M., Dong, X. (2011). The distinct roles of two GPCRs, MrgprC11 and PAR2, in itch and hyperalgesia. *Science Signaling*, **4**: 45.
- Liu, T., Li, S., Ying, S., Tang, S., Ding, Y., Li, Y., Qiao, J., Fang, H. (2020). The IL-23/IL-17 Pathway in Inflammatory Skin Diseases: From Bench to Bedside. *Frontiers in Immunology*, **11**: 2971.
- Liu, Y., Yang, F.C., Okuda, T., Dong, X., Zylka, M.J., Chen, C.L., Anderson, D.J., Kuner, R., Ma, Q. (2008). Mechanisms of compartmentalized expression of Mrg class G-protein-coupled sensory receptors. *Journal of Neuroscience*, **28**: 125–132.
- Lo, I.C., Chan, H.C., Qi, Z., Ng, K.L., So, C., Tsang, S.Y. (2016). TRPV3 Channel Negatively Regulates Cell Cycle Progression and Safeguards the Pluripotency of Embryonic Stem Cells. *Journal of Cellular Physiology*, **231**: 403–413.
- De Logu, F., Landini, L., Janal, M.N., Li Puma, S., De Cesaris, F., Geppetti, P., Nassini, R. (2019). Migraine-provoking substances evoke periorbital allodynia in mice. *Journal of Headache and Pain*, **20**: 18.
- Loh, T.Y., Hsiao, J.L., Shi, V.Y. (2020). Therapeutic potential of lebrikizumab in the treatment of atopic dermatitis. *Journal of Asthma and Allergy*, **13**: 109–114.
- Lonsdale, J., Thomas, J., Salvatore, M., Phillips, R., Lo, E., Shad, S., Hasz, R., Walters, G., Garcia, F., Young, N., Foster, B., Moser, M., Karasik, E., Gillard, B., Ramsey, K., Sullivan, S., Bridge, J., Magazine, H., Syron, J., Fleming, J., Siminoff, L., Traino, H., Mosavel, M., Barker, L., Jewell, S., Rohrer, D., Maxim, D., Filkins, D., Harbach, P., Cortadillo, E., Berghuis, B., Turner, L., Hudson, E., Feenstra, K., Sobin, L., Robb, J., Branton, P., Korzeniewski, G., Shive, C., Tabor, D., Qi, L., Groch, K., Nampally, S., Buia, S., Zimmerman, A., Smith, A., Burges, R., Robinson, K., Valentino, K., Bradbury, D., Cosentino, M., Diaz-Mayoral, N., Kennedy, M., Engel, T., Williams, P., Erickson, K., Ardlie, K., Winckler, W., Getz, G., DeLuca, D., Daniel MacArthur, Kellis, M., Thomson, A., Young, T., Gelfand, E., Donovan, M., Meng, Y., Grant, G., Mash, D., Marcus, Y., Basile, M., Liu, J., Zhu, J., Tu, Z., Cox, N.J., Nicolae, D.L., Gamazon, E.R., Im, H.K., Konkashbaev, A., Pritchard, J., Stevens, M., Flutre, T., Wen, X., Dermitzakis, E.T., Lappalainen, T., Guigo, R., Monlong, J., Sammeth, M., Koller, D., Battle, A., Mostafavi, S., McCarthy, M., Rivas, M., Maller, J., Rusyn, I., Nobel, A., Wright, F., Shabalina, A., Feolo, M., Sharopova, N., Sturcke, A., Paschal, J., Anderson, J.M., Wilder, E.L., Derr, L.K., Green, E.D., Struwing, J.P., Temple, G., Volpi, S., Boyer, J.T., Thomson, E.J., Guyer, M.S., Ng, C., Abdallah, A., Colantuoni, D., Insel, T.R., Koester, S.E., A Roger Little, Bender, P.K., Lehner, T., Yao, Y., Compton, C.C., Vaught, J.B., Sawyer, S., Lockhart, N.C., Demchok, J., Moore, H.F. (2013). The Genotype-Tissue Expression (GTEx) project. *Nature Genetics*, **45**: 580–585.
- Lu, D., Chen, L., Shi, X., Zhang, Xiaoting, Ling, X., Chen, X., Xie, L., Jiang, L., Ding, L., He, Y.,

- Zhang, Xingqi. (2013). A functional polymorphism in interleukin-1 α (IL1A) gene is associated with risk of alopecia areata in Chinese populations. *Gene*, **521**: 282–286.
- Luetteke, N.C., Phillips, H.K., Qiu, T.H., Copeland, N.G., Shelton Earp, H., Jenkins, N.A., Lee, D.C. (1994). The mouse waved-2 phenotype results from a point mutation in the EGF receptor tyrosine kinase. *Genes and Development*, **8**: 399–413.
- Luetteke, N.C., Qiu, T.H., Peiffer, R.L., Oliver, P., Smithies, O., Lee, D.C. (1993). TGF α deficiency results in hair follicle and eye abnormalities in targeted and waved-1 mice. *Cell*, **73**: 263–278.
- Luo, J., Feng, J., Liu, S., Walters, E.T., Hu, H. (2015). Molecular and cellular mechanisms that initiate pain and itch. *Cellular and Molecular Life Sciences*, **72**: 3201–3223.
- Luo, J., Feng, J., Yu, G., Yang, P., Mack, M.R., Du, J., Yu, W., Qian, A., Zhang, Y., Liu, S., Yin, S., Xu, A., Cheng, J., Liu, Qingyun, O’Neil, R.G., Xia, Y., Ma, L., Carlton, S.M., Kim, B.S., Renner, K., Liu, Qin, Hu, H. (2018). Transient receptor potential vanilloid 4-expressing macrophages and keratinocytes contribute differentially to allergic and nonallergic chronic itch. *Journal of Allergy and Clinical Immunology*, **141**: 608–619.
- Luo, J., Stewart, R., Berdeaux, R., Hu, H. (2012). Tonic inhibition of TRPV3 by Mg²⁺ in mouse epidermal keratinocytes. *Journal of Investigative Dermatology*, **132**: 2158–2165.
- Luostarinen, S., Hämäläinen, M., Moilanen, E. (2021). Transient receptor potential ankyrin 1 (Trpa1)—an inflammation-induced factor in human hacat keratinocytes. *International Journal of Molecular Sciences*, **22**: 3322.
- Lutsey, P.L., Cushman, M., Steffen, L.M., Green, D., Barr, R.G., Herrington, D., Ouyang, P., Folsom, A.R. (2006). Plasma hemostatic factors and endothelial markers in four racial/ethnic groups: The MESA study. *Journal of Thrombosis and Haemostasis*, **4**: 2629–2635.
- Ma, F., Plazyo, O., Billi, A.C., Tsoi, L.C., Xing, X., Wasikowski, R., Gharaee-Kermani, M., Hile, G., Jiang, Y., Harms, P.W., Xing, E., Kirma, J., Xi, J., Hsu, J.E., Sarkar, M.K., Chung, Y., Di Domizio, J., Gilliet, M., Ward, N.L., Maverakis, E., Klechevsky, E., Voorhees, J.J., Elder, J.T., Lee, J.H., Kahlenberg, J.M., Pellegrini, M., Modlin, R.L., Gudjonsson, J.E. (2023). Single cell and spatial sequencing define processes by which keratinocytes and fibroblasts amplify inflammatory responses in psoriasis. *Nature Communications*, **14**: 1–19.
- Ma, Q. (2010). Labeled lines meet and talk: Population coding of somatic sensations. *Journal of Clinical Investigation*, **120**: 3773–3778.
- Maccardle, R.C., Engman, M.F., Engman, M.F. (1941). XCII. Histology of neurodermatitis. *Archives of Dermatology and Syphilology*, **44**: 161–189.
- Mack, M.R., Kim, B.S. (2018). The Itch–Scratch Cycle: A Neuroimmune Perspective. *Trends in Immunology*, **39**: 980–991.
- Macpherson, L.J., Dubin, A.E., Evans, M.J., Marr, F., Schultz, P.G., Cravatt, B.F., Patapoutian, A. (2007). Noxious compounds activate TRPA1 ion channels through covalent modification of cysteines. *Nature*, **445**: 541–545.
- Mahmoud, E.A., Elgarhy, L.H., Hasby, E.A., Mohammad, L. (2019). Dickkopf-1 expression in androgenetic alopecia and alopecia areata in Male patients. *American Journal of Dermatopathology*, **41**: 122–127.
- Majhi, R.K., Sahoo, S.S., Yadav, M., Pratheek, B.M., Chattopadhyay, S., Goswami, C. (2015). Functional expression of TRPV channels in T cells and their implications in immune regulation. *FEBS Journal*, **282**: 2661–2681.
- Maksimovic, S., Nakatani, M., Baba, Y., Nelson, A.M., Marshall, K.L., Wellnitz, S.A., Firozi, P., Woo, S.H., Ranade, S., Patapoutian, A., Lumpkin, E.A. (2014). Epidermal Merkel cells are mechanosensory cells that tune mammalian touch receptors. *Nature*, **509**: 617–621.
- Mamolo, C., Bissonnette, R., Khan, S., Lan, S., Ports, W., Poulin, Y. (2013). An evaluation of the

- effect of topical tofacitinib (CP-690, 550) on pruritus and patient satisfaction with study medication in a phase IIA trial for plaque psoriasis. *Journal of the American Academy of Dermatology*, **68**: 192.
- Mandadi, S., Sokabe, T., Shibasaki, K., Katanosaka, K., Mizuno, A., Moqrich, A., Patapoutian, A., Fukumi-Tominaga, T., Mizumura, K., Tominaga, M. (2009). TRPV3 in keratinocytes transmits temperature information to sensory neurons via ATP. *Pflugers Archiv European Journal of Physiology*, **458**: 1093–1102.
- Mann, G.B., Fowler, K.J., Gabriel, A., Nice, E.C., Williams, R.L., Dunn, A.R. (1993). Mice with a null mutation of the TGF α gene have abnormal skin architecture, wavy hair, and curly whiskers and often develop corneal inflammation. *Cell*, **73**: 249–261.
- Mao, B., Wu, W., Li, Y., Hoppe, D., Stanek, P., Glinka, A., Niehrs, C. (2001). LDL-receptor-related protein 6 is a receptor for Dickkopf proteins. *Nature*, **411**: 321–325.
- Marson, J., Bhatia, N., Graber, E., Harper, J., Lio, P., Tlougan, B., Nussbaum, D., Baldwin, H. (2022). Supplement Article: The Role of Epidermal Barrier Dysfunction and Cutaneous Microbiome Dysbiosis in the Pathogenesis and Management of Acne Vulgaris and Rosacea. *Journal of drugs in dermatology : JDD*, **21**: SF3502915–SF35029114.
- Martin, G.R., Kleinman, H.K., Terranova, V.P., Ledbetter, S., Hassell, J.R. (1984). The regulation of basement membrane formation and cell-matrix interactions by defined supramolecular complexes. *Ciba Foundation symposium*, **108**: 197–212.
- Maruyama, T., Kanaji, T., Nakade, S., Kanno, T., Mikoshiba, K. (1997). 2APB, 2-aminoethoxydiphenyl borate, a membrane-penetrable modulator of Ins(1,4,5)P₃-induced Ca²⁺ release. *Journal of Biochemistry*, **122**: 498–505.
- Mashiko, S., Mehta, H., Bissonnette, R., Sarfati, M. (2017). Increased frequencies of basophils, type 2 innate lymphoid cells and Th2 cells in skin of patients with atopic dermatitis but not psoriasis. *Journal of Dermatological Science*, **88**: 167–174.
- Matsui, T., Amagai, M. (2017). Erratum: Dissecting the formation, structure and barrier function of the stratum corneum [Int. Immunol., 27, 6, (2015)(269-280)] DOI:10.1093/intimm/dxv013. *International Immunology*, **29**: 243–244.
- Matsumura, H., Mohri, Y., Morinaga, H., Fukuda, M., Kurata, S., Nishimura, E.K. (2017). Hair follicle aging is driven by transepidermal elimination of stem cells via COL17A1 proteolysis. *Journal of Dermatological Science*, **86**: 53.
- Matterne, U., Apfelbacher, C.J., Loerbroks, A., Schwarzer, T., Büttner, M., Ofenloch, R., Diepgen, T.L., Weisshaar, E. (2011). Prevalence, correlates and characteristics of chronic pruritus: A population-based cross-sectional study. *Acta Dermato-Venereologica*, **91**: 674–679.
- Matthews, K.A., Sowers, M.F., Derby, C.A., Stein, E., Miracle-McMahill, H., Crawford, S.L., Pasternak, R.C. (2005). Ethnic differences in cardiovascular risk factor burden among middle-aged women: Study of Women’s Health Across the Nation (SWAN). *American Heart Journal*, **149**: 1066–1073.
- Mayle, K.M., Le, A.M., Kamei, D.T. (2012). The intracellular trafficking pathway of transferrin. *Biochimica et Biophysica Acta - General Subjects*, **1820**: 264–281.
- McMahon, S.B., Koltzenburg, M. (1992). Itching for an explanation. *Trends in Neurosciences*, **15**: 497–501.
- McNeil, B.D., Pundir, P., Meeker, S., Han, L., Udem, B.J., Kulka, M., Dong, X. (2015). Identification of a mast-cell-specific receptor crucial for pseudo-allergic drug reactions. *Nature*, **519**: 237–241.
- Meng, J., Chen, W., Wang, J. (2020). Interventions in the B-type natriuretic peptide signalling pathway as a means of controlling chronic itch. *British Journal of Pharmacology*, **177**: 1025–1040.
- Meng, J., Moriyama, M., Feld, M., Buddenkotte, J., Buhl, T., Szöllösi, A., Zhang, J., Miller, P.,

- Ghetti, A., Fischer, M., Reeh, P.W., Shan, C., Wang, J., Steinhoff, M. (2018). New mechanism underlying IL-31-induced atopic dermatitis. *Journal of Allergy and Clinical Immunology*, **141**: 1677–1689.
- Meng, J., Wang, J., Buddenkotte, J., Buhl, T., Steinhoff, M. (2019). Role of SNAREs in Atopic Dermatitis-Related Cytokine Secretion and Skin-Nerve Communication. *Journal of Investigative Dermatology*, **139**: 2324–2333.
- Meng, J., Wang, J., Steinhoff, M., Dolly, J.O. (2016). TNF α induces co-trafficking of TRPV1/TRPA1 in VAMP1-containing vesicles to the plasmalemma via Munc18-1/syntaxin1/SNAP-25 mediated fusion. *Scientific Reports*, **6**: 1–15.
- Metcalf, D.D., Baram, D., Mekori, Y.A. (1997). Mast cells. *Physiological Reviews*, **77**: 1033–1079.
- Mevorah, B., Goldberg, I., Sprecher, E., Bergman, R., Metzker, A., Luria, R., Gat, A., Brenner, S. (2005). Olmsted syndrome: Mutilating palmoplantar keratoderma with periorificial keratotic plaques. *Journal of the American Academy of Dermatology*, **53**: 266–272.
- Meyer, T., Begitt, A., Vinkemeier, U. (2007). Green fluorescent protein-tagging reduces the nucleocytoplasmic shuttling specifically of unphosphorylated STAT1. *FEBS Journal*, **274**: 815–826.
- Migliorini, P., Italiani, P., Pratesi, F., Puxeddu, I., Boraschi, D. (2020). The IL-1 family cytokines and receptors in autoimmune diseases. *Autoimmunity Reviews*, **19**: 102617.
- Mikesell, A.R., Isaeva, O., Moehring, F., Sadler, K.E., Menzel, A.D., Stucky, C.L. (2022). Keratinocyte PIEZO1 modulates cutaneous mechanosensation. *eLife*, **11**.
- Min, J.K., Han, K.Y., Kim, E.C., Kim, Y.M., Lee, S.W., Kim, O.H., Kim, K.W., Gho, Y.S., Kwon, Y.G. (2004). Capsaicin Inhibits in Vitro and in Vivo Angiogenesis. *Cancer Research*, **64**: 644–651.
- Misery, L., Brenaut, E., Le Garrec, R., Abasq, C., Genestet, S., Marcorelles, P., Zagnoli, F. (2014). Neuropathic pruritus. *Nature Reviews Neurology*, **10**: 408–416.
- Mishra, S.K., Hoon, M.A. (2010). Ablation of TrpV1 neurons reveals their selective role in thermal pain sensation. *Molecular and Cellular Neuroscience*, **43**: 157–163.
- Mishra, S.K., Hoon, M.A. (2013). The cells and circuitry for itch responses in mice. *Science*, **340**: 968–971.
- Mishra, S.K., Tisel, S.M., Orestes, P., Bhangoo, S.K., Hoon, M.A. (2011). TRPV1-lineage neurons are required for thermal sensation. *EMBO Journal*, **30**: 582–593.
- Miyamoto, T., Petrus, M.J., Dubin, A.E., Patapoutian, A. (2011). TRPV3 regulates nitric oxide synthase-independent nitric oxide synthesis in the skin. *Nature Communications*, **2**: 1–12.
- Mohamed-Ali, V., Pinkney, J.H., Coppack, S.W. (1998). Adipose tissue as an endocrine and paracrine organ. *International Journal of Obesity*, **22**: 1145–1158.
- Mölter, J., Avitan, L., Goodhill, G.J. (2018). Detecting neural assemblies in calcium imaging data. *BMC Biology*, **16**: 143.
- Montell, C., Birnbaumer, L., Flockerzi, V. (2002). The TRP channels, a remarkably functional family. *Cell*, **108**: 595–598.
- Moore, C., Gupta, R., Jordt, S.E., Chen, Y., Liedtke, W.B. (2018). Regulation of Pain and Itch by TRP Channels. *Neuroscience Bulletin*, **34**: 120–142.
- Moqrich, A., Hwang, S.W., Earley, T.J., Petrus, M.J., Murray, A.N., Spencer, K.S.R., Andahazy, M., Story, G.M., Patapoutian, A. (2005). Impaired thermosensation in mice lacking TRPV3, a heat and camphor sensor in the skin. *Science*, **307**: 1468–1472.
- Morginson, W.J., Rich, C.O., Eskelson, Y.D., Kirkman, L.W., Utterback, M., Burton, A.M., Coletti, J.M. (1956). Dyclonine hydrochloride: a new topical antipruritic agent. *Postgraduate medicine*, **19**: 605–607.

- Morita, T., McClain, S.P., Batia, L.M., Pellegrino, M., Wilson, S.R., Kienzler, M.A., Lyman, K., Olsen, A.S.B., Wong, J.F., Stucky, C.L., Brem, R.B., Bautista, D.M. (2015). HTR7 Mediates Serotonergic Acute and Chronic Itch. *Neuron*, **87**: 124–138.
- Moriyama, T., Higashi, T., Togashi, K., Iida, T., Segi, E., Sugimoto, Y., Tominaga, T., Narumiya, S., Tominaga, M. (2005). Sensitization of TRPV1 by EP1 and IP reveals peripheral nociceptive mechanism of prostaglandins. *Molecular Pain*, **1**: 3.
- Morizane, S., Yamasaki, K., Kajita, A., Ikeda, K., Zhan, M., Aoyama, Y., Gallo, R.L., Iwatsuki, K. (2012). TH2 cytokines increase kallikrein 7 expression and function in patients with atopic dermatitis. *Journal of Allergy and Clinical Immunology*, **130**: 259–261.
- Moro, K., Yamada, T., Tanabe, M., Takeuchi, T., Ikawa, T., Kawamoto, H., Furusawa, J.I., Ohtani, M., Fujii, H., Koyasu, S. (2010). Innate production of TH 2 cytokines by adipose tissue-associated c-Kit⁺ Sca-1⁺ lymphoid cells. *Nature*, **463**: 540–544.
- Moses, L., Pachter, L. (2022). Museum of spatial transcriptomics. *Nature Methods*, **19**: 534–546.
- Mosley, B., Urdal, D.L., Prickett, K.S. (1987). The interleukin-1 receptor binds the human interleukin-1 α precursor but not the interleukin-1 β precursor. *Journal of Biological Chemistry*, **262**: 1–4.
- Murillas, R., Larcher, F., Conti, C.J., Santos, M., Ullrich, A., Jorcano, J.L. (1995). Expression of a dominant negative mutant of epidermal growth factor receptor in the epidermis of transgenic mice elicits striking alterations in hair follicle development and skin structure. *EMBO Journal*, **14**: 5216–5223.
- Murphy-Ullrich, J.E. (2019). Thrombospondin 1 and Its Diverse Roles as a Regulator of Extracellular Matrix in Fibrotic Disease. *Journal of Histochemistry and Cytochemistry*, **67**: 683–699.
- Naba, A., Clauser, K.R., Ding, H., Whittaker, C.A., Carr, S.A., Hynes, R.O. (2016). The extracellular matrix: Tools and insights for the ‘omics’ era. *Matrix Biology*, **49**: 10–24.
- Naba, A., Clauser, K.R., Hoersch, S., Liu, H., Carr, S.A., Hynes, R.O. (2012). The matrisome: In silico definition and in vivo characterization by proteomics of normal and tumor extracellular matrices. *Molecular and Cellular Proteomics*, **11**: M111.014647.
- Nakamura, N., Tamagawa-Mineoka, R., Yasuie, R., Masuda, K., Matsunaka, H., Murakami, Y., Yokosawa, E., Katoh, N. (2019). Stratum corneum interleukin-33 expressions correlate with the degree of lichenification and pruritus in atopic dermatitis lesions. *Clinical Immunology*, **201**: 1–3.
- Nakatsuji, T., Chen, T.H., Two, A.M., Chun, K.A., Narala, S., Geha, R.S., Hata, T.R., Gallo, R.L. (2016). Staphylococcus aureus Exploits Epidermal Barrier Defects in Atopic Dermatitis to Trigger Cytokine Expression. *Journal of Investigative Dermatology*, **136**: 2192–2200.
- Nattkemper, L.A., Tey, H.L., Valdes-Rodriguez, R., Lee, H., Mollanazar, N.K., Albornoz, C., Sanders, K.M., Yosipovitch, G. (2018). The Genetics of Chronic Itch: Gene Expression in the Skin of Patients with Atopic Dermatitis and Psoriasis with Severe Itch. *Journal of Investigative Dermatology*, **138**: 1311–1317.
- Nauroy, P., Barruche, V., Marchand, L., Nindorera-Badara, S., Bordes, S., Closs, B., Ruggiero, F. (2017). Human Dermal Fibroblast Subpopulations Display Distinct Gene Signatures Related to Cell Behaviors and Matrisome. *Journal of Investigative Dermatology*, **137**: 1787–1789.
- Nauroy, P., Nyström, A. (2020). Kallikreins: Essential epidermal messengers for regulation of the skin microenvironment during homeostasis, repair and disease. *Matrix Biology Plus*, **6–7**: 100019.
- Neckermann, G., Bavandi, A., Meingassner, J.G. (2000). Atopic dermatitis-like symptoms in hypomagnesaemic hairless rats are prevented and inhibited by systemic or topical SDZ ASM 981. *British Journal of Dermatology*, **142**: 669–679.
- Neuberger, A., Nadezhdin, K.D., Zakharian, E., Sobolevsky, A.I. (2021). Structural mechanism of TRPV3 channel inhibition by the plant-derived coumarin osthole. *EMBO reports*, **22**: 53233.

- Nguyen, N.D., Memon, T.A., Burrell, K.L., Almestica-Roberts, M., Rapp, E., Sun, L., Scott, A.F., Rower, J.E., Deering-Rice, C.E., Reilly, C.A. (2020). Transient receptor potential ankyrin-1 and vanilloid-3 differentially regulate endoplasmic reticulum stress and cytotoxicity in human lung epithelial cells after pneumotoxic wood smoke particle exposure. *Molecular Pharmacology*, **98**: 586–597.
- Nilius, B., Vriens, J., Prenen, J., Droogmans, G., Voets, T. (2004). TRPV4 calcium entry channel: A paradigm for gating diversity. *American Journal of Physiology - Cell Physiology*, **286**: 195–205.
- Niyonsaba, F., Ushio, H., Hara, M., Yokoi, H., Tominaga, M., Takamori, K., Kajiwar, N., Saito, H., Nagaoka, I., Ogawa, H., Okumura, K. (2010). Antimicrobial Peptides Human β -Defensins and Cathelicidin LL-37 Induce the Secretion of a Pruritogenic Cytokine IL-31 by Human Mast Cells. *The Journal of Immunology*, **184**: 3526–3534.
- Nofal, A., Assaf, M., Nassar, A., Nofal, E., Shehab, M., El-Kabany, M. (2010). Nonmutilating palmoplantar and periorificial keratoderma: A variant of Olmsted syndrome or a distinct entity? *International Journal of Dermatology*, **49**: 658–665.
- Nyström, A., Bruckner-Tuderman, L. (2019). Matrix molecules and skin biology. *Seminars in Cell and Developmental Biology*, **89**: 136–146.
- O'Donnell, B.L., Sanchez-Pupo, R.E., Sayedyahosseini, S., Karimi, M., Bahmani, M., Zhang, C., Johnston, D., Kelly, J.J., Wakefield, C.B., Barr, K., Dagnino, L., Penuela, S. (2023). PANX3 Channels Regulate Architecture, Adhesion, Barrier Function, and Inflammation in the Skin. *Journal of Investigative Dermatology*, **143**: 1509–1519.
- Oetjen, L.K., Mack, M.R., Feng, J., Whelan, T.M., Niu, H., Guo, C.J., Chen, S., Trier, A.M., Xu, A.Z., Tripathi, S. V., Luo, J., Gao, X., Yang, L., Hamilton, S.L., Wang, P.L., Brestoff, J.R., Council, M.L., Brasington, R., Schaffer, A., Brombacher, F., Hsieh, C.S., Gereau, R.W., Miller, M.J., Chen, Z.F., Hu, H., Davidson, S., Liu, Q., Kim, B.S. (2017). Sensory Neurons Co-opt Classical Immune Signaling Pathways to Mediate Chronic Itch. *Cell*, **171**: 217–228.
- Oh, M.-H., Oh, S.Y., Lu, J., Lou, H., Myers, A.C., Zhu, Z., Zheng, T. (2013). TRPA1-Dependent Pruritus in IL-13–Induced Chronic Atopic Dermatitis. *The Journal of Immunology*, **191**: 5371–5382.
- Ohta, T., Imagawa, T., Ito, S. (2007). Novel agonistic action of mustard oil on recombinant and endogenous porcine transient receptor potential V1 (pTRPV1) channels. *Biochemical Pharmacology*, **73**: 1646–1656.
- Okubo, A., Uchida, Y., Higashi, Y., Sato, T., Ogawa, Y., Ryuge, A., Kadomatsu, K., Kanekura, T. (2022). CD147 is essential for the development of psoriasis via the induction of th17 cell differentiation. *International Journal of Molecular Sciences*, **23**: 177.
- Olmsted, H.C. (1927). Keratoderma Palmaris Et Plantaris Congenitalis. *American Journal of Diseases of Children*, **33**: 757.
- Ommori, R., Ojji, N., Mizuno, F., Kita, E., Ikada, Y., Asada, H. (2013). Selective induction of antimicrobial peptides from keratinocytes by staphylococcal bacteria. *Microbial Pathogenesis*, **56**: 35–39.
- Ommori, R., Park, K., Miyagawa, F., Azukizawa, H., Kanno, M., Asada, H. (2018). Epidermal growth factor receptor (EGFR) inhibitory monoclonal antibodies and EGFR tyrosine kinase inhibitors have distinct effects on the keratinocyte innate immune response. *British Journal of Dermatology*, **178**: 796–797.
- Ostadhadi, S., Foroutan, A., Momeny, M., Norouzi-Javidan, A., Azimi, E., Kordjazy, N., Dehpour, A.R. (2016). Evidence for the involvement of nitric oxide in cholestasis-induced itch associated response in mice. *Biomedicine and Pharmacotherapy*, **84**: 1367–1374.
- Ostadhadi, S., Haj-Mirzaian, A., Azimi, E., Mansouri, P., Dehpour, A.R. (2015). Involvement of nitric oxide in serotonin-induced scratching in mice. *Clinical and Experimental Dermatology*, **40**: 647–652.

Pan, H., Fatima, M., Li, A., Lee, H., Cai, W., Horwitz, L., Hor, C.C., Zaher, N., Cin, M., Slade, H., Huang, T., Xu, X.Z.S., Duan, B. (2019). Identification of a Spinal Circuit for Mechanical and Persistent Spontaneous Itch. *Neuron*, **103**: 1135–1149.

Di Paolo, N.C., Shayakhmetov, D.M. (2016). Interleukin 1 α and the inflammatory process. *Nature Immunology*, **17**: 906–913.

Park, C.W., Kim, H.J., Choi, Y.W., Chung, B.Y., Woo, S.Y., Song, D.K., Kim, H.O. (2017). TRPV3 channel in keratinocytes in scars with post-burn pruritus. *International Journal of Molecular Sciences*, **18**: 2425.

Peier, A.M., Reeve, A.J., Andersson, D.A., Moqrich, A., Earley, T.J., Hergarden, A.C., Story, G.M., Colley, S., Hogenesch, J.B., McIntyre, P., Bevan, S., Patapoutian, A. (2002). A heat-sensitive TRP channel expressed in keratinocytes. *Science*, **296**: 2046–2049.

Peng, C., Zhang, S., Lei, L., Zhang, X., Jia, X., Luo, Z., Huang, X., Kuang, Y., Zeng, W., Su, J., Chen, X. (2017). Epidermal CD147 expression plays a key role in IL-22-induced psoriatic dermatitis. *Scientific Reports*, **7**: 44172.

Penuela, S., Bhalla, R., Gong, X.Q., Cowan, K.N., Celetti, S.J., Cowan, B.J., Bai, D., Shao, Q., Laird, D.W. (2007). Pannexin 1 and pannexin 3 are glycoproteins that exhibit many distinct characteristics from the connexin family of gap junction proteins. *Journal of Cell Science*, **120**: 3772–3783.

Perez, G.I.P., Gao, Z., Jourdain, R., Ramirez, J., Gany, F., Clavaud, C., Demaude, J., Breton, L., Blaser, M.J. (2016). Body site is a more determinant factor than human population diversity in the healthy skin microbiome. *PLoS ONE*, **11**: 151990.

Pezzolo, E., Naldi, L. (2020). Epidemiology of major chronic inflammatory immune-related skin diseases in 2019. *Expert Review of Clinical Immunology*, **16**: 155–166.

Phelps, C.B., Wang, R.R., Choo, S.S., Gaudet, R. (2010). Differential regulation of TRPV1, TRPV3, and TRPV4 sensitivity through a conserved binding site on the ankyrin repeat domain. *Journal of Biological Chemistry*, **285**: 731–740.

Philippeos, C., Telerman, S.B., Oulès, B., Pisco, A.O., Shaw, T.J., Elgueta, R., Lombardi, G., Driskell, R.R., Soldin, M., Lynch, M.D., Watt, F.M. (2018). Spatial and Single-Cell Transcriptional Profiling Identifies Functionally Distinct Human Dermal Fibroblast Subpopulations. *Journal of Investigative Dermatology*, **138**: 811–825.

Pirazzini, M., Rossetto, O., Eleopra, R., Montecucco, C. (2017). Botulinum neurotoxins: Biology, pharmacology, and toxicology. *Pharmacological Reviews*, **69**: 200–235.

Piscitelli, S.C., Pavel, A.B., McHale, K., Jett, J.E., Collins, J., Gillmor, D., Tabolt, G., Li, R., Song, T., Zhang, N., Tallman, A.M., Guttman-Yassky, E. (2021). A Phase 1b, Randomized, Single-Center Trial of Topical Cerdulatinib (DMVT-502) in Patients with Mild-to-Moderate Atopic Dermatitis. *Journal of Investigative Dermatology*, **141**: 1847–1851.

Pogatzki-Zahn, E.M., Pereira, M.P., Cremer, A., Zeidler, C., Dreyer, T., Riepe, C., Wempe, C., Lotts, T., Segelcke, D., Ringkamp, M., Kremer, A.E., Agelopoulos, K., Ständer, S. (2020). Peripheral Sensitization and Loss of Descending Inhibition Is a Hallmark of Chronic Pruritus. *Journal of Investigative Dermatology*, **140**: 203–211.

Pop, T.L., Sîrbe, C., Bența, G., Mititelu, A., Grama, A. (2022). The Role of Vitamin D and Vitamin D Binding Protein in Chronic Liver Diseases. *International Journal of Molecular Sciences*, **23**: 10705.

Prescott, S.A., Ma, Q., De Koninck, Y. (2014). Normal and abnormal coding of somatosensory stimuli causing pain. *Nature Neuroscience*, **17**: 183–191.

Proksch, E., Nissen, H.P., Bremgartner, M., Urquhart, C. (2005). Bathing in a magnesium-rich Dead Sea salt solution improves skin barrier function, enhances skin hydration, and reduces inflammation in atopic dry skin. *International Journal of Dermatology*, **44**: 151–157.

- Provitera, V., Nolano, M., Pagano, A., Caporaso, G., Stancanelli, A., Santoro, L. (2007). Myelinated nerve endings in human skin. *Muscle and Nerve*, **35**: 767–775.
- Qi, H., Shi, Y., Wu, H., Niu, C., Sun, X., Wang, K.W. (2022). Inhibition of temperature-sensitive TRPV3 channel by two natural isochlorogenic acid isomers for alleviation of dermatitis and chronic pruritus. *Acta Pharmaceutica Sinica B*, **12**: 723–734.
- Qu, Y., Wang, G., Sun, X., Wang, K.W. (2019). Inhibition of the warm temperature-activated Ca²⁺-permeable transient receptor potential vanilloid TRPV3 channel attenuates atopic dermatitis. *Molecular Pharmacology*, **96**: 393–400.
- Ranade, S.S., Woo, S.H., Dubin, A.E., Moshourab, R.A., Wetzel, C., Petrus, M., Mathur, J., Bégay, V., Coste, B., Mainquist, J., Wilson, A.J., Francisco, A.G., Reddy, K., Qiu, Z., Wood, J.N., Lewin, G.R., Patapoutian, A. (2014). Piezo2 is the major transducer of mechanical forces for touch sensation in mice. *Nature*, **516**: 121–125.
- Rau, K.K., McIlwrath, S.L., Wang, H., Lawson, J.J., Jankowski, M.P., Zylka, M.J., Anderson, D.J., Koerber, H.R. (2009). Mrgprd enhances excitability in specific populations of cutaneous murine polymodal nociceptors. *Journal of Neuroscience*, **29**: 8612–8619.
- Reddy, V.B., Iuga, A.O., Shimada, S.G., LaMotte, R.H., Lerner, E.A. (2008). Cowhage-evoked itch is mediated by a novel cysteine protease: A ligand of protease-activated receptors. *Journal of Neuroscience*, **28**: 4331–4335.
- Reddy, V.B., Shimada, S.G., Sikand, P., Lamotte, R.H., Lerner, E.A. (2010). Cathepsin S elicits itch and signals via protease-activated receptors. *Journal of Investigative Dermatology*, **130**: 1468–1470.
- Reddy, V.B., Sun, S., Azimi, E., Elmariah, S.B., Dong, X., Lerner, E.A. (2015). Redefining the concept of protease-activated receptors: Cathepsin S evokes itch via activation of Mrgprs. *Nature Communications*, **6**: 1–10.
- Reynders, A., Moqrich, A. (2015). Analysis of cutaneous MRGPRD free nerve endings and C-LTMRs transcriptomes by RNA-sequencing. *Genomics Data*, **5**: 132–135.
- Rivers, J.K., Duke, E.E., Justus, D.W. (1985). Etretnate: Management of keratoma hereditaria mutilans in four family members. *Journal of the American Academy of Dermatology*, **13**: 43–49.
- Rognoni, E., Gomez, C., Pisco, A.O., Rawlins, E.L., Simons, B.D., Watt, F.M., Driskell, R.R. (2016). Inhibition of β -catenin signalling in dermal fibroblasts enhances hair follicle regeneration during wound healing. *Development (Cambridge)*, **143**: 2522–2535.
- Roosterman, D., Goerge, T., Schneider, S.W., Bunnett, N.W., Steinhoff, M. (2006). Neuronal control of skin function: The skin as a neuroimmunoendocrine organ. *Physiological Reviews*, **86**: 1309–1379.
- Rossbach, K., Nassenstein, C., Gschwandtner, M., Schnell, D., Sander, K., Seifert, R., Stark, H., Kietzmann, M., Bäumer, W. (2011). Histamine H₁, H₃ and H₄ receptors are involved in pruritus. *Neuroscience*, **190**: 89–102.
- Rothman, S. (1922). Beiträge zur Physiologie der Juckempfindung. *Archiv für Dermatologie und Syphilis*, **139**: 227–234.
- ROWLEY, D.A., BENDITT, E.P. (1956). 5-Hydroxytryptamine and histamine as mediators of the vascular injury produced by agents which damage mast cells in rats. *The Journal of experimental medicine*, **103**: 399–412.
- Ru, F., Sun, H., Jurcakova, D., Herbstsomer, R.A., Meixong, J., Dong, X., Udem, B.J. (2017). Mechanisms of pruritogen-induced activation of itch nerves in isolated mouse skin. *Journal of Physiology*, **595**: 3651–3666.
- Ruzicka, T., Hanifin, J.M., Furue, M., Pulka, G., Mlynarczyk, I., Wollenberg, A., Galus, R., Etoh, T., Mihara, R., Yoshida, H., Stewart, J., Kabashima, K. (2017). Anti-Interleukin-31 Receptor A Antibody for Atopic Dermatitis. *New England Journal of Medicine*, **376**: 826–835.

- Sahu, R.P., Goswami, C. (2023). Presence of TRPV3 in macrophage lysosomes helps in skin wound healing against bacterial infection. *Experimental Dermatology*, **32**: 60–74.
- Sakai, K., Akiyama, T. (2020). New insights into the mechanisms behind mechanical itch. *Experimental Dermatology*, **29**: 680–686.
- Sakai, S., Kawakami, K. (2007). Synthesis and characterization of both ionically and enzymatically cross-linkable alginate. *Acta Biomaterialia*, **3**: 495–501.
- Sameshima, T., Nabeshima, K., Toole, B.P., Yokogami, K., Okada, Y., Goya, T., Koono, M., Wakisaka, S. (2000). Glioma cell extracellular matrix metalloproteinase inducer (EMMPRN) (CD147) stimulates production of membrane-type matrix metalloproteinases and activated gelatinase A in co-cultures with brain-derived fibroblasts. *Cancer Letters*, **157**: 177–184.
- Sanchez-Pupo, R.E., O'Donnell, B.L., Johnston, D., Gyenis, L., Litchfield, D.W., Penuela, S. (2022). Pannexin 2 is expressed in murine skin and promotes UVB-induced apoptosis of keratinocytes. *Molecular Biology of the Cell*, **33**: 1–14.
- Sanders, K.M., Nattkemper, L.A., Rosen, J.D., Andersen, H.H., Hsiang, J., Romanelli, P., Bernigaud, C., Guillot, J., Chosidow, O., Yosipovitch, G. (2019). Non-Histaminergic Itch Mediators Elevated in the Skin of a Porcine Model of Scabies and of Human Scabies Patients. *Journal of Investigative Dermatology*, **139**: 971–973.
- Sanjel, B., Maeng, H.J., Shim, W.S. (2019). BAM8-22 and its receptor MRGPRX1 may attribute to cholestatic pruritus. *Scientific Reports*, **9**: 1–13.
- Saotome, K., Murthy, S.E., Kefauver, J.M., Whitwam, T., Patapoutian, A., Ward, A.B. (2018). Structure of the mechanically activated ion channel Piezo1. *Nature*, **554**: 481–486.
- Savage, S.R., Zhang, B. (2020). Using phosphoproteomics data to understand cellular signaling: A comprehensive guide to bioinformatics resources. *Clinical Proteomics*, **17**: 1–18.
- Savin, J.A. (1998). How should we define itching? *Journal of the American Academy of Dermatology*, **39**: 268–269.
- Savinko, T., Matikainen, S., Saarialho-Kere, U., Lehto, M., Wang, G., Lehtimäki, S., Karisola, P., Reunala, T., Wolff, H., Lauerma, A., Alenius, H. (2012). IL-33 and ST2 in atopic dermatitis: Expression profiles and modulation by triggering factors. *Journal of Investigative Dermatology*, **132**: 1392–1400.
- Sawada, Y., Hosokawa, H., Matsumura, K., Kobayashi, S. (2008). Activation of transient receptor potential ankyrin 1 by hydrogen peroxide. *European Journal of Neuroscience*, **27**: 1131–1142.
- Schmeer, K.K., Tarrence, J. (2018). Racial-ethnic Disparities in Inflammation: Evidence of Weathering in Childhood? *Journal of Health and Social Behavior*, **59**: 411–428.
- Schmelz, M., Schmidt, R., Bickel, A., Handwerker, H.O., Torebjörk, H.E. (1997). Specific C-receptors for itch in human skin. *Journal of Neuroscience*, **17**: 8003–8008.
- Schmidt, B.A., Horsley, V. (2013). Intradermal adipocytes mediate fibroblast recruitment during skin wound healing. *Development (Cambridge)*, **140**: 1517–1527.
- Schneider, M.R., Werner, S., Paus, R., Wolf, E. (2008). Beyond wavy hairs: The epidermal growth factor receptor and its ligands in skin biology and pathology. *American Journal of Pathology*, **173**: 14–24.
- Schoenborn, J.R., Wilson, C.B. (2007). Regulation of Interferon- γ During Innate and Adaptive Immune Responses. *Advances in Immunology*, **96**: 41–101.
- Schut, C., Dalgard, F.J., Halvorsen, J.A., Gieler, U., Lien, L., Aragones, L.T., Poot, F., Jemec, G.B.E., Misery, L., Kemény, L., Sampogna, F., van Middendorp, H., Balieva, F., Linder, D., Szepletowski, J.C., Lvov, A., Marron, S.E., Altunay, İ.K., Finlay, A.Y., Salek, S., Kupfer, J. (2019). Occurrence, chronicity and intensity of itch in a clinical consecutive sample of patients with skin

- diseases: A multi-centre study in 13 european countries. *Acta Dermato-Venereologica*, **99**: 146–151.
- Seifert, O., Söderman, J., Skarstedt, M., Dienus, O., Matussek, A. (2015). Increased expression of the wnt signalling inhibitor Dkk-1 in nonlesional skin and peripheral blood mononuclear cells of patients with plaque psoriasis. *Acta Dermato-Venereologica*, **95**: 407–410.
- Seo, S.H., Kim, S., Kim, S.E., Chung, S., Lee, S.E. (2020). Enhanced Thermal Sensitivity of TRPV3 in Keratinocytes Underlies Heat-Induced Pruritogen Release and Pruritus in Atopic Dermatitis. *Journal of Investigative Dermatology*, **140**: 2199–2209.
- Sharif, B., Ase, A.R., Ribeiro-da-Silva, A., Séguéla, P. (2020). Differential Coding of Itch and Pain by a Subpopulation of Primary Afferent Neurons. *Neuron*, **106**: 940–951.
- Shaw, J.L.V., Diamandis, E.P. (2007). Distribution of 15 human kallikreins in tissues and biological fluids. *Clinical Chemistry*, **53**: 1423–1432.
- Shelley, W.B., Arthur, R.P. (1957). The Neurohistology and Neurophysiology of the Itch Sensation in Man. *A. M. A. Archives of Dermatology*, **76**: 296–323.
- Shim, W.S., Tak, M.H., Lee, M.H., Kim, Minjung, Kim, Minkyung, Koo, J.Y., Lee, C.H., Kim, Misook, Oh, U. (2007). TRPV1 mediates histamine-induced itching via the activation of phospholipase A2 and 12-lipoxygenase. *Journal of Neuroscience*, **27**: 2331–2337.
- Shimizu, T., Nishihira, J., Mizue, Y., Nakamura, H., Abe, R., Watanabe, H., Ohkawara, A., Shimizu, H. (2001). High macrophage migration inhibitory factor (MIF) serum levels associated with extended psoriasis [1]. *Journal of Investigative Dermatology*, **116**: 989–990.
- Shinohara, T., Harada, M., Ogi, K., Maruyama, M., Fujii, R., Tanaka, H., Fukusumi, S., Komatsu, H., Hosoya, M., Noguchi, Y., Watanabe, T., Moriya, T., Itoh, Y., Hinuma, S. (2004). Identification of a G protein-coupled receptor specifically responsive to β -alanine. *Journal of Biological Chemistry*, **279**: 23559–23564.
- Sibilia, M., Wagner, E.F. (1995). Strain-dependent epithelial defects in mice lacking the EGF receptor. *Science*, **269**: 234–238.
- Sideris, N., Vakirlis, E., Tsentemidou, A., Kourouklidou, A., Ioannides, D., Sotiriou, E. (2020). Under Development JAK Inhibitors for Dermatologic Diseases. *Mediterranean Journal of Rheumatology*, **31**: 137–144.
- Sikand, P., Dong, X., LaMotte, R.H. (2011). BAM8-22 peptide produces itch and nociceptive sensations in humans independent of histamine release. *Journal of Neuroscience*, **31**: 7563–7567.
- Singh, A.K., McGoldrick, L.L., Sobolevsky, A.I. (2018). Structure and gating mechanism of the transient receptor potential channel TRPV3. *Nature Structural and Molecular Biology*, **25**: 805–813.
- Sinha, S., Lin, G., Ferenczi, K. (2021). The skin microbiome and the gut-skin axis. *Clinics in Dermatology*, **39**: 829–839.
- Smith, G.D., Gunthorpe, M.J., Kelsell, R.E., Hayes, P.D., Reilly, P., Facer, P., Wright, J.E., Jerman, J.C., Walhin, J.P., Ooi, L., Egerton, J., Charles, K.J., Smart, D., Randall, A.D., Anand, P., Davis, J.B. (2002). TRPV3 is a temperature-sensitive vanilloid receptor-like protein. *Nature*, **418**: 186–190.
- Solé-Boldo, L., Raddatz, G., Schütz, S., Mallm, J.P., Rippe, K., Lonsdorf, A.S., Rodríguez-Paredes, M., Lyko, F. (2020). Single-cell transcriptomes of the human skin reveal age-related loss of fibroblast priming. *Communications Biology*, **3**: 1–12.
- Solinski, H.J., Dranchak, P., Oliphant, E., Gu, X., Earnest, T.W., Braisted, J., Inglese, J., Hoon, M.A. (2019). Inhibition of natriuretic peptide receptor 1 reduces itch in mice. *Science Translational Medicine*, **11**: 5464.
- Solinski, H.J., Kriegbaum, M.C., Tseng, P.Y., Earnest, T.W., Gu, X., Barik, A., Chesler, A.T., Hoon, M.A. (2019). Nppb Neurons Are Sensors of Mast Cell-Induced Itch. *Cell Reports*, **26**: 3561–3573.
- Solis, A.G., Bielecki, P., Steach, H.R., Sharma, L., Harman, C.C.D., Yun, S., de Zoete, M.R.,

Warnock, J.N., To, S.D.F., York, A.G., Mack, M., Schwartz, M.A., Dela Cruz, C.S., Palm, N.W., Jackson, R., Flavell, R.A. (2019). Mechanosensation of cyclical force by PIEZO1 is essential for innate immunity. *Nature*, **573**: 69–74.

Song, Z., Chen, X., Zhao, Q., Stanic, V., Lin, Z., Yang, S., Chen, T., Chen, J., Yang, Y. (2021). Hair Loss Caused by Gain-of-Function Mutant TRPV3 Is Associated with Premature Differentiation of Follicular Keratinocytes. *Journal of Investigative Dermatology*, **141**: 1964–1974.

Soumelis, V., Reche, P.A., Kanzler, H., Yuan, W., Edward, G., Homey, B., Gilliet, M., Ho, S., Antonenko, S., Lauerma, A., Smith, K., Gorman, D., Zurawski, S., Abrams, J., Menon, S., McClanahan, T., De Waal-Malefyt, R., Bazan, F., Kastelein, R.A., Liu, Y.J. (2002). Human epithelial cells trigger dendritic cell-mediated allergic inflammation by producing TSLP. *Nature Immunology*, **3**: 673–680.

Southall, M.D., Li, T., Gharibova, L.S., Pei, Y., Nicol, G.D., Travers, J.B. (2003). Activation of epidermal vanilloid receptor-1 induces release of proinflammatory mediators in human keratinocytes. *Journal of Pharmacology and Experimental Therapeutics*, **304**: 217–222.

Sprague, J., Harrison, C., Rowbotham, D.J., Smart, D., Lambert, D.G. (2001). Temperature-dependent activation of recombinant rat vanilloid VR1 receptors expressed in HEK293 cells by capsaicin and anandamide. *European Journal of Pharmacology*, **423**: 121–125.

Ständer, S., Grundmann, S.A. (2012). Chronic pruritus. *Giornale Italiano di Dermatologia e Venereologia*, **147**: 161–169.

Ständer, S., Luger, T.A., Cappelleri, J.C., Bushmakin, A.G., Mamolo, C., Zielinski, M.A., Tallman, A.M., Yosipovitch, G. (2018). Validation of the itch severity item as a measurement tool for pruritus in patients with psoriasis: Results from a phase 3 tofacitinib program. *Acta Dermato-Venereologica*, **98**: 340–345.

Ständer, S., Moormann, C., Schumacher, M., Buddenkotte, J., Artuc, M., Shpacovitch, V., Brzoska, T., Lippert, U., Henz, B.M., Luger, T.A., Metzger, D., Steinhoff, M. (2004). Expression of vanilloid receptor subtype 1 in cutaneous sensory nerve fibers, mast cells, and epithelial cells of appendage structures. *Experimental Dermatology*, **13**: 129–139.

Stanley, E.R., Berg, K.L., Einstein, D.B., Lee, P.S.W., Pixley, F.J., Wang, Y., Yeung, Y.G. (1997). Biology and action of colony-stimulating factor-1. *Molecular Reproduction and Development*, **46**: 4–10.

Steele, H.R., Xing, Y., Zhu, Y., Hilley, H.B., Lawson, K., Nho, Y., Niehoff, T., Han, L. (2021). MrgprC11+ sensory neurons mediate glabrous skin itch. *Proceedings of the National Academy of Sciences of the United States of America*, **118**: 2022874118.

Story, G.M., Peier, A.M., Reeve, A.J., Eid, S.R., Mosbacher, J., Hricik, T.R., Earley, T.J., Hergarden, A.C., Andersson, D.A., Hwang, S.W., McIntyre, P., Jegla, T., Bevan, S., Patapoutian, A. (2003). ANKTM1, a TRP-like channel expressed in nociceptive neurons, is activated by cold temperatures. *Cell*, **112**: 819–829.

Subramanian, H., Gupta, K., Lee, D., Bayir, A.K., Ahn, H., Ali, H. (2013). β -Defensins Activate Human Mast Cells via Mas-Related Gene X2. *The Journal of Immunology*, **191**: 345–352.

Sugiura, T., Bielefeldt, K., Gebhart, G.F. (2004). TRPV1 function in mouse colon sensory neurons is enhanced by metabotropic 5-hydroxytryptamine receptor activation. *Journal of Neuroscience*, **24**: 9521–9530.

Sulk, M., Seeliger, S., Aubert, J., Schwab, V.D., Cevikbas, F., Rivier, M., Nowak, P., Voegel, J.J., Buddenkotte, J., Steinhoff, M. (2012). Distribution and expression of non-neuronal transient receptor potential (TRPV) ion channels in rosacea. *Journal of Investigative Dermatology*, **132**: 1253–1262.

Sun, S., Dong, X. (2016). Trp channels and itch. *Seminars in Immunopathology*, **38**: 293–307.

Sun, X., Qi, H., Wu, H., Qu, Y., Wang, K.W. (2020). Anti-pruritic and anti-inflammatory effects of natural verbascoside through selective inhibition of temperature-sensitive Ca²⁺-permeable TRPV3

- channel. *Journal of Dermatological Science*, **97**: 229–231.
- Sun, X.Y., Sun, L.L., Qi, H., Gao, Q., Wang, G.X., Wei, N.N., Wang, K.W. (2018). Antipruritic effect of natural coumarin osthole through selective inhibition of thermosensitive TRPV3 channel in the skin. *Molecular Pharmacology*, **94**: 1164–1173.
- Swain, S.M., Liddle, R.A. (2021). Piezo1 acts upstream of TRPV4 to induce pathological changes in endothelial cells due to shear stress. *Journal of Biological Chemistry*, **296**: 100171.
- Syeda, R., Xu, J., Dubin, A.E., Coste, B., Mathur, J., Huynh, T., Matzen, J., Lao, J., Tully, D.C., Engels, I.H., Michael Petrassi, H., Schumacher, A.M., Montal, M., Bandell, M., Patapoutian, A. (2015). Chemical activation of the mechanotransduction channel Piezo1. *eLife*, **4**.
- Szőllősi, A.G., Vasas, N., Angyal, Á., Kistamás, K., Nánási, P.P., Mihály, J., Béke, G., Herczeg-Lisztes, E., Szegedi, A., Kawada, N., Yanagida, T., Mori, T., Kemény, L., Bíró, T. (2018). Activation of TRPV3 Regulates Inflammatory Actions of Human Epidermal Keratinocytes. *Journal of Investigative Dermatology*, **138**: 365–374.
- Tabib, T., Morse, C., Wang, T., Chen, W., Lafyatis, R. (2018). SFRP2/DPP4 and FMO1/LSP1 Define Major Fibroblast Populations in Human Skin. *Journal of Investigative Dermatology*, **138**: 802–810.
- Tadala, L., Langenbach, D., Dannborg, M., Cervantes-Rivera, R., Sharma, A., Vieth, K., Rieckmann, L.M., Wanders, A., Cisneros, D.A., Puhar, A. (2022). Infection-induced membrane ruffling initiates danger and immune signaling via the mechanosensor PIEZO1. *Cell Reports*, **40**: 111173.
- Tal, M., Liberman, R. (1997). Local injection of nerve growth factor (NGF) triggers degranulation of mast cells in rat paw. *Neuroscience Letters*, **221**: 129–132.
- Talagas, M., Lebonvallet, N., Leschiera, R., Siquin, G., Elies, P., Haftek, M., Pennec, J.P., Ressenkoff, D., La Padula, V., Le Garrec, R., L'herondelle, K., Mignen, O., Le Pottier, L., Kerfant, N., Reux, A., Marcorelles, P., Misery, L. (2020). Keratinocytes Communicate with Sensory Neurons via Synaptic-like Contacts. *Annals of Neurology*, **88**: 1205–1219.
- Tang, Y., Kesavan, P., Nakada, M.T., Yan, L. (2004). Tumor-Stroma Interaction: Positive Feedback Regulation of Extracellular Matrix Metalloproteinase Inducer (EMMPRIN) Expression and Matrix Metalloproteinase-Dependent Generation of Soluble EMMPRIN. *Molecular Cancer Research*, **2**: 73–80.
- Tani, E., Ishikawa, T. (1990). Histamine Acts Directly on Calcitonin Gene-Related Peptide- and Substance P-Containing Trigeminal Ganglion Neurons as Assessed by Calcium Influx and Immunocytochemistry. *Auris Nasus Larynx*, **17**: 267–274.
- Tao, J., Huang, C.Z., Yu, N.W., Wu, Y., Liu, Y.Q., Li, Y., Tian, J., Yang, L.Y., Zhang, J., Li, J.W., Zhou, Y.W., Tu, Y.T. (2008). Olmsted syndrome: A case report and review of literature. *International Journal of Dermatology*, **47**: 432–437.
- Taylor, P.M., Woodfield, R.J., Hodgkin, M.N., Pettitt, T.R., Martin, A., Kerr, D.J., Wakelam, M.J.O. (2002). Breast cancer cell-derived EMMPRIN stimulates fibroblast MMP2 release through a phospholipase A2 and 5-lipoxygenase catalyzed pathway. *Oncogene*, **21**: 5765–5772.
- Terhorst, D., Kalali, B.N., Ollert, M., Ring, J., Mempel, M. (2010). The role of toll-like receptors in host defenses and their relevance to dermatologic diseases. *American Journal of Clinical Dermatology*, **11**: 1–10.
- Thakur, M., Crow, M., Richards, N., Davey, G.I.J., Levine, E., Kelleher, J.H., Agley, C.C., Denk, F., Harridge, S.D.R., McMahon, S.B. (2014). Defining the nociceptor transcriptome. *Frontiers in Molecular Neuroscience*, **7**: 87.
- Théréne, C., Brenaut, E., Barnetche, T., Misery, L. (2018). Efficacy of Systemic Treatments of Psoriasis on Pruritus: A Systemic Literature Review and Meta-Analysis. *Journal of Investigative Dermatology*, **138**: 38–45.

Threadgill, D.W., Dlugosz, A.A., Hansen, L.A., Tennenbaum, T., Lichti, U., Yee, D., LaMantia, C., Mourton, T., Herrup, K., Harris, R.C., Barnard, J.A., Yuspa, S.H., Coffey, R.J., Magnuson, T. (1995). Targeted disruption of mouse EGF receptor: Effect of genetic background on mutant phenotype. *Science*, **269**: 230–234.

Tibshirani, R., Walther, G., Hastie, T. (2001). Estimating the number of clusters in a data set via the gap statistic. *Journal of the Royal Statistical Society. Series B: Statistical Methodology*, **63**: 411–423.

Tohyama, M., Matsumoto, A., Tsuda, T., Dai, X., Shiraishi, K., Sayama, K. (2021). Suppression of IL-17A-induced CCL20 production by cytokine inducible SH2-containing protein 1 in epidermal keratinocytes. *Journal of Dermatological Science*, **101**: 202–209.

Toledo Mauriño, J.J., Fonseca-Camarillo, G., Furuzawa-Carballeda, J., Barreto-Zuñiga, R., Martínez Benítez, B., Granados, J., Yamamoto-Furusho, J.K. (2020). TRPV Subfamily (TRPV2, TRPV3, TRPV4, TRPV5, and TRPV6) Gene and Protein Expression in Patients with Ulcerative Colitis. *Journal of Immunology Research*, **2020**: 2906845.

Tsagareli, M.G., Nozadze, I. (2020). An overview on transient receptor potential channels superfamily. *Behavioural Pharmacology*, **31**: 413–434.

Tseng, P.Y., Hoon, M.A. (2022). Specific β -Defensins Stimulate Pruritus through Activation of Sensory Neurons. *Journal of Investigative Dermatology*, **142**: 594–602.

Tzanetakou, V., Kanni, T., Giatrakou, S., Katoulis, A., Papadavid, E., Netea, M.G., Dinarello, C.A., Van Der Meer, J.W.M., Rigopoulos, D., Giamarellos-Bourboulis, E.J. (2016). Safety and efficacy of anakinra in severe hidradenitis suppurativa a randomized clinical trial. *JAMA Dermatology*, **152**: 52–59.

Uhlén, M., Fagerberg, L., Hallström, B.M., Lindskog, C., Oksvold, P., Mardinoglu, A., Sivertsson, Å., Kampf, C., Sjöstedt, E., Asplund, A., Olsson, I.M., Edlund, K., Lundberg, E., Navani, S., Szigyanto, C.A.K., Odeberg, J., Djureinovic, D., Takanen, J.O., Hober, S., Alm, T., Edqvist, P.H., Berling, H., Tegel, H., Mulder, J., Rockberg, J., Nilsson, P., Schwenk, J.M., Hamsten, M., Von Feilitzen, K., Forsberg, M., Persson, L., Johansson, F., Zwahlen, M., Von Heijne, G., Nielsen, J., Pontén, F. (2015). Tissue-based map of the human proteome. *Science*, **347**: 1260419.

Ui, H., Andoh, T., Lee, J.B., Nojima, H., Kuraishi, Y. (2006). Potent pruritogenic action of tryptase mediated by PAR-2 receptor and its involvement in anti-pruritic effect of nafamostat mesilate in mice. *European Journal of Pharmacology*, **530**: 172–178.

Usoskin, D., Furlan, A., Islam, S., Abdo, H., Lönnerberg, P., Lou, D., Hjerling-Leffler, J., Haeggström, J., Kharchenko, O., Kharchenko, P. V., Linnarsson, S., Ernfors, P. (2015). Unbiased classification of sensory neuron types by large-scale single-cell RNA sequencing. *Nature Neuroscience*, **18**: 145–153.

Varadi, M., Anyango, S., Deshpande, M., Nair, S., Natassia, C., Yordanova, G., Yuan, D., Stroe, O., Wood, G., Laydon, A., Zidek, A., Green, T., Tunyasuvunakool, K., Petersen, S., Jumper, J., Clancy, E., Green, R., Vora, A., Lutfi, M., Figurnov, M., Cowie, A., Hobbs, N., Kohli, P., Kleywegt, G., Birney, E., Hassabis, D., Velankar, S. (2022). AlphaFold Protein Structure Database: Massively expanding the structural coverage of protein-sequence space with high-accuracy models. *Nucleic Acids Research*, **50**: 439–444.

Vasas, N., Péntzes, Z., Kistamás, K., Nánási, P.P., Molnár, S., Szegedi, A., Szöllösi, A.G., Bíró, T. (2022). Transient receptor potential vanilloid 3 expression is increased in non-lesional skin of atopic dermatitis patients. *Experimental Dermatology*, **31**: 807–813.

Vieira-de-Abreu, A., Calheiros, A.S., Mesquita-Santos, F.P., Magalhães, E.S., Mourão-Sá, D., Castro-Faria-Neto, H.C., Bozza, M.T., Bandeira-Melo, C., Bozza, P.T. (2011). Cross-talk between macrophage migration inhibitory factor and eotaxin in allergic eosinophil activation forms leukotriene C4-synthesizing lipid bodies. *American Journal of Respiratory Cell and Molecular Biology*, **44**: 509–516.

Voets, T., Prenen, J., Vriens, J., Watanabe, H., Janssens, A., Wissenbach, U., Bödding, M.,

- Droogmans, G., Nilius, B. (2002). Molecular determinants of permeation through the cation channel TRPV4. *Journal of Biological Chemistry*, **277**: 33704–33710.
- Vogt-Eisele, A.K., Weber, K., Sherkheli, M.A., Vielhaber, G., Panten, J., Gisselmann, G., Hatt, H. (2007). Monoterpenoid agonists of TRPV3. *British Journal of Pharmacology*, **151**: 530–540.
- Voisin, T., Perner, C., Messou, M.A., Shiers, S., Ualiyeva, S., Kanaoka, Y., Price, T.J., Sokol, C.L., Bankova, L.G., Frank Austen, K., Chiu, I.M. (2021). The CysLT2R receptor mediates leukotriene C4-driven acute and chronic itch. *Proceedings of the National Academy of Sciences of the United States of America*, **118**: 2022087118.
- Wallace, R.G., Kenealy, M.R., Brady, A.J., Twomey, L., Duffy, E., Degryse, B., Caballero-Lima, D., Moyna, N.M., Custaud, M.A., Meade-Murphy, G., Morrin, A., Murphy, R.P. (2020). Development of dynamic cell and organotypic skin models, for the investigation of a novel viscoelastic burns treatment using molecular and cellular approaches. *Burns*, **46**: 1585–1602.
- Wallmeyer, L., Dieter, K., Sochorová, M., Gruber, A.D., Kleuser, B., Vávrová, K., Hedtrich, S. (2017). TSLP is a direct trigger for T cell migration in filaggrin-deficient skin equivalents. *Scientific Reports*, **7**: 1–12.
- Walsh, C.M., Hill, R.Z., Schwendinger-Schreck, J., Deguine, J., Brock, E.C., Kucirek, N., Rifi, Z., Wei, J., Gronert, K., Brem, R.B., Barton, G.M., Bautista, D.M. (2019). Neutrophils promote CXCR3-dependent itch in the development of atopic dermatitis. *eLife*, **8**.
- Wang, F., Kim, B.S. (2020). Itch: A Paradigm of Neuroimmune Crosstalk. *Immunity*, **52**: 753–766.
- Wang, Fang, Trier, A.M., Li, F., Kim, S., Chen, Z., Chai, J.N., Mack, M.R., Morrison, S.A., Hamilton, J.D., Baek, J., Yang, T.L.B., Ver Heul, A.M., Xu, A.Z., Xie, Z., Dong, Xintong, Kubo, M., Hu, H., Hsieh, C.S., Dong, Xinzhong, Liu, Q., Margolis, D.J., Ardeleanu, M., Miller, M.J., Kim, B.S. (2021). A basophil-neuronal axis promotes itch. *Cell*, **184**: 422–440.
- Wang, F., Yang, T.L.B., Kim, B.S. (2020). The Return of the Mast Cell: New Roles in Neuroimmune Itch Biology. *Journal of Investigative Dermatology*, **140**: 945–951.
- Wang, Haiyuan, Yang, P., Lu, Y., Wang, J., Jeon, J., Wang, Q., Tian, J. Bin, Zang, B., Yu, Y., Zhu, M.X. (2021). Mechanisms of proton inhibition and sensitization of the cation channel TRPV3. *Journal of General Physiology*, **153**: 1–16.
- Wang, L., Zhou, H., Zhang, M., Liu, W., Deng, T., Zhao, Q., Li, Y., Lei, J., Li, X., Xiao, B. (2019). Structure and mechanogating of the mammalian tactile channel PIEZO2. *Nature*, **573**: 225–229.
- Wang, X.N., McGovern, N., Gunawan, M., Richardson, C., Windebank, M., Siah, T.W., Lim, H.Y., Fink, K., Li, J.L.Y., Ng, L.G., Ginhoux, F., Angeli, V., Collin, M., Haniffa, M. (2014). A three-dimensional atlas of human dermal leukocytes, lymphatics, and blood vessels. *Journal of Investigative Dermatology*, **134**: 965–974.
- Wang, Y., Dong, C., Han, Y., Gu, Z., Sun, C. (2022). Immunosenescence, aging and successful aging. *Frontiers in Immunology*, **13**: 1–18.
- Wang, Yujing, Li, H., Xue, C., Chen, H., Xue, Y., Zhao, F., Zhu, M.X., Cao, Z. (2021). TRPV3 enhances skin keratinocyte proliferation through EGFR-dependent signaling pathways. *Cell Biology and Toxicology*, **37**: 313–330.
- Warnock, J.K., Morris, D.W. (2002). Adverse cutaneous reactions to antidepressants. *American Journal of Clinical Dermatology*, **3**: 329–339.
- Watanabe, A., Takeuchi, M., Nagata, M., Nakamura, K., Nakao, H., Yamashita, H., Makino, S., Harada, M., Hirasawa, T. (2003). Role of the Nh (Non-hair) mutation in the development of dermatitis and hyperproduction of IgE in DS-Nh mice. *Experimental Animals*, **52**: 419–423.
- Watanabe, N., Hanabuchi, S., Soumelis, V., Yuan, W., Ho, S., de Waal Malefyt, R., Liu, Y.J. (2004). Human thymic stromal lymphopoietin promotes dendritic cell-mediated CD4⁺ T cell homeostatic expansion. *Nature Immunology*, **5**: 426–434.

- Watt, F.M. (1989). Terminal differentiation of epidermal keratinocytes. *Current Opinion in Cell Biology*, **1**: 1107–1115.
- Wee, P., Wang, Z. (2017). Epidermal growth factor receptor cell proliferation signaling pathways. *Cancers*, **9**: 52.
- Wei, Z., Lin, B.J., Chen, T.W., Daie, K., Svoboda, K., Druckmann, S. (2020). A comparison of neuronal population dynamics measured with calcium imaging and electrophysiology. *PLoS Computational Biology*, **16**: 1008198.
- Weisshaar, E. (2016). Epidemiology of Itch. *Current Problems in Dermatology (Switzerland)*, **50**: 5–10.
- Wells, A. (1999). EGF receptor. *International Journal of Biochemistry and Cell Biology*, **31**: 637–643.
- Whang, K.A., Khanna, R., Williams, K.A., Mahadevan, V., Semenov, Y., Kwatra, S.G. (2021). Health-Related QOL and Economic Burden of Chronic Pruritus. *Journal of Investigative Dermatology*, **141**: 754–760.
- Wilson, S.R., Gerhold, K.A., Bifolck-Fisher, A., Liu, Q., Patel, K.N., Dong, X., Bautista, D.M. (2011). TRPA1 is required for histamine-independent, Mas-related G protein-coupled receptor-mediated itch. *Nature Neuroscience*, **14**: 595–603.
- Wilson, S.R., Nelson, A.M., Batia, L., Morita, T., Estandian, D., Owens, D.M., Lumpkin, E.A., Bautista, D.M. (2013). The ion channel TRPA1 is required for chronic itch. *Journal of Neuroscience*, **33**: 9283–9294.
- Wilson, S.R., Thé, L., Batia, L.M., Beattie, K., Katibah, G.E., McClain, S.P., Pellegrino, M., Estandian, D.M., Bautista, D.M. (2013). The epithelial cell-derived atopic dermatitis cytokine TSLP activates neurons to induce itch. *Cell*, **155**: 285–295.
- Wolstenholme, A.J., Williamson, S.M., Reaves, B.J. (2011). TRP channels in parasites. *Advances in Experimental Medicine and Biology*, **704**: 359–371.
- Woo, S.H., Ranade, S., Weyer, A.D., Dubin, A.E., Baba, Y., Qiu, Z., Petrus, M., Miyamoto, T., Reddy, K., Lumpkin, E.A., Stucky, C.L., Patapoutian, A. (2014). Piezo2 is required for Merkel-cell mechanotransduction. *Nature*, **509**: 622–626.
- Woodbury, C.J., Zwick, M., Wang, S., Lawson, J.J., Caterina, M.J., Koltzenburg, M., Albers, K.M., Koerber, H.R., Davis, B.M. (2004). Nociceptors lacking TRPV1 and TRPV2 have normal heat responses. *Journal of Neuroscience*, **24**: 6410–6415.
- Wooten, M., Weng, H.J., Hartke, T. V., Borzan, J., Klein, A.H., Turnquist, B., Dong, X., Meyer, R.A., Ringkamp, M. (2014). Three functionally distinct classes of C-fibre nociceptors in primates. *Nature Communications*, **5**: 1–12.
- Wu, L.S., Li, F.F., Sun, L.D., Li, D., Su, J., Kuang, Y.H., Chen, G., Chen, X.P., Chen, X. (2011). A miRNA-492 binding-site polymorphism in BSG (basigin) confers risk to psoriasis in Central South Chinese population. *Human Genetics*, **130**: 749–757.
- Xiao, R., Tang, J., Wang, C., Colton, C.K., Tian, J., Zhu, M.X. (2008). Calcium plays a central role in the sensitization of TRPV3 channel to repetitive stimulations. *Journal of Biological Chemistry*, **283**: 6162–6174.
- Xiao, R., Tian, J., Tang, J., Zhu, M.X. (2008). The TRPV3 mutation associated with the hairless phenotype in rodents is constitutively active. *Cell Calcium*, **43**: 334–343.
- Xie, Y., Chen, D., Jiang, K., Song, L., Qian, N., Du, Y., Yang, Y., Wang, F., Chen, T. (2022). Hair shaft miniaturization causes stem cell depletion through mechanosensory signals mediated by a Piezo1-calcium-TNF- α axis. *Cell Stem Cell*, **29**: 70–85.
- Xie, Y., Yang, L. (2016). Calcium and Magnesium Ions Are Membrane-Active against Stationary-

- Phase Staphylococcus aureus with High Specificity. *Scientific Reports*, **6**: 1–8.
- Xie, Z., Hu, H. (2018). TRP channels as drug targets to relieve itch. *Pharmaceuticals*, **11**: 100.
- Xu, H., Delling, M., Jun, J.C., Clapham, D.E. (2006). Oregano, thyme and clove-derived flavors and skin sensitizers activate specific TRP channels. *Nature Neuroscience*, **9**: 628–635.
- Xu, H., Ramsey, I.S., Kotecha, S.A., Moran, M.M., Chong, J.A., Lawson, D., Ge, P., Lilly, J., Silos-Santiago, I., Xie, Y., DiStefano, P.S., Curtis, R., Clapham, D.E. (2002). TRPV3 is a calcium-permeable temperature-sensitive cation channel. *Nature*, **418**: 181–186.
- Xu, Xiaojun, Xu, Hao, Y., Zhu, X., Lu, J., Ouyang, X., Lu, Y., Huang, X., Li, Y., Wang, J., Shen, X. (2020). Antispasmodic Drug Drofenine as an Inhibitor of Kv2.1 Channel Ameliorates Peripheral Neuropathy in Diabetic Mice. *iScience*, **23**.
- Yamaguchi, T., Nagasawa, T., Satoh, M., Kuraishi, Y. (1999). Itch-associated response induced by intradermal serotonin through 5-HT₂ receptors in mice. *Neuroscience Research*, **35**: 77–83.
- Yamaguchi, Y., Morita, A., Maeda, A., Hearing, V.J. (2009). Regulation of skin pigmentation and thickness by dickkopf 1 (DKK1). *Journal of Investigative Dermatology Symposium Proceedings*, **14**: 73–75.
- Yamaguchi, Y., Passeron, T., Hoashi, T., Watabe, H., Rouzaud, F., Yasumoto, K.K.-I., Hara, T., Tohyama, C., Katayama, I., Miki, T., Hearing, V.J. (2008). Dickkopf 1 (DKK1) regulates skin pigmentation and thickness by affecting Wnt/ β -catenin signaling in keratinocytes. *The FASEB Journal*, **22**: 1009–1020.
- Yamamoto-Kasai, E., Imura, K., Yasui, K., Shichijou, M., Oshima, I., Hirasawa, T., Sakata, T., Yoshioka, T. (2012). TRPV3 as a therapeutic target for itch. *Journal of Investigative Dermatology*, **132**: 2109–2112.
- Yamamoto-Kasai, E., Yasui, K., Shichijo, M., Sakata, T., Yoshioka, T. (2013). Impact of TRPV3 on the development of allergic dermatitis as a dendritic cell modulator. *Experimental Dermatology*, **22**: 820–824.
- Yan, D., Issa, N., Afifi, L., Jeon, C., Chang, H.W., Liao, W. (2017). The Role of the Skin and Gut Microbiome in Psoriatic Disease. *Current Dermatology Reports*, **6**: 94–103.
- Yan, K., Sun, X., Wang, G., Liu, Y., Wang, K.W. (2019). Pharmacological activation of thermo-transient receptor potential vanilloid 3 channels inhibits hair growth by inducing cell death of hair follicle outer root sheath. *Journal of Pharmacology and Experimental Therapeutics*, **370**: 299–307.
- Yan, L., Zhang, X., Fu, J., Liu, Q., Lei, X., Cao, Z., Zhang, J., Shao, Y., Tong, Q., Qin, W., Liu, X., Liu, C., Liu, Z., Li, Z., Lu, J., Xu, X. (2021). Inhibition of the transient receptor potential vanilloid 3 channel attenuates carbon tetrachloride-induced hepatic fibrosis. *Biochemical and Biophysical Research Communications*, **558**: 86–93.
- Yang, G., Seok, J.K., Kang, H.C., Cho, Y.Y., Lee, H.S., Lee, J.Y. (2020). Skin barrier abnormalities and immune dysfunction in atopic dermatitis. *International Journal of Molecular Sciences*, **21**: 2867.
- Yang, Hua, Chen, W., Zhu, R., Wang, J., Meng, J. (2022). Critical Players and Therapeutic Targets in Chronic Itch. *International Journal of Molecular Sciences*, **23**: 1–27.
- Yang, R., Xiong, Z., Liu, C., Liu, L. (2014). Inhibitory effects of capsaicin on voltage-gated potassium channels by TRPV1-independent pathway. *Cellular and Molecular Neurobiology*, **34**: 565–576.
- Yang, Yudie, Qu, L., Mijakovic, I., Wei, Y. (2022). Advances in the human skin microbiota and its roles in cutaneous diseases. *Microbial Cell Factories*, **21**: 1–14.
- Yang, Y.S., Cho, S.I., Choi, M.G., Choi, Y.H., Kwak, I.S., Park, C.W., Kim, H.O. (2015). Increased Expression of Three Types of Transient Receptor Potential Channels (TRPA1, TRPV4 and TRPV3) in Burn Scars with Postburn Pruritus. *Acta Dermato-Venereologica*, **95**: 20–24.

Yap, J.M.G., Ueda, T., Kanemitsu, Y., Takeda, N., Fukumitsu, K., Fukuda, S., Uemura, T., Tajiri, T., Ohkubo, H., Maeno, K., Ito, Y., Oguri, T., Ugawa, S., Niimi, A. (2021). AITC inhibits fibroblast-myofibroblast transition via TRPA1-independent MAPK and NRF2/HO-1 pathways and reverses corticosteroids insensitivity in human lung fibroblasts. *Respiratory Research*, **22**: 1–12.

Yasuda, C., Enomoto, A., Ishiwatari, S., Mori, N., Kagoyama, K., Matsunaga, K., Yoshihisa, Y., Matsukuma, S., Shimizu, T. (2014). Macrophage migration inhibitory factor (MIF) in the stratum corneum: A marker of the local severity of atopic dermatitis. *Experimental Dermatology*, **23**: 764–766.

Yoneda, M., Suzuki, H., Hatano, N., Nakano, S., Muraki, Y., Miyazawa, K., Goto, S., Muraki, K. (2019). PIEZO1 and TRPV4, which are distinct mechano-sensors in the osteoblastic MC3T3-E1 cells, modify cell-proliferation. *International Journal of Molecular Sciences*, **20**: 1–20.

Yoshioka, T., Hikita, I., Matsutani, T., Yoshida, R., Asakawa, M., Toyosaki-Maeda, T., Hirasawa, T., Suzuki, R., Arimura, A., Horikawa, T. (2003). DS-Nh as an experimental model of atopic dermatitis induced by *Staphylococcus aureus* producing staphylococcal enterotoxin C. *Immunology*, **108**: 562–569.

Yoshioka, T., Imura, K., Asakawa, M., Suzuki, M., Oshima, I., Hirasawa, T., Sakata, T., Horikawa, T., Arimura, A. (2009). Impact of the Gly573Ser substitution in TRPV3 on the development of allergic and pruritic dermatitis in mice. *Journal of Investigative Dermatology*, **129**: 714–722.

Yosipovitch, G., Reaney, M., Mastey, V., Eckert, L., Abbé, A., Nelson, L., Clark, M., Williams, N., Chen, Z., Ardeleanu, M., Akinlade, B., Graham, N.M.H., Pirozzi, G., Staudinger, H., Plaum, S., Radin, A., Gadkari, A. (2019). Peak Pruritus Numerical Rating Scale: psychometric validation and responder definition for assessing itch in moderate-to-severe atopic dermatitis. *British Journal of Dermatology*, **181**: 761–769.

Yosipovitch, G., Samuel, L.S. (2008). Neuropathic and psychogenic itch. *Dermatologic Therapy*, **21**: 32–41.

Yu, X., Yan, N., Li, Z., Hua, Y., Chen, W. (2019). FGF19 sustains the high proliferative ability of keratinocytes in psoriasis through the regulation of Wnt/GSK-3 β / β -catenin signalling via FGFR4. *Clinical and Experimental Pharmacology and Physiology*, **46**: 761–769.

Zhang, H., Sun, X., Qi, H., Ma, Q., Zhou, Q., Wang, W., Wang, K.W. (2019). Pharmacological inhibition of the temperature-sensitive and Ca²⁺-permeable transient receptor potential vanilloid TRPV3 channel by natural forsythoside B attenuates pruritus and cytotoxicity of keratinocytes. *Journal of Pharmacology and Experimental Therapeutics*, **368**: 21–31.

Zhang, L., McNeil, B.D. (2019). Beta-defensins are proinflammatory pruritogens that activate Mrgprs. *Journal of Allergy and Clinical Immunology*, **143**: 1960–1962.

Zhang, S., Liu, B., Wang, W., Lv, L., Gao, D., Chai, M., Li, M., Wu, Z., Zhu, Y., Ma, J., Leng, L. (2021). The “Matrisome” reveals the characterization of skin keloid microenvironment. *FASEB Journal*, **35**: 21237.

Zhao, J., Munanairi, A., Liu, X.Y., Zhang, J., Hu, L., Hu, M., Bu, D., Liu, L., Xie, Z., Kim, B.S., Yang, Y., Chen, Z.F. (2020). PAR2 Mediates Itch via TRPV3 Signaling in Keratinocytes. *Journal of Investigative Dermatology*, **140**: 1524–1532.

Zhao, Q., Zhou, H., Chi, S., Wang, Y., Wang, Jianhua, Geng, J., Wu, K., Liu, W., Zhang, T., Dong, M.Q., Wang, Jiawei, Li, X., Xiao, B. (2018). Structure and mechanogating mechanism of the Piezo1 channel. *Nature*, **554**: 487–492.

Zhu, F., Yang, S., Meng, F., Zheng, Y., Ku, X., Luo, C., Hu, G., Liang, Z. (2022). Leveraging Protein Dynamics to Identify Functional Phosphorylation Sites using Deep Learning Models. *Journal of Chemical Information and Modeling*, **62**: 3331–3345.

Zhu, T., Guo, J., Wu, Y., Lei, T., Zhu, J., Chen, H., Kala, S., Wong, K.F., Cheung, C.P., Huang, X., Zhao, X., Yang, M., Sun, L. (2023). The mechanosensitive ion channel Piezo1 modulates the

migration and immune response of microglia. *iScience*, **26**: 105993.

Zhu, Z., Chen, J., Lin, Y., Zhang, C., Li, W., Qiao, H., Fu, M., Dang, E., Wang, G. (2020). Aryl Hydrocarbon Receptor in Cutaneous Vascular Endothelial Cells Restricts Psoriasis Development by Negatively Regulating Neutrophil Recruitment. *Journal of Investigative Dermatology*, **140**: 1233–1243.

Zimmerman, A., Bai, L., Ginty, D.D. (2014). The gentle touch receptors of mammalian skin. *Science*, **346**: 950–954.

Zou, Z., Long, X., Zhao, Q., Zheng, Y., Song, M., Ma, S., Jing, Y., Wang, S., He, Y., Esteban, C.R., Yu, N., Huang, J., Chan, P., Chen, T., Izpisua Belmonte, J.C., Zhang, W., Qu, J., Liu, G.H. (2021). A Single-Cell Transcriptomic Atlas of Human Skin Aging. *Developmental Cell*, **56**: 383–397.

Zubcevic, L., Herzik, M.A., Wu, M., Borschel, W.F., Hirschi, M., Song, A.S., Lander, G.C., Lee, S.Y. (2018). Conformational ensemble of the human TRPV3 ion channel. *Nature Communications*, **9**: 4773.

Zylka, M.J., Dong, X., Southwell, A.L., Anderson, D.J. (2003). Atypical expansion in mice of the sensory neuron-specific Mrg G protein-coupled receptor family. *Proceedings of the National Academy of Sciences of the United States of America*, **100**: 10043–10048.